CURRENT CHALLENGES IN PROVIDING EARLY WARNING OF HARMFUL ALGAL AND MICROBIOLOGICAL RISK TO AQUACULTURE

EDITED BY: Marcos Mateus, Joe Silke, Keith Davidson and Patricia Neira Del Río

PUBLISHED IN: Frontiers in Marine Science

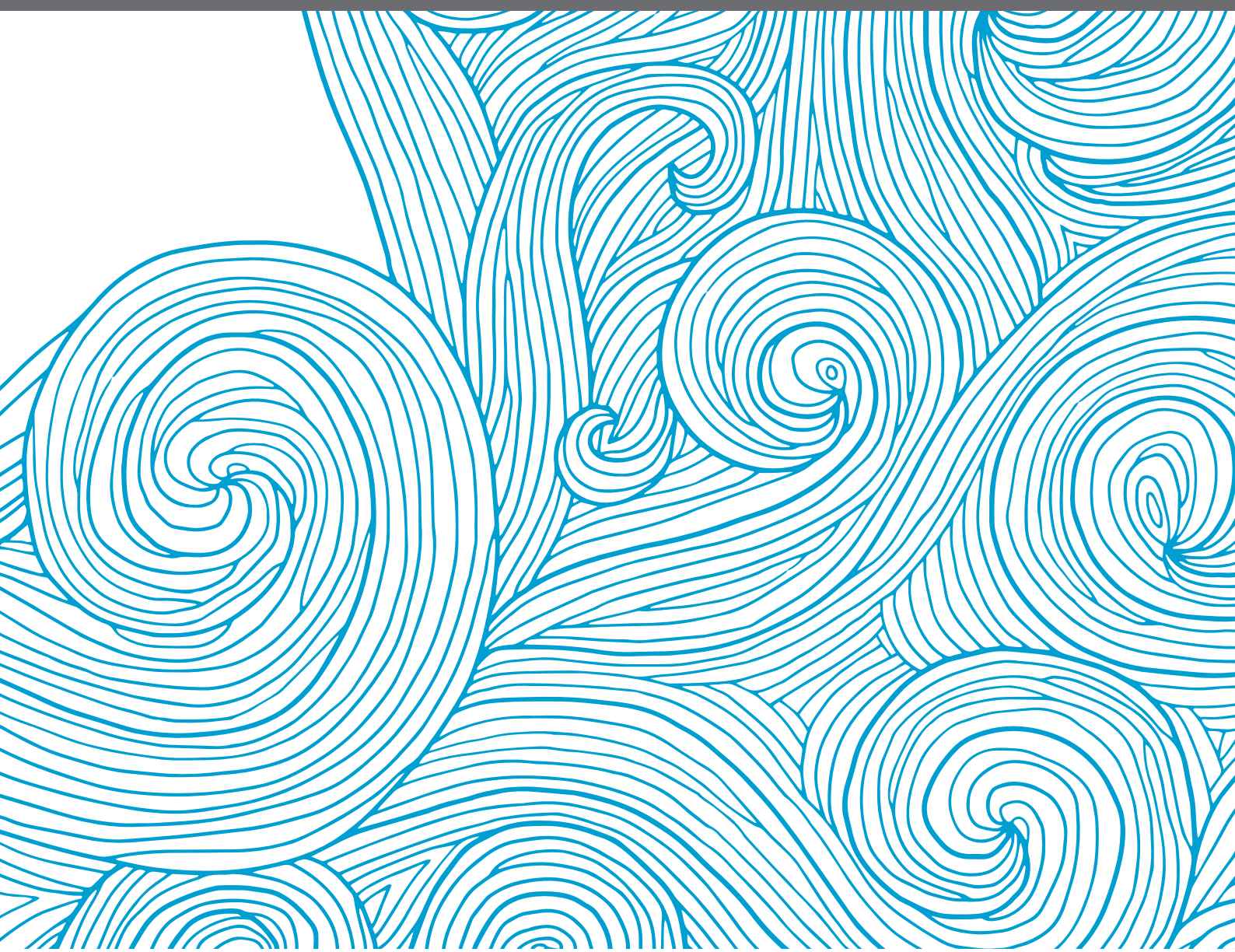

frontiers Research Topics

frontiers

ISSN 1664-8714
ISBN 978-2-88976-887-5
DOI 10.3389/978-2-88976-887-5

About Frontiers

Frontiers is more than just an open-access publisher of scholarly articles: it is a pioneering approach to the world of academia, radically improving the way scholarly research is managed. The grand vision of Frontiers is a world where all people have an equal opportunity to seek, share and generate knowledge. Frontiers provides immediate and permanent online open access to all its publications, but this alone is not enough to realize our grand goals.

Frontiers Journal Series

The Frontiers Journal Series is a multi-tier and interdisciplinary set of open-access, online journals, promising a paradigm shift from the current review, selection and dissemination processes in academic publishing. All Frontiers journals are driven by researchers for researchers; therefore, they constitute a service to the scholarly community. At the same time, the Frontiers Journal Series operates on a revolutionary invention, the tiered publishing system, initially addressing specific communities of scholars, and gradually climbing up to broader public understanding, thus serving the interests of the lay society, too.

Dedication to Quality

Each Frontiers article is a landmark of the highest quality, thanks to genuinely collaborative interactions between authors and review editors, who include some of the world's best academicians. Research must be certified by peers before entering a stream of knowledge that may eventually reach the public - and shape society; therefore, Frontiers only applies the most rigorous and unbiased reviews.
Frontiers revolutionizes research publishing by freely delivering the most outstanding research, evaluated with no bias from both the academic and social point of view. By applying the most advanced information technologies, Frontiers is catapulting scholarly publishing into a new generation.

What are Frontiers Research Topics?

Frontiers Research Topics are very popular trademarks of the Frontiers Journals Series: they are collections of at least ten articles, all centered on a particular subject. With their unique mix of varied contributions from Original Research to Review Articles, Frontiers Research Topics unify the most influential researchers, the latest key findings and historical advances in a hot research area! Find out more on how to host your own Frontiers Research Topic or contribute to one as an author by contacting the Frontiers Editorial Office: frontiersin.org/about/contact

CURRENT CHALLENGES IN PROVIDING EARLY WARNING OF HARMFUL ALGAL AND MICROBIOLOGICAL RISK TO AQUACULTURE

Topic Editors:
Marcos Mateus, Universidade de Lisboa, Portugal
Joe Silke, Marine Institute, Ireland
Keith Davidson, Scottish Association For Marine Science, United Kingdom
Patricia Neira Del Río, Marine Institute, Ireland

Citation: Mateus, M., Silke, J., Davidson, K., Del Río, P. N., eds. (2022). Current Challenges in Providing Early Warning of Harmful Algal and Microbiological Risk to Aquaculture. Lausanne: Frontiers Media SA. doi: 10.3389/978-2-88976-887-5

Table of Contents

frontiers | Frontiers in Marine Science

TYPE Editorial
PUBLISHED 27 July 2022
DOI 10.3389/fmars.2022.973925

OPEN ACCESS

EDITED AND REVIEWED BY
Stephen J Newman,
Department of Primary Industries and Regional Development of Western Australia (DPIRD), Australia

*CORRESPONDENCE
Keith Davidson
kda@sams.ac.uk

SPECIALTY SECTION
This article was submitted to Marine Fisheries, Aquaculture and Living Resources, a section of the journal Frontiers in Marine Science

RECEIVED 20 June 2022
ACCEPTED 04 July 2022
PUBLISHED 27 July 2022

CITATION
Neira Del Río P, Mateus M, Silke J and Davidson K (2022) Editorial: Current challenges in providing early warning of harmful algal and microbiological risk to aquaculture.
Front. Mar. Sci. 9:973925.
doi: 10.3389/fmars.2022.973925

Editorial: Current challenges in providing early warning of harmful algal and microbiological risk to aquaculture

Patricia Neira Del Río[1], Marcos Mateus[2], Joe Silke[1] and Keith Davidson[3]*

[1]Marine Institute, Galway, Ireland, [2]Marine, Environment and Technology Centre/Laboratory for Robotics and Engineering Systems (MARETEC/LARSyS), Instituto Superior Técnico, Universidade de Lisboa, Lisbon, Portugal, [3]Scottish Association for Marine Science, Scottish Marine Institute, Oban, United Kingdom

KEYWORDS

Harmful algal blooms, biotoxins, early warning, remote sensing, mathematical modelling

Editorial on the research topic

Current Challenges in Providing Early Warning of Harmful Algal and Microbiological Risk to Aquaculture

The aquaculture sector is a major industry in Europe's Atlantic Arc. Its continued sustainable growth is required to meet the increasing demand for farmed fish and shellfish. However, such expansion faces several microbiological challenges, with harmful algal blooms (HABs) being prominent among these.

A few species of naturally occurring marine microalgae can produce biotoxins. When conditions are favourable, these organisms can rapidly increase in abundance generating a HAB event. Farmed shellfish feed on these microalgae and can concentrate the biotoxins within their flesh. While the shellfish themselves are not harmed, their consumption poses a risk to human consumers. The impact of shellfish poisoning can range from mild gastrointestinal symptoms to neurological issues and, in extreme cases, may even lead to death.

Blooms of other harmful phytoplankton species have a damaging effect on farmed fish through deoxygenation, toxicity, or damage to the gills. In most cases, consumption of these fish would not be harmful to humans, but the associated production losses can be economically significant for the industry.

HAB and pathogen events are spatially and temporally variable. The aquaculture industry, therefore, relies on early warning indicators of these events to allow for the best possible mitigation measures to be put in place.

The Interreg Atlantic Area funded project PRIMROSE built on the existing HAB forecasting systems developed within the award-winning EU FP7 funded project ASIMUTH (Maguire et al., 2016). The project PRIMROSE delivered improved forecasts of HABs, microbial risks and climate impacts in aquaculture locations encompassing the length of Europe's Atlantic Arc, from the Shetland Islands in the north to the Canary Islands in the South.

The transnational cooperation within PRIMROSE allowed for the generation of best practices and methodologies for HAB, biotoxin and microbial early warning indicators to be shared among the partner countries, allowing enhanced risk assessment.

This special issue summarises the developments in HAB early warning indicators through PRIMROSE in the European Atlantic Arc, while also showcasing similar developments in other geographical regions.

Early detection of HABs is key to providing the aquaculture industry with sufficient time to undertake mitigative measures. Several authors highlighted the role of remote sensing in this process. Martinez-Vicente et al. presented results from laboratory experiments that were conducted to improve existing algorithms for the satellite detection of the important fish killing dinoflagellate *Karenia mikimotoi*. The application of the laboratory-derived training dataset improved the ability of the algorithm to distinguish between high turbidity and high chlorophyll (phytoplankton) concentrations.

A different approach to the use of remote sensing for the detection of *K. mikimotoi* was undertaken by Jordan et al., who demonstrated the potential use of the "red band difference" algorithm, that was originally developed to monitor a different harmful species of the same genus (*Karenia brevis*) in the US. The study found success with this approach in European waters, with the potential to couple the remote sensing to a Lagrangian particle tracking model to then predict the future progression of the bloom as it advects across the shelf. Lin et al. also addressed satellite-derived ocean colour measurements and Lagrangian particle tracking. In this work the authors developed a prediction scheme to merge the satellite observations and the model data, thus enhancing the capability to interpret HAB risk.

The use of Lagrangian modelling approaches was prominent in other studies in this issue. Beddington et al. reviewed the performance of three different modelling systems against historical bloom events, confirming that such particle tracking tools can be usefully integrated operationally into HAB early warning systems. Hariri et al. discuss the combination of Lagrangian modelling with molecular analyses that can provide more information on the species composition of the taxa of interest. In another case, the role of molecular approaches combined with flow cytometry was evaluated by Mirasbekov et al. as a means for better identification of HAB taxa.

Operational early warning indication using a FVCOM based high-resolution unstructured grid mathematical model for Scottish waters was demonstrated by Davidson et al. This contribution also summarised the Scottish HAB early warning system and its use by the aquaculture industry. The need for such reactive early warning approaches was confirmed by Gianella et al. who used PCA and K-means to statistically demonstrate the spatial and temporal variability of HABs in Scottish waters.

The status of HAB and shellfish biotoxin EWS approaches Europe-wide, and an evaluation of the similarities and differences in separate regions was summarised by Fernandes-Salvador et al. Their paper considered the potential to further improve these EWS through multi-disciplinary approaches combining heterogeneous sources of information.

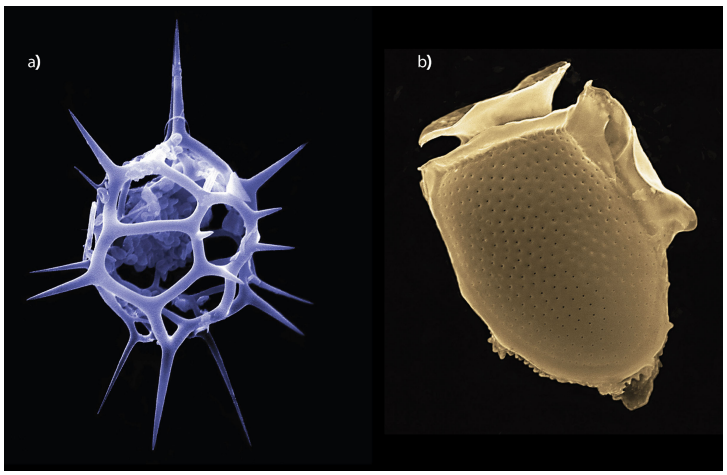

GRAPHICAL ABSTRACT
Enhanced colour image scanning electron microscope of two harmful phytoplankton **(A)** *Dictyocha* sp. and **(B)** *Dinophysis acuminata*.

Mitigation of HABs is problematic and was not ignored within this Research Topic, being addressed by Zhang et al., who examined the effects of natural extracts of the edible brown algae *Sargassum fusiforme* on the growth of some important HAB species as one possible method of intervention.

Microbial pathogens such as *Vibrio* or *Ecoli* can also accumulate in shellfish. Occurrences of these pathogens can lead to gastrointestinal health implications for anyone who consumes contaminated shellfish. But novel microbial challenges may also pose a risk to aquaculture. In this issue, for instance, Mateus et al. discuss the potential for shellfish to be a reservoir for the SARS-CoV-2 virus and the potential need to consider the incorporation of SARS-CoV-2 detection strategies within regulatory shellfish monitoring programmes.

The development of new technologies for harmful algal blooms is likely to be key to the enhancement of early warning systems for HABs to protect aquaculture. A range of novel technologies applied within PRIMORE are described by Ruiz-Villarreal et al.

The articles of this Research Topic demonstrate the 'state of the art' in HAB early warning systems in European waters. Remote sensing and molecular approaches continue to develop to supplement the "core" microscope-based methods for HAB detection. Early warning systems are targeted to the specific challenges in different countries and regions but utilise similar approaches with data sharing in different countries. The issue demonstrates the considerable developments and success in the application of Lagrangian mathematical model-based alerts for the HAB taxa that are transported advectively on oceanographic currents.

Author contributions

All authors listed have made a substantial, direct, and intellectual contribution to the work and approved it for publication.

Funding

This work was funded by the EU Interreg project "Predicting the Impact of Regional Scale Events on the Aquaculture Sector" (PRIMROSE) Grant No. EAPA_182/2016.

Conflict of interest

The authors declare that the research was conducted in the absence of any commercial or financial relationships that could be construed as a potential conflict of interest.

Publisher's note

Reference

Maguire, J., Cusack, C., Ruiz-Villarreal, M., Silk, J., McElligott, D., and Davidson, K. (2016). Applied simulations and integrated modelling for the understanding of toxic and harmful algal blooms (ASIMUTH): Integrated HAB forecast systems for europe's Atlantic arc. *Harmful Algae* 53, 160–165. doi: 10.1016/j.hal.2015.11.006.

frontiers in Marine Science

ORIGINAL RESEARCH
published: 09 December 2020
doi: 10.3389/fmars.2020.582960

Sensitivity of a Satellite Algorithm for Harmful Algal Bloom Discrimination to the Use of Laboratory Bio-optical Data for Training

Victor Martinez-Vicente[1]*, *Andrey Kurekin*[1], *Carolina Sá*[2], *Vanda Brotas*[2], *Ana Amorim*[2], *Vera Veloso*[2], *Junfang Lin*[1] and *Peter I. Miller*[1]

[1] Remote Sensing Group, Plymouth Marine Laboratory, Plymouth, United Kingdom, [2] MARE, Centro de Ciências Do Mar e Ambiente, Faculdade de Ciências, Universidade de Lisboa, Lisbon, Portugal

Early detection of dense harmful algal blooms (HABs) is possible using ocean colour remote sensing. Some algorithms require a training dataset, usually constructed from satellite images with a priori knowledge of the existence of the bloom. This approach can be limited if there is a lack of *in situ* observations, coincident with satellite images. A laboratory experiment collected biological and bio-optical data from a culture of *Karenia mikimotoi*, a harmful phytoplankton dinoflagellate. These data showed characteristic signals in chlorophyll-specific absorption and backscattering coefficients. The bio-optical data from the culture and a bio-optical model were used to construct a training dataset for an existing statistical classifier. MERIS imagery over the European continental shelf were processed with the classifier using different training datasets. The differences in positive rates of detection of *K. mikimotoi* between using an algorithm trained with purely manually selected areas on satellite images and using laboratory data as training was overall <1%. The difference was higher, <15%, when using modeled optical data rather than laboratory data, with potential for improvement if local average chlorophyll concentrations are used. Using a laboratory-derived training dataset improved the ability of the algorithm to distinguish high turbidity from high chlorophyll concentrations. However, additional *in situ* observations of non-harmful high chlorophyll blooms in the area would improve testing of the ability to distinguish harmful from non-harmful high chlorophyll blooms. This approach can be expanded to use additional wavelengths, different satellite sensors and different phytoplankton genera.

Keywords: phytoplankton, English channel, MERIS, optical backscattering, *Karenia mikimotoi*, harmful algal blooms, ocean color

OPEN ACCESS

Edited by:
Joe Silke,
Marine Institute, Ireland

Reviewed by:
Richard P. Stumpf,
National Centers for Coastal Ocean Science (NOAA), United States
Michelle Christine Tomlinson,
National Centers for Coastal Ocean Science (NOAA), United States
Jennifer Cannizzaro,
University of South Florida, United States

***Correspondence:**
Victor Martinez-Vicente
vmv@pml.ac.uk

Specialty section:
This article was submitted to Marine Fisheries, Aquaculture and Living Resources, a section of the journal Frontiers in Marine Science

Received: *13 July 2020*
Accepted: *18 November 2020*
Published: *09 December 2020*

Citation:
Martinez-Vicente V, Kurekin A, Sá C, Brotas V, Amorim A, Veloso V, Lin J and Miller PI (2020) Sensitivity of a Satellite Algorithm for Harmful Algal Bloom Discrimination to the Use of Laboratory Bio-optical Data for Training. Front. Mar. Sci. 7:582960. doi: 10.3389/fmars.2020.582960

1. INTRODUCTION

Toxic phytoplankton species impact human health and the economy world wide (Kudela et al., 2015; Sanseverino et al., 2016). Events of enhanced growth of toxic phytoplankton (or Harmful algal blooms, HABs) are expected to be more frequent in a climate change scenario (Griffith and Gobler, 2020). Because of their event-like nature it is difficult to design monitoring and early-warning systems using solely *in situ* sampling (Babin et al., 2008). However, the optical properties of some HABs species favor the use of ocean colour satellite remote sensing as a tool for detection

(Cullen et al., 1997; Dierssen et al., 2015). In order to improve HABs satellite algorithms, a better understanding of the variability of the phytoplankton inherent optical properties (IOP) is, therefore, crucial.

The variability of optical properties among phytoplankton species has been studied through laboratory experiments (Bricaud et al., 1983, 1988; Ahn et al., 1992). In the context of HAB species, some authors have focused on the absorption coefficient, showing potential for detection using the fourth-derivative of the phytoplankton absorption coefficient (a_{phy}, m^{-1}) (Millie et al., 1995, 1997; Stæhr and Cullen, 2003). Indeed, this technique has been applied to the discrimination among phytoplankton groups using hyperspectral remote sensing reflectance, (R_{rs}, sr^{-1}), in preparation for new sensors (Xi et al., 2015, 2017). Other laboratory studies have taken into account the optical backscattering coefficient (b_{bp}, m^{-1}) (Vaillancourt et al., 2004; Whitmire et al., 2010; Harmel et al., 2016), including the effects of different light regimes (Stramski and Morel, 1990; Poulin et al., 2018).

However, few studies have implemented bio-optical knowledge into practical remote sensing applications for HAB detection. From *in situ* sampling, a HAB dominated by dinoflagellate *Karenia brevis* in the Eastern Gulf of Mexico (Cannizzaro et al., 2008) presented lower than expected chlorophyll-specific backscattering coefficient and backscattering ratio (i.e., $\tilde{b}_{bp} = b_{bp}/b_p$), which was used to establish a HAB detection criteria. These criteria were not applicable to the East China Sea (Shang et al., 2014), and a different index had to be developed regionally. Further, laboratory experiments showed a wide dispersion among phytoplankton species for chlorophyll-specific backscattering and demonstrated a relationship between $\tilde{b}_{bp}$ and cell size (Whitmire et al., 2010). Given the regional and biological differences recorded, it is therefore necessary to develop algorithms and approaches that can take into account these sources of variability to further develop HAB detection capabilities.

A regional HAB detection algorithm developed for the European Shelf (Kurekin et al., 2014) was developed to allow for these factors. It employs a fully automatic data-driven approach to identify key characteristics of R_{rs} and derived quantities, and then applies these characteristics to classify pixels in satellite images into *no bloom*, *non-harmful bloom*, and *harmful bloom* categories (Miller et al., 2006). The performance of this algorithm depends on the choice of the training data. In the original implementation (Kurekin et al., 2014), the training data were defined by manually selecting regions of interest with *a priori* harmful phytoplankton species (i.e., *Karenia mikimotoi* and *Phaeocystis globosa*) from MODIS and MERIS sensor measurements. Thus, the algorithm was adapted to specific optical conditions, phytoplankton species and sensor characteristics. If any of these changed, the algorithm would need to be re-trained, in addition to the subjective component introduced by the manual selection of the areas in the image.

In this study, we propose an alternative approach to constructing a training dataset for the Kurekin et al. (2014) algorithm in the European Shelf by using laboratory bio-optical experiments, aiming to incorporate regional and species-specific variability of optical properties. In particular, we focused as an example species on the dinophyceae *K. mikimotoi* as it is known to occur in blooms on the Western English Channel on the European continental shelf (Barnes et al., 2015). Laboratory experiments on this species were used to retrieve chlorophyll specific IOP. These in turn were used to compute simulations of R_{rs} to augment the training dataset for the classifier by incorporating other optically active components and making it more representative of natural conditions. We further performed a numerical experiment, a sensitivity study, using different configurations of the training datasets to investigate the benefit of using laboratory and modeled data. Simulations included a range of phytoplankton concentrations, as well as other optically active components (detritus and yellow substance or gelbstoff) in the absence of other blooms of non-harmful algae. The results of our sensitivity study confirm the potential of this approach to detect HABs based on species-specific bio-optical information, which is applicable to many ocean color sensors.

2. METHODS

The Kurekin et al. (2014) algorithm is a statistic operator that requires training data based on spectral features of the targeted phytoplankton species. It then calculates discrimination function parameters in the feature hyperspace (Miller et al., 2006). The original set of ocean color features was limited to arbitrary combinations of R_{rs} from specific spectral bands of a particular satellite sensor. In this study, spectral ratios of R_{rs} were also used.

The features are then automatically processed to select a reduced subset of the most relevant features by applying a Stepwise Discriminant Analysis (SDA) algorithm implemented in the statistical package "klaR" (Weihs et al., 2005). The best combination of features is selected iteratively, by adding more significant or removing less significant features one by one. The significance of features is estimated by applying the probability of correct classification criterion. By reducing the number of classification features, improvement of accuracy and computational efficiency was achieved. The features are used to classify pixels into the original classes *no bloom*, *non-harmful*, and *harmful*. For the current study, the *unknown* class has been added to represent data that cannot be related to any of known classes.

For this kind of statistical algorithm, in addition to the statistical method, the choice of training datasets representative of the different classes is critical and is the focus of this work. In the Kurekin et al. (2014) work the training datasets were subjectively defined from satellite images. Here, alternative ways to produce training datasets are presented using modeled and experimental data.

2.1. Model of R_{rs}

As in previous studies (Shang et al., 2014), the above surface remote sensing reflectance (R_{rs}) was calculated with (Gordon et al., 1988):

$$R_{rs}(\lambda) = \frac{0.52 \times r_{rs}(\lambda)}{1 - 1.7 \times r_{rs}(\lambda)} \quad (1)$$

where the remote sensing reflectance just below the water surface (r_{rs}) is modeled as a function of the absorption ($a(\lambda)$) and backscattering ($b_b(\lambda)$) coefficients:

$$r_{rs}(\lambda) = \left(g_0 + g_1 \times \frac{b_b(\lambda)}{a(\lambda) + b_b(\lambda)}\right) \times \frac{b_b(\lambda)}{a(\lambda) + b_b(\lambda)} \quad (2)$$

with g_0= 0.089 and g_1 = 0.125, respectively. The spectrally varying a (m^{-1}) and b_b(m^{-1}) were modeled as:

$$a = a_w + a_{bg} + a_{km} \quad (3)$$

$$b_b = b_{bw} + b_{bp,bg} + b_{bp,km} \quad (4)$$

Here a_w and b_{bw} were the absorption and backscattering coefficients of pure seawater (Pope and Fry, 1997), the *km* sub-index refers to *K. mikimotoi*, and the *bg* sub-index refers to the *background* component. The *background* component was assumed to covary with chlorophyll concentration including: phytoplankton, gelbstoff (or colored dissolved organic matter) and detritus. The *background* component was therefore modeled using a generic phytoplankton model: the "new Case I model" as described in Hydrolight (Mobley and Sundman, 2016), where the inherent optical properties of particles solely co-vary with chlorophyll concentration, $TChla_{bg}$ in mgm^{-1}(Bricaud et al., 1998; Loisel and Morel, 1998). With this assumption, Equation (3) was rewritten as:

$$a = a_w + a_{p,bg} + a_{g,bg} + a_{p,km} + a_{g,km} \quad (5)$$

$$b_b = b_{bw} + b_{bp,bg} + b_{bp,km} \quad (6)$$

where the contributions to *background* and *K. mikimotoi* to the particulate (p), and dissolved (g), compartments were modeled as follows. The absorption coefficients of *background* had contributions from living phytoplankton and detrital components ($a_{p,bg}$= $a_{phy,bg}$+$a_{det,bg}$) as well as from dissolved matter ($a_{g,bg}$). Only phytoplankton ($a_{phy,km}$) and dissolved matter ($a_{g,km}$) were considered as contributors to the absorption coefficient due to *K. mikimotoi*, but not particulate detritus. Particle backscattering for the *background* ($b_{bp,bg}$) and for *K. mikimotoi* were not further separated in other particulate compartments. Optical absorption and backscattering coefficients for *background* were described as a function of $TChla_{bg}$ using well validated models (see **Supplementary Material**, section 1).

Absorption and particle backscattering coefficients for *K. mikimotoi* were computed using the formulae below and parameterized using results from a laboratory experiment (section 2.2).

The $a_{ph,km}$ was modeled as a function of its chlorophyll concentration ($TChla_{km}$):

$$a_{ph,km}(\lambda) = A_a(\lambda) \times (TChla_{km})^{B_a(\lambda)} \quad (7)$$

where the values of $A_a(\lambda)$ and $B_a(\lambda)$ were derived from measurements. The $a_{dg,km}$ was modeled in the same way as $a_{g,bg}$ (see **Supplementary Material**, section 1) but with a range of f from 0.2 to 1.0 with a step of 0.2, to cover more variability of $a_{g,km}$.

The backscattering coefficient of *K. mikimotoi* ($b_{bp,km}$) was modeled as Equation (7):

$$b_{bp,km}(\lambda) = A_{bb}(\lambda)(TChla_{km})^{B_{bb}(\lambda)} \quad (8)$$

where the values of parameters $A_{bb}(\lambda)$ and $B_{bb}(\lambda)$ were derived from measurements. Data from the reflectance model were re-sampled to 0.1 nm spectral resolution by spline interpolation, multiplied by MERIS spectral response coefficients and integrated over the full wavelength range to obtain band-averaged R_{rs}.

2.2. Laboratory Measurements of Optical Properties of *Karenia mikimotoi*

The optical properties and $TChla_{km}$ were obtained through sequential additions of a *Karenia mikimotoi* culture to a flow-through system (Slade et al., 2010; Browning et al., 2015) following the method detailed in this section.

Karenia mikimotoi is a naked unicellular dinoflagellate with diameter between 15 and 40 μm (K-0260, SCCAP). For this experiment it was grown at the University of Lisbon, where also the optical measurements took place. The culturing chamber had a light:dark cycle of 14:10 h. *Karenia mikimotoi* was grown at a temperature of 15°C and salinity of 30 psu, in a L1 media and a photon flux density of 43 $\mu molm^{-2}s^{-1}$. The health of the culture was monitored using microscopy counts and the optical experiment was performed when they reached exponential growth phase. The experimental setup consisted of a peristaltic pump (Watson Marlow 603S) connected to a hyperspectral absorption and attenuation meter (Wetlabs *acs*), and to a black chamber housing a three wavelengths backscatter meter (Wetlabs ECO-BB3). The system was cleaned successively with de-ionized water, diluted Extran and diluted HCl, then rinsed with de-ionized water previous to the experiment. After the cleaning cycle, the system was filled with pre-filtered seawater (Pall Acropak 0.2 μm/0.2 μm) and recirculated at 1 $lmin^{-1}$ (or 30 r.p.m.) for the whole experiment. Different flow speed were tested (10 and 60 r.p.m.) with no significant changes in the data. Data were recorded for at least 3 min for each addition of culture (Browning et al., 2015). After each addition of the culture into the experimental setup the system was left to stabilize for 1–2 min, then data were recorded for 3 min with the *acs* and ECO-BB3, and finally water was collected for laboratory analysis.

Temperature, T, and salinity, S, were measured with a probe (YSI-85, Model 85/50 FT) before and after each culture addition and the average was used to correct the optical measurements.

Data from the *acs* and ECO-BB3 instruments were processed following standard protocols (Wetlabs, 2009; Whitmire et al., 2010). Median and interquartile range (IQR) for the inherent optical properties were calculated for each concentration of culture and the median values from the blank were subtracted (see **Supplementary Material**, section 2 for further details on data processing and data quality control procedures).

Water samples (100–500 ml) were collected from the system after each *Karenia mikimotoi* culture addition for particulate absorption, pigment analysis, and microscopy. Samples for spectrophotometric and HPLC pigment analysis were filtered

TABLE 1 | Summary of combination of training datasets for the simulation experiments.

Class	Experiment 1	Experiment 2	Experiment 3
No bloom	Satellite	Satellite	Satellite
Non-harmful bloom	Satellite	Satellite	*Background*
Harmful bloom	Satellite	*Background* and laboratory	*Background* and laboratory

Satellite indicates where only MERIS data have been used to characterize the optical signature of a class. Background indicates where modeled data have been used (section 2.1 and ***Supplementary Material****). Laboratory indicates where optical measurements specific to Karenia mikimotoi have been used (section 2.2).*

onto Whatman GF/F 25 mm filters using low pressure pumps, flash frozen in liquid nitrogen and kept at −80°C for <3 months. Spectrophotometric measurements (Shimazdu UV2450 with 0.5 nm resolution) of the particulate absorption coefficient of the sample retained on the filter ($a_{p,km}$) was used to derive the phytoplankton ($a_{ph,km}$) and particulate detritus, ($a_{d,km}$) absorption coefficients (Tassan and Ferrari, 1995) with β-correction from laboratory experiments (Finkel and Irwin, 2001). High performance liquid chromatography (HPLC) analysis was done to determine phytoplankton pigments concentrations (Zapata et al., 2000; Mendes et al., 2007). Total chlorophyll a concentration ($TChla_{km}$) was defined as the sum of Chl-a + Chl-a allomers + Chl-a epimers concentrations. The health of the cultures was confirmed as the percentage of phaeopigments to $TChla_{km}$ plus phaeopigments, which was always $\leq$ 3%. Cell concentration of the culture was determined by microscopy counts. Depending on cell size and cell concentration, different counting chambers were used (Palmer-Maloney and Sedgwick-Rafter) following the standard procedures (Andersen, 2005).

Linear regressions on the log_{10}-transformed inherent optical data and $TChla_{km}$ were used to compute the coefficients needed for Equations (5) and (6). Spectral interpolation was necessary to match the inherent optical properties. Backscattering coefficient ($b_{bp,km}$) was interpolated to 0.5 nm interval to match the spectrophotometric $a_{phy,km}$ measurements by fitting a power-law (i.e., $b_{bp,km}(\lambda) = b_{bp,km}(532) \times (\lambda/532)^{-\gamma}$).

2.3. Simulation Experiments and Evaluation

Three separate simulation experiments were performed using different training datasets combinations (**Table 1**). This section describes the training datasets for each Experiment, the evaluation dataset and the statistics used to measure algorithm performance.

2.3.1. Training Datasets

The training dataset in Experiment 1 was taken as the reference. It was generated from MERIS sensor measurements of R_{rs} at wavelengths 413, 443, 490, 510, 560, 620, 665, 681, and 709 nm. Absorption and backscattering coefficients derived from inversion algorithms (e.g., Smyth et al., 2007) were not used in this training dataset. Using IOP derived from MERIS data introduced additional uncertainty (Defoin-Platel and Chami, 2007; Werdell et al., 2018). Historical MERIS scenes with documented *K. mikimotoi* bloom events in the English Channel in years 2002–2004, were selected (Kelly-Gerreyn et al., 2004; Vanhoutte-Brunier et al., 2008). Areas of these scenes were manually delineated and labeled into *no bloom*, *non-harmful*, and *harmful* classes. In total five MERIS scenes were selected on 19 July 2002, 1 and 7 July 2003, 10 and 23 July 2004. To compose a training dataset the images were first sub-sampled by a factor of 4. Overall, 6.25% of satellite pixels were used for training and 93.75% were used for evaluation (section 2.3.2). The data in the training dataset were arranged in a 2D table format with R_{rs} values and class labels of individual image pixels stored in rows. In total the training table contained 14,072 records of *no bloom* class, 12,116 records of *non-harmful bloom* class, and 10,294 records of *harmful bloom* class.

In Experiment 2, the records in the training table labeled as *harmful bloom* were removed. R_{rs} spectra *harmful bloom* class results from the addition of the *background* optical properties from bio-optical models (section 2.1) to the *K. mikimotoi* optical properties derived from laboratory experiments (section 2.2), to include in the training dataset the effect of a mixed particle assemblage in a HAB event. Values used for $TChla_{km}$ varied from 1 to 15 mgm^{-3} with a constant step in logarithm scale resulting in 500 concentrations. $TChla_{bg}$ varied from 0.01 to 2 mgm^{-3} having 10 concentrations with an identical interval in logarithm scale, therefore a total of 5,000 combinations were obtained.

Experiment 3, was the same as Experiment 2 but with the *non-harmful bloom* class defined by the *background* optical properties from bio-optical models (section 2.1), with $TChla_{bg}$ between 1 and 10 mgm^{-3}. From each experiment, a set of classifier coefficients was obtained after training. In all the Experiments, the *no bloom* class was defined using the manual selection of parts of the satellite images.

2.3.2. Evaluation Dataset

Due to lack of *in situ* data to perform an independent validation of the classification, the results from each Experiment were evaluated with the part of the training images that had been reserved (i.e., not used for training). The performance was quantified through statistical comparisons with the manually classified pixels. The same 5 MERIS scenes as those used for training were used to generate training and evaluation datasets for the HAB classifier (see section 2.3.1). The same evaluation dataset was applied in all three experiments, but the classification results were different because the training data were different.

The measures of performance included a confusion matrix and derived statistical measures: overall accuracy, kappa coefficient, errors of commission, and producer accuracy. Overall accuracy was calculated as the number of correctly classified pixels divided by the total number of classified pixels. The kappa coefficient measures the agreement between the evaluation

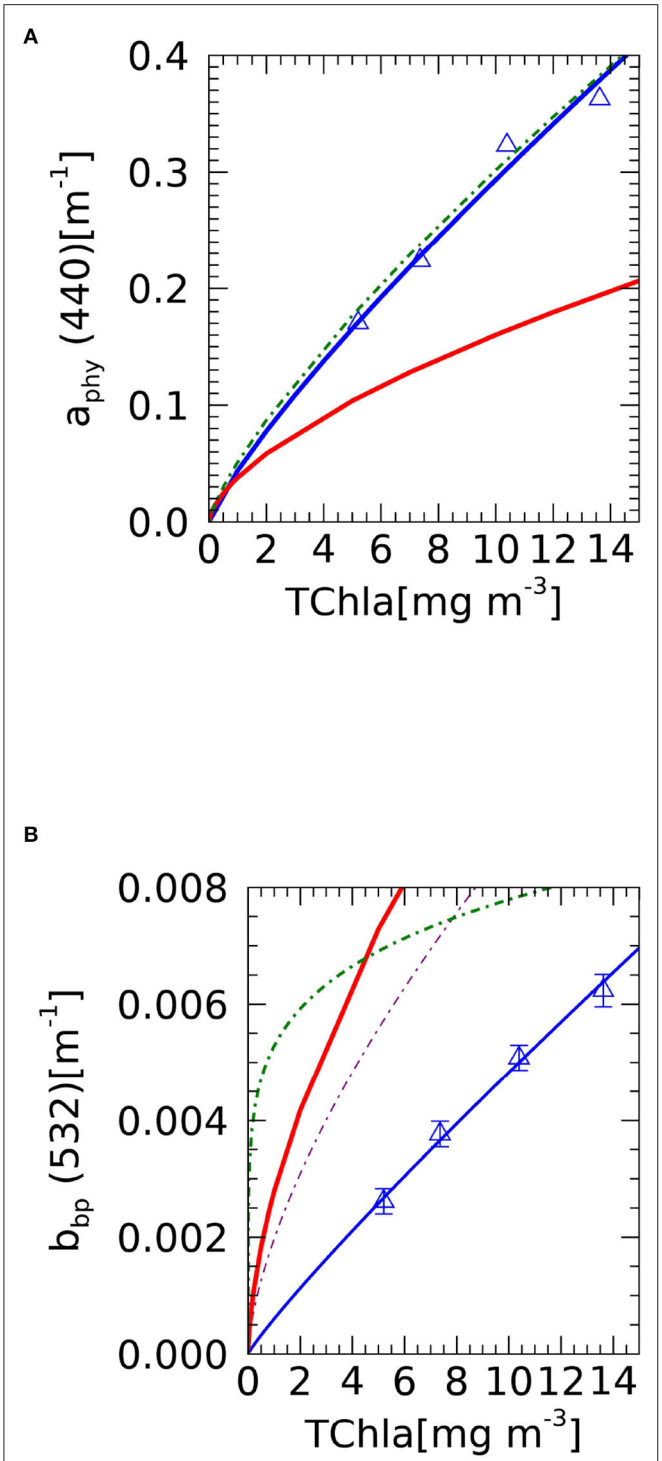

FIGURE 1 | Relationship between measured *TChla* and optical properties at a given wavelength. Red solid line is the *background* model and blue solid triangles and line are experimental results from this study for *Karenia mikimotoi*: **(A)** Phytoplankton absorption. Green dot-dash line are Cannizzaro et al. (2008) predictions of $a_{phy}(443)$ for $>10^{-4}$ cells l^{-1}; **(B)** $b_{bp,km}(532)$. Green dotted-dash line are Cannizzaro et al. (2008) predictions of $b_{bp}(532)$ for $>10^{-4}$ cells l^{-1}; purple alternate-dash is Antoine et al. (2011). Symbols are median experimental values and error bars are IQR. Solid lines are power law fit to these data (**Table 2**).

dataset and the classification results in the range from 0 to 1. The data can be considered to be in perfect statistical agreement when kappa is 1 and disagree when kappa equals 0. *Errors of commission* is the measure of false positive, estimated for each class as the fraction of pixels that were classified incorrectly. *Producer accuracy* is calculated for each class as the probability that the pixels in this class were classified correctly.

Not all of the classified image pixels were used for estimation of the confusion matrix. If the probability of *unknown* class was higher than 0.6 or the probability of any of other three classes was lower that 0.6, the pixel was considered as unreliable and discarded.

3. RESULTS AND DISCUSSION

3.1. Optical Properties: Modeled Data for *Background* and Laboratory Experiments for *Karenia mikimotoi*

The *background* model is constructed with the underlying hypothesis that at lower $TChl_{bg}$, the smaller phytoplankton sizes dominate the optical properties. For absorption (**Figure 1A**) this means that there is a higher slope for lower chlorophyll concentrations (i.e., less than ∼2 mg Chla m^{-3}). Larger cells are expected to have lower per-chlorophyll absorption due to the package effect (Bricaud et al., 2004). Values from this laboratory experiment are greater than those predicted by the model, pointing toward higher *TChla* per cell in the culture. However, the values are close to other studies for HAB-forming dinoflagellates (Cannizzaro et al., 2008).

The backscattering coefficient is also modeled as a power law for the *background* (**Figure 1B**), following the same underlying assumption of smaller cells dominating optical properties of lower chlorophyll concentrations (Loisel and Morel, 1998). Measurements from the current laboratory experiment are lower than those predicted by the *background* model, but similar to other laboratory experiments. For example, $b^*_{bp,km}(470)$ = 0.000525 m^{-2} mg $Chla^{-1}$ is comparable to the lower values obtained for other species of dinophyceae ($b^*_{bp}(442)$ from 0.0005786 to 0.0009194 m^{-2} mg $Chla^{-1}$) (Whitmire et al., 2010). These laboratory values are low in comparison with other field studies in coastal waters (Antoine et al., 2011) and in areas with HAB blooms (Cannizzaro et al., 2008). This disagreement is to be expected, as the *in situ* studies incorporate the b_{bp} signal from the whole population, which is an assemblage of phytoplankton and other particles (Stramski et al., 2001; Martinez-Vicente et al., 2010, 2012). In fact, for Experiment 2, the *harmful* class $b_{bp}(532)$ can vary from 0.00718 m^{-1} for 1.01 mg Chla m^{-3} to 0.01112 m^{-1} for 17 mg Chla m^{-3}, when the contributions of *background* and *K. mikimotoi* were added. As a comparison, Cannizzaro et al. (2008) predicts $b_{bp}(532)$ = 0.00855 m^{-1} for 17 mg Chla m^{-3}. The coefficients resulting from the power law fit to the laboratory data, used by the classifier, are summarized in **Table 2**.

The second set of parameters needed in Equations (7) and (8) are the chlorophyll-specific spectrally varying inherent optical properties (**Supplementary Figure 1**). For chlorophyll-specific absorption, the model predicts a flattening of the spectra at higher

TABLE 2 | Regression coefficients and statistics of the fit for $a_{phy,km}(440)$ and $b_{bp,km}(532)$, as a function of chlorophyll concentration, *TChla*.

Optical properties	A(C.I.)	B(C.I.)	r^2	RMSE
$a_{phy,km}(440)$	0.0438 (0.0420)	0.83 (0.04)	0.98	1.52
$b_{bp,km}(532)$	0.0006 (0.0244)	0.90 (0.03)	0.99	3.31

Data were fitted to the power function $Y = A \times X^B$, (see Equations 7, 8) using a Type-II linear regression (major axis), on $\log_{10}$-transformed variables. All regressions are significant ($p < 0.005$), 95% confidence intervals (C.I.) of the coefficients are given in parenthesis. The determination coefficient, r^2, and the root mean square error, RMSE, are calculated from the $\log_{10}$-transformed variables. Considered four TChla concentrations after data quality control.

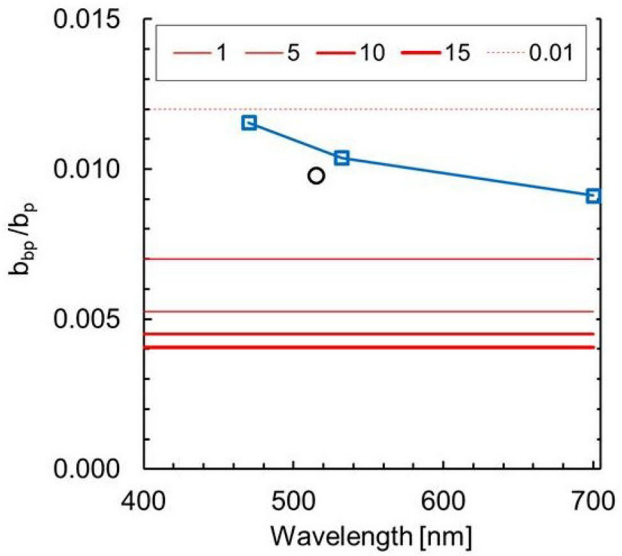

FIGURE 2 | Spectral backscattering ratio ($\tilde{b}_{bp} = b_{bp}/b_p$) for *background* model and for *Karenia mikimotoi* from laboratory. Red lines are modeled values at different *TChla*. Blue squares and line are median values from experimental data. Black circle is value reported by Harmel et al. (2016).

chlorophyll concentrations. The median values obtained from the laboratory experiment are consistent with this prediction for the blue part of the spectra (400–500 nm) but they are higher for the red. However, the experiment is in close agreement with previous laboratory experiments, in particular with observations under low light conditions (see Figure 4 in Stæhr and Cullen, 2003). Concerning the spectral chlorophyll-specific backscattering coefficient (**Supplementary Figure 1**), modeled values for the *background* follow also the assumption of smaller phytoplankton sizes dominating at lower $TChl_{bg}$. This leads to higher chlorophyll-specific backscattering values (i.e., smaller phytoplankton is more efficient at backscattering light) and more features due to absorption effects on the backscattering spectral shape.

Backscattering ratio (**Figure 2**) shows that the laboratory measurements are 6% higher than other experimental data from the literature specific to the same species (Harmel et al., 2016), and within range for other dinophyceae algae [$\tilde{b}_{bp}(442)$ from 0.0061 to 0.0210] (Whitmire et al., 2010). The laboratory experiment results also aligns with *in situ* observations (Whitmire et al., 2007; Cannizzaro et al., 2008).

3.2. Training Dataset From Modeled and Laboratory Data

The forward calculated R_{rs} from *background* and laboratory experiments are shown in **Figure 3**, for different chlorophyll concentrations, alongside the training dataset derived from pixels in the satellite image manual selection. The *no bloom* class is defined in all Experiments from the manual selection in the satellite image. **Figures 3B,D** display the results for the *background* model reflectances. Increase in *TChla* controls the shape of the spectra. These data are used for training class *non-harmful bloom* and *harmful bloom* (**Table 1**). **Figure 3F** shows modeled R_{rs} spectra for *K. mikimotoi* using the specific optical properties derived from the laboratory experiments.

The median R_{rs} spectrum for the *no bloom* class from satellite (**Figure 3A**) compares well in magnitude and shape to R_{rs} modeled for the lower $TChl_{bg}$ (**Figure 3B**). Median *TChla* for *no bloom* from satellite, computed using OC5, is 0.35 mg Chla m^{-3} and dispersion (half the inter-decile range = (Q90-Q10)/2) is 0.13 mg Chla m^{-3}. The *harmful* class from satellite (**Figure 3E**) and from the laboratory experiments (**Figure 3F**) are also in agreement of scale and spectral shape. *TChla* from the satellite is 8.15 ± 10.6 mg Chla m^{-3}, which encompasses the range of $TChla_{km}$ simulated. However, R_{rs} spectra of the *harmless bloom* class from satellite (**Figure 3C**) is lower than the R_{rs} modeled (**Figure 3D**). Satellite *TChla* is 1.01 ± 0.52 mg Chla m^{-3} and is representative of the lower limit of the simulated range (i.e., from 1 mg Chla m^{-3}) for the *background*, which could explain some differences in the results below. The classifier coefficients are available and attached to this paper (**Supplementary Material**, section 3).

3.3. Detection of HABs in Satellite Data

Figure 4 presents two examples of MERIS scenes with documented *K. mikimotoi* blooms. These scenes were selected to train and to compare the sensitivity of the classifier to training datasets in Experiments 1, 2, and 3 (see section 2.3). The enhanced MERIS *true color* images of the bloom are shown in **Figures 4A,B**. The *harmful bloom* class can be seen in the images as a reddish patch close to the center of the images. **Figures 4C,D** show the *TChla* as retrieved by standard chlorophyll algorithm for the area, highlighting the co-location of elevated *TChla* with *harmful bloom* class. The manual delineation of the area around those blooms for *harmful bloom* is shown in red in **Figures 4E,F**.

The turquoise and darker greenish colors, mostly toward the Atlantic Ocean, are associated with *no bloom* and *non-harmful bloom* classes (**Figures 4A,B**). They match low to medium *TChla* (**Figures 4C,D**). The manually selected areas for these classes are blue and green respectively (**Figures 4E,F**). In these examples, the pixels manually selected for the *non-harmful bloom* class are mostly toward the Atlantic Ocean, with *TChla*∼1 mgm^{-3}, which explains the R_{rs} (**Figure 3C**). A special case is the white

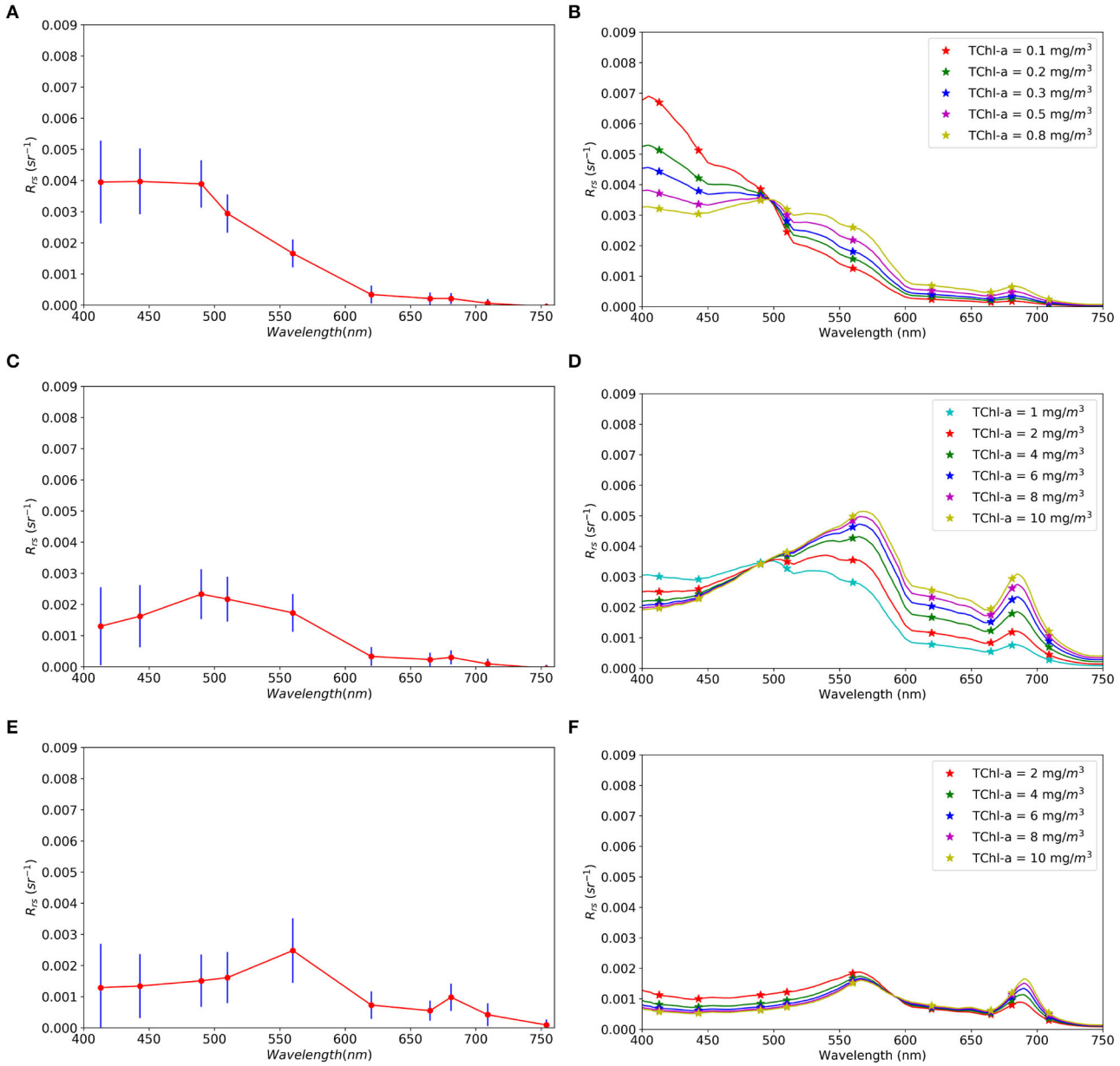

FIGURE 3 | R_{rs} spectra used for training the HAB classifier. **(A,C,E)** Median and standard deviation R_{rs} from MERIS pixels for *no bloom*, *no harmful*, and *harmful* classes, respectively (section 2.3). **(B,D,F)** R_{rs} spectra at different *TChla* concentrations for *background* **(B,D)** and *Karenia mikimotoi* **(F)** datasets used to train the classifier in Experiments 2 and 3. MERIS bands are indicated by stars.

bright patch on the Western English Channel, close to the coast of England (**Figure 4A**). This corresponds to a bloom of non-toxic coccolithophores species, which has not been identified as high *TChla* (**Figure 4C**) and has not been labeled as a separate class in the classifier. However, the chlorophyll algorithm is not always capable to discern "bright" waters from high chlorophyll concentrations. For instance, toward the North, in the Bristol Channel, an orangy-white patch, is a well documented location of high riverine contributions of suspended particulate matter (Neil et al., 2011) (**Figures 4A,B**). Finally, at the center of the Western English Channel, dark red patches (**Figures 4A,B**) match the corresponding extremely high chlorophyll concentration images (**Figures 4C,D**) from documented blooms (Kelly-Gerreyn et al., 2004; Vanhoutte-Brunier et al., 2008). These patches were used to define the *harmful bloom* class manually from satellite (**Figures 4E,F**). are distinguishable. Overall, high *TChla* can be considered a good indicator of areas with potential HAB, however, highly turbid waters in coastal areas can produce misleading high *TChla* when chlorophyll algorithms fail. Lack of *in situ* data to verify high-chlorophyll non-harmful bloom areas,

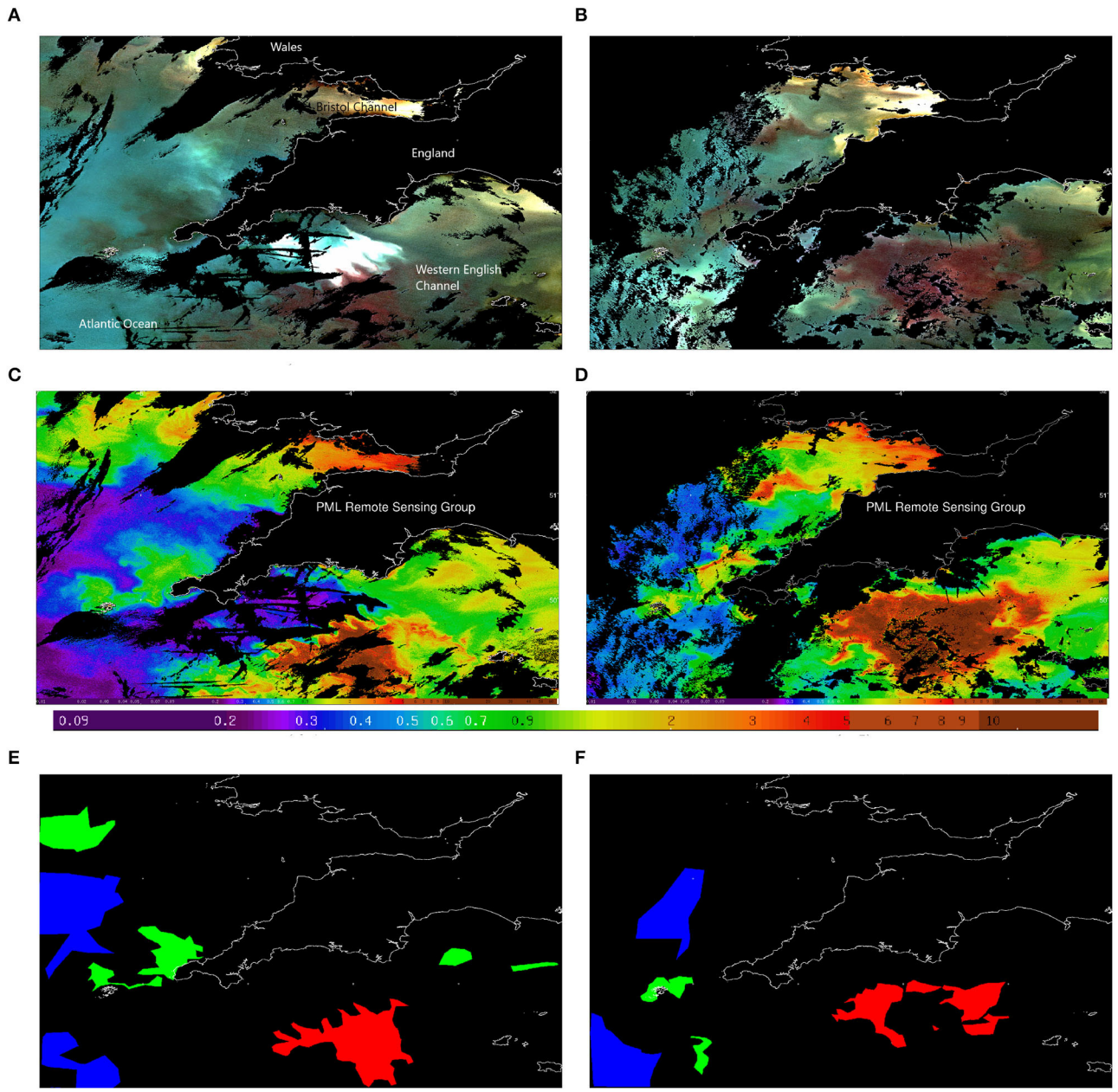

FIGURE 4 | MERIS images showing a *Karenia mikimotoi* bloom in the English Channel on 19 July 2002 **(A,C,E)** and 1 July 2003 **(B,D,F)**. Enhanced true colour images **(A,B)** and chlorophyll concentration from Algorithm OC5 for MERIS **(C,D)** (Tilstone et al., 2017). Image masks used for training and evaluation of *Karenia mikimotoi* HAB classifier **(E,F)**. Blue areas indicate data selected to construct the training dataset for *no bloom* class. Green areas are for *non-harmful bloom* training dataset. Red areas for a generic *harmful bloom* class training dataset.

preclude drawing any conclusion about the validity of using the current algorithm and training datasets to identify those, and it is an extension for this study.

The scenes in **Figure 4** were further processed using the *K. mikimotoi* classifier, trained with the datasets in Experiments 1–3 to generate risk maps (**Figure 5**). Qualitatively, the three experiments produced overall similar maps with some interesting localized differences (**Figure 5**). The classification results were different in the Bristol Channel, where concentration of sediments was relatively high. No collocated *in situ* suspended particulate matter are available, but this is well known area of intense bottom resuspension of sediments and river runoff (Uncles, 2010; Uncles et al., 2015). In Experiment 1 (**Figures 5A,B**) the classifier, trained on satellite data, discriminated this region as HAB. This false positive detection disappeared in Experiments 2 and 3 (**Figures 5C–F**),

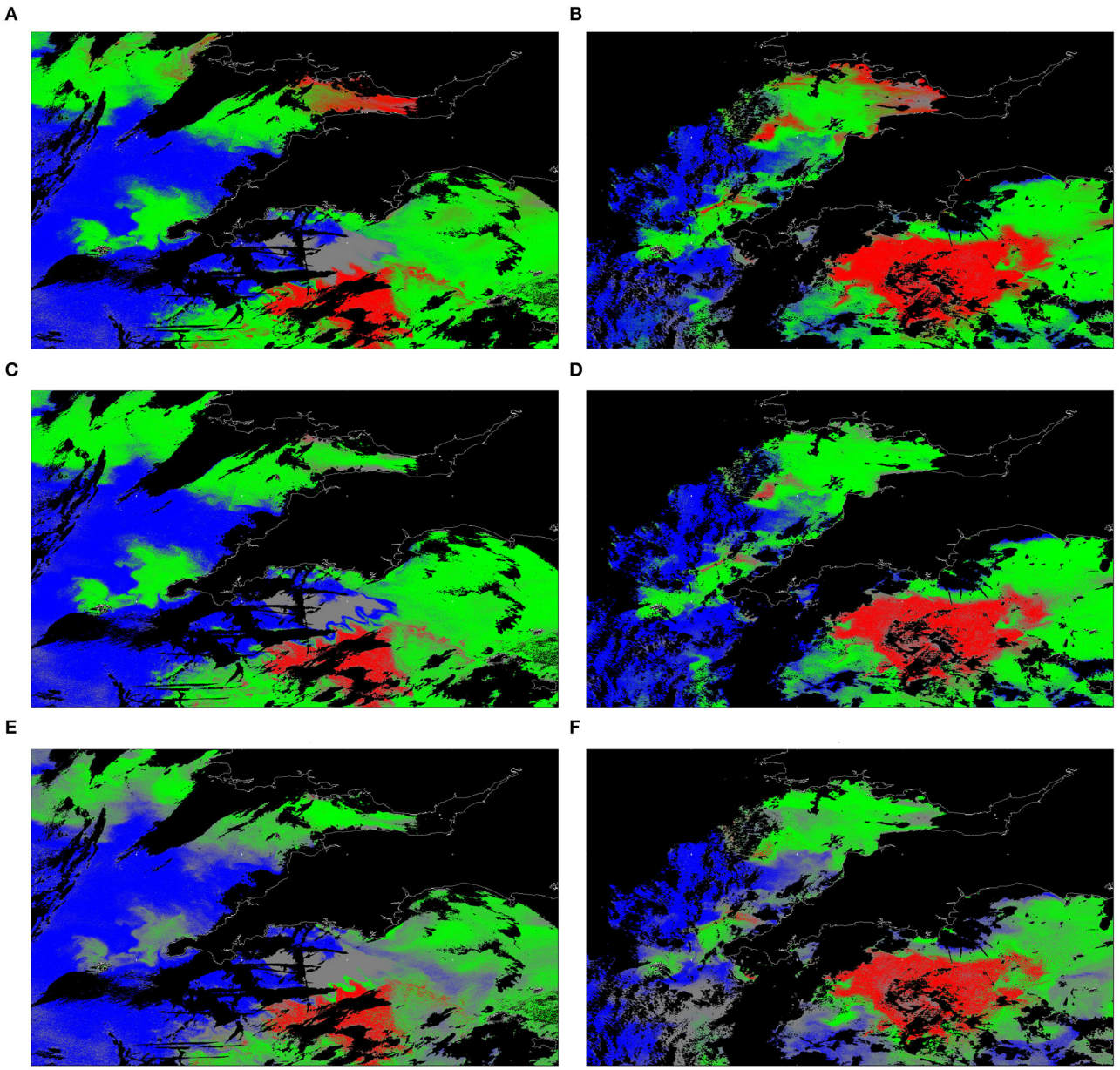

FIGURE 5 | *Karenia mikimotoi* HAB classification maps of the English Channel on 19 July 2002 (left column) and 1 July 2003 (right column): **(A,B)** Experiment 1, **(C,D)** Experiment 2, and **(E,F)** Experiment 3. Pixels classified as *Harmful bloom* are shown in red, *non-harmful bloom* in green, and *no bloom* in blue. Pixels classified as *unknown*, are presented in gray and black is land within contours and missing data over water, due to cloud cover or sun glint.

highlighting an improvement of performance in this optically complex region. Another observation in these examples is that the coverage by grey areas increased from Experiments 1 to 3. Indeed, the percentage of *unknown* class pixels (**Table 3**) shows a slight increase from Experiment 1 to Experiment 2. It has the highest value for Experiment 3, indicating where the algorithm fails to classify a pixel among one of the known categories. **Figures 5E,F** point to greater areas of grey (*unknown* class) coinciding with areas of lower *TChla* (**Figures 4C,D**). The increase in *unknown* class for Experiment 3 can be related to using a range of chlorophyll for modeling the *non-harmful* class with higher values than what is normally encountered in the area (i.e., ∼1.5 mg Chla m^{-3} from Smyth et al., 2010). It is worth noting that the coccolithophore bloom was classified as unknown in **Figures 5A,C,E** for the three Experiments. None of the satellite training images or simulated data for the three training classes included the coccolithophore bloom examples and in all three experiments the algorithm correctly discriminated these data as *unknown* class.

TABLE 3 | The percentage of image pixels, classified as *unknown*.

Scene(Date)	Experiment 1(%)	Experiment 2(%)	Experiment 3(%)
19 July 2002	8.81	11.15	36.61
1 July 2003	9.93	11.50	40.93

TABLE 4 | The confusion matrix for *Karenia mikimotoi* classifier.

	Classified as (%)		
True class	***Harmful bloom***	***Non-harmful bloom***	***No bloom***
	Experiment 1		
Harmful bloom	98.6	1.41	0.00
Non-harmful bloom	2.84	96.0	1.20
No bloom	0.00	0.61	99.4
	Experiment 2		
Harmful bloom	97.7	2.29	0.06
Non-harmful bloom	2.52	95.6	1.88
No bloom	0.00	0.66	99.3
	Experiment 3		
Harmful bloom	84.1	15.9	0.00
Non-harmful bloom	4.62	78.6	16.8
No bloom	0.00	0.00	100

The matrix was normalized by the number of elements in each class.

Numerically, the comparisons of the classification algorithm was assessed using the confusion matrix and statistical measures derived from the confusion matrix. The results of classifier assessment in Experiments 1–3 are summarized in **Tables 4**, **5**. Due to the limited availability of *in situ* data for validation, the evaluation of the experiments has been made using satellite data (see section 2.3), the focus being on the relative changes in the results.

Overall, there are small differences among the results from the Experiments. Importantly, Experiment 1 and 2 percentage classification of *harmful bloom* class is <1% and the greatest difference is <15% (**Table 4**). The confusion matrix demonstrates that the accuracy of *non-harmful bloom* classification is lower for the Experiment 3. The differences in results between Experiment 1 and 3 may be due to the difference in the range of R_{rs} for the ranges of *TChla* considered for the *non-harmful bloom* class, as discussed above. The small differences between Experiment 1 and 2 may point to expected variability of the optical properties within the *K. mikimotoi* culture. It follows from **Table 4** that the classifier results in Experiment 2 have the lowest false positive rate for *non-harmful blooms* being classified as *K. mikimotoi* (i.e., 2.52). This observation is in good agreement with the classified maps in **Figure 5** that showed reduced false alarms in the Bristol Channel for Experiment 2 and even fewer in Experiment 3.

According to the results, all three classifiers performed well, achieving overall accuracy above 0.91 and kappa value above 0.85 (**Table 5**). The best performance was demonstrated by the classifier in Experiment 1 and the worst for the classifier in Experiment 3 with 7% lower overall accuracy, highlighting the importance of the choice of ranges in chlorophyll adapted to the region of study. However, the fact that the difference among using different training datasets was low (i.e., subjective in Experiment 1 vs. laboratory-derived in Experiment 2), supports the use of laboratory data to train this type of classifier.

The *errors of commission* and *producer accuracy* statistical measures for different classes are summarized in **Table 5**. These values are quite similar for Experiment 1 and Experiment 2, indicating that the performance loss is relatively small when the satellite training data for *harmful bloom* are replaced with laboratory derived data in Experiment 2. This points to a small degradation of the classification accuracy using laboratory data. A more significant loss in accuracy can be observed in Experiment 3, where the *producer accuracy* for *non-harmful bloom* class is reduced by almost 20% by using the bio-optical model instead of satellite-derived data for training.

Overall, the results demonstrate that the novel approach based on laboratory experiments can be used for simulation of R_{rs} values and training of a HAB classifier with only slight degradation of the classification accuracy while reducing false positives due to turbid coastal waters. This study has highlighted the impact of the selection ranges for *no bloom* conditions that should be fit to simulate *TChla* similar to those found in the environment where the model is deployed. A smaller source of uncertainty could be related to the use of laboratory conditions as representative of natural conditions for *K. mikimotoi*. A wider set of culture conditions of the phytoplankton could allow for increasing the training dataset to be able to deal with the natural environmental variability to which the phytoplankton is exposed in the real ocean. We speculate that the low light culture conditions in our experiment could have affected the optical properties of the phytoplankton. While they are in agreement with other studies under similar conditions (Whitmire et al., 2010; Harmel et al., 2016), the variability with light intensity and adaptation should be considered and included in subsequent training datasets (Poulin et al., 2018). More complex modeling of R_{rs} by different mixes of phytoplankton species and use of more advanced radiative transfer modeling (Mobley and Stramski, 1997; Stramski and Mobley, 1997) could also make our training dataset more robust. However, it is the lack of *in situ* observations co-incident with either radiometry from *in situ* and/or satellite platforms that limits further advance (Tomlinson et al., 2009), as we were unable to validate our results against real-world observations. Therefore, more efforts to collate existing data and to gather new ones are required.

4. CONCLUSIONS AND FURTHER WORK

In this work, a novel approach, tested through a sensitivity study, to produce training datasets for HAB classification using machine learning methods has been proposed. The novelty of the approach consists in injecting the bio-optical knowledge from the literature and from a purpose built laboratory experiment into a training dataset for detection of a specific phytoplankton species that can cause health and economic harm to the coastal communities.

TABLE 5 | Performance measures derived from the confusion matrix.

True class	Errors of commission	Producer accuracy	Overall accuracy	Kappa coefficient
		Experiment 1		
Harmful bloom	0.027	0.986		
Non-harmful bloom	0.023	0.960	0.981	0.972
No bloom	0.009	0.994		
		Experiment 2		
Harmful bloom	0.029	0.976		
Non-harmful bloom	0.030	0.956	0.978	0.966
No bloom	0.013	0.993		
		Experiment 3		
Harmful bloom	0.024	0.841		
Non-harmful bloom	0.310	0.786	0.915	0.858
No bloom	0.047	0.999		

The potential advantages of this approach include moving away from subjectivity in terms of selection of training datasets as well as not being sensor or even region specific. It is easy to envisage that this approach can be applied to radiometric sensors installed in multiple platforms such as ferries, drones or different satellites.

Laboratory measurements of absorption and backscattering coefficients for different concentrations of *K. mikimotoi* chlorophyll have been performed, matching existing observations at low light conditions of the culture. When these data were used to train a HABs classifier and applied to MERIS images from the European coastal shelf, there was <1% degradation of the capacity to detect the harmful bloom in comparison to using satellite data, but there was a better discrimination of false positives in turbid coastal waters. Further tests on the ability to separate non-harmful from harmful algal blooms when both have high chlorophyll concentrations are needed. Even replacing most of the training datasets with a combination of modeled and laboratory derived R_{rs} did not degrade HAB detection significantly, although regional average chlorophyll concentrations need to be known a priory to improve the results.

The limited availability of suitable datasets to ground truth the results, constrains the conclusions of this study to a sensitivity analysis. If HAB detection from satellite is to progress to become an operational satellite product, in a similar way radiometry or *Chla* products are, the construction and open availability of standardized and purpose built relevant validation datasets should be the focus of future work. Indeed, when *in situ* observations are available (Caballero et al., 2020), local tuning of an algorithm can be achieved. The approach proposed here could be ported to different species by modifying the training datasets.

DATA AVAILABILITY STATEMENT

The datasets presented in this study can be found in online repositories. The names of the repository/repositories and accession number(s) can be found at: https://doi.org/10.5281/zenodo.4075095.

AUTHOR CONTRIBUTIONS

VM-V designed the experiment, carried out the experiment, and wrote the first draft of the manuscript. VB, CS, AA, and VV helped out with the experiment in the laboratory. AK and JL did the numerical experiments. PM discussed initial ideas. All co-authors provided comments to the manuscript.

FUNDING

This work benefited from funding from EC-FP7 AQUA-USERS (Grant 607325), Interreg Atlantic Area project PRIMROSE (Grant EAPA 182/2016), NERC ShellEye (Grant NE/P011004/1), Fundação para a Ciência e Tecnologia through the strategic project UIDB/04292/2020. This work was also supported by funding from the European Union's Horizon 2020 Research and Innovation Programme under grant agreement N 810139: Project Portugal Twinning for Innovation and Excellence in Marine Science and Earth Observation—PORTWIMS. Also supported by HABWAVE project LISBOA-01-0145-FEDER-031265, co-funded by EU ERDF funds, within the PT2020 Partnership Agreement and Compete 2020, and national funds through FCT, I.P.

ACKNOWLEDGMENTS

Thanks to C. Beltran for the analysis of HPLC samples and G.Dall'Olmo for initial advice on the setup of the optical chamber. We acknowledge the comments and suggestions from three reviewers who have contributed to improve this work.

SUPPLEMENTARY MATERIAL

The Supplementary Material for this article can be found online at: https://www.frontiersin.org/articles/10.3389/fmars.2020.582960/full#supplementary-material

REFERENCES

Ahn, Y. H., Bricaud, A., and Morel, A. (1992). Light backscattering efficiency and related properties of some phytoplankters. *Deep-Sea Res. Part A Oceanogr. Res. Pap*. 39, 1835–1855. doi: 10.1016/0198-0149(92)90002-B

Andersen, R. A. (2005). *Algal Culturing Techniques*. London: Elsevier.

Antoine, D., Siegel, D. A., Kostadinov, T. S., Maritorena, S., Nelson, N. B., Gentili, B., et al. (2011). Variability in optical particle backscattering in contrasting bio-optical oceanic regimes. *Limnol. Oceanogr.* 56, 955–973. doi: 10.4319/lo.2011.56.3.0955

Babin, M., Roesler, C., and Cullen, J. J. (2008). *Real-Time Coastal Observing Systems for Marine Ecosystem Dynamics and Harmful Algal Blooms*. Oceanographic Methodology Series. Paris: UNESCO.

Barnes, M. K., Tilstone, G. H., Smyth, T. J., Widdicombe, C. E., Gloël, J., Robinson, C., et al. (2015). Drivers and effects of *Karenia mikimotoi* blooms in the western English channel. *Prog. Oceanogr.* 137, 456–469. doi: 10.1016/j.pocean.2015.04.018

Bricaud, A., Bedhomme, A. L., and Morel, A. (1988). Optical-properties of diverse phytoplanktonic species - experimental results and theoretical interpretation. *J. Plankt. Res.* 10, 851–873. doi: 10.1093/plankt/10.5.851

Bricaud, A., Claustre, H., Ras, J., and Oubelkheir, K. (2004). Natural variability of phytoplanktonic absorption in oceanic waters: influence of the size structure of algal populations. *J. Geophys. Res.* 109:C11010. doi: 10.1029/2004JC002419

Bricaud, A., Morel, A., Babin, M., Allali, K., and Claustre, H. (1998). Variations of light absorption by suspended particles with chlorophyll a concentration in oceanic (case 1) waters: analysis and implications for bio-optical models. *J. Geophys. Res.* 103, 31033–31044. doi: 10.1029/98JC02712

Bricaud, A., Morel, A., and Prieur, L. (1983). Optical-efficiency factors of some phytoplankters. *Limnol. Oceanogr.* 28, 816–832. doi: 10.4319/lo.1983.28.5.0816

Browning, T. J., Stone, K., Bouman, H. A., Mather, T. A., Pyle, D. M., Moore, C. M., et al. (2015). Volcanic ash supply to the surface ocean?remote sensing of biological responses and their wider biogeochemical significance. *Front. Mar. Sci.* 2:14. doi: 10.3389/fmars.2015.00014

Caballero, I., Fernández, R., Escalante, O. M., Mamán, L., and Navarro, G. (2020). New capabilities of sentinel-2a/b satellites combined with in situ data for monitoring small harmful algal blooms in complex coastal waters. *Sci. Rep.* 10:8743. doi: 10.1038/s41598-020-65600-1

Cannizzaro, J. P., Carder, K. L., Chen, F. R., Heil, C. A., and Vargo, G. A. (2008). A novel technique for detection of the toxic dinoflagellate, karenia brevis, in the Gulf of Mexico from remotely sensed ocean color data. *Contin. Shelf Res.* 28, 137–158. doi: 10.1016/j.csr.2004.04.007

Cullen, J. J., Ciotti, u. M., Davis, R. F., and Lewis, M. R. (1997). Optical detection and assessment of algal blooms. *Limnol. Oceanogr.* 42(5 Part 2), 1223–1239. doi: 10.4319/lo.1997.42.5_part_2.1223

Defoin-Platel, M. and Chami, M. (2007). How ambiguous is the inverse problem of ocean color in coastal waters? *J. Geophys. Res.* 112, 1–16. doi: 10.1029/2006JC003847

Dierssen, H., McManus, G. B., Chlus, A., Qiu, D., Gao, B.-C., and Lin, S. (2015). Space station image captures a red tide ciliate bloom at high spectral and spatial resolution. *Proc. Natl. Acad. Sci. U.S.A.* 112, 14783–14787. doi: 10.1073/pnas.1512538112

Finkel, Z., and Irwin, A. (2001). Light absorption by phytoplankton and the filter amplification correction: cell size and species effects. *J. Exp. Mar. Biol. Ecol.* 259, 51–61. doi: 10.1016/S0022-0981(01)00225-8

Gordon, H. R., Brown, O. B., Evans, R. H., Brown, J. W., Smith, R. C., Baker, K. S., et al. (1988). A semianalytic radiance model of ocean color. *J. Geophys. Res.* 93, 10909–10924. doi: 10.1029/JD093iD09p10909

Griffith, A. W., and Gobler, C. J. (2020). Harmful algal blooms: A climate change co-stressor in marine and freshwater ecosystems. *Harmf. Algae* 91:101590. doi: 10.1016/j.hal.2019.03.008

Harmel, T., Hieronymi, M., Slade, W., Rottgers, R., Roullier, F., and Chami, M. (2016). Laboratory experiments for inter-comparison of three volume scattering meters to measure angular scattering properties of hydrosols. *Opt. Exp.* 24, A234–A256. doi: 10.1364/OE.24.00A234

Kelly-Gerreyn, B., Qurban, M., Hydes, D., Miller, P., and Fernand, L. (2004). "Coupled ferrybox ship of opportunity and satellite data observations of plankton succession across the European shelf sea and Atlantic Ocean," in *International Council for the Exploration of the Sea (ICES) Annual Science Conference*, Vigo.

Kudela, R. M., Berdelet, E., Bernard, S., Burford, M., Fernand, L., Lu, S., et al. (2015). *Harmful Algal Blooms. A Scientific Summary for Policy Makers*. Paris: IOC/UNESCO, (IOC/INF-1320).

Kurekin, A., Miller, P. I., and Van der Woerd, H. J. (2014). Satellite discrimination of *Karenia mikimotoi* and phaeocystis harmful algal blooms in European coastal waters: Merged classification of ocean colour data. *Harmf. Algae* 31, 163–176. doi: 10.1016/j.hal.2013.11.003

Loisel, H., and Morel, A. (1998). Light scattering and chlorophyll concentration in case 1 waters: a reexamination. *Limnol. Oceanogr.* 43, 847–858. doi: 10.4319/lo.1998.43.5.0847

Martinez-Vicente, V., Land, P. E., Tilstone, G. H., Widdicombe, C., and Fishwick, J. R. (2010). Particulate scattering and backscattering related to water constituents and seasonal changes in the western English channel. *J. Plankton Res.* 32, 603–619. doi: 10.1093/plankt/fbq013

Martinez-Vicente, V., Tilstone, G. H., Sathyendranath, S., Miller, P. I., and Groom, S. B. (2012). Contributions of phytoplankton and bacteria to the optical backscattering coefficient over the mid-Atlantic ridge. *Mar. Ecol. Prog. Ser.* 445, 37–51. doi: 10.3354/meps09388

Mendes, C. R., Cartaxana, P., and Brotas, V. (2007). HPLC determination of phytoplankton and microphytobenthos pigments: comparing resolution and sensitivity of a C18 and a C8 method. *Limnol. Oceanogr.* 5, 363–370. doi: 10.4319/lom.2007.5.363

Miller, P. I., Shutler, J. D., Moore, G. F., and Groom, S. B. (2006). Seawifs discrimination of harmful algal bloom evolution. *Int. J. Rem. Sens.* 27, 2287–2301. doi: 10.1080/01431160500396816

Millie, D. F., Schofield, O. M., Kirkpatrick, G. J., Johnsen, G., Tester, P. A., and Vinyard, B. T. (1997). Detection of harmful algal blooms using photopigments and absorption signatures: a case study of the florida red tide dinoflagellate, gymnodinium breve. *Limnol. Oceanogr.* 42(5 Part 2), 1240–1251. doi: 10.4319/lo.1997.42.5_part_2.1240

Millie, F, D., Kirkpatrick, J, G., Vinyard, and T, B. (1995). Relating photosynthetic pigments and *in vivo* optical density spectra to irradiance for the florida red-tide dinoflagellate gymnodinium breve. *Mar. Ecol. Prog. Ser.* 120, 65–75. doi: 10.3354/meps120065

Mobley, C., and Sundman, L. (2016). *HydroLight 5.3.0- EcoLight 5.3.0 Technical Documentation*. Sequoia Inc.

Mobley, C. D., and Stramski, D. (1997). Effects of microbial particles on oceanic optics: methodology for radiative transfer modeling and example simulations. *Limnol. Oceanogr.* 42, 550–560. doi: 10.4319/lo.1997.42.3.0550

Neil, C., Cunningham, A., and McKee, D. (2011). Relationships between suspended mineral concentrations and red-waveband reflectances in moderately turbid shelf seas. *Rem. Sens. Environ.* 115, 3719–3730. doi: 10.1016/j.rse.2011.09.010

Pope, R., and Fry, E. (1997). Absorption spectrum (380-700 nm) of pure water. II. integrating cavity measurements. *Appl. Opt.* 36, 8710–8723. doi: 10.1364/AO.36.008710

Poulin, C., Antoine, D., and Huot, Y. (2018). Diurnal variations of the optical properties of phytoplankton in a laboratory experiment and their implication for using inherent optical properties to measure biomass. *Opt. Exp.* 26, 711–729. doi: 10.1364/OE.26.000711

Sanseverino, I., Conduto, D., Pozzoli, L., Dobricic, S., and Lettieri, T. (2016). *Algal Bloom and Its Economic Impact*. Number EUR 27905 EN. Library Catalog: ec.europa.eu.

Shang, S., Wu, J., Huang, B., Lin, G., Lee, Z., Liu, J., et al. (2014). A new approach to discriminate dinoflagellate from diatom blooms from space in the East China Sea. *J. Geophys. Res.* 119, 4653–4668. doi: 10.1002/2014JC009876

Slade, W. H., Boss, E., Dall'Olmo, G., Langner, M. R., Loftin, J., Behrenfeld, M. J., et al. (2010). Underway and moored methods for improving accuracy in measurement of spectral particulate absorption and attenuation. *J. Atmos. Ocean. Technol.* 27, 1733–1746. doi: 10.1175/2010JTECHO755.1

Smyth, T. J., Fishwick, J. R., AL-Moosawi, L., Cummings, D. G., Harris, C., Kitidis, V., et al. (2010). A broad spatio-temporal view of the western English channel observatory. *J. Plankton Res.* 32, 585–601. doi: 10.1093/plankt/fbp128

Smyth, T. J., Moore, G. F., Hirata, T., and Aiken, J. (2007). Semianalytical model for the derivation of ocean color inherent optical properties: description,

implementation, and performance assessment: erratum. *Appl. Opt.* 46, 429–430. doi: 10.1364/AO.46.000429

Stæhr, P. A., and Cullen, J. J. (2003). Detection of *Karenia mikimotoi* by spectral absorption signatures. *J. Plankton Res.* 25, 1237–1249. doi: 10.1093/plankt/fbg083

Stramski, D., Bricaud, A., and Morel, A. (2001). Modeling the inherent optical properties of the ocean based on the detailed composition of the planktonic community. *Appl. Opt.* 40, 2929–2945. doi: 10.1364/AO.40.002929

Stramski, D., and Mobley, C. D. (1997). Effects of microbial particles on oceanic optics: a database of single-particle optical properties. *Limnol. Oceanogr.* 42, 538–549. doi: 10.4319/lo.1997.42.3.0538

Stramski, D., and Morel, A. (1990). Optical properties of photosynthetic picoplankton in different physiological states as affected by growth irradiance. *Deep Sea Res. Part A Oceanogr. Res. Pap.* 37, 245–266. doi: 10.1016/0198-0149(90)90126-G

Tassan, S., and Ferrari, G. M. (1995). An alternative approach to absorption measurements of aquatic particles retained on filters. *Limnol. Oceanogr.* 40, 1358–1368. doi: 10.4319/lo.1995.40.8.1358

Tilstone, G., Mallor-Hoya, S., Gohin, F., Couto, A. B., Sá, C., Goela, P., et al. (2017). Which ocean colour algorithm for MERIS in North West European waters? *Rem. Sens. Environ.* 189, 132–151. doi: 10.1016/j.rse.2016.11.012

Tomlinson, M. C., Wynne, T. T., and Stumpf, R. P. (2009). An evaluation of remote sensing techniques for enhanced detection of the toxic dinoflagellate, Karenia Brevis. *Rem. Sens. Environ.* 113, 598–609. doi: 10.1016/j.rse.2008.11.003

Uncles, R. J. (2010). Physical properties and processes in the Bristol channel and Severn estuary. *Mar. Pollut. Bull.* 61, 5–20. doi: 10.1016/j.marpolbul.2009.12.010

Uncles, R. J., Stephens, J. A., and Harris, C. (2015). Estuaries of southwest England: salinity, suspended particulate matter, loss-on-ignition and morphology. *Prog. Oceanogr.* 137, 385–408. doi: 10.1016/j.pocean.2015.04.030

Vaillancourt, R. D., Brown, C. W., Guillard, R. R. L., and Balch, W. M. (2004). Light backscattering properties of marine phytoplankton: relationships to cell size, chemical composition and taxonomy. *J. Plankton Res.* 26, 191–212. doi: 10.1093/plankt/fbh012

Vanhoutte-Brunier, A., Fernand, L., Ménesguen, A., Lyons, S., Gohin, F., and Cugier, P. (2008). Modelling the *Karenia mikimotoi* bloom that occurred in the western English channel during summer 2003. *Ecol. Model.* 210, 351–376. doi: 10.1016/j.ecolmodel.2007.08.025

Weihs, C., Ligges, U., Luebke, K., and Raabe, N. (2005). "KLAR analyzing German business cycles," in *Data Analysis and Decision Support*, eds D. Baier, R. Decker, and L. Schmidt-Thieme (Berlin: Springer-Verlag), 335–343. doi: 10.1007/3-540-28397-8_36

Werdell, P. J., McKinna, L. I. W., Boss, E., Ackleson, S. G., Craig, S. E., Gregg, W. W., et al. (2018). An overview of approaches and challenges for retrieving marine inherent optical properties from ocean color remote sensing. *Prog. Oceanogr.* 160, 186–212. doi: 10.1016/j.pocean.2018.01.001

Wetlabs (2009). *Ac-Meter Protocol Revision p*. Technical report.

Whitmire, A. L., Boss, E., Cowles, T. J., and Pegau, W. S. (2007). Spectral variability of the particulate backscattering ratio. *Opt. Exp.* 15, 7019–7031. doi: 10.1364/OE.15.007019

Whitmire, A. L., Pegau, W. S., Karp-Boss, L., Boss, E., and Cowles, T. J. (2010). Spectral backscattering properties of marine phytoplankton cultures. *Opt. Exp.* 18, 15073–15093. doi: 10.1364/OE.18.015073

Xi, H., Hieronymi, M., Krasemann, H., and Röttgers, R. (2017). Phytoplankton group identification using simulated and *in situ* hyperspectral remote sensing reflectance. *Front. Mar. Sci.* 4:272. doi: 10.3389/fmars.2017.00272

Xi, H., Hieronymi, M., Röttgers, R., Krasemann, H., and Qiu, Z. (2015). Hyperspectral differentiation of phytoplankton taxonomic groups: a comparison between using remote sensing reflectance and absorption spectra. *Remote Sens.* 7:14781. doi: 10.3390/rs71114781

Zapata, M., Rodríguez, F., and Garrido, J. (2000). Separation of chlorophylls and carotenoids from marine phytoplankton: a new HPLC method using a reversed phase C8 column and pyridine-containing mobile phases. *Mar. Ecol. Prog. Ser.* 195:29-45. doi: 10.3354/meps195029

Conflict of Interest: The authors declare that the research was conducted in the absence of any commercial or financial relationships that could be construed as a potential conflict of interest.

frontiers in Marine Science

ORIGINAL RESEARCH
published: 09 April 2021
doi: 10.3389/fmars.2021.631732

HABreports: Online Early Warning of Harmful Algal and Biotoxin Risk for the Scottish Shellfish and Finfish Aquaculture Industries

Keith Davidson[1], Callum Whyte[1], Dmitry Aleynik[1], Andrew Dale[1], Steven Gontarek[1], Andrey A. Kurekin[2], Sharon McNeill[1], Peter I. Miller[2], Marie Porter[1], Rachel Saxon[1] and Sarah Swan[1]*

[1] Scottish Association for Marine Science, Oban, United Kingdom, [2] Plymouth Marine Laboratory, Plymouth, United Kingdom

We present an on-line early warning system that is operational in Scottish coastal waters to minimize the risk to humans and aquaculture businesses in terms of the human health and economic impacts of harmful algal blooms (HABs) and their associated biotoxins. The system includes both map and time-series based visualization tools. A "traffic light" index approach is used to highlight locations at elevated HAB/biotoxin risk. High resolution mathematical modelling of cell advection, in combination with satellite remote sensing, provides early warning of HABs that advect from offshore waters to the coast. Expert interpretation of HAB, biotoxin and environmental data in light of recent and historical trends is used to provide, on a weekly basis, a forecast of the risk from HABs and their biotoxins to allow mitigation measures to be put in place by aquaculture businesses, should a HAB event be imminent.

Keywords: harmful algal blooms, biotoxins, early warning, remote sensing, modelling

OPEN ACCESS

Edited by:
Jose Luis Iriarte, Austral University of Chile, Chile

Reviewed by:
Rowena Fay Stern, Marine Biological Association of the United Kingdom, United Kingdom
Gustaaf Marinus Hallegraeff, University of Tasmania, Australia
Jorge I. Mardones, Instituto de Fomento Pesquero (IFOP), Chile

****Correspondence:***
Keith Davidson
keith.davidson@sams.ac.uk

Specialty section:
This article was submitted to Marine Fisheries, Aquaculture and Living Resources, a section of the journal Frontiers in Marine Science

Received: *20 November 2020*
Accepted: *18 March 2021*
Published: *09 April 2021*

Citation:
Davidson K, Whyte C, Aleynik D, Dale A, Gontarek S, Kurekin AA, McNeill S, Miller PI, Porter M, Saxon R and Swan S (2021) HABreports: Online Early Warning of Harmful Algal and Biotoxin Risk for the Scottish Shellfish and Finfish Aquaculture Industries. Front. Mar. Sci. 8:631732. doi: 10.3389/fmars.2021.631732

INTRODUCTION

Harmful algal blooms (HABs) are primarily natural phenomena that are characterized by increases in the density of certain phytoplankton species that are harmful to human use of the marine environment (Smayda, 1990). In many locations, these blooms are of particular concern to the finfish and shellfish aquaculture industries. The phytoplankton genera that are detrimental to these two related sectors are, in general, distinct.

Some HAB species cause "shellfish poisoning" that results from the human consumption of shellfish that have ingested toxic cells and then bio-accumulated the toxin within their flesh (Davidson and Bresnan, 2009; Berdalet et al., 2016). This significant danger has led to an extensive monitoring effort to minimize human health risk. For example, in the EU it is a regulatory requirement to monitor both the abundance of the causative phytoplankton and the concentration of biotoxins within shellfish flesh on a regular basis (Davidson et al., 2011). Harvesting restrictions are applied until toxins return below safe threshold levels and the shellfish are again fit for consumption.

Farmed fish are impacted, in general, by different HAB species through physical interference, de-oxygenation or ichthyotoxicity. While the vectoring of toxin to humans through fish consumption can occur (Berdalet et al., 2016), this is of most concern to wild fisheries in tropical latitudes (e.g., ciguatera fish poisoning). Hence, the impact of HABs on the large fish aquaculture operations of

high latitude fjordic countries (Norway, Scotland, Chile, and Canada) is primarily economic, as a result of fish kills.

Early warning of the timing, location and magnitude of HABs and their associated biotoxins is of great value to coastal zone managers and the aquaculture industry, informing business planning and ensuring the protection of both human and fish health (Anderson et al., 2001, 2016; Davidson et al., 2016). Martino et al. (2020) demonstrated that blooms of the toxin producing dinoflagellate *Dinophysis* result in the loss of 15% of turnover of the Scottish shellfish industry, a value of ∼ £ (GBP) 1.4 million. The Scottish finfish aquaculture sector is considerably larger in value, £ (GBP) 468 million direct gross value added (Scottish Government, 2020), but the financial impact of HABs are less easily determined due to the commercial sensitivity of fish kill data. However, studies in similar fjordic regions elsewhere have demonstrated the significant impact of HABs on the fish farming sector. For example, a HAB event killed eight million salmon in northern Norway in 2019 with a direct value of over 850 million NOK (Davidson et al., 2020), and a massive fish kill in Chile in 2016 following a bloom of the dictyochophyte *Pseudochattonella* caused the mortality of 39 million salmon with $ (USD) 800 million of economic impact (Anderson and Rensel, 2016).

Regulatory monitoring for shellfish biotoxin producing HAB species and their associated toxins is undertaken in most shellfish producing countries, typically on a weekly basis. In Scotland, this is overseen by the competent authority, Food Standards Scotland (FSS), and operated by CEFAS (biotoxins) and SAMS (phytoplankton), respectively.

The financial cost of HAB and biotoxin monitoring at all shellfish farms is prohibitive. Regulators therefore typically monitor only a representative sub-set of farms. In Scotland, this is carried out according to a "Pod" system. A Pod usually includes a number of relatively closely located shellfish-producing sites, for example, all the farms within a single fjordic sea loch. Within each Pod, a Representative Monitoring Point (RMP) is chosen that is considered representative of the Pod as a whole. A biotoxin result over the regulatory limit at this point will result in the closure of all the farms within the Pod.

While this approach is generally capable of safeguarding human health, it is not infallible. For example, in 2013, a large bloom of *Dinophysis* impacted the Scottish Shetland Islands where much of the country's shellfish aquaculture is concentrated. It resulted in a very rapid increase in shellfish toxicity to high levels in less than the 1-week monitoring window (**Figure 1**). This led to toxin-contaminated mussels being harvested and consumed. Seventy people reported shellfish toxicity symptoms to food safety authorities, although the number affected is likely to be substantially higher. Subsequent analysis of this bloom (Whyte et al., 2014) indicated that it developed offshore and was rapidly advected by strong wind-driven westerly currents to the coastline where it impacted the aquaculture businesses.

Given, the significance of this event in terms of human health and public perception of shellfish safety, it led to increased effort to develop an early warning system for HABs in Scottish waters. Achieving this goal is, however, far from straightforward as different HAB genera exhibit different life cycles and changing density and toxicity (Berdalet et al., 2016; Wells et al., 2020). Variability in local or regional oceanography or hydrography is also thought to be critical to bloom location and timing (Gowen et al., 1998; Smayda, 2002; Paterson et al., 2017).

In Scottish waters there are eight different species/genera of HABs that are of concern in relation to their capacity to cause shellfish poisoning (Davidson et al., 2011), the most prevalent being *Dinophysis, Pseudo-nitzschia,* and *Alexandrium;* responsible for diarrhetic, amnesic and paralytic shellfish poisoning, respectively. The dinoflagellate *Karenia mikimotoi* (Davidson et al., 2009) and dense (spiny) diatom blooms (Bruno et al., 1989; Treasurer et al., 2003) are of greatest concern in relation to the health of farmed fish.

MATERIALS AND METHODS

The EU FP7 "Applied Simulations and Integrated Modelling for the Understanding of Harmful Algal Blooms" (ASIMUTH) project developed a prototype HAB alert system for various locations on the western seaboard of Europe. This was achieved by combining regulatory phytoplankton monitoring and biotoxin data with satellite remote sensing and other information on current, recent, or modelled future marine conditions. In Scotland, HAB risk bulletins were prepared weekly, based on expert interpretation of the various data streams, for use by the aquaculture industry. Through a number of subsequent grants plus Scottish Government and aquaculture industry funding, we have further developed these early warning tools to provide a more advanced HAB and biotoxin alert system for Scottish waters as described here.

We produce four linked products all freely available to the aquaculture industry, other stakeholders and the general public through the https://www.HABreports.org/website. These are:

(1) An interactive, web-map based, spatial and temporal display of current and historical trends in HABs and biotoxins.

The website is written in HTML5, PHP and JavaScript: it utilizes the OpenLayers JavaScript Library to provide the main mapping functionality, along with the Proj4 JS Library to provide on-the-fly projection functionality between GPS Longitude\Latitude and the British National Grid projection. In addition, it uses a number of other JavaScript libraries to provide layout and charting capabilities. The backend data source for the map data is a PostgreSQL\PostGIS database, hosted on the SAMS Scientific Database server.

The monitoring data used to create the interactive web map are updated weekly from two sources: an excel format report detailing FSS regulatory monitoring biotoxin results generated by CEFAS, and the most recent regulatory HAB counts generated by SAMS. The data are consolidated by loading both into a single Microsoft Access database, where the data are checked for errors. Static map images (png) can then be bulk-exported for each species and toxin, for use in the weekly PDF bulletin (see section "Materials and Methods" below).

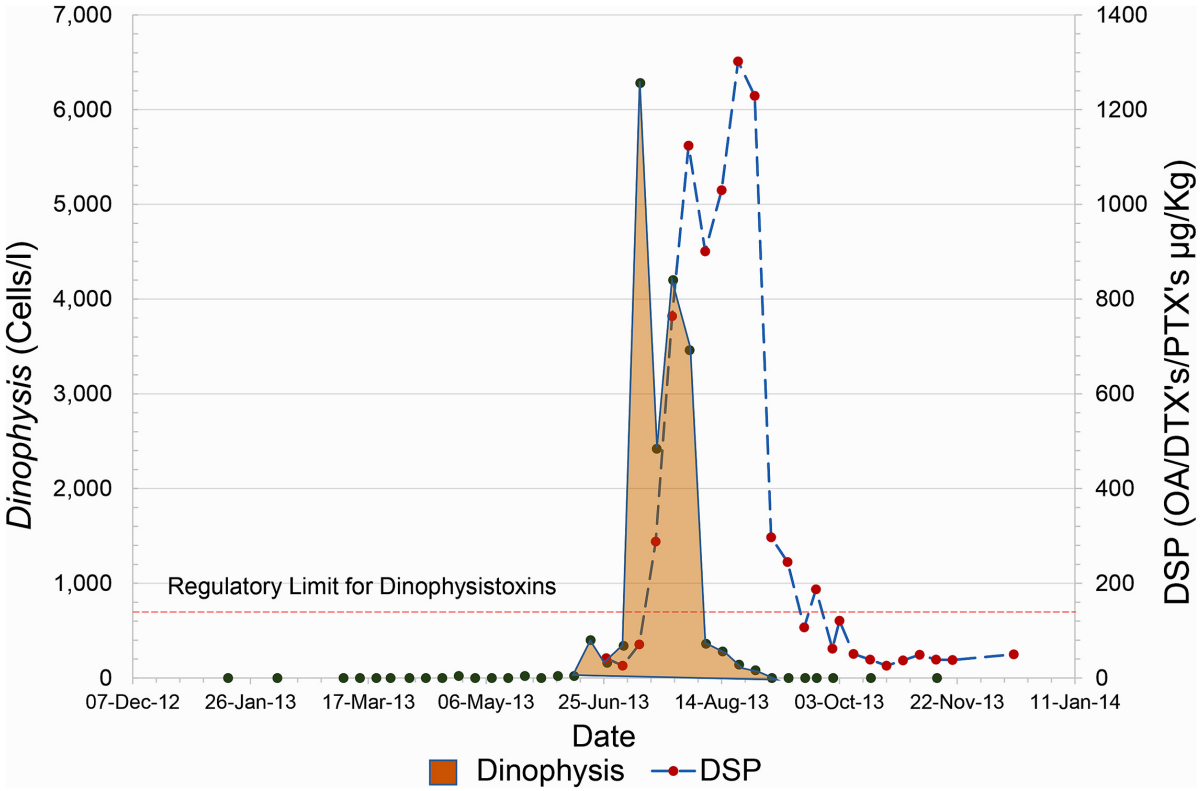

FIGURE 1 | An example of the rapid rise of *Dinophysis* and associated toxins that occurred during the summer of 2013. The plot shown represents the evolution of the bloom in the site, East of Linga, however, this rapid increase was mirrored in sites along the West coast of the Shetland Islands.

Forecast data for areas of interest, in the form of modelled particle tracking (see section "Discussion" below) is retrieved from the SAMS modelling cluster and incorporated into the Access database. These data are then uploaded to the backend database of the HABreports website, along with the PDF report, and are made available for download.

(2) A detailed risk assessment and HAB/biotoxin forecast bulletin for the Shetland Islands, which has the country's greatest density of shellfish aquaculture.

The content of the bulletin, and the approach to data interpretation and display within it, was determined through discussion with industry (primarily the trade association Seafood Shetland) at a range of stakeholder meetings over several years. The bulletin takes the form of a PDF document that is available for download from the HABreports website and is also emailed directly to registered stakeholders.

The bulletin summarizes the current information relating to HAB and biotoxin concentrations in the Shetland Islands and includes a suite of data products that industry have indicated are of use to them when making harvesting and husbandry decisions.

Harmful algal bloom events can be advective in nature with blooms developing offshore and then being driven to the coast by means of winds and currents. While we can use a combination of remote sensing and modelling to forecast high biomass, fish killing *K. mikimotoi*, the low biomass shellfish toxin producers such as *Dinophysis* are not suitable for this approach as they cannot be detected by satellite. The bulletin therefore includes information on their densities at coastal monitoring sites and meteorological and oceanographic conditions, to provide an indication of when conditions may be suitable to promote onshore advection of these genera and hence when risk is elevated. Wind information is updated, using a combination of the wind direction and speed from the Shetland meteorological stations at Sumburgh and Scatsa. These data are presented as wind roses for the current time and for the preceding 3 weeks. A summary of the previous month is also provided. We also subset forecast currents from the Mercator-IBI36 model (Sotillo et al., 2015).

Industry is also interested in water temperature, as temperature-based stratification can often promote harmful blooms and relates to, for example, increases in the abundance of the parasites that cause amoebic gill disease. Hence, daily sea surface temperatures maps produced with the Multi-Satellite aggregated MUR-SST 1 km gridded dataset (Armstrong et al., 2012) provided by NASA Jet Propulsion Laboratory in Pasadena CA are also presented for the previous 5 days.

Charts of six-hourly wind, rain and temperature predictions for the next 3 days over the Shetland and Orkney region are based on localized implementation of a high-resolution 3-level nested

Weather Research Forecasting WRF v4 model (Skamarock et al., 2008) run operationally at SAMS.

Satellite chlorophyll images that provide an indication of total phytoplankton biomass are generated using the OCEANCOLOUR_ATL_CHL_L4_NRT_OBSERVATIONS_009_0937 product obtained from the CMEMS[1] portal and based on satellite observations daily interpolated onto a 1 km grid by merging data from sensors on board SeaWiFS, MODIS-Aqua, MERIS, VIIRSN, and OLCI-S3A satellites.

These data also assist in the provision, within the bulletin, of an "expert interpretation" based forecast that applies our ecological understanding of HAB dynamics in Scottish waters. Expert interpretation is by its very nature at least a partially qualitative process, but one that relies on scientific understanding of the ecological and hydrodynamic processes underpinning blooms of the different harmful genera impacting a region.

(3) A web-based application of the FSS Toxin Traffic Light Guidance (TTLG) that quantifies risk at individual shellfish harvesting sites.

In 2014 FSS (then as part of the United Kingdom wide Food Standards Agency) developed a decision matrix to help food business operators (FBOs) in Scotland assess the safety of the shellfish they produce for human consumption (FSA, 2014). The matrix is populated with FSS Official Control monitoring program data from the Access database outlined in Section "Introduction" above. A flow diagram outlining the steps required to calculate the index (for *Dinophysis*) is presented in **Supplementary Figure 1**. The calculated output of the matrix known as the "Toxin Traffic Light Guidance" (TTLG) indicates the harvesting action and testing considerations that should follow. Based on the outcome of the TTLG decision matrix a green, amber or red risk is generated. Associated actions are:

- Green: no increase in end-product testing, the FBO should maintain routine verification checks.
- Amber: increased frequency of end-product testing or positive release.
- Red: cease harvesting unless there is evidence available that the product is safe.

(4) A mathematical model/satellite/coastal monitoring-based early warning system for advective HABs.

Our approach to achieve early warning of blooms that develop offshore is the satellite remote sensing-based detection of the bloom, followed by the application of a mathematical model to predict its subsequent temporal and spatial evolution. Within the HABreports website, we therefore currently provide an early warning system for fish killing *K. mikimotoi*, as this species can reach sufficiently high cell densities that it can be detected by satellite.

Remote sensing is undertaken using the HAB classification methodology of Kurekin et al. (2014), in which a linear discriminant analysis classifier is trained to identify ocean colour characteristics of known *K. mikimotoi* bloom events. The classifier is designed to identify HAB species in satellite images that dominate the phytoplankton ensemble and have a high cell concentration. It uses a machine learning approach to identify classification features from example satellite images of algal blooms, selected manually by browsing for matchups with historical records of HAB events. Visual masking of the location of "harmful bloom," "non-harmful bloom," and "no bloom" pixels forms the training dataset that is applied to calculate the parameters of the LDA classifier.

The classification is based on spectral features of the target phytoplankton species. In this study, the set of features comprised combinations of remote sensing reflectance (Rrs) from specific spectral bands of the MODIS sensor and spectral ratios of Rrs. A reduced subset of the most relevant features was automatically identified by an iterative Stepwise Discriminant Analysis (SDA) algorithm implemented in the statistical package "klaR" (Weihs et al., 2005). The selected features were used to classify satellite image pixels into "no bloom," "non-harmful," and "harmful" categories. An "unknown" class was added to represent water classes that are significantly different in spectral characteristics from any of known classes (Kurekin et al., 2014).

This classification methodology demonstrated its efficiency in solving complex HAB discrimination tasks with many unknown factors and errors in satellite measurements. The statistical approach based on the LDA classifier reduced the effect of errors in ocean colour measurements. Training of the classifier using examples of HAB events allowed us to incorporate different HAB properties and adapt to variability in pigment content and community size structure. Introduction of the "unknown" class contributed to better discrimination of water classes with high sediment or dissolved organic matter concentration, resulting in fewer false alarms.

We then classify each MODIS ocean colour scene in near-real time and compile a median composite HAB risk map for the last 7 days, in order to gain cloud-free coverage of most areas. We identify 'particles' that represent areas with an elevated HAB risk from the satellite classifier using a three-stage algorithm. Firstly, the "HAB risk" and "unknown class" likelihood maps are smoothed by applying a median filter of size 10×10 pixels (11×11 km). Secondly, map regions with "HAB risk" >0.6 and "unknown" likelihood <0.5 are selected as regions of elevated HAB risk. Finally, the image pixels in the selected regions are replaced with particles located on a regular grid of 22 km spacing. Each particle records the coordinates, HAB risk ("harmful" likelihood) value, date and time.

Shellfish biotoxin producing genera do not reach a sufficiently high cell density in Scottish waters to be visible from satellite remote sensing and hence their offshore detection is not possible. However, weekly cell counts obtained from the FSS regulatory monitoring program can be used to identify developing blooms in coastal locations. Modelling of the development of these blooms gives information on their potential to impact other aquaculture sites through transport on the coastal current.

Harmful algal bloom alerts from either remote sensing or coastal monitoring are then used to initiate the mathematical model-based HAB alert systems that predict the offshore-onshore

[1] marine.copernicus.eu

advection or along-coast movement of these blooms within the aquaculture regions of Scotland.

On the west coast of the mainland (and adjacent islands) we use the WeStCOMS v2 model (Aleynik et al., 2016). This unstructured grid, free-surface, hydrostatic model is based on the open source Finite Volume Community Ocean Model (FVCOM) (Chen et al., 2011). As the WeStCOMS domain does not reach the Shetland Islands, an alternative approach was taken for this region using the 1/36° Iberian-Biscay-Irish Mercator-Ocean daily forecasting model IBI36QV5R1 with a regular horizontal grid spacing of approximately 2 km (Sotillo et al., 2015). This model will be referred to as Mercator-IBI36.

WeStCOMS-FVCOM provides the flexibility in mesh size distribution required to resolve the complex fjordic coastline and islands of the region, allowing enhanced predictions of bloom progression. The model's open lateral boundaries are forced with output from a relatively high resolution (2 km) North-East Atlantic ROMS operational model, provided by the Marine Institute, Ireland (Dabrowski et al., 2016). Tides at the boundaries are derived from the Oregon State University inverse barotropic tidal solution (Egbert and Erofeeva, 2002). Fresh-water discharge and sea-surface forcing are supplied from a coupled regional Weather Research Forecasting (WRF v4) (Skamarock et al., 2008) system which we run simultaneously using a High Performance Computing system at SAMS.

To have confidence in our model predictions we validated the predictions and reliability of each model. Statistical evaluation of WeStCOMS performance is presented in Aleynik et al. (2016). A further validation of diffusion characteristics was performed in October 2019 in Loch Linnhe on the Scottish west coast using Rhodamine-WT dye, which was released into surface waters near the eastern shore (Dale et al., 2020). A CTD equipped with a rhodamine fluorometer was used to trace the dye during sequential transects.

To validate the performance of the Mercator-IBI36 model in Scottish waters, we undertook the deployment of 16 drifters east of the southern tip of Shetland, between 3°W and 4°W on 28th September 2015. The drifters consisted of eight Coastal Ocean Dynamics Experiment (CODE) style surface drifters and eight Surface Velocity Program (SVP) style drifters, drogued to follow the water at 15 m. Drifters were released in pairs of 'surface' and 'drogued.' Both styles of drifter followed the water with a downwind slip of approximately 0.1% of the wind speed (Niiler et al., 1995; Poulain and Gerin, 2019). In the model, we seeded the same number of neutrally buoyant virtual drifters at the same times, depths and locations as the actual drifters.

In the "Results" Section below, we demonstrate the use of the HABreports products through a series of examples.

RESULTS

Map and Time Series Display

The right-hand panel of the front page of the HABreports website consists of an interactive map of Scotland. Two exemplar versions of the front page are presented in **Figure 2**.

For easy interpretation, each monitored site is identified by one of three symbols. A green circle indicates that all HAB genus/species and associated biotoxins are below regulatory threshold. An amber diamond indicates that at least one HAB species or shellfish biotoxin is elevated, but still below regulatory threshold. A red star indicates that a parameter (HAB or biotoxin) exceeds regulatory threshold at the site (**Figure 2a**).

A drop-down menu allows the user to interrogate this information more closely by selecting any monitored species or toxin using a further system of colour- and size-coded circular symbols (**Figure 2b**). Blue indicates that the site was not monitored for the particular parameter in the week of interest. Green represents a zero count, yellow represents non-zero but low concentration, amber represents elevated concentrations that remain below regulatory threshold, and red indicates that the site is above regulatory threshold. The size of these red symbols increases with concentration, to allow easy identification of areas with the greatest risk. By hovering the cursor over a particular site in the map view, the user is able to confirm the site name and its unique FSS Site Identification Number (SIN). Information is also presented on the indicator shellfish species, the date of sample collection and the concentration of the parameter of choice (i.e., HAB genus/species or biotoxin).

There is also an option to interrogate the data for specific areas of the country in more detail. For any selected site, the HABreports website displays an 8-week summary of the status of each toxin and HAB organism (**Figures 2a,b** left-hand panel). By clicking on a specific parameter it is then possible to see the time series in both graphical and numerical form back to 2005 when monitoring began in its current form (not shown). This facility allows users to evaluate the inter-annual trends at particular locations.

Risk Assessment Forecast

On the basis of current funding, the detailed weekly risk assessment and forecast "bulletin" for the shellfish and finfish aquaculture industries is produced for the Shetland Islands, which account for ∼75% of Scotland's shellfish production, but is easily extendable to other regions.

The bulletin currently runs to 12 pages summarizing HAB, biotoxin and environmental information and hence is not fully reproduced here. Rather, the pages that summarize HAB and shellfish biotoxin concentrations from the week of 1st July 2019 are presented as an example. These data are displayed in both map (**Figure 3A**) and schematic (**Figure 3B**) form. This graphical display allows industry to easily interpret results at their farm(s) in light of data from adjacent sites. Maps are also produced for the previous 3 weeks to allow easy visualization and interpretation of temporal trends. Maps of each HAB organism and associated toxin are displayed on an individual page, one above the other, to allow comparison between cells and associated toxicity and their temporal and spatial evolution.

Each weekly bulletin contains a summary page that reports the current state of the major HAB organisms and shellfish toxins. Based on expert interpretation of these data and the associated environmental information detailed above we provide a forecast for the following week of the HAB/biotoxin

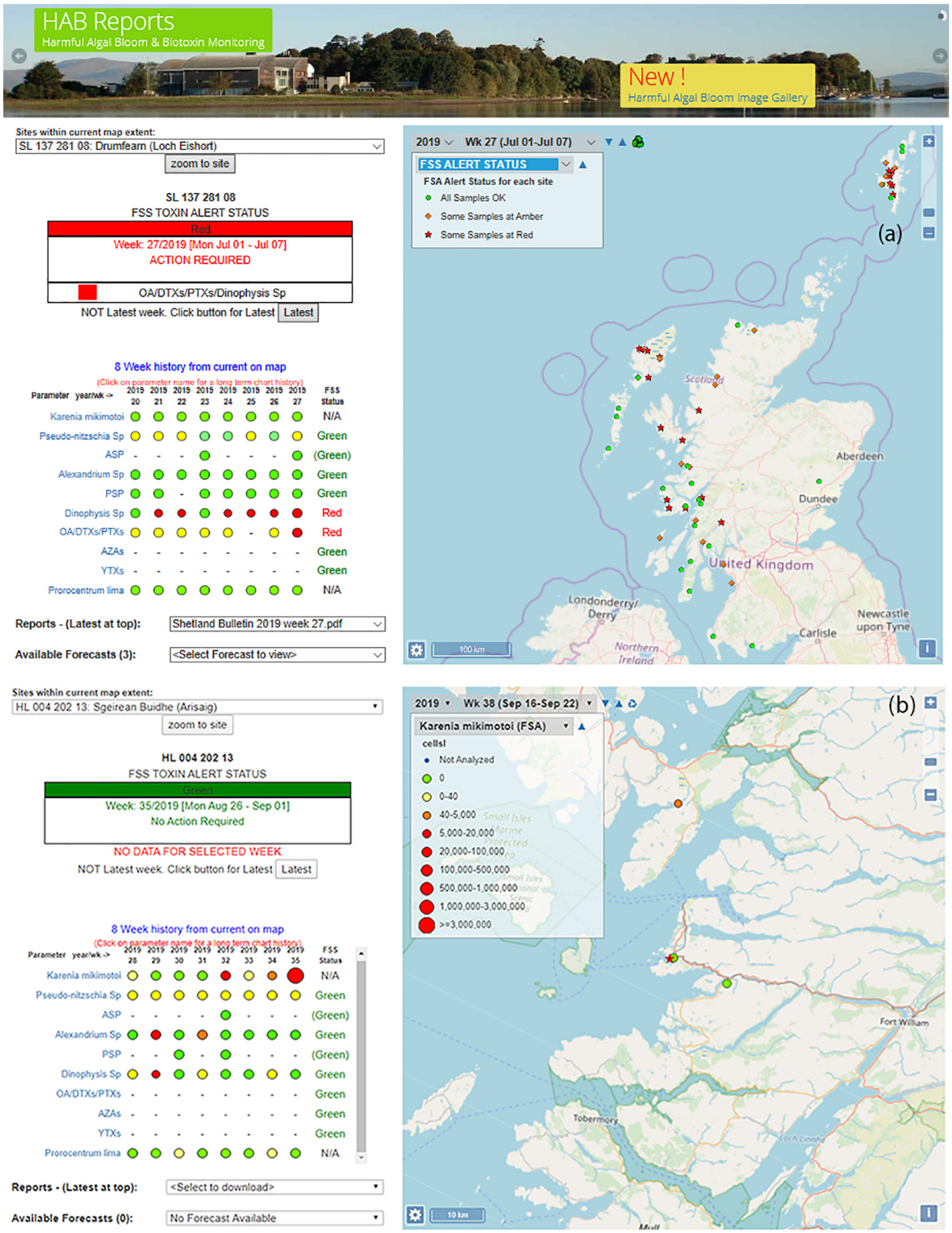

FIGURE 2 | Views **(a)** of front page of the of HABreports.org website for **(a)** the week of 1st of July 2019 at which time the selected site (Loch Eishort) had a red TTLG alert due to elevated concentration of *Dinophysis* and its associated toxins and **(b)** an enlarged view of the map component of the HABreports web site in which the abundance concentration of *Karenia mikimotoi* exceed 2.5 M cells·L^{-1} for the week of 26th of August 2019 at the Arisaig site (star).

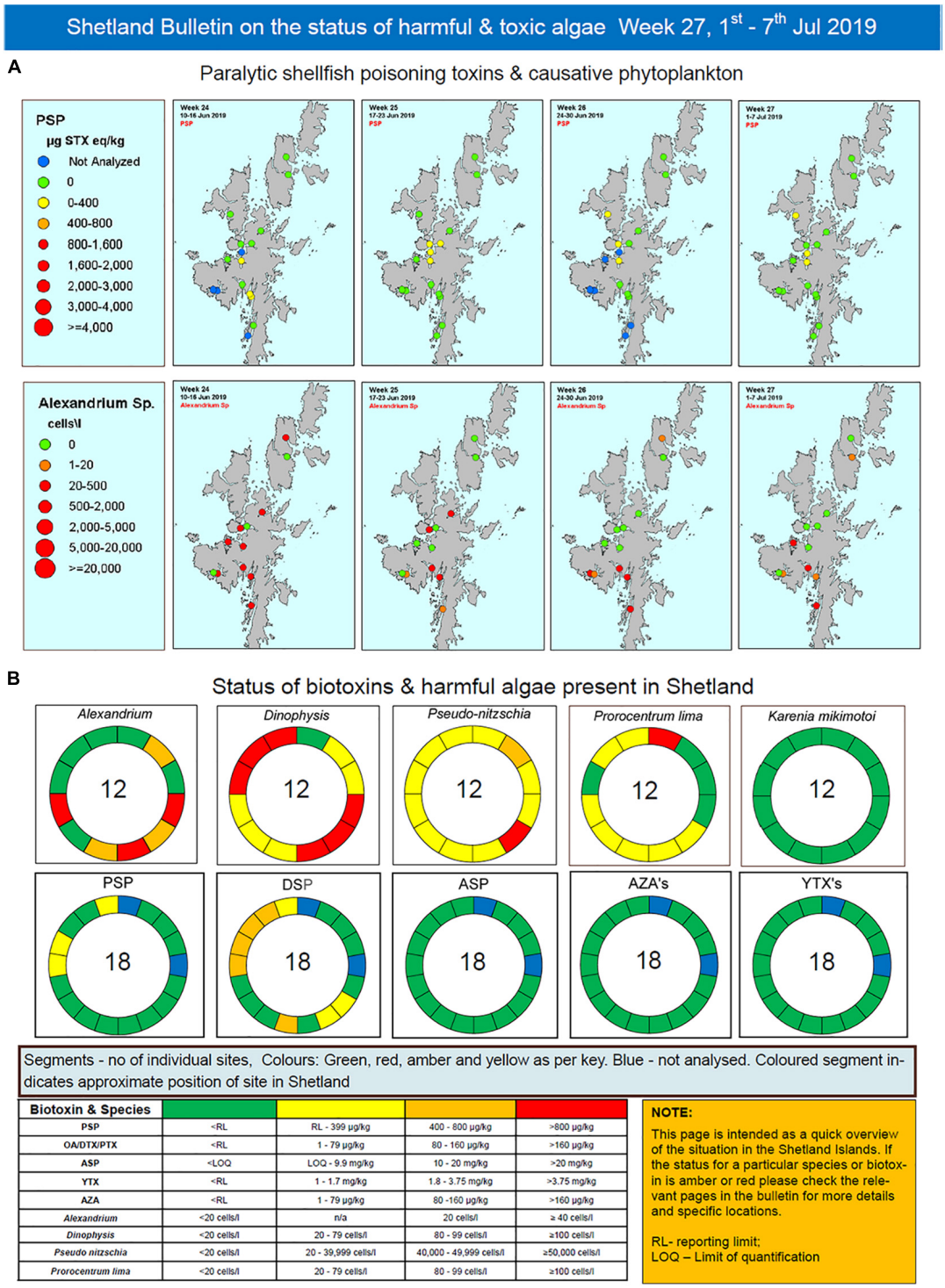

FIGURE 3 | Exemplar pages from the detailed Shetland Islands bulletin for the week of 1st of July 2019 representing **(A)** a map based view of paralytic shellfish toxins and their causative phytoplankton (*Alexandrium* sp.) and **(B)** a schematic "donut" presentation of the Shetland Islands representing the locations and concentrations of the different species and toxins present.

risk for the region. **Figure 4** illustrates the combination of different relevant data streams that an "expert" might use in conjunction with their ecological understanding of a harmful species to produce a bloom/biotoxin forecast for the following week. Our success rate for predicting incidences of the three major shellfish toxin syndromes [Diarrhetic Shellfish Poisoning

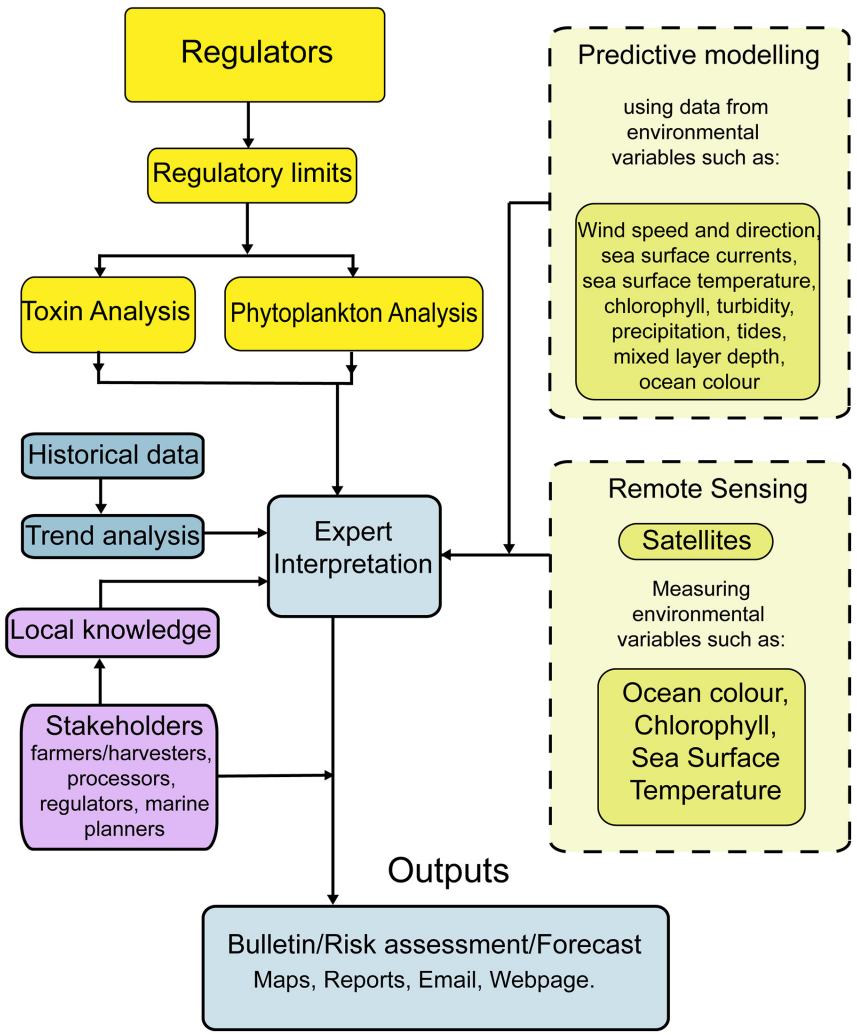

FIGURE 4 | Data streams that contribute to the expert interpretation based HAB/biotoxin forecast.

(DSP) from *Dinophysis*, Paralytic Shellfish Poisoning (PSP) from *Alexandrium* and Amnesic Shellfish Poisoning (ASP) from *Pseudo-nitzschia*] is presented in **Table 1**.

Case Study: Combining Data Sources and Expert Interpretation to Forecast Risk

Supplementary Figure 4 illustrates a range of the predictive tools included within HABreports that may be used when determining the likelihood of an algal bloom. Below follows an example of how these sources of data may be used to support the development of a risk forecast. **Supplementary Figures 4B,C** show the forecasted sea surface currents for two consecutive days during week 26 (22–28 June 2020). A strong shelf-edge current can be seen in the top left of the diagram. Within the region of interest for forecasting, shown in close up in **Supplementary Figure 4C**, relatively strong surface currents can be seen flowing around the top of the Shetland Islands and down the eastern coast. Experience tells us that these currents often bring phytoplankton cells into the eastern voes. Additionally, from chlorophyll concentration measured in the waters around the Shetland Islands on the 23rd of June (**Supplementary Figure 4A**), we can see what appears to be a tongue of chlorophyll stretching along the edge of the Faroes-Shetland trough and extending around the northern coast of the Shetland Islands. This corresponds to an area of warmer, stratified surface water that can be seen in **Supplementary Figure 4E**. Finally, **Supplementary Figure 4D** shows the mean wind direction observed at the meteorological stations at Sumburgh and Scatsa airports on Shetland for the previous week. We can see that the prevailing winds came from the South East. Indeed, the prevailing wind for the previous 2 weeks was also from the East. Combining information from these various sources led us to predict that

TABLE 1 | Expert interpretation success for the HABreports system 2017–2019.

	DSP			PSP			ASP		
Year	Correct (%)	False positive (%)	False negative (%)	Correct (%)	False positive (%)	False negative (%)	Correct (%)	False positive (%)	False negative (%)
2017	67	33	0	76	24	0	62	38	0
2018	80	20	0	50	47	3	97	3	0
2019	70	30	0	70	30	0	94	6	0

		Toxin	Areas move to higher alert status if any one condition is met	
		Green	Amber	Red
Information	Official Control (OC) results for flesh or data available from harvesters own testing (EPT)	Levels less than amber trigger level detected in OC/EPT for the Pod over previous 4 weeks	OC/EPT at or above amber trigger level but below red trigger level over previous 4 weeks	OC/EPT results are at red trigger levels or above
	Phytoplankton Monitoring	Phytoplankton samples at green e.g. *Dinophysis* spp. at 0-100 cells/litre over previous 4 weeks	Phytoplankton samples at amber trigger level e.g. *Dinophysis* spp. greater than 100 cells/litre over previous 4 weeks	Harvester may want to consider critical levels based on experience
	Wider area considerations	Neighbouring area at green status i.e at levels defined above	Adjacent areas showing shellfish flesh or phytoplankton at amber trigger levels	Adjacent areas showing shellfish flesh or phytoplankton at red trigger levels
Actions	Harvesting actions	All harvesting can continue subject to routine OC sampling	Harvesting can continue with increased EPT or positive release	farmers should consider suspending harvesting unless they have evidence for product safety
	Post toxic event considerations	Area returns to green status if criteria are met and 4 weeks have passed since red criteria was applied	Area should remain at amber alert for a minimum of 4 weeks before returning to green	Harvesting suspended, unless there is evidence that product is safe, until levels fall below red trigger level

FIGURE 5 | The TLTG decision matrix: separate specific matrices are used for each toxin/phytoplankton group based on their relevant trigger levels. Each matrix is split into two sections. The top three rows describe the information that should be available to the shellfish farmers regarding phytoplankton and toxin analysis at their site and in adjacent sites. The bottom two rows describe the recommended actions taken following a toxic outbreak.

there would be a moderate to high probability of an accumulation of *Pseudo-nitzschia* cells in the north-easterly facing voes on Shetland during Week 26. As we can see in **Supplementary Figure 4F**, such an event did indeed occur with *Pseudo-nitzschia* reaching high concentrations in Dales Voe (red dot).

Toxin Traffic Lights

The TTLG decision matrix is presented in **Figure 5**. The left-hand side of the front page of the HABreports site (**Figure 2**) displays the calculated value of the TTLG for any selected location as red/amber/green.

Should there be a red or amber warning, the HABreports site also displays which parameters are elevated in concentration and hence have led to this result. In the example presented in **Figure 2a** the data generate a red TTLG warning on the basis of elevated *Dinophysis* and its toxins. **Figure 2b** demonstrates high abundance of *K. mikimotoi*, but this organism is not a shellfish toxin producer and hence does not influence the

TTLG. *Pseudo-nitzschia* abundance is somewhat elevated, but only modestly, and as ASP toxins are low, the TTLG index is green in this case.

The TTLG and the map/time series displays give information on the current and historical status of HAB and biotoxin concentrations within a Pod. From this, a user can identify the course of action to take based on the current HAB/biotoxin status of their site, and assess current trends (for example, identify a developing harmful bloom) or evaluate historical precedent for harmful events at a particular location or time of year. However, while valuable, these tools are effectively a "now-cast." To provide a forward-looking forecast it is necessary to utilize both mathematical modelling and expert interpretation, as discussed below.

Satellite/Mathematical Model Early Warning

The WeStCOMS model domain extends from the Isle of Man in the south to Cape Wrath in the north and about 30 miles west of the Hebrides (**Figure 6**). As noted above, validation of this model is reported by Aleynik et al. (2016). In the additional dye release experiments reported here, winds increased substantially from 2–3 ms^{-1} to 10 ms^{-1}, with direction favorable for driving fresh surface waters across the loch toward the experimental region. This led to freshening of surface waters and downward displacement of dye-laden water, the timing of which were well represented in the model (**Figure 7**).

For the Mercator-IBI36 model, validation also demonstrated good agreement between the reported drifter GPS location every hour from deployment as they tracked toward and beyond Shetland (**Supplementary Figure 2**). The tracks from real drifter fixes were sub-sampled to the nearest mid-day (12:00) and a 'virtual drifter' was advected for the next 24 h starting from the observed drifter location, then the iterations were repeated over several days as shown in **Supplementary Figure 3**. Thus, the model has a finite-difference scheme in space and an explicit 4^{th} order Runge-Kutta scheme in time with the assumption that the modelled velocity field was stationary during discreet (hour-long) tracking time intervals. The distances between observed and 'virtual' drifter positions are summarized in **Table 2**. Good agreement between model and experiment was achieved with the modelling performance of the deeper drifters exceeding the shallow ones in terms of the virtual-observed separation distances after 2–3 weeks with averaged values (deep) Δr_{15} = 8.4 ± 6.0 and (shallow) Δr_0 = 11.3 ± 8.7 km. After removal of the outliers ($>2\sigma$ exceeding the averaged), model prediction deviations from the observed tracks further reduced (5.7 ± 2.9 and 7.3 ± 3.8 km, respectively, for lowered and sub-surface drifters). These estimates provide the expected error range in the predictions of virtual particle advection using the daily-averaged, sub-surface velocity field of the Mercator-IBI36 model. In complicated coastal environments, unstructured grid solutions often demonstrate better skill and a narrower range of separation distances (2.7–8 km) was achieved for WeStCOMS-based simulations of SVP drifters released during the summer 2013 FASTNET experiment (Aleynik et al., 2016), which remained within the cloud of virtual drifters over several days in relatively calm weather and tide conditions.

Should a developing harmful bloom be flagged by either remote sensing analysis or from *in situ* samples from coastal monitoring, the timing, location and magnitude of this event is identified. An example satellite derived HAB risk map is shown in **Figure 8**. The map uses colour coding to represent the risk for three classes: "harmful" bloom in red; "non-harmful" bloom in green and "no bloom" in blue. The saturation of red and other colours in the map indicates the degree of HAB risk. The "unknown" class in **Figure 8** is shown in gray, representing data with spectral signatures that cannot be discriminated by the classifier, for example water types with high concentration of suspended particulate matter (SPM) and coloured dissolved organic matter (CDOM), coccolithophore blooms, etc. Land and missing data over water due to cloud cover or sun glint are shown in black. This automatically initiates a model run, with virtual particles being placed at the center of bloom location. The trajectory of these particles is then displayed as an animation on the HABreports website. In 2019 three *K. mikimotoi* events were detected, allowing us to provide 5-day early warning simulations of their predicted trajectories. Simulation of cell advection over 5 days with the Mercator-IBI36 model (left) and with enhanced details in WeStCOMS-FVCOM model (right) are shown in **Figure 9**.

DISCUSSION

Harmful algal bloom prediction has many similarities to weather forecasting. In the same way as we expect northern hemisphere summers to be warmer than winters, we expect most HAB events in these regions in summer months as a result of the increased temperature, irradiance and resultant stratification of the water column: conditions that promote (harmful) dinoflagellate growth (Smayda and Reynolds, 2003). However, for useful forecasts we require more spatially and temporally resolved predictions of short-term harmful events and a methodology to rapidly inform interested stakeholders.

While the HAB and biotoxin monitoring that is required in the EU and by other food safety authorities is generally sufficient to safeguard human health, as demonstrated by the 2013 Scottish shellfish poisoning event, it is not capable of providing 100% consumer protection. As the costs and logistical constraints of monitoring all aquaculture sites are significant, in Scotland sentinel sites (RMPs) that represent a number of farming locations (Pods) are sampled. A risk assessment by FSS indicated that the current weekly monitoring program reduces risk of HAB generated human illness from shellfish poisoning to less than 1% (Holtrop et al., 2016). As FBOs, the responsibility to ensure that harvested shellfish is safe for human consumption falls on the shellfish growers and hence methods to further reduce this risk are required.

As illustrated by the 2013 human toxicity incident, it is possible for shellfish to become toxic very rapidly and hence the industry often undertakes end-product testing of shellfish toxicity

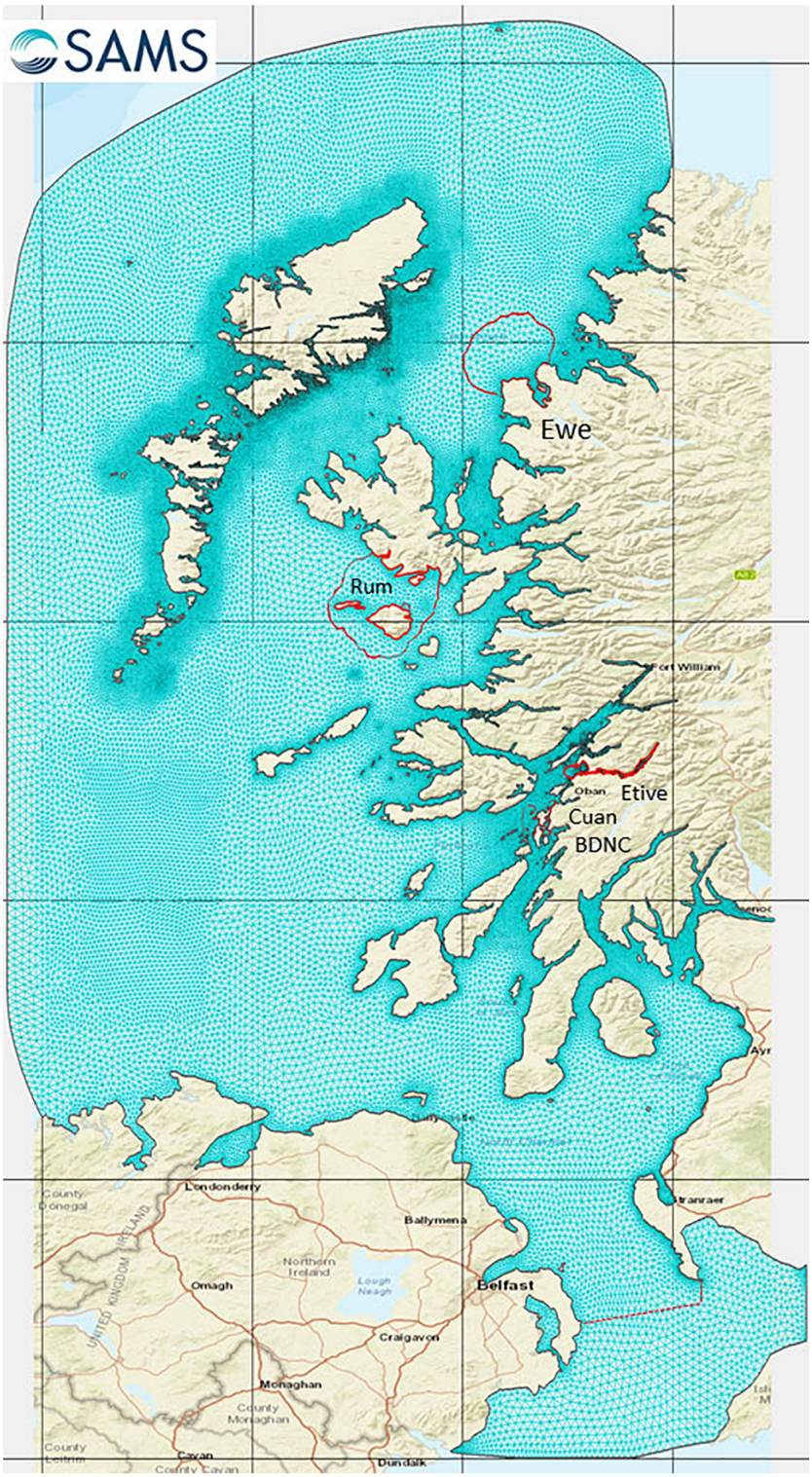

FIGURE 6 | The West Scotland Coastal Ocean Modelling System (WeStCOMS-FVCOM) model domain.

as a positive release system. However, such testing is both time consuming and expensive and hence HAB forecasts allow this to be undertaken in a targeted rather than blanket manner.

Regulatory HAB monitoring does not safeguard shellfish aquaculture businesses from the economic impacts of HAB events such as extended farm closures or product recalls.

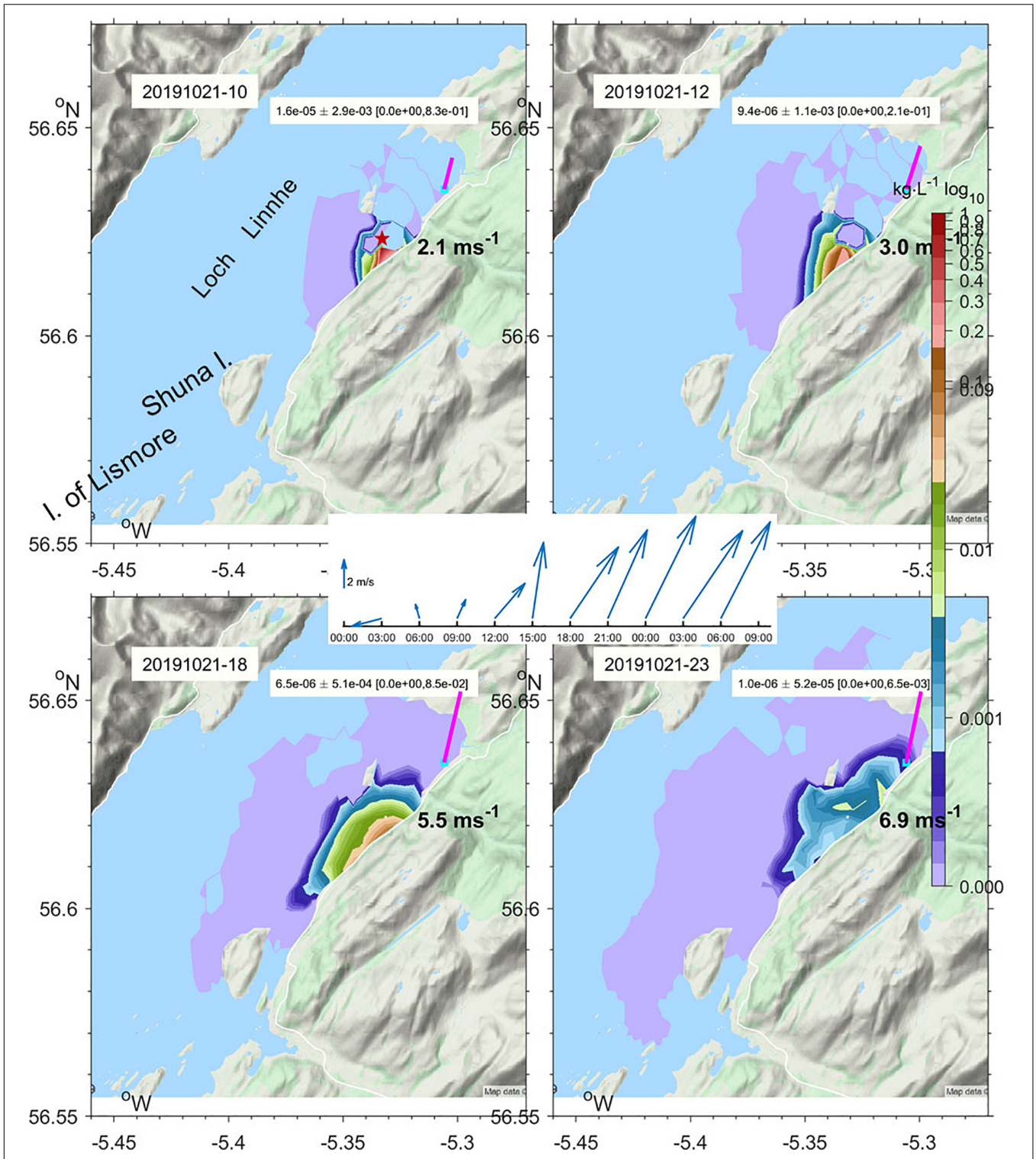

FIGURE 7 | Subsurface maximum concentration of Rhodamine-WT Dye under the tide and prevailing wind (vectors) predicted by WeStCOMS v2 model on 21st October 2019 at 10, 12, 18, and 23 GMT. The site where dye was released at 09:21 is marked with a star.

Furthermore, as fish killing HAB events in Scotland and Europe are not thought to have human health implications, regulatory monitoring does not extend to finfish aquaculture. HAB and biotoxin forecasting systems are therefore required to minimize health and business risk, allowing operators to take mitigation measures such as extra end-product testing, moving harvesting to

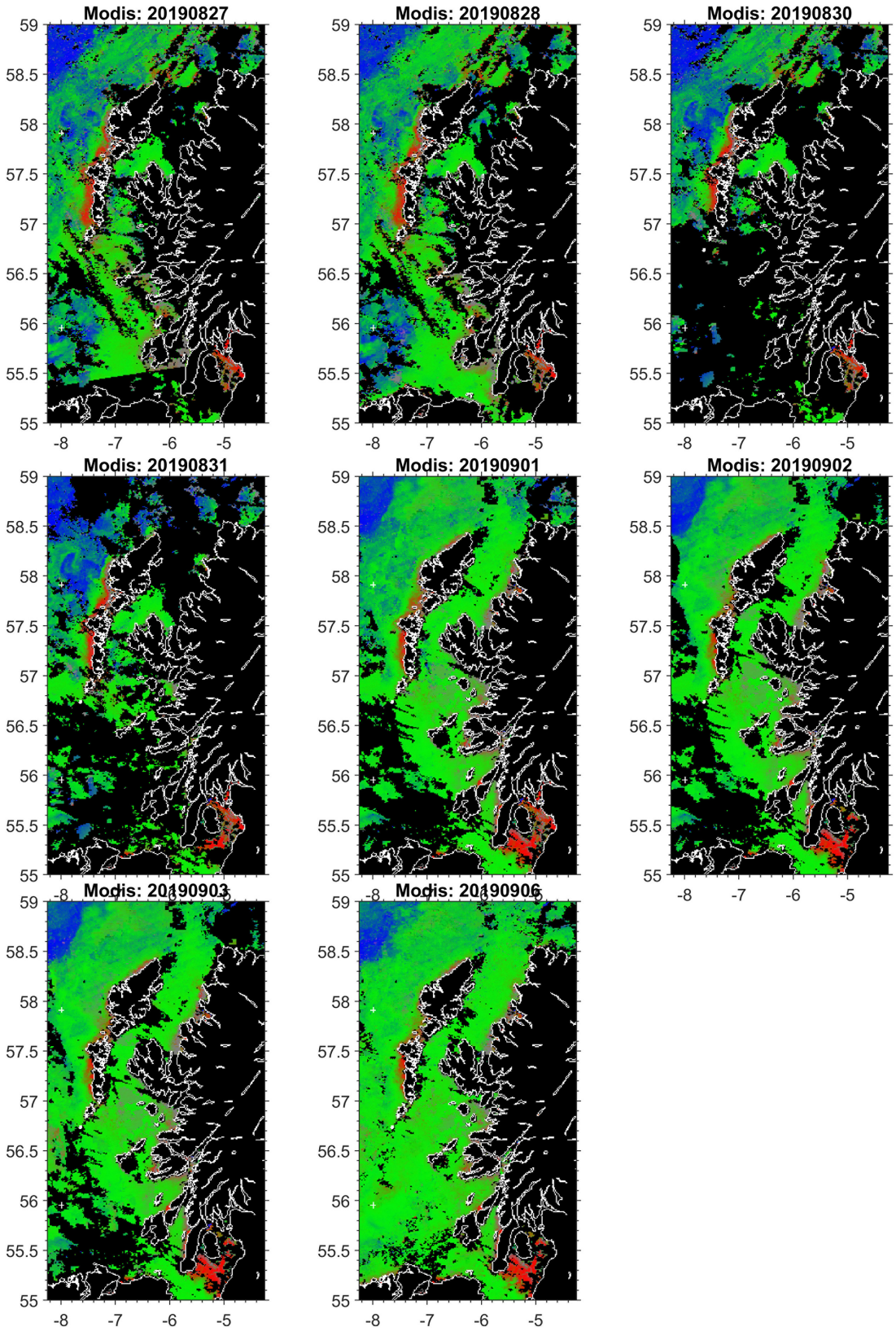

FIGURE 8 | An exemplar remote sensing based HAB risk map: elevated HABs-risk for *Karenia mikimotoi* was detected in Modis-satellite sea-surface colour analysis charts over 2 weeks (35 and 36) in August–September 2019 along the western coast of Hebrides and the 'false alarm' in the Sea of Clyde.

TABLE 2 | Statistical estimates of the Mercator-IBI36 daily-averaged model skill based on the 24-h track separation distances of 16 observed and model drifters and their averaged $<\Delta r>$ values shown separately for deep (15 m) and the near-surface (0.5 m) layers for all samples (left) and excluding values exceeding 2 standard deviations (right).

Drf#	Mean	Min	Max	Std	Nd	Drf#	Mean	Min	Max	Std	Nd < 2σ
Deep 15 m	**15 m**										
1	11.6	0.5	31.7	8.5	30	1	8.0	0.5	16.0	4.1	24
2	7.1	0.8	35.8	6.4	32	2	5.3	0.8	12.4	2.6	28
3	7.6	0.8	28.6	5.9	32	3	5.7	0.8	11.3	3.0	27
4	8.2	3.3	16.2	3.2	21	4	4.6	3.3	6.1	1.1	6
5	8.3	0.1	30.3	6.9	23	5	5.8	0.1	11.6	3.4	19
6	8.3	1.0	21.5	5.4	23	6	5.5	1.0	10.0	3.0	16
7	7.4	0.5	17.9	5.1	21	7	4.4	0.5	7.9	2.4	14
8	8.3	0.4	30.4	6.9	22	8	6.2	0.4	12.8	4.0	19
Surface 0.5 m	**0.5 m**										
9	9.1	0.7	29.5	6.9	23	9	6.4	0.7	13.4	4.1	18
10	10.9	2.5	39.6	7.8	25	0.10	8.3	2.5	14.2	3.4	21
11	12.8	4.1	35.6	9.2	15	11	8.1	4.1	16.6	3.6	11
12	14.2	4.2	27.6	12.1	3	12	7.5	4.2	10.8	4.7	2
14	11.0	2.8	43.4	9.3	23	14	8.0	2.8	15.1	3.4	20
15	10.1	2.8	18.4	7.9	3	15	5.9	2.8	9.1	4.5	2
16	10.9	3.5	30.7	7.8	15	16	7.0	3.5	12.5	3.1	11
<> km	9.7	1.9	29.2	7.3		<> km	6.4	1.9	12.0	3.4	
<> 15 m	**8.4**	0.9	26.6	**6.0**		<> 15 m	**5.7**	0.9	11.0	**2.9**	
<> 0.5 m	**11.3**	2.9	32.1	**8.7**		<> 0.5 m	**7.3**	2.9	13.1	**3.8**	

The values in bold highlight the main result of the data analysis.

a different location until toxins have depurated from shellfish, or deploying barrier methods such as bubble curtains or tarpaulins at fish farms (Brown et al., 2019; Gallardo-Rodríguez et al., 2019).

Regulatory monitoring results are released by the regulator in a spreadsheet format that can be difficult to interpret spatially and includes no temporal information. Hence, in discussion with the aquaculture industry, we developed our map-based approach so that information can easily be interpreted in time and space. The TTLG system was evaluated by McLeod and McLeod (2016), who found that it provided an improved level of protection for consumers of shellfish in Scotland. However, the work also highlighted that only around 50% of Scotland's FBOs undertook their own calculation of the TTLG. Given that negative public perception of shellfish related human health events will impact the industry indiscriminately, this low take-up was of concern. McLeod and McLeod (2016) demonstrated that smaller FBOs were less likely to follow the TTLG. This may be through lack of confidence in their ability to undertake the calculations on a weekly basis, and/or lack of staff resource. Hence, the calculation and dissemination of the TTLG index for all actively monitored shellfish harvesting sites in Scottish waters via HABreports mitigates risk for all operators.

For some HAB organisms, we have sufficient data to be able to forecast regional or even local patterns and trends at a seasonal level. For example, a link between the initiation of *Dinophysis* blooms and the upwelling season in north west Spain has been established (Diaz et al., 2016), as has a seasonal separation of *Pseudo-nitzschia delicatissima* and *seriata* taxonomic groups. The former is thought to be non-toxic in Scottish waters and is primarily observed in spring and the latter is potentially toxic and primarily observed in summer and autumn (Fehling et al., 2006; Rowland-Pilgrim et al., 2019). However, this understanding is rarely sufficient to allow forecast of risk in a specific location. As many HAB events are spatially and temporally variable, often differing in magnitude and location from year to year, "useful" HAB risk assessment requires a greater resolution than seasonal. An understanding of the underlying ecology and drivers of bloom events, along with the observational platforms and predictive approaches to identify and forecast developing blooms, is therefore necessary for useful expert interpretation.

Scotland has not experienced the major raphidophyte blooms that impact other salmon farming regions. The last reported incident was a bloom of "flagellate X" in 1982 (Smayda, 2006). The dinoflagellate *Karenia mikimotoi* is the organism of greatest concern, with periodic blooms being observed in Scotland and adjacent regions (Silke et al., 2005; Davidson et al., 2009). Spiney diatoms may also cause fish kills (Bruno et al., 1989; Treasurer et al., 2003) in the region, but these are typically identified by "in house" fish farm cell counts and are not routinely reported in the scientific literature or regulatory monitoring and are therefore less easy to include in our forecasts.

In contrast to shellfish biotoxin producing species there are no accepted threshold densities of concern for fish killing HABs. *Karenia mikimotoi* is thought to result in fish kills at cell densities in excess of 10 million cells L^{-1} (Davidson et al., 2009), but clearly industry wishes an early warning before this density is reached. Hence, when our satellite classifier "HAB risk" exceeds > 0.6 with "unknown" likelihood of less than 0.5 a bloom is identified as being of elevated HAB risk, triggering a model run. When *K. mikimotoi* densities in coastal monitoring samples exceed

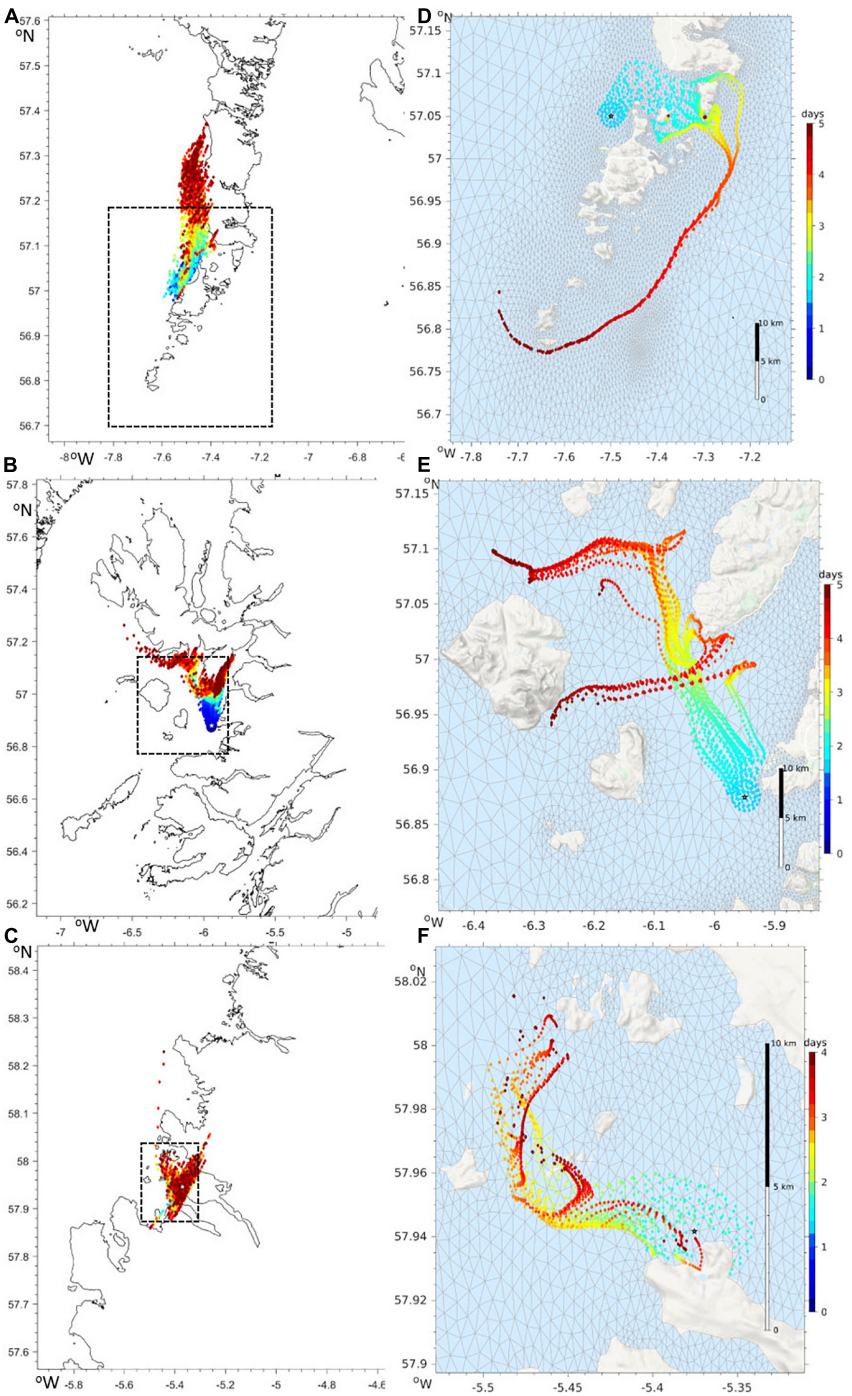

FIGURE 9 | Advection of virtual particles driven by surface currents in the Mercator-IBI36 **(A–C)** and WeStCOMS-FVCOM **(D–F)** hydrodynamic models. The colours show the forecast over next 5 days since after noon of 2019/08/27. Modelled particles were launched from the locations with the highest abundances of *Karenia-mikimotoi* near the Isle of Barra **(A,D)**, on Arisaig **(B,E)** and in Loch Kinnaird **(C,F)**. The areas on the right hand WeStCOMS simulations are highlighted in the left-hand Mercator-IBI36 plots by a dashed rectangle.

background levels this is reported in the bulletin, with cell densities exceeding 100,000 L^{-1} generating a model run.

Harmful algal blooms may develop *in situ* or be advected from another location. In Scottish waters blooms of at least three of the four most important genera, *Dinophysis, Pseudo-nitzschia*, and *Karenia* are thought to develop offshore and be advected to the coast (Fehling et al., 2012; Whyte et al., 2014; Gillibrand et al., 2016; Paterson et al., 2017). While the fourth important

genus, *Alexandrium*, develops from local cyst beds, *Alexandrium* blooms have been shown to be advected long distances when conditions are favorable (Anderson et al., 2014). Historically, the use of mathematical models in HAB forecasting was limited by physical and biological constraints (Davidson et al., 2016). Shelf wide physical oceanographic models lacked the necessary spatial resolution of model grid to resolve the complexities of the near coast environments where aquaculture is located. The physiology of many HAB organisms is insufficiently understood to produce credible operational biological models, particularly if they exist as a minor component of the biomass of a complex food web. Hence, while the development of biologically based operational HAB models remains a major challenge, even for high biomass blooms, physical models have developed such that robust operational models exist for most shelf seas. The use of such models to simulate the Lagrangian transport of known HABs provides a further potential mechanism for HAB early warning. However, as HAB events are controlled by the biological response to the environment, detailed forward prediction is limited to the timescale that we might hope to predict environmental change to a reasonable level of accuracy, i.e., likely a maximum of ∼1–2 weeks.

Examples of operational forecast systems are relatively few, but those that exist typically include a combination of monitoring, modelling and expert interpretation. For example, the Gulf of Maine *Alexandrium catenella* (as. *A. fundyense*) forecasts include both cyst surveys and high-resolution mathematical modelling of the region (McGillicuddy et al., 2005; He et al., 2008) to predict transport of excysted cells. In the Gulf of Mexico and the east coast of Florida, NOAA produce HAB nowcasts of *Karenia brevis* bloom location and 3- to 4-day forecasts of respiratory irritation risk from the aerosols that are generated by this species (Stumpf et al., 2009). Similarly, the California-Harmful Algae Risk Mapping (C-HARM) model estimates the probability of *Pseudo-nitzschia* blooms on the basis of physical circulation models, satellite remote-sensing of the ocean colour and chlorophyll and statistical models (Anderson et al., 2016). In Ireland, the Marine Institute releases alerts similar to those we report here for Scotland, including modelled HAB prediction for Bantry Bay for the following 3 days, based on a detailed understanding of the water exchange in that location (Raine et al., 2010; Cusack et al., 2016; Dabrowski et al., 2016).

The Scottish west coast is the second longest coastline in Europe and the waters to the west of Scotland, in common with other fjordic aquaculture regions, are complex. The region contains water masses from the Irish Sea and Atlantic (Ellett, 1979; McKay et al., 1986) supplemented by local freshwater runoff and Irish shelf waters (Fernand et al., 2006). Existing medium and low-resolution hydrodynamic models that use a structured (i.e., evenly spaced) computational grid are incapable of resolving important features (islands, fjords) and interconnections (straits). The development of the WeStCOMS unstructured grid model was therefore crucial to our ability to forecasts HABs in this region as it provided the necessary resolution on the fjordic coastline. While the coast of Shetland is also complex, it does not exhibit the large number of coastal islands that are found adjacent to the Scottish mainland and hence adequate simulation of HABs advecting from offshore to the coastal zone was achieved with the Mercator-IBI36 model.

Expert interpretation is a critical component of our forecasts, allowing the synthesis of a number of different (and sometimes contradictory) indicators to evaluate risk. In the three full years of operation of our system (2017–2019) our mean success rate for predicting incidences of the three major shellfish toxin syndromes, DSP from *Dinophysis*, PSP from *Alexandrium* and ASP from *Pseudo-nitzschia,* was 74% (**Table 1**). Greatest success (97%) has been with *Pseudo-nitzschia* mediated events that are often related to periods of poor summer weather in which water stratification may partially break down. Our lowest success rate is for *Alexandrium* mediated PSP toxicity. However, this is partly due to the severity (possible fatality) of PSP and hence the need to take a very conservative approach to risk assessment, in this case resulting in a higher proportion of false positives. This ensures that false negatives, that have a potentially serious health implication, are minimized.

Regulatory HAB monitoring is conducted to genus level, but the three HAB genera of greatest concern to the shellfish aquaculture industry in Scotland all exhibit variable toxicity at the species level. For example, Swan et al. (2018) demonstrated different shellfish toxicity resulting from blooms of *Dinophysis acuminata* and *Dinophysis acuta* in the Clyde Sea. Touzet et al. (2010) found both toxic and non-toxic strains of *Alexandrium* in the Shetland Islands, and Fehling et al. (2005, 2004) demonstrated that the toxicity of *Pseudo-nitzschia* can vary in response to the availability of nutrients and change in other environmental conditions. Hence alerts and forecasts are undertaken on a precautionary basis on the assumption that a bloom may be toxic.

For our Lagrangian particle models to be effective, they require accurate information on bloom size and location sufficiently far in advance that early warning can be provided. Satellite derived remote sensing is currently able to report areas of high phytoplankton biomass in near surface waters, and in some cases identify which organism is present. A challenge is therefore to develop complementary observational approaches, particularly for the shellfish biotoxin producing organisms that rarely dominate the phytoplankton biomass. For example, studies have demonstrated that some HAB species can be present in thin (potentially <1 m in thickness) layers of limited geographical extent, often associated with strong density interfaces in the water column, and at a depth not detectable by satellite remote sensing (Gowen et al., 1998; Touzet et al., 2010).

Developments in marine autonomous vehicles offer the potential for advances in HAB detection, potentially being able to identify HABs that display such sub-surface maxima (Seegers et al., 2015) or occur in thin layers (Farrell et al., 2012). For example, Siemering (2017) was able to identify a *Phaeocystis* bloom to the west of Scotland from a sea-glider deployment in 2015. Going forward, sensors capable of discriminating harmful from benign phytoplankton at low concentrations are required. Examples of this technology include the Environmental Sample Processor developed that provides *in situ* collection and analysis of water samples (Scholin et al., 2017) and the imaging Flowcytobot (Olson and Sosik, 2007), although further

development is required to make such instruments affordable for routine application.

Our system is currently operational for Scottish waters. However, most of the techniques are easily applied elsewhere. The TTLG approach is being trialed in other European countries thought the Atlantic Arc Interreg project PRIMROSE and we are currently developing a HABreports system for Malaysia to provide enhanced early warning of HAB events in that country.

DATA AVAILABILITY STATEMENT

The datasets presented in this study can be found in online repositories. The names of the repository/repositories and accession number(s) can be found below: https://thredds.sams.ac.uk/thredds/catalog/scoat-drifters/catalog.html.

AUTHOR CONTRIBUTIONS

KD designed the study and wrote the manuscript. SS was responsible for biological data collection. CW, SG, SM, and RS undertook bulletin production and dissemination. AD, MP, and DA were responsible for physical oceanography and modelling. PM and AK undertook the remote sensing. All authors contributed to the article and approved the submitted version.

FUNDING

This work was funded by the BBSRC/NERC Sustainable Aquaculture program grant "Minimizing the risk of harm to aquaculture and human health from advective harmful algal blooms through early warning" BB/M025934/1 (KD, CW, AD, DA, MP, RS, SS, and SM). It has also benefited from support from the EU Interreg projects "Predicting the Impact of Regional Scale Events on the Aquaculture Sector" (PRIMROSE) (KD, CW, AK, SG, and PM), "Collaborative Oceanography and Monitoring for Protected Areas and Species" (COMPASS) (AD) and the UKRI projects "Satellite-based monitoring of harmful algal blooms and water quality for aquaculture farms" (Shelleye) NE/P011004/1 (PM, AK, and KD), "Combining Autonomous Observations and Models for Predicting and Understanding Shelf Seas" (CAMPUS) NE/R00675X/1 (KD and DA) and "Evaluating the Environmental Conditions Required for the Development of Offshore Aquaculture (Off-Aqua)" BB/S004246/1 (KD, AD, and DA).

SUPPLEMENTARY MATERIAL

The Supplementary Material for this article can be found online at: https://www.frontiersin.org/articles/10.3389/fmars.2021.631732/full#supplementary-material

Supplementary Figure 1 | This flow chart illustrates the steps taken to determine the toxin traffic light guidance status for a given week for the toxin/causative phytoplankton pair Okadaic acids/*Dinophysis*.

Supplementary Figure 2 | The paths of drifters released to the west of Shetland in September 2015. Black shows 15-m-drogued SVP-style drifters. Magenta shows surface CODE-style drifters.

Supplementary Figure 3 | Daily tracks of the observed (red) and virtual (blue) drifters seeded into **(a)** the surface and **(b)** 15 m depth at the times and locations of observed drifters. Virtual drifters were advected by currents derived from the daily-averaged Mercator-IBI36 model velocity field.

Supplementary Figure 4 | This figure displays the various panels referred to in the case study (see section "Case Study: Combining Data Sources and Expert Interpretation to Forecast Risk"). Panel **(A)** shows chlorophyll concentrations observed around Shetland on the 21st June 2020, data courtesy the CMEMS (marine.copernicus.eu) portal. Panel **(B)** shows forecasted sea surface currents for the 23rd June 2020. Data courtesy Mercator-IBI36 model (Sotillo et al., 2015). Panel **(C)** shows a magnified section of panel **(B)**. Panel **(D)** shows a wind rose of wind directions and wind speeds around the Shetland Islands during week 26. Panel **(E)** illustrates sea surface temperatures around the Shetland Islands on the 22nd of June, data courtesy Multi-Satellite aggregated MUR-SST 1 km gridded dataset, JPL, NASA (Armstrong et al., 2012). Panel **(F)** is a map of Shetland with the concentrations of observed *Pseudo-nitzschia* in actively monitored shellfish harvesting sites indicated by yellow and red dots. Yellow dots indicate locations where low concentrations were found whereas red dots indicate locations where concentrations were in excess of official control monitoring trigger levels.

REFERENCES

Aleynik, D., Dale, A. C., Porter, M., and Davidson, K. (2016). A high resolution hydrodynamic model system suitable for novel harmful algal bloom modelling in areas of complex coastline and topography. *Harmful Algae* 53, 102–117. doi: 10.1016/j.hal.2015.11.012

Anderson, C. R., Kudela, R. M., Kahru, M., Chao, Y., Rosenfeld, L. K., Bahr, F. L., et al. (2016). Initial skill assessment of the california harmful algae risk mapping (C-HARM) system. *Harmful Algae* 59, 1–18. doi: 10.1016/j.hal.2016.08.006

Anderson, D., Anderson, P., Bricelj, V., Cullen, J., and Rensel, J. E. J. (2001). *Monitoring and management strategies for harmful algal blooms in coastal waters. APEC #201-MR-01.1, Asia PacificEconomic Program*. Paris: Singapore, and Intergovernmental Oceanographic Commission.

Anderson, D., and Rensel, J. (2016). *Harmful Algal Blooms Assessing Chile's Historic HAB Events of 2016 A Report Prepared for the. Glob. Aquac. Alliance 19*. Available Online at: https://www.aquaculturealliance.org/wp-content/ (accessed March 24, 2021).

Anderson, D. M., Keafer, B. A., Kleindinst, J. L., McGillicuddy, D. J., Martin, J. L., Norton, K., et al. (2014). Alexandrium fundyense cysts in the gulf of maine: long-term time series of abundance and distribution, and linkages to past and future blooms. *Deep. Res. Part II Top. Stud. Oceanogr.* 103, 6–26. doi: 10.1016/j.dsr2.2013.10.002

Armstrong, E. M., Wagner, G., Vazquez-Cuervo, J., and Chin, T. M. (2012). Comparisons of regional satellite sea surface temperature gradients derived from MODIS and AVHRR sensors. *Int. J. Remote Sens.* 33, 6639–6651. doi: 10.1080/01431161.2012.692832

Berdalet, E., Fleming, L. E., Gowen, R., Davidson, K., Hess, P., Backer, L. C., et al. (2016). Marine harmful algal blooms, human health and wellbeing: challenges and opportunities in the 21st century. *J. Mar. Biol. Assoc. U.K.* 2015, 61–91. doi: 10.1017/S0025315415001733

Brown, A. R., Lilley, M., Shutler, J., Lowe, C., Artioli, Y., Torres, R., et al. (2019). Assessing risks and mitigating impacts of harmful algal blooms on mariculture and marine fisheries. *Rev. Aquac.* 12, 1663–1688. doi: 10.1111/raq.12403

Bruno, D. W., Dear, G., and Seaton, D. D. (1989). Mortality associated with phytoplankton blooms amongst farmed atlantic salmon, *Salmo salar* L., in Scotland. *Aquaculture* 78, 217–222. doi: 10.1016/0044-8486(89)90099-9

Chen, C., Beardsley, R., and Cowles, G. (2011). *An Unstructured Grid Finite-Volume Coastal Ocean Model: FVCOM User Manual*. Amherst, MA: University of Massachusetts.

Cusack, C., Cusack, C., Dabrowski, T., Lyons, K., Berry, A., and Westbrook, G. (2016). Harmful algal bloom forecast system for SW Ireland . part II: Are operational oceanographic models useful in a HAB warning system? harmful algal bloom forecast system for SW Ireland . Part II Are operational oceanographic models useful in a HAB warnin. *Harmful Algae* 53, 86–101. doi: 10.1016/j.hal.2015.11.013

Dabrowski, T., Lyons, K., Nolan, G., and Berry, A. (2016). Harmful algal bloom forecast system for SW Ireland . Part I: description and validation of an operational forecasting model harmful algal bloom forecast system for SW ireland . part I: description and validation of an operational forecasting model. *Harmful Algae* 53, 64–76. doi: 10.1016/j.hal.2015.11.015

Dale, A. C., Allen, C., Venables, E., Beaton, J., and Aleynik, D. (2020). *Dye tracer dispersion studies in support of bath treatment models for fish farms*. Scotland: Scottish Aquaculture Research Forum.

Davidson, K., Anderson, D. M., Mateus, M., Reguera, B., Silke, J., Sourisseau, M., et al. (2016). Forecasting the risk of harmful algal blooms. *Harmful Algae* 53, 1–7. doi: 10.1016/j.hal.2015.11.005

Davidson, K., and Bresnan, E. (2009). Shellfish toxicity in UK waters: a threat to human health? *Environ. Health* 8:S12. doi: 10.1186/1476-069X-8-S1-S12

Davidson, K., Jardine, S., Martino, S., Myre, G., Peck, L., Raymond, R., et al. (2020). "The Economic Impacts of Harmful Algal Blooms on Salmon Cage Aquaculture," in *GlobalHAB. Evaluating, Reducing and Mitigating the Cost of Harmful Algal Blooms: A Compendium of Case Studies*, ed. V. L. Trainer 84–94.

Davidson, K., Miller, P., Wilding, T. A., Shutler, J., Bresnan, E., Kennington, K., et al. (2009). A large and prolonged bloom of *Karenia mikimotoi* in scottish waters in 2006. *Harmful Algae* 8, 349–361. doi: 10.1016/j.hal.2008.07.007

Davidson, K., Tett, P., and Gowen, R. (2011). "Harmful Algal Blooms," in *Marine Pollution & Human Health*, eds R. Hester and R. Harrison 95–127.

Diaz, P., Ruiz-villarreal, M., Pazos, Y., Moita, T., Dı, P. A., and Reguera, B. (2016). Climate variability and *Dinophysis acuta* blooms in an upwelling system. *Harmful Algae* 53, 145–159. doi: 10.1016/j.hal.2015.11.007

Egbert, G. D., and Erofeeva, S. Y. (2002). Efficient inverse modeling of barotropic ocean tides. *J. Atmos. Ocean. Technol.* 19, 183–204. doi: 10.1175/1520-04262002019<0183:EIMOBO<2.0.CO;2

Ellett, D. (1979). Some oceanographic features of hebridean waters. *Proc. R. Soc. Edinburgh* 77B, 61–74. doi: 10.1017/s026972700001263x

Farrell, H., Gentien, P., Fernand, L., Lunven, M., Reguera, B., González-Gil, S., et al. (2012). Scales characterising a high density thin layer of *Dinophysis acuta* ehrenberg and its transport within a coastal jet. *Harmful Algae* 15, 36–46. doi: 10.1016/j.hal.2011.11.003

Fehling, J., Davidson, K., and Bates, S. S. (2005). Growth dynamics of non-toxic *Pseudo-nitzschia delicatissima* and toxic *P. seriata* (Bacillariophyceae) under simulated spring and summer photoperiods. *Harmful Algae* 4, 763–769. doi: 10.1016/j.hal.2004.11.002

Fehling, J., Davidson, K., Bolch, C., and Tett, P. (2006). Seasonality of *Pseudo-nitzschia* spp. (*Bacillariophyceae*) in western Scottish waters. *Mar. Ecol. Prog. Ser.* 323, 91–105. doi: 10.3354/meps323091

Fehling, J., Davidson, K., Bolch, C. J., and Bates, S. S. (2004). Growth and domoic acid production by *Pseudo-nitzschia seriata* (*Bacillariophyceae*) under phosphate and silicate limitation. *J. Phycol.* 40, 674–683. doi: 10.1111/j.1529-8817.2004.03213.x

Fehling, J., Davidson, K., Bolch, C. J. S., Brand, T. D., and Narayanaswamy, B. E. (2012). The relationship between phytoplankton distribution and water column characteristics in north west european shelf sea waters. *PLoS One* 7:e34098. doi: 10.1371/journal.pone.0034098

Fernand, L., Nolan, G. D., Raine, R., Chambers, C. E., Dye, S. R., White, M., et al. (2006). The irish coastal current: a seasonal jet-like circulation. *Cont. Shelf Res.* 26, 1775–1793. doi: 10.1016/j.csr.2006.05.010

FSA (2014). *Managing Shellfish Toxin Risks, Guidance for harvesters and Processors*. Available Online at: https://www.foodstandards.gov.scot/downloads/managing-shellfish-toxins-guidance.pdf (accessed March 24, 2021).

Gallardo-Rodríguez, J. J., Astuya-Villalón, A., Llanos-Rivera, A., Avello-Fontalba, V., and Ulloa-Jofré, V. (2019). A critical review on control methods for harmful algal blooms. *Rev. Aquac.* 11, 661–684. doi: 10.1111/raq.12251

Gillibrand, P. A., Siemering, B., Miller, P. I., and Davidson, K. (2016). Individual-based modelling of the development and ttansport of a *Karenia mikimotoi* bloom on the north-west european continental shelf. *Harmful Algae* 53, 118–134. doi: 10.1016/j.hal.2015.11.011

Gowen, R. J. R., Raine, R., Dickey-Collas, M., and White, M. (1998). Plankton distributions in relation to physical oceanographic features on the southern malin shelf, august 1996. *ICES J. Mar. Sci.* 55, 1095–1111. doi: 10.1006/jmsc.1998.0418

He, R., McGillicuddy, D. J., Keafer, B. A., and Anderson, D. (2008). Historic 2005 toxic bloom of *Alexandrium fundyense* in the western gulf of maine: 2. coupled biophysical numerical modeling. *J. Geophys. Res.* 113:C07040. doi: 10.1029/2007JC004602

Holtrop, G., Swan, S. C., Duff, B., Wilding, T., Narayanaswamy, B. E., and Davidson, K. (2016). *Risk assessment of the Scottish monitoring programme for the marine biotoxins in shellfish harvested from classified production areas: review of the current sampling scheme to develop an improved programme based on evidence of risk*. Available Online at: https://www.foodstandards.gov.scot/publications-and-research/publications/risk-assessment-of-the-scottish-monitoring-programme-for-the-marine-biotoxi (accessed March 24, 2021).

Kurekin, A. A., Miller, P. I., and Van der Woerd, H. J. (2014). Satellite discrimination of *Karenia mikimotoi* and *Phaeocystis* harmful algal blooms in european coastal waters: merged classification of ocean colour data. *Harmful Algae* 31, 163–176. doi: 10.1016/j.hal.2013.11.003

Martino, S., Gianella, F., and Davidson, K. (2020). An approach for evaluating the economic impacts of harmful algal blooms: the effects of blooms of toxic *Dinophysis* spp. on the productivity of scottish shellfish farms. *Harmful Algae* 99:101912. doi: 10.1016/j.hal.2020.101912

McGillicuddy, D. J., Anderson, D. M., Lynch, D. R., and Townsend, D. W. (2005). Mechanisms regulating large-scale seasonal fluctuations in *Alexandrium fundyense* populations in the gulf of maine: results from a physical–biological model. *Deep Sea Res. Part II Top. Stud. Oceanogr.* 52, 2698–2714. doi: 10.1016/j.dsr2.2005.06.021

McKay, W. A., Baxter, J. M., Ellett, D., and Meldrum, D. T. (1986). Radiocaesium and circulation patterns west of scotland. *J. Environ. Radioact.* 4, 205–232. doi: 10.1016/0265-931x(86)90011-1

McLeod, C., and McLeod, D. (2016). *Evaluation of the Shellfish Traffic Light Toxin Guidance for Food Standards Scotland*. Scotland, USA: Food Standards Scotland.

Niiler, P. P., Sybrandy, A. S., Bi, K., Poulain, P. M., and Bitterman, D. (1995). Measurements of the water-following capability of holey-sock and TRISTAR drifters. Deep sea res. part I oceanogr. *Res. Pap.* 42, 1951–1964. doi: 10.1016/0967-0637(95)00076-3

Olson, R. J., and Sosik, H. M. (2007). A submersible imaging-in-flow instrument to analyze nano-and microplankton: imaging flowcytobot. *Limnol. Oceanogr. Methods* 5, 195–203. doi: 10.4319/lom.2007.5.195

Paterson, R. F., McNeill, S., Mitchell, E., Adams, T., Swan, S. C., Clarke, D., et al. (2017). Environmental control of harmful dinoflagellates and diatoms in a fjordic system. *Harmful Algae* 69, 1–17. doi: 10.1016/j.hal.2017.09.002

Poulain, P.-M., and Gerin, R. (2019). Assessment of the water-following capabilities of CODE drifters based on direct relative flow measurements. *J. Atmos. Ocean. Technol.* 36, 621–633. doi: 10.1175/JTECH-D-18-0097.1

Raine, R., McDermott, G., Silke, J., Lyons, K., Nolan, G., and Cusack, C. (2010). A simple short range model for the prediction of harmful algal events in the bays of southwestern ireland. *J. Mar. Syst.* 83, 150–157. doi: 10.1016/j.jmarsys.2010.05.001

Rowland-Pilgrim, S., Swan, S. C., O'Neill, A., Johnson, S., Coates, L., Stubbs, P., et al. (2019). Variability of amnesic shellfish toxin and *Pseudo-nitzschia* occurrence in bivalve molluscs and water samples–analysis of ten years of the official control monitoring programme. *Harmful Algae* 87:101623. doi: 10.1016/j.hal.2019.101623

Scholin, C., Birch, J., Jensen, S., Massion, E., Pargett, D., Preston, C., et al. (2017). The quest to develop ecogenomic sensors: A 25-Year history of the

environmental sample processor (ESP) as a case study. *Oceanography* 30, 100–113. doi: 10.5670/oceanog.2017.427

Scottish Government. (2020). *Estimation of the Wider Economic Impacts of the Aquaculture Sector in Scotland*. Available Online at: https://www.scottishsalmon.co.uk/sites/default/files/2020-09/estimation-wider-economic-impacts-aquaculture-sector-scotland.pdf (accessed March 24, 2021).

Seegers, B. N., Birch, J. M., Marin, R., Scholin, C. A., Caron, D. A., Seubert, E. L., et al. (2015). Subsurface seeding of surface harmful algal blooms observed through the integration of autonomous gliders, moored environmental sample processors, and satellite remote sensing in southern california. *Limnol. Oceanogr.* 60, 754–764. doi: 10.1002/lno.10082

Siemering, B. (2017). *Environmental drivers and advective transport of harmful phytoplankton in North West European Shelf Seas*. Scotland: Univeristy of Aberdeen.

Silke, J., O'Beirn, F., and Cronin, M. (2005). *Karenia mikimotoi*: an exceptional dinoflagellate bloom in western Irish waters, summer 2005. *Mar. Envon. Health series* 21, 1649–1653.

Skamarock, W. C., Klemp, J. B., Dudhia, J., Gill, D. O., Barker, D. M., Duda, M. G., et al. (2008). *A Description of the Advanced Research WRF Version 3. NCAR Technical Note (475)*. Colorado, U S A: University Corporation for Atmospheric Research, 125.

Smayda, T. J. (1990). "Novel and nuisance phytoplankton blooms in the sea - evidence for a global epidemic," in *ler, L., Anderson, D. (Eds.), Toxic Marine Phytoplankton*, eds E. Granéli and B. Sundstrom (New York: Elsevier), 29–40.

Smayda, T. J. (2002). Turbulence, watermass stratification and harmful algal blooms: an alternative view and frontal zones as "pelagic seed banks.". *Harmful Algae* 1, 95–112. doi: 10.1016/S1568-9883(02)00010-0

Smayda, T. J. (2006). *Scottish Executive Environment Group Harmful Algal Bloom Communities in Scottish Coastal Waters: Relationship to Fish Farming and Regional Comparisons – A Review*. Available online at www.scotland.gov.uk/Publications/2006/02/03095327/0 (accessed March 24, 2021).

Smayda, T. J., and Reynolds, C. S. (2003). Strategies of marine dinoflagellate survival and some rules of assembly. *J. Sea Res.* 49, 95–106. doi: 10.1016/S1385-1101(02)00219-8

Sotillo, M. G., Cailleau, S., Lorente, P., Levier, B., Aznar, R., Reffray, G., et al. (2015). The myocean IBI ocean forecast and Reanalysis systems: operational products and roadmap to the future copernicus service. *J. Oper. Oceanogr.* 8, 63–79. doi: 10.1080/1755876X.2015.1014663

Stumpf, R. P., Tomlinson, M. C., Calkins, J. A., Kirkpatrick, B., Fisher, K., Nierenberg, K., et al. (2009). Skill assessment for an operational algal bloom forecast system. *J. Mar. Syst.* 76, 151–161. doi: 10.1016/j.jmarsys.2008.05.016

Swan, S. C., Turner, A. D., Bresnan, E., Whyte, C., Paterson, R. F., McNeill, S., et al. (2018). *Dinophysis acuta* in scottish coastal waters and its influence on diarrhetic shellfish toxin profiles. *Toxins* 10:399. doi: 10.3390/toxins10100399

Touzet, N., Davidson, K., Pete, R., Flanagan, K., McCoy, G. R., Amzil, Z., et al. (2010). Co-occurrence of the west european (Gr.III) and north american (Gr.I) ribotypes of *Alexandrium tamarense* (dinophyceae) in shetland, scotland. *Protist* 161, 370–384. doi: 10.1016/j.protis.2009.12.001

Treasurer, J. W., Hannah, F., and Cox, D. (2003). Impact of a phytoplankton bloom on mortalities and feeding response of farmed atlantic salmon, salmo salar, in west scotland. *Aquaculture* 218, 103–113. doi: 10.1016/S0044-8486(02)00516-1

Weihs, C., Ligges, U., Luebke, K., and Raabe, N. (2005). "klaR analyzing German business cycles," in *Data Analysis and Decision Support*, eds D. Baier, R. Decker, and L. Schmidt-Thieme (Berlin: Springer-Verlag), 335–343. doi: 10.1007/3-540-28397-8_36

Wells, M. L., Karlson, B., Wulff, A., Kudela, R., Trick, C., Asnaghi, V., et al. (2020). Future HAB science: directions and challenges in a changing climate. *Harmful Algae* 91:101632. doi: 10.1016/j.hal.2019.101632

Whyte, C., Swan, S., and Davidson, K. (2014). Changing wind patterns linked to unusually high *Dinophysis* blooms around the shetland islands, scotland. *Harmful Algae* 39, 365–373. doi: 10.1016/j.hal.2014.09.006

Conflict of Interest: The authors declare that the research was conducted in the absence of any commercial or financial relationships that could be construed as a potential conflict of interest.

frontiers in Marine Science

ORIGINAL RESEARCH
published: 30 April 2021
doi: 10.3389/fmars.2021.638889

Using the Red Band Difference Algorithm to Detect and Monitor a *Karenia* spp. Bloom Off the South Coast of Ireland, June 2019

Catherine Jordan[1,2], Caroline Cusack[2], Michelle C. Tomlinson[3], Andrew Meredith[4], Ryan McGeady[2,5], Rafael Salas[2], Clynton Gregory[1] and Peter L. Croot[1]*

[1] Earth and Ocean Sciences, School of Natural Sciences and Ryan Institute, National University of Ireland Galway, Galway, Ireland, [2] Marine Institute, Galway, Ireland, [3] National Centers for Coastal Ocean Science (NCCOS, NOAA), Silver Spring, MD, United States, [4] Consolidated Safety Services Inc., Fairfax, VA, United States, [5] Zoology, School of Natural Sciences and Ryan Institute, National University of Ireland Galway, Galway, Ireland

During the months of May, June, July and August 2019 the Red Band Difference algorithm was tested over Irish waters to assess its suitability for the Irish harmful algal bloom alert system. Over the 4 weeks of June an extensive localised surface phytoplankton bloom formed in the Celtic Sea, south of Ireland. Satellite imagery from the Sentinel-3a's Ocean and Land Colour Instrument, processed using the Red Band Difference algorithm detected the bloom in surface shelf waters and helped monitor its movement. Daily satellite images indicated that the bloom appeared at the sea surface on the 2nd June 2019 and peaked in size and surface abundance in offshore shelf waters within 4 weeks, remnants remained at the surface into July. A particle tracking approach was used to replicate oceanic circulation patterns in the vicinity of the observed algal bloom and estimate its trajectory. The initial horizontal distribution of particles in the tracking model were based on a satellite imagery polygon of the bloom when it first appeared in surface waters. Good agreement was observed between satellite imagery of the bloom and the particle tracking model. *In situ* sampling efforts from a research cruise and the national inshore phytoplankton monitoring programme confirmed that *Karenia mikimotoi* was the causative organism of the bloom. This pilot study shows great potential to use the Red Band Difference algorithm in the existing Irish harmful algal bloom alert system. In addition, satellite ocean colour data combined with particle tracking model estimates can be a useful tool to monitor high biomass harmful algal bloom forming species, such as *Karenia mikimotoi,* in surface coastal waters around Ireland and elsewhere.

Keywords: harmful algal bloom, Red Band Difference, OLCI, remote sensing, aquaculture, ocean colour, particle tracking, monitoring programme

OPEN ACCESS

Edited by:
Keith Davidson, Scottish Association for Marine Science, United Kingdom

Reviewed by:
Peter I. Miller, Plymouth Marine Laboratory, United Kingdom
Marcos Mateus, University of Lisbon, Portugal

****Correspondence:***
Catherine Jordan
Catherine.Jordan@marine.ie

Specialty section:
This article was submitted to Marine Fisheries, Aquaculture and Living Resources, a section of the journal Frontiers in Marine Science

Received: *07 December 2020*
Accepted: *01 April 2021*
Published: *30 April 2021*

Citation:
Jordan C, Cusack C, Tomlinson MC, Meredith A, McGeady R, Salas R, Gregory C and Croot PL (2021) Using the Red Band Difference Algorithm to Detect and Monitor a Karenia spp. Bloom Off the South Coast of Ireland, June 2019. Front. Mar. Sci. 8:638889. doi: 10.3389/fmars.2021.638889

INTRODUCTION

Aquaculture is extremely important for providing food, nutrition and employment around the world. According to the FAO (2020), aquaculture production reached a record high in 2018. There has been a 527% increase in global aquaculture production from 1990 to 2018. Due to wild fish stocks declining and the population increasing globally, the role of aquaculture in society is more

important than ever (FAO, 2020). Aquaculture is a highly valuable industry to the Irish economy. Production in Ireland had a net gain from under €100 million in 2009 to €180 million in 2018 with aquaculture outputs between 30,000 and 50,000 tonnes mainly from salmon and bivalve farming (Dennis and Jackson, 2019). The success of aquaculture is influenced by a range of conditions, both environmental and biological such as temperature, salinity, oxygen and food availability to name a few (Mydlarz et al., 2006). Harmful Algae Blooms (HABs) are a concern for both finfish and bivalve aquaculture (Callaway et al., 2012). In most cases, the proliferation of microscopic algae is beneficial to the overall ecosystem, e.g., as a source of food for wild fisheries and aquaculture (Tweddle et al., 2018). However, a small minority of algal bloom forming species have negative impacts on their surrounding environment. HABs, caused by either small or large biomass blooms, and depending on the species, can result in serious economic losses to marine sectors such as tourism, aquaculture and fisheries with additional, often unquantifiable, impacts on ocean health (Anderson et al., 2015).

In order to mitigate against and prepare for the impacts of HABs, it is essential to detect, monitor, track and forecast their development and movement in real time (Stumpf and Tomlinson, 2005). Collecting samples in the field alone has limitations as the samples or measurements are collected at discrete points and times, and while this method generally offers high quality data from a specific point in time, temporal and spatial limitations are a challenge. Combining different observational methods can greatly help managers detect and monitor HAB hazards. For example, satellite remote sensing techniques are powerful tools to detect and monitor the movement of surface phytoplankton blooms due to the vast area covered in one single swath measurement (Stumpf and Tomlinson, 2005. Emerging remote sensing techniques for Europe should positively impact the aquaculture industry. Ocean colour sensors and the algorithms designed to detect phytoplankton blooms or HABs have been continually improving since the launch of the first ocean colour sensor, the Coastal Zone Colour Scanner in 1978 and the most recent launch of ESA Sentinel 3B OLCI in 2018 (Groom et al., 2019). Satellite technology has proven very useful in mapping the geographical extent of blooms and movement (Miller et al., 2006; Stumpf et al., 2009). To determine the concentration of chlorophyll-*a* (Chl-*a*) or other optically active constituents such as coloured dissolved organic matter (CDOM) or suspended particulate matter (SPM), different types of algorithms have been developed by measuring the water leaving radiance, or reflectance (Groom et al., 2019). The use of satellite technology focussed on Chl-*a* and sea surface temperature (SST) combined with field sampling can support early warning systems for certain HAB types.

Standard ocean colour algorithms that estimate chlorophyll concentration or HABs from satellite sensors use the blue and green spectral bands of the visible spectrum to monitor the colour of the ocean. These algorithms are very useful, especially in open ocean water, which are classified as Case 1 waters. The algorithms are not as accurate in the more complex Case 2 waters, situated close to the coast and inland. The two water types were originally introduced by Morel and Prieur (1977). These descriptions have since been refined (Gordon and Morel, 1983; Morel, 1988; IOCCG, 2000; Mobley et al., 2004). Mobley et al. (2004) describe case 1 waters whose inherent optical properties (IOPs) are dominated by phytoplankton. Case 2 waters generally contain higher concentrations of CDOM, SPM, and inorganic particles in addition to phytoplankton. In Case 2 waters, as the band selection used for the standard algorithms is highly influenced by non-living suspensions, CDOM and sediment and can be misinterpreted as chlorophyll concentration.

Standard algorithms that use the blue green ratio are very important and valid methods of retrieving chlorophyll concentrations. Due to the problems with CDOM and sediment interference it is also useful to have an algorithm measuring chlorophyll fluorescence using the red bands. Chlorophyll fluorescence can be defined by red light re-emitted by chlorophyll molecules when excited by light (Zeng and Li, 2015). Chlorophyll fluorescence in the red band of the visible spectrum has proven successful to monitor HABs in coastal areas of the United States. A good example is the Gulf of Mexico where ocean colour is used to detect *Karenia brevis* blooms (Amin et al., 2009). As described by Amin et al. (2009) the Red Band Difference (RBD) relative fluorescence algorithm is less sensitive to CDOM, SPM, and atmospheric corrections and useful in coastal waters. Vandersea et al. (2020) describe how the RBD algorithm is also suitable for *Karenia mikimotoi* blooms and demonstrates how it was applied to monitor a 2013 bloom in Kachemak Bay, Alaska alongside field sampling and lab techniques. The RBD algorithm is also used off the east coast of the United States and can detect several HAB dinoflagellates of interest in Chesapeake Bay, the largest estuary in the United States and a location with very turbid waters. Scattering by sediments may interfere with algorithms in environments like this (Wolny et al., 2020). The benefits of using the RBD algorithm in a turbid environment is that the algorithm is less sensitive to interference by non-algal pigments as it was designed to detect Chl-*a* fluorescence in the HAB blooming species *K. brevis* without interference from sediment, the algorithm is designed to return positive values in waters where blooms occur and negative values in high scattering waters (Amin et al., 2009). This is currently used as a HAB monitoring tool for coastal managers who support aquaculture in Chesapeake Bay for a range of dinoflagellate blooms (Wolny et al., 2020). There are currently no studies using this RBD algorithm in Irish waters.

While *K. brevis* blooms were never recorded in Irish waters, *K. mikimotoi* blooms frequently occur in Irish waters (Ottway et al., 1979; Silke et al., 2005) and have been recorded historically and in recent years, reviewed recently by Li et al. (2019). Gentien (1998) describes *K. mikimotoi* as a common "red tide" or large bloom forming dinoflagellates in shelf waters of the northeast Atlantic. Previously referred to as *Gyrodinium aureolum, Gymnodinium cf. aureolum, Gymnodinium nagasakiense,* and *Gymnodinium mikimotoi* in the literature *K. mikimotoi* blooms are commonly associated with marine fauna kills (Brand et al., 2012; Li et al., 2019). *Karenia* are thought to overwinter in low numbers as motile cells and when favourable biogeochemical and physical conditions arrive in early to late summer *Karenia* will grow and bloom (Gentien, 1998). Globally, *K. mikimotoi* has adapted to a wide range of temperatures ranging between

4 and 30°C but the European isolate has a narrower range of 6–20°C. The salinity ranges *K. mikimotoi* can survive in are also quite extensive ranging from 9 to 35 ppt, therefore suited to a range of environments (Li et al., 2019). Li et al., 2019 also describe that *K. mikimotoi* is known to grow well in low light environments, however, it is not photo inhibited by high light intensities, therefore capable of adapting to conditions at both the surface and at the bottom. One important feature of *K. mikimotoi* behaviour in the environment is that, like many dinoflagellates that are capable of vertically migrating over a diurnal cycle, beginning from depth before sunrise and reaching the surface before midday. This is known as diurnal vertical migration (DVM) (Olsson and Graneli, 1991; Koizumi et al., 1996; Park et al., 2001; Shikata et al., 2014, 2015, 2016). This phenomenon is likely why the RBD approach is so applicable to satellite detection of blooms of *K. mikimotoi* as the cells will be in the upper part of the water column at midday, close to the over pass time of the satellite, with a significant number of cells in the upper 2 m of the water column corresponding to the observable signal depth for red light in seawater (Doerffer, 1993).

The true toxicity of *K. mikimotoi* is unknown but the dinoflagellate is known to produce toxins including haemolysin (Neely and Campbell, 2006) and gymnocin A and gymnocin B (Satake et al., 2002, 2005). *Karenia mikimotoi* is not known to create shellfish related biotoxins, but mass mortalities of shellfish have been associated with blooms of this species. Causes of mortalities include inhibiting larval settling rates, immune functions, gut tissue damage and larval spat mortalities. The blooms may not only impact the survival rate of shellfish but also affect the developmental processes, therefore blooms can greatly impact wild and farmed shellfish (Li et al., 2019). The effects of these blooms are not limited to shellfish but also wild and farmed fish and a range of invertebrates. *Karenia mikimotoi* senescent blooms are known to deplete the water of oxygen levels when bacterial respiration associated with the breakdown of the bloom begins, and when macro-organisms start to decay, and biochemical oxygen demand rises. Diaz and Rosenberg (2008) observed mass mortalities of benthic organisms when the water became anoxic after a *Karenia* bloom. *Karenia mikimotoi* also secrete mucus (with high concentrations of extracellular polysaccharide) that can increase the likelihood of mortalities, for example, when fish gills become clogged (Gentien et al., 2007). Li et al. (2019) describe how even at low algal densities gill damage and mortality in both wild and cultured salmon, rainbow trout and turbot were reported, even in waters with high dissolved oxygen levels. Mortalities of a range of invertebrates, are also linked to blooms of this unarmoured dinoflagellate in European waters and evident in the literature since 1966 (Jones et al., 1982). The earliest published Irish report of a *Karenia* spp. bloom related to marine life mortalities off the south coast of Ireland was made by Ottway et al. (1979). Two Irish examples of exceptional *Karenia* spp. blooms include the months of May, June, and July of 2005 (Silke et al., 2005) and more recently, a *K. mikimotoi* bloom in the summer (May to September) of 2012 (O'Boyle et al., 2016). In July 2012, *Karenia* spp. were at high concentrations, greater than one million cells per litre, in the surface waters at the Malin shelf off northwest Ireland suggesting a potential offshore origin for these blooms (Bresnan et al., 2013).

Ireland has a weekly HAB bulletin, published to assist aquaculture business managers, helping them make practical decisions to mitigate against potential HAB impacts. The bulletin contains several data products based on historical and recent biotoxin and phytoplankton profiles, satellite and oceanographic *in situ* and modelled forecasting data. Products used by local scientists help to develop HAB alerts for the days ahead. In this paper, we show the potential of introducing a new bio-optical chlorophyll fluorescence algorithm to the Irish HAB monitoring system, which is currently being used successfully in the United States, to detect *K. brevis* and several other HAB species and asses the suitability of the RBD algorithm to detect and monitor HABs around the Irish coast.

During the months of May, June, July and August 2019 the RBD algorithm was tested in Irish waters for the first time. During this time a phytoplankton bloom appeared in the Celtic Sea, south of Ireland.

The objectives of this pilot study were:

1. To test the RBD algorithm in Irish waters and assess its suitability for use in the Irish HAB monitoring system.
2. To determine the phytoplankton taxa responsible for the bloom by analysing the drift trajectory of the bloom by using local water circulation patterns in a particle tracking model and analysing in situ phytoplankton data from the national inshore monitoring programme and an offshore phytoplankton survey.

MATERIALS AND METHODS

Study Area

Figure 1 presents the study area where the phytoplankton bloom was identified via satellite imagery, including *in situ* sampling locations described in section "*In situ* Data." The samples were from three inshore stations: Cork Harbour, Oysterhaven and Kinsale, and from eight offshore stations from the research cruise CV19018; 138, 139, 140, 141, 142, 143, 144, and 148 as described in section "*In situ* Data." Also illustrated in **Figure 1** is the polygon that was created based on manual interpretation of satellite imagery from when the bloom first appeared at the surface. This polygon was used for the horizontal distribution of particles deployed in the Lagrangian Particle Tracking model as described in section "Lagrangian Particle Tracking." The study area was in the Celtic Sea, an area of the NE Atlantic Ocean bordered by Ireland in the north, The United Kingdom in the east and the Bay of Biscay (47°N) in the south. The Celtic Sea is relatively shallow with depths ranging between 100 and 200 m and decreasing in depth near the coast as illustrated in **Figure 1**. Tidal circulation across the Celtic Sea is weak, water movement is primarily due to wind action (Raine, 2014). In the Celtic Sea, the water tends to stabilise in April when the seasonal thermocline becomes established. Throughout the summer months, there is a deepening of the thermocline due to continued heating of the surface layer until the Autumn when the cooling phase begins,

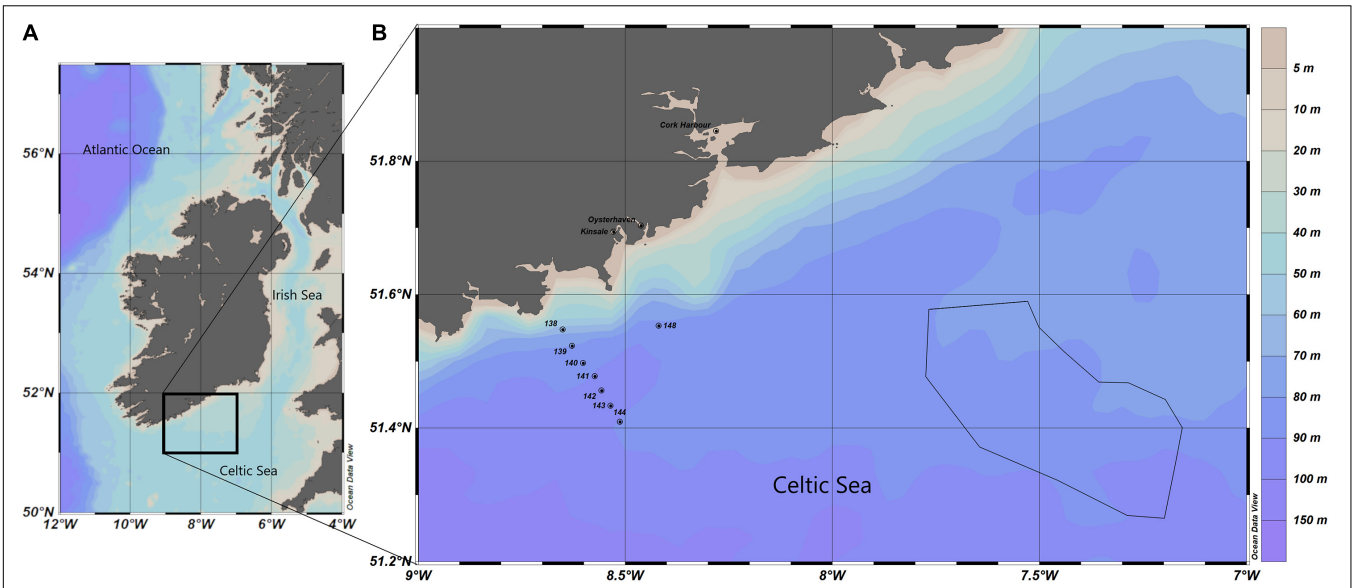

FIGURE 1 | (A) Map of study area in the Celtic Sea. **(B)** *In situ* sample locations are noted as points and the polygon location for the particle tracking model is outlined by the black line. Bathymetry is represented in metres.

and the water column becomes well mixed again. Within the Celtic Sea there are exceptions to this in areas of tidally mixed fronts, these are found at the boundaries between thermally stratified and tidally mixed areas such as the entrance to the Irish Sea, where the Celtic Sea Front is located and at the Ushant front, located between the southwest United Kingdom and northwest France (Raine, 2014).

Satellite Imagery

The Red Band Difference satellite imagery was generated from the study area with geographic latitude and longitude limits of 47°N to 58°N, 2°W to 12°W. The region of interest covers all coastal waters around the island of Ireland. Satellite data from the Ocean and Land Colour Instrument (OLCI) sensor on Sentinel 3A were obtained from The European Organisation of Meteorological Satellites (EUMETSAT). The multispectral OLCI sensor has 21 spectral bands from 0.4 to 1.0 μm and has a spatial resolution of 300 m. The bands are optimised to measure ocean colour over open ocean and coastal zones. The whole field-of-view is shifted across track by 12.6° away from the sun to minimise the impact of sun glint. Once the OLCI L1B data were downloaded from EUMETSAT, the data were processed to L2 using the NOAA, National Centres for Coastal Ocean Science (NCCOS) satellite automated processing system which utilises NASA's l2gen software included in the Sea-viewing Wide Field-of-view Sensor (SeaWiFS) Data Analysis System (SeaDAS) package (version 7.5.3). The l2gen processing produced a surface reflectance product (R_{rhos}) that is corrected for top-of-atmosphere solar irradiance, Rayleigh radiance and molecular absorption (Wynne et al., 2018).

The RBD algorithm used to highlight areas of high fluorescence, indicative of high algal biomass, uses only pixels within the valid R_{rhos} range (0–1) described by Amin et al., 2009 and modified for OLCI R_{rhos} bands as follows:

$$RBD = R_{rhos}(681) - R_{rhos}(665).$$

Due to the increase in reflectance caused by Chl-*a* fluorescence at 681 nm, the RBD is positive in areas of Chl-*a* fluorescence. The RBD data products were mapped to Universal Transverse Mercator (WGS 84) projection at 300 m horizontal resolution using a nearest neighbour interpolation. A land mask was applied, and the product saved to a GeoTiFF (an image file with georeferencing information embedded in the file as metadata) and stored in a database at NCCOS. Weekly mean composites of the daily images were created using a custom ArcGIS python toolbox, RS_Tools, that was developed specifically for working with products from the NOAA-NCCOS satellite processing system.

Satellite imagery was produced for the weekly HAB bulletin using an algorithm developed by Ifremer, known as the OC5 product. The level 4 Chl-*a* product is extracted from the IFREMER FTP site[1]. Matlab (MathWorks) is used to convert the level 4 Netcdf files to *.grd files. Matlab is then used to calculate chlorophyll anomalies from the 60-day median value calculated using data between current date minus 74 and current date minus 14. This anomaly data is rendered as .png files (Leadbetter et al., 2018).

Lagrangian Particle Tracking

To examine the effect of local water circulation patterns on the drift trajectory of the *Karenia* bloom, a particle

[1]ftp://ftp.ifremer.fr/ifremer/cersat/products/gridded/ocean-color/atlantic/EUR-L4-CHL-ATL-v01/

tracking simulation was conducted using outputs from a 3D hydrodynamic numerical ocean model. The northeast Atlantic Regional Ocean Modelling System (ROMS) model encompasses a large area of the northwestern European continental shelf including Irish territorial waters (NE_Atlantic model; Dabrowski et al., 2016). This model has a horizontal resolution of 1.1 to 1.6 km in Irish coastal waters with 40 terrain-following vertical layers (Dabrowski et al., 2016). The ROMS model output data was coupled with an offline 3D Lagrangian particle tracking mass-preserving scheme called ICHTHYOP; an individual-based model (Ichthyop v3; Lett et al., 2008). This was used to simulate particle transport from the *Karenia* bloom location (i.e., the potential HAB surface transport pathways). Particle tracking simulations were conducted using hourly ROMS ocean current speed and direction outputs using a Runge–Kutta 4th order numerical scheme and a 5-min time step. The initial horizontal distribution of the particles, representing *K. mikimotoi* cells, was based on a polygon created from satellite observations of the bloom when it was first identified at the water surface as (**Figure 1**). In total, 50,000 particles were released with a random vertical distribution between 0 and 20 m depth in the Celtic Sea. The 50,000 particles were selected as this is the limit of detection for *K. brevis* (cells per litre) in the Gulf of Mexico, by legacy satellites (Tester et al., 1998). Particles were neutrally buoyant, so any movement of particles between depths was due to vertical currents. The model simulation did not include growth or grazing of the phytoplankton. In the simulation the particles were transported for a fixed duration of 27 days from 2 to 29 June 2019. Maps were generated to show the density distribution of particles on different dates to show bloom progression and to compare with satellite imagery.

In situ Data

Availability of biological data in the region where the bloom occurred according to satellite imagery was investigated to establish the predominant phytoplankton in the area at the time. **Figure 1** shows the locations where phytoplankton samples were collected at the time of the bloom.

The Irish Marine Institute runs the national biotoxin and phytoplankton monitoring programme and releases a weekly HAB bulletin[2]. Phytoplankton abundance and composition results (freely available at http://webapps.marine.ie/HABs/Locations/Inshore) from southern stations close to where the bloom occurred were downloaded for this study. When the results of the particle tracking model confirmed the direction the bloom travelled, Cork Harbour, Oysterhaven, and Kinsale inshore stations were selected. Local officers from the Sea-Fisheries Protection Authority and other assigned personnel collect water and shellfish samples, at weekly intervals, from designated shellfish production areas. Samples are sent to the Marine Institute where the analyses are carried out. The programme carries an ISO 17025 quality accreditation. A 25 mL Lugol's iodine fixed seawater sample is used to determine the abundances of biotoxin producing or problematic phytoplankton using the Utermöhl test method, a recognised standard method, described in detail in UNESCO, 2010, references therein. The limit of detection is 40 cells/L^{-1}.

Coincidentally a phytoplankton field survey aboard the RV *Celtic Voyager* was being conducted in the Celtic Sea when the bloom was still visible via satellite imagery in July 2019. Water samples were collected at the periphery of the bloom at stations 135–144 and 148 (see **Figure 1**) on 10 July. A phytoplankton net vertically deployed to a maximum depth of 50 m at each station determined the predominant phytoplankton in the water column. A SeaBird 9/11 plus CTD integrated with a carousel water sampler for real-time auto-fire operations was lowered to approximately 5 m above sea floor level. Niskin water bottles were fired on the up cast at discrete depths where peaks of relative fluorescence and temperature gradients were evident on the depth profile. A fine scale sampler (FSS) was used to study the vertical thin layer distributions of dinoflagellates and to examine the correlation to the thin layer water properties. The FSS was lowered to the depth of the desired thin layer and all 15 bottles were fired simultaneously. Water samples were fixed in Lugol's iodine and stored in sterile 50 mL Sarstedt© water sampling bottles. Phytoplankton species were identified with an inverted microscope, Olympus CKX4. Aliquots and cells counted following the Utermöhl method (UNESCO, 2010).

RESULTS

Red Band Difference satellite imagery show a phytoplankton bloom (**Figure 2**), appearing in surface waters in the Celtic Sea, off southern Ireland on 2 June 2019. Weekly composites of satellite images show the bloom steadily increase in size (spatially) and magnitude (elevated surface pigment), the warmer colours on the images represent higher fluorescence which indicate higher bloom concentration in the weeks that followed (**Figure 2**). The images also show the extent of the bloom geographically. The surface bloom peaked in magnitude on the 27 June 2019 (**Figure 2**) (Daily file for 27th June 2019 in **Supplementary Material**). Following this, the bloom began to disperse and dissipate in early July 2019, however, remnants remained visible in the satellite imagery until late July (**Figure 2**).

Figure 3 displays satellite imagery from the weekly HAB bulletin, weeks 24–28 (4th June, 2019–8th July 2019) (see text footnote 2). Focussing on the study area in the Celtic Sea it is clear the increase in chlorophyll concentration at the surface was detected using both algorithms. In both **Figures 2**, **3**B there is a noticeable rise in chlorophyll concentration in the location the bloom was detected using the RBD algorithm. There is an increase from 1 mg/m^3 to 3 mg/m^3 between weeks 24 and 25 in **Figure 3**. Chlorophyll concentration peaks in concentration between dates 23 June 2019 between and 30 June 2019 (D) and (E) using both algorithms. Comparing both **Figures 2**, **3** it is evident the increase in chlorophyll concentration was detected in the Celtic Sea using both algorithms, but **Figure 2** displays a clearer series of images displaying the bloom's progression and movement.

[2]https://www.marine.ie/Home/site-area/data-services/interactive-maps/weekly-hab-bulletin

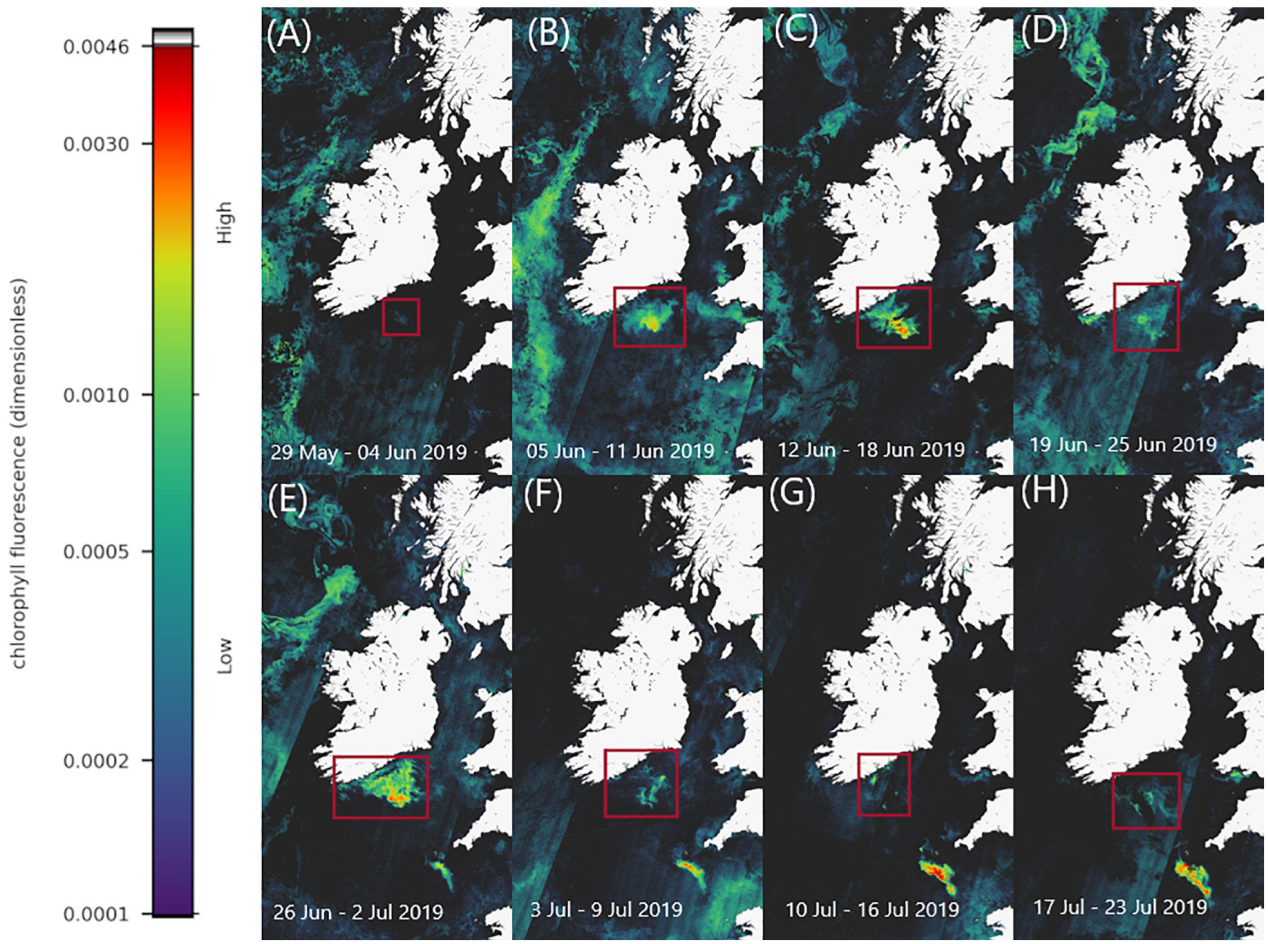

FIGURE 2 | Sentinel-3a OLCI images with RBD algorithm displaying the phytoplankton bloom progression between 29th May 2019 and 23rd July 2019 **(A–H)**. Colours indicate relative fluorescence, with warmer colours representing higher fluorescence indicative of higher bloom concentration.

The exact reason for the stripe artefacts in the RBD satellite imagery are not resolved at present, typically this is due to detector striping where radiometric miscalibration in the detector array elements can result in along track striping. However, it can also arise from solar glint or the "smile effect."

Trajectories from the particle tracking simulation produced a similar pattern to that of the surface bloom in the RBD satellite images at the end of June 2019. Virtual particles that represent the bloom increase in spatial extent over the 4-week period, eventually a significant percentage of particles move toward the south coast of Ireland toward the last week of June in agreement with the Sentinel-3a OLCI RBD satellite imagery (**Figure 4**). Data from an inshore sampling station, in Cork Harbour confirm *Karenia* spp. as the predominant taxa recorded from late June to late July. The cell counts for *Karenia* spp. in Cork Harbour were 2,471,168 cells/L on the 30 June, 117,234 cells/L on 14 July and 257,634 cells/L on 28 July. Between June and July, *Karenia* spp. cell counts at three inshore coastal stations (Cork Harbour, Oysterhaven, Kinsale; see **Figure 1** for locations) positioned along the south coast of Ireland, showed a dramatic cell increase after being undetected at Cork Harbour and Kinsale coastal stations prior to the bloom detection in offshore waters. *Karenia* spp. had been detected in very low numbers in Oysterhaven in April 2019 (8,800 cells/L) and wasn't recorded again until the 2 June (120 cells/L). Highest cell densities of *Karenia* spp. occurred on different days at each coastal station (Cork Harbour, Oysterhaven and Kinsale) and in a westward direction. Cork Harbour displayed the highest *Karenia* spp. cell count on the 30 June (2,471,168 cells/L), Oysterhaven on the 14 July (255,432 cells/L), and Kinsale on 28 July (398,736 cells/L) (**Figure 5**).

In 2019, the first inshore phytoplankton record of *Karenia* spp. (13,840 cells/L) in Cork Harbour was detected on 23 June. On 30 June the sharp rise in cell densities (2,471,168 cells/L) was detected, 3 days after the bloom peaked offshore. Around the same time (30 June) to the west in Oysterhaven, 80,000 cells/L were recorded in water samples. These numbers increased to 260,000 cells/L by mid-July. Further west in Kinsale cell numbers rose from approximately 71,000 cells/L on 14 July to 398,736 by the 28 July. Many other phytoplankton taxa were identified during the above dates but *Karenia* spp. was consistently the highest cells/L recorded in each instance (Full

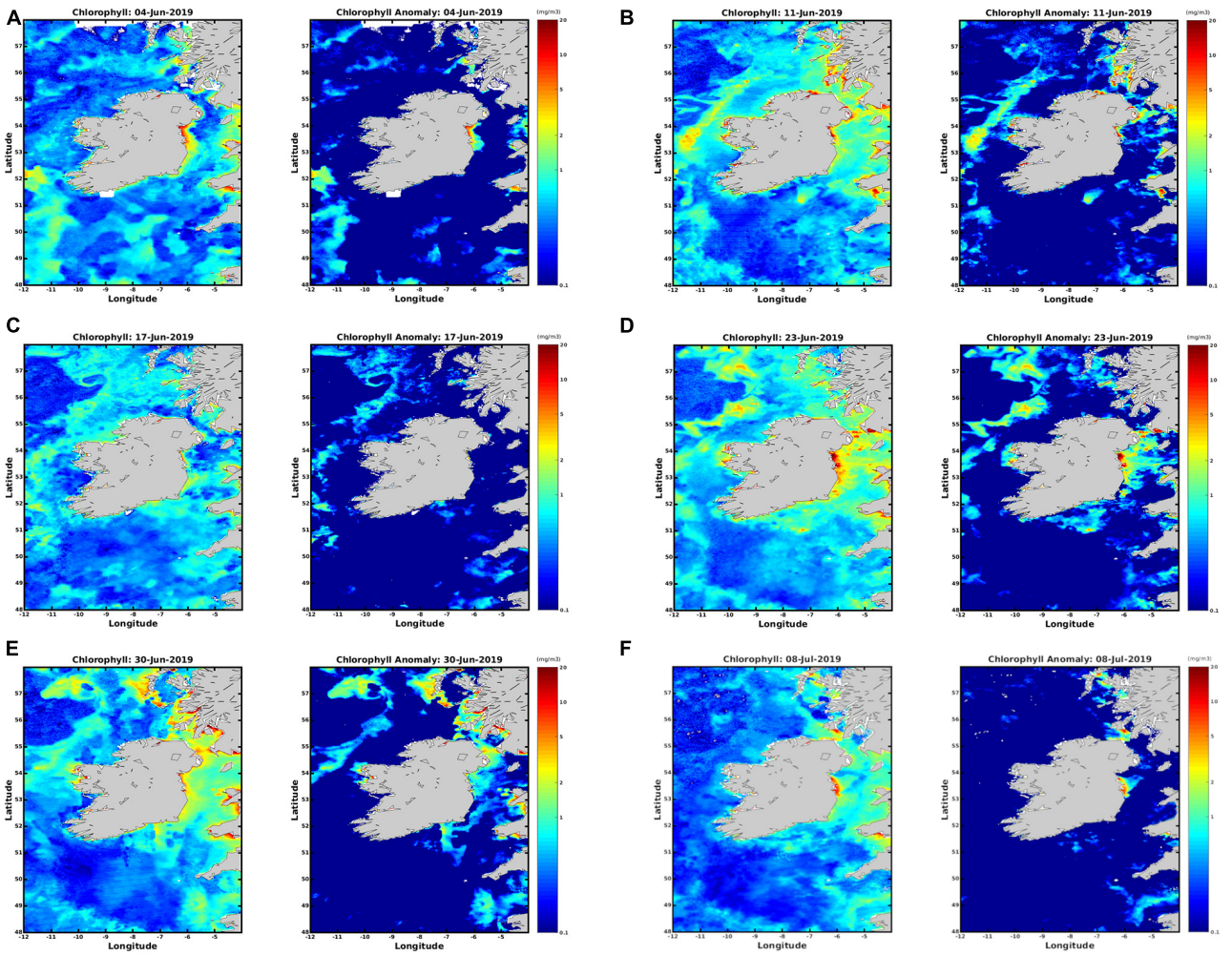

FIGURE 3 | OC5 IFREMER Level 4 Chlorophyll a data from the HAB bulletin weeks 24–28 **(A–F)** 4th June 2019 to 8th July 2019.

cell counts for the three southern stations can be viewed in **Supplementary Material**).

In July, phytoplankton cell counts from the research cruise CV19018, that coincided with the time of the offshore bloom confirmed the predominant taxa observed was *K. mikimotoi*. The satellite imagery showed that stations ST134-144 were on the outer edge of the bloom and that station at ST148 was located in a high-density area of the bloom (**Figure 6**), the values in this graphic represent values closest to the surface. *K. mikimotoi* values of 1,710,000 cells/L at station 148 were recorded at deeper depths but may not have been visible to satellite at that time due to the time the samples were taken and the behaviour of the phytoplankton.

Water samples collected with the CTD at stations 135–148 had an array of phytoplankton taxa identified (e.g., *Dinophysis acuminata*, *Prorocentrum*, *Ceratium lineatum*, *Ceratium fusus*, *Ceratium furca*, *Ceratium tripos*, *Ceratium macroceros*, *Protoperidinium*, *Gyrodinium*, *Ceratium inflatum*, *Dinophysis acuta*, *Noctiluca*) with *Karenia mikimotoi* present and the most abundant taxa recorded at stations sampled. The FSS bottles were deployed at 17–19 m at station 148 at 16:48 after a thin layer was identified on the CTD cast. *K. mikimotoi* was again the predominant taxa observed throughout the 5 bottles with cell counts of 3,146,000 cells/L, 4,258,000 cells/L, 3,842,000 cells/L, 3,276,000 cells/L and 2,474,000 recorded (Full cell counts for CV19018 can be viewed in **Supplementary Material**).

In situ K. mikimotoi cell counts from stations 138–148 closest to the surface were used to clarify whether there were any potential associations between the satellite derived RBD value, and *in situ* cell counts. While sampling was conducted over the course of the day from 09:03 to 16:34, it was difficult to determine the exact surface counts at the time of the satellite data acquisition given the DVM behaviour of *Karenia* spp. A linear regression was calculated, (Cells/L) = 1.97×10^8 (RBD) – 1.49×10^4, with an R^2 value of 0.93 (n = 8) was determined (linear regression and data for this conclusion in **Supplementary Material**). This suggests to us that an RBD value greater than approximately 0.0005 makes a useful early threshold for bloom formation as it is roughly equivalent to 1×10^6 cells/L. However, given that there are several unknowns with regard to fluorescence characteristics

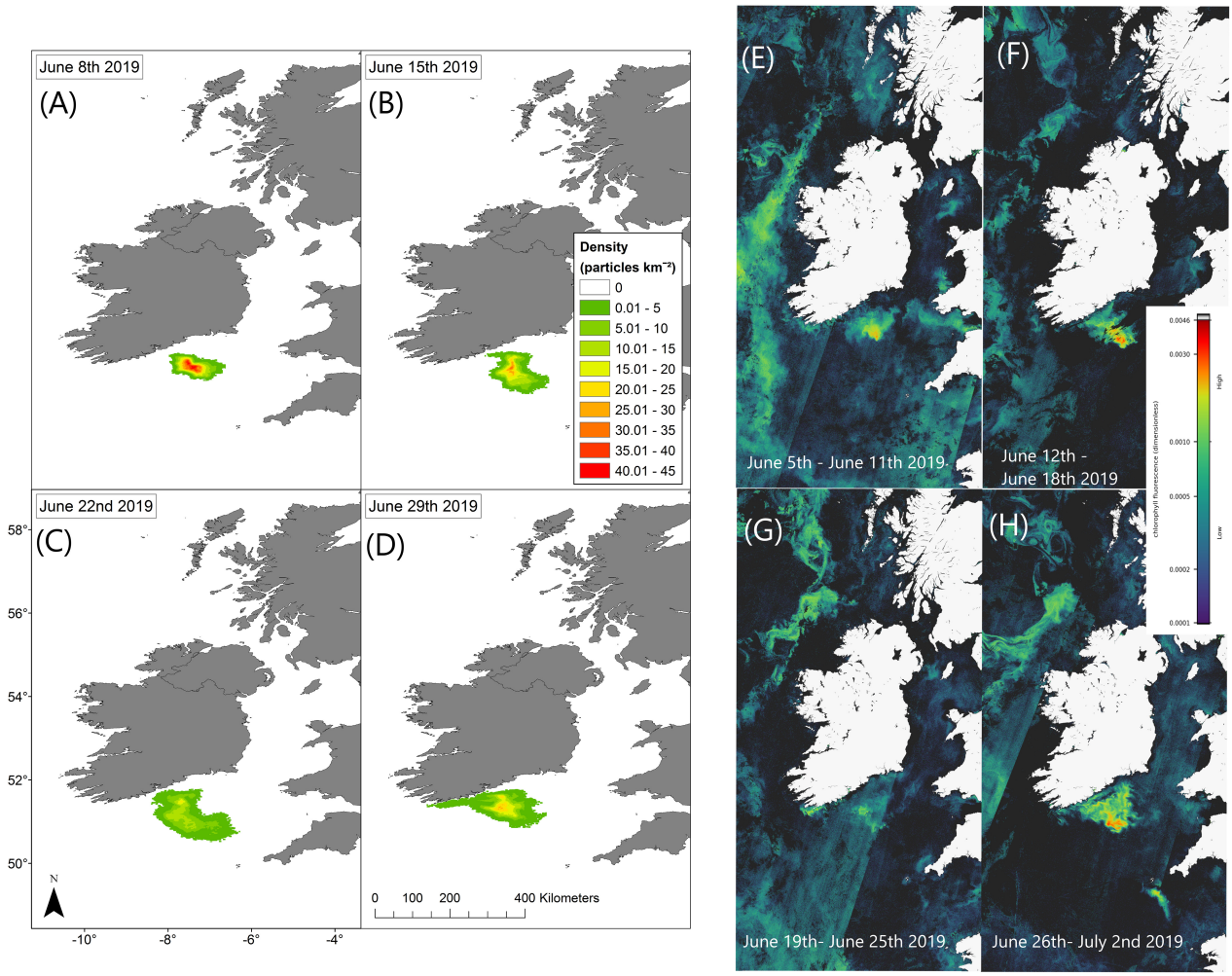

FIGURE 4 | Particle tracking model simulation results display current driven bloom dispersal on the left **(A–D)**. Maps show the density distribution of particles on 08/06/2019, 15/06/2019, 22/06/2019, and 29/06/2019 compared with Sentinel-3a OLCI images with RBD weekly composites on the right **(E–H)**.

and the DVM nature of *K. mikimotoi*, the timing of satellite measurement, *in situ* sample timing, and the low sample size the high correlation value could have been fortuitous as the samples acquired for this study were opportunistic therefore there are spatial and temporal mismatches involved.

Future work to clarify this would require more dedicated *in situ* sampling at the time of satellite-measurement acquisition and an estimate of the *Karenia* spp. position within the water column at that time. The findings of such studies will help determine a threshold for a warning system.

DISCUSSION

The RBD algorithm was tested in Irish waters for the first time during the months of May, June, July, and August 2019 to assess its suitability for adding to the established HAB monitoring system. A phytoplankton bloom occurred off the south coast at this time and was visible using the RBD satellite images. The results we have presented here show the RBD algorithm was proficient in assessing the timing of the initiation, movement, geographical extent, locations of the peak abundances and duration of the bloom. Although this study demonstrates the RBD's use in detecting *Karenia* spp. blooms, the algorithm would be useful for monitoring HAB events in general as the detection of bloom presence with the RBD algorithm indicates some Chl-*a* fluorescence, as the radiance returned at 681 nm is greater than that returned from 665 nm, even though 681 nm also includes strong Chl-*a* absorption (Wolny et al., 2020) and already used for Chesapeake Bay for monitoring a range of dinoflagellates.

Unfortunately, there was not enough offshore data to do a rigorous validation, but, we were able to confirm the predominant phytoplankton in an area when the bloom appeared on satellite imagery using data from an offshore survey that coincided with the bloom in July. Having confirmed the drift trajectory of the bloom based on local water circulation patterns using the particle tracking model we were confident in using the inshore data from the southern stations Cork Harbour,

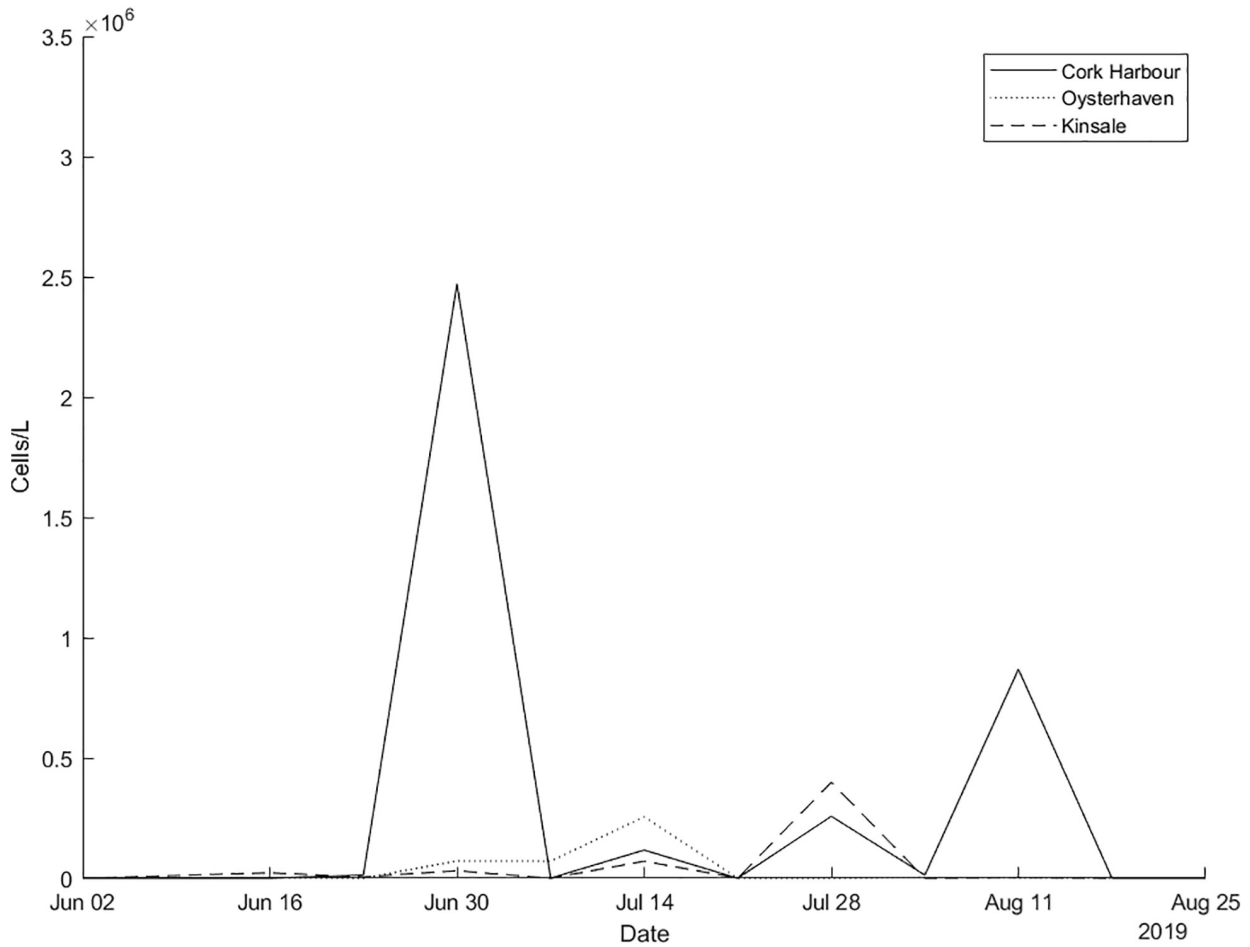

FIGURE 5 | *In situ Karenia* spp. cells/L counts for inshore stations in Cork Harbour, Oysterhaven, and Kinsale from the national monitoring programme June–August 2019.

Oysterhaven, and Kinsale and confirmed that *Karenia* spp. was the predominate taxa identified.

Although the authors are not trying to replace the current standard chlorophyll algorithm, it is hoped the preliminary use of RBD algorithm will become an extra monitoring tool within the HAB alert system. This paper presents the results from a pilot study and future studies will help improve methodologies with the implementation of more validation methods such as the use of hyperspectral radiometry from the national research vessel.

The acquisition of new technical skills will further help support a sustainable aquaculture industry in Ireland. The use of satellite technology for observing the movement of phytoplankton blooms are well documented throughout the world (Stumpf et al., 2003, 2009; Stumpf and Tomlinson, 2005; Miller et al., 2006; Davidson et al., 2016; Groom et al., 2019). Of course, there are going to be limitations to using earth observation data, some of which include: clouds, difficulty differentiating between phytoplankton species and, depth limitations (Ruddick et al., 1999). As discussed, blue-green ratio chlorophyll algorithms can overestimate chlorophyll in waters close to the coast due to contamination of CDOM and sediment in the measurements. Satellite measurements of chlorophyll fluorescence are considered proficient to detect blooms in areas like this (Gower and King, 2012; Gower et al., 2013). Introducing new methods of monitoring is useful to improve current mitigation efforts, given the diversity and complexity of HAB events and the different behaviours of phytoplankton functional types (Moisan et al., 2017). Understanding the history and behaviours of the most problematic species that are responsible for HAB events can help detect what type of bloom is forming offshore before it is possible to collect samples. This can be done by using algorithms with trained datasets (Martinez-Vicente et al., 2020) and also it is vital to understand the typical behaviour of the species. It is established that blooms of *Karenia* spp. originate in regions of the continental shelf that have weak tidal currents and are stratified in the summer (Brand et al., 2012). For example, in the Celtic Sea close to the Nymphe bank, where tidal streams are weak, the spring bloom develops earliest (Pingree et al., 1976; Raine, 2014). In this area, high densities of *K. mikimotoi* have been observed as early as May (Pemberton et al., 2004). The Nymphe Bank is located at 51°30′0″ N 7°30′0″W, an area where the centre of the bloom

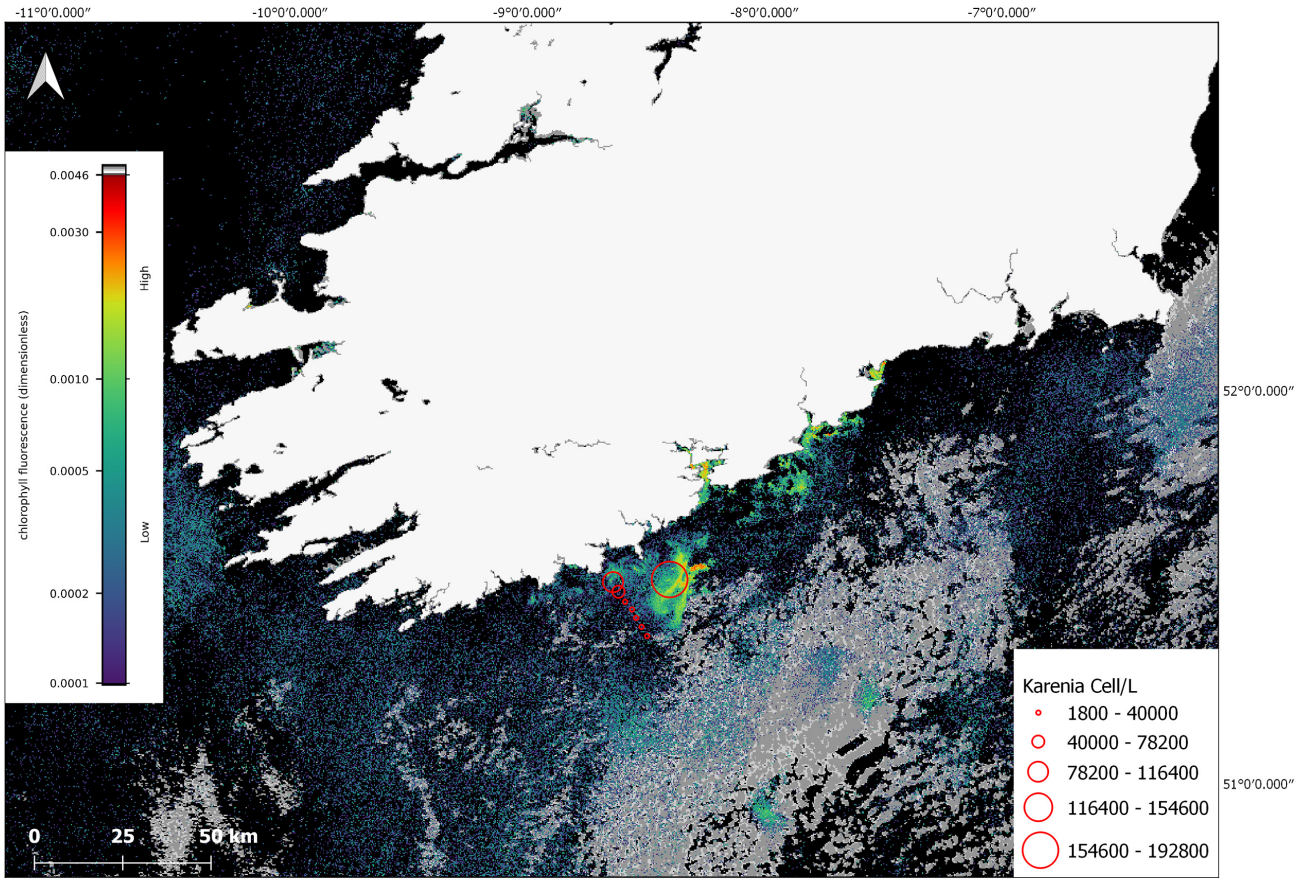

FIGURE 6 | Sentinel-3a OLCI image with RBD algorithm from 10 July 2019. The red circles indicate cell concentrations determined using light microscopy for *in situ* samples collected on CV19018 on the same date. The grey colour in the image represents cloud cover.

first appeared on satellite imagery, see **Figure 1**; 51°23′24″ N 7°23′18″W. Large blooms of *Karenia* spp. have been recorded around Ireland in regions with similar slack circulation, areas such as the southern Malin shelf and the Irish shelf to the west of the Aran Islands (Gowen et al., 1998; Silke et al., 2005). Subsequent growth and transport in coastal currents can spread their impact over large areas of the coastal zone (Davidson et al., 2009). Due to the proximity to land, the development of these blooms are difficult to detect without satellite technology.

Many harmful algae display diurnal vertical migration behaviour (Park et al., 2001; Kononen et al., 2003). The algae are known to swim toward the surface at dawn and to deeper depths at dusk (Olsson and Graneli, 1991; Koizumi et al., 1996; Park et al., 2001). *Karenia mikimotoi* are known to vertically migrate within an estimated daily depth range of 15–20 m (Koizumi et al., 1996; Li et al., 2019) they migrate before sunrise and reach the surface before midday (Li et al., 2019). When the cells assemble at the surface during upward migration, this has been shown to promote the formation of the red tide (Honjo, 2004). Previous observations have suggested that *K. mikimotoi* are frequently found in thin layers near the pycnocline (Brand et al., 2012) developing at or directly below the thermocline (Holligan et al., 1984) particularly at frontal regions between well-mixed and stratified waters (Pingree et al., 1977). Results from the FSS at station 148 on CV19018 show *Karenia* spp. between 17 and 19 m in a thin layer in extremely high densities. These samples were taken at 16:34, due to the DVM behaviour of the species, they were travelling to deeper depths before dusk and higher concentrations could have been identified at the surface if the samples were taken around midday. Knowing *Karenia* spp. exhibit these behaviours of surfacing around midday, it is a good reason to choose a fluorescence algorithm to monitor coastal waters. Fluorescence penetration depth is shallow because oceanic waters attenuate fluorescence and the signal only returns information of Chl-*a* in the subsurface waters of approximately 2 m (Xing et al., 2007).

Additionally, in order to predict movement of the bloom, it is important we understand the water circulation patterns. The RBD images show the bloom was detected by satellite on the 2 June, 14 days before *Karenia* spp. was identified in the inshore samples. Historically, *K. mikimotoi* blooms are known to occur in shelf and coastal waters off the south, southwest, west and northwest of Ireland. Water circulation around these coastal areas is heavily influenced by the Irish Coastal Current that flows in a clockwise direction around the Irish Atlantic coastline (Raine, 2014). This coastal current is an important

transport pathway in the northern Celtic Sea. In summer, the westward transport of planktonic organisms is heavily influenced by the Irish Coastal Current with faster flows, in a density driven current, found at depths of ∼25 m (Farrell et al., 2012). In this study, relatively calm weather was reported in June with weak wind speeds and low significant wave heights (average 1.2 m) recorded at the M5 data buoy in the Celtic Sea, conditions suitable for the development of the *K. mikimotoi* bloom observed in offshore surface waters. The numerical hydrodynamic model used in this study was tightly coupled to meteorological data and the particle tracking model shows the advection of the *K. mikimotoi* bloom into inshore regions when the bloom was fully developed. Wind driven advection is important in this region. For example, in 1998, weak wind driven upwelling in the region uplifted a subsurface *K. mikimotoi* bloom into surface waters off the SW coast, wind also played an important part in the transport of the bloom eastwards across the Celtic Sea where it was advected into coastal areas; this bloom was recorded using satellite ocean colour and thermal infra-red sea surface temperature images alongside *in situ* measurements (Raine et al., 2001). The results from the particle tracking model confirm the bloom followed the pattern of the clockwise coastal current when *Karenia* spp. counts peaked in the three southern inshore stations at different times. Cork Harbour first, Oysterhaven and then Kinsale.

The method explained in this study shows high-biomass blooms, like *Karenia* spp. can be detected and monitored with the RBD algorithm like in the Gulf of Mexico and Alaska (Amin et al., 2009; Vandersea et al., 2020) and now this study confirms it is a useful product to use in Irish waters. Wolny et al. (2020) describes how the RBD method is used to monitor the most common marine and estuarine HABs in Chesapeake Bay indicating the potential for other HAB blooms of interest in Ireland. Further discrimination of genus or species level is difficult with just satellite technology, but combined with particle tracking and routine monitoring programmes, can further develop a more robust warning system. Aquaculture business owners can limit damage to their stock by avoiding moving, harvesting and/or planting new seed while warning systems are in place.

Quantitative application of the RBD approach examined here, requires more data to better constrain the relationship between RBD values and cell numbers of *Karenia mikimotoi* as the observed reflectance/fluorescence is influenced by a suite of external variables which may change with time (e.g., irradiance, photosynthetic efficiency, cell size, etc.). One such key parameter is the chlorophyll per cell of *Karenia mikimotoi*, with laboratory studies indicating it decreases with increasing irradiance and covers a wide range of values in the literature; 2–27 pg Chl cell^{-1} (Stæhr and Cullen, 2003; Chang and Gall, 2013; Wang et al., 2019; Zhao et al., 2019). Values of 2–6 pg Chl cell^{-1} (Stæhr and Cullen, 2003; Zhao et al., 2019) have been found under high light conditions similar to what was observed in the Celtic Sea at the time of our study, using the Cell numbers of ∼3,000,000 cells/L from the centre of the bloom at that time would indicate a value of 6–18 μg Chl/L potentially associated with *Karenia mikimotoi*.

There was limited availability of offshore data to do a full validation for this study. If this algorithm was to be used as an operational satellite product, future work will investigate combinations of inshore and offshore sampling and combining hyperspectral radiometry data.

CONCLUSION

- We analysed remotely sensed data for the period of May–August 2019 testing the RBD algorithm in Irish waters for the first time.
- The phytoplankton bloom we identified using the satellite technology was localised and was reflected in the inshore phytoplankton samples from around Ireland.
- Both the satellite imagery and the particle tracking simulation results confirm the movement and the direction the bloom travelled.
- *Karenia* spp. was present in high numbers only at southern stations at the time of the bloom and was not identified anywhere else along the Irish coastline.
- A sudden increase of *Karenia* spp. in Cork Harbour, Oysterhaven and Kinsale occurred shortly after the bloom developed in offshore waters.
- The appearance of *Karenia* spp. at the southern coastal stations followed an east to west pattern in line with what the expected transport of the Irish coastal current.
- We established that the predominant phytoplankton observed in offshore samples was *K. mikimotoi.*
- We describe the potential for Ireland to use the Red Band Difference algorithm as an extra monitoring tool within the established HAB alert system to provide an early warning method of HABs and in particular, *Karenia* spp. blooms.

DATA AVAILABILITY STATEMENT

The original contributions presented in the study are included in the article/**Supplementary Material**, further inquiries can be directed to the corresponding author/s.

AUTHOR CONTRIBUTIONS

CJ wrote the first draft of the manuscript under the guidance of PC and CC. AM, MT, and CJ participated in the analysis and presentation of ocean colour satellite data. RM carried out the particle tracking model simulation. RS and CG participated in the collection and analysis of the field *in situ* data. All authors contributed to the manuscript revisions.

FUNDING

This project (Grant-aid Agreement No. CF/17/03/01) is carried out with the support of the Marine Institute and funded under the Marine Research Programme by the Irish Government. Further funding was provided by the Marine Institute Networking and Research Communication Awards, Networking and Travel Grant, and Ryan Institute Travel Awards for CJ visit to NCCOS, NOAA in October 2019. This work was partially supported by the

INTERREG Atlantic Area Work Programme project PRIMROSE Project Number: EAPA_182/2016.

ACKNOWLEDGMENTS

We thank Richard Stumpf and his team at NCCOS, NOAA for their guidance that helped create this study. We thank the phytoplankton team at the Marine Institute for analysing the inshore samples made available for this study. We also thank Dr. Robin Raine (Chief Scientist), researchers and crew of CV19018 for the offshore phytoplankton data used in this study, Kieran Lyons from the Marine Institute for providing the data for the particle tracking model, and the reviewers for their comments and suggestions which have helped improve this manuscript.

SUPPLEMENTARY MATERIAL

The Supplementary Material for this article can be found online at: https://www.frontiersin.org/articles/10.3389/fmars.2021.638889/full#supplementary-material

Supplementary Image 1 | 27 June 2019 RBD daily image.

Supplementary Table 1 | Cork Harbour, Oysterhaven, Kinsale phytoplankton counts June - August 2019.

Supplementary Table 2 | Cork Harbour, Oysterhaven, Kinsale Karenia cell counts June - August 2019.

Supplementary Table 3 | CV19018 phytoplankton cell counts 10 July 2019.

Supplementary Data Sheet 1 | Linear regression of RBD and in situ Karenia mikimotoi cell counts.

REFERENCES

Amin, R., Zhou, J., Gilerson, A., Gross, B., Moshary, F., and Ahmed, S. (2009). Novel optical techniques for detecting and classifying toxic dinoflagellate Karenia brevis blooms using satellite imagery. *Opt. Express* 17, 9126–9144. doi: 10.1364/oe.17.009126

Anderson, C. R., Moore, S. K., Tomlinson, M. C., Silke, J., and Cusack, C. K. (2015). "Living with harmful algal blooms in a changing world: strategies for modeling and mitigating their effects in coastal marine ecosystems," in *Coastal and Marine Hazards, Risks, and Disasters*, eds J. T. Ellis and D. J. Sherman (Amsterdam: Elsevier), 495–561. doi: 10.1016/b978-0-12-396483-0.00017-0

Brand, L. E., Campbell, L., and Bresnan, E. (2012). Karenia: the biology and ecology of a toxic genus. *Harmful Algae* 14, 156–178. doi: 10.1016/j.hal.2011.10.020

Bresnan, E., Davidson, K., Edwards, M., Fernand, L., Gowen, R., Hall, A., et al. (2013). Impacts of climate change on harmful algal blooms. *MCCIP Sci. Rev.* 2013, 236–243. doi: 10.14465/2013.arc24.236-243

Callaway, R., Shinn, A. P., Grenfell, S. E., Bron, J. E., Burnell, G., and Cook, E. J. (2012). Review of climate change impacts on marine aquaculture in the UK and Ireland. *Aquatic Conserv. Mar. Freshw. Ecosyst.* 22, 389–421.

Chang, F. H., and Gall, M. (2013). Pigment compositions and toxic effects of three harmful Karenia species, *Karenia concordia*, *Karenia brevisulcata* and *Karenia mikimotoi* (Gymnodiniales, Dinophyceae), on rotifers and brine shrimps. *Harmful Algae* 27, 113–120. doi: 10.1016/j.hal.2013.05.005

Dabrowski, T., Lyons, K., Cusack, C., Casal, G., Berry, A., and Nolan, G. D. (2016). Ocean modelling for aquaculture and fisheries in Irish waters. *Ocean Sci.* 12, 101–116. doi: 10.5194/os-12-101-2016

Davidson, J., Mateus, M., Reguera, B., Silke, J., and Sourisseau, M. (2016). Applied simulations and integrated modelling for the understanding of toxic and harmful algal blooms (ASIMUTH). *Harmful Algae* 53, 1–166. doi: 10.1007/978-0-387-75865-7_1

Davidson, K., Miller, P., Wilding, T. A., Shutler, J., Bresnan, E., Kennington, K., et al. (2009). A large and prolonged bloom of *Karenia mikimotoi* in Scottish waters in 2006. *Harmful Algae* 8, 349–361. doi: 10.1016/j.hal.2008.07.007

Dennis, J., and Jackson, E. (2019). *BIM National Seafood Survey Aquaculture Report*.

Diaz, R. J., and Rosenberg, R. (2008). Spreading dead zones and consequences for marine ecosystems. *Science* 321, 926–929. doi: 10.1126/science.1156401

Doerffer, R. (1993). Estimation of primary production by observation of solar-stimulated fluorescence ICES mar. *Sci. Symp.* 197, 104–113.

Farrell, H., Gentien, P., Fernand, L., Lunven, M., Reguera, B., González-Gil, S., et al. (2012). Scales characterising a high density thin layer of *Dinophysis acuta* Ehrenberg and its transport within a coastal jet. *Harmful Algae* 15, 36–46. doi: 10.1016/j.hal.2011.11.003

FAO (2020). *The State of World Fisheries and Aquaculture 2020. Sustainability in Action*. Rome: FAO.

Gentien, P. (1998). "Bloom dynamics and ecophysiology of the Gymnodinium mikimotoi species complex," in *Physiological Ecology of Harmful Algal Blooms*, eds D. Anderson, A. D. Cembella, and G. M. Hallegraeff (Berlin: Springer).

Gentien, P., Lunven, M., Lazure, P., Youenou, A., and Crassous, M. P. (2007). Motility and autotoxicity in *Karenia mikimotoi* (Dinophyceae). *Philos. Trans. R. Soc. B Biol. Sci.* 362, 1937–1946. doi: 10.1098/rstb.2007.2079

Gordon, H. R., and Morel, A. Y. (1983). *Remote Assessment of Ocean Color for Interpretation of Satellite Visible Imagery: a Review*. Berlin: Springer-Verlag.

Gowen, R. J., Raine, R., Dickey-Collas, M., and White, M. (1998). Plankton distributions in relation to physical oceanographic features on the southern Malin Shelf, August 1996. *ICES J. Mar. Sci.* 55, 1095–1111. doi: 10.1006/jmsc.1998.0418

Gower, J., and King, S. (2012). Use of satellite images of Chlorophyll fluorescence to monitor the spring bloom in coastal waters. *Int. J. Remote Sens.* 33, 7469–7481. doi: 10.1080/01431161.2012.685979

Gower, J., King, S., Statham, S., Fox, R., and Young, E. (2013). The malaspina dragon: a newlydiscovered pattern of the early spring bloom in the strait of georgia, British Columbia, Canada. *Prog. Oceanogr.* 115, 181–188. doi: 10.1016/j.pocean.2013.05.024

Groom, S. B., Sathyendranath, S., Ban, Y., Bernard, S., Brewin, B., and Brotas, V. (2019). Satellite ocean colour: current status and future perspective. *Front. Mar. Sci.* 6:485.

Holligan, P., Williams, P., Purdie, D., and Harris, R. (1984). Photosynthesis, respiration and nitrogen supply of plankton populations in stratified, frontal and tidally mixed shelf waters. *Mar. Ecol. Prog. Ser.* 17, 201–213. doi: 10.3354/meps017201

Honjo, T. (2004). "Karenia (formerly Gymnodinium) mikimotoi," in *Red Tides. New Zealand: Terra Scientific Publishing Company*, ed. T. Okaichi (Dordrecht: Kluwer Academic Publishers), 345–357.

IOCCG (2000). "Remote sensing of ocean colour in coastal, and other optically-complex, waters," in *Reports of the International Ocean-Colour Coordinating Group, No. 3*, ed. S. Sathyendranath (Dartmouth: IOCCG).

Jones, K. J., Ayres, P., Bullock, A. M., Roberts, R. J., and Tett, P. (1982). A red tide of Gyrodinium aureolum in sea lochs of the firth of Clyde and associated mortality of pond-reared salmon. *J. Mar. Biol. Assoc. U.K.* 62, 771–782. doi: 10.1017/s0025315400044040

Koizumi, Y., Uchida, T., and Honjo, T. (1996). Diurnal vertical migration of Gymnodinium mikimotoi during a red tide in Hoketsu Bay, Japan. *J. Plank. Res.* 18, 289–294. doi: 10.1093/plankt/18.2.289

Kononen, K., Huttunen, M., Hällfors, S., Gentien, P., Lunven, M., Huttula, T., et al. (2003). Development of a deep chlorophyll maximum of *Heterocapsa triquetra* Ehrenb. at the entrance to the Gulf of Finland. *Limnol. Oceanogr.* 48, 594–607. doi: 10.4319/lo.2003.48.2.0594

Leadbetter, A., Silke, J., and Cusack, C. (2018). *Creating a Weekly Harmful Algal Bloom Bulletin. Version 1*. Ireland: Marine Institute.

Lett, C., Verley, P., Mullon, C., Parada, C., Brochier, T., Penven, P., et al. (2008). A lagrangian tool for modelling ichthyoplankton dynamics. *Environ. Modell. Softw.* 23, 1210–1214. doi: 10.1016/j.envsoft.2008.02.005

Li, X., Yan, T., Yu, R., and Zhou, M. (2019). A review of *karenia mikimotoi*: bloom events, physiology, toxicity and toxic mechanism. *Harmful Algae* 90:101702. doi: 10.1016/j.hal.2019.101702

Martinez-Vicente, V., Kurekin, A., Sá, C., Brotas, V., Amorim, A., Veloso, V., et al. (2020). Sensitivity of a satellite algorithm for harmful algal bloom discrimination to the use of laboratory bio-optical data for training. *Front. Mar. Sci.* 7:582960.

Miller, P., Shutler, J., Moore, G., and Groom, S. (2006). SeaWiFS discrimination of harmful algal bloom evolution. *Int. J. Remote Sens.* 27, 2287–2301. doi: 10.1080/01431160500396816

Mobley, C. D., Stramski, D., Bissett, W. P., and Boss, E. (2004). Optical modeling of ocean waters: is the Case 1 - Case 2 classification still useful? *Oceanography* 17, 60–67. doi: 10.5670/oceanog.2004.48

Moisan, T. A., Rufty, K. M., Moisan, J. R., and Linkswiler, M. A. (2017). Satellite observations of phytoplankton functional type spatial distributions, phenology, diversity, and ecotones. *Front. Mar. Sci.* 4, 1–24.

Morel, A. (1988). Optical modeling of the upper ocean in relation to its biogenous matter content (case I waters). *J. Geophys. Res.* 93:10749. doi: 10.1029/jc093ic09p10749

Morel, A., and Prieur, L. (1977). Analysis of variations in ocean color1. *Limnol. Oceanogr.* 22, 709–722. doi: 10.4319/lo.1977.22.4.0709

Mydlarz, L. D., Jones, L. E., and Harvell, C. D. (2006). Innate immunity, environmental drivers and disease ecology of marine and freshwater Invertebrates. *Annu. Rev. Ecol. Evol. Syst.* 37, 251–288. doi: 10.1146/annurev.ecolsys.37.091305.110103

Neely, T., and Campbell, L. (2006). A modified assay to determine hemolytic toxin variability among Karenia clones isolated from the Gulf of Mexico. *Harmful Algae* 5, 592–598. doi: 10.1016/j.hal.2005.11.006

O'Boyle, S., McDermott, G., Silke, J., and Cusack, C. (2016). Potential impact of an exceptional bloom of *Karenia mikimotoi* on dissolved oxygen levels in waters off western Ireland. *Harmful Algae* 53, 77–85. doi: 10.1016/j.hal.2015.11.014

Olsson, P., and Graneli, E. (1991). Observations on diurnal vertical migration and phased cell division for three coexisting marine dinoflagellates. *J. Plankton Res.* 13, 1313–1324. doi: 10.1093/plankt/13.6.1313

Ottway, B., Parker, M., McGrath, D., and Crowley, M. (1979). Observations on a bloom of Gyrodinium aureolum Hulbert on the south coast of Ireland 1976, associated with mortalities of littoral and sub-littoral organisms. *Ir. Fish. Invest Ser. B* 18, 3–9.

Park, J. G., Jeong, M. K., Lee, J. A., Cho, K.-J., and Kwon, O.-S. (2001). Diurnal vertical migration of a harmful dinoflagellate, *Cochlodinium polykrikoides* (Dinophyceae), during a red tide in coastal waters of Namhae Island, Korea. *Phycologia* 40, 292–297. doi: 10.2216/i0031-8884-40-3-292.1

Pemberton, K., Rees, A. P., Miller, P. I., Raine, R., and Joint, I. (2004). The influence of water body characteristics on phytoplankton diversity and production in the Celtic Sea. *Cont. Shelf Res.* 24, 2011–2028. doi: 10.1016/j.csr.2004.07.003

Pingree, R. D., Holligan, P. M., and Head, R. N. (1977). Survival of dinoflagellate blooms in the western English channel. *Nature* 265, 266–269. doi: 10.1038/265266a0

Pingree, R. D., Holligan, P. M., Mardell, G. T., and Head, R. N. (1976). The influence of physical stability on spring, summer and autumn phytoplankton blooms in the Celtic sea. *J. Mar. Biol. Assoc. U. K.* 56, 845–873. doi: 10.1017/s0025315400020919

Raine, R. (2014). A review of the biophysical interactions relevant to the promotion of HABs in stratified systems: the case study of Ireland. *Deep Sea Res. II Top. Stud. Oceanogr.* 101, 21–31. doi: 10.1016/j.dsr2.2013.06.021

Raine, R., O'Boyle, S., O'Higgins, T., White, M., Patching, J., Cahill, B., et al. (2001). A satellite and field portrait of a *Karenia mikimotoi* bloom off the south coast of Ireland, August 1998. *Hydrobiologia* 465, 187–193. doi: 10.1007/978-94-010-0434-3_19

Ruddick, K., Park, Y., Cauwer, V., Debruyn, W., and Sterckx, S. (1999). *Overview of Ocean Colour: theoretical background, sensors and applicability for the detection and monitoring of harmful algae blooms (capabilities and limitations) Kevin. UNESCO Monographs on Oceanographic Methodology Series, Manual on Harmful Marine Microalgae Overview, 1–50*.

Satake, M., Shoji, M., Oshima, Y., Naoki, H., Fujita, T., and Yasumoto, T. (2002). Gymnocin-A, a cytotoxic polyether from the notorious red tide dinoflagellate, Gymnodinium mikimotoi. *Tetrahedron Lett.* 43, 5829–5832. doi: 10.1016/s0040-4039(02)01171-1

Satake, M., Tanaka, Y., Ishikura, Y., Oshima, Y., Naoki, H., and Yasumoto, T. (2005). Gymnocin-B with the largest contiguous polyether rings from the red tide dinoflagellate, Karenia (formerly Gymnodinium) mikimotoi. *Tetrahedron Lett.* 46, 3537–3540. doi: 10.1016/j.tetlet.2005.03.115

Shikata, T., Matsunaga, S., Nishide, H., Sakamoto, S., Onistuka, G., and Yamaguchi, M. (2015). Diurnal vertical migration rhythms and their photoresponse in four phytoflagellates causing harmful algal blooms. *Limnol. Oceanogr.* 60, 1251–1264. doi: 10.1002/lno.10095

Shikata, T., Onitsuka, G., Abe, K., Kitatsuji, S., Yufu, K., Yoshikawa, Y., et al. (2016). Relationships between light environment and subsurface accumulation during the daytime in the red-tide dinoflagellate *Karenia mikimotoi*. *Mar. Biol.* 164:18.

Shikata, T., Sakamoto, S., Onitsuka, G., Aoki, K., and Yamaguichi, M. (2014). Effects of salinity on diel vertical migration behavior in two red-tide algae, Chattonella antiqua and *Karenia mikimotoi*. *Plankton Benthos Res.* 9, 42–50. doi: 10.3800/pbr.9.42

Silke, J., O'Beirn, F., and Cronin, M. (2005). *Karenia mikimotoi: an Exceptional Dinoflagellate Bloom in Western Irish Waters, Summer 2005*. Ireland: Marine Institute.

Stæhr, P. A., and Cullen, J. J. (2003). Detection of *Karenia mikimotoi* by spectral absorption signatures. *J. Plankton Res.* 25, 1237–1249. doi: 10.1093/plankt/fbg083

Stumpf, R. P., and Tomlinson, M. C. (2005). "Remote sensing of harmful algal blooms," in *Remote Sensing of Coastal Aquatic Environments*, eds R. L. Miller, C. E. del Castillo, and B. A. McKee (Dordrecht: Springer), 347.

Stumpf, R. P., Culver, M. E., Tester, P. A., Tomlinson, M. C., Kirkpatrick, G. J., and Pederson, B. A. (2003). Monitoring Karenia brevis blooms in the Gulf of Mexico using satellite ocean color imagery and other data. *Harmful Algae* 2, 147–160. doi: 10.1016/s1568-9883(02)00083-5

Stumpf, R. P., Tomlinson, M. C., Calkins, J. A., Kirkpatrick, B., Fisher, K., Nierenberg, K., et al. (2009). Skill assessment for an operational algal bloom forecast system. *J. Mar. Syst.* 76, 151–161. doi: 10.1016/j.jmarsys.2008.05.016

Tester, P. A., Stumpf, R. P., and Steidinger, K. A. (1998). ""Ocean color imagery: what is the minimum detection level for *Gymnodinium breve* blooms?"," in *Harmful Algae, Proceedings of the VII International Conference on Harmful Algae*, eds B. Reguera, J. Blanco, and M. Fernandez (Paris: Xunta de Galicia and Intergovernmental Oceanographic Commission of UNESCO), 149–151.

Tweddle, J. F., Gubbins, M., and Scott, B. E. (2018). Should phytoplankton be a key consideration for marine management? *Mar. Policy* 97, 1–9. doi: 10.1016/j.marpol.2018.08.026

UNESCO (2010). *Microscopic and Molecular Methods for Quantitative Phytoplankton Analysis*. Paris: UNESCO.

Vandersea, M., Tester, P., Holderied, K., Hondolero, D., Kibler, S., and Powell, K. (2020). An extraordinary *Karenia mikimotoi* "beer tide" in Kachemak Bay Alaska. *Harmful Algae* 92:101706. doi: 10.1016/j.hal.2019.101706

Wang, X., Feng, X., Zhuang, Y., Lu, J., Wang, Y., Gonçalves, R. J., et al. (2019). Effects of ocean acidification and solar ultraviolet radiation on physiology and toxicity of dinoflagellate *Karenia mikimotoi*. *Harmful Algae* 81, 1–9. doi: 10.1016/j.hal.2018.11.013

Wolny, J. L., Tomlinson, M. C., Schollaert, Uz, S., Egerton, T. A., McKay, J. R., et al. (2020). Current and future remote sensing of harmful algal blooms in the chesapeake bay to support the shellfish industry. *Front. Mar. Sci.* 7:337.

Wynne, T. T., Meredith, A., Briggs, T., Litaker, W., and Stumpf, R. P. (2018). *Harmful Algal Bloom Forecasting Branch Ocean Color Satellite Imagery Processing Guidelines*. Silver Spring, MD: NOAA.

Xing, X. G., Zhao, D. Z., Liu, Y. G., Yang, J. H., Xiu, P., and Wang, L. (2007). An overview of remote sensing of chlorophyll fluorescence. *Ocean Sci. J.* 42, 49–59.

Zeng, L., and Li, D. (2015). Development of in situ sensors for chlorophyll concentration measurement. *J. Sensors* 2015, 1–16. doi: 10.1155/2015/903509

Zhao, T., Tan, L., Huang, W., and Wang, J. (2019). The interactions between micro polyvinyl chloride (mPVC) and marine dinoflagellate *Karenia mikimotoi*: The inhibition of growth, chlorophyll and photosynthetic efficiency. *Environ. Pollut.* 247, 883–889. doi: 10.1016/j.envpol.2019.01.114

Conflict of Interest: AM was employed by Consolidated Safety Services Inc.

The remaining authors declare that the research was conducted in the absence of any commercial or financial relationships that could be construed as a potential conflict of interest.

frontiers in Marine Science

OPINION
published: 10 May 2021
doi: 10.3389/fmars.2021.669402

Monitoring SARS-CoV-2 as a Microbiological Risk in Shellfish Aquaculture

Marcos Mateus[1]*, *Miguel Remondes*[2], *Lígia Pinto*[1] and *Alexandra Silva*[3]

[1] Marine, Environment and Technology Centre/Laboratory for Robotics and Engineering Systems (MARETEC/LARSyS), Instituto Superior Técnico, Universidade de Lisboa, Lisbon, Portugal, [2] Instituto de Medicina Molecular João Lobo Antunes, Faculdade de Medicina, Universidade de Lisboa, Lisbon, Portugal, [3] IPMA, I.P—Instituto Português do Mar e da Atmosfera, Lisbon, Portugal

Keywords: SARS-CoV-2, COVID-19, gastrointestinal infection, transmission, shellfish safety, early warning systems

INTRODUCTION

Coronaviruses (CoVs) are a large family of viruses known to induce respiratory and gastrointestinal (GI) infection in animals and humans. These viruses are persistent in the environment (Guillier et al., 2020; Ren et al., 2020), and known to resist the (mild) food production processes routinely used to inactivate or control bacterial pathogens (Goli, 2020). Until recently, CoVs were not assumed to be highly pathogenic in humans (Zaki et al., 2012), but this perception changed after the recent Severe Acute Respiratory Syndrome CoV (SARS-CoV), Middle East Respiratory Syndrome CoV (MERS-CoV), and the current severe acute respiratory syndrome (SARS-CoV-2) outbreaks.

The most recently identified coronavirus, SARS-CoV-2, first isolated in late December 2019 among patients with severe pneumonia at Wuhan City, China (Zhu et al., 2020), revealed a significant gap in knowledge about CoVs. Since then, scientists have been trying to understand its transmission pathways and infection dynamics, and how the virus shapes the resulting pathology, the coronavirus disease (COVID-19). A significant number of scientific breakthroughs related to SARS-CoV-2 have been published over the past year, but there are still many unknows and unanswered questions, and countless others will surely arise as new data is collected, and new strains revealed.

So far, the contribution of foodborne transmission for the maintenance and recurrence of SARS-CoV-2 infection is still disputed (Amirian, 2020; Donà et al., 2020; Li et al., 2021). Such possibility, however, should be considered as an emerging risk with potential public health impact, demanding the implementation, or adaptation, of effective strategies to protect at-risk populations in the face of emerging epidemiologic data.

Shellfish are particularly relevant in such assessment. Often consumed uncooked, shellfish are a long-standing source of foodborne illness, frequently associated with foodborne outbreaks with substantial impact on human health (Jones, 2009). For instance, norovirus (NoV) accumulation by shellfish, and the ensuing risks to human health associated with shellfish consumption are well-documented (Bellou et al., 2013). Similarly, the accumulation of other infectious agents of human-associated waste sources, and its repercussion on human health, is well-reported (Fleming et al., 2014).

Facing a hypothetical foodborne transmission of COVID-19 *via* the consumption of raw shellfish, we briefly address possible reasons to consider the incorporation of SARS-CoV-2 detection strategies on regular shellfish monitoring programs and include this risk on early warning

OPEN ACCESS

Edited by:
Jose Luis Iriarte, Austral University of Chile, Chile

Reviewed by:
Soizick Le Guyader, Institut Français de Recherche pour l'Exploitation de la Mer (IFREMER), France

***Correspondence:**
Marcos Mateus
marcos.mateus@tecnico.ulisboa.pt

Specialty section:
This article was submitted to Marine Fisheries, Aquaculture and Living Resources, a section of the journal Frontiers in Marine Science

Received: *18 February 2021*
Accepted: *09 April 2021*
Published: *10 May 2021*

Citation:
Mateus M, Remondes M, Pinto L and Silva A (2021) Monitoring SARS-CoV-2 as a Microbiological Risk in Shellfish Aquaculture. Front. Mar. Sci. 8:669402. doi: 10.3389/fmars.2021.669402

systems to the aquaculture industry and public health. Our opinion is based on current knowledge about the SARS-CoV-2 and long-established facts about the role of wastewater and shellfish on the transmission of viral infections to humans (**Figure 1**).

SARS-COV-2 AND GASTROINTESTINAL FUNCTION IN HUMANS

Though the respiratory system is most severely impacted by CoVs, these viruses are found in the sweat glands, kidney, and intestinal tract, and therefore may spread *via* sweat, urine, and fecal excretion (Ding et al., 2004). In addition, their presence in the alimentary tract (Huang et al., 2021), suggests that this is an entry route for viruses present in food or water.

Information about other potential pathways of SARS-CoV-2 transmission is relatively scarce, but there is accumulating evidence in support of fecal-mediated transmission (Amirian, 2020; Cuicchi et al., 2021; Heneghan et al., 2021). SARS-CoV-2 GI tract infection has been repeatedly reported (Guan et al., 2020; Hindson, 2020; Lo et al., 2020; Mao et al., 2020; Pan et al., 2020; Xiao et al., 2020). Accordingly, viable viruses were detected in feces, implicating these as a potential source of SARS-CoV-2 transmission by fecal contamination (Wang et al., 2020). Paradoxically, some studies also infer that most of the viral particles excreted in feces are no longer infectious (Walsh et al., 2020; Senatore et al., 2021).

A recent study in children found that positive detection of SARS-CoV-2 on rectal swabs outlasts even negative nasopharyngeal testing, suggesting that the GI tract might be the primary apparatus to be infected, with higher incidence of fecal-oral transmission (Xu et al., 2020). SARS-CoV-2 was also recovered from nasal washes, saliva, urine, and feces of infected animals (ferrets) up to 8 days post-infection (Kim et al., 2020). Thus, while still poorly understood, the GI symptoms reported from the start of COVID-19 epidemic at least suggest that fecal–oral transmission of SARS-CoV-2 may occur (Yeo et al., 2020).

THE PRESENCE OF VIRUSES IN SEWAGE

NoV enter aquatic environments by contaminated overland run-off after heavy rainfall, hydraulic overload in sewage treatment plants, and combined sewer overflow (Kim et al., 2016). These routes are shared by most other pathological agents. The presence of SARS-CoV-2 in wastewater, reported worldwide, suggests that this may also be the case for this infectious agent (La Rosa et al., 2020; Mallapaty, 2020; Medema et al., 2020; Wu et al., 2020).

Early studies showed that coronaviruses rapidly become inactive in wastewater (Sherchan et al., 2020), but can remain infectious up to 4 days if contained within fecal matter (Gundy et al., 2009). Recent assessments agree with these observations, reporting that the virus can survive hours to days in untreated wastewater (Arslan et al., 2020; Orive et al., 2020; Kumar et al., 2021; Patel et al., 2021), and even much longer periods in cold climates (Bhowmick et al., 2020). Studies have reported that SARS-CoV-2 remains active for 25 days in wastewater at 5°C (Shutler et al., 2021) and can persist in wastewater at room temperature for ∼6 days (Bivins et al., 2020).

DISCUSSION

The evidence reviewed here suggests the possibility of fecal–oral transmission of SARS-CoV-2. If confirmed, the novel CoV can share foodborne infection pathways with other CoVs, and even NoV (Lopman et al., 2012; Li et al., 2021). Shellfish such as oysters can selectively accumulate NoV strains as they have human-like viral carbohydrate ligands (Le Guyader et al., 2012). If indeed this, or a similar, process is shared by SARS-CoV-2, then shellfish can potentially act as a vector for fecal-oral transmission to humans, similarly, and even concurrently, to norovirus, with the predictable devastating consequences (**Figure 1**).

Due to significant knowledge gaps, the potential role of wastewater in SARS-CoV-2 transmission has been underappreciated (Kitajima et al., 2020; Lodder and de Roda Husman, 2020), and little is known about the infective power of SARS-CoV-2 particles found in sewage waters. Respiratory droplets are the main human-to-human mechanism of transmission, but fecal shedding with environmental contamination is increasingly seen as having an important role in viral spread (Bhowmick et al., 2020; Donà et al., 2020).

Until now, the viability of SARS-CoV-2 in wastewater has not been proven (Senatore et al., 2021), and further studies are needed to investigate its fate in wastewater (Collivignarelli et al., 2020) and in natural water bodies receiving treated or untreated wastewater (Kumar et al., 2021). The WHO, for instance, assumes that it is unlikely that wastewater will become an important transmission pathway for coronaviruses like SARS-CoV-2 (WHO/UNICEF, 2020). However, ruling out such possibility at such early stage may prove disastrous, as SARS-CoV-2 remains viable for significantly longer periods in stool samples than in respiratory and serum samples. Such resilience highlights the need to strengthen the public management of sewage waters in the prevention and control of the epidemic (Zheng et al., 2020; Senatore et al., 2021).

A recent monitoring study made in several sites along the coast of France reported the absence of SARS-CoV-2 in oysters (Desdouits et al., 2021). The authors, nonetheless, do not exclude shellfish as potential agents of transmission, but highlight the need for more monitoring studies before reaching such conclusion. Food industry and regulatory agencies should take such knowledge into account, despite its preliminary stage, to regulate and implement food safety principles and practices that prevent the spread of SARS-CoV-2 *via* shellfish consumption, all the while protecting the economy and livelihood of human populations therein dependent.

Given the high infection and rapid transmission of SARS-CoV-2 (Kim et al., 2020), shellfish commerce and consumption can rapidly and effectively propagate infection over long distances, and sustain its endemic persistence. To prevent such occurrence, the following questions must necessarily be addressed and unequivocally answered as part of an integrative approach to mitigate COVID-19:

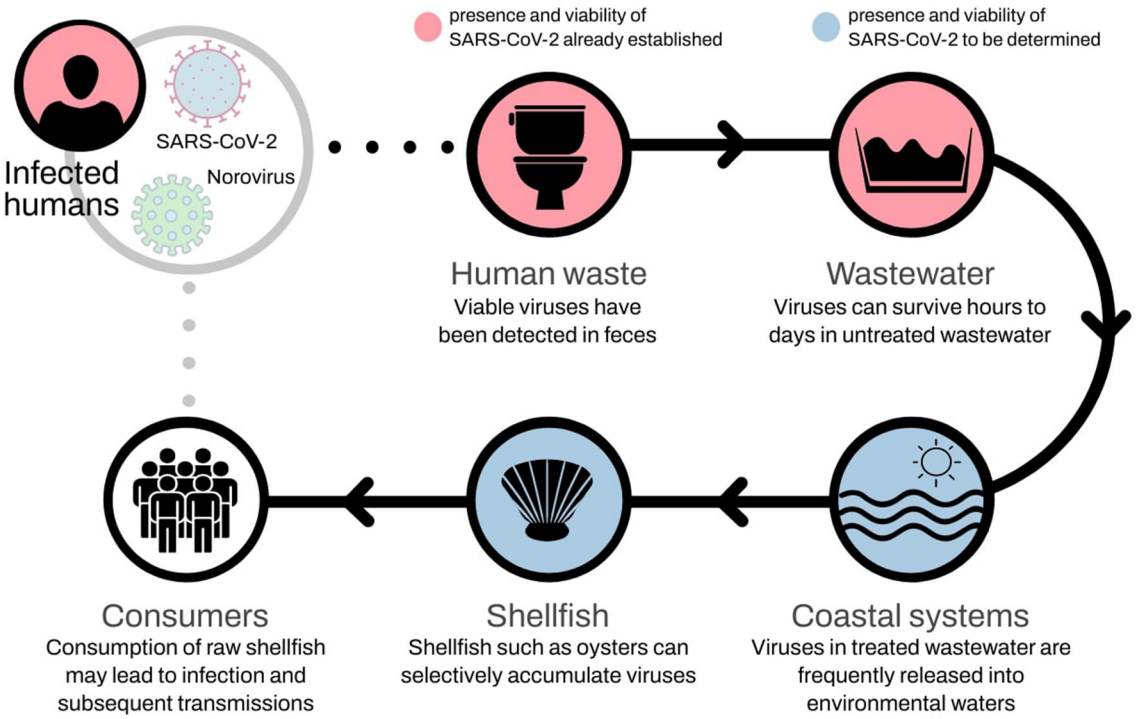

FIGURE 1 | Potential foodborne transmission of SARS-CoV-2 *via* shellfish. Such transmission route is known to occur with norovirus.

1. Is SARS-CoV-2 found in coastal waters, under the influence of urban pollution, still infectious?
2. Are shellfish production/growth conditions and practices (e.g., in oyster beds) enough to allow environmental factors such as osmotic stress in salt water, and UV radiation, to inactivate the virus?
3. Do shellfish accumulate SARS-CoV-2 as they do NoV?
4. If SARS-CoV-2 is found in shellfish:
   a. Is it still viable to infect humans (making shellfish a vector of contamination)?
   b. Is the source environmental or from being handled by infected people (good hygiene practices must be in place)?
   c. Can it be eradicated by depuration?
5. Should government or the regulatory authorities consider a temporary suspension of production and/or commercialization of shellfish before the answers to the above questions are reached?

Seafood-born infection and toxicity is presently met by effective good-practices in most developed countries. The current COVID-19 epidemic threatens to be a "game-changer" to the effect that failing to address the topics discussed here might perpetuate the threat of infection, albeit in a much smaller scale than by direct contact with infected humans, but still, one capable of triggering an outbreak of serious consequences. SARS-CoV-2 transmission *via* shellfish unfolds over multiple spatial scales, as freshly harvested products can be consumed locally, but also commercialized world-wide. Oysters pose a particular threat, as they are one of the most commercialized group of shellfish over the past few years (FAO, 2020), and they are often consumed raw.

For the time being, the possibility of transmission through the food sector is considered negligible, and its assessment is not seen as a priority by public authorities (Bilal et al., 2020; Rizou et al., 2020). However, until such hypothesis is discarded, there are reasons to consider the inclusion of SARS-CoV-2 in monitoring programs and early warning systems currently implemented in the shellfish industry. We note, nonetheless, that economic consequences may be expected if bans to shellfish harvesting and consumptions arise from such policies, impacting different sectors of activity, from artisanal shellfish harvesters, to aquaculture producers, and ultimately across all levels of shellfish industry.

Finally, the above considerations are pertinent, not just to shellfish, but also to other food sources at risk of contamination with liquid or solid human waste potentially carrying SARS-CoV-2.

AUTHOR CONTRIBUTIONS

MM and MR contributed equally to the design and development of the manuscript. LP provided insights on early warning systems for the aquaculture sector. AS contributed with expertise on monitoring programs and early warning systems for shellfish areas. LP and AS were actively involved in the manuscript preparation. All authors contributed to the article and approved the submitted version.

FUNDING

This work was supported by the Interreg Atlantic Area Operational Programme, Grant Agreement No: EAPA 182/2016 (Project PRIMROSE, https://www.shellfish-safety.eu). AS supported by Grant IPMA-BCC-2016-35 from project SNMxB-Monitor-16.02.01-FEAMP-0043. Publication fees were supported by FCT/MCTES (PIDDAC) through project LARSyS—FCT Pluriannual funding 2020–2023 (UIDB/EEA/50009/2020).

REFERENCES

Amirian, E. S. (2020). Potential fecal transmission of SARS-CoV-2: current evidence and implications for public health. *Int. J. Infect. Dis.* 95, 363–370. doi: 10.1016/j.ijid.2020.04.057

Arslan, M., Xu, B., and Gamal El-Din, M. (2020). Transmission of SARS-CoV-2 via fecal-oral and aerosols–borne routes: environmental dynamics and implications for wastewater management in underprivileged societies. *Sci. Total Environ.* 743:140709. doi: 10.1016/j.scitotenv.2020.140709

Bellou, M., Kokkinos, P., and Vantarakis, A. (2013). Shellfish-borne viral outbreaks: a systematic review. *Food Environ. Virol.* 5, 13–23. doi: 10.1007/s12560-012-9097-6

Bhowmick, G. D., Dhar, D., Nath, D., Ghangrekar, M. M., Banerjee, R., Das, S., et al. (2020). Coronavirus disease 2019 (COVID-19) outbreak: some serious consequences with urban and rural water cycle. *NPJ Clean Water* 3:32. doi: 10.1038/s41545-020-0079-1

Bilal, M., Nazir, M. S., Rasheed, T., Parra-Saldivar, R., and Iqbal, H. M. N. (2020). Water matrices as potential source of SARS-CoV-2 transmission – an overview from environmental perspective. *Case Stud. Chem. Environ. Eng.* 2:100023. doi: 10.1016/j.cscee.2020.100023

Bivins, A., Greaves, J., Fischer, R., Yinda, K. C., Ahmed, W., Kitajima, M., et al. (2020). Persistence of SARS-CoV-2 in water and wastewater. *Environ. Sci. Technol. Lett.* 7, 937–942. doi: 10.1021/acs.estlett.0c00730

Collivignarelli, M. C., Collivignarelli, C., Carnevale Miino, M., Abbà, A., Pedrazzani, R., and Bertanza, G. (2020). SARS-CoV-2 in sewer systems and connected facilities. *Process Saf. Environ. Prot.* 143, 196–203. doi: 10.1016/j.psep.2020.06.049

Cuicchi, D., Lazzarotto, T., and Poggioli, G. (2021). Fecal-oral transmission of SARS-CoV-2: review of laboratory-confirmed virus in gastrointestinal system. *Int. J. Colorectal Dis.* 36, 437–444. doi: 10.1007/s00384-020-03785-7

Desdouits, M., Piquet, J.-C., Wacrenier, C., Le Mennec, C., Parnaudeau, S., Jousse, S., et al. (2021). Can shellfish be used to monitor SARS-CoV-2 in the coastal environment? *Sci. Total Environ.* 778:146270. doi: 10.1016/j.scitotenv.2021.146270

Ding, Y., He, L., Zhang, Q., Huang, Z., Che, X., Hou, J., et al. (2004). Organ distribution of severe acute respiratory syndrome (SARS) associated coronavirus (SARS-CoV) in SARS patients: implications for pathogenesis virus transmission pathways. *J. Pathol.* 203, 622–630. doi: 10.1002/path.1560

Donà, D., Minotti, C., Costenaro, P., Da Dalt, L., and Giaquinto, C. (2020). Fecal-oral transmission of SARS-CoV-2 in children: is it time to change our approach? *Pediatr. Infect. Dis. J.* 39, e133–134. doi: 10.1097/INF.0000000000002704

FAO (2020). *FAO - Fisheries and Aquaculture Information and Statistics Branch*. Available at: http://www.fao.org/fishery/statistics/en (accessed May 7, 2020).

Fleming, L. E., McDonough, N., Austen, M., Mee, L., Moore, M., Hess, P., et al. (2014). Oceans and human health: a rising tide of challenges and opportunities for Europe. *Mar. Environ. Res.* 99, 16–19. doi: 10.1016/j.marenvres.2014.05.010

Goli, M. (2020). Review of novel human β-coronavirus (2019-nCoV or SARS-CoV-2) from the food industry perspective—appropriate approaches to food production technology. *Food Sci. Nutr.* 8, 5228–5237. doi: 10.1002/fsn3.1892

Guan, W., Ni, Z., Hu, Y., Liang, W., Ou, C., He, J., et al. (2020). Clinical characteristics of coronavirus disease 2019 in China. *N. Engl. J. Med.* 382, 1708–1720. doi: 10.1056/NEJMoa2002032

Guillier, L., Martin-Latil, S., Chaix, E., Thébault, A., Pavio, N., Le Poder, S., et al. (2020). Modeling the inactivation of viruses from the coronaviridae family in response to temperature and relative humidity in suspensions or on surfaces. *Appl. Environ. Microbiol.* 86, e01244–e01220. doi: 10.1128/AEM.01244-20

Gundy, P. M., Gerba, C. P., and Pepper, I. L. (2009). Survival of coronaviruses in water and wastewater. *Food Environ. Virol.* 1:10. doi: 10.1007/s12560-008-9001-6

Heneghan, C., Spencer, E. A., Brassey, J., and Jefferson, T. (2021). SARS-CoV-2 and the role of orofecal transmission: systematic review. *F1000Research* 10:231. doi: 10.1101/2020.08.04.20168054

Hindson, J. (2020). COVID-19: faecal–oral transmission? *Nat. Rev. Gastroenterol. Hepatol.* 17:259. doi: 10.1038/s41575-020-0295-7

Huang, N., Pérez, P., Kato, T., Mikami, Y., Okuda, K., Gilmore, R. C., et al. (2021). SARS-CoV-2 infection of the oral cavity and saliva. *Nat. Med.* doi: 10.1038/s41591-021-01296-8. [Epub ahead of print].

Jones, S. (2009). "1 - Microbial contamination and shellfish safety," in *Woodhead Publishing Series in Food Science, Technology and Nutrition*, eds S. E. Shumway and G. E. Rodrick (Cambridge: Woodhead Publishing), 3–42.

Kim, M. S., Koo, E. S., Choi, Y. S., Kim, J. Y., Yoo, C. H., Yoon, H. J., et al. (2016). Distribution of human norovirus in the coastal waters of South Korea. *PLoS ONE* 11:e0163800. doi: 10.1371/journal.pone.0163800

Kim, Y. I., Kim, S. G., Kim, S. M., Kim, E. H., Park, S. J., Yu, K. M., et al. (2020). Infection and rapid transmission of SARS-CoV-2 in ferrets. *Cell Host Microbe* 27, 704–709. doi: 10.1016/j.chom.2020.03.023

Kitajima, M., Ahmed, W., Bibby, K., Carducci, A., Gerba, C. P., Hamilton, K. A., et al. (2020). SARS-CoV-2 in wastewater: state of the knowledge and research needs. *Sci. Total Environ.* 739:139076. doi: 10.1016/j.scitotenv.2020.139076

Kumar, M., Alamin, M., Kuroda, K., Dhangar, K., Hata, A., Yamaguchi, H., et al. (2021). Potential discharge, attenuation and exposure risk of SARS-CoV-2 in natural water bodies receiving treated wastewater. *NPJ Clean Water* 4:8. doi: 10.1038/s41545-021-00098-2

La Rosa, G., Iaconelli, M., Mancini, P., Bonanno Ferraro, G., Veneri, C., Bonadonna, L., et al. (2020). First detection of SARS-CoV-2 in untreated wastewaters in Italy. *Sci. Total Environ.* 736:139652. doi: 10.1016/j.scitotenv.2020.139652

Le Guyader, F. S., Atmar, R. L., and Le Pendu, J. (2012). Transmission of viruses through shellfish: when specific ligands come into play. *Curr. Opin. Virol.* 2, 103–110. doi: 10.1016/j.coviro.2011.10.029

Li, D., Zhao, M. Y., and Hsern, M. T. T. (2021). What makes a foodborne virus: comparison between coronaviruses with human noroviruses. *Curr. Opin. Food Sci.* 42, 1–7. doi: 10.1016/j.cofs.2020.04.011

Lo, I. L., Lio, C. F., Cheong, H. H., Lei, C. I., Cheong, T. H., Zhong, X., et al. (2020). Evaluation of SARS-CoV-2 RNA shedding in clinical specimens and clinical characteristics of 10 patients with COVID-19 in Macau. *Int. J. Biol. Sci.* 16, 1698–1707. doi: 10.7150/ijbs.45357

Lodder, W., and de Roda Husman, A. M. (2020). SARS-CoV-2 in wastewater: potential health risk, but also data source. *Lancet Gastroenterol. Hepatol.* 1253:30087. doi: 10.1016/S2468-1253(20)30087-X

Lopman, B., Gastañaduy, P., Park, G. W., Hall, A. J., Parashar, U. D., and Vinjé, J. (2012). Environmental transmission of norovirus gastroenteritis. *Curr. Opin. Virol.* 2, 96–102. doi: 10.1016/j.coviro.2011.11.005

Mallapaty, S. (2020). How sewage could reveal true scale of coronavirus outbreak. *Nature* 580, 176–177. doi: 10.1038/d41586-020-00973-x

Mao, R., Liang, J., Shen, J., Ghosh, S., Zhu, L. R., Yang, H., et al. (2020). Implications of COVID-19 for patients with pre-existing digestive diseases. *Lancet Gastroenterol. Hepatol.* 5, 426–428. doi: 10.1016/S2468-1253(20)30076-5

Medema, G., Heijnen, L., Elsinga, G., Italiaander, R., and Brouwer, A. (2020). Presence of SARS-coronavirus-2 RNA in sewage and correlation with reported COVID-19 prevalence in the early stage of the epidemic in The Netherlands. *Environ. Sci. Technol. Lett.* 7, 511–516. doi: 10.1021/acs.estlett.0c00357

Orive, G., Lertxundi, U., and Barcelo, D. (2020). Early SARS-CoV-2 outbreak detection by sewage-based epidemiology. *Sci. Total Environ.* 732:139298. doi: 10.1016/j.scitotenv.2020.139298

Pan, L., Mu, M., Yang, P., Sun, Y., Wang, R., Yan, J., et al. (2020). Clinical characteristics of COVID-19 patients with digestive symptoms in Hubei, China:

a descriptive, cross-sectional, multicenter study. *Am. J. Gastroenterol.* 11, 766–773. doi: 10.14309/ajg.0000000000000620

Patel, M., Chaubey, A. K., Pittman, C. U., Mlsna, T., and Mohan, D. (2021). Coronavirus (SARS-CoV-2) in the environment: occurrence, persistence, analysis in aquatic systems and possible management. *Sci. Total Environ.* 765:142698. doi: 10.1016/j.scitotenv.2020.142698

Ren, S.-Y., Wang, W.-B., Hao, Y.-G., Zhang, H.-R., Wang, Z.-C., Chen, Y.-L., et al. (2020). Stability and infectivity of coronaviruses in inanimate environments. *World J. Clin. Cases* 8, 1391–1399. doi: 10.12998/wjcc.v8.i8.1391

Rizou, M., Galanakis, I. M., Aldawoud, T. M. S., and Galanakis, C. M. (2020). Safety of foods, food supply chain and environment within the COVID-19 pandemic. *Trends Food Sci. Technol.* 102, 293–299. doi: 10.1016/j.tifs.2020.06.008

Senatore, V., Zarra, T., Buonerba, A., Ho, K., Shadi, C., and Gregory, W. H. (2021). Indoor versus outdoor transmission of SARS - COV - 2 : environmental factors in virus spread and underestimated sources of risk. *Euro Mediterranean J. Environ. Integr.* 6:30. doi: 10.1007/s41207-021-00243-w

Sherchan, S. P., Shahin, S., Ward, L. M., Tandukar, S., Aw, T. G., Schmitz, B., et al. (2020). First detection of SARS-CoV-2 RNA in wastewater in North America: a study in Louisiana, USA. *Sci. Total Environ.* 743:140621. doi: 10.1016/j.scitotenv.2020.140621

Shutler, J. D., Zaraska, K., Holding, T., Machnik, M., Uppuluri, K., Ashton, I. G. C., et al. (2021). Rapid Assessment of SARS-CoV-2 Transmission Risk for Fecally Contaminated River Water. *ACS EST Water*. 1, 949–957. doi: 10.1021/acsestwater.0c00246

Walsh, K. A., Jordan, K., Clyne, B., Rohde, D., Drummond, L., Byrne, P., et al. (2020). SARS-CoV-2 detection, viral load and infectivity over the course of an infection. *J. Infect.* 81, 357–371. doi: 10.1016/j.jinf.2020.06.067

Wang, W., Xu, Y., Gao, R., Lu, R., Han, K., Wu, G., et al. (2020). Detection of SARS-CoV-2 in different types of clinical specimens. *JAMA* 323, 1843–1844. doi: 10.1001/jama.2020.3786

WHO/UNICEF (2020). *Water, Sanitation, Hygiene and Waste Management for the COVID-19 Virus*.

Wu, F., Xiao, A., Zhang, J., Gu, X., Lee, W. L., Kauffman, K., et al. (2020). SARS-CoV-2 titers in wastewater are higher than expected from clinically confirmed cases. *mSystems* 5:e00614-20. doi: 10.1128/mSystems.00614-20

Xiao, F., Tang, M., Zheng, X., Liu, Y., Li, X., and Shan, H. (2020). Evidence for gastrointestinal infection of SARS-CoV-2. *Gastroenterology* 158, 1831–1833.e3. doi: 10.1053/j.gastro.2020.02.055

Xu, Y., Li, X., Zhu, B., Liang, H., Fang, C., Gong, Y., et al. (2020). Characteristics of pediatric SARS-CoV-2 infection and potential evidence for persistent fecal viral shedding. *Nat. Med.* 26, 502–505. doi: 10.1038/s41591-020-0817-4

Yeo, C., Kaushal, S., and Yeo, D. (2020). Enteric involvement of coronaviruses: is faecal–oral transmission of SARS-CoV-2 possible? *Lancet Gastroenterol. Hepatol.* 5, 335–337. doi: 10.1016/S2468-1253(20)30048-0

Zaki, A. M., van Boheemen, S., Bestebroer, T. M., Osterhaus, A. D. M. E., and Fouchier, R. A. M. (2012). Isolation of a novel coronavirus from a man with pneumonia in Saudi Arabia. *N. Engl. J. Med.* 367, 1814–1820. doi: 10.1056/NEJMoa1211721

Zheng, S., Fan, J., Yu, F., Feng, B., Lou, B., Zou, Q., et al. (2020). Viral load dynamics and disease severity in patients infected with SARS-CoV-2 in Zhejiang province, China, January-March 2020: retrospective cohort study. *BMJ* 369, m1443. doi: 10.1136/bmj.m1443

Zhu, N., Zhang, D., Wang, W., Li, X., Yang, B., Song, J., et al. (2020). A novel coronavirus from patients with pneumonia in China, 2019. *N. Engl. J. Med.* 382, 727–733. doi: 10.1056/NEJMoa2001017

Conflict of Interest: The authors declare that the research was conducted in the absence of any commercial or financial relationships that could be construed as a potential conflict of interest.

frontiers in Marine Science

REVIEW
published: 10 June 2021
doi: 10.3389/fmars.2021.666583

Current Status of Forecasting Toxic Harmful Algae for the North-East Atlantic Shellfish Aquaculture Industry

Jose A. Fernandes-Salvador[1], Keith Davidson[2], Marc Sourisseau[3], Marta Revilla[1], Wiebke Schmidt[4,5], Dave Clarke[4], Peter I. Miller[6], Paola Arce[2], Raúl Fernández[7], Luz Maman[7], Alexandra Silva[8], Callum Whyte[2], Maria Mateo[1], Patricia Neira[4], Marcos Mateus[9], Manuel Ruiz-Villarreal[10], Luis Ferrer[1] and Joe Silke[4]*

[1] AZTI, Marine Research, Basque Research and Technology Alliance, Pasaia, Spain, [2] Scottish Association for Marine Science, Scottish Marine Institute, Oban, United Kingdom, [3] French Research Institute for Exploitation of the Sea, Ifremer DYNECO PELAGOS, Plouzané, France, [4] Marine Institute, Galway, Ireland, [5] Environment Agency, Chief Scientist's Group, Bristol, United Kingdom, [6] Plymouth Marine Laboratory, Plymouth, United Kingdom, [7] Laboratorio de Control de Calidad de los Recursos Pesqueros, Agencia de Gestión Agraria y Pesquera de Andalucía, Consejería de Agricultura, Ganadería, Pesca y Desarrollo Sostenible, Junta de Andalucía, Cartaya, Spain, [8] Phytoplankton Laboratory, Division of Oceanography and Marine Environment, Instituto Português do Mar e da Atmosfera, Lisbon, Portugal, [9] MARETEC – Marine, Environment and Technology Centre, LARSyS, Instituto Superior Técnico, Universidade de Lisboa, Lisbon, Portugal, [10] Centro Oceanográfico de A Coruña, Instituto Español de Oceanografía (IEO,CSIC), A Coruña, Spain

Across the European Atlantic Arc (Scotland, Ireland, England, France, Spain, and Portugal) the shellfish aquaculture industry is dominated by the production of mussels, followed by oysters and clams. A range of spatially and temporally variable harmful algal bloom species (HABs) impact the industry through their production of biotoxins that accumulate and concentrate in shellfish flesh, which negatively impact the health of consumers through consumption. Regulatory monitoring of harmful cells in the water column and toxin concentrations within shellfish flesh are currently the main means of warning of elevated toxin events in bivalves, with harvesting being suspended when toxicity is elevated above EU regulatory limits. However, while such an approach is generally successful in safeguarding human health, it does not provide the early warning that is needed to support business planning and harvesting by the aquaculture industry. To address this issue, a proliferation of web portals have been developed to make monitoring data widely accessible. These systems are now transitioning from "nowcasts" to operational Early Warning Systems (EWS) to better mitigate against HAB-generated harmful effects. To achieve this, EWS are incorporating a range of environmental data parameters and developing varied forecasting approaches. For example, EWS are increasingly utilizing satellite data and the results of oceanographic modeling to identify and predict the behavior of HABs. Modeling demonstrates that some HABs can be advected significant distances before impacting aquaculture sites. Traffic light indices are being developed to provide users with an easily interpreted

OPEN ACCESS

Edited by:
Jose Luis Iriarte, Austral University of Chile, Chile

Reviewed by:
Bernd Krock, Alfred Wegener Institute, Helmholtz Centre for Polar and Marine Research (AWI), Germany
Eileen Bresnan, Marine Scotland, United Kingdom
Grant Colborne Pitcher, Department of Agriculture, Forestry and Fisheries, South Africa

***Correspondence:**
Jose A. Fernandes-Salvador
jfernandes@azti.es

Specialty section:
This article was submitted to Marine Fisheries, Aquaculture and Living Resources, a section of the journal Frontiers in Marine Science

Received: *10 February 2021*
Accepted: *10 May 2021*
Published: *10 June 2021*

Citation:
Fernandes-Salvador JA, Davidson K, Sourisseau M, Revilla M, Schmidt W, Clarke D, Miller PI, Arce P, Fernández R, Maman L, Silva A, Whyte C, Mateo M, Neira P, Mateus M, Ruiz-Villarreal M, Ferrer L and Silke J (2021) Current Status of Forecasting Toxic Harmful Algae for the North-East Atlantic Shellfish Aquaculture Industry. Front. Mar. Sci. 8:666583. doi: 10.3389/fmars.2021.666583

assessment of HAB and biotoxin risk, and expert interpretation of these multiple data streams is being used to assess risk into the future. Proof-of-concept EWS are being developed to combine model information with *in situ* data, in some cases using machine learning-based approaches. This article: (1) reviews HAB and biotoxin issues relevant to shellfish aquaculture in the European Atlantic Arc (Scotland, Ireland, England, France, Spain, and Portugal; (2) evaluates the current status of HAB events and EWS in the region; and (3) evaluates the potential of further improving these EWS though multi-disciplinary approaches combining heterogeneous sources of information.

Keywords: modeling, machine learning, toxins, phytoplankton, food production, short-term, regulation, early warning systems

INTRODUCTION

Phytoplankton provide key ecosystem services to humans by providing food for marine life, oxygen and sequestering CO_2 (Billett et al., 1983; Smetacek, 1999; Irigoien et al., 2004). However, some naturally occurring phytoplankton species can produce a range of marine biotoxins that accumulate in shellfish tissues through filter feeding (Vale et al., 2008; Wang, 2008). Thus, blooms of these harmful algal species (HABs) can negatively impact fisheries and aquaculture (Smayda, 1990; Berdalet et al., 2016; Sanseverino et al., 2016; FAO, 2018). The risk of intoxication causes significant economic losses for the aquaculture industry due to the temporary suspension of harvesting when toxin concentrations exceed the permissible regulatory limits as laid down in regulation EU853/2004 (Rodríguez-Rodríguez et al., 2011; Mardones et al., 2020; Martino et al., 2020). These temporary suspensions in harvesting cannot be prevented, but Early Warning Systems (EWS), such as bulletins issued to local harvesters to warn them of upcoming HAB events, aim to forecast their occurrence and reduce their socio-economic impact. Existing EWS have focused on some of the mechanisms/conditions that trigger the onset of blooms (e.g., nutrient availability) (Sverdrup, 1953), their transport (Farrell et al., 2012; Fehling et al., 2012; Whyte et al., 2014), and the conditions that favor the different functional groups of phytoplankton (Glibert et al., 2014; Wyatt, 2014). However, an EWS framework requires refinement to forecast the occurrence of harmful/toxic species affecting these regions. Predicting which species from a functional group will dominate, and where and when they will bloom presents major challenges (Huisman and Weissing, 1999).

The North-eastern Atlantic (NEA) region is heterogeneous in terms of which blooms are problematic and their associated triggering conditions. For example, upwelling conditions along the Spanish and Portuguese coasts can cause the rapid onset of HAB events that impact local shellfish harvesting sites (Díaz et al., 2016). Stratified (Raine, 2014), mixed (Gowen et al., 2012), and frontal water masses (Simpson et al., 1979) all exist within the Atlantic areas providing contrasting conditions for HAB development (Rathaille and Raine, 2011; Berdalet et al., 2017; Paterson et al., 2017). Early instances of EWS have focused mainly on detecting blooms, sometimes without considering whether the algae are actually producing toxins or how the bio-accumulation of toxins within shellfish tissues may result in harmful impacts at low cell densities (Hallegraeff, 2003; Davidson et al., 2011).

An improved ability to forecast HAB events would result in a significant benefit for the aquaculture industry. The potential to develop early warning systems has for a long time been a goal of HAB science, with early attempts to achieve this in European waters being discussed by Maguire et al. (2016). The EU shellfish hygiene directives require Atlantic Area countries to operate monitoring programs for the presence of harmful algae and shellfish biotoxins to ensure shellfish safety. In practice, monitoring methodology varies by country (Anderson, 1998) and is designed to protect human health rather than the economic viability of the aquaculture industry. However, in all cases these programs provide a "now-cast" upon which more sophisticated remote sensing, modeling or expert interpretation-based risk assessment or forecast systems can be built (Davidson et al., 2016).

Shellfish production is an important industry across the European Atlantic Arc, providing both healthy food and important economic support for remote family and small businesses in rural coastal areas (Munro and Wallace, 2018; Mardones et al., 2020). The distribution and effects of HABs in combination with other environmental and economic threats has reduced European shellfish production over the last two decades (Avdelas et al., 2021). HABs are sometimes associated with large-scale marine fish mortality events but are more frequently associated with various types of shellfish poisoning in humans (Sanseverino et al., 2016; Bresnan et al., 2021). The significant economic impact of shellfish biotoxins are reviewed by Mardones et al. (2020), with Martino et al. (2020) demonstrating that the harmful dinoflagellate *Dinophysis* and its toxins alone reduce shellfish production in Scotland by 15% per annum. Shellfish producers are not allowed to harvest and sell their product until it is deemed fit for human consumption. This can result in significant economic losses for the farmers (Rodríguez-Rodríguez et al., 2011; LeBihan et al., 2019; Theodorou et al., 2020; Karlson et al., 2021).

In order to address the challenges and potential benefits of HAB and biotoxin EWS we must first understand the shellfish aquaculture industry in this region. Scotland, England, Ireland, France, Portugal, and Spain are the main shellfish aquaculture

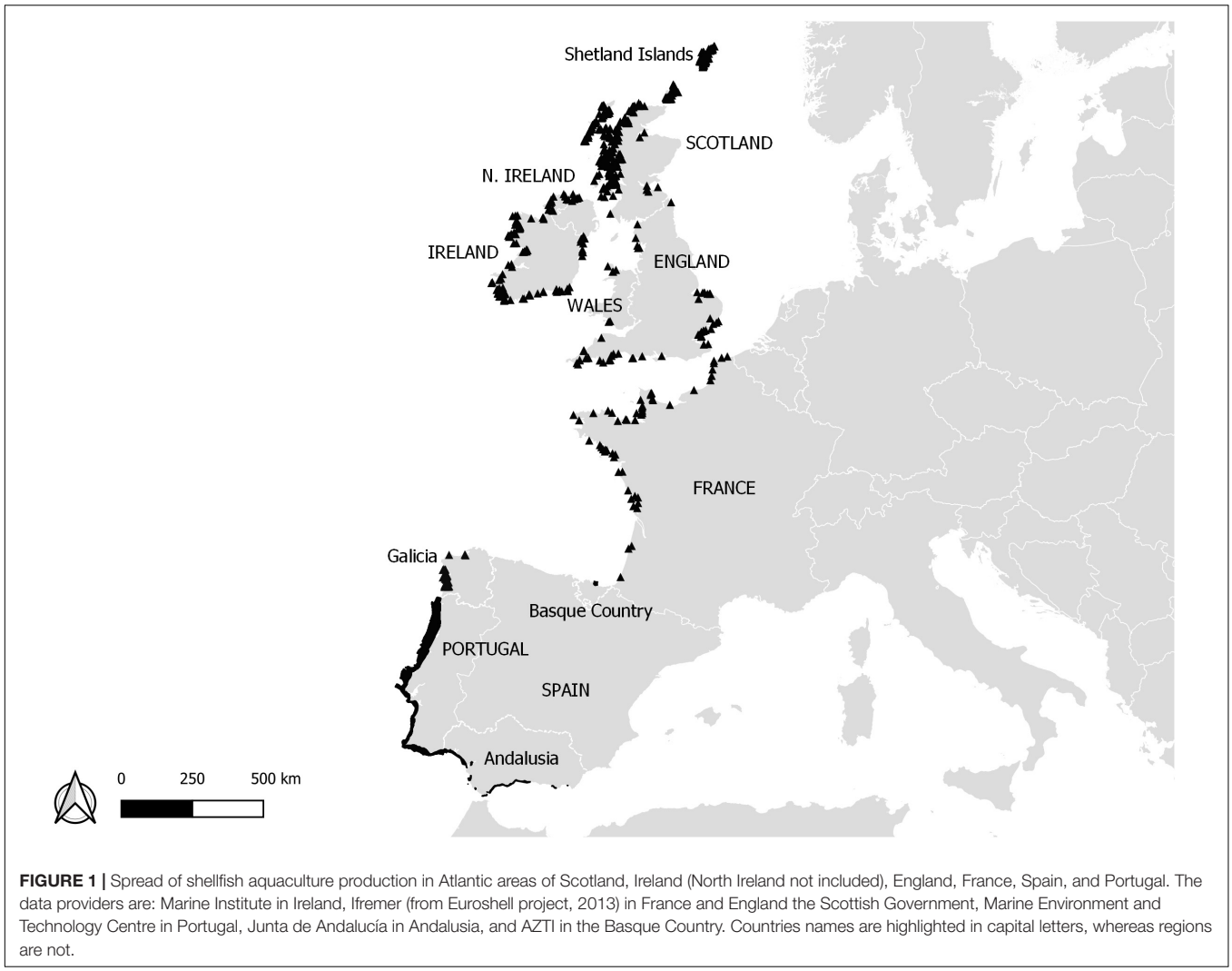

FIGURE 1 | Spread of shellfish aquaculture production in Atlantic areas of Scotland, Ireland (North Ireland not included), England, France, Spain, and Portugal. The data providers are: Marine Institute in Ireland, Ifremer (from Euroshell project, 2013) in France and England the Scottish Government, Marine Environment and Technology Centre in Portugal, Junta de Andalucía in Andalusia, and AZTI in the Basque Country. Countries names are highlighted in capital letters, whereas regions are not.

producers (FAO, 2019) in the NEA regions (**Figure 1**). Pacific oysters (*Crassostrea gigas*) and blue mussels (Atlantic *Mytilus edulis* and Mediterranean *Mytilus galloprovincialis*) are the dominant shellfish aquaculture species in terms of production volume, although other species have high economic value such as native oysters (*Ostrea edulis*), and scallops (*Aequipecten opercularis* and *Pecten maximus*). As the latitude decreases other bivalve species start to gain greater importance such as *Spisula* spp. and *Ensis* spp. in Ireland or *Ruditapes philippinarum* in France. Clams and cockles dominate in southern countries of the NEA arc (Portugal and South Spain) with a high diversity of species (*Ruditapes* spp., *Chamelea gallina*, *Donax trunculus*, *Callista chione,* and *Acanthocardia tuberculata*).

Scottish production primarily occurs in the fjordic sea lochs that are typical of its west coast and islands and is dominated by mussels followed by Pacific oysters (Munro and Wallace, 2018). The value of the industry in 2017 was estimated at £12.4 million, with Atlantic mussels contributing £10.1m (8,232 tons) and Pacific oysters £2.0m. Production is regionally variable, and the northerly Shetland Islands accounted for ∼80% of the total. In **England and Wales** cultured shellfish species are primarily mussels and Pacific and native oysters (Hambrey and Evans, 2016; Defra, 2019). Besides these, wild species Queen scallop (*Aequipecten opercularis*) and Scallop (*Pecten maximus*) are harvested by dredging. Mussels and Pacific oysters dominate English production, and mussels in Wales (Ellis et al., 2015). In 2020 the **Irish** shellfish aquaculture industry was worth an estimated total of €51 million with an output of 24,000 tons. There is diverse variety of marine bivalve molluscan species produced from 97 production areas around the coast. mainly mussels, worth €11 million through both rope longline (10,300 tons) and bottom cultivation (4,400 tons) as well as Pacific and native oysters worth €37 million, with a smaller production of clam species (*Spisula solida*/*Venerupis* spp.). Some areas along the east and west coasts concentrate on dredging for razor clams (*Ensis siliqua*/*magnus*). Dredging of scallops occurs mainly on the southwest and west coasts, however, a large number dredged from the United Kingdom and French coastlines

are landed in Ireland. In **France**, shellfish farming is mainly represented by Pacific oysters and mussels, although scallop and Manila clam *Tapes philippinarum* from the Atlantic coastline also contribute significantly to the overall production. On the **Basque Coast (Spain)**, at the south-eastern part of the Bay of Biscay mussel farming is in its infancy. In contrast, **Galicia** is an area of intensive mussel (*Mytilus galloprovincialis*) aquaculture, approx. 250,000T per year. More than 90% of all mussels in Spain are produced in Galicia on 3,350 rafts operated by 2,300 families (estimates from 2012). Galician farmers harvest from natural beds and cultured bivalves (clams, cockles, scallops). The socio-economic importance of these activities in Galicia is very high. In **Andalusia**, shellfish are mainly harvested from the wild, principally clams, and cockles (*Chamelea gallina, Donax trunculus, Callista chione,* and *Acanthocardia tuberculata*). Aquaculture production focuses on mussels (*Mytilus galloprovincialis*), oysters (*Crassostrea gigas* and *Crassostrea angulata*), and some clam species (*Ruditapes decussatus* and *Ruditapes philippinarum*) and is undertaken in the marshes of large rivers and estuaries. Since 2000, mussel aquaculture has been undertaken in the open sea.

In this article, we first discuss the regional occurrence of toxin-producing HABs and their environmental drivers. We then consider early warning approaches to best mitigate HAB impacts for both producers and consumers of shellfish in the NEA countries, noting that the EWS must adapt to regional heterogeneity in the ecology of HABs and the structure of the aquaculture industry.

MONITORING OF MARINE BIOTOXIN OCCURRENCE AND CAUSATIVE ORGANISMS

Regulations to Avoid Human Poisoning

There are several EU food safety legislative requirements laid down for the production, harvesting and analysis for contaminants of live bivalve molluscs from classified production areas for human consumption. Specifically, EU regulations (853/2004, 854/2004, and 627/2019) specify the maximum permissible regulatory limits for the presence of marine biotoxins (**Table 1**). In compliance with the regulations, EU member states monitor for the presence and quantify the concentration of marine biotoxins in shellfish from classified production areas. These areas have specific sampling sites known as "representative monitoring points" (RMPs) which are routinely sampled all year round (weekly to monthly). The monitoring frequency may be increased: following the onset of, and throughout a toxic event; during identified high-risk periods; during the presence of causative toxigenic phytoplankton species in the water column; or during the occurrence of biotoxins in adjacent shellfish areas. When the regulatory marine biotoxin concentrations are exceeded in a particular shellfish species, this results in a mandatory closure for the harvesting of the affected shellfish species in the area.

According to Regulation (EC) No 854/2004 (Annex II, Chapter II, B, 7) and Articles 59 and 61 in EC 627/2019, plankton samples for regulatory monitoring purposes are to be

TABLE 1 | Summary of toxins typically analyzed in Europe with the analytical methods and the regulatory limits (maximum quantities allowed in bivalve molluscs placed on the market).

Risk for humans	Reference methods	Lipophilic toxins[a]	Analytes	Regulatory limits[b]	Units
Amnesic shellfish poisoning (ASP)	HPLC-UV	–	Domoic acid (DA)	20	mg DA kg^{-1}
Paralytic shellfish poisoning (PSP)	HPLC-FLD	–	Saxitoxin (STX) and its analogs	800	μg STX diHCl eq. kg^{-1}
Diarrheic shellfish poisoning (DSP)	LC-MS/MS	Okadaic acid (OA) group	OA	160[c]	μg OA eq. kg^{-1}
			DTX1		
			DTX2		
			DTX3		
Not-completely known		Pectenotoxin (PTX) group	PTX1		
			PTX2		
Azaspiracid shellfish poisoning (AZP)		Azaspiracid (AZA) group	AZA1	160[d]	μg AZA eq. kg^{-1}
			AZA2		
			AZA3		
Cardiotoxicity		Yessotoxin (YTX) group	YTX	3.75[e]	mg YTX eq. kg^{-1}
			homo-YTX		
			45-hydroxy-YTX		
			45-hydroxyhomo-YTX		

Methods: HPLC, High Performance Liquid Chromatography; UV, Ultraviolet detection; FLD, Fluorescence detection; LC-MS/MS, Liquid Chromatography-Mass Spectrometry. Toxins: DA, Domoic Acid; STX, Saxitoxin; OA, Okadaic Acid; DTX, Dinophysistoxin; PTX, Pectenotoxin; AZA, Azaspiracid; YTX, Yessotoxin. These methods are similar across regions, but other internationally recognised validated methods may be applied (EU 627/2019).

[a] *Until December 2014 lipophilic toxins could be analyzed together, by means of mouse bioassay.*

[b] *European Legislation: CE 853/2004; UE 15/2011; EU 786/2013, and EU 627/2019.*

[c] *Sum of OA, dinophysistoxins (DTXs), and PTXs.*

[d] *Sum of AZAs.*

[e] *Sum of YTXs.*

representative of the water column and to provide information on the presence of toxic species as well as population trends. For shallow stations (depth <5 m), a water sample taken using a bucket, oceanographic bottle or a pole sampler is considered suitable for quantification purposes. Sampling should avoid the disturbance of the bottom sediment. In locations where depths are >5 m depth sampling should be integrated by means of a hose (Lindahl, 1986), which is considered more suitable for species that present heterogeneous vertical distribution (e.g., Raine, 2014). Net sampling (10–20 μm) can be used to take an integrated sample of the water column, pulling it from the bottom up to the surface. The methodology for hose and bottle sampling, and net hauls is described in the European Standard EN 15972:2011. For identification and quantification of toxin-producing phytoplankton, there is no specific method required by EU legislation, although an EU NRL best practice guide is due to be published soon[1]. Post collection phytoplankton are enumerated by microscopy, with inverted microscopy after sedimentation of fixed samples (Utermöhl, 1958) being the widely used standard. The Utermöhl procedure is described in the European Standard En 15204, 2006. Monitoring toxigenic phytoplankton potentially provides an indication and early insight of the potential subsequent onset of toxification of shellfish above regulatory levels (Davidson et al., 2016; Maguire et al., 2016; Botelho et al., 2019). The abundance of harmful phytoplankton generally follows a seasonal cycle with the greatest abundance in spring and summer, and to a lesser extent in autumn months (Coates et al., 2018).

Main Groups of Poisoning Syndromes and Associated Toxins

Recently, Bresnan et al., 2021 used the IOC-ICES-PICES Harmful Algal Event Database (HAEDAT) to describe the diversity of harmful algal events along the Atlantic margin of Europe from 1987 to 2018 (**Figure 2**). Closures of shellfish production areas are mainly due to the regular annual occurrence of Diarrhetic Shellfish Toxins (DSTs) with protracted closure periods typical over the summer months. Paralytic Shellfish Toxins (PSTs) and Amnesic Shellfish Toxins (ASTs) occur less frequently and usually result in shorter closure periods. The occurrence of Azaspiracid toxins (AZA's), in the arc area, although observed from the Southwest along the West and through to the Northwest coast of Ireland, is not a regular occurrence in the region. The length of closure periods associated with AZAs is also extremely variable. Most events recorded were due to DSTs produced by species of the *Dinophysis acuminata* complex and *Dinophysis acuta*. Their seasonal patterns have been thoroughly described in European Atlantic waters (e.g., Reguera et al., 2012; Batifoulier et al., 2013; Fernández et al., 2019; Salas and Clarke, 2019). However, there is strong interannual variability in the timing and duration of shellfishery closures, which can respond to physical factors such as temperature, stratification and water circulation. Therefore, four main poisoning syndromes (DSP, AZ, ASP, and PSP) and group of associated toxins (DST, AZA, AST, and PST) have been identified as most problematic to the shellfish industry in the European Atlantic Arc countries (**Figure 2**). These are introduced in the following paragraphs in order from the greatest to least concern. **Table 2** shows a more comprehensive summary of syndromes and associated causative species; for an exhaustive review see Bresnan et al. (2021).

DSP – Diarrhetic Shellfish Poisoning; **DST** – Diarrhetic Shellfish Toxins: *Dinophysis* spp. are common in European waters where cell densities are highest in summer and generally absent or below the detection threshold in the winter months (November to February). Blooms are thought to mainly develop in open waters, possibly at frontal regions and then be advected to coastal aquaculture sites (Delmas et al., 1993; Batifoulier et al., 2013; Whyte et al., 2014; Raine et al., 2016). In Scotland, early season blooms are typically related to *D. acuminata*, whereas occasional late summer blooms are related to *D. acuta* (Swan et al., 2018). Recently Paterson et al. (2017) demonstrated the potential for a frontal region to limit the transport of a *D. acuta* bloom, preventing it from significantly impacting aquaculture sites in Loch Fyne. In Ireland, *D. acuminata* starts to appear from late May, and usually peaks in late June–July. Similar to Scotland *D. acuta* starts to appear in Irish waters from June/July onward and tends to peak later in the summer during August (Salas and Clarke, 2019) and can result in prolonged closure periods for mussel harvesting. Additional events can occur in September/October with occasional winter closures as observed in 2012–2013 (Clarke, 2020). In France, *Dinophysis* spp. are also responsible for the highest number of closure periods, the main causative species being *D. acuminata*, *Dinophysis sacculus*, *D. acuta,* and *Dinophysis caudata*. *Dinophysis* blooms occur from April to October, but start later in the English Channel when compared- to the south in the Bay of Biscay. In Spanish Galician waters, *D. acuminata* occur every year, although there is strong interannual variability in the duration of the closures related to this species (Reguera et al., 2012; Moita et al., 2016). In the autumn transition, from upwelling to downwelling conditions at the end of summer, blooms of *D. acuta* appear in some years (Díaz et al., 2016, 2019; Ruiz-Villarreal et al., 2016). A recent review of 30 years data show that there has been no increase in frequency or intensity of *D. acuta* in Galician Rias (Díaz et al., 2016). *Dinophysis ovum*, *D. sacculus,* and *Dinophysis fortii* (with a preference for mild and warm temperatures) are also common in the south of Spain and Portugal. In Spanish Andalusian waters, the *Dinophysis acuminata* complex is present most of the year, but concentrations are seasonal with two or three peaks occurring in spring and autumn (Fernández et al., 2019). *Dinophysis acuta* reaches peak concentrations in summer and the beginning of autumn (Fernández et al., 2019). In Portugal, *Dinophysis* blooms are observed from April to October (spring to autumn) during the upwelling season and particularly during the autumn transition, associated with periods of thermohaline stratification between moderate pulses of upwelling or during downwelling events (Moita et al., 2006; Trainer et al., 2010; Reguera et al., 2012, 2014).

PSP – Paralytic Shellfish Poisoning; **PST** – Paralytic Shellfish Toxins: Several members of this genus *Alexandrium* contain the

[1]Monitoring of Toxin-producing Phytoplankton in Bivalve Mollusc Harvesting Areas; Guide to Good Practice: Technical Application; and, EU Working Group on Toxin-producing Phytoplankton Monitoring in Bivalve Mollusc Harvesting Areas.

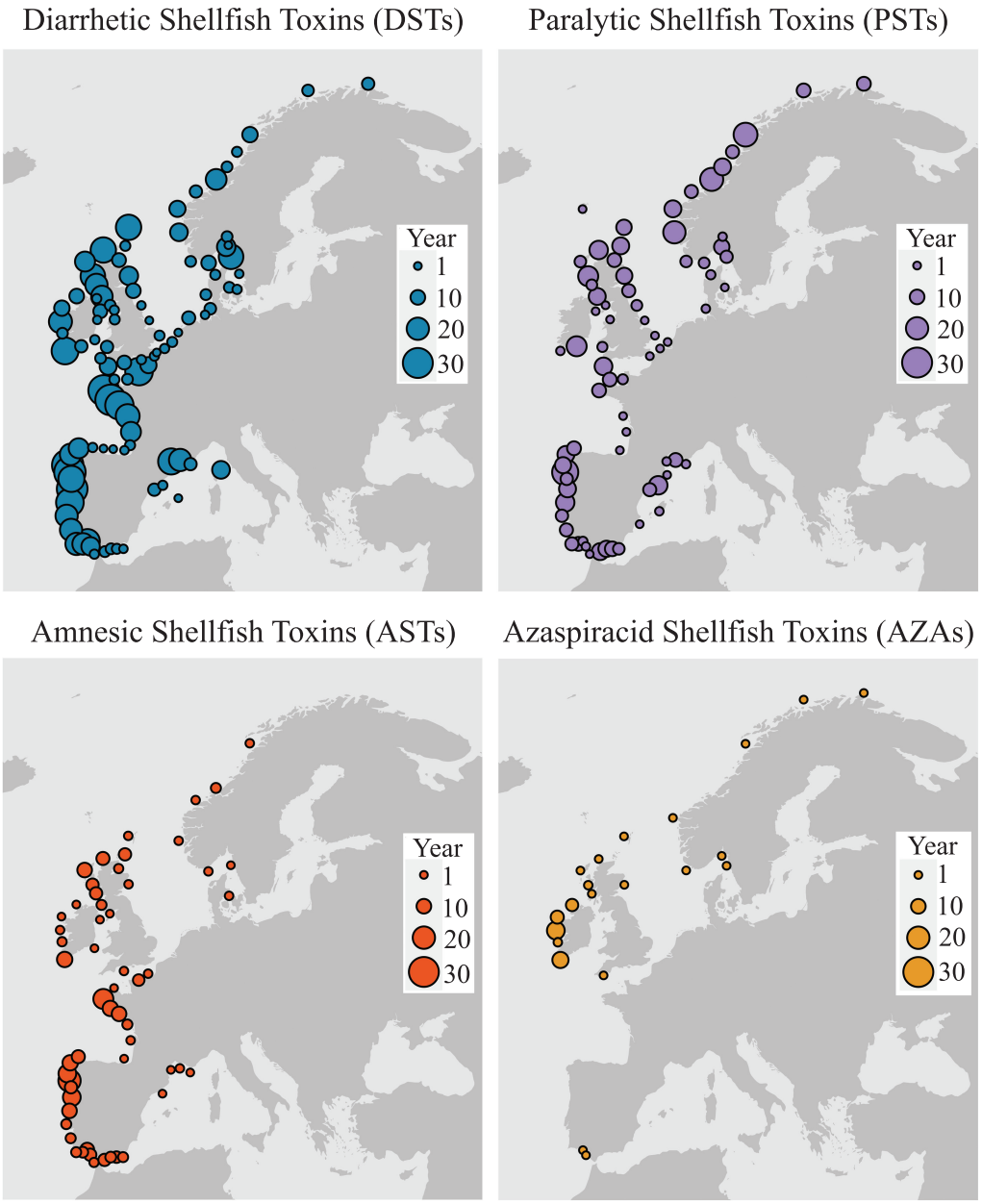

FIGURE 2 | Number of years where events associated with harmful algae have been recorded in IOC-ICES-PICES HAEDAT database. The majority of events are management actions closing shellfish harvesting areas to protect human health.

gene-specific to produce STX and its mere presence implies a risk (Swan and Davidson, 2012). The highly toxic PST producing species *Alexandrium catenella* (formerly identified as *Gonyaulax excavata*, *Alexandrium fundyense,* and/or Group I ribotype/N. American *Alexandrium tamarense)* occurs in Scottish waters and can result in shellfish flesh samples above regulatory threshold limits at low cell densities. However, indistinguishable (at least by light microscopy) non-toxic *Alexandrium tamarense* can co-occur (Touzet et al., 2010). *Alexandrium minutum* is the primary causative organism responsible for PSP in Irish shellfish and in the south west of England, although non-toxin-producing strains have been recorded in Ireland (Touzet et al., 2007; Clarke, 2020) and Scotland (Brown et al., 2010; Lewis et al., 2018). In 2020 in southwest Ireland, the highest ever PSP concentrations were observed in mussels and oysters, where unusually the PSP event lasted for several weeks. Along the French Atlantic coast, the main toxic species is also *A. minutum* with regular blooms in bays and semi-enclosed areas around French Brittany (e.g., Penze estuary, Bay of Brest, and Rance) resulting in closures (Santos et al., 2014; Chapelle, 2016). The *Alexandrium* occurrence, bloom and regulation in each bay is, however, driven by different biological processes such as

TABLE 2 | Main toxification syndromes and main associated species worldwide.

Syndrome	Causative organism	Toxin group	Clinical symptom	Impact
ASP	*Pseudo-nitzschia abrensis*	Domoic acid (DA)	Neurological	Food safety
	Pseudo-nitzschia australis			
	Pseudo-nitzschia brasiliana			
	Pseudo-nitzschia cacianthe			
	Pseudo-nitzschia calliantha			
	Pseudo-nitzschia cuspidata			
	Pseudo-nitzschia delicatissima			
	Pseudo-nitzschia fraudulenta			
	Pseudo-nitzschia hasleana			
	Pseudo-nitzschia multiseries			
	Pseudo-nitzschia multistriata			
	Pseudo-nitzschia plurisecta			
	Pseudo-nitzschia pseudodelicatissima			
	Pseudo-nitzschia pungens			
	Pseudo-nitzschia seriata			
	Pseudo-nitzschia subpacifica			
DSP	*Dinophysis acuminata*	Okadaic acid (OA), Dinophysis and pectenotoxins	Gastrointestinal	Food safety
	Dinophysis acuta			
	Dinophysis caudata			
	Dinophysis fortii			
	Dinophysis infundibulum			
	Dinophysis norvegica			
	Dinophysis ovum			
	Dinophysis sacculus			
	Dinophysis tripos			
	Phalacroma rotundatum			
	Prorocentrum hoffmannianum			
	Prorocentrum lima			
AZP	*Amphidoma languida*	Azaspiracids (AZA)	Gastrointestinal	Food safety
	Azadinium dexteroporum			
	Azadinium poporum			
	Azadinium spinosum			
PSP	*Alexandrium andersonii*	Saxitoxins (STX) and analogs	Neurological	Food safety
	Alexandrium catenella			
	Alexandrium minutum			
	Alexandrium ostenfeldii			
	Centrodinium punctatum			
	Gymnodinium catenatum			
NSP	*Karenia brevis*	Brevetoxins (BTX)	Neurological, respiratory irritations	Food safety, Food security (fish kills), Human health (aerosols)
	Karenia papilionacea			
YTX	*Gonyaulax spinifera*	Yessotoxins (YTX), [also adriatoxin]	n.e.p.	Food safety
	Lingulodinium polyedra			
	Protoceratium reticulatum			

This is a non exhaustive list that does not consider less frequent species or species of questionable impacts. N.e.p., no effect proven in humans (EFSA, 2008). The list of all HAB species is reviewed and regularly updated at IOC-UNESCO Taxonomic Reference List of Harmful Microalgae (http://www.marinespecies.org/hab/).

water temperature, dilution rates, river inputs, and/or pathogens (Chambouvet et al., 2008; Chapelle et al., 2015; Sourisseau et al., 2017). The population of *A. minutum* is also heterogeneous along the coast with sub-populations having different physiologies and levels of toxicity (Le Gac et al., 2016). The species *Alexandrium ostenfeldii* has been identified in various locations in the region including Spain, France, United Kingdom, and Ireland (Bresnan et al., 2021). In addition to saxitoxins this species can produce spirolides (Davidson et al., 2015) and other toxins including gonyautoxins (Martens et al., 2017), but with spirolides being the dominant toxins in European and North Atlantic *A. ostenfeldii* populations (Sopanen et al., 2011).

Paralytic Shellfish Toxins are also associated with *Gymnodinium catenatum* (Visciano et al., 2016). This species is prevalent in Iberian waters (Galician and Andalusian waters in Spain, and Portugal) and poses a concern. However, it has not been identified in the Basque Country area (Muñiz et al., 2017). The timing of *G. catenatum* blooms is associated with relaxation of upwelling events from late summer and subsequent advection into coastal areas, (Bravo et al., 2010) which are more common on the Mediterranean side than on the Atlantic side of Andalusia. In the Gulf of Cadiz and the Iberian Peninsula, the dominant organisms are *Gymnodinium catenatum* and *Alexandrium minutum* (Vale et al., 2008), the former being almost exclusive in the Atlantic coasts of Spain and Portugal, from mid-summer to autumn.

ASP – Amnesic Shellfish Poisoning; **AST** – Amnesic Shellfish Toxins: The genus *Pseudo-nitzschia* contains species or strains capable of producing domoic acid (DA) (Landsberg, 2002; Moestrup et al., 2009). In Scotland, similar to *Dinophysis*, this genus is thought to be transported advectively by oceanographic currents (Fehling et al., 2012; Siemering et al., 2016). *Pseudo-nitzschia* is categorized within the low toxin producing *Pseudo-nitzschia delicatissima* group and the (usually) toxic *Pseudo-nitzschia seriata* group. Typically blooms of the *P. delicatissima* group start earlier in the year (March–April), with blooms of the *P. seriata* group occurring in July–August when most toxicity is expected (Fehling et al., 2006; Rowland-Pilgrim et al., 2019). Analysis of *Pseudo-nitzschia* blooms in Loch Creran (Argyll and Bute, Scotland) has suggested that these are related to periods of poor weather (low air pressure and rainfall preceding the blooms). In Ireland, *Pseudo-nitzschia australis* blooms, observed from March to May, from the southwest up along the west coast, are the common cause of harvesting closures (usually short 1–2 weeks) (Clarke, 2020). DA producing species *P. seriata* and *Pseudo-nitzschia multiseries* have also been detected in Irish waters. In France, blooms of *Pseudo-nitzschia* species, including *P. australis*, are regularly observed from the Bay of Biscay to the English Channel (Nezan et al., 2010; Thorel et al., 2017), from March to November. These blooms appear linked to the seasonal and interannual frequency (Husson et al., 2016) of physical and hydrological processes (i.e., river discharge, upwelling, vertical mixing). In Galicia, blooms of *Pseudo-nitzschia* have been reported for decades (Míguez , 1996; Velo-Suarez et al., 2008), but with only one report of human intoxification, involving two people, in 2004 (HAEDAT database). In the Basque Country, the detection of toxins in April 2017 coincided with a bloom of *Pseudo-nitzschia* spp., but the causative species could not be elucidated. During the upwelling season in Portugal, from spring to late summer, blooms of *Pseudo-nitzschia* spp. are recurrent (Palma et al., 2010) although harvesting closures are very few per year and of short term duration (1 month maximum). *P. australis* (Costa and Garrido, 2004) and *P. multiseries* (Godinho et al., 2018) have been reported associated with these events.

AZP – Azaspiracids Shellfish Poisoning; **AZA** – Azaspiracid Toxins: In Ireland, *Azadinium spinosum* is the causative species of Azaspiracids, which can occur all around the Irish coastline, but predominantly cause closures around the northwest, west and southwest coasts. Similar to DSP, significant and prolonged closure periods are caused by AZA events, and on occasion can carry over from 1 year to the next, as observed in 2005–2006, and in 2013–2014 (Clarke, 2020). *Azadinium* has also been observed in Scottish and southwest of England waters (Paterson, 2017; Dhanji-Rapkova et al., 2019). The genus has also been detected in France (Brittany) and Spain (Galicia) since early 2000s (Magdalena et al., 2003) with a recent event in south Spain (Tillmann et al., 2017). However, reports of human illness have been sporadic in the NEA region (Bresnan et al., 2021). Also occurring in Irish waters, producing different AZA compounds (not currently legislated for), is the closely related *Amphidoma languida*. In Portugal, the genus is routinely monitored but no blooms or associated impacts have occurred to date.

We now describe typical patterns of HAB shellfish closures using as examples a northern (Ireland) and southern region (Portugal) since other countries around them follow similar patterns:

In Ireland, it is not unusual to have site closures due to toxins above regulatory levels from all four main toxin groups ASTs, AZAs, DSTs and PSTs (**Table 2**). Most years shellfish production area closures are due to DST and AZA. However, the extent, the maximum concentrations observed, and the length of the closure varies considerably from year to year, and occasionally intoxication of shellfish occurs late in the year (Clarke, 2020). The number of closures due to AST and PST is variable, with some years having no closures at all due to concentrations below regulatory levels. When there is an AST or PST event, it is usually short-lived with closures in place for 1–2 weeks (**Table 3**).

In Portugal, events occur mainly from spring to autumn and are associated with upwelling (AST) or the subsequent stratification after wind relaxation (DST and PST) (**Table 4**). Closures can last 9 months from the beginning of the year. AST events are less frequent where the *Pseudo-nitzschia genus* is always present in Iberian waters. PST events usually occur between September and December/February associated with *Gymnodinium catenatum* blooms, at the end of the upwelling season (Moita et al., 2003; Pitcher et al., 2010) until January in northern Portuguese waters (Pazos et al., 2006). *Pseudo-nitzschia* species were regularly observed in water samples and during spring-summer upwelling episodes (Palma et al., 2010).

The Historical Evolution of EWS

This section has shown that there is a heterogeneity of toxic events that can be harmful for human health and lead to shellfish area closures that have a direct, negative impact on the industry. Risk and uncertainty (Mousavi and Gigerenzer, 2014) represents a management challenge that impacts the industry throughout the year, not just when outbreaks occur. Therefore, the need for reducing this uncertainty is great, but shellfish farms are generally small businesses without the capacity to develop their own EWS. Therefore, most EWS developments have been initiated by the scientific community after noting the needs of the industry and regulatory authorities, and the scientific potential. For example, in Ireland, farming closures since the late 1980s especially in the southwest, have been a major concern for the continual development of the sector and drove the development of forecasting approaches in that location. Initially, as part of

TABLE 3 | Closure table of Irish production areas in 2018 due to toxins concentrations above regulatory levels.

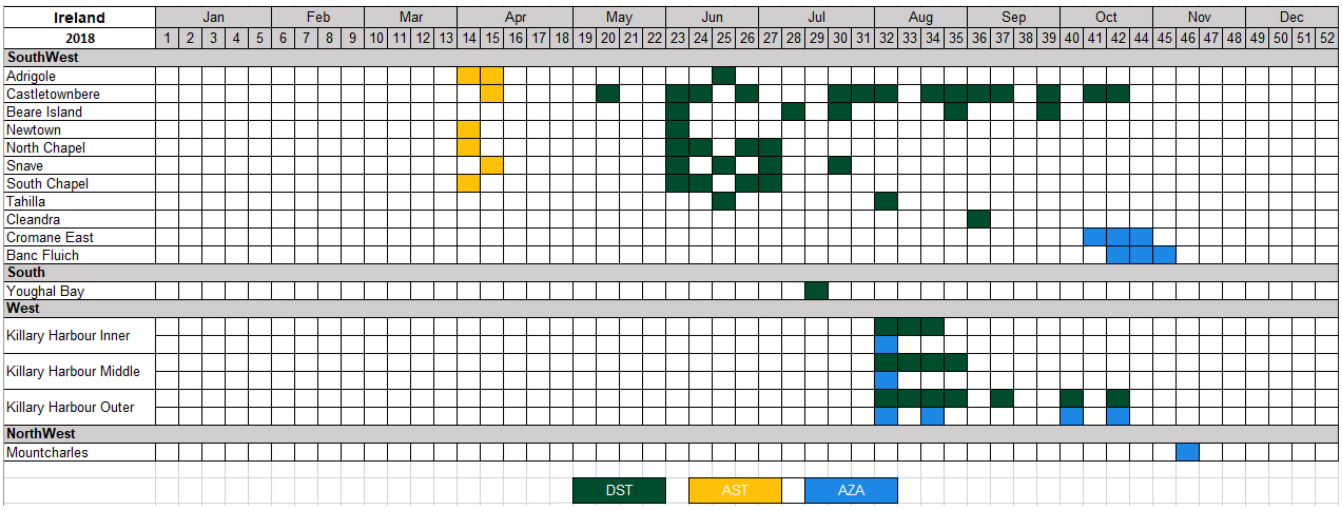

TABLE 4 | An overview of the spatial and temporal distribution of ban-on-harvesting periods in Portugal during 2018.

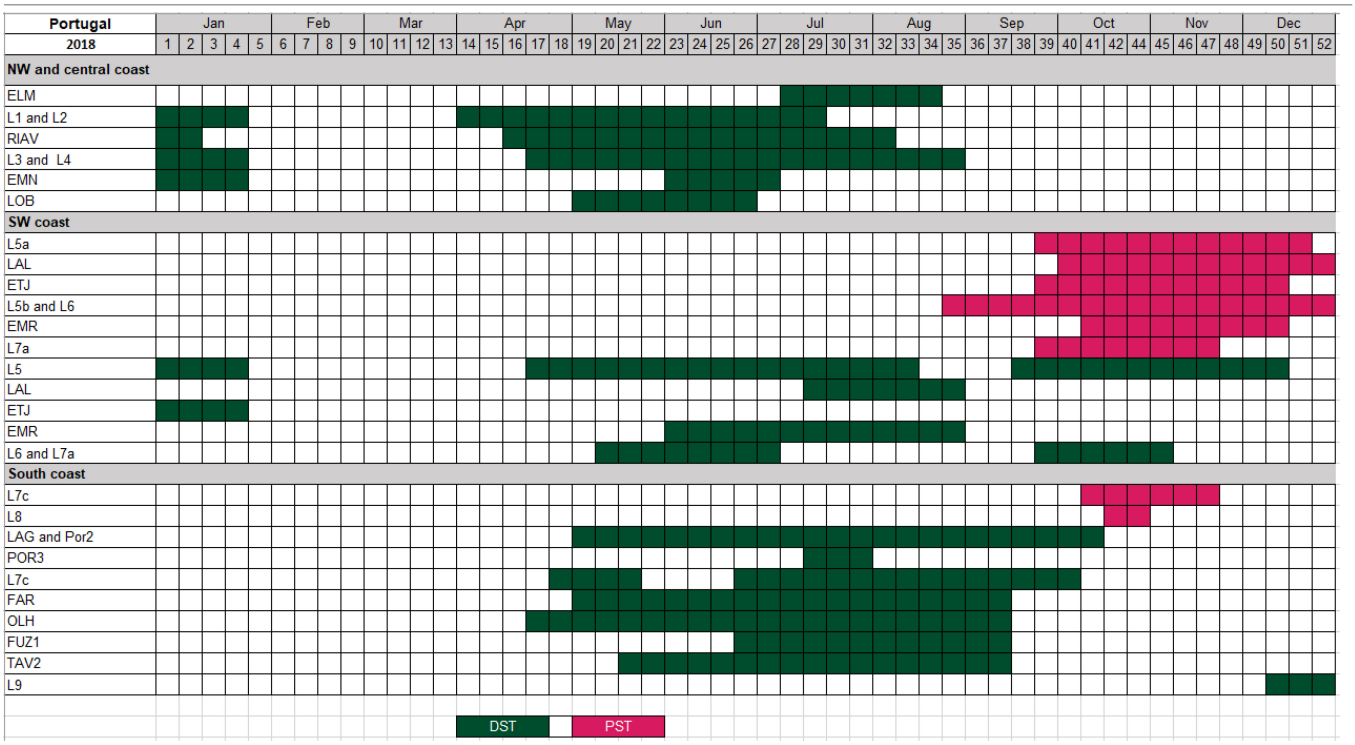

the ASIMUTH project, several institutes in Scotland, Ireland, France, Spain, and Portugal developed risk assessments, models and algorithms to assess the probability of occurrence of a HAB event and disseminated this information to stakeholders in "bulletins" (Davidson et al., 2016; Maguire et al., 2016). This was the precursor of the PRIMROSE project, which has improved these bulletins and added additional operational models (https://www.shellfish-safety.eu/).

Operational or pre-operational systems have previously been trialed in Scotland, France, Ireland, the Basque country, and the wider United Kingdom as described below:

In Scotland, the introduction of weekly HAB bulletins and assessments came after the trade association Seafood Shetland approached SAMS following a large, advected bloom of *Dinophysis* in 2013, that impacted all the active shellfish harvesting sites on the West coast of Shetland. The bloom, exacerbated by strong westerly winds, caused *Dinophysis* numbers in the affected sites to accumulate rapidly, raising toxin concentrations in the shellfish above actionable levels within 2–3 days of the bloom's arrival (Whyte et al., 2014). This time span was shorter than the weekly frequency of the regulatory monitoring program and hence intoxicated shellfish reached market. As a result, seventy people reported illnesses associated with symptoms of diarrhetic shellfish poisoning. The approach to reporting HABs in Shetland has developed iteratively through dialogue between local stakeholders and scientists at SAMS. The Scottish bulletin has been well received by industry who continue to be regularly updated on its development through local stakeholder workshops.

By contrast, in France EWS development has mainly been driven by scientific interest, but, unfortunately, has failed to attract enough interest from the industry. As an example, a French oceanographic forecasting system (PREVIMER; Charria et al., 2014) was built 10 years ago, and although some scientific developments related to HABs were progressed within this system through several joint projects (EASYCO, ASIMUTH) there was little industry interest was noted in its use.

As in Scotland, the Irish bulletin seems to have attracted the interest of the industry. The bulletin is usually prepared on Monday–Tuesday each week and then uploaded to the public access website from where it is publicly accessible and available for download. The bulletin is weighted to those areas where impacts from HABs are greatest, primarily the aquaculture sites of the southwest and west. However, bulletins and the forecasts they contain are assembled and issued for the whole country. There is an increase in the use of the bulletin during the bloom season where detectable amounts of biotoxins are more likely to occur. Besides the weekly bulletin, the Marine Institute provides up-to-date information on its website, https://webapps.marine.ie/habs related to the concentration of phytoplankton and biotoxins for the inshore and offshore production areas.

The ShellEye project was funded for 4 years by the United Kingdom Biotechnology and Biological Sciences Research Council (BBSRC) and Natural Environment Research Council (NERC) to develop a water quality bulletin service specifically for the shellfish industry, using the latest satellite and modeling technologies. ShellEye was driven by industry demand with the bulletin service being trialed by a number of shellfish farmers and related stakeholders, focused on four pilot sites in England, Wales, and Scotland: St Austell Bay, Menai Straits, Morecambe Bay, and Loch Ryan. Feedback obtained from shellfish farmers demonstrated the potential for the service, confirming they were able to use the information in the day-to-day management of their farm, and were interested to continue receiving bulletins, e.g., "We enjoyed the bulletins hugely and find it amazing to be able to see so clearly. We actually harvested our first batch of oysters this week, so the emails were very useful."

The Basque country is a special case since aquaculture activity is very recent and has been driven by a coordinated group of local industries, local institutions, and local scientists. Therefore, the need for an EWS has been, from the beginning, driven by industry, institutions and scientists together. As farming is offshore, the EWS is required to include, not only harmful events, but also information on extreme events (e.g., winds and waves).

SHORT-TERM FORECAST OF HAB OCCURRENCE AND TOXIN PRESENCE IN SHELLFISH

A development within modern alert systems is the use of a range of approaches to provide a forecast rather than a "now cast" of HAB and biotoxin conditions. These can be summarized into several major types (Davidson et al., 2016; Maguire et al., 2016; Mateus et al., 2019).

1. Type 1: Industry alert "bulletin" reports, which are compiled from datasets including data generated from biotoxin and/or phytoplankton monitoring programs, and include, where available, additional environmental variables. These parameters are often synthesized into graphical and map images for easy interpretation by stakeholders. The simplest bulletins are only warning systems reporting current findings, and do not necessarily function as early warning systems. However, through an "expert interpretation" to assess current and short-term future evolution of HAB and biotoxin risk, these bulletins can function as forecast systems for aquaculture businesses.
2. Type 2: Particle tracking based systems. These systems rely on Lagrangian dispersion modeling approaches. They aim to identify key production points of toxic phytoplankton and track their dispersal using oceanographic modeling. Lagrangian particle tracking models are a useful tool to predict the transport of HAB events once they have been observed. Particle tracking models, coupled to circulation models, are used in all NEA arc countries.
3. Type 3: Statistical models based on remote sensing. These models aim to improve the inference of presence from environmental conditions (e.g., sea surface temperature and surface chlorophyll) from satellite images and the statistical relationship with the presence of toxic phytoplankton. The approach aims to forecast the presence of toxic events under particular environmental conditions, even if the cause-effect relationships are not fully understood.

4. Type 4: Statistical (e.g., Generalized Additive Models, GAMs) and machine learning models (e.g., Bayesian networks) based on the fusion of multiple sources of data. These types of model analyze environmental conditions during historic toxic events to establish relationships between environmental factors and the development of toxic events.
5. Type 5: Mechanistic full-low trophic ecosystem models. These systems rely on the use of the mechanistic understanding of the relationships between environmental conditions and the presence of toxin-producing phytoplankton. As such, the relationships of environmental conditions with the proliferation of toxic phytoplankton, its dispersion and assimilation by bivalves is explicitly addressed. However, most of these models work at aggregated trophic levels and hence struggle to differentiate between harmful and benign phytoplankton. The degree of complexity of these systems varies, dependent on the complexity of the models they rely on.

Forecasting systems are rarely comprised of just one approach, but instead are a combination of shared information from different multiple approaches. For example, the boundary between type 4 and type 5 models may not be clear, since statistical modeling always uses some of the mechanistic knowledge available (e.g., variables to include), whereas mechanistic models use statistical inference of equations and parameters. The above approaches are currently incorporated in "bulletin" reports from each region utilizing the various datasets and data products available (**Supplementary Table 1**). Most of this information in Atlantic arc countries, especially HAB *in situ* data, had not been previously available publicly. However, this information is now becoming available through public bulletins, datasets, websites and media platforms providing access to monitoring data and data products in combination with forecasting models (**Table 5**). The current status of forecasting systems in Atlantic Arc countries is summarized below.

In Scotland, the alert system includes a "traffic light" based risk index and a number of other data products that summarize current and historical HAB and shellfish biotoxin risk for the country as a whole. In addition, a more detailed "expert interpretation" based risk assessment is provided for the Shetland Islands. Bulletins have been produced weekly since 2014 (type 1 system) and are available via www.HABreports.org in pdf format providing a summary of HAB and biotoxin concentrations in the current and previous 3 weeks. Additional information is provided on relevant environmental conditions allowing for expert interpretation-based risk assessment for the week ahead to be generated. This additional information includes mean wind direction in the current and three preceding weeks from local meteorological stations, forecasted sea surface currents from the Mercator Ocean model, sea surface temperature from JPL and Chlorophyll from Copernicus. HAB predictions based on the WeStCOMS mathematical model (type 2) are also integrated within the HABreports web site with the aim of predicting the likely impact on coastal aquaculture of any blooms that have been detected offshore by remote sensing (type 2 system). The effectiveness of the early warning of the Scottish system has been evaluated by Davidson et al. (2021) who found predictions to be 74% accurate.

The Scottish HABreports alert system also includes model based HAB predictions from the WeStCOMS mathematical model (type 2 system) with the aim of predicting the likely impact on coastal aquaculture of any blooms that have been detected offshore by remote sensing (type 2 system). The WeStCOMS mathematical model is a coupled meteorological/oceanographic model that includes meteorological forcing using the open-source Weather Research and Forecasting (WRF) model v. 3.5.1 (Skamarock and Klemp, 2008). This is a non-hydrostatic atmospheric model, nested within the NOAA National Centers for Environmental Prediction (NCEP) operational forecast model with 1° spatial resolution (Juang, 2000). The WRF model domain covers Scotland and its neighboring seas with a grid of 140 × 240 points. The finest resolution is around 2 km in the central part. The oceanographic model is a Finite-Volume Coastal Ocean Model (FVCOM) based hydrodynamic model. Model bathymetry was based on gridded data from SeaZone (2007) and refined in certain key areas using Admiralty charts and some multi-beam surveys. Vertical eddy viscosity and diffusivity were computed using the Mellor-Yamada 2.5 scheme (Mellor and Yamada, 1982). Horizontal diffusion was represented using a Smagorinsky (1963) eddy parameterization with a fixed coefficient (C = 0.2). The bottom boundary layer was parameterized with a logarithmic wall-layer law using a drag coefficient. The hydrodynamic model was integrated numerically using a time-split method with an external time step of 0.6 s. Boundary conditions: Water movement within hydrodynamic models is predominantly driven by tidal forcing applied at the "open" (water) boundaries. The tidal forcing was derived from the 1/30° degree implementation of the Oregon State University Tidal Prediction Software (OTIS) for the European shelf (Egbert and Erofeeva, 2002). At each of the domain's open boundary nodes, the 11 primary tidal constituents were used to derive sea surface elevation time series. Open boundaries also included a 6-km-wide "sponge layer" to filter high-frequency numerical wave reflection noise using a Blumberg-Kantha implicit gravity wave radiation condition (Wu et al., 2011). The use of this model to operationally simulate HABs is explained more fully by Aleynik et al. (2016) and Davidson et al. (2021).

In England, since the completion of the ShellEye project outlined above, there is currently no operational forecasting of HABs undertaken for this region. However, the project demonstrated the potential for a water quality monitoring service for the aquaculture industry, using satellite ocean color products to provide early warning of the growth or decline of certain high-biomass HAB species in a weekly bulletin (Miller et al., in press). Of the marine biotoxin producing genera, only *Pseudo-nitzschia* spp. can form a dense enough bloom to affect ocean color; but not all blooms of this species release toxins meaning that careful interpretation of results is required.

The unstructured grid hydrodynamic model FVCOM is also run operationally for a domain covering the Southwest United Kingdom, producing 3-day predictive forecasts. The model is forced by an operational WRF for surface forcing and the lateral boundary data are obtained from the CMEMS

AMM15 model. The river input is modeled from the WRF temperature and precipitation. The Lagrangian particle tracking model PyLAG (Uncles et al., 2020) is run offline on saved hourly outputs from FVCOM. This Lagrangian model uses a Milstein numerical scheme for advection and diffusion, with the diffusivities provided directly from the hydrodynamic model. There are no biological behaviors, and the virtual particles are modeled as buoyant, however, it is possible to set up with 3D advection and some simple behaviors (e.g., temperature dependence). Particles are seeded based on the HAB-risk product (Kurekin et al., 2014) in a 200-m radius around identified high risk areas. These are advected until the end of the forecast period and the results of the model are served as both a gridded particle density and probability field: this takes into consideration both the uncertainty from the identification algorithm and the drifting particles.

ShellEye also investigated single site statistical models of the environmental conditions that promote the release of algal toxins (Type 3 models). It was found that sea surface temperature (SST), solar radiation, wind speed, time-lagged rainfall and wind direction, were useful in predicting the onset of DSP toxins (Schmidt et al., 2018).

In Ireland, since 2013, the Marine Institute has produced a weekly HAB bulletin which is published and publicly available in PDF format through the in-house developed HABs database and website platform. The objective of the bulletin is to provide a short-term (3–5 days) predictive forecast on the likelihood of the occurrence of a HAB event around the Irish coastline and inshore areas. This prediction is based on current and historical data of HABs species and marine biotoxin occurrence from the national monitoring programs, incorporating observed trends and patterns with data input from satellite data and hydrodynamic models.

The bulletin provides information on the potential development and occurrence of toxins in shellfish and/or harmful phytoplankton species (type 1 system) in aquaculture areas, based on *in situ* monitoring and data generated over the preceding 3 weeks. In detail, the bulletin contains geographical maps of the cell densities of the major HAB phytoplankton species (*Pseudo-nitzschia* spp., *Azadinium*-type spp., *Dinophysis* spp., and *Alexandrium* spp.) and their associated causative biotoxin concentration in shellfish [Domoic Acid (AST), Azaspiracids (AZA), Okadaic Acid and Dinophysistoxins 1, -2 (DST), and Saxitoxin and related compounds (PST)]. The number and region of any closures of shellfish aquaculture production areas due to these toxin concentrations exceeding regulatory levels in shellfish are presented as doughnut charts with accompanying text comments as regards the observations based on the preceding 3 weeks of data. Other HAB species are also detailed, particularly the bloom-forming species types, commonly observed in Irish waters, including *Karenia mikimotoi, Phaeocystis* spp., and *Noctiluca scintillans*. Data and results are mapped and tabulated from historical trends of observed biotoxin concentrations per geographical region from the beginning of the current year to date and also for the current week and additionally the historical occurrence of toxicity per region over the last 10 years per toxin group. Furthermore, a list of the top five phytoplankton species per geographical region from the preceding to the current week is also displayed.

Satellite imagery detailing chlorophyll-*a* concentration and its anomaly (in comparison to the average of the past 60 days) and sea surface temperature (SST) are also displayed. The method used to calculate the chlorophyll-*a* anomaly uses the

TABLE 5 | EWS for HABs and Biotoxins in the Atlantic arc regions: features and components.

NEA arc countries	EWS Type 1	EWS Type 2	EWS Type 3	EWS Type 4	Warning frequency	Warning focus	Bulletins and/or demo links
Ireland	Operational	Operational	Operational	None	Weekly	DST, PST, AST, and AZA	http://webapps.marine.ie/HABs/
Scotland	Operational	Operational	None	None	Weekly (spring to autumn)	DST, PST, and AST	https://www.habreports.org/
England	Operational	None	Operational	None	Weekly (spring to autumn)	*Karenia,* and *Pseudo-nitzschia*	*ShellEye* email bulletin subscription service: https://www.shelleye.org S-3 EUROHAB for Channel: https://www.s3eurohab.eu
France	Operational	None	Developing	None	Weekly	DST, PST, and AST	Monitoring bulletins: https://envlit-alerte.ifremer.fr/accueil Demonstration: https: //www.s3eurohab.eu/portal/?state=07513e
Spain – Basque Country	Operational	Developing	None	Proof-of-concept	Monthly	DST, PST, and AST	Temporally offline due to system reconfiguration (www.euskoos.eus)
Spain – Galicia	Operational	Operational	None	None	Weekly	DST, PST, and AST	http://centolo.co.ieo.es/primrose/Galician_ HAB_bulletins/
Spain – Andalusia	Operational	None	Proof-of-concept	Proof-of-concept	Weekly	DST, PST, AST, AZA, and YTX	https://www.juntadeandalucia.es/ agriculturaypesca/moluzonasprodu/
Portugal	Operational	Operational	None	None	Weekly	DST, PST, and AST	http://www.ipma.pt/pt/bivalves/index.jsp http://www.ipma.pt/pt/bivalves/fito/index-map-dia-chart.jsp

60-day median chlorophyll-*a* concentration, not including the last 2 weeks to prevent a potential recent bloom skewing the median field (Stumpf et al., 2003 and Tomlinson et al., 2004). For SST, the information provided by the Irish Weather Buoy Network (IMOS) on the 10-year weekly average temperature is used and compared with the same week of the past 10 years, so the anomaly is based on the long-term weekly average and each measured sea surface temperature value has the appropriate weekly average value.

Over many years, hydrodynamic models for three Irish sites (Bantry Bay in the Southwest of Ireland, Killary Harbour and Cleggan at the West coast of Ireland) have been developed within the Marine Institute. These provide information on water flow, particle tracking and physical oceanographic features (type 2 system). For this, hydrodynamic forecasts from a Regional Ocean Modeling System (ROMS) for 3 days in Irish coastal waters is created. ROMS is an evolution of the S-Coordinate Rutgers University Model (SCRUM), as described by Song and Haidvogel (1994). The numerical aspects of ROMS have been described in detail by Shchepetkin and McWilliams (2005), where the ROMS AGRIF version developed in France (Debreu et al., 2012) is used. The downscale models of areas of particular interest (Bantry Bay, Killary Harbour, and Cleggan Bay) incorporate online particle tracking with virtual particles released at pre-defined transects at the start of each model run (Leadbetter et al., 2018). The operational model also produces an estimate of the ocean state as a 3–7 days forecast of the dominant regional physical processes that result in water exchange events between the bay and its adjacent shelf for these three areas. Upwelling and downwelling signals indicate potential for future toxic contamination of shellfish in certain bays in the south-west of Ireland. The skill of the model in simulating toxic HAB episodes up to 10 days in advance is demonstrated by Cusack et al. (2016). Similar to the preparation of the weekly Scottish bulletin the data summary graphics are produced using automated routines, which are then assessed by an expert evaluator. This evaluator provides expert opinion and analysis based on the datasets and all the parameters described above, and provides text to the weekly bulletin to provide a national forecast for the current week (3–5 days forecast), describing the cautionary predictive risk of a potential new HAB event occurring, or an existing event continuing/dissipating per toxin group or for bloom forming species (Dabrowski et al., 2016; Maguire et al., 2016; Leadbetter et al., 2018).

In France, Ifremer produces publicly available (type 1) weekly HAB bulletins based only on toxins and/or phytoplankton monitoring for all areas of the coast. Despite previous short-term forecast attempts (type 2 and 5), there is currently no operational forecasting included in bulletins, however, a new alert system remains in development as outlined below.

For the PST producing *Alexandrium minutum*, the retention time in the bays, water temperature, riverine nutrient input and resources competition were identified as the main abiotic drivers of blooms (Guallar et al., 2017). Subsequently, mechanistic approaches (type 5) based on these observations were evaluated (Sourisseau et al., 2017) but forecasting capacity has decreased over the years since the first intoxification event (2012), suggesting some evolution of the plankton communities.

Modeling studies (type 5) of the fish-killing dinoflagellate *Karenia mikimotoi* suggested that stratification (Gentien et al., 2007; Vanhoutte-Brunier et al., 2008) may not be the only driver of these blooms and that transport in the coastal current, as well as seeding from offshore blooms influence the incidence, consistent with modeling of this species in Scottish waters (Gillibrand et al., 2016; Sourisseau et al., 2016). A HAB forecasting exercise (simulating *K. mikimotoi* and also *Pseudo-nitzschia* spp., and *Phaeocystis* spp.) based on such mechanistic models (type 5) over a short time scale (∼ 4 days) was conducted during the PREVIMER project (Ménesguen et al., 2014) with mixed success prior to this operational model being terminated in 2017.

Currently, there is no specific hydrodynamic model in operation to forecast HABs advection in France. However, hydrodynamic condition forecasts at different frequencies (hourly to daily) are provided at several resolutions (from 4 km to 500 m) up to 4 days in advance. These 3D field solutions are used to forecast advections of exceptional events by using tools such as the Lagrangian particle tracking model Ichthyop (Lett et al., 2008).

Using type 4 approaches, a range of statistical relationships between HABs and environmental variables were obtained using different methodologies (Díaz et al., 2013; Hernandez Farinas et al., 2015; Husson et al., 2016; Guallar et al., 2017; Barraquand et al., 2018; Karasiewicz et al., 2018). These studies suggest that the whole planktonic community (species interactions and ecological niches) should be taken into account to fully understand HABs dynamic (Karasiewicz et al., 2018). In particular it is important to represent large functional groups (diatoms vs. dinoflagellates) which appeared to be linked with decadal variability of river inputs.

Work in different Spanish regions occurs autonomously and hence each is considered separately. For the **Basque Country (North of Spain, Southeast Bay of Biscay waters)**, several systems are being developed: (i) a bulletin or report based on sampling (type 1 system); (ii) an operational hydrodynamic model based on the Regional Ocean Modeling System (type 2), with a mean horizontal resolution of 670 m and 32 vertical levels (Ferrer et al., 2007, 2009, 2013); and, (iii) a machine learning system (type 4) based on supervised classification and Bayesian networks (Fernandes et al., 2010, 2013, 2015).

The ROMS hydrodynamic model is used to obtain a 4-day forecast of current, temperature, and salinity fields in the south-eastern Bay of Biscay. ROMS has been used in several studies to model the water circulation in the study area (e.g., Ferrer et al., 2007, 2009, 2015; Ferrer and Caballero, 2011; Caballero et al., 2014; Laiz et al., 2014; Legorburu et al., 2015). The ROMS domain used in the EuskOOS modeling system covers the southeast Bay of Biscay, extending from 43.24 to 44°N and from 3.4 to 1.3°W, with a mean horizontal resolution of 670 m. Vertically, the water column is divided into 32 sigma-coordinate levels. These levels are more concentrated within the surface waters, where most of the variability occurs. The bathymetry was obtained from the European Marine Observation and Data network (Vasquez

et al., 2015), smoothed to ensure stable and accurate simulations (Haidvogel et al., 2000). The atmospheric forcing used in ROMS is obtained from the Weather Research and Forecasting model (WRF) run by Euskalmet (Basque Meteorological Agency). The boundary conditions are obtained from the 3-D hourly data provided by the NEMO model for the Iberian-Biscay-Ireland region. The online 3-D Lagrangian particle tracking module existing in ROMS is activated and is generating forecasts of the 4-day evolution of several virtual particles released at fixed points and at 00:00 UTC in the ROMS domain at high temporal resolution (1 min). These virtual particles are initially located at the sea surface to forecast the drift of HABs from and to the pilot aquaculture farm (located in the Mendexa region). For the analysis of specific events in the past, the Sediment, Oil spill, and Fish Tracking model (SOFT) is used with the ROMS outputs and satellite-derived information.

A machine learning approach was used to find non-linear correlations (*Symmetrical Uncertainty Score*; SUS; Hall, 1999) and key non-correlated predictors (*Correlated-based feature subset selection*; CFS; Hall and Smith, 1997; Hall, 2000) between environmental conditions across the region and the presence of DSTs in shellfish in aquaculture sites. The presence of these toxins is often correlated with higher concentrations of phytoplankton cell density (blooms), but it is also observed that toxins in shellfish can occur at low cell densities (**Table 6**). The model has been validated using 10-fold cross-validation with an accuracy of 67% and only 3% of false positives. If we use the presence of *D. acuminata* as a predictor, the accuracy increments to 83%, without increasing the false positives. The relationships found by the model have been observed in other areas of the world (Zhu et al., 2017). Relationships between toxins, nutrients, and productivity are common (Bates et al., 1989; Hutchins and Bruland, 1998; Pan et al., 1998; Sunda et al., 2005; Anderson et al., 2008; Sun et al., 2011; Lelong et al., 2012; Tatters et al., 2012; Schnetzer et al., 2013; Sison-Mangus et al., 2014; McCabe et al., 2016; Drakulović et al., 2017; Grzebyk et al., 2017; Zhu et al., 2017). Surprisingly, temperature is not a selected predictor of toxin presence (Zhu et al., 2017; Smith et al., 2018), but it might be because there have not been significant changes in the temperature range in the region (Revilla et al., 2010). Negative correlations with silicates might be due to previous blooms of diatoms. The presence of toxins is correlated with nutrient concentrations outside of the aquaculture site. In the region, there is an important bathymetric gradient with a transition from a coastal current from West to East to a weaker oceanic current in the opposite direction. In the west, limited eddies that transport nutrient-rich waters to the open sea are common (Ferrer and Caballero, 2011). Therefore, these eddies facilitate water mixing and nutrient upwelling, supporting the proliferation of toxic phytoplankton species as well as their transport to other coastal areas (**Figure 3**). This transport can take between 1 and 4 weeks depending on oceanographic and meteorological conditions (Ferrer and Caballero, 2011). This type of phytoplankton species transport mechanism has been previously documented in northern areas of the Bay of Biscay (Batifoulier et al., 2013). Similarly, some Scottish harmful algal bloom genera/species are thought to develop offshore and be advected by winds and currents to the coast. An example of this was the exceptional *Dinophysis* bloom in the Shetland Islands in 2013 that resulted in an outbreak of shellfish poisoning (Whyte et al., 2014).

Along the Spanish coast, the general tendency at the sea surface is a flow from west/northwest to east/southeast, this occurs at least 90% of the time (based on small buoys trajectories analysis). CTD data indicates that this flow is evident at 10–15 m where peaks of chlorophyll appear. Thus, most HABs are expected to come from the western Spanish coast (or offshore areas with eddies such as the Cape Ortegal longitude, 8°W, as predicted in the Bayesian network model) than from the French coast.

In Galicia, an oceanographic system (type 2) has been developed to forecast *Dinophysis* spp. presence (Ruiz-Villarreal et al., 2016). A HAB bulletin was designed to provide information on the current and potential future state of HABs and biotoxins in Galicia within a 3-day forecast. This early warning system supports decisions of the Galician regulatory monitoring system operated by INTECMAR as well as providing forecasts to the Galician aquaculture industry. The system integrates HAB information from monitoring programs with hydrodynamical models and both physical and biochemical data from *in situ* networks along with satellite imagery. It has been shown to be capable of making predictions of bloom transport, but not the initiation of a toxic event, especially for low biomass HAB species. Additionally, it has been shown that early warning of the risk of autumn toxic dinoflagellate blooms in the Galician Rías is feasible by combining Lagrangian particle tracking simulations with HAB data from Portuguese monitoring (Ruiz-Villarreal et al., 2016). The Lagrangian particle tracking model Ichthyop (Lett et al., 2008) is used for Galicia. Ichthyop runs offline forced by the hourly results of the Meteogalicia ROMS nowcast and forecast simulations[2]. In common with approaches elsewhere in the Atlantic Arc, the HAB cells are considered as passive particles that move with the flow and do not have "behavior" (Velo-Suárez et al., 2010; Dippner et al., 2011; Aoki et al., 2012; Ruiz-Villarreal et al., 2016). Approximately 1000 virtual particles are randomly released each day in the first 20 m of the water column at six locations/configurations: Inside the Galician Rías (Vigo, Pontevedra, Arousa, and Muros). Along the Portuguese shelf, 10,000 particles are released inside two polygons: (1) between 40.8024° N and 41.27° N and inshore the 200-m isobath; and (2) between 41.27° N and 41.87° N and inshore of the 200-m isobath. This allows forecasting of the transport from the northern Portuguese shelf to the Galician rías, where the harvesting areas are located.

In **Andalusia**, type 1 bulletins based on *in situ* monitoring are used. Upwelling is thought to be important to HAB development in this region (García et al., 2002; Navarro and Ruiz, 2006; Prieto et al., 2006, 2009; Navarro et al., 2012). In 2006, a neural network model was developed to forecast *Dinophysis acuminata* (Velo-Suárez and Gutiérrez-Estrada, 2007), but is not regularly

[2]http://mandeo.meteogalicia.es/thredds/catalogos/ROMS/catalog.html

TABLE 6 | Selection of potential predictors using cross-validation showing the percentage of times that each predictor has been selected (Freq. Selec.).

D. acuminata			Okadaic acid (diarrheic toxin)			Yessotoxins (cardiotoxicity)		
SUS	**Freq. Selec. (%)**	**Predictor**	**SUS**	**Freq. Selec. (%)**	**Predictor**	**SUS**	**Freq. Selec. (%)**	**Predictor**
0.72	40	Fe	0.61	100	Fe	0.73	90	Fe
0.68	70	PP	0.51	100	PP	0.53	90	PP
0.68	80	PhyC	0.61	100	PhyC	0.50	10	PhyC
0.71	50	Si	0.61	50	Si	0.67	90	Si
0.68	50	CHL	0.51	90	CHL	0.64	90	PO_4
				20	O_2	0.57	50	NO_3
				10	*D. Acuminata*			

SUS corresponds with the non-parametric Symmetrical Uncertainty Score which values range between 0 and 1. AO, okadaic acid; YTX, yessotoxin; Fe, iron; PP, primary production; PhyC, phytoplankton concentration as carbon in water; Si, silicate; CHL, Chlorophyll; O_2, oxygen; PO_4, phosphate; NO_3, nitrate.

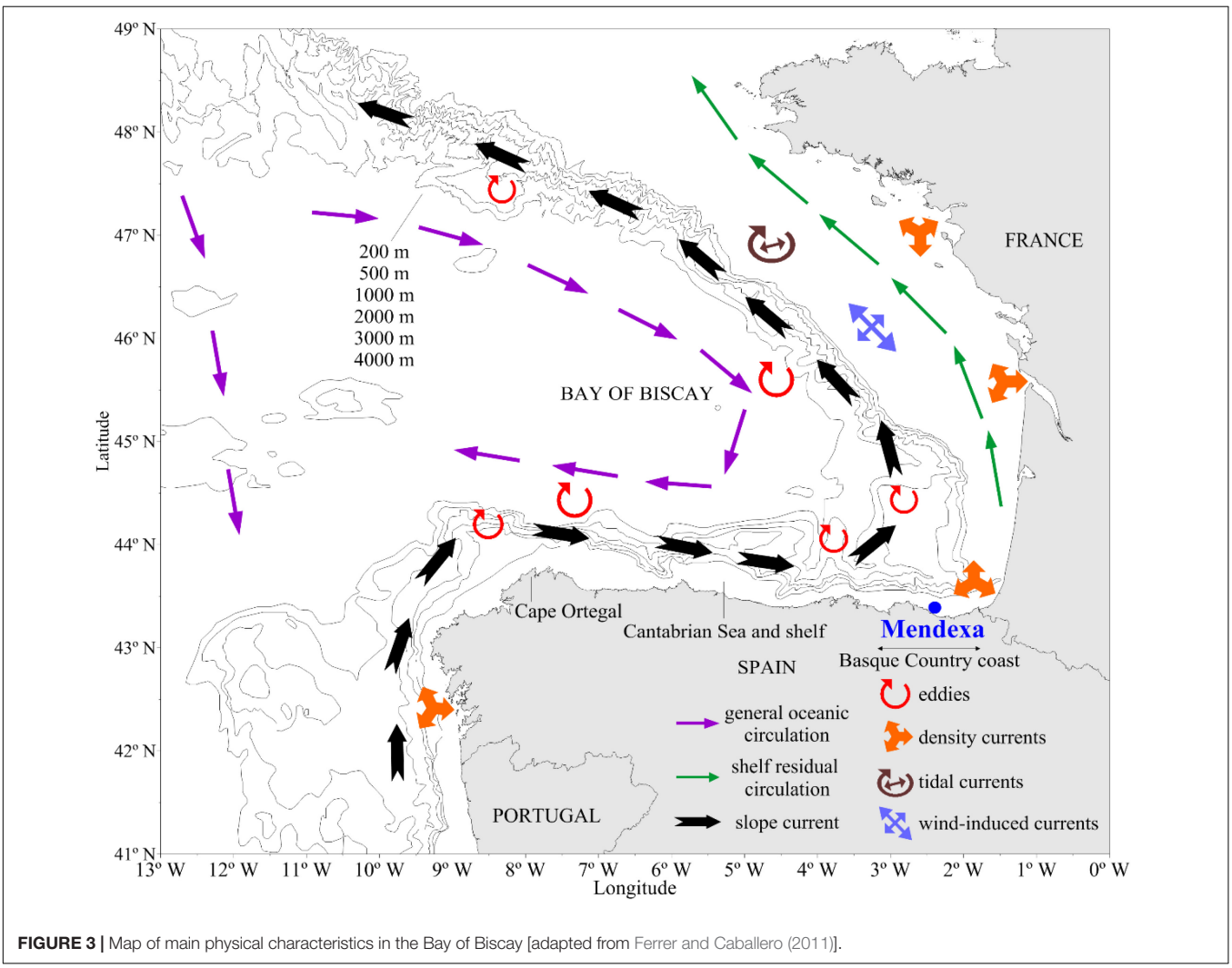

FIGURE 3 | Map of main physical characteristics in the Bay of Biscay [adapted from Ferrer and Caballero (2011)].

used in bulletins. Recently a proof-of-concept based on satellite information has been developed (Caballero et al., 2020).

In Portugal, a prototype oceanographic system (type 2) is being updated to forecast HAB and shellfish closures areas. The system has been developed by IPMA and IST within the ASIMUTH project (Pinto et al., 2016; Silva et al., 2016). Originally, it operated for a test period of 1 year, producing weekly bulletins with an illustration of open and closed production areas, along with a forecast for potentially impacted areas, based on the ocean circulation and toxin concentrations. The updated version of the bulletin follows the same approach, with the forecast relying on a combination of field data

and model results. The system relies on the hydrodynamic forecast, simulating tri-dimensional velocity fields and thermal distribution, coupled to a model of Lagrangian elements to simulate the passive transport of particles, without incorporating any biological processes. Results from the national weekly shellfish and toxin sampling program are the starting point of the forecast. The Lagrangian model is then triggered to simulate the transport of particles from those areas impacted by HABs to determine the pathways of dispersion/retention along the coast and assess the impact on neighboring areas. Model predictions with a 4-day forecast capacity rely on the PCOMS model (Mateus et al., 2012). The model setup consists of 50 vertical layers, with 43 cartesian-coordinate layers at the bottom, and seven sigma coordinate layers in the top 10 m. The model simulates the 3D thermohaline structure and velocity fields for the West Iberian coast and is systematically validated with tidal gauge data and sea surface temperature from remote sensing. The particle tracking model runs offline, relying on the previously computed hydrodynamic solutions. Particles move in two dimensions (x and y), according to local current fields pre-calculated by the hydrodynamic model. Production areas are defined as polygons along the Portuguese coast, corresponding to major bivalve production areas by the regulatory authority in Portugal (IPMA), also responsible for the national monitoring program. All polygons are populated with particles and their movement along the coast to adjacent polygons is monitored. The risks to each production area are then assessed based on the possibility of receiving particles from known contaminated areas. Two new pilot areas are being tested for local prediction, namely the Ria Formosa (in the south) and Ria de Aveiro (on the northwest coast). The Portuguese bulletin is planned to be made available in a web page format, updated twice a week (Wednesday and Friday). In addition to the modeled surface currents, wind and particle transport, it will also include monitoring results for HABs (and microbiology), oceanographic information, remote sensing data for SST and Chlorophyll-*a*. A warning trigger for neighboring monitoring laboratories (Galicia and Andalusia) is also planned to be included in the system.

DISCUSSION

Effectiveness of Current Early Warning Systems

This study describes the range of toxin-producing phytoplankton, their associated toxins, the impact they can have on shellfish aquaculture in the Atlantic arc countries and the various EWS that are being developed to safeguard the industry and human health. It demonstrates that in most countries in the region, EWS are still in the early stages of development and testing. Some systems only have the capacity to provide end users with a warning based on current official control monitoring programs, while others, such as Ireland and the Shetland Islands in Scotland, are providing both risk assessments and forecasts. However, several proof-of-concept systems are under development and show promise as illustrated by the examples in section "Short-Term Forecast of HAB Occurrence and Toxin Presence in Shellfish" and those in the literature (Vilas et al., 2014; Torres Palenzuela et al., 2019; Caballero et al., 2020). Much of the current development of EWS is centered around *in situ* regulatory monitoring data of harmful species and their toxins at aquaculture sites. These data are designed to be used for operational decisions on whether a harvesting area should be closed to protect human health and are therefore not designed to provide the early warning needed to manage aquaculture business risk. Environmental data comes from different sources, ranging from programs that monitor the state of the ocean to numerical models of ocean physics and biology. Combining approaches, often involving huge volumes of data with very different spatial and temporal resolution into information systems to support end-users therefore poses significant technological challenges.

When it comes to ascertaining the best fit model approach the choice of model is driven by the species of concern and the topography of each region. For example, in Scotland, the type 2 particle tracking model using is based on an unstructured grid FVCOM system. This was chosen because of the complex fjordic nature of the Scottish coastline and hence the need to be able to track the advective movement of HAB events at high spatial resolution.

Particle tracking models (ROMS, FVCOM, and MOHID) are among the simplest models, since they consider only physical components and hence are suitable for many toxic HABs that are known to be driven by advection processes. However, these models cannot be applied to all toxigenic species and information is required to know where and when the HAB event starts to initiate the model. At present, this is achieved by a combination of remote sensing and coastal monitoring, but neither are ideal for optimal early warning. Coastal monitoring can provide limited early warning, where satellite methods appear to be able to distinguish and differentiate between only a few (high biomass) species, and cloud cover can limit their operability. Combining with the additional approach of machine learning, this can integrate all this model information together with other sources of data (e.g., *in situ* observations or other models from Copernicus services) and result in a probabilistic forecast with the information and data available. The example of the Basque probabilistic model presented above, highlights that with enough data integration over 80% accuracy can be reached with almost no false positives. However, extension of this proof-of-concept will require a level of data gathering in near real time, which is not yet realistic, given the difficulties to identify the target species (*D. acuminata*) species *in situ*.

Lagrangian models play a central role in many current HAB early warning systems, as they provide information on the oceanographic transport of potentially toxic blooms, once identified by *in situ* observation. While the most probable origin of the blooms can potentially be determined by inverse drift computation (Abascal et al., 2012), in a similar fashion to that used in other oceanographic disciplines (Breivik et al., 2012; Drévillon et al., 2013; Suneel et al., 2016; Chen, 2019) this is not currently operational. Hence, initiation of Lagrangian model predictions of advective bloom transport requires information on

the location and size of a potentially harmful bloom before it has reached the shellfishery.

One cost-effective method of obtaining this information is through satellite ocean color imagery, which can provide coverage of large marine areas at a resolution of a few hundred meters. Unfortunately, cloud cover obscures data collection and hence is their primary limitation. Satellite monitoring offers the potential to identify an advective bloom before it reaches the coast. This approach focuses mainly on the detection of chlorophyll and hence is suitable for detecting large blooms of phytoplankton at the water surface (Spyrakos et al., 2011). Satellite-based approaches increasingly use machine learning methods for discriminating certain dense HABs from harmless blooms (Velo-Suárez and Gutiérrez-Estrada, 2007; Gokaraju et al., 2011; Xu et al., 2014; Guallar et al., 2016). However, large blooms of phytoplankton do not necessarily lead to toxic events, and others, such as the dinoflagellate *Dinophysis* spp., responsible for DSP, can cause harm at concentrations of only a few hundred or thousand cells per liter, far too low to be observable from space (Broullón et al., 2020). This is common to many shellfish toxin producing species of *Alexandrium*, *Dinophysis* and *Azadinium* genus which do not produce the main biomass component of a bloom that a satellite image can detect. Satellites can also provide useful information on sea surface temperature (SST) highlighting the onset and extension of an upwelling event, a process often linked to the triggering of a toxic bloom.

Model initiation would therefore benefit from remote sensing approaches capable of better discriminating harmful from benign species, and a more holistic approach to combine data from multiple sources, for example using machine learning. This study shows the potential of combining satellite, modeled, laboratory, and *in situ* data (e.g., Basque Country example). It also shows that an effective early warning system needs to consider a complex array of parameters including the presence or absence of toxins, the presence or absence of specific phytoplankton species, oceanographic dispersal models, satellite data models and biogeochemical and meteorological data or model forecasts. The use of such models could be extended to estimate the origin of blooms, not just to establish potential pathways of dispersion or retention.

New data gathering methodologies that are currently under development to enhance our ability to identify blooms offshore, including enhanced remote sensing approaches, autonomous observation platforms and data assimilation techniques will be key to enhancing the model skill.

Of course, the further ahead we look the less reliable these forecasts become. Currently the Irish and Scottish forecasts predict the occurrence of HABs up to a week ahead. Given that official control monitoring takes place weekly, this is usually sufficient to prevent intoxicated shellfish being harvested. Trend analysis of previous years can also provide some information on the seasonal occurrence of toxin-producing phytoplankton, but this is generally limited by significant inter-annual variation. As a comparison, advances in meteorological forecasting have been slow, increasing in duration by a day each decade (Alley et al., 2019), and now give a reasonably accurate forecast up to 2 weeks in advance. The marine ecosystem that controls the growth of toxic phytoplankton is every bit as complex. This creates a quandary: the aquaculture industry wants long term forecasts, though this will lead to more false positives, and forecasting a toxic event that does not happen will reduce industry confidence in the process. At the moment, model systems are still a long way from being able to produce long-term predictions for the industry and rely instead on expert opinion to draw together the various data streams needed to produce a meaningful forecast.

How Can the Aquaculture Industry Use HAB Early Warning Systems?

Early warning systems offers several potential benefits to the industry. In the case of a possible closure, they allow shellfish farmers to source product from alternative, healthy sites, an important factor in maintaining important market supply chains. It also gives industry the opportunity to implement mitigation strategies such as erecting physical barriers and increasing the frequency of end product testing (EPT), to verify the presence of toxins in their shellfish. Giving farmers the ability to make better management decisions over harvesting and planned husbandry work minimizes costly product recall and reduces human health incidents, both of which have long-lasting detrimental effects on consumer confidence.

Future Considerations for Early Warning Systems

Looking ahead, the integration of multiple observational platforms at the right scale combined with real-time processing capacity is required to unlock the potential of forecasting systems. The term big data was coined to capture this emerging trend (Hu et al., 2014). In addition to its sheer volume, big data exhibits other unique characteristics when compared with traditional data. The need for real-time storage, processing and visualization is crucial for an effective system beyond previous proofs-of-concept. This development calls for new system architectures for data acquisition, transmission, storage, and large-scale data processing mechanisms from computer science (LeCun et al., 2015). Big data techniques enhanced by machine learning methods can increase the value of such data and its applicability to societal, industrial and management challenges. Such methods have proven their potential in fisheries forecasting (Fernandes et al., 2010) and automatic classification of zooplankton samples (Fernandes et al., 2009). The Probabilistic Graphical Models (PGMs) paradigm (Pearl, 1988; Castillo et al., 1997), based on probability theory and graph theory (Buntine, 1991), is such a tool. Machine learning and statistical methods have a wide literature of model validation and performance estimation that is needed for end-user trust and interpretation of model forecasts (Fernandes et al., 2010; Witten et al., 2017). To take these forecasts further a multi-disciplinary approach joining domain experts and artificial intelligence experts is key (Grosjean et al., 2004; Fernandes et al., 2012, 2013; Trifonova et al., 2015; Uusitalo et al., 2016; Hernández-González et al., 2019; Taconet et al., 2019; Cruz et al., 2021).

Data consolidation is a major challenge in developing a machine learning based system. As noted above, data sources

may include *in situ* regulatory monitoring, sensors, meteorology, models and satellite: often provided in different formats, undocumented or with missing information. EWS developments will accelerate and reach their full potential only with FAIR data: findability, accessibility, interoperability, and reusability (Wilkinson et al., 2016; Bax et al., 2019; Stall et al., 2019). These curated datasets incorporate training information and so provide an opportunity to improve the efficiency and strength of statistical models. This method is already employed for essential biodiversity variables (EBVs), to study global biodiversity (Kissling et al., 2018), and to collect essential ocean variables (EOVs, Miloslavich et al., 2018) needed to monitor the ocean. Each owner and provider of data related to HABs should also consider contributing their data to these frameworks, as international networks such as HAEDAT currently focus on harmful events (**Figure 2**), rather than the distribution of toxin-producing algal species.

Climate change will also bring increased toxin threats from species such as *Gymnodinium catenatum* and *Azadinium* spp. (Higman et al., 2013; Turner et al., 2015), and from other toxin-producing organisms currently present elsewhere in Europe and in similar environments worldwide (Davidson et al., 2015). Evidence on climate change impacts on HABs have been described by Edwards et al. (2006) who noted shifts in the distribution of HABs in the North-East Atlantic since the 1960s. Links between increasing sea surface temperatures and wind intensity have led to an increase in the potentially toxic diatom *Pseudo-nitzschia* in the NEA since the mid-1990s (Hinder et al., 2012). Climate change effect on the timing and severity of toxic events is still uncertain (Wells et al., 2019) with model predictions and *in situ* data not always coinciding (Dees et al., 2017; Gobler et al., 2017).

As we have seen, the shellfish aquaculture industry differs between and even within countries in the NEA: hydrography may be very different; toxic species may change as may the toxicity of a particular species; and there is a great deal of inter-annual and seasonal variation. This creates a challenge when developing models which must be adapted and fitted to these divergent conditions. Over the past decade EWS have been implemented with varying degrees of success in different countries. Some, such as those in Ireland and Scotland are fully functional while others are still in the developmental proof of concept and trial stage. This heterogeneity means the overall value of these EWS systems to industry, while, regionally important, is currently low but rapidly increasing as cross region cooperation and method sharing increases.

AUTHOR CONTRIBUTIONS

JF-S, KD, MS, MR, WS, DC, MR-V, and LF contributed to the initial idea, data analysis, and the manuscript writing. PM, RF, AS, MiM, and JS contributed to the initial idea and manuscript writing. PA, LM, CW, McM, and PN contributed to the data analysis and manuscript writing. All authors contributed to the article and approved the submitted version.

FUNDING

Interreg Atlantic Area Programme Project PRIMROSE (Grant No. EAPA_182/2016, https://www.shellfish-safety.eu/). The national monitoring program of bivalve molluscs in Portugal is funded by project SNMB—MONITOR (Monitor-16.02.01-FEAMP-0043): Competitiveness and sustainable development for the shellfish sector of mainland Portugal co-financed by the Portuguese Government, Operational Program (OP) March 2020, Portugal 2020 and European Union through the European Structural Funds and Investment Funds (FEEI) and European Maritime and Fisheries Fund (EMFF), AS acknowledges funding from IPMA fellowship (IPMA-BCC-2016-35). This study was partially supported by the project EGRECOST CALIDAD – Control de Calidad de Aguas Cultivos Marinos (Departamento de Desarrollo Económico e Infraestructuras del Gobierno Vasco) and by the UKRI projects CAMPUS (Grant No. NE/R00675X/1) and Off-Aqua (Grant No. BB/S004246/1). This study was partially supported by the European H2020 project FutureMARES (Grant No. 869300).

ACKNOWLEDGMENTS

IOC-ICES-PICES HAEDAT maps courtesy of Pieter Provoost, IOC project office for IODE, Ostend, Belgium. The authors thank three reviewers for their constructive comments that have improved the manuscript. This is contribution number 1037 from the Marine Research Division (AZTI-BRTA).

SUPPLEMENTARY MATERIAL

The Supplementary Material for this article can be found online at: https://www.frontiersin.org/articles/10.3389/fmars.2021.666583/full#supplementary-material

REFERENCES

Abascal, A. J., Castanedo, S., Fernández, V., and Medina, R. (2012). Backtracking drifting objects using surface currents from high-frequency (HF) radar technology. *Ocean Dyn.* 62, 1073–1089. doi: 10.1007/s10236-012-0546-4

Aleynik, D., Dale, A. C., Porter, M., and Davidson, K. (2016). A high resolution hydrodynamic model system suitable for novel harmful algal bloom modelling in areas of complex coastline and topography. *Harmful Algae* 53, 102–117.

Alley, R. B., Emanuel, K. A., and Zhang, F. (2019). Advances in weather prediction. *Science* 363:342.

Anderson, C. R., Siegel, D. A., Brzezinski, M. A., and Guillocheau, N. (2008). Controls on temporal patterns in phytoplankton community structure in the Santa Barbara Channel, California. *J. Geophys. Res.* 113:C04038. doi: 10.1029/2007JC004321

Anderson, D. M. (1998). Physiology and bloom dynamics of toxic *Alexandrium* species, with emphasis on life cycle transitions. *Nato Asi Ser. G Ecol. Sci.* 41, 29–48.

Aoki, K., Onitsuka, G., Shimizu, M., Kuroda, H., Matsuyama, Y., Kimoto, K., et al. (2012). Factors controlling the spatio-temporal distribution of the 2009 *Chattonella antiqua* bloom in the Yatsushiro Sea, Japan. *Estuar. Coast. Shelf Sci.* 114, 148–155. doi: 10.1016/j.ecss.2012.08.028

Avdelas, L., Avdic−Mravlje, E., Borges Marques, A. C., Cano, S., Capelle, J. J., Carvalho, N., et al. (2021). The decline of mussel aquaculture in the European Union: causes, economic impacts and opportunities. *Rev. Aquac.* 13, 91–118. doi: 10.1111/raq.12465

Barraquand, F., Picoche, C., Maurer, D., Carassou, L., and Auby, I. (2018). Coastal phytoplankton community dynamics and coexistence driven by intragroup density-dependence, light and hydrodynamics. *Oikos Nordic Ecol. Soc.* 127, 1834–1852. doi: 10.1111/oik.05361

Bates, S. S., Bird, C. J., de Freitas, A. S. W., Foxall, R., Gilgan, M., Hanic, L. A., et al. (1989). Pennate diatom *Nitzschia pungens* as the primary source of momoic acid, a toxin in shellfish from Eastern Prince Edward Island, Canada. *Can. J. Fish. Aquat. Sci.* 46, 1203–1215. doi: 10.1139/f89-156

Batifoulier, F., Lazure, P., Velo-Suarez, L., Maurer, D., Bonneton, P., Charria, G., et al. (2013). Distribution of *Dinophysis* species in the Bay of Biscay and possible transport pathways to Arcachon Bay. *J. Mar. Syst.* 109, S273–S283. doi: 10.1016/j.jmarsys.2011.12.007

Bax, N. J., Miloslavich, P., Muller-Karger, F. E., Allain, V., Appeltans, W., Batten, S. D., et al. (2019). A response to scientific and societal needs for marine biological observations. *Front. Mar. Sci.* 6:395. doi: 10.3389/fmars.2019.00395

Berdalet, E., Fleming, L. E., Gowen, R., Davidson, K., Hess, P., Backer, L. C., et al. (2016). Marine harmful algal blooms, human health and wellbeing: challenges and opportunities in the 21st century. *J. Mar. Biol. Assoc.* 96, 61–91. doi: 10.1017/S0025315415001733

Berdalet, E., Montresor, M., Reguera, B., Roy, S., Yamazaki, H., Cembella, A., et al. (2017). Harmful algal blooms in fjords, coastal embayments, and stratified systems: recent progress and future research. *Oceanography* 30, 46–57. doi: 10.5670/oceanog.2017.109

Billett, D. S. M., Lampitt, R. S., and Mantoura, R. F. C. (1983). Seasonal sedimentation of phytoplankton to the deep-sea benthos. *Nature* 302, 520–522. doi: 10.1038/302520a0

Botelho, M. J., Vale, C., and Ferreira, J. G. (2019). Seasonal and multi-annual trends of bivalve toxicity by PSTs in Portuguese marine waters. *Sci. Total Environ.* 664, 1095–1106. doi: 10.1016/j.scitotenv.2019.01.314

Bravo, I., Fraga, S., Figueroa, R. I., Pazos, Y., Massanet, A., and Ramilo, I. (2010). Bloom dynamics and life cycle strategies of two toxic dinoflagellates in a coastal upwelling system (NW Iberian Peninsula). *Deep Sea Res. Part II Top. Stud. Oceanogr.* 57, 222–234. doi: 10.1016/j.dsr2.2009.09.004

Breivik, Ø, Bekkvik, T. C., Wettre, C., and Ommundsen, A. (2012). BAKTRAK: backtracking drifting objects using an iterative algorithm with a forward trajectory model. *Ocean Dyn.* 62, 239–252. doi: 10.1007/s10236-011-0496-2

Bresnan, E., Arévalo, F., Belin, C., Branco, M. A., Cembella, A. D., Clarke, D., et al. (2021). Diversity and regional distribution of harmful algal events along the Atlantic margin of Europe. *Harmful Algae* 102:101976. doi: 10.1016/j.hal.2021.101976

Broullón, E., López-Mozos, M., Reguera, B., Chouciño, P., Doval, M. D., Fernández-Castro, B., et al. (2020). Thin layers of phytoplankton and harmful algae events in a coastal upwelling system. *Prog. Oceanogr.* 189:102449. doi: 10.1016/j.pocean.2020.102449

Brown, L., Bresnan, E., Graham, J., Lacaze, J. P., Turrell, E., and Collins, C. (2010). Distribution, diversity and toxin composition of the genus *Alexandrium* (Dinophyceae) in Scottish waters. *Eur. J. Phycol.* 45, 375–393. doi: 10.1080/09670262.2010.495164

Buntine, W. (1991). "Theory refinement on Bayesian networks", in *Uncertainty Proceedings*, Elsevier, 52–60. doi: 10.1016/B978-1-55860-203-8.50010-3

Caballero, A., Ferrer, L., Rubio, A., Charria, G., Taylor, B. H., and Grima, N. (2014). Monitoring of a quasi-stationary eddy in the Bay of Biscay by means of satellite, *in situ* and model results. *Deep Sea Res. Part II* 106, 23–37. doi: 10.1016/j.dsr2.2013.09.029

Caballero, I., Fernández, R., Escalante, O. M., Mamán, L., and Navarro, G. (2020). New capabilities of Sentinel-2A/B satellites combined with in situ data for monitoring small harmful algal blooms in complex coastal waters. *Sci. Rep.* 10, 1–14. doi: 10.1038/s41598-020-65600-1

Castillo, E., Gutierrez, J., and Hadi, A. (1997). *Expert Systems and Probabilistic Network Models*. New York, NY: Springer Verlag.

Chambouvet, A., Morin, P., Marie, D., and Guillou, L. (2008). Control of toxic marine dinoflagellate blooms by serial parasitic killers. *Science* 322, 1254–1257. doi: 10.1126/science.1164387

Chapelle, A. (2016). *Modélisation du Phytoplancton Dans Les Écosystèmes Côtiers. Application À L'eutrophisation et Aux Proliférations D'algues Toxiques*. Brest: Université de Bretagne Occidentale.

Chapelle, A., Le Gac, M. L. C., Siano, R., Quere, J., Caradec, F., Le Bec, C., et al. (2015). The Bay of Brest (France), a new risky site for toxic *Alexandrium minutum* blooms and PSP shellfish contamination. *Harmful Algae News* 51, 4–5.

Charria, G., Repecaud, M., Quemener, L., Menesguen, A., Rimmelin Maury, P., et al. (2014). PREVIMER: a contribution to in situ coastal observing systems. *Mercator Ocean Q. Newslett.* 49, 9–20.

Chen, H. (2019). Performance of a simple backtracking method for marine oil source searching in a 3D 101 ocean. *Mar. Pollut. Bull.* 142, 321–334. doi: 10.1016/j.marpolbul.2019.03.045

Clarke, D. (2020). "New insights and perspectives from 20 years of monitoring algal events in Irish coastal waters," in *Proceedings of the 11th Irish Shellfish Safety Workshop, Marine Environment and Health Series No. 41*, eds D. Clarke and M. Gilmartin (Galway: Marine Institute).

Coates, L., Swan, S., Davidson, K., Turner, A., Maskrey, B., and Algoet, M. (2018). *Annual Report on the Results of the Biotoxin and Phytoplankton Official Control Monitoring Programmes for Scotland - 2017*. Lowestoft: Cefas.

Costa, P. R., and Garrido, S. (2004). Domoic acid accumulation in the sardine *Sardina pilchardus* and its relationship to *Pseudo-nitzschia* diatom ingestion. *Mar. Ecol. Prog. Ser.* 284, 261–268. doi: 10.3354/meps284261

Cruz, R. C., Reis Costa, P., Vinga, S., Krippahl, L., and Lopes, M. B. (2021). A Review of recent machine learning advances for forecasting harmful algal blooms and shellfish contamination. *J. Mar. Sci. Eng.* 9:283. doi: 10.3390/jmse9030283

Cusack, C., Dabrowski, T., Lyons, K., Berry, A., Westbrook, G., Salas, R., et al. (2016). Harmful algal bloom forecast system for SW Ireland. Part II: are operational oceanographic models useful in a HAB warning system. *Harmful Algae* 53, 86–101. doi: 10.1016/j.hal.2015.11.013

Dabrowski, T., Lyons, K., Nolan, G., Berry, A., Cusack, C., and Silke, J. (2016). Harmful algal bloom forecast system for SW Ireland. Part I: description and validation of an operational forecasting model. *Harmful Algae* 53, 64–76. doi: 10.1016/j.hal.2015.11.015

Davidson, K., Anderson, D. M., Mateus, M., Reguera, B., Silke, J., Sourisseau, M., et al. (2016). Forecasting the risk of harmful algal blooms: preface to the Asimuth special issue. *Harmful Algae* 53, 1–7. doi: 10.1016/j.hal.2015.11.005

Davidson, K., Baker, C., Higgins, C., Higman, W., Swan, S., Veszelovszki, A., et al. (2015). Potential threats posed by new or emerging marine biotoxins in UK waters and examination of detection methodologies used for their control: cyclic imines. *Mar. Drugs* 13, 7087–7112. doi: 10.3390/md13127057

Davidson, K., Tett, P., and Gowen, R. J. (2011). "Harmful algal blooms," in *Marine Pollution & Human Health*, eds R. M. Harrison and R. E. Hester (Cambridge: RSC publishing), 95–127.

Davidson, K., Whyte, C., Aleynik, D., Kurekin, A., Gontarek, S., McNeill, S., et al. (2021). HABreports: online early warning of harmful algal and biotoxin risk for the Scottish shellfish and finfish aquaculture industries. *Front. Mar. Sci.* 8:631732. doi: 10.3389/fmars.2021.631732

Debreu, L., Marchesiello, P., Penven, P., and Cambon, G. (2012). Two-way nesting in split-explicit ocean models: algorithms, implementation and validation. *Ocean Model.* 49–50, 1–21. doi: 10.1016/j.ocemod.2012.03.003

Dees, P., Bresnan, E., Dale, A. C., Edwards, M., Johns, D., Mouat, B., et al. (2017). Harmful algal blooms in the Eastern North Atlantic ocean. *Proc. Natl. Acad. Sci. U.S.A.* 114, E9763–E9764. doi: 10.1073/pnas.1715499114

Defra (2019). *MAGIC Interactive Mapping Tool: Geographic Information About the Natural Environment From Across Government*. London: Defra.

Delmas, D., Herbland, A., and Maestrini, S. Y. (1993). "Do *Dinophysis* spp. come from the "open sea" along the French Atlantic coast?," in *Toxic Phytoplankton Blooms in the Sea*, eds T. Smayda and Y. Shimizu (Amsterdam: Elsevier Science), 489–494.

Dhanji-Rapkova, M., O'Neill, A., Maskrey, B. H., Coates, L., Swan, S. C., Alves, M. T., et al. (2019). Variability and profiles of lipophilic toxins in bivalves

from Great Britain during five and a half years of monitoring: azaspiracids and yessotoxins. *Harmful Algae* 87:101629. doi: 10.1016/j.hal.2019.101629

Díaz, P. A., Reguera, B., Moita, T., Bravo, I., Ruiz-Villarreal, M., and Fraga, S. (2019). Mesoscale dynamics and niche segregation of two *Dinophysis* species in Galician-Portuguese coastal waters. *Toxins* 11:37.

Díaz, P. A., Reguera, B., Ruiz-Villarreal, M., Pazos, Y., Velo-Suarez, L., Berger, H., et al. (2013). Climate variability and oceanographic settings associated with interannual variability in the initiation of *Dinophysis acuminata* blooms. *Mar. Drugs* 11, 2964–2981. doi: 10.3390/md11082964

Díaz, P. A., Ruiz-Villarreal, M., Pazos, Y., Moita, T., and Reguera, B. (2016). Climate variability and *Dinophysis acuta* blooms in an upwelling system. *Harmful Algae* 53, 145–159. doi: 10.1016/j.hal.2015.11.007

Dippner, J. W., Nguyen-Ngoc, L., Doan-Nhu, N., and Subramaniam, A. (2011). A model for the prediction of harmful algae blooms in the Vietnamese upwelling area. *Harmful Algae* 10, 606–611. doi: 10.1016/j.hal.2011.04.012

Drakulović, D., Gvozdenović, S., Joksimović, D., Mandić, M., and Pestorić, B. (2017). Toxic and potentially toxic phytoplankton in the mussel and fish farms in the transitional area of Montenegrin Coast (South-Eastern Adriatic Sea). *Turkish J. Fish. Aqu. Sci.* 17, 885–900. doi: 10.4194/1303-2712-v17_5_05

Drévillon, M., Greiner, E., Paradis, D., Payan, C., Lellouche, J.-M., Reffray, G., et al. (2013). A strategy for producing refined currents in the Equatorial Atlantic in the context of the search of the AF447 wreckage. *Ocean Dyn.* 63, 63–82. doi: 10.1007/s10236-012-0580-2

Edwards, M., Johns, D. G., Leterme, S. C., Svendsen, E., and Richardson, A. J. (2006). Regional climate change and harmful algal blooms in the northeast Atlantic. *Limnol. Oceanogr.* 51, 820–829. doi: 10.4319/lo.2006.51.2.0820

EFSA (2008). Opinion of the scienti fi c panel on contaminants in the food chain on a request from the European commission on marine biotoxins in shell fish–azaspiracids. *EFSA J.* 723, 1–52. doi: 10.2903/j.efsa.2009.907

Ellis, T., Gardiner, R., Gubbins, M., Reese, A., and Smith, D. (2015). *Aquaculture Statistics for the UK, with a Focus on England and Wales: 2012*. Lowestoft: Cefas, 18.

Egbert, G. D., and Erofeeva, S. Y. (2002). Efficient inverse modeling of barotropic ocean tides. *J. Atmos. Oceanic Technol.* 19, 183–204. doi: 10.1175/1520-0426(2002)019<0183:EIMOBO>2.0.CO;2

En 15204 (2006). *Water Quality - Guidance Standard on the Enumeration of Phytoplankton Using Inverted Microscopy (Utermöhl technique)*. Brussels: European Committee for Standardization.

FAO (2018). *The State of World Fisheries and Aquaculture 2018. Meeting the Sustainable Development Goals*. Rome: Food and Agriculture Organization of the United Nations.

FAO (2019). *FAO Yearbook. Fishery and Aquaculture Statistics 2017/FAO Annuaire. Statistiques des Pêches et De l'aquaculture 2017/FAO Anuario. Estadísticas de Pesca y Acuicultura 2017*. Rome: Food and Agriculture Organization of the United Nations.

Farrell, H., Gentien, P., Fernand, L., Lunven, M., Reguera, B., González-Gil, S., et al. (2012). Scales characterising a high density thin layer of *Dinophysis acuta* Ehrenberg and its transport within a coastal jet. *Harmful Algae* 15, 36–46. doi: 10.1016/j.hal.2011.11.003

Fehling, J., Davidson, K., Bolch, C. J., and Tett, P. (2006). Seasonality of *Pseudo-nitzschia* spp. (Bacillariophyceae) in western Scottish waters. *Mar. Ecol. Prog. Ser.* 323, 91–105. doi: 10.3354/meps323091

Fehling, J., Davidson, K., Bolch, C. J., Brand, T., and Narayanaswamy, B. E. (2012). The relationship between phytoplankton distribution and water column characteristics in North West European Shelf Sea Waters. *PLoS One* 7:e34098. doi: 10.1371/journal.pone.0034098

Fernandes, J. A., Irigoien, X., Boyra, G., Lozano, J. A., and Inza, I. (2009). Optimizing the number of classes in automated zooplankton classification. *J. Plankt. Res.* 31, 19–29. doi: 10.1093/plankt/fbn098

Fernandes, J. A., Irigoien, X., Goikoetxea, N., Lozano, J. A., Inza, I., Pérez, A., et al. (2010). Fish recruitment prediction, using robust supervised classification methods. *Ecol. Model.* 221, 338–352. doi: 10.1016/j.ecolmodel.2009.09.020

Fernandes, J. A., Irigoien, X., Lozano, J. A., Inza, I., Goikoetxea, N., and Pérez, A. (2015). Evaluating machine-learning techniques for recruitment forecasting of seven North East Atlantic fish species. *Ecol. Inform.* 25, 35–42. doi: 10.1016/j.ecoinf.2014.11.004

Fernandes, J. A., Kauppila, P., Uusitalo, L., Fleming-Lehtinen, V., Kuikka, S., and Pitkänen, H. (2012). Evaluation of reaching the targets of the water framework directive in the Gulf of Finland. *Environ. Sci. Technol.* 46, 8220–8228. doi: 10.1021/es300126b

Fernandes, J. A., Lozano, J. A., Inza, I., Irigoien, X., Pérez, A., and Rodríguez, J. D. (2013). Supervised pre-processing approaches in multiple class variables classification for fish recruitment forecasting. *Environ. Model. Softw.* 40, 245–254. doi: 10.1016/j.envsoft.2012.10.001

Fernández, R., Mamán, L., Jaén, D., Fernández Fuentes, L., Ocaña, M. A., and Gordillo, M. M. (2019). *Dinophysis* species and diarrhetic shellfish toxins: 20 years of monitoring program in Andalusia, South of Spain. *Toxins* 11:189. doi: 10.3390/toxins11040189

Ferrer, L., and Caballero, A. (2011). Eddies in the Bay of Biscay: a numerical approximation. *J. Mar. Syst.* 87, 133–144. doi: 10.1016/j.jmarsys.2011.03.008

Ferrer, L., Fontán, A., Chust, G., Mader, J., González, M., Valencia, V., et al. (2009). Low-salinity plumes in the oceanic region of the Basque Country. *Cont. Shelf Res.* 29, 970–984.

Ferrer, L., González, M., Valencia, V., Mader, J., Fontán, A., Uriarte, A. D., et al. (2007). "Operational coastal systems in the Basque Country region: modelling and observations," in *Proceedings 17th International Offshore (Ocean) and Polar Eng. Conference*, eds J. S. Chung, M. Kashiwagi I, J. Losada, and L.-K. Chien (Lisbon: ISOPE), 1736–1743.

Ferrer, L., Zaldua-Mendizabal, N., Del Campo, A., Franco, J., Mader, J., Cotano, U., et al. (2015). Operational protocol for the sighting and tracking of Portuguese man-of-war in the southeastern Bay of Biscay: observations and modelling. *Cont. Shelf Res.* 95, 39–53. doi: 10.1016/j.csr.2014.12.011

Ferrer, L., Zaldua-Mendizabal, N., Del Campo, A., Franco, J., Mader, J., Cotano, U., et al. (2013). Protocolo operacional para el avistamiento y seguimiento del cnidario *Physalia physalis* (carabela portuguesa) en el sureste del golfo de Bizkaia. *Rev. Invest. Mar.* 20, 88–102.

García, C. M., Prieto, L., Vargas, M., Echevarría, F., García-Lafuente, J., Ruiz, J., et al. (2002). Hydrodynamics and the spatial distribution of plankton and TEP in the Gulf of Cadiz (SW Iberian Peninsula). *J. Plankt. Res.* 24, 817–833. doi: 10.1093/plankt/24.8.817

Gentien, P., Lunven, M., Lazure, P., Youenou, A., and Crassous, M. P. (2007). Motility and Autotoxicity in *Karenia Mikimotoi* (Dinophyceae). *Philos. Trans. R. Soc. B Biol.* Sci. 362, 1937–1946. doi: 10.1098/rstb.2007.2079

Gillibrand, P. A., Siemering, B., Miller, P. I., and Davidson, K. (2016). Individual-based modelling of the development and transport of a *Karenia mikimotoi* bloom on the North-West European continental shelf. *Harmful Algae* 53, 118–134. doi: 10.1016/j.hal.2015.11.011

Glibert, P. M., Wilkerson, F. P., Dugdale, R. C., Parker, A. E., Alexander, J., Blaser, S., et al. (2014). Phytoplankton communities from San Francisco Bay Delta respond differently to oxidized and reduced nitrogen substrates—even under conditions that would otherwise suggest nitrogen sufficiency. *Front. Mar. Sci.* 1:17. doi: 10.3389/fmars.2014.00017

Gobler, C. J., Doherty, O. M., Hattenrath-Lehmann, T. K., Griffith, A. W., Kang, Y., and Litaker, R. W. (2017). Ocean warming since 1982 has expanded the niche of toxic algal blooms in the North Atlantic and North Pacific oceans. *Proc. Natl. Acad. Sci. U.S.A.* 114, 4975–4980. doi: 10.1073/pnas.1619575114

Godinho, L., Silva, A., Branco, M. A. C., Marques, A., and Costa, P. R. (2018). Evaluation of intracellular and extracellular domoic acid content in *Pseudo-nitzschia multiseries* cell cultures under different light regimes. *Toxicon* 155, 27–31. doi: 10.1016/j.toxicon.2018.10.003

Gokaraju, B., Durbha, S. S., King, R. L., and Younan, N. H. (2011). A machine learning based spatio-temporal data mining approach for detection of harmful algal blooms in the Gulf of Mexico. *IEEE J. Select. Top. Appl. Earth Observ. Remote Sens.* 4, 710–720. doi: 10.1109/JSTARS.2010.2103927

Gowen, R. J., Tett, P., Bresnan, E., Davidson, K., and McKinney, A. (2012). Anthropogenic nutrient enrichment and blooms of harmful phytoplankton. *Oceanogr. Mar. Biol.* 50, 65–126. doi: 10.1201/b12157-3

Grosjean, P., Picheral, M., Warembourg, C., and Gorsky, G. (2004). Enumeration, measurement, and identification of net zooplankton samples using the ZOOSCAN digital imaging system. *ICES J. Mar. Sci.* 61, 518–525. doi: 10.1016/j.icesjms.2004.03.012

Grzebyk, D., Audic, S., Lasserre, B., Abadie, E., de Vargas, C., and Bec, B. (2017). Insights into the harmful algal flora in northwestern Mediterranean coastal lagoons revealed by pyrosequencing metabarcodes of the 28S rRNA gene. *Harmful Algae* 68, 1–16. doi: 10.1016/j.hal.2017.06.003

Guallar, C., Bacher, C., and Chapelle, A. (2017). Global and local factors driving the phenology of *Alexandrium minutum* (Halim) blooms and its toxicity. *Harmful Algae* 67, 44–60. doi: 10.1016/j.hal.2017.05.005

Guallar, C., Delgado, M., Diogene, J., and Fernandez-Tejedor, M. (2016). Artificial neural network approach to population dynamics of harmful algal blooms in Alfacs Bay (NW Mediterranean): case studies of *Karlodinium* and *Pseudo-nitzschia*. *Ecol. Model.* 338, 37–50. doi: 10.1016/j.ecolmodel.2016.07.009

Haidvogel, D. B., Arango, H. G., Hedström, K., Beckmann, A., Malanotte-Rizzoli, P., and Shchepetkin, A. F. (2000). Model evaluation experiments in the North Atlantic Basin: simulations in nonlinear terrain-following coordinates. *Dyn. Atmos. Oceans* 32, 239–281. doi: 10.1016/S0377-0265(00)00049-X

Hall, M. A. (1999). *Correlation-Based Feature Selection for Machine Learning*. Dissertation thesis. Waikato: The University of Waikato.

Hall, M. A. (2000). "Correlation-based feature selection of discrete and numeric class machine learning," in *Proceedings of the Seventeenth International Conference on Machine Learning* (Stanford, CA: Stanford University), 359–366.

Hall, M. A., and Smith, L. A. (1997). "Feature subset selection: a correlation based filter approach," in *Proceedings of the International Conference on Neural Information Processing and Intelligent Information Systems* (Berlin: Springer), 855–858.

Hallegraeff, G. M. (2003). "Harmful algal blooms: a global overview," in *Manual on Harmful Marine Microalgae*, eds G. Hallegraeff, D. Anderson, A. Cembella, and H. Enevoldsen (Paris: IOC Manuals and Guides UNESCO), 1–22.

Hambrey, J., and Evans, S. (2016). *Aquaculture in England, Wales and Northern Ireland: An Analysis of the Economic Contribution and Value of the Major Subsectors and the Most Important Farmed Species. Report SR694*. Edinburgh: Sea Fish Industry Authority, 162.

Hernandez Farinas, T., Bacher, C., Soudant, D., Belin, C., and Barille, L. (2015). Assessing phytoplankton realized niches using a French national phytoplankton monitoring network. *Estuar. Coast. Shelf Sci.* 159, 15–27. doi: 10.1016/j.ecss.2015.03.010

Hernández-González, J., Inza, I., Granado, I., Basurko, O. C., Fernandes, J. A., and Lozano, J. A. (2019). Aggregated outputs by linear models: an application on marine litter beaching prediction. *Inform. Sci.* 481, 381–393. doi: 10.1016/j.ins.2018.12.083

Higman, W., Turner, A., Baker, C., Higgins, C., Veszelovszki, A., and Davidson, K. (2013). *Research to Support the Development of a Monitoring Programme for New or Emerging Marine Biotoxins in Shellfish in UK waters*. London: Report to the Food Standards Agency, 437.

Hinder, S. L., Hays, G. C., Edwards, M., Roberts, E. C., Walne, A. W., and Gravenor, M. B. (2012). Changes in marine dinoflagellate and diatom abundance under climate change. *Nat. Clim. Change* 2, 271–275. doi: 10.1038/nclimate1388

Hu, H., Wen, Y., Chua, T. S., and Li, X. (2014). Toward scalable systems for big data analytics: a technology tutorial. *IEEE Access* 2, 652–687. doi: 10.1109/ACCESS.2014.2332453

Huisman, J., and Weissing, F. J. (1999). Biodiversity of plankton by species oscillations and chaos. *Nature* 402, 407–410. doi: 10.1038/46540

Husson, B., Hernández-Fariñas, T., Le Gendre, R., Schapira, M., and Chapelle, A. (2016). Two decades of *Pseudo-nitzschia* spp. blooms and king scallop (*Pecten maximus*) contamination by domoic acid along the French Atlantic and English channel coasts: seasonal dynamics, spatial heterogeneity and interannual variability. *Harmful Algae* 51, 26–39. doi: 10.1016/j.hal.2015.10.017

Hutchins, D. A., and Bruland, K. W. (1998). Iron-limited diatom growth and Si:N uptake ratios in a coastal upwelling regime. *Nature* 393, 561–564. doi: 10.1038/31203

Irigoien, X., Huisman, J., and Harris, R. P. (2004). Global biodiversity patterns of marine phytoplankton and zooplankton. *Nature* 429, 863–867. doi: 10.1038/nature02593

Juang, H. M. H. (2000). The NCEP mesoscale spectral model: a revised version of the nonhydrostatic regional spectral model. *Mon. Weather Rev.* 128, 2329–2362. doi: 10.1175/1520-0493(2000)128<2329:TNMSMA>2.0.CO;2

Karasiewicz, S., Breton, E., Lefebvre, A., Hernandez Farinas, T., and Lefebvre, S. (2018). Realized niche analysis of phytoplankton communities involving HAB: Phaeocystis spp. as a case study. *Harmful Algae* 72, 1–13. doi: 10.1016/j.hal.2017.12.005

Karlson, B., Andersen, P., Arneborg, L., Cembella, A., Eikrem, W., John, U., et al. (2021). Harmful algal blooms and their effects in coastal seas of Northern Europe. *Harmful Algae* 102:101989. doi: 10.1016/j.hal.2021.101989

Kissling, W. D., Ahumada, J. A., Bowser, A., Fernandez, M., Fernández, N., García, E. A., et al. (2018). Building essential biodiversity variables (EBV s) of species distribution and abundance at a global scale. *Biol. Rev.* 93, 600–625. doi: 10.1111/brv.12359

Kurekin, A. A., Miller, P. I., and Van der Woerd, H. J. (2014). Satellite discrimination of *Karenia mikimotoi* and *Phaeocystis* harmful algal blooms in European coastal waters: Merged classification of ocean colour data. *Harmful Algae* 31, 163–176. doi: 10.1016/j.hal.2013.11.003

Laiz, I., Ferrer, L., Plomaritis, T. A., and Charria, G. (2014). Effect of river runoff on sea level from in-situ measurements and numerical models in the Bay of Biscay. *Deep Sea Res. Part II* 106, 49–67. doi: 10.1016/j.dsr2.2013.12.013

Landsberg, J. H. (2002). The effects of harmful algal blooms on aquatic organisms. *Rev. Fish. Sci.* 10, 113–390. doi: 10.1080/20026491051695

Le Gac, M., Metegnier, G., Chomérat, N., Malestroit, P., Quéré, J., Bouchez, O., et al. (2016). Evolutionary processes and cellular functions underlying divergence in *Alexandrium minutum*. *Mol. Ecol.* 25, 5129–5143.

Leadbetter, A., Silke, J., and Cusack, C. (2018). *Creating a Weekly Harmful Algal Bloom Bulletin*. Galway: Marine Institute, 63.

LeBihan, V., Guillotreau, B., Morineau, B., and Pardo, S. (2019). "The impact of shellfish trade bans caused by Harmful Algal Blooms (HABs) on a french regional economy: an input-output approach," in *Proceedings of the Oceanext-Interdisciplinary Conference*, Nantes.

LeCun, Y., Bengio, Y., and Hinton, G. (2015). Deep learning. *Nature* 521, 436–444. doi: 10.1038/nature14539

Legorburu, I., Ferrer, L., Galparsoro, I., and Larreta, J. (2015). Distribution of river-borne particulate Pb in the Basque continental shelf (Bay of Biscay). *Environ. Earth Sci.* 74, 4261–4279. doi: 10.1007/s12665-015-4495-3

Lelong, A., Hégaret, H., Soudant, P., and Bates, S. S. (2012). *Pseudo-nitzschia* (Bacillariophyceae) species, domoic acid and amnesic shellfish poisoning: revisiting previous paradigms. *Phycologia* 51, 168–216. doi: 10.2216/11-37.1

Lett, C., Verley, P., Mullon, C., Parada, C., Brochier, T., Penven, P., et al. (2008). A Lagrangian tool for modelling ichthyoplankton dynamics. *Environ. Modell. Softw.* 23, 1210–1214. doi: 10.1016/j.envsoft.2008.02.005

Lewis, A. M., Coates, L. N., Turner, A. D., Percy, L., and Lewis, J. (2018). A review of the global distribution of *Alexandrium minutum* (Dinophyceae) and comments on ecology and associated paralytic shellfish toxin profiles, with a focus on Northern Europe. *J. Phycol.* 54, 581–598. doi: 10.1111/jpy.12768

Lindahl, O. (1986). "A dividable hose for phytoplankton sampling," in *Proceedings of the International Council for the Exploration of the Sea Report of the Working Group on Exceptional Algal Blooms*, Copenhagen.

Magdalena, A. B., Lehane, M., Krys, S., Fernández, M. L., Furey, A., and James, K. J. (2003). The first identification of azaspiracids in shellfish from France and Spain. *Toxicon* 42, 105–108. doi: 10.1016/S0041-0101(03)00105-3

Maguire, J., Cusack, C., Ruiz-Villarreal, M., Silke, J., McElligott, D., and Davidson, K. (2016). Applied simulations and integrated modelling for the understanding of toxic and harmful algal blooms (ASIMUTH): integrated HAB forecast systems for Europe's Atlantic Arc. *Harmful Algae* 53, 160–166. doi: 10.1016/j.hal.2015.11.006

Mardones, J. I., Holland, D. S., Anderson, L., Le Bihan, V., Gianella, F., Clément, A., et al. (2020). *Estimating and Mitigating the Economic Costs of Harmful Algal Blooms on Commercial and Recreational Shellfish Harvesters*. Belgium: GlobalHAB, 66.

Martens, H., Tillmann, U., Harju, K., Dell'Aversano, C., Tartaglione, L., and Krock, B. (2017). Toxin variability estimations of 68 Alexandrium ostenfeldii (Dinophyceae) strains from The Netherlands reveal a novel abundant gymnodimine. *Microorganisms* 5:29. doi: 10.3390/microorganisms5020029

Martino, S., Gianella, F., and Davidson, K. (2020). An approach for evaluating the economic impacts of harmful algal blooms: the effects of blooms of toxic *Dinophysis* spp. on the productivity of Scottish shellfish farms. *Harmful Algae* 99:101912. doi: 10.1016/j.hal.2020.101912

Mateus, M., Fernandes, J., Revilla, M., Ferrer, L., Villarreal, M. R., Miller, P., et al. (2019). "Early warning systems for shellfish safety: the pivotal role of computational science," in *Proceedings of the*

International Conference on Computational Science (Cham: Springer), 361–375.

Mateus, M., Riflet, G., Chambel, P. C., Fernandes, L., Fernandes, R., Juliano, M., et al. (2012). An operational model for the West Iberian coast: products and services. *Ocean Sci.* 8, 713–732. doi: 10.5194/os-8-713-2012

McCabe, R. M., Hickey, B. M., Kudela, R. M., Lefebvre, K. A., Adams, N. G., Bill, B. D., et al. (2016). An unprecedented coastwide toxic algal bloom linked to anomalous ocean conditions. *Geophys. Res. Lett.* 43, 10366–10376. doi: 10.1002/2016GL070023

Mellor, G. L., and Yamada, T. (1982). Development of a turbulence closure model for geophysical fluid problems. *Rev. Geophys.* 20, 851–875. doi: 10.1029/RG020i004p00851

Ménesguen, A., Dussauze, M., Lecornu, F., Dumas, F., and Thouvenin, B. (2014). Operatonial modelling of nutrients and phytoplankton in the Bay of Biscay and english channel. *Mercator Ocean Q. Newslett.* 49, 87–93.

Míguez, A., Fernlindez, L., and Fraga, S. (1996). "First detection of domoic acid in Galicia (NW of Spain)", in *Harmful Toxic Algal Blooms*, eds T. Yasumoto, Y. Oshima, and Y. Fukuyo, Paris, 143–145.

Miller, P. I., Kurekin, A., Evers-King, H., Lockett, J., Davidson, K.-M., Calder-Potts, R., et al. (in press). Satellite monitoring and modelling for early warning of water quality risks to shellfish farms. *Bull. Am. Meteorol. Soc.*

Miloslavich, P., Bax, N. J., Simmons, S. E., Klein, E., Appeltans, W., Aburto−Oropeza, O., et al. (2018). Essential ocean variables for global sustained observations of biodiversity and ecosystem changes. *Glob. Change Biol.* 24, 2416–2433. doi: 10.1111/gcb.14108

Moestrup, Ø, Akselman, R., Cronberg, G., Elbraechter, M., Fraga, S., Halim, Y., et al. (2009). *IOC-UNESCO Taxonomic Reference List of Harmful Micro Algae*. Available online at: http://www.marinespecies.org/hab (accessed January 27, 2021).

Moita, M. T., Oliveira, P. B., Mendes, J., and Palma, A. (2003). Distribution of Chlorophyll a and *Gymnodinium catenatum* associated with coastal upwelling plumes off central Portugal. *Acta Oecol.* 24, 125–132. doi: 10.1016/S1146-609X(03)00011-0

Moita, M. T., Pazos, Y., Rocha, C., Nolasco, R., and Oliveira, P. B. (2016). Toward predicting *Dinophysis* blooms off NW Iberia: a decade of events. *Harmful Algae* 53, 17–32. doi: 10.1016/j.jbusres.2014.02.013

Moita, M. T., Sobrinho-Gonçalves, L., Oliveira, P. B., Palma, S., and Falcao, M. (2006). A bloom of *Dinophysis acuta* in a thin layer off north-west Portugal. *Afr. J. Mar. Sci.* 28, 265–269. doi: 10.2989/18142320609504160

Mousavi, S., and Gigerenzer, G. (2014). Risk, uncertainty, and heuristics. *J. Bus. Res.* 67, 1671–1678.

Muñiz, O., Revilla, M., Rodríguez, J. G., Laza-Martínez, A., Seoane, S., Franco, J., et al. (2017). Evaluation of phytoplankton quality and toxicity risk based on a long-term time series previous to the implementation of a bivalve farm (Basque coast as a case study). *Reg. Stud. Mar. Sci.* 10, 10–19. doi: 10.1016/j.rsma.2016.12.012

Munro, L. A., and Wallace, I. S. (2018). *Scottish Shellfish Farm Production Survey 2017*. Aberdeen: Marine Scotland Science.

Navarro, G., and Ruiz, J. (2006). Spatial and temporal variability of phytoplankton in the Gulf of Cadiz through remote sensing images. *Deep Sea Res. Part II* 53, 1241–1260. doi: 10.1016/j.dsr2.2006.04.014

Navarro, G., Caballero, I., Prieto, L., Vázquez, A., Flecha, S., Huertas, I. E., et al. (2012). Seasonal-to-interannual variability of Chlorophyll-a bloom timing associated with physical forcing in the Gulf of Cádiz. *Adv. Space Res.* 50, 1164–1172. doi: 10.1016/j.asr.2011.11.034

Nezan, E., Chomerat, N., Bilien, G., Boulben, S., Duval, A., and Ryckaert, M. (2010). *Pseudo-nitzschia australis* on French Atlantic coast-an unusual toxic bloom. *Harmful Algae News* 41, 1–2.

Palma, S., Mouriño, H., Silva, A., Barão, M. I., and Moita, M. T. (2010). Can *Pseudo-nitzschia* blooms be modeled by coastal upwelling in Lisbon Bay? *Harmful Algae* 9, 294–303. doi: 10.1016/j.hal.2009.11.006

Pan, Y., Bates, S. S., and Cembella, A. (1998). Environmental stress and domoic acid production by *Pseudo-nitzschia*: a physiological perspective. *Nat. Toxins* 6, 127–135. doi: 10.1002/(SICI)1522-7189(199805/08)6:3/43.0.CO

Paterson, R. F. (2017). *Investigating the Distribution, Seasonal Dynamics and Toxicity of Azadinium spinosum in Scottish waters using qPCR*. Dissertation thesis. Aberdeen: The University of Aberdeen.

Paterson, R. F., McNeill, S., Mitchell, E., Adams, T., Swan, S. C., Clarke, D., et al. (2017). Environmental control of harmful dinoflagellates and diatoms in a fjordic system. *Harmful Algae* 69, 1–17. doi: 10.1016/j.hal.2017.09.002

Pazos, Y., Moroño, A., Triñanes, J., Doval, M., Montero, P., and Vilarinho, M. G. (2006). "Early detection and intensive monitoring during an unusual toxic bloom of *Gymnodinium catenatum* advected into the Galician Rías (NW, Spain)," in *Proceedings of the 12th International Conference on HABs*, Copenhagen.

Pearl, J. (1988). *Probabilistic Reasoning in Intelligence Systems: Networks of Plausible Inference*. San Francisco, CA: Morgan Kaufmann Publishers Inc.

Pinto, L., Mateus, M., and Silva, A. (2016). Modeling the transport pathways of harmful algal blooms in the Iberian coast. *Harmful Algae* 53, 8–16. doi: 10.1016/j.hal.2015.12.001

Pitcher, G. C., Figueiras, F. G., Hickey, B. M., and Moita, M. T. (2010). The physical oceanography of upwelling systems and the development of harmful algal blooms. *Prog. Oceanogr.* 85, 5–32. doi: 10.1016/j.pocean.2010.02.002

Prieto, L., Navarro, G., Cózar, A., Echevarria, F., and García, C. M. (2006). Distribution of TEP in the euphotic and upper mesopelagic zones of the southern Iberian coasts. *Deep Sea Res. Part II Top. Stud. Oceanogr.* 53, 1314–1328. doi: 10.1016/j.dsr2.2006.03.009

Prieto, L., Navarro, G., Rodríguez-Gálvez, S., Huertas, I. E., Naranjo, J. M., and Ruiz, J. (2009). Oceanographic and meteorological forcing of the pelagic ecosystem on the Gulf of Cadiz shelf (SW Iberian Peninsula). *Cont. Shelf Res.* 29, 2122–2137. doi: 10.1016/j.csr.2009.08.007

Raine, R. (2014). A review of the biophysical interactions relevant to the promotion of HABs in stratified systems: the case study of Ireland. *Deep Sea Res. Part II Top. Stud. Oceanogr.* 101, 21–31. doi: 10.1016/j.dsr2.2013.06.021

Raine, R., Cosgrove, S., Fennell, S., Gregory, C., Bernett, M., Purdie, D., et al. (2016). "Origins of Dinophysis blooms which impact Irish aquaculture," in *Proceedings of the 17th International Conference of Harmful Algae*, eds L. A. O. Proença and G. M. Hallegraeff (Florianópolis: International Society for the Study of Harmful Algae), 46–49.

Rathaille, A. N., and Raine, R. (2011). Seasonality in the excystment of *Alexandrium minutum* and *Alexandrium tamarense* in Irish coastal waters. *Harmful Algae* 10, 629–635. doi: 10.1016/j.hal.2011.04.015

Reguera, B., Riobó, P., Rodríguez, F., Díaz, P. A., Pizarro, G., Paz, B., et al. (2014). *Dinophysis* toxins: causative organisms, distribution and fate in shellfish. *Mar. Drugs* 12, 394–461. doi: 10.3390/md12010394

Reguera, B., Velo-Suárez, L., Raine, R., and Park, M. G. (2012). Harmful *Dinophysis* species: a review. *Harmful Algae* 14, 87–106. doi: 10.1016/j.hal.2011.10.016

Revilla, M., Borja, A., Fontán, A., Franco, J., Manuel, G., Valencia, V., et al. (2010). Phytoplankton biomass and temperature trends in offshore waters of the Basque country. *Globec Int. Newslett.* 10:12.

Rodríguez-Rodríguez, G., Villasante, S., and García-Negro, M. C. (2011). Are red tides affecting economically the commercialization of the Galician (NW Spain) mussel farming? *Mar. Policy* 35, 252–257. doi: 10.1016/j.marpol.2010.08.008

Rowland-Pilgrim, S., Swan, S. C., O'Neill, A., Johnson, S., Coates, L., Stubbs, P., et al. (2019). Variability of amnesic shellfish toxin and *Pseudo-nitzschia* occurrence in bivalve molluscs and water samples–analysis of ten years of the official control monitoring programme. *Harmful Algae* 87:101623. doi: 10.1016/j.hal.2019.101623

Ruiz-Villarreal, M., García-García, L. M., Cobas, M., Díaz, P. A., and Reguera, B. (2016). Modelling the hydrodynamic conditions associated with *Dinophysis* blooms in Galicia (NW Spain). *Harmful Algae* 53, 40–52. doi: 10.1016/j.hal.2015.12.003

Salas, R., and Clarke, D. (2019). Review of DSP toxicity in Ireland: long-term trend impacts, biodiversity and toxin profiles from a monitoring perspective. *Toxins* 11:61. doi: 10.3390/toxins11020061

Sanseverino, I., Conduto, D., Pozzoli, L., Dobricic, S., and Lettieri, T. (2016). *Algal Bloom and its Economic Impact*. Luxembourg: European Union.

Santos, M., Costa, P. R., Porteiro, F. M., and Moita, M. T. (2014). First report of a massive bloom of *Alexandrium minutum* (Dinophyceae) in middle North Atlantic: a coastal lagoon in S. Jorge Island, Azores. *Toxicon* 90, 265–268. doi: 10.1016/j.toxicon.2014.08.065

Schmidt, W., Evers-King, H. L., Campos, C. J. A., Jones, D. B., Miller, P. I., Davidson, K., et al. (2018). A generic approach for the development of short-term predictions of *Escherichia coli* and biotoxins in shellfish. *Aquac. Environ. Interact.* 10, 173–185. doi: 10.3354/aei00265

Schnetzer, A., Jones, B. H., Schaffner, R. A., Cetinic, I., Fitzpatrick, E., Miller, P. E., et al. (2013). Coastal upwelling linked to toxic *Pseudo-nitzschia australis* blooms in Los Angeles coastal waters, 2005–2007. *J. Plankt. Res.* 35, 1080–1092. doi: 10.1093/plankt/fbt051

Shchepetkin, A. F., and McWilliams, J. C. (2005). The regional oceanic modeling system (ROMS): a split-explicit, free-surface, topography-following-coordinate oceanic model. *Ocean Model.* 9, 347–404. doi: 10.1016/j.ocemod.2004.08.002

Siemering, B., Bresnan, E., Painter, S. C., Daniels, C. J., Inall, M., and Davidson, K. (2016). Phytoplankton distribution in relation to environmental drivers on the NorthWest European Shelf Sea. *PLoS One* 11:e0164482. doi: 10.1371/journal.pone.0164482

Silva, A., Pinto, L., Rodrigues, S. M., de Pablo, H., Santos, M., Moita, T., et al. (2016). A HAB warning system for shellfish harvesting in Portugal. *Harmful Algae* 53, 33–39. doi: 10.1016/j.hal.2015.11.017

Simpson, J. H., Edelsten, D. J., Edwards, A., Morris, N. C. G., and Tett, P. B. (1979). The Islay front: physical structure and phytoplankton distribution. *Estuar. Coast. Mar. Sci.* 9:713. doi: 10.1016/S0302-3524(79)80005-5

Sison-Mangus, M., Jiang, S., Tran, K., and Kudela, R. M. (2014). Host-specific adaptation governs the interaction of the marine diatom. Pseudo-nitzschia and their microbiota. *ISME J.* 8, 63–76. doi: 10.1038/ismej.2013.138

Skamarock, W. C., and Klemp, J. B. (2008). A time-split nonhydrostatic atmospheric model for weather research and forecasting applications. *J. Comput. Phys.* 227, 3465–3485. doi: 10.1016/j.jcp.2007.01.037

Smagorinsky, J. (1963). General circulation experiments with the primitive equations: I. The basic experiment. *Mon. Weather Rev.* 91, 99–164. doi: 10.1175/1520-0493(1963)091<0099:GCEWTP>2.3.CO;2

Smayda, T. J. (1990). "Novel and nuisance phytoplankton blooms in the sea: evidence for a global epidemic," in *Toxic Marine Phytoplankton*, eds E. Granéli, B. Sundstrøm, L. Edler, and D. M. Anderson (Amsterdam: Elsevier), 29–40.

Smetacek, V. (1999). Diatoms and the ocean carbon cycle. *Protist* 150, 25–32.

Smith, M. E., Robertson Lain, L., and Bernard, S. (2018). An optimized Chlorophyll a switching algorithm for MERIS and OLCI in phytoplankton-dominated waters. *Remote Sens. Environ.* 215, 217–227. doi: 10.1016/j.rse.2018.06.002

Song, Y. T., and Haidvogel, D. B. (1994). A semi-implicit ocean circulation model using a generalized topography-following coordinate system. *J. Comp. Phys.* 115, 228–244. doi: 10.1006/jcph.1994.1189

Sopanen, S., Setälä, O., Piiparinen, J., Erler, K., and Kremp, A. (2011). The toxic dinoflagellate *Alexandrium ostenfeldii* promotes incapacitation of the calanoid copepods *Eurytemora affinis* and *Acartia bifilosa* from the northern Baltic Sea. *J. Plankt. Res.* 33, 1564–1573. doi: 10.1093/plankt/fbr052

Sourisseau, M., Jegou, K., Lunven, M., Quere, J., Gohin, F., and Bryere, P. (2016). Distribution and dynamics of two species of Dynophiceae producing high biomass blooms over the French Atlantic Shelf. *Harmful Algae* 53, 53–63. doi: 10.1016/j.hal.2015.11.016

Sourisseau, M., Le Guennec, V., Le Gland, G., Plus, M., and Chapelle, A. (2017). Resource competition affects plankton community structure; evidence from trait-based modeling. *Front. Mar. Sci.* 4:52. doi: 10.3389/fmars.2017.00052

Spyrakos, E., Vilas, L. G., Palenzuela, J. M. T., and Barton, E. D. (2011). Remote sensing chlorophyll a of optically complex waters (rias Baixas, NW Spain): application of a regionally specific chlorophyll a algorithm for MERIS full resolution data during an upwelling cycle. *Remote Sens. Environ.* 115, 2471–2485. doi: 10.1016/j.rse.2011.05.008

Stall, S., Yarmey, L., Cutcher-Gershenfeld, J., Hanson, B., Lernhert, K., Nosek, B., et al. (2019). Make scientific data FAIR'. *Nature* 570, 27–29. doi: 10.1038/d41586-019-01720-7

Stumpf, R. P., Culver, M. E., Tester, P. A., Tomlinson, M., Kirkpatrick, G. J., Pederson, B. A., et al. (2003). Monitoring Karenia brevis blooms in the Gulf of Mexico using satellite ocean color imagery and other data. *Harmful Algae* 2, 147–160. doi: 10.1016/S1568-9883(02)00083-5

Sun, C.-C., Wang, Y.-S., Wu, M.-L., Dong, J.-D., Wang, Y.-T., Sun, F.-L., et al. (2011). Seasonal variation of water quality and phytoplankton response patterns in Daya Bay, China. *Int. J. Environ. Res. Public Health* 8, 2951–2966. doi: 10.3390/ijerph8072951

Sunda, W. G., Price, N. M., and Morel, F. M. M. (2005). "Trace metal ion buffers and their use in culture studies," in *Algal Culturing Techniques*, ed. R. A. Anderson (Cambridge, MA: Elsevier Academic Press), 35–63.

Suneel, V., Ciappa, A., and Vethamony, P. (2016). Backtrack modeling to locate the origin of tar balls depositing along the west coast of India. *Sci. Total Environ.* 569–570, 31–39. doi: 10.1016/j.scitotenv.2016.06

Sverdrup, H. U. (1953). On conditions for the vernal blooming of phytoplankton. *ICES J. Mar. Sci.* 18, 287–295. doi: 10.1093/icesjms/18.3.287

Swan, S. C., Turner, A. D., Bresnan, E., Whyte, C., Paterson, R. F., McNeill, S., et al. (2018). *Dinophysis acuta* in Scottish Waters and its influence on diarrhetic shellfish toxin profiles. *Toxins* 10:399. doi: 10.3390/toxins10100399

Swan, S., and Davidson, K. (2012). *Monitoring Programme for the Presence of Toxin Producing Plankton in Shellfish Production Areas in Scotland*. Scotland: Food Standards Agency.

Taconet, M., Kroodsma, D., and Fernandes, J. A. (2019). *Global Atlas of AIS-based fishing activity - Challenges and opportunities*. Rome: FAO.

Tatters, A. O., Fu, F. X., and Hutchins, D. A. (2012). High CO2 and silicate limitation synergistically increase the toxicity of *Pseudo-nitzschia fraudulenta*. *PLoS One* 7:e32116. doi: 10.1371/journal.pone.0032116

Theodorou, J. A., Moutopoulos, D. K., and Tzovenis, I. (2020). Semi-quantitative risk assessment of Mediterranean mussel (*Mytilus galloprovincialis* L.) harvesting bans due to harmful algal bloom (HAB) incidents in Greece. *Aquac. Econ. Manag.* 24, 273–293. doi: 10.1080/13657305.2019.1708994

Thorel, M., Claquin, P., Schapira, M., Le Gendre, R., Riou, P., Goux, D., et al. (2017). Nutrient ratios influence variability in *Pseudo-nitzschia* species diversity and particulate domoic acid production in the Bay of Seine (France). *Harmful Algae* 68, 192–205. doi: 10.1016/j.hal.2017.07.005

Tillmann, U., Jaén, D., Fernández, L., Gottschling, M., Witt, M., Blanco, J., et al. (2017). *Amphidoma languida* (Amphidomatacea, Dinophyceae) with a novel azaspiracid toxin profile identified as the cause of molluscan contamination at the Atlantic coast of southern Spain. *Harmful Algae* 62, 113–126. doi: 10.1016/j.hal.2016.12.001

Tomlinson, M. C., Stumpf, R. P., Ransibrahmanakul, V., Truby, E. W., Kirkpatrick, G. J., Pederson, B. A., et al. (2004). Evaluation of the use of SeaWiFS imagery for detecting *Karenia brevis* harmful algal blooms in the eastern Gulf of Mexico. *Remote Sens. Environ.* 91, 293–303. doi: 10.1016/j.rse.2004.02.014

Torres Palenzuela, J. M., González Vilas, L., Bellas, F. M., Garet, E., González-Fernández, Á, et al. (2019). *Pseudo-nitzschia* blooms in a coastal upwelling system: Remote sensing detection, toxicity and environmental variables. *Water* 11:1954. doi: 10.3390/w11091954

Touzet, N., Davidson, K., Pete, R., Flanagan, K., McCoy, G. R., Amzil, Z., et al. (2010). Co-occurrence of the West European (Gr. III) and North American (Gr. I) ribotypes of *Alexandrium tamarense* (Dinophyceae) in Shetland, Scotland. *Protist* 161, 370–384. doi: 10.1016/j.protis.2009.12.001

Touzet, N., Franco, J. M., and Raine, R. (2007). 'Characterization of nontoxic and toxin-producing strains of Alexandrium minutum (Dinophyceae) in Irish coastal waters'. *Appl. Environ. Microbiol.* 73, 3333–3342. doi: 10.1128/AEM.02161-06

Trainer, V. L., Pitcher, G. C., Reguera, B., and Smayda, T. J. (2010). The distribution and impacts of harmful algal bloom species in eastern boundary upwelling systems. *Prog. Oceanogr.* 85, 33–52. doi: 10.1016/j.pocean.2010.02.003

Trifonova, N., Kenny, A., Maxwell, D., Duplisea, D., Fernandes, J., and Tucker, A. (2015). Spatio-temporal Bayesian network models with latent variables for revealing trophic dynamics and functional networks in fisheries ecology. *Ecol. Inform.* 30, 142–158. doi: 10.1016/j.ecoinf.2015.10.003

Turner, A., Higgins, C., Veszelovski, A., Payne, D., Davidson, K., Hungerford, J., et al. (2015). Monitoring of new or emerging marine biotoxins in UK waters: Brevetoxins. *Mar. Drugs* 13, 1224–1254. doi: 10.3390/md13031224

Uncles, R. G., Clark, J. R., Bedington, M., and Torres, R. (2020). "On sediment dispersal in the Whitsand Bay marine conservation zone: neighbour to a closed dredge-spoil disposal site," in *Marine Protected Areas: Evidence, Policy, and Practise*, eds R. Clark and J. Humphreys (Amsterdam: Elsevier Inc.), 599–569.

Utermöhl, H. (1958). Zur Vervollkommnung der quantitativen Phytoplankton-Methodik. Mitt. int. Verein. *Theor. Angew. Limnol.* 9, 1–38.

Uusitalo, L., Fernandes, J. A., Bachiller, E., Tasala, S., and Lehtiniemi, M. (2016). Semi-automated classification method addressing marine strategy framework

directive (MSFD) zooplankton indicators. *Ecol. Indic.* 71, 398–405. doi: 10.1016/j.ecolind.2016.05.036

Vale, P., Botelho, M. J., Rodrigues, S. M., Gomes, S. S., and Sampayo, M. A. M. (2008). Two decades of marine biotoxin monitoring in bivalves from Portugal (1986–2006): a review of exposure assessment. *Harmful Algae* 7, 11–25. doi: 10.1016/j.hal.2007.05.002

Vanhoutte-Brunier, A., Fernand, L., Ménesguen, A., Lyons, S., Gohin, F., and Philippe, C. (2008). Modelling the *Karenia mikimotoi* bloom that occurred in the western english channel during summer 2003. *Ecol. Model.* 210, 351–376. doi: 10.1016/j.ecolmodel.2007.08.025

Vasquez, M., Mata Chacón, D., Tempera, F., O'Keeffe, E., Galparsoro, I., Sanz Alonso, J. L., et al. (2015). Broad-scale mapping of seafloor habitats in the north-east Atlantic using existing environmental data. *J. Sea Res.* 100, 120–132. doi: 10.1016/j.seares.2014.09.011

Velo-Suárez, L., and Gutiérrez-Estrada, J. C. (2007). Artificial neural network approaches to one-step weekly prediction of *Dinophysis acuminata* blooms in Huelva (Western Andalucía, Spain). *Harmful Algae* 6, 361–371. doi: 10.1016/j.hal.2006.11.002

Velo-Suarez, L., Gonzalez-Gil, S., Gentien, P., Lunven, M., Bechemin, C., Fernand, L., et al. (2008). Thin layers of *Pseudo-nitzschia* spp. and the fate of Dinophysis acuminata during an upwelling–downwelling cycle in a Galician Ria. *Limnol. Oceanogr.* 53:1816. doi: 10.4319/lo.2008.53.5.1816

Velo-Suárez, L., Reguera, B., González-Gil, S., Lunven, M., Lazure, P., Nézan, E., et al. (2010). Application of a 3D Lagrangian model to explain the decline of a *Dinophysis acuminata* bloom in the Bay of Biscay. *J. Mar. Syst.* 83, 242–252. doi: 10.1016/j.jmarsys.2010.05.011

Vilas, L. G., Spyrakos, E., Palenzuela, J. M. T., and Pazos, Y. (2014). Support Vector Machine-based method for predicting *Pseudo-nitzschia* spp. blooms in coastal waters (Galician rias, NW Spain). *Prog. Oceanogr.* 124, 66–77. doi: 10.1016/j.pocean.2014.03.003

Visciano, P., Schirone, M., Berti, M., Milandri, A., Tofalo, R., and Suzzi, G. (2016). Marine biotoxins: occurrence, toxicity, regulatory limits and reference methods. *Front. Microbiol.* 7:1051. doi: 10.3389/fmicb.2016.01051

Wang, D. Z. (2008). Neurotoxins from marine dinoflagellates: a brief review. *Mar. Drugs* 6, 349–371. doi: 10.3390/md20080016

Wells, M. L., Karlson, B., Wulff, A., Kudela, R., Trick, C., Asnaghi, V., et al. (2019). Future HAB science: Directions and challenges in a changing climate. *Harmful Algae* 91:101632. doi: 10.1016/j.hal.2019.101632

Whyte, C., Swan, S., and Davidson, K. (2014). Changing wind patterns linked to unusually high Dinophysis blooms around the coast of the Shetland Islands, Scotland. *Harmful Algae* 39, 365–373. doi: 10.1016/j.hal.2014.09.006

Wilkinson, M. D., Dumontier, M., Aalbersberg, I. J., Appleton, G., Axton, M., Baak, A., et al. (2016). The FAIR guiding principles for scientific data management and stewardship. *Sci. Data* 3:160018. doi: 10.1038/sdata.2016.18

Witten, I. H., Frank, E., Hall, M., and Pal, C. J. (2017). *Data Mining: Practical Machine Learning Tools and Techniques With Java Implementations*, 4th Edn. Burlington, MA: Morgan Kaufmann Series in Data Management Systems.

Wu, L., Chen, C., Guo, P., Shi, M., Qi, J., and Ge, J. (2011). A FVCOM-based unstructured grid wave, current, sediment transport model, I. Model description and validation. *J. Ocean Univ. China* 10, 1–8. doi: 10.1007/s11802-011-1788-3

Wyatt, T. (2014). Margalef's mandala and phytoplankton bloom strategies. *Deep Sea Res. Part II Top. Stud. Oceanogr.* 101, 32–49. doi: 10.1016/j.dsr2.2012.12.006

Xu, X., Pan, D., Mao, Z., and Tao, B. (2014). A new algorithm based on the background field for red tide monitoring in the East China Sea. *Acta Oceanol. Sin.* 33, 62–71. doi: 10.1007/s13131-014-0404-y

Zhu, Z., Qu, P., Fu, F., Tennenbaum, N., Tatters, A. O., and Hutchins, D. A. (2017). *Harmful Algae* 67, 36–43. doi: 10.1016/j.hal.2017.06.004

Conflict of Interest: The authors declare that the research was conducted in the absence of any commercial or financial relationships that could be construed as a potential conflict of interest.

The reviewer EB declared a past co-authorship with the authors to the handling editor.

frontiers in Marine Science

ORIGINAL RESEARCH
published: 21 July 2021
doi: 10.3389/fmars.2021.680482

Combining Imaging Flow Cytometry and Molecular Biological Methods to Reveal Presence of Potentially Toxic Algae at the Ural River in Kazakhstan

Yersultan Mirasbekov[1†], Aigerim Abdimanova[1†], Kuanysh Sarkytbayev[1†], Kanat Samarkhanov[1,2], Aidyn Abilkas[1,3], Daria Potashnikova[4], Galina Arbuz[1], Zhanpeis Issayev[5], Ivan A. Vorobjev[1,3], Dmitry V. Malashenkov[6] and Natasha S. Barteneva[1,3,7]**

[1] Department of Biology, School of Sciences and Humanities, Nazarbayev University, Nur-Sultan, Kazakhstan, [2] Xinjiang Institute of Ecology and Geography, University of Chinese Academy of Sciences, Beijing, China, [3] Laboratory of Biophotonics and Imaging, National Laboratory Astana, Nazarbayev University, Nur-Sultan, Kazakhstan, [4] Department of Cell Biology and Histology, Lomonosov Moscow State University, Moscow, Russia, [5] Core Facilities, Nazarbayev University, Nur-Sultan, Kazakhstan, [6] Department of General Ecology and Hydrobiology, Lomonosov Moscow State University, Moscow, Russia, [7] The Environmental Research and Efficiency Cluster (EREC), Nazarbayev University, Nur-Sultan, Kazakhstan

Algal blooms occur in freshwater bodies throughout the world, often leading to fish kills. Cases of these kills along the Ural River were reported in 2018–2019, involving significant amount of sturgeon in fish farming areas. In this study, the analysis of algal samples from the delta of the Ural River up to 100 km inland was carried out from August to December 2019 using imaging flow cytometry (IFC), molecular biological, and microscopic techniques. We identified the filamentous cyanobacteria *Cuspidothrix issatschenkoi*, *Dolichospermum* cf. *flos-aquae*, *Dolichospermum* cf. *macrosporum*, *Pseudanabaena limnetica*, and *Planktothrix* spp. as the dominant potentially toxic phytoplankton species, and we also found minor quantities of *Cylindrospermopsis raciborskii*. For the first time, molecular phylogenetic investigations of field clones of cyanobacteria from Ural River were carried out to establish the taxa of the dominant species and to identify the presence of genes encoding toxins. The complementary analysis with nanopore-based next-generation sequencing overlapped with the results of IFC and was instrumental in revealing minor cyanobacteria taxa. Real-time PCR analysis and sequencing indicated the presence of *Microcystis* and ADA-clade spp. as well as genes associated with the production of microcystin (*mcyE*) and the algal neurotoxin saxitoxin (*sxtA*) originating from cyanobacteria. These findings suggest that toxin-producing cyanobacteria could become a threat in the Ural River near Atyrau, which can significantly affect aquaculture in the region.

Keywords: toxic algae, cyanobacteria, imaging flow cytometry, next-generation sequencing, MinION, real-time PCR, satellite data analysis, *Cylindrospermopsis raciborskii*

OPEN ACCESS

Edited by:
Joe Silke, Marine Institute, Ireland

Reviewed by:
Khor Waiho, University of Malaysia Terengganu, Malaysia
Nor Azman Kasan, University of Malaysia Terengganu, Malaysia

***Correspondence:**
Dmitry V. Malashenkov
dvmalashenkov@gmail.com
Natasha S. Barteneva
natalie.barteneva@nu.edu.kz; bartene@yahoo.com

† These authors have contributed equally to this work

Specialty section:
This article was submitted to Marine Fisheries, Aquaculture and Living Resources, a section of the journal Frontiers in Marine Science

Received: *14 March 2021*
Accepted: *10 June 2021*
Published: *21 July 2021*

Citation:
Mirasbekov Y, Abdimanova A, Sarkytbayev K, Samarkhanov K, Abilkas A, Potashnikova D, Arbuz G, Issayev Z, Vorobjev IA, Malashenkov DV and Barteneva NS (2021) Combining Imaging Flow Cytometry and Molecular Biological Methods to Reveal Presence of Potentially Toxic Algae at the Ural River in Kazakhstan. Front. Mar. Sci. 8:680482. doi: 10.3389/fmars.2021.680482

INTRODUCTION

The incidence and intensity of harmful algal blooms (HABs) as well as the associated economic impact have increased worldwide with warming water temperatures in recent years (Paerl and Paul, 2012; Jeppesen et al., 2017; Griffith and Gobler, 2020; Wells et al., 2020; Fernandes-Salvador et al., 2021). HABs are complex events typically caused by multiple factors occurring simultaneously, may threaten ecosystems, and lead to the degradation of water quality for recreation, drinking, and aquaculture (Heisler et al., 2008; Oliver et al., 2012; Jeppesen et al., 2017) with further changes in temperature, nutrient load, and oxygenation of aquatic environments. The toxin production by certain cyanobacteria (e.g., *Dolichospermum circinalis*, *Cylindrospermopsis raciborskii*, and *Microcystis aeruginosa*) during algal blooms causes the accumulation of toxins in the tissues of fresh- and saltwater mussels, fish, and mammals (Rapala et al., 1997; Codd et al., 2005; Wilson et al., 2005; Carmichael, 2008; Mihali et al., 2009; Oliver et al., 2012; De Pace et al., 2014; Gibble et al., 2016; Li et al., 2016; Luerling et al., 2017; Meriluoto et al., 2017; Chernova et al., 2019). The harmful effects can be caused by either direct effects from toxins or changes in the water chemistry, such as oxygen depletion or hydrogen sulfide production (Eriksson et al., 1986; Tornazo et al., 1990). Together with nutrients, the temperature is considered an essential factor in the growth, metabolism of cyanobacteria (Reynolds, 2008), and the adaptation of invasive potentially toxic cyanobacterial species, particularly *Cylindrospermopsis* (=*Raphidiopsis*) *raciborskii* (Padisák, 1997; Thomas and Litchman, 2016). In the last decade, the increasing contamination of freshwater bodies by anthropogenic pollution, as well as the upward temperature gradient have had major effects on further expansion of cyanobacteria in freshwater bodies (Sukenik et al., 2015). Although most studies are focused on the seasonal algal blooms in summer and spring seasons, cold weather and winter cyanobacterial blooms have been documented throughout the literature (Naselli-Flores et al., 2007; Babanazarova et al., 2013; Wejnerowski et al., 2018). Water temperature directly affects rates of respiration, photosynthesis, and algal growth in aquatic ecosystems (Regier et al., 1990). The link between temperature and toxin production by cyanobacteria remains elusive and is governed by the complex interaction among all environmental factors.

Importantly, improving the ability to monitor and detect HABs and cyanobacterial toxins are required for better documentation and understanding of algal blooms and the prevention of their effects on fisheries and farmed aquaculture (Shumway, 1990; Pearl and Tucker, 1995; GEOHAB, 2001; Ramsdell et al., 2005; Anderson et al., 2012). Strong species-specific interactions between the environment and phytoplankton communities make HAB predictions difficult (Griffith and Gobler, 2020). Monitoring programs for HABs were developed initially for marine HABs and generally relied on the microscopic identification and manual time-consuming counting of phytoplankton (Anderson et al., 2012). The inability of conventional flow cytometry to determine species composition is one of the major reasons why flow cytometry could not be adopted as a standard tool for monitoring harmful algae (Rutten et al., 2005). In the HAB monitoring and research, there are several different approaches to identify causative species and relevant toxins, including the development of nucleic-based biosensors in microarray and real-time polymerase-chain reaction (PCR) formats (Dierks-Horn et al., 2011; rev. McPartlin et al., 2017), imaging flow cytometry (IFC) (Buskey and Hyatt, 2006; Campbell et al., 2010, 2013), and satellite analysis-based algorithms. The FlowCAM (Yokogawa Fluid Imaging Technologies, United States) is an imaging flow cytometer designed to characterize microplankton size range particles (Sieracki et al., 1998) and used by different research groups for semi-automated monitoring of algal blooms (Buskey and Hyatt, 2006; Lehman et al., 2013; Dashkova et al., 2017). FlowCAM software have been allowed to discriminate and quantitate different potentially toxic algae within complex natural assemblages, including *Microcystis* colonies (Buskey and Hyatt, 2006; Lehman et al., 2013, 2017; Sukenik et al., 2015; Graham et al., 2018; Kurobe et al., 2018; Mirasbekov et al., 2021).

In common HAB monitoring strategies, the number of field samples required to be analyzed by light microscopy for taxonomical species identification dramatically reduces the possibilities of early detection of HAB initiation and dispersion phases (Antonella and Luca, 2013). In addition, the optical-based methods of identifying toxic cyanobacteria (light microscopy or IFC) do not differentiate toxin-producing from non-toxin-producing species. By taking in the account these limitations of traditional imaging approaches (microscopy and cytometry) in monitoring programs, molecular methods have been implemented for detection of pre-bloom algal abundances. That includes many real-time PCR protocols to monitor toxic cyanobacteria (rev. Martins and Vasconcelos, 2011). Identifying and quantifying of the potentially toxic species present may not suffice to estimate the potential toxic risk, because not all of the strains may produce toxins. Screening based on molecular targeting is more precise and sensitive with advantage of distinguishing non-toxic and toxic strains (Pearson and Neilan, 2008). Within most important cyanotoxins, PCR-based methods were used to identify toxic genotypes of cyanobacteria-producing microcystins, cylindrospermopsin, paralytic shellfish toxins (PSTs), anatoxins, and other toxins (Pomati et al., 2000; Foulds et al., 2002; Vaitomaa et al., 2003; Kurmayer and Christiansen, 2010; Pearson et al., 2010; Martins and Vasconcelos, 2011; Antonella and Luca, 2013). Microcystin production has been the most studied between cyanobacteria and is well known among several genera of cyanobacteria, including *Microcystis*, *Anabaena*, *Pseudoanabaena*, *Planktothrix*, and others (Kurmayer and Christiansen, 2010; Pearson et al., 2010). Cylindrospermopsin (CYN) is the second most widely occurring hepatotoxin produced by cyanobacteria species, including *C. raciborskii* and *Aphanizomenon*/*Cuspidothrix* spp. (Pearson et al., 2010). Several species of freshwater filamentous cyanobacteria have been reported to produce PSTs (saxitoxins) (Humpage et al., 1984; Mahmood and Carmichael, 1986). Although initially thought to be rare, cyanobacterial anatoxin-a (ANTX) has been detected in many freshwater habitats (Bruno et al., 2016; Ballot et al., 2018). Real-time PCR protocols can be helpful in defining the

presence of toxic cyanobacteria genotypes during bloom- and non-bloom seasons (Martins and Vasconcelos, 2011; Antonella and Luca, 2013). However, molecular probes and PCR primers are designed for specific targets and may overlook unknown members of an algal community. In freshwater cyanobacteria research, next-generation sequencing (NGS) has been recently used to assess the general diversity mostly based on 16S rRNA gene amplicons analysis (Liao et al., 2016; Woodhouse et al., 2016; Lezcano et al., 2017; Scherer et al., 2017). Lately, the portable MinION device offered a unique solution for dinoflagellates HAB microbiome research (Hatfield et al., 2020). Recently released, the Oxford Nanopore MinION device (United Kingdom) is a third-generation portable sequencing platform valuable for applications with a large number of samples or where portability is more important than increased error rate (5–15%, Pfeiffer et al., 2018) (Castro-Wallace et al., 2017; Johnson et al., 2017; Gowers et al., 2019; Burton et al., 2020). However, only a few studies focused on harmful algae in water bodies combining NGS assessment with toxic genotype analysis by real-time PCR (Fortin et al., 2015; Lee et al., 2015).

Although most studies are focused on the seasonal algal blooms in summer and spring seasons, cold-weather and winter cyanobacterial blooms have been documented throughout the literature (Naselli-Flores et al., 2007; Babanazarova et al., 2013; Wejnerowski et al., 2018). Water temperature directly affects rates of respiration, photosynthesis, and algal growth in aquatic ecosystems (Regier et al., 1990; Joehnk et al., 2008). The link between temperature and toxin production by cyanobacteria remains elusive and is governed by the complex interaction among all environmental factors. It was found that the highest toxin contents, such as microcystin (MC), cylindrospermopsin, and other toxic compounds, are not associated with temperature conditions most favorable for cyanobacteria growth (Saker and Griffiths, 2000 for cylindrospermopsin; Savadova et al., 2018 for MC).

In this work, a combination of high-resolution IFC, NGS, and PCR-based methods were used to evaluate the presence of potentially toxic cyanobacteria along the Ural River, including the places of recent fish kills. Initial detection and identification of potentially toxic algae was done with IFC, and then confirmed with molecular methods. This combination of methodological approaches will be a valuable way to determine the presence and frequency of potentially toxic detectable cyanobacteria. Additionally, metagenomic analysis with the Nanopore sequencing platform provided an alternative, complementary way to identify and characterize potential harmful algae strains.

MATERIALS AND METHODS

Water Sampling

Ural River is the third river in terms of its length among European rivers, and it flows from the Ural mountains to the delta of the Caspian Sea. The temperature in this area can be as low as −38°C and as high as 46°C (Kazhydromet Climate Monitoring Bulletin, 2016). This project had covered the region of the river within the borders of Atyrau city, upstream from the city border (100 km away), and downstream to the delta of the Caspian Sea. The sampling sites are illustrated in **Figure 1**, and they were assigned as follows: S1 Delta > S2 Channel > S3 Ship > S4 low Peretaska > S5 Balykshy > S6 Peretaska > S7 Oil refinery water intake-ANPZ > S8 Atyrau Su Arnasy > S9 Geolog > S10 Almaly > S11 Saraishyk > S12 low Makhambet > S13 upper Makhambet > S14 Ural River 100 km (distances are as follows: S1–S2 14.8 km; S2–S3 21.2 km; S3–S4 9.2 km; S4–S5 8.6 km; S5–S6 2.1 km; S6–S7 1.6 km; S7–S8 6.7 km; S8–S9 5.1 km; S9–S10 16 km; S10–S11 45 km; S11–S12 23.2 km; S12–S13 17.5 km; S13–S14 24.6 km) The samples were collected across the length of the river in August–December 2019, noting that sampling in October and December was limited by two sampling points at Peretaska duct, near a local cogeneration plant and oil refinery.

Shortly, the surface water sampling was carried out, and samples for IFC analysis of the phytoplankton communities and hydrochemistry were collected at each location in plastic 5-L bottles from surface water horizon (0.5 m depth) in plastic 5-L bottles. Water turbidity was checked by the Secchi disk. Phytoplankton samples were fixed in triplicates with different fixators: paraformaldehyde (0.5%), glutaraldehyde (0.5%), and Lugol's solution. Fresh, live samples were preserved in the cold box until delivered to the laboratory and then kept in the refrigerator at 4°C. Water parameters such as dissolved oxygen, salinity, conductivity, temperature, and total dissolved solids at the sampling site were measured on-site. The phosphate concentration was calculated by the standard molybdate method (Motomizu et al., 1983).

Satellite Data Analysis

Land surface temperature is one of the physical observation remote sensing parameters which are of great importance for different disciplines, such as environmental studies, hydrology, etc., which contributes to a better understanding of energy and water exchange. NASA's Landsat mission has collected a huge amount of relatively high spatial resolution thermal data as it has a thermal infrared (TIR) sensor onboard since 1984 (Barsi et al., 2003). In this study, Landsat 8 data were used on Atyrau city to retrieve land surface temperature for recent dates as it is the source of new images. Landsat 8 has two thermal bands with a spatial resolution of 100 m and a 16-day revisit time (Rozenstein et al., 2014). The data included bands 4, 5, and 10 of scenes LC08_L1TP_166027_20181201_20181211_01_T1 (December 01, 2018), LC08_L1TP_167027_20181208_20181211_01_T1 (December 08, 2018), LC08_L1TP_167027_20190314_20190325_01_T1 (March 14, 2019), and LC08_L1TP_167027_20191211_20191217_01_T1 (December 01, 2019).

The Land Surface Temperature Calculation

The main workflow is based on the algorithms proposed by Chander and Markham (2003), Chander et al. (2009), and Walawender et al. (2012). Band ten from Landsat 8 images was used to calculate the top of the atmospheric radiance (TOR) first, and then it was converted into the at-sensor temperature.

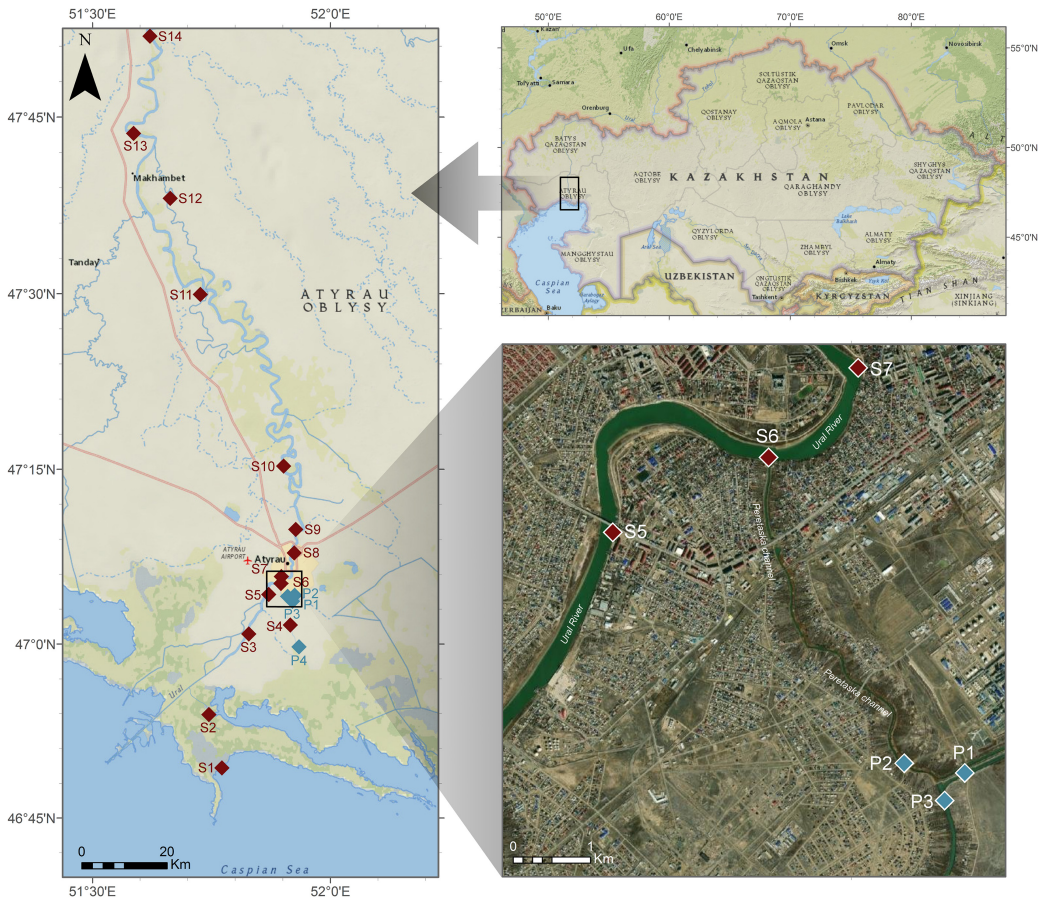

FIGURE 1 | Representation of sampling points on the Ural River. Sampling points from S1 to S3 were taken near the Ural delta, sampling points S4–S9 were taken within the city boundaries, where most of the fish die-off happened at the end of 2018–beginning 2019, sampling points S10–S14 were taken above the city boundaries upstream of the Ural River. Sampling points P1–P4 are taken during October 2019 expedition.

In parallel, the red and the near-infrared bands were used to calculate NDVI. The NDVI was used to calculate the ground emissivity. Both derivatives were integrated into the final land surface temperature products for each date. The time series covering the period between December 2018 and December 2019 were processed using Python 3 codes.

Ion Chromatography

To determine the ionic composition of water, ion chromatography technique (IC) was used. Before the IC analysis, samples were filtered with 0.22 μm cellulose acetate filters using a vacuum pump. The analysis of fluoride, chloride, nitrite, bromide, nitrate, phosphate, and sulfate ions in water samples was performed using a Dionex ICS-6000 HPIC system (Thermo Fisher Scientific, Waltham, MA, United States) equipped with a conductivity detector, two chromatographic columns: for the separation of cations and anions, and Chameleon 6.0 software. Anion separation was carried out using a Dionex IonPac AS11-HC-4 μm capillary, analytical, and guard column (2 × 250 mm) and 30 mmol potassium hydroxide solution as eluent. To determine the cations, we used a Dionex IonPac CS12A-5 mSm IC column (3 × 150 mm). A calibration chart was built from 1 to 30 ppb; the correlation coefficient was 0.998. Quality control was acquired at 15 ppb with 40 times diluted samples.

Ultra High-Performance Liquid Chromatography Coupled With Diode Array Detection

An UHPLC-diode array detection (DAD) method was chosen because it can quickly confirm the presence of microcystin (MC-LR) and nodularin in aqueous samples (Rapala et al., 2002; Thuret-Benoist et al., 2019). The UHPLC system used was an Ultimate 3000 instrument (Thermo Fisher Scientific, United States) equipped with DAD detector. UV-spectra were drawn from 200 to 300 nm. Separation of the toxins was achieved on reversed-phase C18 analytical column thermostated at 35°C. Both the aqueous, water (A), and organic, acetonitrile (B), mobile phases contained 0.025% trifluoroacetic acid (TFA). The following linear gradient program was used: 0 min 70% A, 1.2 min 70% A, 6.2 min 30% A, 7 min 0% A, 7.4 min 70% A; stop time 10 min. The sample injection volume was 5 μl. The

flow rate was 0.350 ml/min. For identification of cyanotoxins in water samples, we used standards of MC-LR and nodularin (Thermo Fisher Scientific, United States) with a concentration of 500 μg/L. Stock solution of the toxins was prepared in methanol and stored at −20°C. For solid-phase extraction (SPE), C18 cartridges HyperSep Phenyl, 500 mg (Thermo Fisher Scientific, United States) were used. All solvents (distilled water, methanol, and acetonitrile) were UHPLC gradient grade. TFA was at least of analytical reagent grade. The filtered samples were passed through a SPE cartridge. Analytes were eluted from the solid phase with a small amount of 90:10 methanol:reagent water (*v*/*v*). The extract were concentrated to dryness by evaporation with SP Genevac Rocket Synergy 2 evaporator (SP Inc., Anchorage, AK, United States), and then adjusted to a 1-ml volume with 90:10 methanol:reagent water (*v*/*v*). The HPLC method was optimized by using ultrapure grade water with diluted MC-LR and nodularin standards (Thermo Fisher Scientific, United States).

Light Microscopy

For the morphological identification of organisms, samples were analyzed with a Leica DM2500 microscope (Leica, Wetzlar, Germany) with ×100, ×200, and ×400 magnifications. The plankton organisms were classified at the genus level and species level, where possible. *Dolichospermum* and *Aphanizomenon*/*Cuspidothrix* could not always be determined to species level because of the lack of akinetes that are a key feature in the morphological identification of nostocalean cyanobacteria. In such cases, the *Dolichospermum* spp. were classified according to the filament type as "curved" or "straight."

Imaging Flow Cytometry

Cell abundance was counted using FlowCAM VS-4 (Yokogawa Fluid Imaging Technologies, United States). A mixture of 5, 10, and 25 μm size beads (Yokogawa Fluid Imaging Technologies, United States) was used for the calibration of the instrument. The FlowCAM was run in autoimage and/or laser-triggered mode using a ×10 objective and a 100-μl flow cell. The results from the FlowCAM were analyzed using VisualSpreadsheet software version 4.0 (Yokogawa Fluid Imaging Technologies, United States). Classification of the dominant genera of phytoplankton was conducted using a semi-manual mode of the software and manual selection of the representative training set of images. To create the subsets within the classification process, statistical filtering, which takes the highest score value as a threshold, was used. Each run of statistical filtering chooses particles with the value of likeness higher than the threshold value. The results of the automated classification were manually rechecked in case of erroneous or missed particles. Classification included subsets of the following major cyanobacterial genera: *Dolichospermum*, *Microcystis*, *Pseudanabaena*, *Aphanizomenon*/*Cuspidothrix*, *Cylindrospermopsis*, and *Sphaerospermopsis* (representative images in **Figure 2**).

MinION Sequencing

Based on FlowCAM IFC analysis, water samples from five different Ural River locations were selected for NGS. More specifically, samples were taken from the delta of river Ural, inside Atyrau town line (Peretaska artificial stream), and near Makhambet village in August 2019 field expedition. DNA extraction was performed using PowerWater DNA Isolation Kit (Qiagen, United States). The resulting DNA concentrations were in a range of 2–10 ng/μl as defined by measurement with a Nanodrop spectrophotometer (Thermo Fisher Scientific, United States) set at 260 nm. The methodology was adapted from manufacturer's instructions in the protocol library of Oxford Nanopore Technologies website. The 16S Barcoding Kit (SQK-RAB204) was used for library preparation, which included PCR reactions and attachment of sequencing adapters. The former procedure was performed by preparation of reaction mixture that included nuclease-free water (14 μl), DNA sample (10 ng, diluted with nuclease-free water to reach 10 μl), DreamTaq Hot Start PCR Master Mix (25 μl), and 16S barcode primer at 10 μM (1 μl). There were 12 different 16S barcodes, and they were assigned for defined samples from Ural River. For instance, Barcode 01 was used for the sample site S1. The thermocycler was set for the following parameters: 1 min at 95°C, followed by 25 cycles with 20 s at 95°C, 30 s at 55°C, 2 min at 65°C for and ended by a final extension of 5 min at 65°C. PCR products were then cleaned up by AMPure XP beads (Beckman Coulter, United States), and the mixture of PCR products (with different barcodes) was prepared. The sequencing adapters were added to this mixture and incubated for 5 min in room temperature. After the library preparation, the DNA library was mixed with loading beads and sequencing buffer (provided by the manufacturer). The MinION device was used for sequencing with flow cell R9.4. DNA library was transferred to the flow cell according to the manufacturer's recommendations, and sequencing run continued for about 14 h. The basecalling was turned on during the run, and the produced data (Fastq files) were analyzed by EPI2ME cloud-based data analysis platform. The "Fastq 16S r2020.04.06" workflow was used to build 16S classification taxonomy.

PCR Analysis of Toxic Cyanobacteria in Ural River Environmental Samples

Based on FlowCAM IFC analysis, water samples from five different locations in the Ural River were selected for molecular analysis (labeled as samples S1, S4, S6, S12, and S13). Primers were designed for the identification of microcystin synthetase gene E (*mcyE*), the aspartate aminotransferase domain for saxitoxin synthesis (*sxtA*), amidinotransferase gene for cylindrospermopsin synthesis (*cyrA*), and genes for the biosynthetic production of anatoxin-a (*anaC*), according to Vaitomaa et al. (2003), Al-Tebrineh et al. (2012), and Rantala-Ylinen et al. (2011). Primers are listed in **Table 1**, and their parameters were verified by OligoAnalyzer Tool (Integrated DNA Technologies, Coralville, IA, United States).

The end-point PCR was performed by mixing of 3 μl of the extracted DNA sample, 25 μl of DreamTaq Hot Start PCR Master Mix, 0.5 μl of each primer (10 μM), and dH_2O up to a final

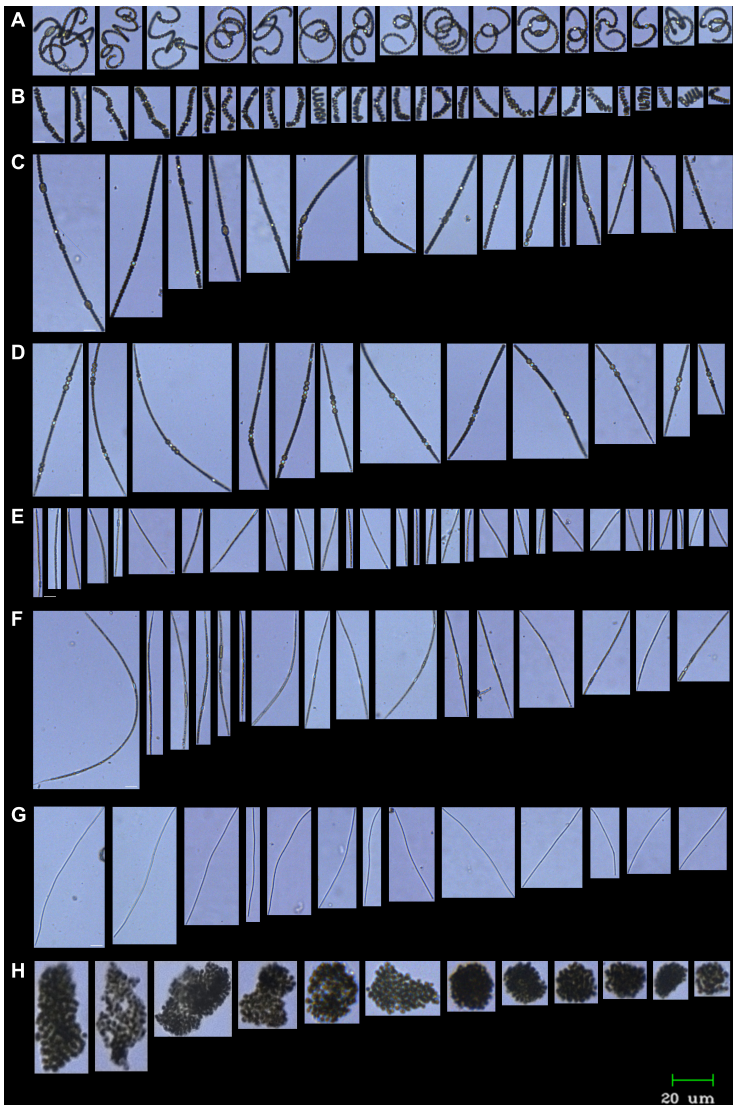

FIGURE 2 | FlowCAM image galleries of most abundant cyanobacteria in River Ural in August 2019. Samples preserved with 0.5% glutaraldehyde; ×10 objective, 100 μm flow cell. **(A,B)** Curved *Dolichospermum* filaments (**A** *Dolichospermum* cf. *flos-aquae*, **B** *Dolichospermum* cf. *compactum*); **(C)** straight *Dolichospermum* filaments (*Dolichospermum* cf. *macrosporum*); **(D)** *Sphaerospermopsis aphanizomenoides*; **(E)** *Cylindrospermopsis raciborskii*; **(F)** *Cuspidothrix issatschenkoi*; **(G)** *Pseudanabaena limnetica*; **(H)** *Microcystis* sp. Scale bar, 20 μm.

reaction volume of 50 μl. All reaction tubes were transferred to a thermocycler (Bio-Rad, Hercules, CA, United States) for a 3-min initial denaturation step at 95°C. That was followed by 40 reaction cycles, with one cycle consisting of 30 s at 95°C, 30 s at temperature depending on T_m of primers, and 60 s at 72°C. The PCR steps were followed by a final extension step at 72°C for 5 min. Length of PCR products were analyzed by DNA electrophoresis using 1% agarose gel with SYBR Safe DNA Gel Stain (Life Sciences, United States). Samples with PCR products were purified and sequenced. The resulted DNA sequences were used for the identification of *Microcystis*-specific toxin synthase genes. Sanger sequencing was performed by commercial entity (Evrogen, RF).

Real-Time PCR

The real-time SYBR Green I qPCR was performed using the Bio-Rad CFX96 Touch Real-Time PCR instrument (Bio-Rad, United States). All reagents were provided by Syntol (Moscow, Russian Federation) and used according to the manufacturer's protocol. The reaction volume of 20 μl included 5 μl of extracted DNA [concentration range of 2–10 ng/μl as defined by measurement with a Nanodrop spectrophotometer (Thermo Fisher Scientific, United States)], 5 μl of nuclease-free water, 2.5 μl of vortexed $MgCl_2$ solution, 2.5 μl of dNTP, 2.5 μl of SYBR Green buffer, 1 μl of each primer (10 μM), and 0.5 μl of SynTaq-polymerase. The reaction protocol included an initial denaturation step at 95°C for 3 min, and 40 cycles of denaturation

(30 s, 95°C), annealing (30 s, T_m of primers), and extension (60 s, 72°C) were followed by melting curve assessment. Each reaction was performed in triplicates. *Microcystis* genome DNA extracted from toxic strain served as a positive control, and a no-DNA reaction well served as a negative control.

Statistical Analysis

Multivariate analysis techniques provide appropriate statistical tools for analysis of environmental parameters and their effects on ecological communities (Greenacre and Primicerio, 2013). The principal component analysis (PCA) was performed to identify the significant environmental conditions influencing distribution detected by IFC cyanobacterial genera in Ural River sampling sites. The analysis was performed using STATISTICA vs. 8 (StatSoft, Tulsa, OK, United States). Environmental parameters included temperature, pH, conductivity, solids (referred as TDS), dissolved oxygen (referred as DO), and NO_3^- and NH_4^+ concentrations as explanatory data (**Supplementary File 1**). Correlations between the abundances of different cyanobacteria and environmental factors were analyzed by Spearman correlation analysis (STATISTICA vs. 8, StatSoft, United States).

RESULTS

Sample Sites Description and Environmental Parameters

Sampling sites S1–S3 were located downstream the Ural River, closer to the Caspian Sea basin. Sampling sites S4–S9 were located within the city area, and sampling sites S10–S14 were located upstream 20–100 km away from the city. The main hotbed of the fish kills was in the urban region of the city, starting from sampling point S5 Balykshy until sampling point S9 Geolog. The area corresponds to the residential districts of the city, as well as the industrial districts. For instance, there is an artificially created water channel called Peretaska (S6), the main purpose of which is water intake by the local thermal power station and oil refinery. Water then exits at a higher temperature (from our measurements at 30°C on October 10 and 26°C on December 24, 2019) and is returned to the upper part of the Peretaska, which then heads in the direction of the Caspian Sea. The temperature difference between the upper and lower Peretaska is significant. Water in the upper part of the Peretaska channel differs from that in the Ural River in terms of its greenish color and high turbidity. The river flow is minimal and unobservable. Sampling points S4–S8 are located near the industrial areas, while S9 Geolog is a residential area near the border of the city.

By applying the satellite analysis approach described in the section "Materials and Methods," we derived the land surface temperature of the study, referring to the four dates indicated above. Results demonstrate a strong thermal anomaly near Atyrau's power plant and oil refinery on December 1 and 8, 2018 (**Figures 3A,B**) and December 2019 (**Figure 3D**), while images acquired in the spring show a significant decrease in the surface temperature for the same area (**Figure 3C**). Furthermore, the locations of a fish kill in December 2018 and 2019 were mapped and combined with the land surface temperature map, derived from the images acquired by Landsat 8 on December 1, 2018 (closer to the date of initial fish kills).

The detailed information on ion concentration is provided in **Supplementary File 1**. The highest concentration of nitrates in water was detected in the artificial water duct S6 Peretaska at 4.69 mg/L of water leading to the cogeneration plant. Accordingly, the oil refining plant's water intake system from the Ural River directly corresponds to the sampling site S7 Oil Refinery Water Intake, where a nitrate concentration of 3.92 mg/L was detected. Phosphate concentrations were slightly increased in the Peretaska locations than the Ural River (Atyrau Su) location. Oxygen concentrations were significantly low in the Peretaska duct (6.5 mg/L). No differences in chloride concentrations between Peretaska sites and the Ural River were detected in water samples in August–December 2019.

Identification and Abundances of Potential Toxic Algae in the River Ural Region

We have identified the cyanobacteria *Cylindrospermopsis* (=*Raphidiopsis*) *raciborskii*, *Sphaerospermopsis aphanizomenoides*, *Dolichospermum* spp., *Aphanizomenon*/*Cuspidothrix* spp., and *Pseudanabaena limnetica* as dominant potentially toxic phytoplankton species in the Ural River using light microscopy and IFC (**Figure 2**). The genera of these potentially toxic cyanobacteria were earlier described as forming algal blooms with the capability of releasing life-threatening toxic compounds (e.g., Codd et al., 2005; Paerl and Otten, 2013; Rastogi et al., 2015). According to the classification results, the most abundant species of potentially toxic cyanobacteria in the Ural River were *Dolichospermum* and *Aphanizomenon*/*Cuspidothrix* spp. Sampling site S1 is the delta of the Caspian Sea, which correspondingly encountered the lowest abundance of cells and a higher water salinity of 0.42%. The S2 channel sampling site is a shallow artificial channel connecting the Caspian Sea to the Ural River with brackish water (0.15%) and a higher abundance of the target species.

The abundance of cells of potentially toxic algae was high in the mouth of the river duct Peretaska, an area with low circulation rates and increased water temperature. The parameters of water in the S6 Peretaska site included a heightened NO_3 concentration (4.69 mg) and a slight increase compared with the sampling point temperature (23°C) at the Ural River. The low Peretaska was low in biodiversity, and *Dolichospermum* spp. was most abundant among potential harmful algae with a cell count equal to 10 filaments/ml. The temperature of this sampling site was 30°C in August and October and decreased to 26°C by the end of December.

The maximum number of cells of *Aphanizomenon*/*Cuspidothrix* spp. reached almost 900 particles/ml at the S11 Saraishyk sampling site (**Figure 4**; **Supplementary File 2**). The site was distinguished by the high NH_4 content in the water (1.19 mg/L). In addition, both the S11 Saraishyk and S10 Almaly sites showed low numbers of *C. raciborskii*. The S12 low Mahambet site had a high

TABLE 1 | List of consensus primers used in the study.

Target gene	Sequence name	Sequence (5′ to 3′)
mcyE for *Microcystis*-specific microcystin synthesis	mcyE-F2	GAAATTTGTGTAGAAGGTGC
	MicmcyE-R8	CAATGGGAGCATAACGAG
sxtA for saxitoxin synthesis	sxtA_F	GGAGTGGATTTCAACACCAGAA
	sxtA_R	GTTTCCCAGACTCGTTTCAGG
cyrA for cylindrospermopsin synthesis	cyrA_F	GTCTGCCCACGTGATGTTATGAT
	cyrA_R	CGTGACCGCCGTGACA
anaC for anatoxin-a synthesis	anaC_F	ATGGTCAGAGGTTTTACAAG
	anaC_R	CGACTCTTAATCATGCGATC

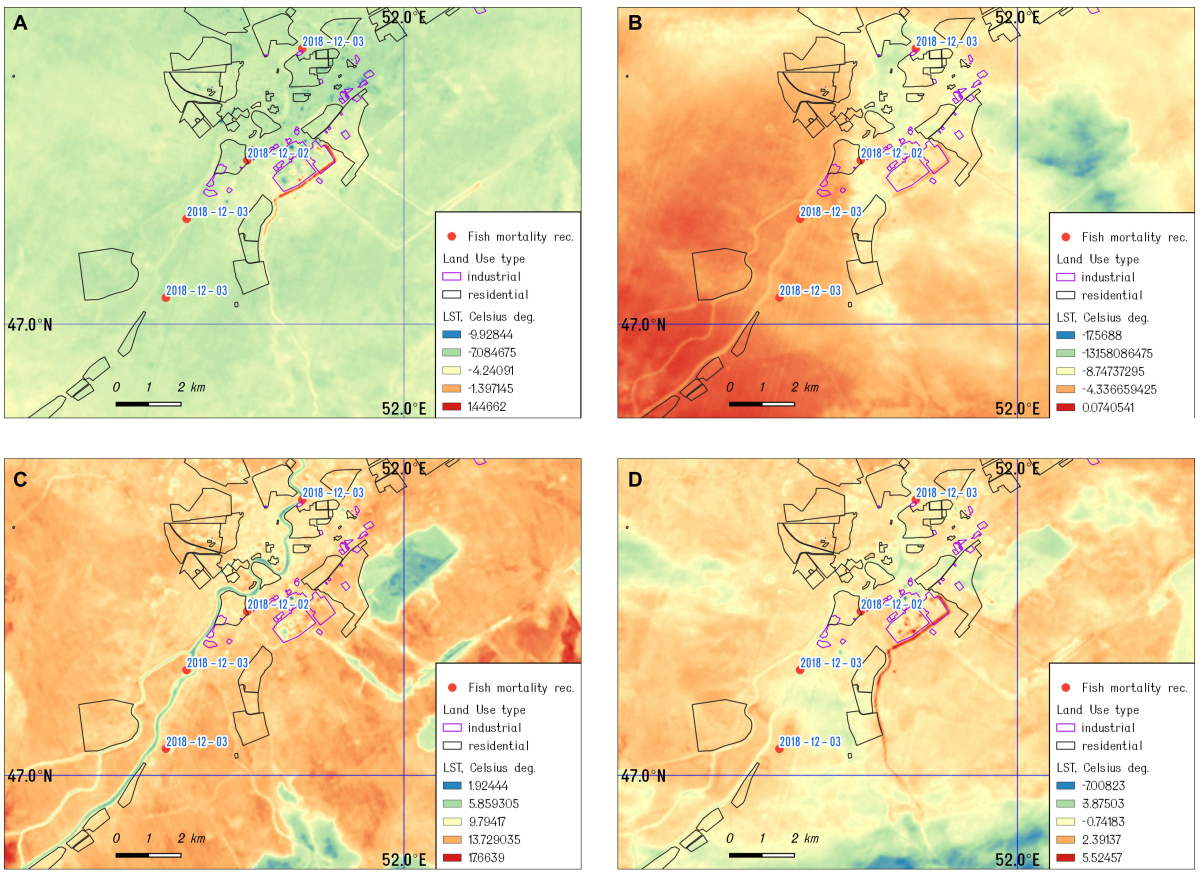

FIGURE 3 | The land surface temperature of the study area: **(A)** December 01, 2018; **(B)** December 08, 2018; **(C)** March 14, 2019; and **(D)** December 01, 2019.

concentration of NH_4 (3.25 mg/L) and is the only sampling point where *Microcystis* sp. was detected by IFC.

The PCA was conducted with environmental parameters (e.g., pH, temperature, DO, conductivity; NO_3^-, NH_4^+) (**Figure 5**). Two principal components with the highest percentages were shown on the plots, which explained 51.7 and 21.62% of variations. For variance analysis, the appearance of *Aphanizomenon*/*Cuspidotrix* sp. was positively correlated with DO ($r = 0.612$, $p < 0.05$; Spearman), and *Microcystis* sp. positively correlated with $NH4^+$ ($r = 0.426$; Spearman). Moreover, there are significant positive correlation between *Dolichospermum*, *Aphanizomenon*/*Cuspidotrix*, and *Pseudoanabaena* spp. ($r = 0.685$; $r = 0.765$; $r = 0.726$, $p < 0.05$, Spearman) which are belonging to ADA-clade (Driscoll et al., 2018; Teikari et al., 2019; Oesterholm et al., 2020), as well as *Dolichospermum* and *Sphaerospermopsis* sp. and *C. raciborskii* ($r = 0.726$; $r = 0.792$; $p < 0.05$, Spearman).

MinION-Based Sequencing

After the sequencing run of 14 h, it resulted in 1,088,000 passed reads with a total yield of 1.6 gigabase pairs of sequencing data. The average sequence length was 1,485 base pairs with an average quality score of 9.29. The 16S amplicon analysis in EPI2ME platform resulted in 896,029 classified reads with an average

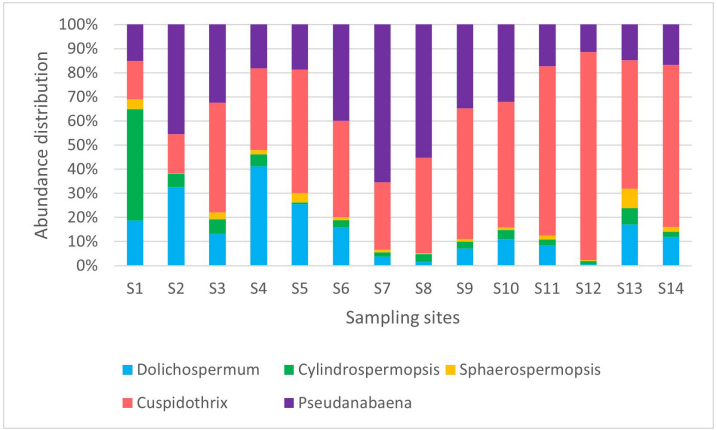

FIGURE 4 | Relative abundances of potentially toxic cyanobacteria (August 2019).

accuracy of 84%, 864,719 of which were used in the further taxonomic analysis in sample sites S1, S4, and S12. The raw sequences from nanopore-based NGS analysis had a significantly higher error rate compared with short-read sequencers, similar to findings by other researchers (Pfeiffer et al., 2018). Large variations in the raw number of reads between different sampling points were observed. The classification was represented by matches in NCBI database (Altschul et al., 1997), and the number of sequencing reads was interpreted to the estimated relative abundance of species in sample sites of the Ural River. **Figure 6** illustrates the relative phylogenetic distribution at the phyla level. The data shows that S1 (Delta) was abundant with cyanobacterial organisms, while the sampling site of S4 (low Peretaska) was mainly inhabited by Proteobacteria and Firmicutes, respectively. A more detailed exploration of cyanobacterial phylum also indicated differences in the distribution within these sites (**Figure 7**). The species-level identification with cyanobacterial origin yielded from one (S4) up to 63 different matches (S1) in NCBI database. According to relative abundance data of these species, *Planktothrix* spp. were predominant, and low quantities of *Microcystis* spp. were also identified at the S12 site. Potentially toxic algae *Nodularia spumigena* was identified by NGS but not by IFC as the most abundant among cyanobacterial species at S1 (delta) site.

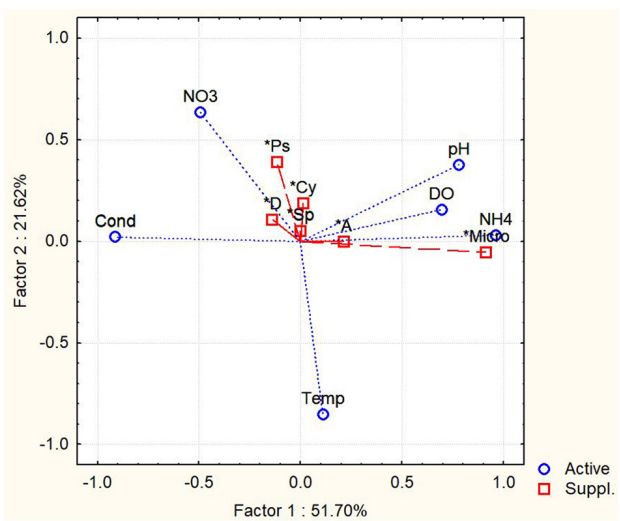

FIGURE 5 | Principal component analysis (PCA) of abundances of potentially toxic cyanobacteria and environmental factors. Temp, temperatures; Cond, conductivity; NO_3, concentration of nitrates; NH_4, ammonium concentration; Micro, *Microcystis* sp.; A, *Aphanizomenon/Cuspidotrix* sp.; D, *Dolichospermum* sp.; Sp, *Sphaerospermopsis* sp.; Cy, *Cylindrospermopsis raciborskii*.

Identification of Toxic Genes in Cyanobacteria Using PCR Methods

Polymerase-chain reaction analysis was used to identify *Microcystis*-specific *mcyE* gene according to the primer design provided by Vaitomaa et al. (2003). The genome assembly of *M. aeruginosa* NIES-843 (Kaneko et al., 2007) was used to find an expected sequence of PCR products. Its size was 247 base pairs, and only S12 sample had a corresponding significant band. The semi-quantitative analysis by SYBR Green I real-time PCR revealed the presence of this gene in sample sites S1 and S12, assessed by the similar melt peak as in positive control. The relative gene abundance data was standardized (ratio-based) by concentration of input DNA extract. Sample S1 contained 2.05-fold more *mcyE* gene per nanograms of total DNA than the S12 sample.

The PCR amplification of the *sxtA* gene had an expected size of 148 base pairs (Rantala-Ylinen et al., 2011) and only sample S13 showed the positive band in the following size range. To validate the presence of this toxin production gene, the real-time PCR analysis was performed with positive control of standards from multiplex qPCR kit (Phytoxigene CyanoDTec^{TM} Toxin Genes Test; Diagnostic Technology, United States). The results showed specific amplification of the *sxtA* gene only in sample S13. The relative *sxtA* gene abundance in site S13 was considerably small with a 1.23×10^{-4}-fold difference, when compared with

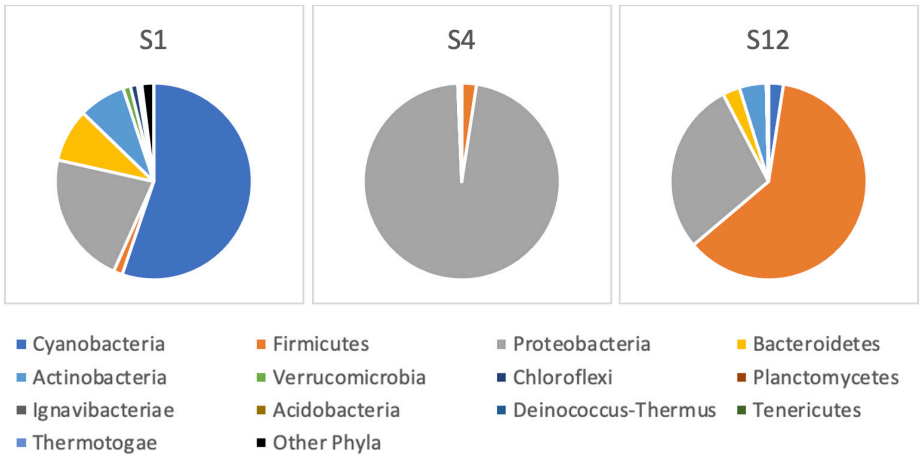

FIGURE 6 | Bacterial community composition at the phylum level based on 16S rRNA next-generation sequencing at the Ural River S1, S4, and S12 sites.

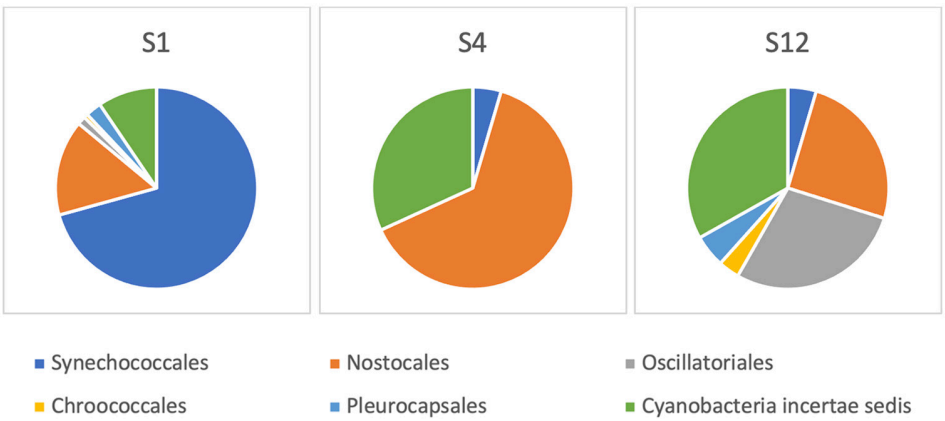

FIGURE 7 | Cyanobacterial community composition based on 16S rRNA next-generation sequencing at the Ural River S1, S4, and S12 sites.

positive control. However, as the positive control from the kit had a known concentration of 100,000 copies/μl, it allowed us to estimate the concentration in S13 sample to 36.8 copies per μl of the extracted total DNA sample.

The presence of cylindrospermopsin (*cyrA*) and anatoxin (*anaC*) genes was not identified by the abovementioned PCR methods. To sum up, the *mcyE* was detected at the environmental samples from S1 and S12 sample sites, below Makhambet village, and the delta of Ural River location, respectively, and *sxtA* gene was detected at S13, upper Makhambet site.

Sanger Sequencing of PCR Products

Polymerase-chain reaction products were purified and sequenced using the forward primer of *Microcystis*-specific *mcyE* gene (Evrogen, Moscow, Russian Federation). Resulted sequence data for S1 and S12 are presented in **Table 2**. Sequencing of samples from S4, S6, and S13 sites did not produce any DNA data of cyanobacterial origin.

Sequence data was analyzed via BLAST algorithm, and the best matches for the two sites are shown in **Table 3**. The sequence homology analysis in NCBI nucleotide database revealed that PCR products from Ural delta (S1) and low Makhambet (S12) matched with *Microcystis*-specific *mcyE* gene with a percentage identity between 88 and 96%, and S13 sample (upper Makhambet) matched with ADA-clade spp. sxtA gene (99%).

DISCUSSION

CyanoHABs are very complex phenomena and early detection and tracking cyanotoxin producers and predicting of the bloom dynamics remain as unsolved challenges for water managers and aquaculture farmers. From December 2018 through March 2019, the significant mortality of farmed sturgeon and other fish species were reported in the Ural River near the town of Atyrau, Kazakhstan, with initial findings of dead fish in the artificial duct of the Peretaska channel, which supplies water to the local power plant and oil refinery. The Peretaska duct was an initial point of a huge fish die-off on the Ural

TABLE 2 | List of DNA sequences of PCR products from Ural River sampling sites.

Sample	Sanger sequencing data
S1-*mcyE*	GCCCGAGCAACGAATACTCATAGACTTAAGATCGAAACTTCTATCCTAGCTTTCTTGATGACAAAAAAGACAATGGAACCGGCGATTTAGG CAAGCAAACTGCTCCCGTGTATCATTGAGTTTATGGGACGAAAAGATAATCAAGTTAAGGTCAATGGTTATCGAATTGACCCCGGAGAAATT CAAACACGACCGTTGCTCCTTGA
S12-*mcyE*	CCTCAATCACTAGCCAACCCTGAAATGACTCAGGAAATGTTAAACCTAGCTTTCTTGAGTGAGACAAAAACTCTCTTTAGAACCGGCGATTT AGGCAAGCAAACTGCTCCGGGTATCATTGAGTTTATGGGACGAAAAGATAATCAAGTTAAGGTCAATGGTTATCGAATTGACCCCGGAGAA ATTGAATATCAATTGACTCGTTATGCTCCCATTGA
S13-*sxtA*	TCGATTAGAGAGTATCCTCTCAGTATTCAATCAGTTACCATTGGAAGAACAGCCCAAATACATTGCTGATATGGGGGTGTGGCGATGGAACTC TCCTGAAACGAGTCTGGGAAACA

TABLE 3 | Origin and identification of *mcyE* and *sxtA* genes in environmental samples from the Ural River.

Sample	Size (bp)	Description of the best match	Max score	*E*-value	Percent. identity
S1-*mcyE*	206	*Microcystis viridis* NIES-102 DNA, complete genome	205	1e-48	88.02%
S12-*mcyE*	218	*Microcystis* sp. GL280646 microcystin synthetase E (mcyE) gene, partial cds	336	2e-88	96.26%
S13-*sxtA*	115	*Anabaena circinalis* AWQC131C saxitoxin (*sxtA*) gene, partial cds	195	7e-46	99.07%
	115	*Aphanizomenon* sp. NH-5 TatA/E (*tatA/E*) and PsbH (*psbH*) genes, complete cds; paralytic shellfish poisoning biosynthesis gene cluster, complete sequence; UbiA (ubiA) gene, complete cds; and unknown gene	195	7e-46	99.07%
	115	Several genome sequences of *Aphanizomenon gracile*	195	7e-46	99.07%

River and aquaculture fish farms in December 2018 (>100 tons of artificially grown sturgeon), and a small fish die-off was observed in December 2019. The temperature anomaly registered by Landsat 8 in this area (**Figures 3A,B,D**) is supported by *in situ* measurements of water temperature in the Peretaska duct below the oil refinery and cogeneration plant. The decrease in temperature in March 2019 coincides with a temporary interruption to the biological treatment plant at the oil refinery due to preventive maintenance (**Figure 3C**). The thermal discharge from power plants leads to an elevation in temperature of the receiving waters (Li et al., 2011) and promotes phytoplankton growth and algal blooms, particularly in cold seasons (Hickman and Klarer, 1975; Jiang et al., 2012, 2019a,b). Thermal discharge plumes near power plants are thermally dynamic environments with strong influences on aquatic organisms. Many scientists report decreasing diversity of aquatic communities, functional and species richness, and even large mortality events of benthos invertebrates near discharge sites or in discharge channels (Suresh et al., 1993; Chuang et al., 2009; Teixeira et al., 2009; de Szechy et al., 2017; Lee et al., 2018; Khosravi et al., 2019). It seems that a shift in temperature is more important than exact temperature numbers, emphasizing a possible role of toxins in quorum sensing. The number of different toxins may increase with changes in growth conditions and temperature shifts (Kleinteich et al., 2012).

In our field expedition, we found a number of potentially toxic cyanobacteria species originally using FlowCAM-based IFC (supported by light microscopy), including invasive *C. raciborskii*, along all of the 100-km stretch of the Ural River–from the delta S1 sampling point up to S14. *C. raciborskii* is a cyanobacterium species with a well-known invasive origin (Padisák, 1997; Moreira et al., 2011), and causes increasing concern because of its potential toxicity (Briand et al., 2004). The presence of *C. raciborskii* was occasionally reported in the region close to the Northern Caspian Sea (Kazakhstan) starting in the twentieth century (Padisák, 1997). However, in the current study, we did not identify the presence of genes encoding cylindrospermopsin in the field samples.

The cyanobacterial blooms are often composed from non-toxic and toxic strains within morphologically identical species, and the reports of multicyanotoxin co-occurrence are becoming increasingly common (Graham et al., 2010; Pitois et al., 2018). The initial choice of detailed analysis of sampling points for the presence of toxic algae was made with IFC, followed by NGS and PCR-based molecular methods. We choose to use a combination of optical methods (IFC) and NGS because the classical optical-based morphological methods may not provide sufficient identification resolution (Eiler et al., 2013; Xiao et al., 2014; Zimmerman et al., 2015; Dzhembekova et al., 2017; Parulekar et al., 2017). Moreover, the traditional cyanobacterial taxonomy has been based on morphological features, but this classification is revised with an accumulation of molecular sequence data (Komárek et al., 2014; Hugenholtz et al., 2021). The taxonomic classification was done with a 16S NCBI database, however, the choice of database may have an effect on the results of taxonomic identification (Park and Won, 2018; Rizal et al., 2020; Winand et al., 2020). Metabarcoding based on 16S rRNA gene revealed a moderately diverse cyanobacterial community at S12 and S1 sampling points, and only a few cyanobacterial species were found at the S4 point (**Figure 6**) where the heated water stream of the artificial Peretaska channel (30°C, October 2019) was represented mostly by Proteobacteria and Firmicutes. Proteobacteria are always present in high-temperature ecosystems and often the dominating phylum in hot springs (Chan et al., 2017; Panda et al., 2017; Adjeroud et al., 2020), as the diversity and richness of microbial communities in thermal springs are negatively affected by temperature (Chan et al., 2017). In the winter, due to the

thermal discharge, the temperature in the Peretaska channel remains high (26°C; December 2019); however, it becomes more permissible for cyanobacteria and other microalgae, which may lead to algal blooming. Temperature increase caused by thermal discharge from power plants may promote phytoplankton growth and blooms, particularly in cold seasons (Jiang et al., 2019a,b).

The structure of the cyanobacterial distribution in the field samples defined by NGS analysis suggested the predominance of filamentous *Planktothrix* sp. and *N. spumigena* in the brackish S1 sampling point. NGS results together with IFC confirmed a predominant presence of *Planktothrix* sp. as well as the presence of low abundant *Microcystis* sp. at the S12 sampling point (low Makhambet). Although there are still common concerns about the nanopore-technology accuracy, mobile sequencing with MinION has already been transformative for bacterial and viral pathogen outbreaks (Quick et al., 2015, 2016; Boykin et al., 2019) and in the context of freshwater analysis (Reddington et al., 2020). We used MinION-based sequencing to complement IFC information on the presence of potentially toxic cyanobacteria at sampling points and found that nanopore amplicon sequencing allowed us to get extended information about the presence of even minor quantities of cyanobacterial genera. Thus, at the S1 sampling point, the predominance of *Planktothrix* sp. and a presence of minor quantities of *N. spumigena* were confirmed by 16S rRNA gene metagenomics, but not by IFC. However, a number of experimental intricacies should be addressed using this approach related to the DNA extraction yields and sample filtrate volumes and database incompleteness that can be curated by adding local species (Abad et al., 2016).

As 16S rRNA-based NGS only provides identification of potentially toxic algae, PCR was required to confirm the presence of toxigenic cyanobacteria species utilizing toxin synthesis genes. Field samples from S12 and S13 (near Makhambet village) demonstrated the presence of strains expressing *mcyE* or *sxtA* genes identified by traditional and real-time PCR. Data from real-time PCR as well as data from Sanger sequencing suggested that low abundant *Microcystis* sp. was the only microcystin producer at the S12 sampling point (low Makhambet), and toxigenic ADA-clade spp. were detected at S13 (upper Makhambet) sampling point (**Figure 4** and **Table 3**). This is in line with other studies, which found that the ADA-clade is a highly significant component of cyanobacterial HABs (Dreher et al., 2021), and dominant microcystin producer is not necessarily the predominant cyanobacterial species in the water stream (Dadheech et al., 2014; Lee et al., 2015; Scherer et al., 2017). In summary, our study demonstrates that potentially toxic cyanobacteria including toxigenic strains widely distributed in Ural River waters. We hypothesize that the presence of potentially toxigenic cyanobacteria in side channels of the Ural River can lead to yearly seasonal fish kills depending on the floods dynamics and winter temperature shifts.

After our manuscript submission to the journal, another fish kill happened in this region (May 02–09, 2021; Baksay) (in the water bodies temporarily connected to Ural River main stream during spring river flooding). The results of UHPLC/DAD analysis of water samples taken a few days later confirmed the presence of MC-LR and nodularin in the water probes (**Supplementary File 2**).

CONCLUSION

During our field study of the Ural River in August–December 2019, we documented the occurrence of potentially toxigenic cyanobacteria in Ural River from the brackish-water delta up to 100 km. *Aphanizomenon*/*Cuspidothrix* spp., *Dolichospermum* spp. (most likely *D.* cf. *flos-aquae* and *D.* cf. *macrosporum*), and, in some locations, *Planktothrix* sp. and *Microcystis* sp. were dominant phytoplankton species, and we also found minor quantities of *C. raciborskii*. The presence in the field samples of toxigenic genotypes (*mcyE*+, *sxtA*+) was confirmed by real-time PCR and Sanger sequencing. The complementary analysis with nanopore sequencing showed potential for using portable and fast NGS for real-time monitoring and research of harmful algae, but currently, a taxonomic identification is still limited by the availability of suitable databases and cost. A combination of IFC with molecular methods demonstrates a potential for monitoring algal blooms and can lay a foundation for addressing these risks in aquaculture and river management of the Ural River region. We, therefore, suggest that the monitoring of toxic algae levels in the Ural River should continue based on the potential of combined IFC and NGS approach among others and on the construction of Ural River-specific database of toxigenic cyanobacteria taxa.

DATA AVAILABILITY STATEMENT

The datasets presented in this study can be found in online repositories. The names of the repository/repositories and accession number(s) can be found below: NCBI BioProject [accession: PRJNA714785].

AUTHOR CONTRIBUTIONS

AAbd, KuS, YM, and NB conducted the field expeditions, collected and analyzed data, and contributed to the funding acquisition. YM, AAbd, KuS, KaS, DP, IV, DM, and NB performed the methodology. YM, KuS, AAbd, AAbi, KaS, DP, GA, ZI, IV, DM, and NB contributed to the data curation and data analysis. KaS contributed to the satellite data analysis. NB performed the supervision of the project. NB and YM wrote a first draft of the manuscript. All of the authors wrote, read, edited, and reviewed a manuscript.

FUNDING

The study was funded by Nazarbayev University grant FDCRGP #110119FD4513 to NB and a research grant to AAbd and KuS from FRIP Program of Young Researchers Alliance. DM was partly working under FPGEC Interdisciplinary Scientific and

Educational School of MSU, and IV was supported by MES #AP05134153/GF4.

ACKNOWLEDGMENTS

We are indebted to Zhasulan Kuzhekov (passed away in January 2020) for his help with field expeditions to Ural River. We are very grateful to the Core Facilities of Nazarbayev University for access to instrumentation, to Yekaterina Dyachenko from Bioline for help with Leica software, and to Veronika Dashkova, Nazarbayev University for training AAbd on FlowCAM imaging cytometer.

SUPPLEMENTARY MATERIAL

The Supplementary Material for this article can be found online at: https://www.frontiersin.org/articles/10.3389/fmars.2021.680482/full#supplementary-material

REFERENCES

Abad, D., Albaina, A., Aguirre, M., Laza-Martínez, A., Uriarte, I., Iriarte, A., et al. (2016). Is metabarcoding suitable for estuarine plankton monitoring? A comparative study with microscopy. *Mar. Biol.* 163, 1–13. doi: 10.1007/s00227-016-2920-0

Adjeroud, M., Escuder-Rodriguez, J.-J., Gonzalez-Siso, M.-I., and Kecha, M. (2020). Metagenomic investigation of bacterial and archaeal diversity of Hammam Essalihine hot spring from Khenchela, Algeria. *Geomicrobiol. J.* 37, 804–817. doi: 10.1080/01490451.2020.1783035

Al-Tebrineh, J., Pearson, L. A., Yasar, S. A., and Neilan, B. A. (2012). A multiplex qPCR targeting hepato-and neurotoxigenic cyanobacteria of global significance. *Harmful Algae* 15, 19–25. doi: 10.1016/j.hal.2011.11.001

Altschul, S. F., Madden, T. L., Schäffer, A. A., Zhang, J., Zhang, Z., Miller, W., et al. (1997). Gapped BLAST and PSI-BLAST: a new generation of protein database search programs. *Nucleic Acids Res.* 25, 3389–3402. doi: 10.1093/nar/25.17.3389

Anderson, D. M., Cembella, A. D., and Hallegraeff, G. M. (2012). Progress in understanding harmful algal blooms paradigm shifts and new technologies for research, monitoring, and management. *Annu. Rev. Mar. Sci.* 4, 143–176. doi: 10.1146/annurev-marine-120308-081121

Antonella, P., and Luca, G. (2013). The quantitative real-time PCR applications in the monitoring of marine harmful algal bloom (HAB) species. *Environ. Sci. Pollut. Res.* 20, 6851–6862. doi: 10.1007/s11356-012-1377-z

Babanazarova, O., Sideley, S., and Schischeleva, S. (2013). The structure of winter phytoplankton in Lake Nero, Russia, a hypertrophic lake dominated by Planktothrix-like Cyanobacteria. *Aquat. Biosyst.* 9:18. doi: 10.1186/2046-9063-9-18

Ballot, A., Scherer, P. I., and Wood, S. A. (2018). Variability in the anatoxin gene clusters of *Cuspidothrix issatschenkoi* from Germany, New Zealand, China and Japan. *PLoS One* 13:e0200774.

Barsi, J. A., Barker, J. L., and Schott, J. R. (2003). "An atmospheric correction parameter calculator for a single thermal band earth-sensing instrument," in *Proceedings of the IGARSS 2003 International Geoscience and Remote Sensing Symposium*, Toulouse. doi: 10.1109/igarss.2003.1294665

Boykin, L. M., Sseruwagi, P., Alicai, T., Ateka, E., Mohammed, I. U., and Stanton, J. L. (2019). Tree lab: portable genomics for early detection of plant viruses and pests in Sub-Saharan Africa. *Genes* 10:632. doi: 10.3390/genes10090632

Briand, J. F., Leboulanger, C., Humbert, J. F., Bernard, C., and Dufuor, P. (2004). *Cylindrospermopsis raciborskii* (Cyanobacteria) invasion at mid-latitudes: selection, wide physiological tolerance, or global warming? *J. Phycol.* 40, 231–238. doi: 10.1111/j.1529-8817.2004.03118.x

Bruno, M., Ploux, O., Metcalf, J. S., Mejean, A., Pawlik-Skowronska, B., and Furey, A. (2016). "Anatoxin-a, Homoanatoxin-a, and Natural Analogues," in *Handbook of Cyanobacterial Monitoring and Cyanotoxin Analysis*, eds J. Meriluoto, L. Spoof, and G. A. Codd (Chichester: Wiley & Sons), 138–147.

Burton, A. S., Stahl, S. E., John, K. K., Jain, M., Juul, S., Turner, D. J., et al. (2020). Off Earth identification of bacterial populations using 16S rDNA nanopore sequencing. *Genes* 11:76. doi: 10.3390/genes11010076

Buskey, E. J., and Hyatt, C. J. (2006). Use of the FlowCAM for semi-automated recognition and enumeration of red tide cells (*Karenia brevis*) in natural plankton samples. *Harmful Algae* 5, 685–692. doi: 10.1016/j.hal.2006.02.003

Campbell, L., Henrichs, D. W., Olson, R. J., and Sosik, H. M. (2013). Continuous automated imaging-in-flow cytometry for detection and early warning of *Karenia brevis* blooms in the Gulf of Mexico. *Environ. Sci. Pollut. Res.* 20, 6896–6902. doi: 10.1007/s11356-012-1437-4

Campbell, L., Olson, R. J., Sosik, H. M., Abraham, A., Henrichs, D. W., Hyatt, C. J., et al. (2010). First harmful Dinophysis (Dinophyceae, Dinophysiales) bloom in the US is revealed by automated imaging flow cytometry. *J. Phycol.* 46, 66–75. doi: 10.1111/j.1529-8817.2009.00791.x

Carmichael, W. W. (2008). A world overview – one hundred twenty seven years of research on toxic cyanobacteria–where do we go from here? *Adv. Exp. Med. Biol.* 619, 105–125.

Castro-Wallace, S. L., Chiu, C. Y., John, K. K., Stahl, S. E., Rubins, K. H., McIntyre, A. B. R., et al. (2017). Nanopore DNA sequencing and genome assembly on the International Space Station. *Sci. Rep.* 7:18022. doi: 10.1038/s41598-017-18364-0

Chan, C. S., Chan, K.-G., Ee, R., Hong, K.-W., Urbieta, M. S., Donati, E. R., et al. (2017). Effects of physico-chemical factors on prokaryotic biodiversity in Malaysian circumneutral hot springs. *Front. Microbiol.* 8:2152. doi: 10.3389/fmicb.2017.01252

Chander, G., and Markham, B. (2003). Revised Landsat-5 TM radiometric calibration procedures and postcalibration dynamic ranges. *IEEE Transact. Geosci. Remote Sens.* 41, 2674–2677. doi: 10.1109/TGRS.2003.818464

Chander, G., Markham, B. L., and Helder, D. L. (2009). Summary of current radiometric calibration for Landsat MSS, TM, ETM+, and EO-1 ALI sensors. *Remote Sens. Environ.* 113, 893–903. doi: 10.1016/j.rse.2009.01.007

Chernova, E., Sidelev, S., Russkikh, I., Voyakina, E., and Zhakovskaya, Z. (2019). First observation of microcystin- and anatoxin-producing cyanobacteria in the easternmost part of the Gulf of Finland (the Baltic Sea). *Toxicon* 157, 18–24. doi: 10.1016/j.toxicon.2018.11.005

Chuang, Y.-L., Yang, H.-H., and Lin, H.-J. (2009). Effects of a thermal discharge from a nuclear power plant on phytoplankton and periphyton in subtropical coastal waters. *J. Sea Res.* 61, 197–205. doi: 10.1016/j.seares.2009.01.001

Codd, G. A., Lindsay, J., Young, F. M., Morrison, L. F., and Metcalf, J. S. (2005). "Harmful cyanobacteria," in *Harmful Cyanobacteria*, eds J. Huisman, H. C. P. Matthijs, and P. M. Visser (Dordrecht: Springer).

Dadheech, P. K., Selmeczy, G. B., Vasas, G., Padisák, J., Arp, W., Tapolczai, K., et al. (2014). Presence of potential toxin-producing cyanobacteria in an oligo-mesotrophic lake in Baltic Lake District, Germany: an ecological, genetic and toxicological survey. *Toxins* 6, 2912–2931. doi: 10.3390/toxins6102912

Dashkova, V., Malashenkov, D., Poulton, N., Vorobjev, I., and Barteneva, N. (2017). Imaging flow cytometry for phytoplankton analysis. *Methods* 112, 188–200. doi: 10.1016/j.ymeth.2016.05.007

De Pace, R., Vita, V., Bucci, M. S., Gallo, P., and Bruno, M. (2014). Microcystin contamination in sea mussel farms from the Italian Southern Adriatic Coast following cyanobacterial blooms in an artificial reservoir. *J. Ecosystems* 2014:374027. doi: 10.1155/2014/374027

de Szechy, M. T. M., de Souza Koutsoukos, V., and de Moura Barboza, C. (2017). Long-term decline of brown algal assemblages from southern Brazil under the influence of a nuclear power plant. *Ecol. Indic.* 80, 258–267. doi: 10.1016/j.ecolind.2017.05.019

Dierks-Horn, S., Metfies, K., Jaeckel, S., and Medlin, L. K. (2011). The ALGADEC device: a semi-automated rRNA biosensor for the detection of toxic algae. *Harmful Algae* 10, 395–401. doi: 10.1016/j.hal.2011.02.001

Dreher, T. W., Davis, E. W. II, and Mueller, R. S. (2021). Complete genomes derived by directly sequencing freshwater bloom populations emphasize the significance of the genus level ADA clade within the Nostocales. *Harmful Algae* 103:102005. doi: 10.1016/j.hal.2021.102005

Driscoll, C. B., Meyer, K. A., Šulčius, S., Brown, N. M., Dick, G. J., Timinskas, A., et al. (2018). A closely-related clade of globally distributed bloom-forming cyanobacteria within the Nostocales. *Harmful Algae* 77, 93–107. doi: 10.1016/j.hal.2018.05.009

Dzhembekova, N., Urusizaki, S., Moncheva, S., and Ivanova, P. (2017). Applicability of massively parallel sequencing on monitoring harmful algae at Varna Bay in the Black Sea. *Harmful Algae* 68, 40–51. doi: 10.1016/j.hal.2017.07.004

Eiler, A., Drakare, S., Bertilsson, S., Pernthaler, J., Peura, S., Rofner, C., et al. (2013). Unveiling distribution patterns of freshwater phytoplankton by a next generation sequencing based approach. *PLoS One* 8:e53516. doi: 10.1371/journal.pone.0053516

Eriksson, J. E., Meriluoto, J. A. O., and Lindholm, T. (1986). "Can cyanobacterial toxins accumulate in aquatic food chains," in *Proceedings of the 4th International Symposium on Microbial Ecology*, Ljubliana, 655–658.

Fernandes-Salvador, J. A., Davidson, K., Sourisseau, M., Revilla, M., Schmidt, W., Clarke, D., et al. (2021). Current status of forecasting toxic harmful algae for the North-East Atlantic shellfish aquaculture industry. *Front. Mar. Sci*. 8:666583. doi: 10.3389/fmars.2021.666583

Fortin, N., Munoz-Ramos, V., Bird, D., Lévesque, B., Whyte, L. G., and Greer, C. W. (2015). Toxic cyanobacterial bloom triggers in Missisquoi Bay, Lake Champlain, as determined by next-generation sequencing and quantitative PCR. *Life* 5, 1346–1380. doi: 10.3390/life5021346

Foulds, I. V., Granacki, A., Xiao, C., Krull, U. J., Castle, A., and Horgen, P. A. (2002). Quantification of microcystin-producing cyanobacteria and *E. coli* in water by 5'-nuclease PCR. *J. Appl. Microbiol*. 93, 825–834.

GEOHAB (2001). "Global ecology and oceanography of harmful algal blooms programme," in *Science Plan*, eds P. Glibert and G. Pitcher (Baltimore, MD: SCOR).

Gibble, C. M., Peacock, M. B., and Kudela, R. M. (2016). Evidence of freshwater algal toxins in marine shellfish: implications for human and aquatic health. *Harmful Algae* 59, 59–66. doi: 10.1016/j.hal.2016.09.007

Gowers, G.-O. F., Vince, O., Charles, J.-H., Klarenberg, I., Ellis, T., and Edwards, A. (2019). Entirely off-grid and solar-powered DNA sequencing of microbial communities during an ice cap traverse expedition. *Genes* 10:902. doi: 10.3390/genes10110902

Graham, J. L., Loftin, K. A., Meyer, M. T., and Ziegler, A. C. (2010). Cyanotoxin mixtures and taste-and-odor compounds in cyanobacterial blooms from the Midwestern United States. *Environ. Sci. Technol.* 44, 7361–7368. doi: 10.1021/es1008938

Graham, M. D., Cook, J., Graydon, J., Kinniburgh, D., Nelson, H., Pilieci, S., et al. (2018). High-resolution imaging particle analysis of freshwater cyanobacterial blooms. *Limnol. Oceanogr. Methods* 16, 669–679. doi: 10.1002/lom3.10274

Greenacre, M., and Primicerio, R. (2013). *Multivariate Analysis of Ecological Data*. (Bilbao: Foundacion BBVA), 331.

Griffith, A. W., and Gobler, C. J. (2020). Harmful algal blooms: a climate change co-stressor in marine and freshwater ecosystems. *Harmful Algae* 91:101590. doi: 10.1016/j.hal.2019.03.008

Hatfield, R. G., Batista, F. M., Bean, T. P., Fonseca, V. G., Santos, A., Turner, A. D., et al. (2020). The application of Nanopore sequencing technology to the study of Dinoflagellates: a proof-of-concept study for rapid sequence-based discrimination of potentially harmful algae. *Front. Microbiol.* 11:844. doi: 10.3389/fmicb.2020.00844

Heisler, J., Glibert, P. M., Burkholder, J. M., Andersond, D. M., Cochlane, W., Dennison, W. C., et al. (2008). Euthrophication and harmful algal blooms: a scientific consensus. *Harmful Algae* 8, 3–13. doi: 10.1016/j.hal.2008.08.006

Hickman, M., and Klarer, D. M. (1975). The effect of the discharge of thermal effluent from a power station on the primary productivity of an epiphytic algal community. *Br. Phycol. J.* 10, 81–91. doi: 10.1080/00071617500650081

Hugenholtz, P., Chuvochina, M., Oren, A., Paks, D. H., and Soo, R. M. (2021). Prokaryotic taxonomy and nomenclature in the age of big sequence data. *ISME J.* doi: 10.1038/s41396-021-00941-x [Epub ahead of print].

Humpage, A. R., Rositano, J., Bretag, A. H., Brown, R., Baker, P. D., Nicholson, B. C., et al. (1984). Paralytic shellfish poisons from Australian cyanobacterial blooms. *Aust. J. Mar. Freshw. Res.* 45, 761–771.

Jeppesen, E., Søndergaard, M., and Liu, Z. (2017). Lake restoration and management in a climate change perspective: an introduction. *Water* 9:122. doi: 10.3390/w9020122

Jiang, Z.-B., Chen, Q.-Z., Zeng, J.-N., Liao, Y.-B., Shou, L., and Liu, J. (2012). Phytoplankton community distribution in relation to environmental parameters in three aquaculture systems in a Chinese subtropical euthrophic bay. *Mar. Ecol. Progr. Ser.* 446, 73–89. doi: 10.3354/meps0949

Jiang, Z., Du, P., Liao, Y., Lio, Q., Chen, Q., Shou, L., et al. (2019a). Oyster farming control on phycoplankton bloom promoted by thermal discharge from a power plant in a eutrophic, semi-enclosed bay. *Water Res.* 159, 1–9. doi: 10.1016/j.watres.2019.04.023

Jiang, Z., Gao, Y., Chen, Y., Du, P., Zhu, X., Liao, Y., et al. (2019b). Spatial heterogeneity of phytoplankton community shaped by a combination of anthropogenic and natural forcings in a long narrow bay in the East China Sea. *Eastuar. Coast. Shelf Sci.* 217, 250–261. doi: 10.1016/j.ecss.2018.11.028

Joehnk, K. D., Huisman, J., Sharples, J., Sommeijer, B., Visser, P. M., and Stroom, J. M. (2008). Summer heatwaves promote blooms of harmful cyanobacteria. *Glob. Change Biol.* 14, 495–512. doi: 10.1111/j.1365-2486.2007.01510.x

Johnson, S. S., Zaikova, E., Goerlitz, D. S., Bai, Y., and Tighe, S. W. (2017). Real-time DNA sequencing in the Antarctic dry valleys using the Oxford Nanopore sequencer. *J. Biomol. Tech.* 28, 2–7. doi: 10.7171/jbt.17-2801-009

Kaneko, T., Nakajima, N., Okamoto, S., Suzuki, I., Tanabe, Y., Tamaoki, M., et al. (2007). Complete genomic structure of the bloom-forming toxic cyanobacterium *Microcystis aeruginosa* NIES-843. *DNA Res*. 14, 247–256. doi: 10.1093/dnares/dsm026

Kazhydromet Climate Monitoring Bulletin (2016). www.kazhydromet.kz (russ.)

Khosravi, M., Nasrolahi, A., Shokri, M. R., Dobretsov, S., and Pansch, C. (2019). Impact of warming on biofouling communities in the Northern Persian Gulf. *J. Thermal Biol.* 85:102403. doi: 10.1016/j.jtherbio.2019.102403

Kleinteich, J., Wood, S. A., Küpper, F. C., Camacho, A., Quesada, A., Frickey, T., et al. (2012). Temperature-related changes in polar cyanobacterial mat diversity and toxin production. *Nat. Clim. Change* 2, 356–360. doi: 10.1038/nclimate1418

Komárek, J., Kaštovský, J., Mareš, J., and Johansen, J. (2014). Taxonomic classification of cyanoprokaryotes (cyanobacterial genera) 2014, using a polyphasic approach. *Preslia* 86, 295–335.

Kurmayer, R., and Christiansen, G. (2010). The genetic basis of toxin production in cyanobacteria. *Freshw. Rev*. 2, 31–50. doi: 10.1608/FRJ-2.1.2

Kurobe, T., Lehman, P. W., Haque, M. E., Sedda, T., Lesmeister, S., and Teh, S. (2018). Evaluation of water quality during successive severe drought years within *Microcystis* blooms using fish embryo toxicity tests for the San Francisco Estuary, California. *Sci. Total Environ.* 610-611, 1029–1037. doi: 10.1016/j.scitotenv.2017.07.267

Lee, P. W., Tseng, L.-C., and Hwang, J.-S. (2018). Comparison of mesozooplankton mortality impacted by the cooling systems of two nuclear power plants at the northern Taiwan coast, southern East China Sea. *Mar. Pollut. Bull.* 136, 114–124. doi: 10.1016/j.marpolbul.2018.09.003

Lee, T. A., Rollwagen-Bollens, G., Bollens, S. M., and Faber-Hammond, J. J. (2015). Environmental influence on cyanobacteria abundance and microcystin toxin production in a shallow temperate lake. *Ecotoxicol. Environ. Saf.* 114, 318–325. doi: 10.1016/j.ecoenv.2014.05.004

Lehman, P. W., Kurobe, T., Lesmeister, S., Baxa, D., Tung, A., and Teh, S. J. (2017). Impacts of the 2014 severe drought on the *Microcystis* bloom in San Francisco estuary. *Harmful Algae* 63, 94–108. doi: 10.1016/j.hal.2017.01.011

Lehman, P. W., Marr, K., Boyer, G. L., Acuna, S., and Teh, S. J. (2013). Long-term trends and causal factors associated with *Microcystis* abundance and toxicity in San Francisco Estuary and implications for climate change impacts. *Hydrobiologia* 718, 141–158. doi: 10.1002/9781118994672.ch2

Lezcano, M. A., Velázquez, D., Quesada, A., and El-Shehawy, R. (2017). Diversity and temporal shifts of the bacterial community associated with a toxic cyanobacterial bloom: an interplay between microcystin producers and degraders. *Water Res.* 125, 52–61. doi: 10.1016/j.watres.2017.08.025

Li, T., Liu, S., Huang, L., Huang, H., Lian, J., Yan, Y., et al. (2011). Diatom to dinoflagellate shift in the summer phytoplankton community in a bay impacted

by nuclear power plant thermal effluent. *Mar. Ecol. Progr. Ser.* 424, 75–85. doi: 10.3354/meps08974

Li, X., Dreher, T. W., and Li, R. (2016). An overview of diversity, occurrence, genetics and toxin production of bloom-forming *Dolichospermum* (*Anabaena*) species. *Harmful Algae* 54, 54–68. doi: 10.1016/j.hal.2015.10.015

Liao, J., Zhao, L., Cao, X., Sun, J., Gao, Z., Wang, J., et al. (2016). Cyanobacteria in lakes on Yungui plateau, China are assembled via niche processes driven by water physicochemical property, lake morphology and watershed land-use. *Sci. Rep.* 6:36357. doi: 10.1038/srep36357

Luerling, M., van Oosterhout, F., and Faasen, E. (2017). Euthrophication and warming boost cyanobacterial biomass and microcystins. *Toxins* 9:64. doi: 10.3390/toxins9020064

Mahmood, N. A., and Carmichael, W. W. (1986). Paralytic shellfish poisons produced by the freshwater cyanobacterium *Aphanizomenon flos-aquae* NH-5. *Toxicon* 24, 175–186. doi: 10.1016/0041-0101(86)90120-0

Martins, A., and Vasconcelos, V. (2011). Use of qPCR for the study of hepatotoxic cyanobacteria population dynamics. *Arch. Microbiol.* 193, 615–627. doi: 10.1007/s00203-011-0724-7

McPartlin, D. A., Loftus, J. H., Crawley, A. S., Silke, J., Murphy, C. S., and O'Kennedy, R. J. (2017). Biosensors for the monitoring of harmful algal blooms. *Curr. Opin. Biotechnol.* 45, 164–169. doi: 10.1016/j.copbio.2017.02.018

Meriluoto, J., Blaha, L., Bojadija, G., Bormans, M., Brient, L., Codd, G. A., et al. (2017). Toxic cyanobacteria and cyanotoxins in European waters – recent progress achieved through the CYANOCOST Action and challenges for further research. *Adv. Oceanogr. Limnol.* 8, 144–161. doi: 10.4081/aiol.2017.6429

Mihali, T. K., Kellmann, R., and Neilan, B. A. (2009). Characterization of the paralytic shellfish toxin biosynthesis gene clusters in *Anabaena circinalis* AWQCI3IC and *Aphanizomenon* sp. NH-5. *BMC Biochem.* 10:8. doi: 10.1186/1471-2091-10-8

Mirasbekov, Y., Zhumakhanova, A., Zhantuyakova, A., Sarkytbayev, K., Malashenkov, D. V., Baishulakova, A., et al. (2021). Semi-automated classification of colonial Microcystis by FlowCAM imaging flow cytometry in mesocosm experiment reveals high heterogeneity during seasonal bloom. *Sci. Rep.* 11, 1–14. doi: 10.1038/s41598-021-88661-2

Moreira, C., Fathalli, A., Vasconcelos, V., and Antunes, A. (2011). Genetic diversity and structure of the invasive toxic cyanobacterium *Cylindrospermopsis raciborskii*. *Curr. Microbiol.* 62, 1590–1595. doi: 10.1007/s00284-011-9900-x

Motomizu, S., Wakimoto, T., and Toei, K. (1983). Spectrophotometric determination of phosphate in river waters with molybdate and malachite green. *Analyst* 108, 361–368. doi: 10.1039/an9830800361

Naselli-Flores, L., Barone, R., Chorus, I., and Kurmayer, R. (2007). Toxic cyanobacterial blooms in reservoirs under a semiarid Mediterranean climate: the magnification of a problem. *Environ. Toxicol.* 22, 399–404. doi: 10.1002/tox.20268

Oesterholm, J., Popin, R. V., Fewer, D. P., and Sivonen, K. (2020). Phylogenomic analysis of secondary metabolism in the toxic cyanobacterial genera *Anabaena*, *Dolichospermum* and *Aphanizomenon*. *Toxins* 12:248. doi: 10.3390/toxins12040248

Oliver, R. L., Hamilton, D. P., Brookes, J. D., et al. (2012). "Physiology, blooms and prediction of planktonic cyanobacteria," in *Ecology of Cyanobacteria II – Their diversity in time and space*, ed. B. A. Whitton (Dordrecht: Publishers'Graphics LLC), 155–194.

Padisák, J. (1997). *Cylindrospermopsis raciborskii* (Woloszynska) Seenayya et Subba Raju, an expanding, highly adaptive cyanobacterium: worldwide distribution and review of its ecology. *Arch. Hydrobiol. Suppl.* 107, 563–593.

Paerl, H. W., and Otten, T. G. (2013). Harmful cyanobacterial blooms causes, consequences, and controls. *Microb. Ecol.* 65, 995–1010. doi: 10.1007/s00248-012-0159-y

Paerl, H. W., and Paul, V. J. (2012). Climate change: links to global expansion of harmful cyanobacteria. *Water Res.* 46, 1349–1363. doi: 10.1016/j.watres.2011.08.002

Panda, A. K., Bisht, S. S., Kaushal, B. R., De Mandal, S., Kumar, N. S., and Basistha, B. C. (2017). Bacterial diversity analysis of Yumthang hot spring, North Sikkim, India by Illumina sequencing. *Big Data Anal.* 2:7. doi: 10.1186/s41044-017-0022-8

Park, S.-C., and Won, S. (2018). Evaluation of 16S rRNA databases for taxonomic assignments using a mock community. *Genomics Inform.* 16:e24. doi: 10.5808/GI.2018.16.4.e24

Parulekar, N. N., Kolekar, P., Jenkins, A., Kleiven, S., Utkilen, H., Johansen, A., et al. (2017). Characterization of bacterial community associated with phytoplankton bloom in a euthrophic lake in South Norway using 16S rRNA gene amplicon sequence analysis. *PLoS One* 12:e0173408. doi: 10.1371/journal.pone.0173408

Pearl, H. W., and Tucker, C. S. (1995). Ecology of blue-green algae in aquaculture ponds. *J. World Aquac. Soc.* 26, 109–131. doi: 10.1111/j.1749-7345.1995.tb00235.x

Pearson, L., Mihali, T., Moffitt, M., Kellmann, R., and Neilan, B. (2010). On the chemistry, toxicology and genetics of the cyanobacterial toxins, microcystin, nodularin, saxitoxin and cylindrospermopsin. *Mar. Drugs* 8, 1650–1680. doi: 10.3390/md8051650

Pearson, L. A., and Neilan, B. A. (2008). The molecular genetics of cyanobacterial toxicity as a basis for monitoring water quality and public health risk. *Curr. Opin. Biotechnol.* 19, 281–288. doi: 10.1016/j.copbio.2008.03.002

Pfeiffer, F., Gröber, C., Blank, M., Händler, K., Beyer, M., Schultze, J. L., et al. (2018). Systematic evaluation of error rates and causes in short samples in next-generation sequencing. *Sci. Rep.* 8:10950. doi: 10.1038/s41598-018-29325-6

Pitois, F., Fastner, J., Pagotto, C., and Dechesne, M. (2018). Multi-toxin occurences in ten French water resource reservoirs. *Toxins* 10:283. doi: 10.3390/toxins10070283

Pomati, F., Sacchi, S., Rossetti, C., and Giovannardi, S. (2000). The freshwater cyanobacterium *Planktothrix* sp. FP1: molecular identification and detection of paralytic shellfish poisoning toxins. *J. Phycol.* 36, 553–562.

Quick, J., Ashton, P., Calus, S., Chatt, C., Gossain, S., Hawker, J., et al. (2015). Rapid draft sequencing and real-time nanopore sequencing in a hospital outbreak of *Salmonella*. *Genome Biol.* 16:114. doi: 10.1186/s13059-015-0677-2

Quick, J., Loman, N. J., Simpson, J. T., Severi, E., Severi, E., Cowley, L., et al. (2016). Real-time, portable genome sequencing for ebola surveillance. *Nature* 530, 228–232. doi: 10.1038/nature16996

Ramsdell, J., Anderson, D., and Glibert, P. (eds) (2005). *HARRNESS (Harmful Algal Research and Response: A National Environmental Science Strategy*). Washington, DC: Ecological Society of America.

Rantala-Ylinen, A., Känä, S., Wang, H., Rouhiainen, L., Wahlsten, M., Rizzi, E., et al. (2011). Anatoxin-a synthetase gene cluster of the cyanobacterium *Anabaena* sp. strain 37 and molecular methods to detect potential producers. *Appl. Environ.l Microbiol.* 77, 7271–7278. doi: 10.1128/AEM.06022-1

Rapala, J., Erkomaa, K., Kukkonen, J., Sivonen, K., and Lahti, K. (2002). Detection of microcystins with protein phosphatase inhibition assay, high-performance liquid chromatography-UV detection and enzyme-linked immunosorbent assay - Comparison of methods. *Anal. Chim. Acta* 466, 213–231. doi: 10.1016/S0003-2670(02)00588-3

Rapala, J., Sivonen, K., Lyra, C., and Niemela, S. I. (1997). Variation of microcystin, cyanobacterial hepatotoxins, in *Anabaena* spp as a function of growth stimulation. *App. Environ. Microbiol.* 63, 2206–2212. doi: 10.1128/aem.63.6.2206-2212.1997

Rastogi, R. P., Madamwar, D., and Incharoensakdi, A. (2015). Bloom dynamics of Cyanobacteria and their toxins: environmental health impacts and mitigation strategies. *Front. Microbiol.* 6:1254. doi: 10.3389/fmicb.2015.01254

Reddington, K., Eccles, D., O'Grady, J., Drown, D. M., Hansen, L. H., Nielsen, T. K., et al. (2020). Metagenomic analysis of planktonic riverine microbial consortia using nanopore sequencing reveals insight into river microbe taxonomy and function. *Gigascience* 9:giaa053. doi: 10.1093/gigascience/giaa053

Regier, H. A., Holmes, J. A., and Pauly, D. (1990). Influence of temperature changes on aquatic ecosystems: an interpretation of empirical data. *Transact. Am. Fish. Soc.* 119, 374–389. doi: 10.1577/1548-8659

Reynolds, C. S. (2008). *Ecology of Phytoplankton*. (Cambridge: Cambridge University Press), 550.

Rizal, N. S. M., Neoh, H.-M., Ramli, R., Periyasamy, P. R., Hanafiah, A., Samat, M. N. A., et al. (2020). Advantages and limitations of 16S rRNA next-generation sequencing for pathogen identification in the diagnostic microbiology laboratory: perspectives from a middle-income country. *Diagnostics* 10:816. doi: 10.3390/diagnostics10100816

Rozenstein, O., Qin, Z., Derimian, Y., and Karnieli, A. (2014). Derivation of land surface temperature for Landsat-8 TIRS using a split window algorithm. *Sensors* 14, 5768–5780. doi: 10.3390/s140405768

Rutten, T. P. A., Sandee, B., and Hofman, A. R. T. (2005). Phytoplankton monitoring by high performance flow cytometry: a successful approach? *Cytometry A* 64, 16–26. doi: 10.1002/cyto.a.20106

Saker, M. L., and Griffiths, D. J. (2000). The effect of temperature on growth and cylindrospermopsin content of seven isolates of *Cylindrospermopsis raciborskii* (Nostocales, Cyanophyceae) from water bodies in northern Australia. *Phycologia* 39, 349–354. doi: 10.2216/i0031-8884-39-4-349.1

Savadova, K., Mazur-Marzec, H., Karosienė, J., Kasperovičienė, J., Vitonytė, I., Torunska-Sitarz, A., et al. (2018). Effect of increased temperature on native and alien nuisance cyanobacteria from temperate lakes: an experimental approach. *Toxins* 10:445. doi: 10.3390/toxins10110445

Scherer, P. I., Millard, A. D., Miller, A., Schoen, R., Raeder, U., Geist, J., et al. (2017). Temporal dynamics of the microbial community composition with a focus on toxic cyanobacteria and toxin presence during harmful algal blooms in two South German lakes. *Front. Microbiol.* 8:2387. doi: 10.3389/fmicb.2017.02387

Shumway, S. E. (1990). A review of the effects of algal blooms on shellfish and aquaculture. *J. World Aquac. Soc.* 21, 65–103. doi: 10.1111/j.1749-7345.1990.tb00529.x

Sieracki, C. K., Sieracki, M. E., and Yentsch, C. S. (1998). An imaging-in-flow system for automated analysis of marine microplankton. *Mar. Ecol. Prog. Ser.* 168, 285–296.

Sukenik, A., Quesada, A., and Salmaso, N. (2015). Global expansion of toxic and non-toxic cyanobacteria: effect on ecosystem functioning. *Biodivers. Conserv.* 24, 889–908. doi: 10.1007/s10531-015-0905-9

Suresh, K., Ahamed, M. S., Durairaj, G., and Nair, K. V. K. (1993). Impact of power plant heated effluent on the abundance of sedentary organisms, off Kalpakkam, East coast of India. *Hydrobiologia* 268, 109–114. doi: 10.1007/BF00006881

Teikari, J. E., Popin, R. V., Hou, S., Wahlsten, M., Hess, W. R., and Sivonen, K. (2019). Insight into the genome and brackish water adaptation strategies of toxic and bloom-forming Baltic Sea *Dolichospermum* sp. UHCC 0315. *Sci. Rep.* 9:4888. doi: 10.1038/s41598-019-40883-1

Teixeira, T. P., Neves, L. M., and Araujo, F. G. (2009). Effect of a nuclear power plant thermal discharge on habitat complexity and fish community structure in Ilha Grande Bay, Brazil. *Mar. Environ. Res.* 68, 188–195. doi: 10.1016/j.marenvres.2009.06.004

Thomas, M. K., and Litchman, E. (2016). Effects of temperature and nitrogen availability on the growth of invasive and native cyanobacteria. *Hydrobiologia* 763, 357–369. doi: 10.1007/s10750-015-2390-2

Thuret-Benoist, H., Pallier, V., and Feuillade-Cathalifaud, G. (2019). Quantification of microcystins in natural waters by HPLC-UV after a pre-concentration step: validation of the analytical performances and study of the interferences. *Environ. Toxicol. Pharmacol.* 72:103223. doi: 10.1016/j.etap.2019.103223

Tornazo, A. E., Nieto, F., and Barja, J. L. (1990). Mortality associated with cyanobacterial bloom in farmed rainbow trout in Galicia (north-western Spain). *Bull. Eur. Assoc. Fish Pathol.* 10, 106–107.

Vaitomaa, J., Rantala, A., Halinen, K., Rouhiainen, L., Tallberg, P., Mokelke, L., et al. (2003). Quantitative Real-Time PCR for determination of microcystin synthetase E copy numbers for *Microcystis* and *Anabaena* in lakes. *Appl. Environ. Microbiol.* 69, 7289–7297. doi: 10.1128/aem.69.12.7289-7297.2003

Walawender, J. P., Hajto, M. J., and Iwaniuk, P. (2012). "A new ArcGIS toolset for automated mapping of land surface temperature with the use of LANDSAT satellite data," in *Proceedings of the 2012 IEEE International Geoscience and Remote Sensing Symposium*, Munich, 4371–4374. doi: 10.1109/IGARSS.2012.6350405

Wejnerowski, L., Rzymski, P., Kokociński, M., and Meriluoto, J. (2018). The structure and toxicity of winter cyanobacterial bloom in a eutrophic lake of the temperate zone. *Ecotoxicology* 27, 752–760. doi: 10.1007/s10646-018-1957-x

Wells, M. L., Karlson, B., Wulff, A., Kudela, R. M., Trick, C., Asnaghi, V., et al. (2020). Future HAB science: directions and challenges in a changing climate. *Harmful Algae* 91, 101632–101650. doi: 10.1016/j.hal.2019.101632

Wilson, A. E., Sarnelle, O., Neilan, B. A., Salmon, T. P., Gehringer, M. M., and Hay, M. E. (2005). Genetic variation of the bloom-forming cyanobacterium *Microcystis aeruginosa* within and among lakes: implications for harmful algal blooms. *Appl. Environ. Microbiol.* 71, 6126–6133. doi: 10.1128/AEM.71.10.6126-6133.2005

Winand, R., Bogaerts, B., Hoffman, S., Lefevre, L., Delvoye, M., Van Braekel, J., et al. (2020). Targeting the 16S rRNA gene for bacterial identification in complex mixed samples: comparative evaluation of second (Illumina) and third (Oxford Nanopore Technologies) generation sequencing technologies. *Int. J. Mol. Sci.* 21:298. doi: 10.3390/ijms21010298

Woodhouse, J. N., Kinsela, A. S., Collins, R. N., Bowling, L. C., Honeyman, G. L., Holliday, J. K., et al. (2016). Microbial communities reflect temporal changes in cyanobacterial composition in a shallow ephemeral freshwater lake. *ISME J* 10, 1337–1351. doi: 10.1038/ismej.2015.218

Xiao, X., Sogge, H., Lagesen, K., Tooming-Klunderud, A., Jakobsen, K. S., and Rohrlack, T. (2014). Use of high throughput sequencing and light microscopy show contrasting results in study of phytoplankton occurrence in a freshwater environment. *PLoS One* 9:e106510. doi: 10.1371/journal.pone.0106510

Zimmerman, J., Gloeckner, G., Regine, J., Neela, E., and Gemeinholzer, B. (2015). Metabarcoding vs. morphological identification to assess diatom diversity in environmental studies. *Mol. Ecol. Resour.* 15, 526–542. doi: 10.1111/1755-0998.12336

Conflict of Interest: The authors declare that the research was conducted in the absence of any commercial or financial relationships that could be construed as a potential conflict of interest.

frontiers in Marine Science

ORIGINAL RESEARCH
published: 22 July 2021
doi: 10.3389/fmars.2021.628095

Effect of the Extracts of *Sargassum fusiforme* on Red Tide Microalgae in East China Sea

Yurong Zhang[1,2], *Nianjun Xu*[1]* *and Yahe Li*[1]

[1] *Key Laboratory of Marine Biotechnology of Zhejiang Province, School of Marine Sciences, Ningbo University, Ningbo, China,* [2] *Key Lab of Mariculture and Enhancement of Zhejiang Province, Zhejiang Marine Fisheries Research Institute, Zhoushan, China*

This study examined the effects of extracts of hijiki (*Sargassum fusiforme*) on the growth and physiology of three species of red tide microalgae (*Prorocentrum donghaiensis*, *Skeletonema costatum*, and *Heterosigma akashiwo*) that commonly grow in the East China Sea. The red tide algae were cultivated with the hijiki extracts at different concentrations to investigate the effects of the extracts on cells growth, chlorophyll *a* content, maximum quantum yield of PSII (*Fv/Fm*), the activities of four oxidoreductases including peroxidase (SOD), glutathione S-transferase (GST), glutathione peroxidase (GSH-Px), glutathione reductase (GR), and the level of the membrane lipid peroxidation product, malondialdehyde (MDA). The sensitivity of red tide algae to the extracts varied among the strains, with *P. donghaiensis* being the most sensitive, followed by *S. costatum*, and then *H. akashiwo*. Furthermore, the extracts had a rapid lethal effect on *P. donghaiensis* at over 1.6 g/L and on *S. costatum* and *P. donghaiensis* at over 8 g/L. From that concentration, increasing amounts of the extracts in cultures of *S. costatum* promoted a reduction in Chl*a* contents and *Fv/Fm* values. In addition, the oxidoreductase activity of *S. costatum* was reduced at 4 and 6 g/L, as shown by the reduced activity of SOD, GR, GSH-Px, GST and MDA content in the cells. The results presented herein will be useful to the development and utilization of hijiki on red tide control, and marine environmental protection.

Keywords: *Sargassum fusiforme*, red tide microalgae, Chl*a*, *Fv/Fm*, oxidoreductase

OPEN ACCESS

Edited by:
Keith Davidson, Scottish Association For Marine Science, United Kingdom

Reviewed by:
Nor Azman Kasan, University of Malaysia Terengganu, Malaysia
Eileen Bresnan, Marine Scotland, United Kingdom

***Correspondence:**
Nianjun Xu
xunianjun@nbu.edu.cn

Specialty section:
This article was submitted to Marine Fisheries, Aquaculture and Living Resources, a section of the journal Frontiers in Marine Science

Received: *11 November 2020*
Accepted: *15 June 2021*
Published: *22 July 2021*

Citation:
Zhang Y, Xu N and Li Y (2021) Effect of the Extracts of Sargassum fusiforme on Red Tide Microalgae in East China Sea. Front. Mar. Sci. 8:628095. doi: 10.3389/fmars.2021.628095

INTRODUCTION

Due to the impact of human activities and changes in the natural environment, eutrophication is increasing along the coast of East China Sea, which is harmful for the biodiversity and ecological functions of the marine ecosystem and resulting in frequent occurrence of red tides. Red tide is a disastrous abnormal marine ecological phenomenon, in which some planktonic microalgae, protozoa, or bacteria suddenly proliferate or gather in a short period of time under certain environmental conditions, resulting in a change in water color. Red tide often leads to water hypoxia, resulting in the deaths of a large number of fish, shellfish, and other marine organisms,

threatening marine ecology and aquaculture. In addition, microcystins produced by harmful algae accumulate in fish and ultimately endanger human health through the food chain (Yu and Chen, 2019). In the first decade of the twenty-first century, the frequency and scale of red tides in China were three times greater than in the late 1950s. During the period between 2000 and 2017, the cumulative area of red tides in China reached 210,000 square kilometers, with the red tide problems in the East China Sea being by far the most serious as compared to that in South China Sea and Bohai Sea (Yu and Chen, 2019). Red tide has become a constraint on the offshore economy development (León-Muñoz et al., 2018; Mascareño et al., 2018), a threat to human food safety (Van Dolah, 2000; McCabe et al., 2016; Daguer et al., 2018), and an ecological disaster damaging marine ecosystems (Yu and Chen, 2019). Consequently, red tide is now an ecological problem that needs to be addressed urgently (Berdalet et al., 2017). Red tide of the Raphidophyta alga *Pseudochattonella* cf. *verruculosa* during the 2016 austral summer (February–March) killed nearly 12% of the Chilean salmon production, causing the worst mass mortality of fish and shellfish ever recorded in the coastal waters of western Patagonia, and the direct economic loss was more than one billion US dollars (León-Muñoz et al., 2018). In October 2017, a red tide of *Karenia brevis* (formerly known as *Gymnodinium breve*), which lasted for 15 months, broke out off the coast of Florida in the United States (Soto et al., 2018). To date, more than 200 toxins have been isolated from red tide species including dinoflagellates, diatoms, and cyanobacteria, resulting in toxic effects including diarrheic shellfish poisoning, azaspiracid poisoning, neurotoxic shellfish poisoning, ciguatera fish poisoning, paralytic shellfish poisoning, tetrodotoxin, and amnesic shellfish poisoning. These toxins pose a great threat to human beings and other organisms (Daguer et al., 2018).

Controlling red tides by means of physical and chemical methods may exert adverse effects on the marine ecosystem (Jeong et al., 2000). Some scholars have proposed that the large-scale cultivation of macroalgae might lead to absorption of nitrogen and phosphorus in water (Ahn et al., 1998), regulating the marine ecosystem and inhibiting the occurrence of red tides (Nakai et al., 1999). Macroalgae cultivation may also provide a spawning ground for fish by providing food and attachment bases for fish eggs; therefore, this activity has the potential to play an important role in ecosystem restoration and increasing the diversity of fishery resources (Yang et al., 2015). Studies have confirmed that seaweeds such as *Gracilaria confervoides*, *Gracilariopsis lemaneiformis*, *Corallina pilulifera*, *Enteromorpha prolifera*, *Ulva lactuca*, *U. fasciata*, *U. pertusa*, and *Sargassum thunbergii* have allelopathic inhibitory effects on red tide microalgae (Jeong et al., 2000; An et al., 2008; Liu et al., 2011; Lu et al., 2011; Tang and Gobler, 2011). Moreover, the growth (Della et al., 2000), cell function, and cell membrane structure (An et al., 2008; Lu et al., 2011; Tang and Gobler, 2011) of red tide algae such as *Skeletonema costatum*, *Amphidinum* sp., and *Karenia mikimoto* can be inhibited and damaged by the dry power, methanol extracts, filtrate and water-soluble extracts obtained from the water used to cultivate these seaweeds. It has been shown that *S. fusiforme* reduced the chlorophyll *a* and maximum chlorophyll fluorescence (*Fv/Fm*) levels in *Karenia mikimotoi* (Ma et al., 2017). Although the inhibitory effects of seaweed extracts on the growth of microalgae have been studied, little is known about their mechanisms of inhibition.

Environmental stress may cause an increase in oxygen free radicals such as superoxide anion radicals, hydrogen peroxide, hydroxyl radicals, and singlet oxygens in plant cells. The radicals usually participate in degrading chloroplasts and reducing the content of ascorbic acid and the activity of ascorbate peroxidase, leading to membrane lipid peroxidation. Some of the free radicals are closely related to the bleaching of photosynthetic pigments and membrane lipid peroxidation. Singlet oxygens in cells react with many macromolecular substances, thereby damaging the normal growth and proliferation of cells (Gill and Tuteja, 2010). During evolution, living organisms have developed an antioxidant system to resist external stressors, including a number of enzymes—superoxide dismutase (SOD), catalase (CAT), ascorbate peroxidase (APX), glutathione reductase (GR), glutathione peroxidase (GPX), and glutathione-S-transferase (GST), and non-enzymatic antioxidants—ascorbic acid (ASH), glutathione (GSH), phenolic compounds, alkaloids, non-protein amino acids, a-tocopherols, and malondialdehyde (MDA) (Gill and Tuteja, 2010). The system can reduce the levels of free radicals caused by environmental stress to protect the cells (Gross, 2003; Hejl and Koster, 2004; Gill and Tuteja, 2010). However, excessively high levels of free radicals cannot be eliminated by the antioxidant system, which can reduce the activity of the enzymes in the antioxidant system. Peroxidation damage is one of the main effects of stressors on living organisms.

Sargassum fusiforme is an edible brown algae with high medicinal value that is widely distributed along the coasts of China, South Korea, and Japan (Hu et al., 2016; Sun et al., 2019; Zhang et al., 2020). In recent years, hijiki has been cultivated on a large scale in Dongtou, Wenzhou, Zhejiang Province. We conducted several investigations in April and June of 2018 and 2019 (data not published), and found that there were significant differences in the community structure of phytoplankton between cultivation and non-cultivation areas, and that the abundance and dominance of *Skeletonema costatum* in the cultivation areas were significantly lower than in non-cultivation areas. In this study, we analyzed the effects of hijiki extracts on the growth, Chl*a* content, maximum quantum yield, and enzyme activity of the red tide algae *Heterosigma akashiwo*, *S. costatum* and *Prorocentrum donghaiensis*, which commonly grow in the East China Sea (Liu et al., 2013; Jiang et al., 2017). We sought to determine the inhibitory effects of *S. fusiforme* on marine microalgae, identify the red tide microalgae that are inhibited by it, as well as to understand the biological mechanism of the inhibitory effects of hijiki on microalgae.

MATERIALS AND METHODS

Microalgae Strains and Cultivation Conditions

The red tide microalgae *Heterosigma akashiwo*, *Skeletonema costatum*, and *Prorocentrum donghaiensis* were purchased from

Shanghai Guangyu Biotechnology Co., Ltd. (Zhejiang, China). These microalgae were cultivated in f/2(+Si) medium and transferred to fresh medium every week for proliferation. Algae cultivation was performed in a smart light growth chamber (Ningbo Southeast Instrument Co., Ltd., Zhejiang, China). The temperature was 23°C ± 0.1 for *H. akashiwo* and *S. costatum*, and 20°C ± 0.1 for *P. donghaiensis*. Light intensity was 4,000 umol.m^{-2}·s^{-1} with a light:dark photoperiod of 12 h:12 h.

Preparation of Seaweed Samples and Extracts

S. fusiforme was collected from Banping Island hijiki culture area, Dongtou, Wenzhou (N 120°59′45″–121°15′58″, E 27°41′19″–28°01′10″). The samples were then washed with pure water and dried at room temperature to a constant weight. The dried hijiki was subsequently pulverized into powder and stored at −20°C until use. Prior to use, the powder was soaked in sterilized seawater for 48 h at a powder-to-seawater ratio of 100 g:1 L. Next, the extracts were filtered through a 400 mesh silk net sieve and centrifuged (15 min at 12,000 rpm). After centrifugation, the supernatant was collected as the stock solution of the hijiki extracts with a concentration of 100 g/L. Both sterilized (121°C, 20 min) and non-sterilized stock solutions were utilized in this study. The concentration of the extracts was expressed as dry weight (g) of *S. fusiforme* per volume (L) of seawater.

Sterilization on the Inhibitory Potential of the Hijiki Extracts Against Microalgae Growth

Either the sterilized or unsterilized hijiki extracts, microalgae in the exponential phase, and enriched f/2 medium prepared with sterilized seawater were added into a 2,000 mL culture flask to a working volume of 1,000 mL with 6 g/L extracts. No extract was added in the control group. The densities of the *P. donghaiensis, S. costatum*, and *H. akashiwo* were 68.3 × 10^6, 70.8 × 10^6, and 65.2 × 10^6 cells/L, respectively. The cultivation of the three strains was performed using both sterilized and unsterilized hijiki extracts; and each treatment was replicated thrice. This gave a total of 6 treatments and 18 experimental runs (**Table 1**). During cultivation, 1 mL samples were collected at 48, 96, and 144 h to measure the density of microalgae. Lugol's solution (0.05 mL) was added to stain the cells. Using a 0.1 mL Sedgewick Rafter cell (**Figure 1**), the density of microalgae was counted under an optical microscope, after which the inhibitory rate (IR) was calculated using the following equation:

$$IR = \left(1 - \frac{Nt}{N0}\right) \times 100\%$$

where N_0 and Nt are control density of microalgae and the density at time t of culture, respectively.

Effect of the Concentration of the Hijiki Extracts on Microalgae Growth

Culture systems with 0, 0.4, 0.8, 1.2, 1.6, 2.0, 4.0, 8.0, and 10.0 g/L extracts were prepared, t to study whether the extracts had the same inhibitory effect on three types of red tide microalgae grown at different densities. The culture systems with 0.4, 0.8, 1.2, and 1.6 g/L extracts were designated as the low-concentration group, in which microalgae grew at normal density. The initial densities of *P. donghaiensis*, *S. costatum*, and *H. akashiwo* in the low-concentration extract groups were 420, 650, and 610 cells/L, respectively. The culture systems with 2.0, 4.0, 8.0, and 10.0 g/L extracts were designated as the high-concentration group, in which the microalgae grew at red tide density. The initial densities of *P. donghaiensis, S. costatum*, and *H. akashiwo* in this group were 75.2 × 10^6, 78.5 × 10^6, and 72.2 × 10^6 cells/L, respectively. The treatment with 0 g/L of hijiki extract was considered as the control group. At 24, 48, 72, 96, 120, 144, and 168 h, 1 mL of culture solution was collected into a centrifuge tube and stained to measure the density of microalgae and calculate the *IR* and the relative growth rate (μ). Another 1 mL of the culture solution was collected to observe the morphology of living cells.

The sample needed to be diluted in order to count it accurately when the cell density was high. The approximate cell density was estimated before dilution. Then, 0.1 ml solution was dropped into the counting plate, and the three squares shown in the green triangle in **Figure 1** were selected to count the number of cells to estimate the approximate cell density because the cell density in the Sedgewick Rafter cell often decreases from the middle to the edge. The dilution factor (d) was selected according to the principle that there should be about 10 cells each square after dilution. The number of cells (n) in 0.1 mL solution after dilution was calculated, and was multiplied by d to obtain the cell density of the solution before dilution.

With <1 cell per 0.1 mL solution, the sample needed to be concentrated to count it accurately. In a test tube, Lugol's reagent was used to stain the cells in 10 mL of solution, and the cells were allowed to settle for 24 h. The stained cells settled to the bottom of the test tube due to the gravity effect. A pipet was used to carefully discard the supernatant until the volume was 1, 0.5, or 0.1 mL for counting. The concentration factor was c. The number of cells (n) in 0.1 mL solution after concentration was calculated, and was divided by c to obtain the cell density of the solution before concentration.

The half inhibitory concentrations (IC_{50}) of the extracts on microalgae at day 5 were calculated using the linear interpolation method.

In this study, the IC_{50} was calculated by the linear interpolation method (Han et al., 2013) between two given points as follows:

TABLE 1 | EC50 (g/L) of hijiki extract on three species of microalgae.

Microalgae	*Prorocentrum donghaiensis*	*Skeletonema costatum*	*Heterosigma akashiwo*
High density (×10^6 cell/L)	2.0 ± 0.5	2.3 ± 0.4	2.9 ± 0.7
Low density (×10^3 cell/L)	0.19 ± 0.06	0.25 ± 0.05	0.35 ± 0.1

Statistics were calculated based on linear interpolation method.

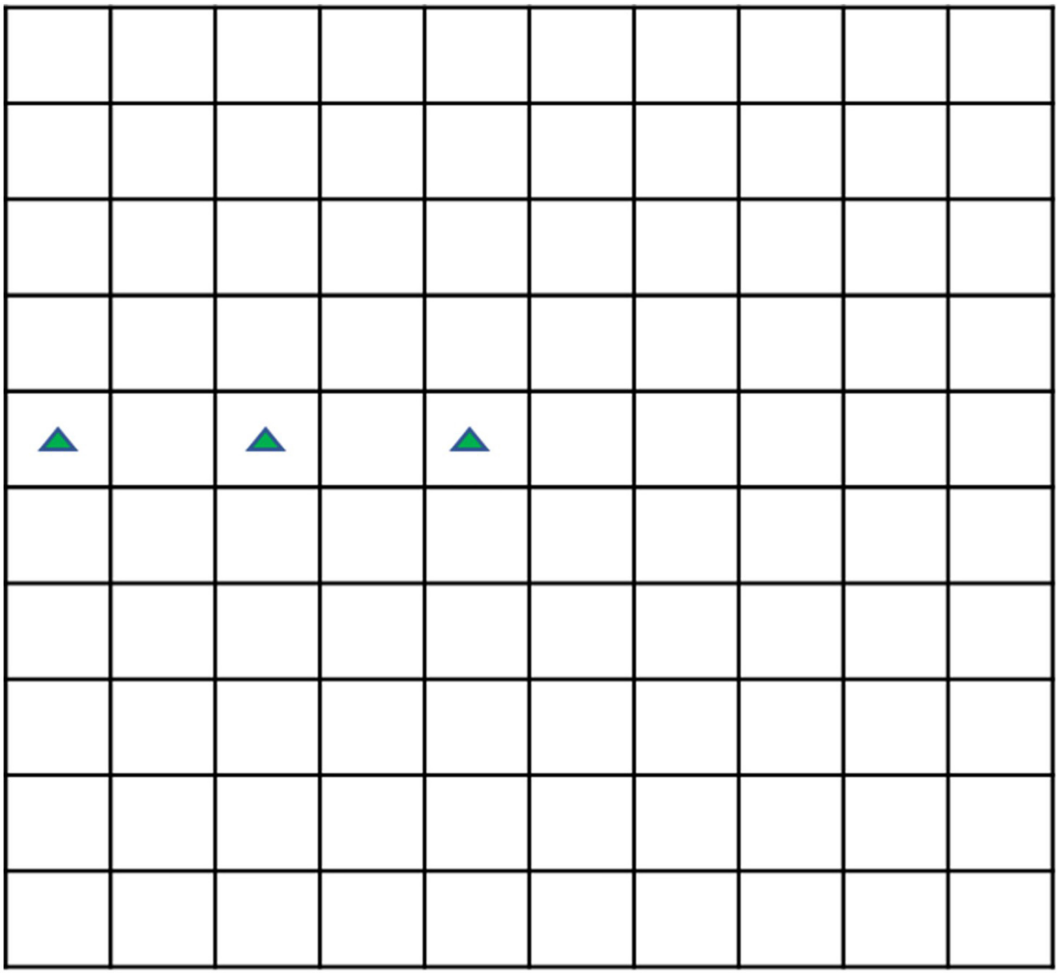

FIGURE 1 | The plane sketch of 0.1 mL Sedgewick Rafter cell.

The cell densities of the two given points were (a, Na) and (b, Nb).

$$\frac{(y - Na)}{(x - a)} = \frac{(Nb - b)}{(b - a)}$$

Solving this equation gives

$$y = Na + \frac{(x - a) \times (Nb - Na)}{(b - a)}$$

If y = 0.5 N_C,

$$IC50 = \mathrm{a} + \frac{(0.5Nc - Na) \times (b - a)}{(Nb - a)}$$

In the equation, a and b are the two given concentrations and Na and Nb are the cell densities at the given concentrations, respectively; x is the unknown concentration; y is the cell density at the unknown concentration; Nc is the cell density of the control at Nh. In this study, the cell density of the control at 144 h was used.

The relative growth rate (μ) was calculated using the following equation:

$$\mu = \frac{lnXn - lnX(n - 1)}{tn - t(n - 1)}$$

where μ is the relative growth rate, h^{-1}; Xn is the density of microalgae at time tn; and X(n−1) is the density of microalgae at time t(n−1).

Determination of Chl*a* and *Fv/Fm*

The culture systems were prepared in the same way as described in the section "Sterilization on the Inhibitory Potential of the Hijiki Extracts against Microalgae Growth," and the final concentrations of the extracts were set to 0, 2.0, 4.0, 8.0, and 10.0 g/L. Each culture system was prepared in triplicate. At 0, 4, 8, 12, 24, 48, 72, 96, 120, 144, and 168 h, 50 mL of the culture solutions were collected into centrifuge tubes and placed in the dark for adaption for 15 min, after which the maximum quantum yield (*Fv/Fm*) (Davide et al., 2016; Guan and Li, 2017) was measured using a handheld chlorophyll fluorometer (AquaPen-C AP-C 100) and the Chl*a* content was determined using a

spectrophotometer. Next, the culture solution was sampled and filtered through a 0.45 μm nitrocellulose filter membrane, after which the filter membrane was placed in a centrifuge tube and 10 mL of 90% acetone was added. After being held for 24 h at 4°C, the tube was centrifuged at 3,000 rpm for 10 minutes and the absorbance of the supernatants was then measured at 750, 664, 647, and 630 nm using 90% acetone as a reference. The content of Chl*a* was calculated using the equation modified by Jeffrey and Humphrey (1975):

$$\rho Chla = (11.85E664 - 1.54E647 - 0.08E630) \times \frac{v}{V.L}$$

where Chl*a* is the concentration (μg/L) of chlorophyll *a*; v is the volume (mL) of the sampled culture solution; V is the actual volume (L) of seawater used; L is the pathlength (cm) of the cuvette; and E664, E647 and E630 are the absorbance values of the solution at 664, 647, and 630 nm, respectively.

Determination of Enzyme Activity

The culture system was prepared in the same way as described in the section "Sterilization on the Inhibitory Potential of the Hijiki Extracts against Microalgae Growth," except that the working volume was 1,250 mL. At 0, 4, 8, 12, 24, 48, 72, 96, 120, 144, and 168 h, 100 mL aliquots of the culture solutions were collected. Before sampling, the culture flask was shaken to evenly distribute the algal cells in the culture solution. After sampling, the culture solution was centrifuged at 1,000 rpm/min for 10 min and pellet cells were collected. Commercial kits A001-1-2, A003-1-3, A004-1-1, A005-1-2, and A062-1-1 were used to determine the activity or content of SOD, MDA, GST, GSH-Px, and GR, respectively.

SPSS Statistical Analysis of Data

Excel 2016 was used to plot the data. SPSS 20.0.0 was used to conduct one-way ANOVA analysis and a $p < 0.05$ was considered to be significant.

RESULTS

The pH Values of the Cultures

The pH values of both sterilized and non-sterilized extracts were 4.967 ± 0.003. The pH values of the high- concentration groups (0, 2, 4, 6, 8, and 10 g/L) were 8.309 ± 0.008, 8.179 ± 0.017, 8.044 ± 0.009, 7.815 ± 0.064, 7.708 ± 0.057, and 7.634 ± 0.065, respectively. The pH values of the low- concentration groups (0, 0.4, 0.8, 1.2, and 1.6 g/L) were 8.293 ± 0.004, 8.281 ± 0.006, 8.267 ± 0.014, 8.246 ± 0.016, and 8.235 ± 0.011, respectively. Therefore, the addition of hijiki extracts reduced the pH value of algae cultures (**Figure 2**).

Inhibitory Effect of Sterilized and Unsterilized Hijiki Extracts on Microalgae Growth

The effects of the sterilized and unsterilized 6 g/L hijiki extracts on the daily growth rates of *P. donghaiensis*, *S. costatum*, and *H. akashiwo* were analyzed. The daily growth rate was determined at 48, 96, and 144 h of culture. The average daily growth rates of three microalgae at different times were slightly higher in the cultures with sterilized extracts than in those with unsterilized extracts, but these differences were not significant ($p > 0.05$) (**Figure 3**), indicating that high temperature and high pressure sterilization did not change the inhibitory effects of the extracts on the red tide microalgae. To prevent contamination by bacteria and protists, the extracts used for all experiments in this study were sterilized.

IC_{50} of Hijiki Extracts on Different Concentration of Microalgae

Based on the linear interpolation method, the IC_{50} of the extracts for inhibiting the growth of three microalgae of high density and low density within 144 h was analyzed. The IC_{50} on high density of *P. donghaiensis*, *S. costatum*, and *H. akashiwo* were 2.0 ± 0.5 g/L, 2.3 ± 0.4 g/L and 2.9 ± 0.7 g/L, respectively, while those on low density *P. donghaiensis*, *S. costatum*, and *H. akashiwo* were 0.19 ± 0.06 g/L, 0.25 ± 0.05 g/L, and 0.35 ± 0.08 g/L (**Table 1**). Therefore, the sequence of the inhibitory effect of the hijiki extracts on three microalgae at both density levels was *P. donghaiensis* > *S. costatum* > *H. akashiwo*.

Effect of Hijiki Extract Concentration on the Growth and Morphology of Microalgae

Effect on the Growth of Microalgae at Low Cell Densities

As the concentration of Hijiki extracts increased, the inhibitory effects on the growth of *P. donghaiensis, S. costatum*, *H. akashiwo* gradually increased. Extract concentrations over 1.6 g/L showed lethal effects on *P. donghaiensis* in 48 h. After 24 h of cultivation, the cell densities of *P. donghaiensis*, *S. costatum*, and *H. akashiwo* cultured with 0.4, 0.8, 1.2, and 1.6 g/L extracts were significantly lower than that of the control groups ($p < 0.05$) (**Figures 4A–C**). The relative growth rates of *P. donghaiensis* (0.0 g/L: 0.014 ± 0.005, 0.4 g/L: 0.010 ± 0.006, 0.8 g/L: 0.004 ± 0.001, 1.2 g/L: −0.023 ± 0.009, and 1.6 g/L: −0.075 ± 0.012), *S. costatum* (0.0 g/L: 0.013 ± 0.005, 0.4 g/L: −0.047 ± 0.010, 0.8 g/L: −0.058 ± 0.011, 1.2 g/L: −0.074 ± 0.015, and 1.6 g/L: −0.078 ± 0.021), and *H. akashiwo* (0.0 g/L: 0.017 ± 0.009, 0.4 g/L: 0.012 ± 0.004, 0.8 g/L: −0.005 ± 0.001, 1.2 g/L: −0.008 ± 0.002, and 1.6 g/L: −0.018 ± 0.008) cultured with 0.4, 0.8, 1.2, and 1.6 g/L extracts at 0–24 h were significantly lower than the control ($p < 0.05$), decreased with the increase in the concentration of the extracts, and recovered after 24 h (**Table 2**). The *P. donghaiensis* cultured with 0.4 and 0.8 g/L maintained a rapid growth during culture, while that cultured with 1.2 g/L extracts grew slowly (**Table 2**). No living cells of *P. donghaiensis* were found at 48 h cultured with 1.6 g/L extracts (**Figure 4A**). The *S. costatum* and *H. akashiwo* cultured with 0.4, 0.8, and 1.2 extracts underwent a rapid growth during culture ($\mu > 0$), while those cultured with 1.6 g/L extracts grew slowly (**Table 2**).

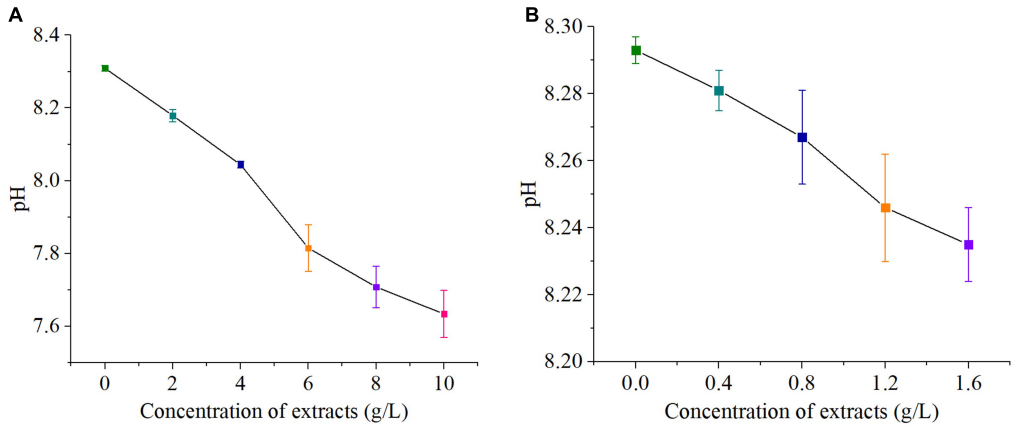

FIGURE 2 | pH value of concentration *S. fusiforme* extracts, high concentration **(A)** and low concentration **(B)**.

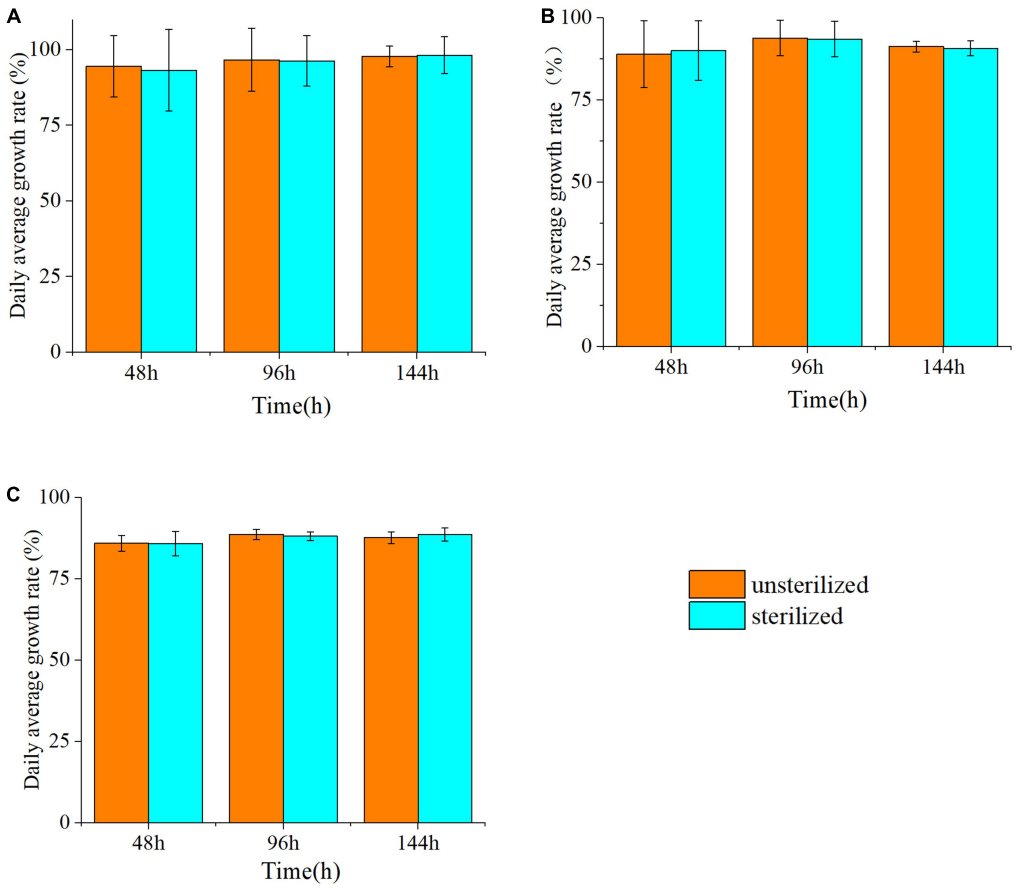

FIGURE 3 | The inhibitory rate (%) of three species of microalgae cultured with unsterilized and sterilized 6 g/L hijiki extract for 48, 96, and 144 h. **(A)** *Prorocentrum donghaiensis*; **(B)** *Skeletonema costatum*; **(C)** *Heterosigma akashiwo.*

Effect on the Growth of Microalgae at High Cell Densities

As the concentration increased, the inhibitory effects of hijiki extracts on the growth of *P. donghaiensis, S. costatum*, and *H. akashiwo* increased. After 24 h of cultivation, the cell densities of *P. donghaiensis*, *S. costatum*, and *H. akashiwo* cultured with 2, 4, 6, 8, and 10 g/L extracts were significantly lower than that of the control groups ($p < 0.05$) (**Figures 4D–F**). The inhibitory effect of extracts on *P. donghaiensis* was stronger than on *S. costatum* and *H. akashiwo*. When cultured with 2, 4, 6, 8, and 10 g/L extracts

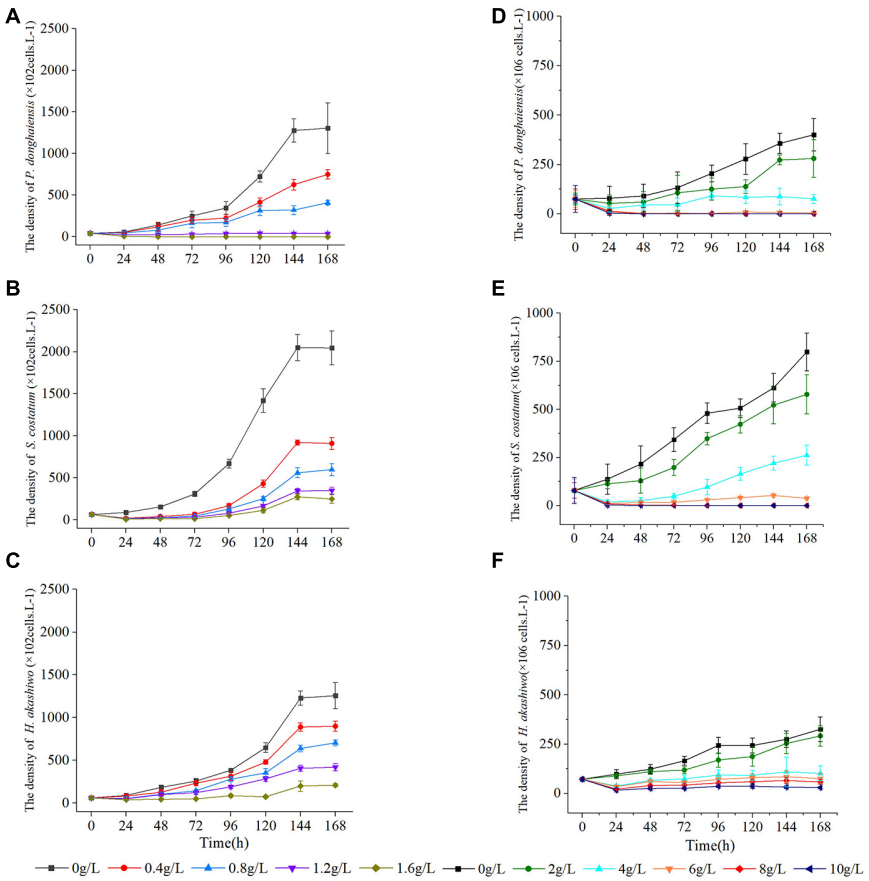

FIGURE 4 | Effect of hijiki extracts on, *Prorocentrum donghaiensis, Skeletonema costatum*, *and Heterosigma akashiw* Low density **(A–C)** and high density **(D–F)**.

TABLE 2 | The relative growth rate of low density microalgae under the influence of different concentrations of extracts (μ) (h^{-1}).

Species	Extracts concentration (g/L)	μ0–24 h	μ24–48 h	μ48–72 h	μ72–96 h	μ96–120 h	μ120–144 h	μ144–16 h
P. donghaiense	0.0	0.014 ± 0.005	0.037 ± 0.0011	0.024 ± 0.014	0.013 ± 0.005	0.031 ± 0.014	0.024 ± 0.009	0.001 ± 0.000
	0.4	0.010 ± 0.006*	0.034 ± 0.0015	0.022 ± 0.010	0.005 ± 0.002*	0.026 ± 0.008	0.017 ± 0.008*	0.007 ± 0.002*
	0.8	0.004 ± 0.001*	0.023 ± 0.009*	0.030 ± 0.019*	0.003 ± 0.000*	0.025 ± 0.012	0.001 ± 0.000*	0.010 ± 0.004*
	1.2	−0.023 ± 0.009*	0.003 ± 0.001*	0.009 ± 0.004*	0.007 ± 0.002*	0.004 ± 0.002*	−0.002 ± 0.001*	0.000 ± 0.001*
	1.6	−0.075 ± 0.012*	/	/	/	/	/	/
S. costatum	0.0	0.013 ± 0.006*	0.023 ± 0.007	0.029 ± 0.017	0.032 ± 0.023	0.031 ± 0.016	0.015 ± 0.006	0.000 ± 0.002
	0.4	−0.047 ± 0.010*	0.029 ± 0.005*	0.020 ± 0.013*	0.038 ± 0.015	0.039 ± 0.020 *	0.032 ± 0.011*	−0.001 ± 0.001
	0.8	−0.058 ± 0.011*	0.026 ± 0.007	0.018 ± 0.007*	0.044 ± 0.018*	0.027 ± 0.018	0.033 ± 0.003*	0.003 ± 0.002*
	1.2	−0.074 ± 0.015*	0.037 ± 0.016*	0.007 ± 0.002*	0.038 ± 0.016	0.031 ± 0.015	0.030 ± 0.019*	0.001 ± 0.001
	1.6	−0.078 ± 0.021*	0.022 ± 0.014*	−0.003 ± 0.001*	0.051 ± 0.023*	0.031 ± 0.014	0.037 ± 0.012*	−0.004 ± 0.002*
H. akashiwo	0.0	0.017 ± 0.009*	0.029 ± 0.010	0.014 ± 0.004	0.017 ± 0.007	0.022 ± 0.008	0.027 ± 0.010	0.008 ± 0.002
	0.4	0.012 ± 0.004*	0.019 ± 0.008*	0.025 ± 0.019*	0.013 ± 0.006*	0.018 ± 0.008	0.026 ± 0.010	0.016 ± 0.005*
	0.8	−0.005 ± 0.001*	0.027 ± 0.006	0.014 ± 0.005	0.027 ± 0.011*	0.010 ± 0.004*	0.025 ± 0.012	0.039 ± 0.023*
	1.2	−0.008 ± 0.002*	0.029 ± 0.009	0.009 ± 0.004*	0.018 ± 0.005	0.017 ± 0.009	0.015 ± 0.007*	−0.005 ± 0.006*
	1.6	−0.018 ± 0.008*	0.005 ± 0.002*	0.004 ± 0.001*	0.023 ± 0.013	−0.006 ± 0.002*	0.041 ± 0.023*	/

*"/" indicates the cell density was zero, so the relative growth rate could not be calculated. *Compared with the control, there was significant difference ($p < 0.05$).*

for 24 h, the relative growth rates of *P. donghaiensis* (0 g/L: 0.002 ± 0.001, 2 g/L: −0.014 ± 0.006, 4 g/L: −0.043 ± 0.020, 6 g/L: −0.067 ± 0.033, 8 g/L: −0.078 ± 0.035, and 10 g/L: −0.128 ± 0.086), *S. costatum* (0 g/L: 0.023 ± 0.008, 2 g/L: 0.015 ± 0.009, 4 g/L: −0.061 ± 0.023, 6 g/L: −0.081 ± 0.025, 8 g/L: −0.090 ± 0.039, and 10 g/L: 0.153 ± 0.061), and *H. akashiwo* (0 g/L: 0.013 ± 0.005, 2 g/L: 0.009 ± 0.004, 4 g/L: −0.027 ± 0.011, 6 g/L: −0.031 ± 0.012, 8 g/L: −0.050 ± 0.019, and 10 g/L: −0.060 ± 0.020) were significantly lower than that of the control ($p < 0.05$), and decreased with the increase in the concentration of the extracts, indicating that those extract concentrations had very strong inhibitory effects on the growth of the three microalgae (**Table 3**). The relative growth rate of *P. donghaiensis* cultured with 2 and 4 g/L extracts recovered after 24 h, and the growth of *P. donghaiensis* cultured with 6 g/L extracts decreased during culture. The growth of *S. costatum* cultured with 4 and 6 g/L extracts recovered after 24 h, and that of *H. akashiwo* cultured with 4, 6, 8, and 10 g/L recovered after 24 h (**Table 3**). *S. costatum* and *H. akashiwo* cultured with 2 g/L grew rapidly during culture. When cultured with 8 and 10 g/L of the extracts, a small number of living cells of *P. donghaiensis* was observed at 24 h, but no living cells were found at 48 h. Similarly, a small number of living cells of *S. costatum* was observed at 24 h, but no living cells were found at 96 h (**Figure 4**).

Effect on the Morphology of Microalgae

The hijiki extracts affected the morphology of *P. donghaiensis* and the growth of *S. costatum*. Normally, *P. donghaiensis* has fusiform cells. However, in this study, cells of *P. donghaiensis* cultured with seaweed extracts showed varying degrees of enlargement. The number of enlarged cells increased with increasing concentrations of hijiki extracts and duration of culture. By day 9 of culture with 6 g/L extracts, almost all algal cells had round or square shapes with enlarged nuclei, some cells grew exospores, and no dividing cells were observed. No living cells were found on day 10 of culture (**Figure 5**). Most of the *S. costatum* cells in the control grew into filaments and were distributed evenly in culture solution, while in the culture with hijiki extracts the cells gathered and grew in clusters that were difficult to disperse. Moreover, higher concentrations of hijiki extracts resulted in more clustering and lower cells survival. For example, at 96 h, living algal cells were still common in the culture with 4 g/L extracts, while they were sporadic in the treatment with 8 g/L extracts and not present in the 10 g/L extract treatment (**Figure 6**).

Effect on Chl*a* Content and Maximum Quantum Yield (*Fv/Fm*)

As the concentration of extracts increased, the Chl*a* content of *S. costatum* gradually decreased. At 12 h of starting the cultivation, there was no significant difference in algal Chl*a* content between the treatments with 2, 4, and 6 g/L extracts and the control ($p > 0.05$), while after 12 h, the algal Chl*a* contents were all significantly lower than that of the control ($p < 0.05$). In the culture with 8 and 10 g/L extracts, Chl*a* content dropped to 0 at 24 h (**Figure 7A**). Additionally, the *Fv/Fm* was significantly higher than that of the control ($p < 0.05$) at 4, 8, and 12 h, after which it gradually decreased relative to the control. At 24 h, the *Fv/Fm* decreased to 0 in the culture with 8 g/L extracts. At 48 h, the *Fv/Fm* in the culture with 10 g/L extracts decreased to 0. In the culture with 2, 4, and 6 g/L extracts, the *Fv/Fm* decreased first, and then gradually increased (**Figure 7B**), but was significantly lower than that of the control at all levels ($p < 0.05$). After 12 h, the *Fv/Fm* value was basically consistent with that of the Chl*a* content.

Effect of Hijiki Extracts on Enzyme Activity

Evaluation of the effects of 4 and 6 g/L extracts on the activity of oxidoreductase of *S. costatum* revealed significant effects on SOD, MDA, GSH-Px, GST, and GR relative to the control. Specifically, the activities of SOD, GR, and GSH-Px all increased, then decreased in response to extract treatment. Moreover, the *S. costatum* culture with 4 g/L extracts showed an increase in SOD activity within 12 h, but this difference was not significant. The activity of SOD was significantly reduced at 24 h ($p < 0.05$), then dropped to the lowest value at 48 h, which was only 33.3% of the control. At 168 h, the activity of SOD increased to about 50% of the control (**Figure 8A**). The hijiki extracts caused an initial increase in the activity of GR of *S. costatum*. At 4 h, the activity of GR in cultures treated with 4 and 6 g/L extracts was significantly higher than that of the control ($p < 0.05$), after which it decreased. At 12 h, the activity of GR in samples treated with 6 g/L extracts was significantly lower than that of the control ($p < 0.05$). At 24 h, the activity of GR in cultures treated with 4 g/L extracts was significantly lower than that of the control ($p < 0.05$) (**Figure 8B**). Cultures treated with 4 and 6 g/L extracts showed significant increases in the activity of GSH-Px at 4 and 8 h compared with that of the control ($p < 0.05$), while they decreased to the same level of the control ($p < 0.05$) at 12 h, and were significantly lower than that of the control at 24 h ($p < 0.05$) (**Figure 8C**). The contents of MDA and GST were lower than that of the control in cultures treated with hijiki extracts. At 4 h, the contents of MDA in the cultures treated with 4 and 6 g/L extracts were significantly lower than that of the control ($p < 0.05$) (**Figure 8D**). The activity of GST in the culture treated with 4 and 6 g/L extracts was also significantly lower than that of the control ($p < 0.05$) (**Figure 8E**).

DISCUSSION

Effect of Hijiki Extracts on the Growth of Red Tide Miroalgae

The hijiki extracts used in the experiment were autoclaved to eliminate the influence of microbes on the growth of microalgae. The IC_{50} of the extracts on growth of the red tide microalgae with both normal and red tide density showed an order of *P. donghaiensis* > *S. costatum* > *H. akashiwo*, indicating that the inhibitory effects of the extracts on the red tide microalgae varied with species and growing densities of the microalgae. Hijiki extracts not only inhibited the growth and proliferation of the microalgae, but also their morphology and dispersion.

TABLE 3 | The relative growth rate of high density microalgae under the influence of different high concentrations of extracts (μ) (h^{-1}).

Species	Extracts concentration (g/L)	μ0–24 h	μ24–48 h	μ48–72 h	μ72–96 h	μ96–120 h	μ120–144 h	μ144–16 h
P. donghaiense	0	0.002 ± 0.001	0.006 ± 0.002	0.016 ± 0.005	0.018 ± 0.009	0.013 ± 0.006	0.010 ± 0.005	0.005 ± 0.002
	2	−0.014 ± 0.006*	0.005 ± 0.002	0.024 ± 0.021	0.007 ± 0.005*	0.004 ± 0.003*	0.028 ± 0.014	0.001 ± 0.002*
	4	−0.043 ± 0.020*	0.021 ± 0.007*	0.001 ± 0.001*	0.029 ± 0.020*	−0.004 ± 0.004*	0.002 ± 0.002	−0.006 ± 0.004*
	6	−0.067 ± 0.033*	−0.084 ± 0.033*	0.023 ± 0.016	−0.023 ± 0.001*	0.063 ± 0.049*	−0.014 ± 0.007	−0.015 ± 0.010*
	8	−0.078 ± 0.035*	/	/	/	/	/	/
	10	−0.128 ± 0.086*	/	/	/	/	/	/
S. costatum	0	0.023 ± 0.008*	0.019 ± 0.008	0.019 ± 0.006	0.014 ± 0.004	0.002 ± 0.003	0.008 ± 0.007	0.011 ± 0.008
	2	0.015 ± 0.009*	0.006 ± 0.002*	0.018 ± 0.013	0.023 ± 0.009*	0.008 ± 0.006*	0.009 ± 0.006	0.004 ± 0.003*
	4	−0.061 ± 0.023*	0.013 ± 0.006*	0.028 ± 0.020	0.028 ± 0.012*	0.022 ± 0.009*	0.012 ± 0.008	0.007 ± 0.002*
	6	−0.081 ± 0.025*	0.013 ± 0.005*	0.004 ± 0.003*	0.024 ± 0.020*	0.014 ± 0.005*	0.010 ± 0.007	−0.014 ± 0.013*
	8	−0.090 ± 0.039*	−0.046 ± 0.024*	−0.026 ± 0.022*	−0.058 ± 0.039*	/	/	/
	10	−0.153 ± 0.061*	−0.033 ± 0.012*	/	/	/	/	/
H. akashiwo	0	0.013 ± 0.005*	0.010 ± 0.004	0.012 ± 0.005	0.016 ± 0.008	0.000 ± 0.005	0.005 ± 0.006	0.007 ± 0.004
	2	0.009 ± 0.004*	0.009 ± 0.003	0.003 ± 0.002*	0.015 ± 0.012	0.004 ± 0.003*	0.013 ± 0.002*	0.006 ± 0.005
	4	−0.027 ± 0.011*	0.023 ± 0.011*	0.005 ± 0.003*	0.009 ± 0.007*	0.000 ± 0.004	0.007 ± 0.003	−0.003 ± 0.004*
	6	−0.031 ± 0.012*	0.024 ± 0.010*	−0.004 ± 0.004*	0.011 ± 0.006*	0.005 ± 0.002*	0.002 ± 0.003*	−0.005 ± 0.006*
	8	−0.050 ± 0.019*	0.025 ± 0.0168	0.002 ± 0.002*	0.010 ± 0.009*	0.004 ± 0.003*	0.004 ± 0.002	−0.005 ± 0.004*
	10	−0.060 ± 0.020*	0.017 ± 0.0088	0.001 ± 0.003*	0.014 ± 0.008	0.001 ± 0.001	−0.005 ± 0.002*	−0.004 ± 0.005*

*"/" indicates the cell density was zero, so the relative growth rate could not be calculated. *Compared with the control, there was significant difference ($p < 0.05$).*

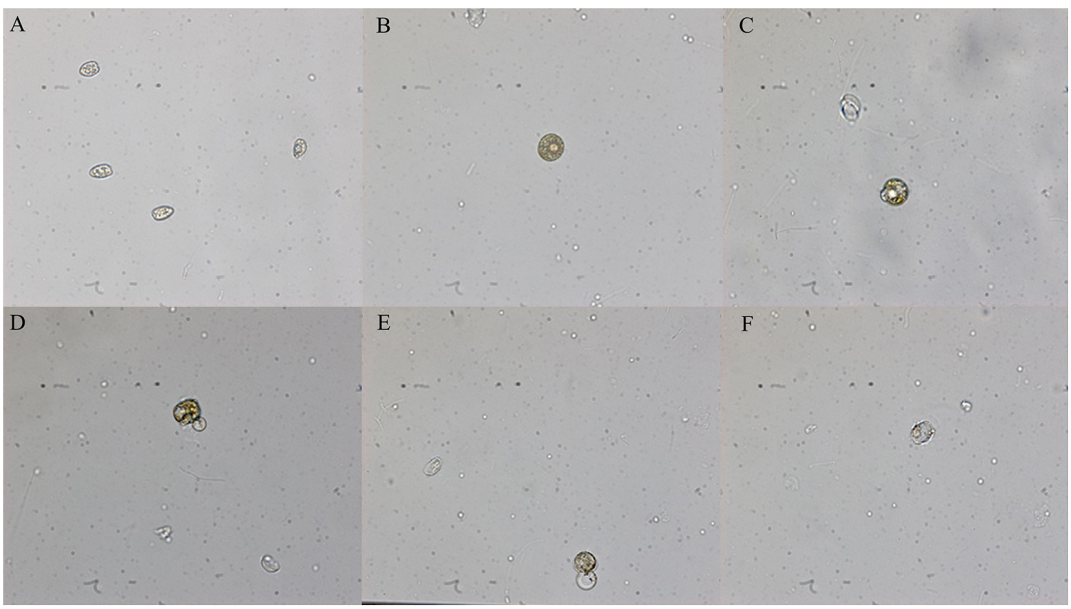

FIGURE 5 | Morphological changes of *Prorocentrum donghaiensis* caused by hijiki extract (40× objective lens). **(A)** Normal cells; **(B)** round cells; **(C)** small exospores; **(D)** medium exospores; **(E)** large exospores; **(F)** dead cells.

Effect of Hijiki Extracts on Chl*a* Content and *Fv/Fm* of *S. costatum*

In this study, hijiki extracts had a significant effect on the Chl*a* content and *Fv/Fm* of *S. costatum*. Although the addition of hijiki extracts reduced the pH value of algae cultures, they were all within the pH range suitable for microalgae growth (Hansen, 2002). Therefore, the inhibitory substances in the extracts are presumably secondary metabolites that have allelopathic effects. The allelochemicals reduced Chl*a* content and damaged the photosynthetic system II (PSII), which prevented the plant from obtaining energy through photosynthesis, ultimately leading to reduced cell proliferation

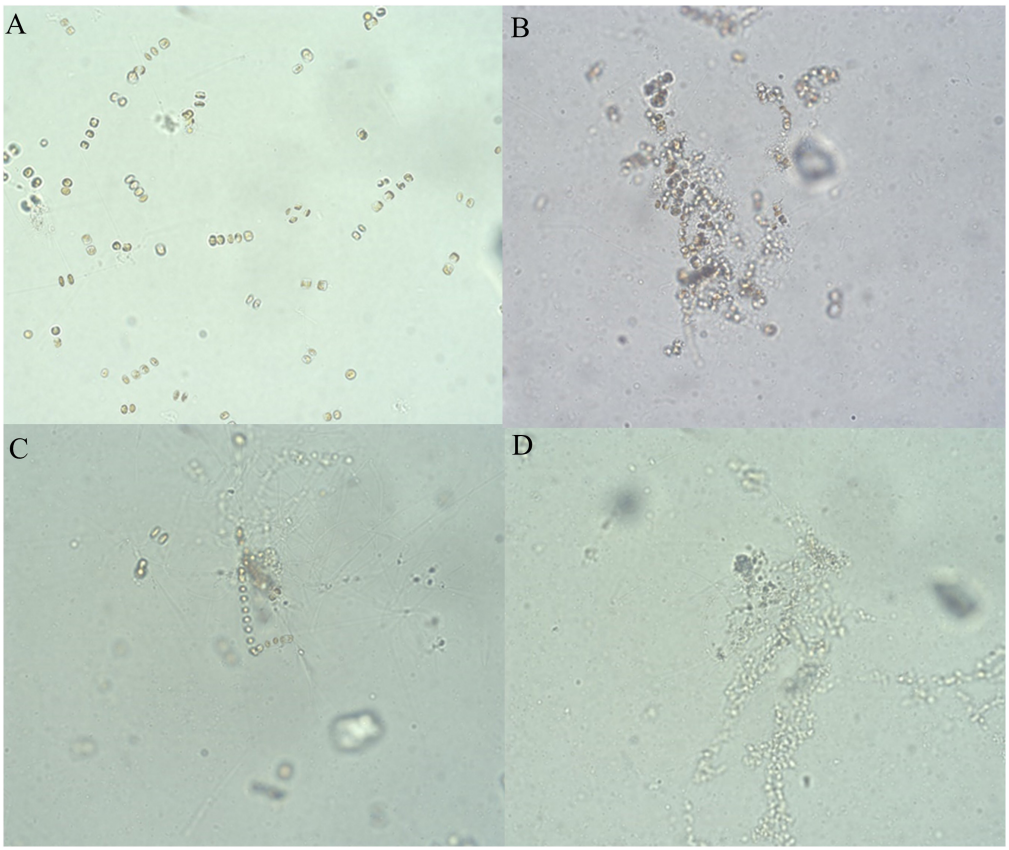

FIGURE 6 | Growth of *Skeletonema costatum* cultured at different concentrations of hijiki extracts for 96 h (20× objective lens). **(A)** Control; **(B)** extract concentration of 4 g/L; **(C)** extract concentration of 8 g/L; **(D)** extract concentration of 10 g/L.

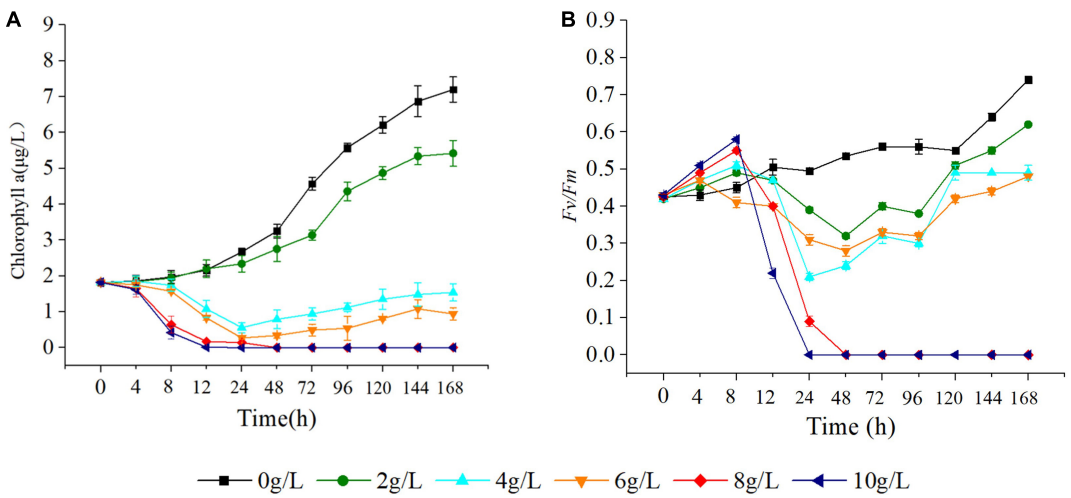

FIGURE 7 | Effect of hijiki extract on chlorophyll *a* content **(A)** and maximum quantum yield **(B)** of *Skeletonema costatum*.

rate and inhibited growth (Gross, 2003). Moreover, the effects of allelochemicals on the photosynthesis of terrestrial plants, freshwater algae, and seaweeds were reflected by reduced Chl*a* contents and *Fv/Fm* values (Körner and Nicklisch, 2002; Sukenik et al., 2002; Śliwińska-Wilczewska et al., 2017; Xu et al., 2019; Zhao et al., 2019). *Eucalyptus* leaf extracts significantly reduced the *Fv/Fm* of *Microcystis aeruginosa* on the third day of treatment (Zhao et al., 2019). Also, allelochemicals of

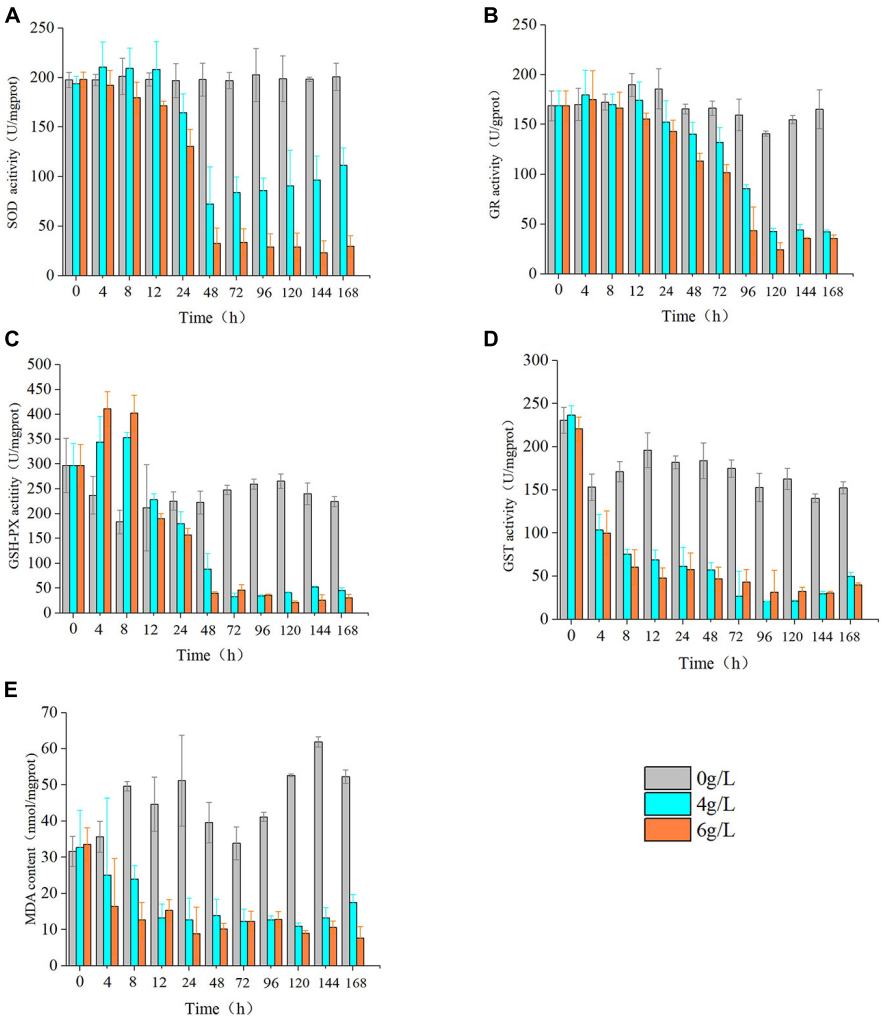

FIGURE 8 | Effect of hijiki extract on the activity of enzymes. **(A)** SOD, **(B)** GR, **(C)** GSH, **(D)** GST, and non-enzymatic antioxidants **(E)** MDA.

picocyanobacterium *Synechococcus* sp. significantly reduced the Chl*a* and *Fv/Fm* of *Phormidium* sp. in 3 days (Śliwińska-Wilczewska et al., 2017). Additionally, exudates of *Myriophyllum spicatum* were able to inhibit the PSII of cyanobacteria, green algae, and diatoms (Körner and Nicklisch, 2002). Moreover, myristic acid ($C_{14}H_{28}O_2$), acrylic acid ($C_3H_4O_2$), and linolenic acid ($C_{18}H_30_2$) isolated from *Enteromorpha prolifera* caused a reduction of Chl*a* content in *S. costatum* and *H. akashiwo* (An et al., 2008). In a recent study, *Cylcellrotheca closterium* extracts reduced the Chl*a* content and *Fv/Fm* of *P. donghaiensis* (Xu et al., 2019).

Chlorophyll *a* is essential for photosynthesis of algal cells. Results from the present study showed that hijiki extracts seriously damaged the photosynthetic system, caused a reduction of Chl*a* content, and inhibited the growth of *S. costatum*, indicating that the allelochemicals of hijiki could directly affect the photosynthetic system.

As a natural probe for photosynthetic energy conversion, *Fv/Fm* contains rich information about photosynthesis and is widely used to analyze the effects of stress on plant photosynthesis (Baker, 2004). *Fv/Fm* denotes the maximum quantum yield of PSII and can be used to indicate the integrity of PSII. When the value of *Fv/Fm* is greater than 0.44, PSII activity decreases with decreasing values of *Fv/Fm*. If the *Fv/Fm* value is less than 0.44, the reaction center is inactivated or destroyed (Schansker and Jack, 1999). In our study, cultures grown with 8 g/L extracts for 24 h or 10 g/L extracts for 48 h caused the *Fv/Fm* of *S. costatum* to decrease to 0 (**Figure 4**). This implied that PSII was damaged, which prevented photosynthesis from proceeding, thereby inhibiting the growth and proliferation of cells or causing the cells to die. The Fv/Fm of the alga cultured with 4, 8, and 10 g/L extracts showed a trend that was initially decreasing and then increasing, which implied that PSII might have a negative feedback regulation that repaired and restored the photosynthetic system. Therefore, it would be useful to determine the effectiveness and effective duration of red tide controlling measures by using a chlorophyll fluorometer to quickly measure the Chl*a* content and *Fv/Fm* value of algae.

Effect of Hijiki Extracts on Oxidoreductase Activity

During culture with hijiki extracts, the contents of SOD, GR, and GSH-Px in microalgae all showed a trend of initial increasing and then decreasing, which indicated that the stress exerted by low concentrations of extracts increased ROS level in the algal cells, while the antioxidant enzymes were unable to eliminate the excessive oxidation products that in turn damaged the enzyme system. The content of GST and MDA decreased throughout the culture, indicating that the algal cells were damaged to a great degree. Therefore, the hijiki extracts had the dual characteristics of enhancing and inhibiting the activity of enzymes. Hijiki extracts damaged the activity of oxidoreductase in the cells of *S. costatum* to varying degrees, which led to a failed removal of ROS over time. The accumulated ROS led to lipid peroxidation, which might have destroyed the cell structure and caused damage or death of algal cells. The performance of oxidoreductase in our study was basically consistent with that reported in terrestrial plants under stress conditions (Gill and Tuteja, 2010). Under abiotic stresses such as salt, drought, water, light, and heavy metal stresses, SOD, GSH-PX, GST, and GR activity of many terrestrial plants increases significantly, and MDA content significantly decreases, to effectively reduce oxidative stress and lipid peroxidation damage (Gill and Tuteja, 2010; Xu et al., 2013; Yousefzadeh-Najafabadi and Ehsanzadeh, 2017; Cengiz et al., 2019).

CONCLUSION

Large-scale cultivation of seaweed can provide potential solutions to global marine environmental problems such as ocean acidification, hypoxia, eutrophication, and harmful algal blooms (Yang et al., 2021). This study was conducted under controlled conditions in the laboratory, and the effects of environmental factors such as temperature and light on the experimental results were excluded. The effects of hijiki extracts on the growth, Chl*a* content, maximum quantum yield, activity of antioxidant enzymes (SOD, GSH-Px, GST, and GR), and content of MDA of red tide microalgae were analyzed. The results showed that the extracts of hijiki dry powder contains substances that have inhibitory effects on the three species of microalgae, and the inhibitory effect increases with the concentration of the extracts. The inhibitory substances could directly affect the photosynthetic system and oxidoreductase system of *S. costatum*, inhibiting the growth of the red tide microalgae. Overall, this research shows a new prospect for the utilization of hijiki on the red tide control, and marine environmental protection.

DATA AVAILABILITY STATEMENT

The raw data supporting the conclusions of this article will be made available by the authors, without undue reservation, to any qualified researcher.

AUTHOR CONTRIBUTIONS

YZ and NX designed the research and wrote the manuscript. YZ performed the research. All authors read and approved the final version of the manuscript.

FUNDING

This work was supported by the Natural Science Foundation of Zhejiang Province (LGF19D060002 and LZ17D060001) and the National Key R&D Program of China (2018YFD0900702).

REFERENCES

Ahn, O., Petrell, R. J., and Harrison, P. J. (1998). Ammonium and nitrate uptake by *Laminaria saccharina* and *Nereocystis leuetkeana* originating from a salmon seacage farm. *J. Appl. Phycol.* 10, 333–340. doi: 10.1023/A:1008092521651

An, Z., Wang, Z. Y., Li, F. M., Tian, Z. J., and Hu, H. Y. (2008). Allelopathic inhibition on red tide microalgae *Skeletonema costatum* by five macroalgal extracts. *Front. Env. Sci. Eng.* 2:297–305. doi: 10.1007/s11783-008-0055-3

Baker, R. (2004). Applications of chlorophyll fluorescence can improve crop production strategies: an examination of future possibilities. *J. Exp. Bot.* 55, 1607–1621. doi: 10.1093/jxb/erz535

Berdalet, E., Kudela, R., Urban, E., Enevoldsen, H., Banas, N. S., Bresnan, E., et al. (2017). Global HAB: a new program to promote international research, observations, and modeling of harmful algal blooms in aquatic systems. *Oceanography* 30, 70–81. doi: 10.5670/oceanog.2017.111

Cengiz, K., Nudrat, A. A., Abdulkadir, S., and Muhammad, A. (2019). Alleviating effect of nitric oxide on oxidative stress and antioxidant defence system in pepper (*Capsicum annuum* L.) plants exposed to cadmium and lead toxicity applied separately or in combination. *Sci. Hortic.* 255, 52–60. doi: 10.1016/j.scienta.2019.05.029

Daguer, H., Hoff, R. B., Molognoni, L., Kleemann, C. R., and Felizardo, L. V. (2018). Outbreaks, toxicology, and analytical methods of marine toxins in seafood. *Curr. Opin. Food Sci.* 24, 43–55. doi: 10.1016/j.cofs.2018.10.006

Davide, I., Alicia, G., Ismael, M., José, M., and Rossella, P. (2016). Outdoor production of *Tisochrysis lutea* in pilot-scale tubular photobioreactors. *J. Appl .Phycol.* 28, 3159–3166. doi: 10.1007/s10811-016-0856-x

Della, G., Antonio, F., and Isidori, M. (2000). Antialgal ent-labdane diterpenes from *Ruppia maritime*. *Phytochemistry* 55, 909–913. doi: 10.1016/S0031-9422(00)00253-3

Gill, S. S., and Tuteja, N. (2010). Reactive oxygen species and antioxidant machinery in abiotic stress tolerance in crop plant. *Plant Physiol. Bioch.* 48, 909–930. doi: 10.1016/j.plaphy.2010.08.016

Gross, E. M. (2003). Allelopathy of aquatic autotrophs. *Crit. Rev. Plant Sci.* 22, 3–4. doi: 10.1080/713610859

Guan, W. C., and Li, L. (2017). Atomic ratio of N to P influences the impact of UV irradiance on photosynthesis and growth in a marine dinoflagellate, *Alexandriu tamarense*. *Photosynthetica* 55, 501–509. doi: 10.1007/s11099-016-0670-3

Han, X. R., Gao, S., Hou, J. N., Li, H. M., and Shi, X. Y. (2013). Allelopathic effects of extracts from Ulva prolifera powders on the growth of *Prorocentrum donghaiense* and *Skeletonema costatum*. *Acta Ecol. Sin.* 33, 7417–7429. doi: 10.1351/PAC-REP-10-07-02

Hansen, P. J. (2002). Effect of high pH on the growth and survival of marine phytoplankton: implications for species succession. *Aquat. Microbial. Ecol.* 28, 279–288.

Hejl, A. M., and Koster, K. L. (2004). Juglone disrupts root plasma membrane H+-ATPase activity and impairs water uptake, root respiration, and growth

in soybean (*Glycine max*) and corn (*Zea mays*). *J. Chem. Ecol.* 30, 453–471. doi: 10.1023/B:JOEC.0000017988.20530.d5

Hu, P., Li, Z. X., Chen, M. C., Sun, Z. L., Ling, Y., Jiang, J., et al. (2016). Structural elucidation and protective role of a polysaccharide from *Sargassum fusiforme* on ameliorating learning and memorydeficiencies in mice. *Carbohyd. Polym.* 139, 150–158. doi: 10.1016/j.carbpol.2015.12.019

Jeffrey, S. W., and Humphrey, G. F. (1975). New spectrophotometric equations for determining chlorophylls *a*, *b*, c_1 and c_2 in higher plants, algae and natural phytoplankton. *Biochem. Physiol. Pflanz.* 167, 191–194. doi: 10.1016/S0015-3796(17)30778-3

Jeong, J. H., Jin, H. J., Sohn, C. H., Suh, K. H., and Hong, Y. K. (2000). Algicidal activity of the seaweed *Corallina pilulifera* against red tide. *J. Appl. Phycol.* 12, 37–43. doi: 10.1023/A:1008139129057

Jiang, B., Li, H., Teng, G., Yan, J., Li, B. X., Li, J. B., et al. (2017). Using GOCI extracting information of red tide for time-series analysing in East China Sea. *J. Zhejiang Univ. SC A* 44, 576–583. doi: 10.3785/j.issn.1008-9497.2017.05.013

Körner, S., and Nicklisch, A. (2002). Allelopathic growth inhibition of selected phytoplankton species by submerged macrophytes. *J. Phycol.* 32, 862–871. doi: 10.1046/j.1529-8817.2002.t01-1-02001.x

León-Muñoz, J., Urbina, M. A., Garreaud, R., and Iriarte, J. L. (2018). Hydroclimatic conditions trigger record harmful algal bloom in western Patagonia (summer 2016). *Sci. Rep.* 8:1330. doi: 10.1038/s41598-018-19461-4

Liu, H. M., Xie, H. M., and Gong, Y. M. (2011). Secondary metabolites from the seaweed Gracilaria lemaneiformis and their allelopathic effects on *Skeletonema costatum*. *Biochem. Syst. Ecol.* 39, 397–400.

Liu, L., Zhou, J., Zheng, B. H., Cai, W. Q., Lin, K. X., and Tang, J. L. (2013). Temporal and spatial distribution of red tide outbreaks in the Yangtze River Estuary and adjacent waters. *China. Mar. Pollut. Bull.* 72, 213–221. doi: 10.1016/j.marpolbul.2013.04.002

Lu, H. M., Xie, H. H., Gong, Y. X., Wang, Q., and Yang, Y. F. (2011). Secondary metabolites from the seaweed *Gracilaria lemaneiformis* and their allelopathic effects on *Skeletonema costatum*. *Biochem. Sys. Eco.* 39, 397–400. doi: 10.1016/j.bse.2011.05.015

Ma, Z., Wu, M., and Lin, L. (2017). Allelopathic interactions between the macroalga *Hizikia fusiformis*(Harvey) and the harmful blooms-forming dinoflagellate *Karenia mikimotoi*. *Harmful Algae* 65, 19–26. doi: 10.1016/j.hal.2017.04.003

Mascareño, A., Cordero, R., Azócar, G., Billi, M., Henríquez, P. A., and Ruz, G. A. (2018). Controversies in social-ecological systems: lessons from a major red tide crisis on Chiloe Island, Chile. *Ecol. Soc.* 23:15. doi: 10.5751/ES-10300-230415

McCabe, R. M., Barbara, M., Hickey, Raphae, M., Kudela Kathi, A., et al. (2016). An unprecedented coastwide toxic algal bloom linked to anomalous ocean conditions. *Geophys. Res. Lett.* 43, 10366–10376. doi: 10.1002/2016GL070023

Nakai, S., Inoue, Y., Hosomi, M., and Murakami, A. (1999). Growth inhibition of blue-green algae by allelopathic effects of macrophytes. *Water Sci. Technol* 39, 47–53. doi: 10.1016/S0273-1223(99)00185-7

Schansker, G., and Jack, J. S. (1999). Performance of active photosystemII centers in photoinhibited pea leaves. *Photosynthesis Res.* 62, 175–184. doi: 10.1023/A:1006374707722

Śliwińska-Wilczewska, S., Maculewicz, J., Felpeto, A. B., Vasconcelos, V., and Latala, A. (2017). Allelopathic activity of picocyanobacterium *Synechococcus* sp. on filamentous cyanobacteria. *J. Exp. Ma. Bio. Ecol* 496, 16–21. doi: 10.1016/j.jembe.2017.07.008

Soto, I. M., Cambazoglu. M. K., and Boyette, A. D. (2018). Advection of *Karenia brevis* blooms from the Florida panhandle towards Mississippi coastal waters. *Harmful Algae* 72, 46–64. doi: 10.1016/j.hal.2017.12.008

Sukenik, A., Eskhol, R., Livne, A., Ora, H., Meir, M., Dani, T., et al. (2002). Inhibition of growth and photosynthesis of the dinoflagellate *Peridinium gatunense* by *Microcystis* sp. (cyanobacteria): a novel allelopathic mechanism. *Limnol. Oceanogr.* 47, 1656–1663. doi: 10.4319/lo.2002.47.6.1656

Sun, Y., Chen, X., Zhang, L., Liu, H., and Li, P. C. (2019). The antiviral property of *Sargassum fusiforme* polysaccharide for avian leukosis virus subgroup in vitro and in vivo. *Int. J. Biol. Macromol.* 138, 70–78. doi: 10.1016/j.ijbiomac.2019.07.073

Tang, Y., and Gobler, C. (2011). The green macroalga, Ulva lactuca, inhibits the growth of seven common harmful algal bloom species via allelopathy. *Harmful Algae* 10, 480–488. doi: 10.1016/j.hal.2011.03.003

Van Dolah, F. M. (2000). Marine algal toxins: origins, health effects, and their increased occurrence. *Environ. Health Persp.* 108 Suppl, 133–141. doi: 10.2307/3454638

Xu, R., Yamada, M., and Fujiyama, H. (2013). Lipid peroxidation and antioxidative enzymes of two turfgrass species under salinity stress. *Pedosphere* 23, 213–222. doi: 10.1016/S1002-0160(13)60009-0

Xu, W. J., Wang, J. T., Tan, L. J., Guo, X., and Xue, Q. N. (2019). Variation in allelopathy of extracellular compounds produced by *Cylindrotheca closterium* against the harmful-algal-bloom dinoflagellate *Prorocentrum donghaiense*. *Mar. Environ. Res.* 148, 19–25. doi: 10.1016/j.marenvres.2019.05.005

Yang, Y., Luo, H., Wang, Q., He, Z., and Long, A. (2021). Large-scale cultivation of seaweed is effective approach to increase marine carbon sequestration and solve coastal environmental problems. *Chin. Acad. Sci.* 36, 1–11. doi: 10.16418/j.issn.1000-3045.20210217103

Yang, Y. F., Liu, Q., Chai, Z. Y., and Tang, Y. Z. (2015). Inhibition of marine coastal bloom-forming phytoplankton by commercially cultivated *Gracilaria lemaneiformis* (*Rhodophyta*). *J. Appl. Phycol.* 27, 2341–2352. doi: 10.1007/s10811-014-0486-0

Yousefzadeh-Najafabadi, M., and Ehsanzadeh, P. (2017). Photosynthetic and antioxidative upregulation in drought-stressed sesame (*Sesamum indicum* L.) subjected to foliar applied salicylic acid. *Photosynthetica* 4, 611–622. doi: 10.1007/s11099-017-0673-8

Yu, Z. M., and Chen, N. S. (2019). Emerging trends in red tide and major research progresses. *Ocean. Limnol. Sin.* 50, 474–486. doi: 10.11693/hyhz20190200041

Zhang, R., Zhang, X. X., Tang, Y. X., and Mao, J. L. (2020). Composition, isolation, purification and biological activities of *Sargassum fusiforme* polysaccharides: A review. *Carbohyd. Polym.* 228:115381. doi: 10.1016/j.carbpol.2019.115381

Zhao, W., Zheng, Z., Zhang, J. L., Roger, S. F., and Luo, X. Z. (2019). Allelopathically inhibitory effects of eucalyptus extracts on the growth of *Microcystis aeruginosa*. *Chemosphere* 225, 424–433. doi: 10.1016/j.chemosphere.2019.03.070

Conflict of Interest: The authors declare that the research was conducted in the absence of any commercial or financial relationships that could be construed as a potential conflict of interest.

frontiers in Marine Science

ORIGINAL RESEARCH
published: 15 November 2021
doi: 10.3389/fmars.2021.736262

Early Warning of Harmful Algal Bloom Risk Using Satellite Ocean Color and Lagrangian Particle Trajectories

Junfang Lin, Peter I. Miller, Bror F. Jönsson and Michael Bedington*

Plymouth Marine Laboratory, Plymouth, United Kingdom

Combining Lagrangian trajectories and satellite observations provides a novel basis for monitoring changes in water properties with high temporal and spatial resolution. In this study, a prediction scheme was developed for synthesizing satellite observations and Lagrangian model data for better interpretation of harmful algal bloom (HAB) risk. The algorithm can not only predict variations in chlorophyll-a concentration but also changes in spectral properties of the water, which are important for discrimination of different algal species from satellite ocean color. The prediction scheme was applied to regions along the coast of England to verify its applicability. It was shown that the Lagrangian methodology can significantly improve the coverage of satellite products, and the unique animations are effective for interpretation of the development of HABs. A comparison between chlorophyll-a predictions and satellite observations further demonstrated the effectiveness of this approach: r^2 = 0.81 and a low mean absolute percentage error of 36.9%. Although uncertainties from modeling and the methodology affect the accuracy of predictions, this approach offers a powerful tool for monitoring the marine ecosystem and for supporting the aquaculture industry with improved early warning of potential HABs.

Keywords: early warning, harmful algal bloom, remote sensing, Lagrangian, particle tracking

OPEN ACCESS

Edited by:
Marcos Mateus,
University of Lisbon, Portugal

Reviewed by:
Nor Azman Kasan,
University of Malaysia Terengganu, Malaysia
Anabella Ferral,
Consejo Nacional de Investigaciones Científicas y Técnicas (CONICET), Argentina

****Correspondence:***
Junfang Lin
Junl@pml.ac.uk

Specialty section:
This article was submitted to Marine Fisheries, Aquaculture and Living Resources, a section of the journal Frontiers in Marine Science

Received: *05 July 2021*
Accepted: *14 October 2021*
Published: *15 November 2021*

Citation:
Lin J, Miller PI, Jönsson BF and Bedington M (2021) Early Warning of Harmful Algal Bloom Risk Using Satellite Ocean Color and Lagrangian Particle Trajectories. Front. Mar. Sci. 8:736262. doi: 10.3389/fmars.2021.736262

INTRODUCTION

Harmful algal blooms (HABs) occur in many coastal regions around the world and appear to be increasing in severity and extent (Hallegraeff, 1993, 2003; Grattan et al., 2016; Gobler, 2020). HABs have caused severe economic losses to aquaculture, fisheries, and tourism while creating major environmental and human health impacts (Anderson et al., 2000; Landsberg, 2002; Heisler et al., 2008). Toxic bloom-forming algae can cause wildlife mortality or human seafood poisoning, and even HAB species that do not produce toxins are able to cause harm through development of high biomass, leading to foams or scums, depletion of oxygen as blooms decay, or destruction of habitat for fish or shellfish by shading of submerged vegetation (Sellner et al., 2003). Such impacts from HABs pose a serious threat to aquatic ecosystems and can disrupt their associated food web (Fogg, 1969; Paerl, 1988). Therefore, considerable attention has been focused on methods to reduce the risks of HAB impacts (Sengco and Anderson, 2004; Anderson, 2009; Anderson et al., 2012).

Satellite ocean color sensors offer a means of detecting and monitoring HABs in the ocean and coastal zone. The potential value of remote sensing for HABs was first described by Mueller (1981), after an experimental ocean color sensor attached to an aircraft detected a bloom of *Karenia brevis*. As the instrument was developed to simulate the Coastal Zone Color Scanner (CZCS), launched

in late 1978, this indicated the capability for satellite detection of blooms. Various approaches were further developed for detection and monitoring of HABs from satellite remote sensing (reviewed by Klemas, 2012; Blondeau-Patissier et al., 2014).

There are many advantages of satellite ocean color products compared to *in situ* monitoring: wide temporal and spatial coverage, and inexpensive; however, there are significant limitations. First, the coarse spectral resolution of current ocean color satellites is only sufficient to distinguish certain clear anomalies in bloom coloring, as the visible spectrum is mostly determined by optical properties of varying concentration of chlorophyll pigments. Second, data from satellite ocean color only reflect the state of the waters at the moment the measurements are taken, whereas the blooms are subject to physical forcing from tidal and wind-driven currents which will advect them away from this state. It is thus very challenging from satellite data alone to provide information regarding the future development and movement of HABs. Another limitation of ocean color remote sensing is that satellite observations are often hampered by weather conditions, such as clouds and sea fog, which can substantially reduce the number of valid ocean color pixels. As a result, satellite imagery may only partially capture features of HABs.

In recent years, the use of Lagrangian particle tracing (or other numerical models) for HAB monitoring has gained more interest (Olascoaga et al., 2008; Wynne et al., 2011; Son et al., 2015; Kwon et al., 2019; Li et al., 2020; Fernandes-Salvador et al., 2021). Lagrangian particle tracing models are useful for determining sources, trajectories, and destinations of drifting water parcels, with high temporal and spatial resolution. Thus, this approach could compensate for some of the limitations of satellite ocean color. However, this approach has so far been used to track particle locations along limited trajectories, preventing a synoptic view of the variability of water properties associated with HABs, e.g., algal concentration. Recently, a new methodology was proposed for synthesizing ocean color data (or *in situ* observations) with ocean circulation velocity fields from an operational model (Jönsson et al., 2009; Jönsson and Salisbury, 2016). This method could significantly improve our capability for monitoring of HABs.

Therefore, this paper aims to expand the Jönsson et al. (2009) scheme for synthesizing satellite observations and Lagrangian data to include extrapolation for better interpretation of the development of HABs. This improved scheme can not only fill gaps in HAB patches in the satellite images captured on cloudy days but also provides an early warning of harmful algal risk. An application example is presented showing the development of a *Karenia mikimotoi* bloom along the southern coast of England.

METHODS AND DATA

Satellite Data

In this study, the prediction scheme is based on the algorithm of Jönsson and Salisbury (2016), which combines simulated velocity fields with ocean color observations to create prediction of biological production in spatial and temporal scales. We applied this prediction scheme to reprocessed Sentinel-3A OLCI Level-3 products, which were downloaded from Plymouth Marine Laboratory (PML) ocean color archive. These products include chlorophyll-a (Chl) and remote sensing reflectance (R_{rs}, sr^{-1}) at 400, 443, 490, 560, 620, 665, 681, 709, 885, and 1020 nm with a spatial resolution of 300 m (Tilstone et al., 2020). The region of interest covers coastal and offshore areas in the southeastern England including the Celtic Sea and English Channel. The satellite passes the study region at around 12:00 a.m. (local time). Two case studies will be presented, covering September 10–15, 2019 and June 29 to July 5, 2019.

Lagrangian Particle Model

The particle tracking model PyLAG (Uncles et al., 2019) is used to produce the Lagrangian trajectories. PyLAG uses a fourth order Runge–Kutta scheme to advect particles, numerically integrated over a 100 s timestep. PyLAG is forced using hourly output from a hydrodynamic model with the horizontal turbulence statistics from the same model used to parameterise the diffusion term as random displacements.

The hydrodynamic forcing is from an operational setup of the Finite Volume Community Ocean Model (FVCOM) (Chen et al., 2003). This solves the prognostic equations on an unstructured grid, allowing higher resolution around complex coastlines and bathymetry, and lower resolution in the open ocean. Horizontal mixing is parameterised through the Smagorinsky scheme (Smagorinsky, 1963) and vertical turbulent mixing is modeled with the General Ocean Turbulence Model (GOTM) using a $\kappa-\omega$ formulation (Umlauf and Burchard, 2005). Lateral boundary conditions for the model are taken from the CMEMS North West Shelf data product (AMM7) and surface forcing from a Weather Forecast and Research (WRF) model which downscales output from the NOAA GFS global forecast model to provide 6-hourly forcing at 1 km resolution over the hydrodynamic model domain. Output of temperature and precipitation from the WRF model is also used to drive a neural network model to provide forecast river flows.

Merging Satellite and Particle Tracking

The algorithm that merges satellite products and velocity fields using Lagrangian particle tracking is described in previous studies (Jönsson et al., 2009, 2011; Jönsson and Salisbury, 2016). Here we summarise the main steps as follows (flowchart shown in **Figure 1**). Satellite products are firstly remapped to a uniform grid with a spatial resolution of 300 m. Virtual particles are then seeded randomly in each grid and advected for 7–10 days at hourly intervals using PyLAG. Next, satellite data are attached to the particle trajectories for the first 5–7 days, where the time difference between ocean color measurements and particle trajectories is limited to 30 min. The attached values are set to missing if satellite data are unavailable. Any particles leaving the model domain are removed to avoid errors. Further, an extrapolation procedure is conducted to predict the values of the satellite data (e.g., Chl) associated with each particle for the remainder of the particle drift, 2–3 days. The extrapolation is similar to the interpolation procedure in Jönsson and Salisbury (2016), but expanded to employ a linear extrapolation to calculate

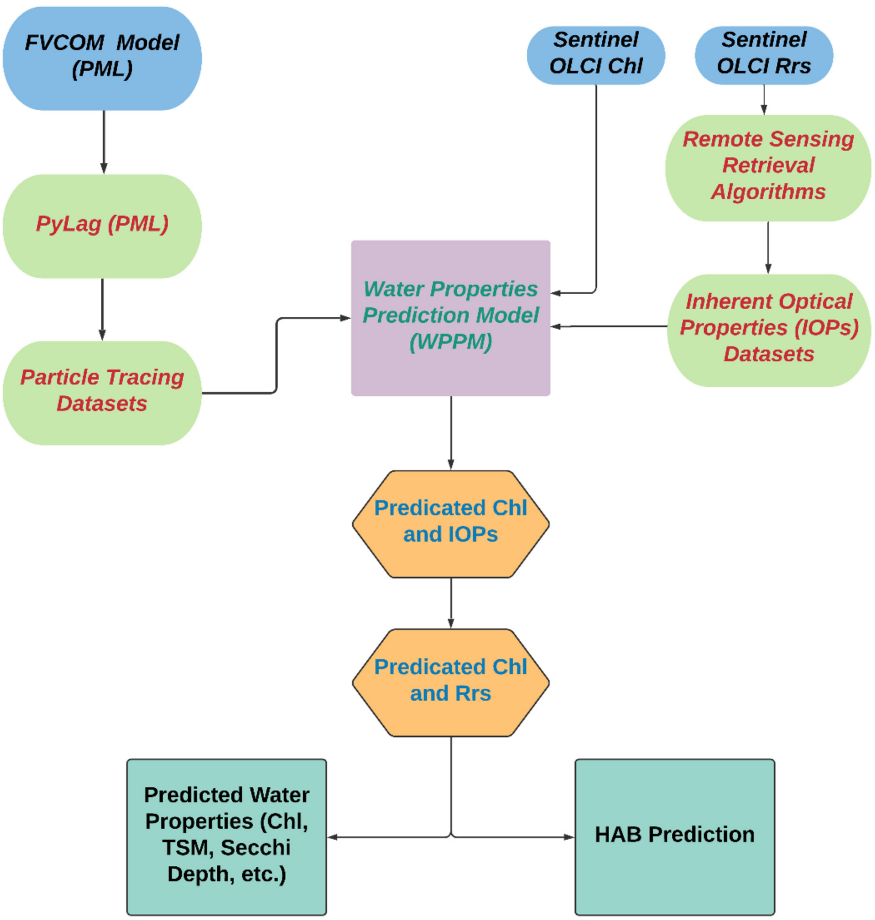

FIGURE 1 | Flowchart of ocean color prediction algorithm for water properties and early warning maps of HAB using Lagrangian particle trajectories and ocean color observations.

a prediction based on any two valid satellite matchups. Note that the extrapolation will be stopped if only one valid matchup is obtained. In most cases there can be more than two matchups, thus an average value of all these extrapolations ($\bar{v}$) is calculated using a weighting function of 1 divided by the days offset according to the following equation:

$$\bar{v} = \sum_{i=1}^{n} w_i v_i \quad (1)$$

$$w_i = \frac{1/d_i}{\sum_{i=1}^{n} 1/d_i} \quad (2)$$

where v_i is the extrapolation value of the ith pair, n is the number of extrapolations, and d is the days offset.

Prediction of Remote Sensing Reflectance

The optical spectra of water bodies provide useful information on its constituents. Hence, the above approach is revised for the capability to predict R_{rs}. It is worth noting that R_{rs} is an apparent optical property (AOP), which highly depends on the light distribution. It would be questionable if R_{rs} is estimated by linear weighting from extrapolations of all trajectories, as the light distribution for the particles along the trajectories could vary significantly. In this study, we propose a revised approach for prediction of R_{rs} based on inherent optical properties (IOPs), which solely depend on optically properties of constituents in the water but are not affected by the changes of light field. The details are described by following steps. In the first step, the quasi-analytical algorithm (QAA) is employed to retrieve IOPs: absorption (a) and backscattering (b_b) coefficients of water (Lee et al., 2002). Then a new set of IOPs is predicted from the retrieved a and b_b. Next, the predicted a and b_b are used to reconstruct R_{rs} with the following equation (Gordon et al., 1988).

$$r_{rs}(\lambda) = \left(g_0 + g_1 \cdot \frac{b_b(\lambda)}{a(\lambda) + b_b(\lambda)}\right) \frac{b_b(\lambda)}{a(\lambda) + b_b(\lambda)} \quad (3)$$

where $g_0 = 0.0949\ \mathrm{sr}^{-1}$, $g_1 = 0.0794\ \mathrm{sr}^{-1}$, and R_{rs} can be converted from r_{rs} with:

$$R_{rs}(\lambda) = \frac{0.52 \cdot r_{rs}(\lambda)}{1 - 1.7 \cdot r_{rs}(\lambda)} \quad (4)$$

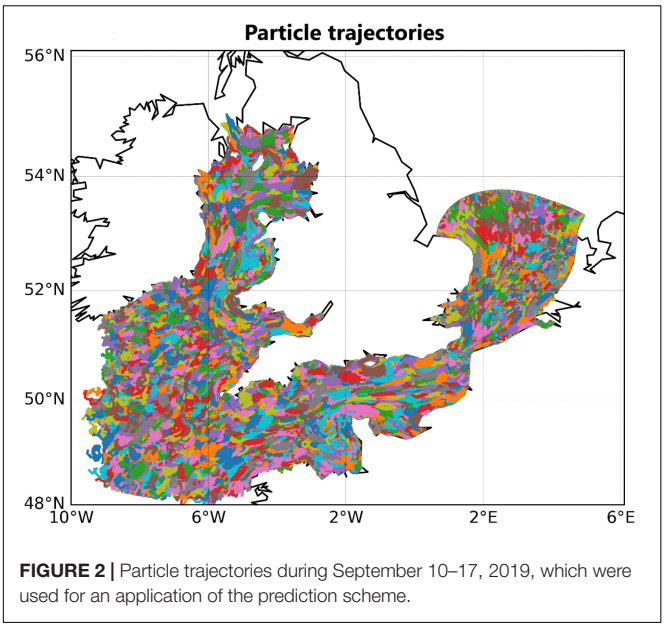

FIGURE 2 | Particle trajectories during September 10–17, 2019, which were used for an application of the prediction scheme.

Following these steps, we are thus provided with time-series images of Chl and R_{rs} at 30-min intervals for the domain. These predictions are important as they will be used by algorithms to determine a quantitative estimate of HAB risk: this will be the focus of a future study. However, here we use R_{rs} to predict the ocean color to enable visual forecasts of bloom development.

Animation of Map Sequences

To demonstrate water property changes over time frames, we combine individual images of Chl by interpolating intermediate timesteps for a smoother appearance using the Matplotlib Animation Python package.[1] To further diagnose more details on various water types, images were composited with red–green–blue (RGB) bands from $R_{rs}(560)$, $R_{rs}(490)$, and $R_{rs}(443)$, respectively, and animated in an analogous way. These wavelengths cover the blue–green section of the optical spectrum, within which most ocean color variability is exhibited; hence this provides an enhanced view of the ocean rather than the true color.

RESULTS

The applicability of this prediction scheme is demonstrated by analyzing the predictions of water properties in two applications in the coastal and offshore regions of southeastern England.

The Celtic Sea and English Channel

Six days of ocean color data were used for this case study (September 9–15, 2019). A total of ∼1 million particles were seeded randomly and advected at hourly intervals for 8 days from September 9 to 17, 2019, including 48 h of predictions following the satellite period, at the same spatial resolution as the ocean color data (300 m × 300 m). **Figure 2** shows a map of all modeled particle trajectories over the 8 days: the path of each particle is represented by a random colored line, which overlap each other

[1]https://imageio.github.io

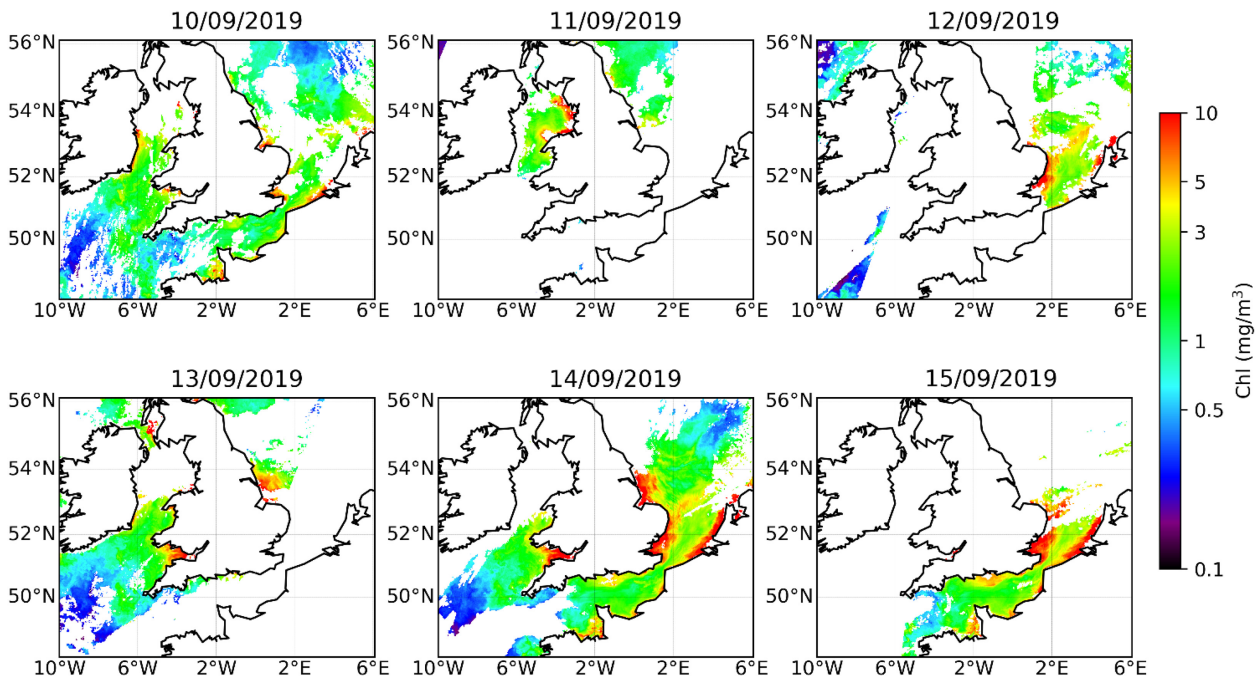

FIGURE 3 | Maps of chlorophyll-a concentration (Sentinel-3 OLCI Level-3 products) during the days with ocean color observations used for prediction of HABs (or other bio-optical parameters).

due to the high density of particles. **Figure 3** shows maps of Sentinel-3 OLCI Level-3 Chl, from which we can identify the variable availability of ocean color during the 6 days due to cloud cover and orbit trajectories. There are some missing pixels in the study region but for most regions there was coverage for at least 50% of the time, e.g., for the region of English Channel, there were 3 days of ocean color observations available (September 9, 10, and 15) out of the 6 days. It is worth mentioning that from these maps we can observe that some algal blooms occurred along the coastal regions of England with high Chl ($>\sim$4 mg/m^3).

Figure 4 presents the time series predictions of Chl that shows the advection of surface waters during the first of the 2-day forecast. The most dynamic feature in this sequence is the movement of an algal bloom along the south coast of England, highlighted within the fixed ellipse in **Figure 4**. The value of this approach can be fully appreciated by viewing the animation of the sequence of predicted Chl maps that accompanies the figure. Advection effects are stronger in regions of the eastern English Channel with significant Chl variabilities over time, consistent with stronger tides in this region. The coastal waters generally demonstrate sharper Chl gradients than open ocean water, which is expected when considering tide, river runoff, and other forces dominating the shelf. The time series and animation of the predicted enhanced ocean-color results is shown in **Figure 5**: the colors in the maps indicate different water types, e.g., yellow colors in river estuaries may indicate high concentration of

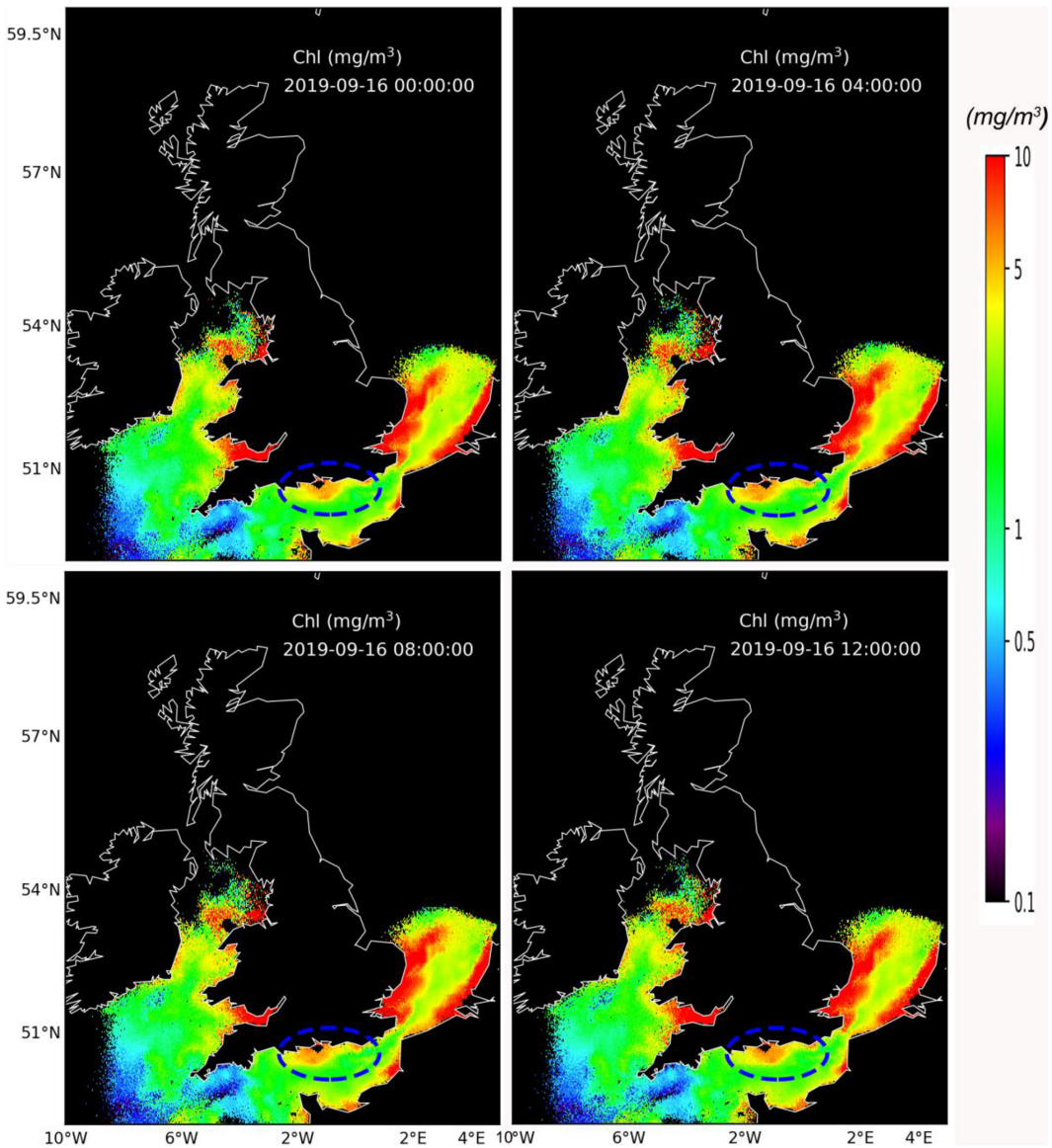

FIGURE 4 | Frames of predicted Chl distribution at 4-h intervals during the first forecast day (September 16, 2019). The dashed ellipse is in the same location in each frame, highlighting the movement of a bloom along the south coast of England. The animation of the complete 2-day forecast can be found *via* https://rsg.pml.ac.uk/shared_files/junl/paper_animation/example1/chl.gif.

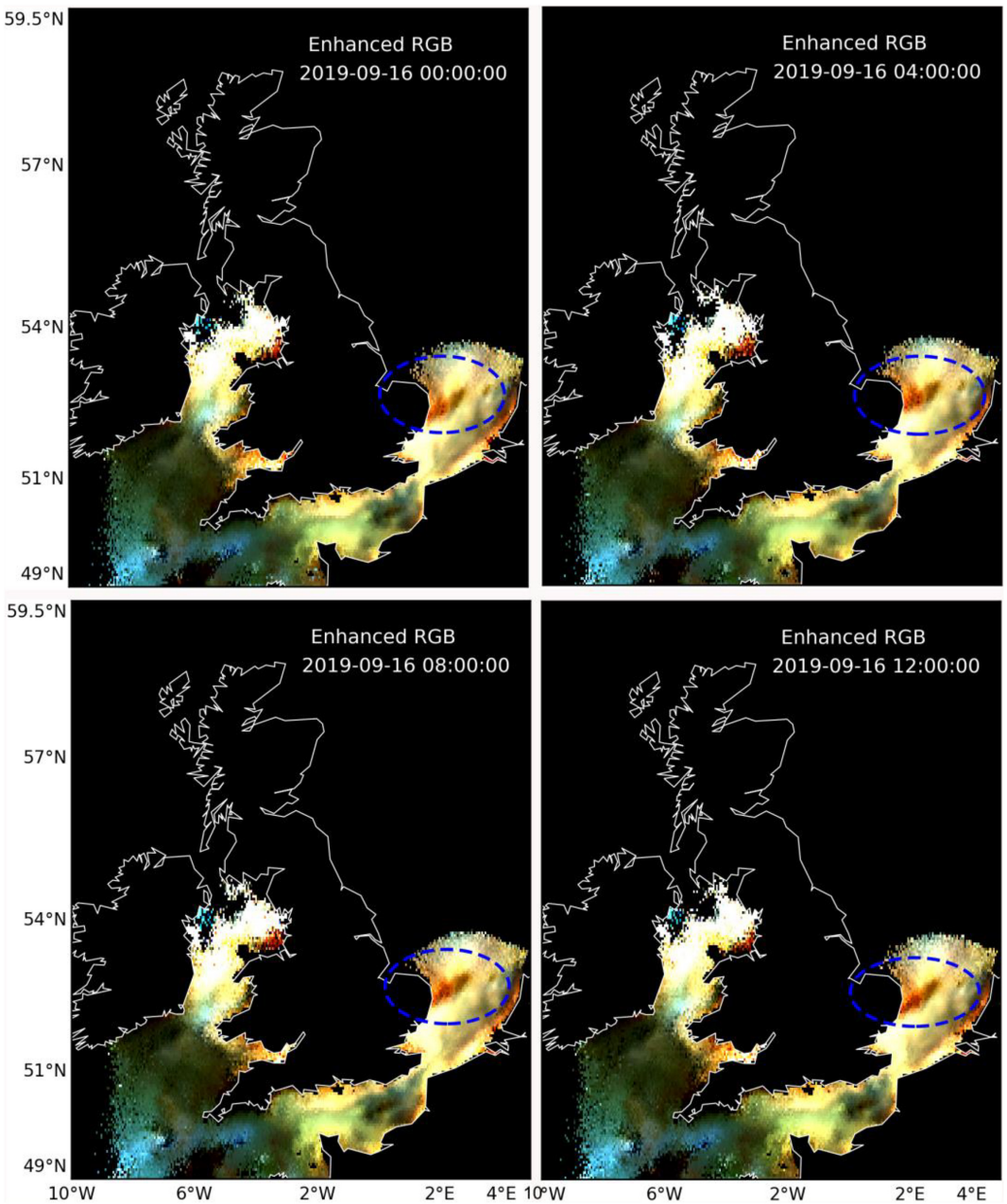

FIGURE 5 | Frames of predicted enhanced ocean-color RGB images indicating variabilities of water types (animation: https://rsg.pml.ac.uk/shared_files/junl/paper_animation/example1/rgb.gif).

sediments, and dark brown colors in the eastern English Channel could be due to a suspected *K. mikimotoi* bloom.

To further demonstrate the efficiency of the prediction approach, the conditions of water quality were also studied by plotting changes over time. Three transects were selected along latitudes 50° N, 51.3° N, and 52.5° N (**Figure 6**), covering possible bloom regions (e.g., estuaries, south-east England coasts). **Figure 7** shows the time series and animation of predicted Chl along the three transects. It was found that Chl varied over a wide range each day, usually with a periodic pattern mainly due to different stages of the tidal cycle that influence the advection of water parcels. In **Figure 7B**, the upward slope indicates a net westward advection of water along the transect.

An error estimation for the prediction algorithm was performed by comparing the predicted Chl on the second forecast day (September 17, 2019 12:00 p.m.) against the satellite-observed Chl scene that day (12:29 p.m.). The scatter plot of cloud-free pixels in the two datasets are shown in **Figure 8**. The predicted Chl agrees well with satellite Chl with an r^2 of 0.81 and a

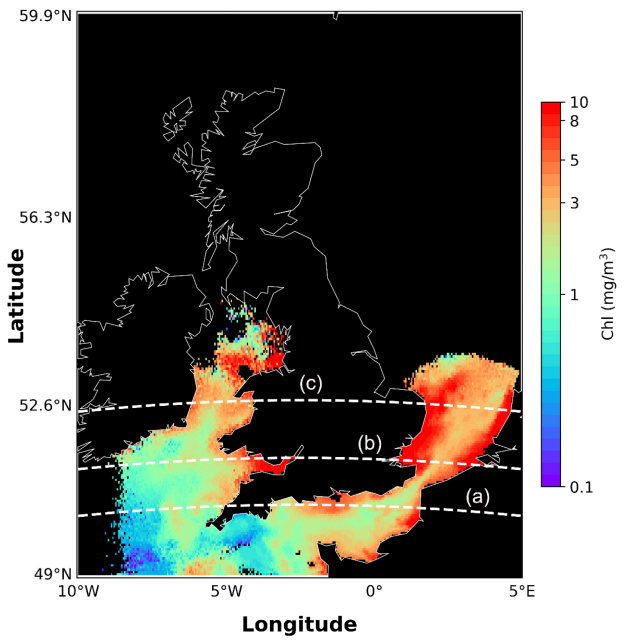

FIGURE 6 | Map showing the distribution of predicted Chl at 15th September 8 p.m. (first predicted image) overlaid with lines of latitudes at 50° N, 51.3° N, and 52.5° N.

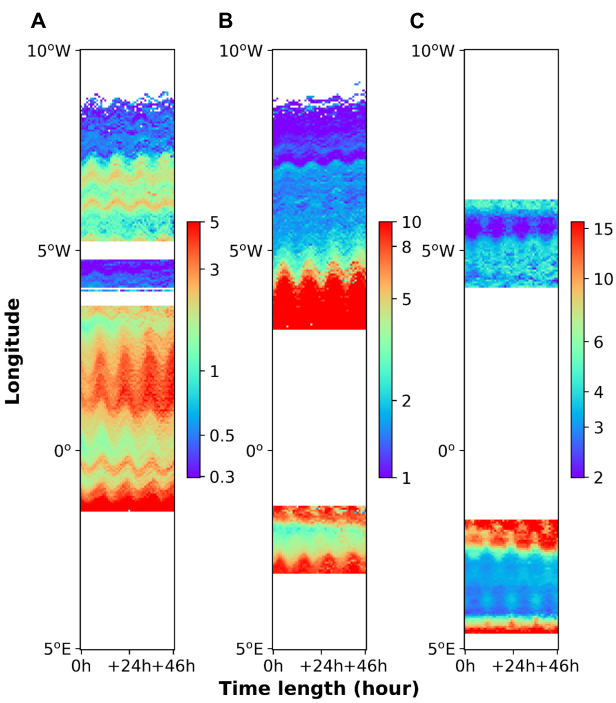

FIGURE 7 | Hovmöller plot showing time series of predicted Chl (mg/m^3) along zonal lines: **(A)** 50° N, **(B)** 51.3° N, and **(C)** 52.5° N.

mean absolute percentage error (MAPE) of 36.9%. The MAPE is defined by

$$MAPE = \frac{1}{n}\sum_{i=1}^{n}\left|\frac{x_p - x_s}{x_s}\right| \quad (5)$$

with x_p and x_s representing predicted and satellite values, respectively, n is the number of values. The results further demonstrate the robust performance of the prediction scheme for changes of water properties.

High Spatial Resolution in English Channel

Monitoring of water bodies at high spatial resolution is of paramount importance, especially in dynamic coastal waters, where the water constituents can vary dramatically over a small distance. To evaluate the ability of the prediction algorithm for high spatial resolution, a further period was studied in the English Channel, June 29 to July 5, 2019 when a large coccolithophore bloom was observed. In this case, many more particles were seeded (∼10 million particles). To demonstrate the techniques using computer time feasible for an operational monitoring system, the region of interest was limited to the English Channel and only 16 h of predictions were generated. The spatial resolution of the resulting prediction images is 100 m with a temporal resolution of 1 h. **Figure 9** shows and animates the changes of Chl distributions over time. Small scale structures are interpreted here (e.g., some fine structures of algae patches were revealed). To gain a precise understanding of water types, the enhanced ocean-color images with high spatial resolution are shown and animated in **Figure 10**. The (harmless) coccolithophorid bloom occurred in the northern English Channel, covering thousands of square kilometers with milky blue. The prediction method here successfully discriminated the locations of the bloom and its advection over time, further demonstrating the value of using this prediction method for monitoring algal blooms.

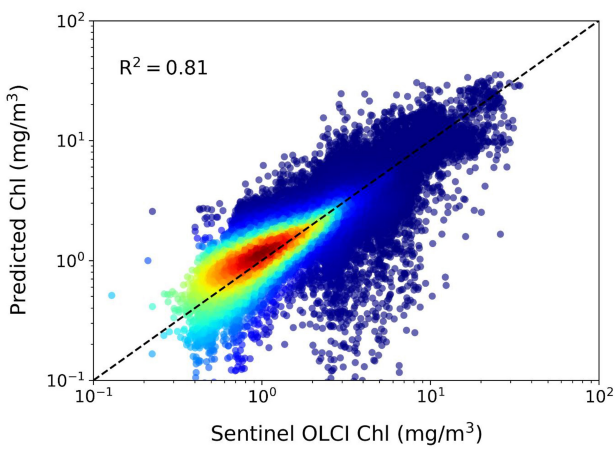

FIGURE 8 | Comparison of Sentinel OLCI Chl with predicted Chl on September 17, 2019 (MAPE = 36.9%); the linear regression between the two datasets is $y = 0.79\,x + 0.28$ ($r^2 = 0.81$).

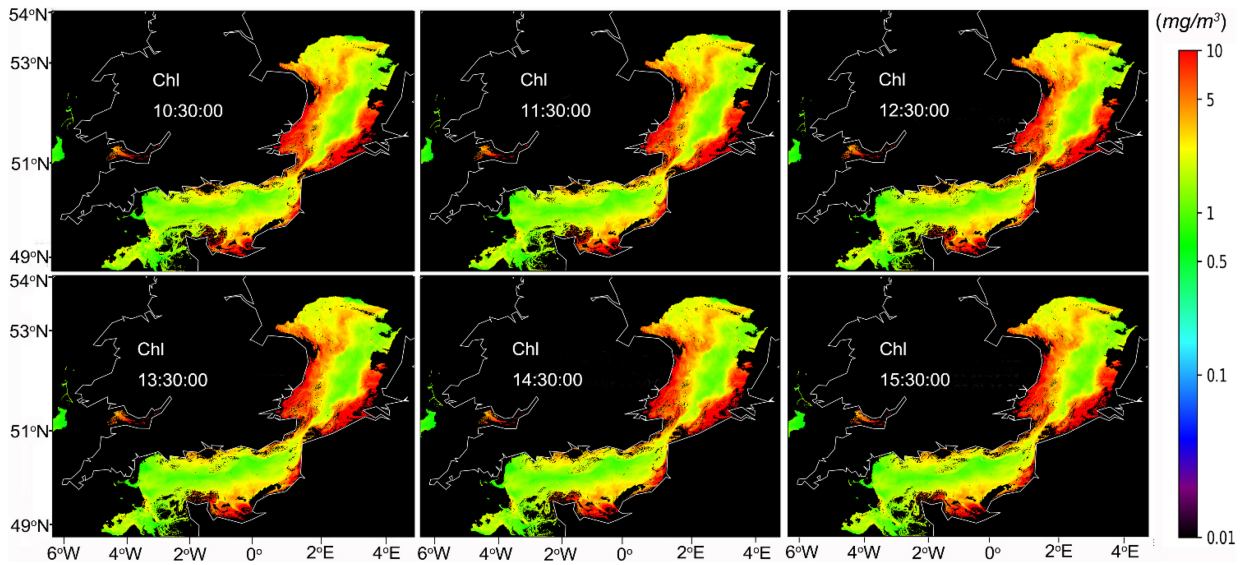

FIGURE 9 | Prediction algorithm applied to the English Channel, June 29 to July 5, 2019: maps showing distribution of predicted Chl at 4-h intervals with high spatial resolution (100 m) (animation: https://rsg.pml.ac.uk/shared_files/junl/paper_animation/example2/chl.gif).

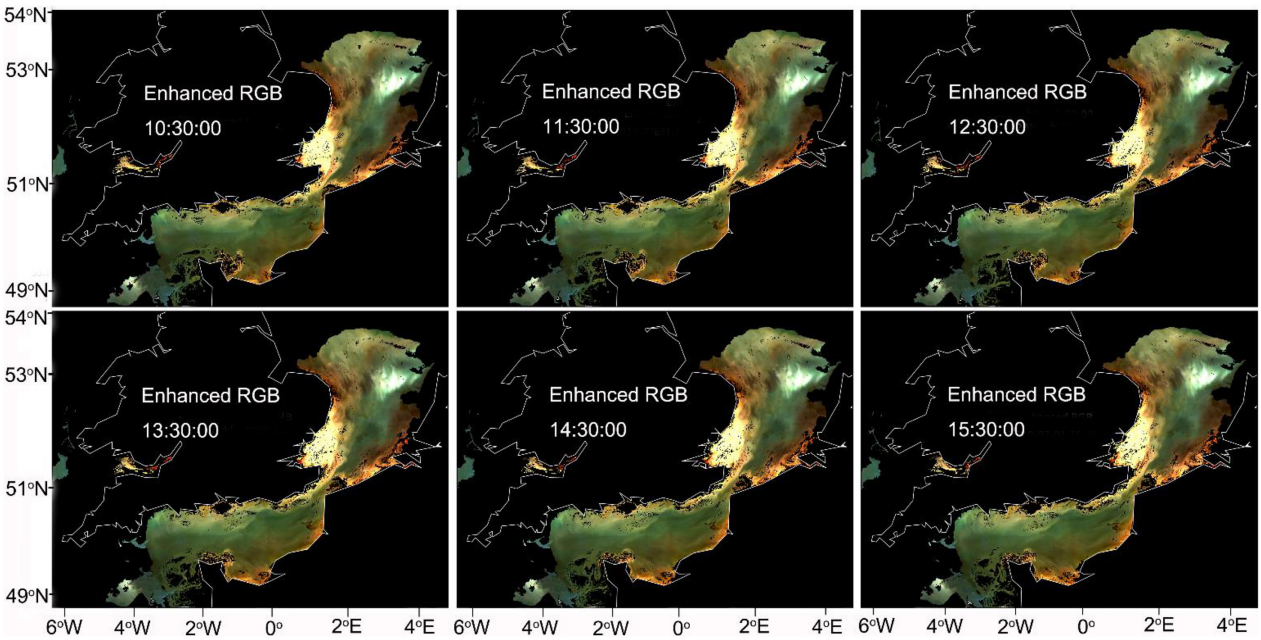

FIGURE 10 | Frames of predicted enhanced ocean-color RGB in the English Channel with high spatial resolution (100 m) showing more details of water properties including the movement of a bright coccolithophore bloom near 53° N (animation: https://rsg.pml.ac.uk/shared_files/junl/paper_animation/example2/rgb.gif).

DISCUSSION

It is quite clear, as seen both in our findings and in earlier studies (e.g., Jönsson et al., 2009; Jönsson and Salisbury, 2016), that biological processes in coastal are strongly affected by physical advection of water parcels, and that combining satellite derived products and simulated velocity fields using particle tracking provides a powerful approach for such analyses. While earlier works by Jönsson et al. (2011) and Jönsson and Salisbury (2016) are primarily focused on estimating the rate of change in satellite properties, we present results showing that the method can be expanded to predict locations and concentrations of the properties. This novel application can be used to better predict HAB events and to identify the extent and location of blooms more precisely, especially in regions with strong tidal cycles where surface currents are predictable.

We find our results to be generally physically coherent and that any patches of high phytoplankton biomass are predicted

and advected in a reasonable way. The nature of the method is such that we expect significant methodological errors to be seen as noise or spurious changes in our predicted fields (see Jönsson et al., 2009 for further discussion). We see for example, as expected, generally sharper Chl gradients in coastal waters compared to the open ocean in the Celtic Sea and English Channel. The method is also able to successfully predict the location of a coccolithophore bloom. The skill of the method discussed here is in line with what earlier studies have reported from the California Current (Jönsson and Salisbury, 2016) and Gulf of Maine (Jönsson et al., 2009) when estimating rates of change, which suggests that the extrapolation approach has a similar ability to provide useful information.

While the prediction tool presented in this study has the potential to improve regional HAB monitoring by more precisely assessing how the current state will develop in the near future, we readily agree that there are limitations. It is inevitable that there will be inaccuracies due to imperfections in the modeling and methodology. Errors in the prediction method could arise from many aspects, e.g., imperfect velocity of fields, extrapolation of model velocities in time and space, numerical integration of the trajectory path, and the omission of vertical velocity.

In this study, Lagrangian particle trajectories were computed according to the effect of both advection and diffusion. However, because each trajectory only contains a limited number of particles, the final locations of simulated particles could not be representative of all possible particle locations due to diffusion. The problem could be especially acute for some areas with large horizontal current shear. Thus, it would be important to keep in mind that uncertainty from diffusion always exists in these areas. The problems could be solved by seeding many more particles at each initial location, though the additional burden of computing their trajectories is currently unfeasible for this real-time application. A practical solution could be to introduce a probability density function indicating possible locations for each traced particle. However, it is beyond the scope of this study and substantial studies of this question are anticipated in the future. Regarding errors from advection, this was assessed in the previous study of Jönsson et al. (2009) by comparing the changes in Chl and sea surface temperature (SST) between the start and end positions of particle trajectories advected between two satellite images. The results showed that the advective errors are small relative to total changes due to other factors.

The extrapolation procedure will also introduce errors to the predictions. The predicted values were estimated *via* linear extrapolation with a weighting function. To reduce error from the extrapolation, when the extrapolated value for a trajectory exceeded 50% of the mean value of all extrapolations, this trajectory was disregarded and was not included for the calculation of final prediction. Considering uncertainty from the IOPs retrieval algorithm, errors in predicted IOPs are inevitable, but errors in R_{rs} could possibly be compensated by reconstruction from these IOPs. Furthermore, it is also worth noting that although individual trajectories have errors, the statistics obtained from thousands of particles are still very informative.

Still, while not perfect, the resulting predictions provide an enhanced set of information for managers and stakeholders to include when assessing the risk of HABs that has not been available until now. The prediction tool is also agnostic to any of its component modules. We are able to easily leverage new improved ocean circulation models and satellite products into the framework to provide as accurate predictions as possible.

CONCLUSION

This study set out to develop a prediction scheme for monitoring HABs by merging satellite observations and Lagrangian particle tracking. Two case studies in regions along the coast of England have shown that the Lagrangian methodology is effective for the interpretation of satellite data for early warning of HAB risk. The accuracy of the predictions relies on many factors. Particularly, the uncertainties from modeling and methodology, e.g., velocity of fields, extrapolation of model velocities in time and space, numerical integration of the trajectory path, and the omission of vertical velocity, may have big impacts on determining the accuracy of final predictions. Notwithstanding these imperfections, this work offers a powerful tool for monitoring and observing the state of the marine ecosystem. The synoptic, time-resolved quantification is invaluable to our understanding of HABs developments. Animated sequences generated by this method promote greater understanding and usage of satellite ocean color data for communicating with aquaculture farmers. Future research will extend the approach to predict quantitative risk maps for key high-biomass HAB species. Hence our future priority is to seek further applications of this new technique to support the aquaculture industry with improved early warning of potential HABs.

DATA AVAILABILITY STATEMENT

The raw data supporting the conclusions of this article will be made available by the authors, without undue reservation.

AUTHOR CONTRIBUTIONS

JL developed the prediction scheme, implemented the code, and wrote the first draft of the manuscript. PM proposed initial ideas and helped shape the research. BJ provided suggestions on code and algorithm development. MB helped carry out numerical simulations. All authors discussed the results and commented on the manuscript.

FUNDING

This study was supported by the Interreg Atlantic Area Programme project "Predicting the Impact of Regional Scale Events on the Aquaculture Sector" (PRIMROSE, Grant No. EAPA_182/2016) and UK BBSRC project "Safe and Sustainable Shellfish: Introducing local testing and management solutions" (reference BB/S004211/1). BJ was in part funded by NASA 80NSSC21K0565 and a Simons Foundation grant (549947, SS).

REFERENCES

Anderson, D. M. (2009). Approaches to monitoring, control and management of harmful algal blooms (HABs). *Ocean Coastal Manage.* 52, 342–347. doi: 10.1016/j.ocecoaman.2009.04.006

Anderson, D. M., Cembella, A. D., and Hallegraeff, G. M. (2012). Progress in understanding harmful algal blooms: paradigm shifts and new technologies for research, monitoring, and management. *Annu. Rev. Mari. Sci.* 4, 143–176. doi: 10.1146/annurev-marine-120308-081121

Anderson, D. M., Hoagland, P., Kaoru, Y., and White, A. W. (2000). *Estimated Annual Economic Impacts From Harmful Algal Blooms (HABs) in the United States*. Woods Hole, MA: WHOI-2000-11Woods Hole Oceanogr Inst.

Blondeau-Patissier, D., Gower, J. F., Dekker, A. G., Phinn, S. R., and Brando, V. E. (2014). A review of ocean color remote sensing methods and statistical techniques for the detection, mapping and analysis of phytoplankton blooms in coastal and open oceans. *Prog. Oceanogr.* 123, 123–144. doi: 10.1016/j.pocean.2013.12.008

Chen, C., Liu, H., and Beardsley, R. C. (2003). An unstructured grid, finite-volume, three-dimensional, primitive equations ocean model: application to coastal ocean and estuaries. *J. Atmospheric Terrest. Phys.* 20, 159–186. doi: 10.1175/1520-0426(2003)020<0159:augfvt>2.0.co;2

Fernandes-Salvador, J. A., Davidson, K., Sourisseau, M., Revilla, M., Schmidt, W., Clarke, D., et al. (2021). Current status of forecasting toxic harmful algae for the north-east Atlantic shellfish aquaculture industry. *Front. Mari. Sci.* 8:666583.

Fogg, G. E. (1969). The physiology of an algal nuisance. *Proc. R. Soc. London Seri. B* 173, 175–189. doi: 10.1098/rspb.1969.0045

Gobler, C. J. (2020). Climate change and harmful algal blooms: insights and perspective. *Harmful Algae* 91:101731. doi: 10.1016/j.hal.2019.101731

Gordon, H. R., Brown, O. B., Evans, R. H., Brown, J. W., Smith, R. C., Baker, K. S., et al. (1988). A semianalytic radiance model of ocean color. *J. Geophy. Res. Atmosph.* 93, 10909–10924. doi: 10.1029/jd093id09p10909

Grattan, L. M., Holobaugh, S., and Morris, J. G. Jr. (2016). Harmful algal blooms and public health. *Harmful Algae* 57, 2–8. doi: 10.1016/j.hal.2016.05.003

Hallegraeff, G. (2003). Harmful algal blooms: a global overview. *Manual Harmful Mari. Microalgae* 33, 1–22. doi: 10.1007/978-0-387-75865-7_1

Hallegraeff, G. M. (1993). A review of harmful algal blooms and their apparent global increase. *Phycologia* 32, 79–99. doi: 10.1186/1476-069X-7-S2-S4

Heisler, J., Glibert, P. M., Burkholder, J. M., Anderson, D. M., Cochlan, W., Dennison, W. C., et al. (2008). Eutrophication and harmful algal blooms: a scientific consensus. *Harmful Algae* 8, 3–13. doi: 10.1016/j.hal.2008.08.006

Jönsson, B. F., and Salisbury, J. E. (2016). Episodicity in phytoplankton dynamics in a coastal region. *Geophy. Res. Lett.* 43, 5821–5828. doi: 10.1002/2016gl068683

Jönsson, B. F., Salisbury, J. E., and Mahadevan, A. J. I. (2009). Extending the use and interpretation of ocean satellite data using *Lagrangian modelling. Int. J. Remote Sen.* 30, 3331–3341. doi: 10.1080/01431160802558758

Jönsson, B., Salisbury, J., and Mahadevan, A. (2011). Large variability in continental shelf production of phytoplankton carbon revealed by satellite. *Biogeosciences* 8:1213. doi: 10.5194/bg-8-1213-2011

Klemas, V. J. (2012). Remote sensing of algal blooms: an overview with case studies. *J. Coas. Res.* 28, 34–43. doi: 10.2112/jcoastres-d-11-00051.1

Kwon, K., Choi, B.-J., Kim, K. Y., and Kim, K. (2019). Tracing the trajectory of pelagic sargassum using satellite monitoring and Lagrangian transport simulations in the East China sea and yellow sea. *Algae* 34, 315–326. doi: 10.4490/algae.2019.34.12.11

Landsberg, J. H. (2002). The effects of harmful algal blooms on aquatic organisms. *Rev. Fish. Science* 10, 113–390. doi: 10.1080/20026491051695

Lee, Z., Carder, K. L., and Arnone, R. A. (2002). Deriving inherent optical properties from water color: a multiband quasi-analytical algorithm for optically deep waters. *Appl. Optics* 41, 5755–5772. doi: 10.1364/ao.41.005755

Li, H., Qin, C., He, W., Sun, F., and Du, P. (2020). Prototyping a numerical model coupled with remote sensing for tracking harmful algal blooms in shallow lakes. *Global Ecol. Conserv.* 22:e00938. doi: 10.1016/j.gecco.2020.e00938

Mueller, J. (1981). *Prospects for Measuring Phytoplankton Bloom Extent and Patchiness Using Remotely Sensed Color Images*. New York: Toxic Dinoflagellate Blooms, Elsevier, North Holland, Inc., 303–330.

Olascoaga, M. J., Beron-Vera, F. J., Brand, L. E., and Koçak, H. J. (2008). Tracing the early development of harmful algal blooms on the west Florida shelf with the aid of lagrangian coherent structures. *J. Geophys. Res. Oceans* 113:c12014. doi: 10.1029/2007JC004533

Paerl, H. W. (1988). Nuisance phytoplankton blooms in coastal, estuarine, and inland waters 1. *Limnol. Oceanogr.* 33, 823–843. doi: 10.4319/lo.1988.33.4_part_2.0823

Sellner, K. G., Doucette, G. J., and Kirkpatrick, G. J. (2003). Harmful algal blooms: causes, impacts and detection. *J. Indust. Microbiol.* 30, 383–406. doi: 10.1007/s10295-003-0074-9

Sengco, M. R., and Anderson, D. M. (2004). Controlling harmful algal blooms through clay flocculation 1. *J. Eukaryotic Microbiol.* 51, 169–172. doi: 10.1111/j.1550-7408.2004.tb00541.x

Smagorinsky, J. (1963). General circulation experiments with the primitive equations: I. the basic experiment. *Monthly Weather Rev.* 91, 99–164. doi: 10.1175/1520-0493(1963)091<0099:gcewtp>2.3.co;2

Son, Y. B., Choi, B.-J., Kim, Y. H., and Park, Y. G. (2015). Tracing floating green algae blooms in the Yellow sea and the East China sea using GOCI satellite data and lagrangian transport simulations. *Remote Sensing Environ.* 156, 21–33. doi: 10.1016/j.rse.2014.09.024

Tilstone, G. H., Pardo, S., Dall'Olmo, G., Brewin, R. J. W., Nencioli, F., Dessailly, D., et al. (2020). Performance of ocean colour chlorophyll a algorithms for sentinel-3 1 OLCI, MODIS-aqua and suomi-VIIRS in open-ocean waters of the Atlantic. *Remote Sens. Environ.* 260:art.112444. doi: 10.1016/j.rse.2021.112444

Umlauf, L., and Burchard, H. (2005). Second-order turbulence closure models for geophysical boundary layers. a review of recent work. *Continental Shelf Res.* 25, 795–827. doi: 10.1016/j.csr.2004.08.004

Uncles, R., Clark, J. R., Bedington, M., and Torres, R. (2019). *Physical Processesl in the Whitsand Bay Marine Conservation Zone: Neighbour to a Closed Dredge-Spoil Disposal Site*. Amsterdam: Marine Protected Areas, Elsevier.

Wynne, T. T., Stumpf, R. P., Tomlinson, M. C., Schwab, D. J., Watabayashi, G. Y., and Christensen, J. D. (2011). Estimating cyanobacterial bloom transport by coupling remotely sensed imagery and a hydrodynamic model. *Ecol. Appl.* 21, 2709–2721. doi: 10.1890/10-1454.1

Conflict of Interest: The authors declare that the research was conducted in the absence of any commercial or financial relationships that could be construed as a potential conflict of interest.

frontiers in Marine Science

ORIGINAL RESEARCH
published: 22 December 2021
doi: 10.3389/fmars.2021.785174

Temporal and Spatial Patterns of Harmful Algae Affecting Scottish Shellfish Aquaculture

Fatima Gianella[1], Michael T. Burrows[1], Sarah C. Swan[1], Andrew D. Turner[2] and Keith Davidson[1]*

[1] Scottish Association for Marine Science, Scottish Marine Institute, Oban, United Kingdom, [2] Centre for Environment, Fisheries and Aquaculture Science, Weymouth, United Kingdom

Consistent patterns of Harmful Algal Bloom (HAB) events are not evident across the scientific literature, suggesting that local or regional variability is likely to be important in modulating any overall trend. This study summarizes Scotland-wide temporal and spatial patterns in a robust 15-year high temporal frequency time series (2006–2020) of the incidence of HABs and shellfish biotoxins in blue Mussels (*Mytilus edulis*), collected as part of the Food Standards Scotland (FSS) regulatory monitoring program. The relationship between the countrywide annual incidence of HAB events and biotoxins with environmental variables was also explored. Temporal patterns exhibited interannual variability, with no year-on-year increase, nor any correlation between annual occurrences. Within years, there was a summer increase in bloom frequency, peaking in July for *Dinophysis* spp. and *Pseudo-nitzschia* spp., and a plateau from May to July for *Alexandrium* spp. Temporal-spatial patterns were analyzed with multivariate statistics on data from monitoring sites aggregated monthly into 50-km grid cells, using Principal Component Analysis (PCA) and cluster K-means analysis. PCA analyses showed correlation between areas with similar temporal dynamics, identifying seasonality as one of the main elements of HAB variability with temporal-spatial patterns being explained by the first and second principal components. Similar patterns among regions in timing and magnitude of blooms were evaluated using K-means clusters. The analysis confirmed that the highest risk from HABs generally occurred during summer, but demonstrated that areas that respond in a similar manner (high or low risk) are not always geographically close. For example, the occurrence of the most prevalent HAB genus, *Dinophysis* spp., is similar countrywide, but there is a regional trend in risk level with "very-high" and "high" clusters located primarily on the southwest coast, the islands of the central and northern west coast and the Shetland Islands. "Early" and "late" blooms were also associated with certain areas and level of risk. Overall, high risk areas mainly face in a southwest direction, whilst low risk locations face a south or southeast direction. We found relatively few countrywide relationships between environmental variables and HABs, confirming the need for regional analysis to support HAB early warning.

Keywords: HAB, shellfish aquaculture, management, *Mytilus edulis*, spatial-temporal trends

OPEN ACCESS

Edited by:
Jose Luis Iriarte, Austral University of Chile, Chile

Reviewed by:
Haifeng Gu, Third Institute of Oceanography, State Oceanic Administration, China
Pedro R. Costa, Portuguese Institute for Sea and Atmosphere (IPMA), Portugal

****Correspondence:***
Fatima Gianella
fatima.gianella@sams.ac.uk

Specialty section:
This article was submitted to Marine Fisheries, Aquaculture and Living Resources, a section of the journal Frontiers in Marine Science

Received: *28 September 2021*
Accepted: *22 November 2021*
Published: *22 December 2021*

Citation:
Gianella F, Burrows MT, Swan SC, Turner AD and Davidson K (2021) Temporal and Spatial Patterns of Harmful Algae Affecting Scottish Shellfish Aquaculture. Front. Mar. Sci. 8:785174. doi: 10.3389/fmars.2021.785174

INTRODUCTION

Harmful algal blooms (HABs), associated with human and shellfish toxicity, are temporally and spatially variable. The occurrence, intensity and distribution of HABs is a problem worldwide (Hallegraeff, 1993, 2010; Van Dolah, 2000; Smayda, 2002; Glibert et al., 2005; Anderson et al., 2017; Gobler et al., 2017; Wells et al., 2019). However, trends of increasing HAB frequency and/or abundance are not evident in all studies (Moore et al., 2009; Díaz et al., 2016; Dees et al., 2017) suggesting that local or regional variability is likely in any overall trend. This is consistent with recent results from Hallegraeff et al. (2021) who used a meta-analysis of Harmful Algae Event Database and Ocean Biodiversity Information system data to demonstrate that there is no empirical support for a global increase in HAB events. Understanding the temporal-spatial variability of HABs and environmental drivers at a regional level is therefore of considerable importance to producers and consumers of shellfish.

The presence of toxic phytoplankton and synthesized biotoxins is a threat for shellfish aquaculture, since the consumption of shellfish that have concentrated these toxins through ingestion of harmful phytoplankton impacts negatively on human health (Smayda, 1990; Berdalet et al., 2016). The economic consequences of HABs for shellfish aquaculture have recently been shown to be significant (Mardones et al., 2020), with Martino et al. (2020) estimating that the incidence of biotoxins associated with Diarrheic Shellfish Poisoning (DSP) causes an annual average loss of 15% in mussel production in Scottish waters, equivalent to £1.37 m.

Scottish waters are impacted by a number of HAB genera, but concern over shellfish toxicity is primarily related to the genera *Dinophysis*, *Alexandrium* and *Pseudo-nitzschia* (Davidson and Bresnan, 2009). *Dinophysis* spp., responsible for the production of Diarrheic Shellfish Toxins (DSTs) by the synthesis of okadaic acid, dinophysistoxins and equivalents (Reguera et al., 2014) have caused prolonged shellfish harvesting closures in Scotland (Whyte et al., 2014; Swan et al., 2018; Bresnan et al., 2021). The toxic *Dinophysis* species most commonly associated with harmful events in Scotland are *D. acuminata* and *D. acuta* (Swan et al., 2018). Some *Alexandrium* spp. cause Paralytic Shellfish Poisoning (PSP) through the synthesis of saxitoxins (Brown et al., 2010; Touzet et al., 2010). The most common toxin producer in Scottish waters is thought to be *Alexandrium catenella* (Bresnan et al., 2021) with *A. minutum* and *A. ostenfeldii* also having been reported (Brown et al., 2010; Lewis et al., 2018). Non-toxic *A. tamarense* (Touzet et al., 2010) and *A. tamutum* (Brown et al., 2010) are also present. *Pseudo-nitzschia* spp. are linked to Amnesic Shellfish Poisoning (ASP) through the production of domoic acid (DA) (Fehling et al., 2006, 2004; Bresnan et al., 2017; Rowland-Pilgrim et al., 2019). In Scottish waters, toxic and non-toxic members are found in the *Pseudo-nitzschia delicatissima* group, with toxic species include *P. calliantha*, *P. pseudodelicatissima* and *P. cf. pseudodelicatissima* (Fehling et al., 2006; Smayda, 2006). The *P. seriata* group includes species that synthesize high levels of DA, *P. australis*, *P. seriata*, *P. fraudulenta*, *P. multiseries* (found occasionally), *P. pungens* and *P.cf. subpacifica* (Fehling et al., 2006; Smayda, 2006). Azaspiracids are infrequently recorded, and as their causative phytoplankton taxa (*Azadinium/Amphidoma*) are not enumerated within the regulatory monitoring program they have not been included in our analyses. The national monitoring program enumerates and reports the main harmful taxa to genus level only. While it is recognized that both toxic and non-toxic species may therefore be enumerated, this approach is used to (a) ensure rapid sample turn around and (b) on a precautionary basis to best protect human health. Hence, the bulk of the analysis and discussion is based on taxonomic resolution to genus level. However, where appropriate, based on other published studies, we comment on how these trends may relate to particular harmful species and their toxins.

Trends observed in Scotland and other site specific studies suggest HABs are spatially and temporally variable, with blooms likely linked to large scale oceanic variations (Belgrano et al., 1999), meteorological or oceanographic anomalies (Moita et al., 2016), and specific environmental conditions, rather than a steady increase every year. Studies involving atmospheric dynamics in the Atlantic Ocean use the North Atlantic Oscillation (NAO) index as the difference between the low pressure system around Iceland and the high pressure of the Azores Islands in the mid North Atlantic Ocean. A positive index indicates a stronger wind intensity predominantly from the southwestern direction, whilst a negative NAO index is related to a smaller difference between the systems leading to lower wind speeds (Phillips et al., 2013). These atmospheric patterns influence the climate and consequently environmental conditions in the water column. Several studies have suggested the NAO index is a useful predictor for the development of HAB events, specifically *Dinophysis* (Belgrano et al., 1999; Báez et al., 2014; Ruiz-Villarreal et al., 2016). Changes in the prevalent wind direction have, through their impact on surface oceanographic currents, led to the development of HAB events in the Shetland Islands (Whyte et al., 2014). In other locations, changes in wind patterns are associated with upwelling/downwelling conditions that cause HAB events, as seen in the northwest coast of Spain (Fraga et al., 1988) and Bay of Bantry, Ireland (Cusack et al., 2016). An increase in sea surface temperature (SST) has also been associated with increased growth rate of phytoplankton, including the toxin-producing taxa *Dinophysis* and *Alexandrium*, found in Scotland (Peperzak, 2003; Gobler et al., 2017; Wells et al., 2019). In some locations, the increase of temperature above a certain limit is the main requirement for blooms of toxic species, such as *Alexandrium minutum* in the Bay of Brest (Chapelle et al., 2015).

Coastal *Dinophysis* and *Pseudo-nitzschia* events have been associated with advective oceanographic transport of blooms that initially develop offshore (Fehling et al., 2012; Whyte et al., 2014; Paterson et al., 2017). Cyst forming *Alexandrium* are more likely to be controlled by local hydrodynamics (Bresnan et al., 2021), with *Alexandrium* blooms potentially related to the germination of cysts introduced into the sediment in previous years (Anderson et al., 2005; Brown et al., 2010). Characterizing the spatial and temporal trends of different HAB genera over multiple years is therefore not straightforward. Many authors have attempted to understand HAB dynamics, using linear modeling in relation to

single or multiple environmental drivers (Hinder et al., 2012; Ruiz-Villarreal et al., 2016; Dees et al., 2017), but such approaches are best suited to the evaluation of decadal trends. Aquaculture practitioners and coastal zone managers have a more pressing need to better understand the likely timing and location of HAB taxa and biotoxins to allow more informed farm management and regulatory decision-making.

High temporal resolution (typically weekly) regulatory monitoring of HABs and their associated shellfish biotoxins in Scottish waters has been undertaken by Food Standards Scotland (FSS) at 143 sites since 2006, generating a unique spatial and temporal dataset of 256 920 observations. Using these data as a regional case study, here we demonstrate the use of statistical techniques to describe, analyze and identify the main HAB and biotoxin patterns in Scottish waters. The relationship between the frequency of HAB events and environmental variables was also assessed. Understanding the dynamics of HABs is useful to support predictive models and other risk assessment approaches to provide early warning of shellfish toxicity (Davidson et al., 2016, 2021). This has the potential to improve measures for safeguarding shellfish consumption and minimize negative impacts in the aquaculture sector.

The statistical approaches used to analyze temporal patterns include the autocorrelation of the frequency of events in the time series. Autocorrelation (or serial correlation) is defined as the correlation of a variable with itself at different times (lag) to examine how current observations relate to those in the past (Cowpertwait and Metcalfe, 2008). Partial autocorrelation is the association with a particular lag, excluding the indirect effect explained by earlier lags. Autocorrelation has previously been used to assess the influence of environmental variables in a HAB time series, with Fischer et al. (2018) finding that cooling temperatures of previous years influenced *Alexandrium* cyst hatching in the Gulf of Maine. In contrast, the abundance of *Pseudo-nitzschia* and the autocorrelation within years presented a non-significant trend from 2008 to 2018 in Scotland (Rowland-Pilgrim et al., 2019), and a study evaluating the toxicity of PSP in Puget Sound did not find a significant correlation between toxicity and year from 1993 to 2007 (Moore et al., 2009).

The clustering analyses uses a descriptive approach to assess similarities between samples and identify patterns. K-means analysis is a method that groups a data set into a specified number of clusters (k) (Macqueen, 1967). Samples associated with a particular mean group together, hence the intra-cluster variation is reduced, differentiating these measurements from those in clusters. This approach has been used in the analysis of phytoplankton patterns and to identify the environmental conditions related to their assemblages and composition (Herrera and Escribano, 2006; Marchese et al., 2019; Barth et al., 2020). It has also been used for assessing clusters of toxin profiles from shellfish samples across geographical areas in Great Britain (Turner et al., 2014). Principal Component Analysis (PCA) is a tool for reducing high-dimensional data to fewer dimensions that explain variance and identify the key variables and their role in this variance (Lever et al., 2017). This method has been used to identify phytoplankton temporal patterns, assess the similarity between annual abundances in the time series, links with environmental variables, and similarity of conditions between sampled stations (Solic et al., 1997; Philippart et al., 2000; Kane, 2011; Fehling et al., 2012; Siemering et al., 2016).

This study therefore sought to examine and describe the temporal patterns of shellfish biotoxin-producing HABs and their biotoxins in Scotland. The spatial patterns and the role of seasonality were analyzed for the phytoplankton taxa only, as the suspension of biotoxin sampling and analysis during periods of shellfish farm closure resulted in missing data and inconsistent spatial patterns. The relationship between the annual HABs frequency, biotoxins and environmental variables was evaluated to identify whether there are countrywide relationships and if these can be used as predictors of a toxin event.

MATERIALS AND METHODS

Data Access and Preparation

Phytoplankton and shellfish biotoxin data were obtained from the Food Standards Scotland (FSS) monitoring program[1]. The FSS scheme is operated by the Centre for Environment, Fisheries and Aquaculture Science (CEFAS) for biotoxins, and the Scottish Association for Marine Science (SAMS) for harmful phytoplankton identification. Samples are collected from representative monitoring points (RMPs), primarily located on the west coast and islands (**Figure 1**) where aquaculture is active. Collection of seawater for phytoplankton analysis is carried out on a weekly basis from March to September and fortnightly in October at all sites, with monthly samples collected from November to February from a reduced number of sites. Harmful phytoplankton genera are identified and enumerated by light microscopy at SAMS. Further details of the program are found in the most recent annual program report (Coates et al., 2020). The following analysis comprises a 15-year time series database, from January 2006 to December 2020.

Phytoplankton samples were collected by officers operating on behalf of several contractors appointed by FSS. This follows the UK National Reference Laboratory (UKNRL) Standard Operating Procedure for the collection of water samples for toxic phytoplankton analysis. These are taken as close to the shellfish bed as possible and at the same location from where shellfish samples for tissue analysis are collected. The sampling method used depends on the depth of water at the site, water samples are usually collected with a 10 m "Lund tube" but occasionally a bucket is used in shallow waters. A well-mixed 500 mL sub-sample of this water is preserved using Lugol's iodine prior to analysis by light microscopy (Uttermöhl method) at SAMS.

Shellfish were collected using UKNRL guidance and shipped to the CEFAS Weymouth laboratory for biotoxin analysis (Coates et al., 2020). These data were available from March 2007 to December 2020. Monitored shellfish species include common mussels (*Mytilus edulis*), common cockles (*Cerastoderma edule*), native oysters (*Ostrea edulis*), Pacific oysters (*Magallana gigas*) and razor clams (*Ensis* spp.).

[1]https://www.foodstandards.gov.scot/business-and-industry/industry-specific-advice

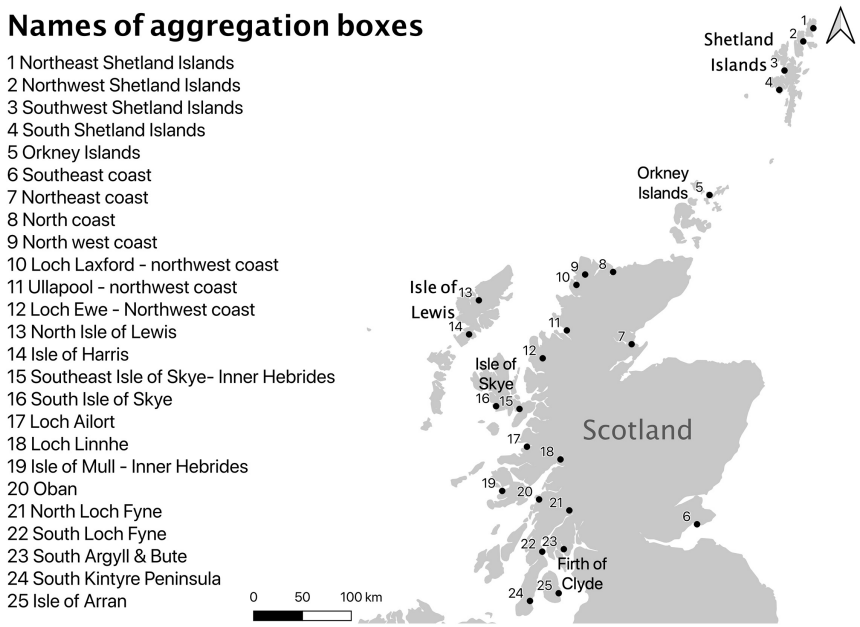

FIGURE 1 | Names and location of the 25 aggregation boxes used (Geographical order North to South).

Common mussels constitute ∼62.2% of the total samples and ∼87.7% of samples with total toxin concentrations above maximum permitted level (MPL). As the diverse mechanisms of assimilation and depuration of biotoxins vary according to the shellfish species, our analysis exclusively selected common mussels as the study species due to the high proportion of samples that exhibited toxicity.

Biotoxins levels were quantified by the use of liquid chromatography with tandem mass spectrometry (LC-MS/MS) for lipophilic toxins (LT), including DSTs (Dhanji-Rapkova et al., 2018), and High Performance Liquid Chromatography (HPLC) with either ultra-violet (domoic acid-DA) (Rowland-Pilgrim et al., 2019) or fluorescence detection (Paralytic Shellfish Toxins—PST) (Turner et al., 2014) following official methods specified in EU regulations (Coates et al., 2020). Biological assays were previously used for the purpose of determining shellfish toxicity for PST and DST, with the year the methods changed to chemical instrumentation methods being specific to each biotoxin class. In the case of PST, HPLC was used from 2007 onward, depending on the shellfish species analyzed, with all PST quantitation performed by HPLC by 2011 (Turner et al., 2014). Quantitative determination of DSTs by LC-MS/MS started from July 2011 (Dhanji-Rapkova et al., 2018) replacing the original qualitative biological assay. The biotoxins laboratory quantifies the total toxin concentrations and uses measurement uncertainties of the methods to report "low," "actual" and "high" values for LT and PST results. FSS uses the latter for risk assessment and as a precautionary measure; this value has been used in the analyses below.

Phytoplankton abundance and biotoxin levels are classified according to the safety threshold value set by the UKNRL following regulation (EC) 2019/627 (**Table 1**). These thresholds were used to categorize whether a HAB or biotoxin event occurred. The proportional frequency of occurrence of an event above the safety threshold was therefore calculated by dividing the frequency of these events by the total number of samples in a time period or at a specific location. Proportional frequencies of occurrence were averaged to evaluate yearly, monthly and the spatial distribution of HABs and toxic events in Scotland. The proportional frequency of these above regulatory threshold events is used in our analyses below.

Spatial Range Studied

The data included information from 130 RMPs. Areas located less than 5 km apart were grouped and averaged due to their close proximity and those with fewer than 10 samples over the time series were excluded. Samples were collected at shellfish farms, some of which moved between 2006 and 2019, in which case the median value of their location was calculated.

Temporal and Spatial Statistical Analysis

The statistical analysis was performed using the R program (R Core Team, 2021). Temporal analysis examined the yearly and monthly autocorrelation in the time series using the ACF function in R. This correlated the proportional frequency of events with previous frequencies, at different time lags (x-axis) in yearly and monthly time series. The partial autocorrelation function (PACF) was applied when the autocorrelation function showed significant lag values.

Sampling effort within and between RMPs varied throughout the time series. Hence, spatial analysis and statistics were applied using "aggregation boxes" ($n = 25$) of 50 km × 50 km to group values after calculating the median (**Figure 1**). Each box contained between one and 15 RMPs. Boxes recording eight or

TABLE 1 | Safety threshold limits delimited for phytoplankton species abundance in water samples and maximum permitted level (MPL) for biotoxin in shellfish tissues in Scotland, set by the UKNRL and EC No 853/2004, respectively.

Species	Threshold cells/liter	Health syndrome	Biotoxins	Maximum permitted level (MPL) per kg of shellfish tissue
Alexandrium spp.	40	Paralytic shellfish poisoning (PSP)	Saxitoxin di-hydrochloride equivalents (PSTs)	800 μg
Dinophysis spp.	100	Diarrheic shellfish poisoning (DSP)	Okadaic acid Dinophysistoxins Pectenotoxins (DSTs)	160 μg
Pseudo-nitzschia spp.	50,000	Amnesic shellfish poisoning (ASP)	Domoic acid (DA)	20 mg

more missing monthly values in the time series were removed from the analysis. The coordinates, corresponding to the samples and estimated values, were rounded into the whole number to group them in the aggregation boxes.

PCA was applied to identify dominant temporal and spatial patterns of the incidence of HAB events throughout the time series, using monthly values of HABs and toxic events. This analysis also sought to evaluate the role of seasonality (temporal) and spatial patterns in the frequency of HAB events, shown by the first and second principal components (PC). These capture the highest proportion of variance and are the main axes of variation in the data set. The loadings (or eigenvectors) indicate the importance of each variable (month, year, and area) according to the PC. The sample scores refer to the correlation between these variables and the loadings for each PC. PCA cannot be performed on datasets with missing values, so these were estimated from generalized least squares models that included year, month and area averages of the time series.

The spatial risk of the blooms was assessed by clustering the aggregation boxes with similar bloom occurrence, timing and intensity. The K-means analysis identified clusters of high and low risk areas according to the bloom occurrence using the kmeans() function (R Core Team, 2021), with the "elbow" method first being used to determine the most appropriate number of clusters for a particular genus/biotoxin. This was assessed by plotting within clusters sum of squares (WSS) against the number of clusters (k) and evaluating the point at which there was a reduction in the slope (the elbow) using the fviz_nbclust function from the "factoextra" library in R (Kassambara and Mundt, 2020). The proportion of variation and K-means for each *k* number were calculated and compared for seasonal (monthly) and annual averages series for each species. The analysis sought to explain a high proportion of variance, maximizing similarity within the clusters and minimizing similarity between clusters, with care being taken not to overfit the values. The annual value was calculated using averaged monthly events. The clusters were categorized as "very-high," "high," "moderate," and "low" risk.

The spatial risk of the taxa was evaluated using the monthly cluster risk classification, ranging from 1 to 4 (1 being "low" risk and 4 "very-high") for quantifying the risk across the taxa and aggregation box. The average risk per aggregation box was calculated and compared to identify the highest and lowest combined risk. The association between HABs risk for all taxa and their location was evaluated using Spearman correlation *rcorr*() function, which does not assume the data follow a normal distribution.

Relationship With Environmental Variables

Our study explored the relationship between HABs occurrence and environmental variables, including SST, the North Atlantic Oscillation (NAO) index (**Supplementary Figure 1**) and wind direction and intensity. To assess the strength and the relationships between annual HABs frequency and the variables we used the correlation [*rcorr*()] function in R. The time series period comprised from 2006 to 2018 for all variables. The SST data was accessed from the Physical Oceanography Distributed Active Archive Center (PODAAC) website[2] carried out by NOAA National Centers for Environmental Information (PO.DAAC, 2020). Daily NAO index database was downloaded from the NOAA data and averaged (NOAA/National Weather Service, 2021). Wind data were taken from the MIDAS database "Open UK hourly weather observation data" (Met Office, 2019). A total of 39 stations located a maximum distance of 5 km from the coast were used. The average wind speed (knots) was calculated, whilst average wind direction (radians) used the directional component of the wind [sine() and cos()]. Linear regression was used to evaluate the relationship between wind direction and intensity, blooms and toxic events.

RESULTS

Temporal Variability of Harmful Algal Blooms and Toxic Events

Temporal Trends

While all the HAB genera of interest exhibit a typical annual pattern of increased abundance in the spring, summer and autumn months, the frequency of events above the safety threshold on a countrywide scale is highly variable between years with no increasing pattern throughout the time series (**Figure 2**) for any of the taxa considered. *Dinophysis* spp. recorded the highest annual frequency of events above the safety threshold ($\geq$100 cells/L) in 2013, reaching 27.53% of events above the safety threshold of the total samples. On a monthly basis, the

[2]https://podaac.jpl.nasa.gov/

maximum frequency of events above the safety threshold was recorded in July 2013 for *Dinophysis* spp. and *Alexandrium* spp., recording ∼69 and 62% of bloom events, respectively; whilst *Pseudo-nitzschia* spp. reached a maximum of ∼38% of monthly bloom events in August 2011 (**Figure 2**). The annual occurrence of blooms of *Dinophysis* spp. and *Alexandrium* spp. followed a similar pattern with a strong positive and statistically significant correlation ($r = 0.61$, $p = 0.02$). Correlation values between annual bloom events of these genera with *Pseudo-nitzschia* spp. were not significant.

Yearly frequencies of HABs and biotoxin events for each taxon and toxin group were not correlated with frequencies in preceding years. The only exception is observed for a lag of 1 year for *Pseudo-nitzschia* spp.

The biotoxins also showed a high variability of monthly occurrence of events above the MPL throughout the time series in a country scale (**Figure 3**), but in contrast to the phytoplankton, not all the biotoxin groups followed a clear seasonal trend, likely caused by the slow depuration of some toxins. The biotoxins sampling was variable across the country and throughout the time series. 8 545 samples analyzed by mouse bioassay (MBA) for DSTs and 760 for PSTs were included in our analysis. Chemical methods superseded the MBA for the analysis of DST s and PSTs during 2011. For these LC-MS/MS analyses we used 16 679 for DSTs, 19 130 for PSTs and 13 694 for DA. There is a clear difference in the frequency of biotoxin events when determined by MBA (2007–2011) and LC-MS/MS (2011–2018), with the chemical analyses displaying a higher frequency of events. DSTs had the highest frequency of events above the safety threshold, with the highest values during summer months, reaching a maximum monthly average in August 2013 (∼54%). PSTs and DA exhibited sporadic events above the MPL throughout the time series. PSTs exceeded regulatory threshold in ∼10.95% of samples in May 2018. DA only exceeded the maximum permitted limit in seven events, in 4 months, reaching a maximum occurrence (∼1.6%) in August 2007.

A comparison between the time series of above regulatory threshold events for monitored HAB taxa and the biotoxins they synthesize does not show a monthly pattern. There is a significant and strong correlation between *Dinophysis* spp. and DSTs ($r = 0.75$, $p < 0.05$), *Alexandrium* spp. and PSTs ($r = 0.60$, $p < 0.05$), whilst *Pseudo-nitzschia* spp. and DA were not significantly correlated ($r = 0.04$, $p > 0.05$).

Seasonal Trends

Countrywide, HAB events above the safety threshold were observed mainly from March to October. HAB occurrence reached maximum monthly median values in July for *Dinophysis* and *Pseudo-nitzschia*; *Alexandrium* reached similar median values in May and June (**Figure 4**). However, the frequency of events and their timing varied, with both early and late year blooms of all organisms. Early season (March) blooms of both *Alexandrium* and *Pseudo-nitzschia* are evident, but in contrast, the average frequency of these early events is nearly zero for *Dinophysis* although a few exceptional years are observed. For *Dinophysis*, the median number of events per month increased as the year progressed and reached its highest value, and the highest amongst all taxa, in July before declining toward the end of the year. *Alexandrium* bloom frequency increased until June, with the frequency remaining high in July before a subsequent decline. *Pseudo-nitzschia* spp. blooms increased in April, before decreasing in May. Following the July peak, a further increase is evident in September and subsequently the frequency of events above the safety threshold decreases.

Elevated shellfish toxins are observed mainly in 8 months of the year (**Figure 4**), with DSTs present at a noticeably higher occurrence in comparison with the other groups. The earliest occurrence of toxicity for DSTs is mainly in June, although there were exceptional toxic events in previous months (March to May). Toxin events above the permitted level reached a peak in August (median above ∼ 13.25%), following a decreasing trend with a low median in October (∼0.88%). PSTs showed a peak of median values in June (∼3.52%); the maximum occurrence decreased in July and presented exceptional cases in August. The occurrence of DA above the safety threshold were mainly zero, with the exception of events in May, July, August, and September.

Relationship Between Monthly Blooms

The apparent seasonal pattern of blooms evident from **Figure 4** was further investigated using autocorrelation analysis in the time series. All of the phytoplankton taxa presented a significant seasonal and cyclical monthly correlation at all monthly lags (**Supplementary Figure 2**). The positive autocorrelation at shorter lags (1–3) suggests the frequency of HABs is linked to their occurrence in the previous month. The negative correlation at lags from 4 to 8 months indicate the different seasonal response. This confirms that seasonality is an important driver for the occurrence of HAB events. While this general trend was confirmed, PACF analysis indicated the seasonal pattern was specific for each HAB taxa. Dinoflagellates *Dinophysis* spp. and *Alexandrium* spp. showed five lags partial negatively autocorrelated (up to 6 months); whilst two and one positive lag, respectively. *Pseudo-nitzschia* spp. showed a low number of autocorrelated lags (three negative and three positive lags), suggesting seasonality has less of an impact in influencing the occurrence of events than for the other two genera.

The biotoxins autocorrelation pattern was group specific (**Supplementary Figure 3**). DSTs and PSTs showed a cyclical pattern by ACF, the former displaying both positive and negative correlations at all lags values while the latter presented only positive autocorrelated lags at 11, 12, and 13 months. DA only showed two positive lags at 1 and 13 months. DSTs showed a higher number of lags autocorrelation by PACF, at low lags and high lags months. PSTs showed one negative partial autocorrelated lag and two positive (10, 11 months). DA only presented one lag autocorrelated (13 months) by PACF.

Temporal-Spatial Analysis

Temporal and Spatial Dynamics

The PCA analysis identified common patterns that emerged from the similarities (correlation) of temporal dynamics and their association with particular aggregation boxes across the coastline. These are portrayed in a low number of dimensions, principal components (PC), that identify the main variables

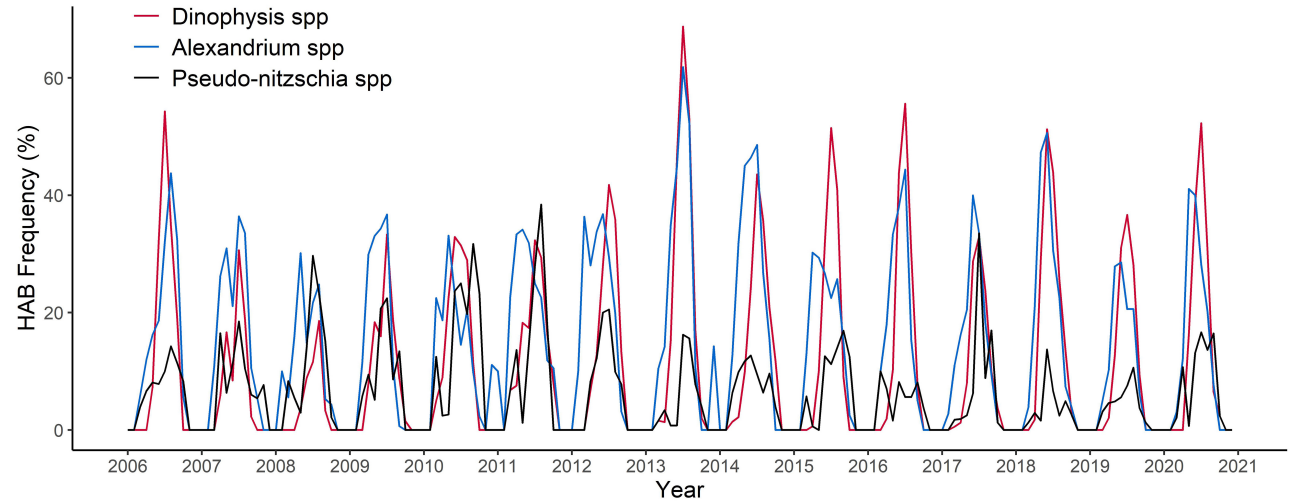

FIGURE 2 | Time series of the proportional frequency of monthly HAB events for genera: *Dinophysis* spp. DSTs -related (red line), *Alexandrium* spp. PSTs-related (blue line), *Pseudo-nitzschia* spp. DA -related (black line) from 2006 to 2020 in Scotland. Total number of samples 16,987.

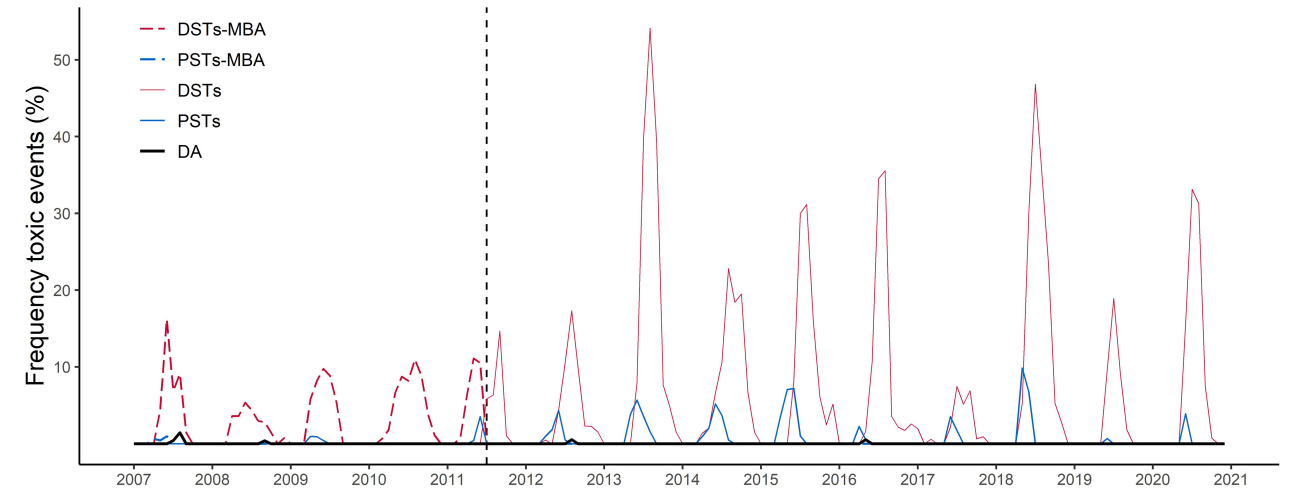

FIGURE 3 | Time series of the proportional frequency of biotoxin monthly events above safety limits from 2007 to 2020 in Scotland, for DSTs-MBA (dashed red line), PSTs-MBA (dashed blue line) (biological assay); DSTs (red line), PSTs (blue line), and DA (black line) (using instrumental method). Vertical dotted line in July 2011 marks the start of the use of the LC-MS/MS method for DSTs quantification in mussels. In previous years, MBA were mainly used. See **Table 1** for definition of abbreviations. Total number of tests performed 58,808.

that play a role in regulating HAB variance. The first principal component (PC1) described ∼56% of *Dinophysis* spp. monthly variance, the highest value amongst the phytoplankton groups. PC1 also described ∼42% of the variance for *Alexandrium* spp. and the lowest ∼27% for *Pseudo-nitzschia* spp. *Dinophysis*, *Alexandrium,* and *Pseudo-nitzschia* showed high and positive PC1 sample scores in years and months of high occurrence of HAB events (**Figures 5A–F**). Thus, PC1 could be related to the common coastal temporal patterns and seasonality marking HABs occurrence. Spatial patterns were assessed using monthly factor loadings (correlations between frequencies and PC1 scores) for the time series in each aggregation box. *Dinophysis* spp. had positive PC1 loadings for all aggregation boxes and a noticeable difference between areas in the southwest coast, the northwest coast, east coast, Isle of Lewis (boxes 13,14), and the Northern Isles (Orkney and Shetland Islands) (**Figure 5G**). This suggests blooms follow a regional pattern, with an important difference in seasonality between southwest and northwest areas. For *Alexandrium,* locations with similar loadings were dispersed throughout the coastline (**Figure 5H**). The highest *Alexandrium* PC1 loadings (0.21–0.3) were in two southwest areas, the central west coast, the northwest coast and the Northern Isles. Lower *Alexandrium* PC1 loadings were found for boxes in sheltered inner lochs of the west coast, Isle of Lewis, east coast and southern areas of the Shetland Islands. Areas showing similar correlations with PC1 for *Pseudo-nitzschia* spp. were

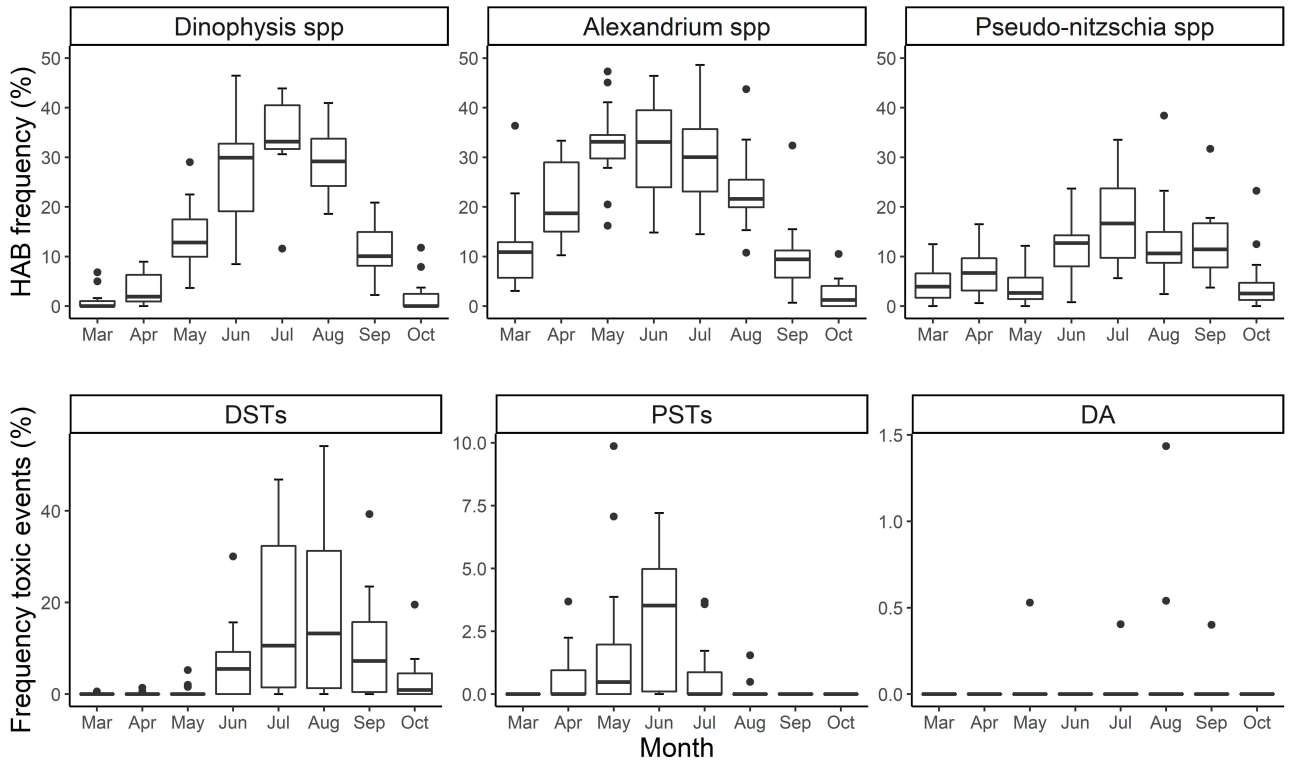

FIGURE 4 | Boxplots of the monthly incidence of HAB taxa: *Dinophysis* spp., *Alexandrium* spp., *Pseudo-nitzschia* spp., and HAB toxins: DSTs, PSTs, DA. Boxplots display the median (bold horizontal line), upper and lower quartile (hinge), maximum and minimum range (whiskers) and outliers (dots above whiskers) of the yearly average of events by month.

widely dispersed with high positive values across the southwest, central coast, northwest, Isle of Lewis and the Shetland Islands (**Figure 5I**). In summary, PC1 for each species captured the temporal pattern of blooms and hence the role of seasonality. The lower proportion of variation explained by PC1 for *Pseudo-nitzschia* spp. suggests local conditions or other variables might have a greater influence on the incidence of HABs for this genus than for *Dinophysis* spp. and *Alexandrium* spp.

The second principal component (PC2) explained a lower proportion of the variance of HAB incidence than PC1: ∼6% for *Dinophysis*, ∼7% for *Alexandrium* and ∼8% for *Pseudo-nitzschia* but was instructive in demonstrating the timing and location of blooms around the country. The PC2 sample scores portray positive or negative scores according to the timing in the year (**Figures 6A–C**). Annual sample scores display an up-down trend of between 1 and 3 years, with no particular association with high incidence years, which could indicate an interannual shifting of bloom location (**Figures 6D–F**). *Dinophysis* showed high and positive monthly PC2 loadings (0.2–0.4) in the southwest and one area in the northeast coast (**Figure 6G**). Negative *Dinophysis* PC2 loadings were rare, the lowest (−0.4–−0.2) observed in the Isle of Harris and Northern Isles (Shetland and Orkney Islands). The pattern suggests there is a temporal shift of bloom location with the high incidence of blooms that peak in July in the Isle of Lewis and the Northern Isles, with "early" (May) and "late" (September) blooms occurring on the southwest coast (Firth of Clyde). *Alexandrium* PC2 loadings were primarily positive in west coast areas, whilst negative values were focused on the Isle of Lewis (aggregation box 13, 14), the Northern Isles (aggregation box 1–5), and two areas in the central west coast (aggregation box 18–20) (**Figure 6H**). This suggests "early" blooms are focused on the south, central and north coast and "summer" blooms are associated with the Isle of Lewis and the Northern Isles (**Figure 6H**). For *Pseudo-nitzschia,* "early" and "late" season blooms (March, April, and September, October, respectively) were associated with negative PC2 sample scores; whilst "summer" blooms during May to August mainly showed positive scores (**Figure 6I**). *Pseudo-nitzschia* PC2 loadings were spatially variable with little regional pattern. For example, negative PC2 were evident in the west coast and near the island of Mull, but the adjacent Loch Fyne (aggregation boxes 21, 22) exhibited high values. "Early" (March-April) and "late" (September-October) blooms were associated with the central west coast (aggregation box 19, 20), east coast (aggregation boxes 6–7) and the south of the Shetlands (aggregation box 4), while "summer" blooms were related to the Isle of Lewis, Orkney Island, Shetland Islands (except the previous mentioned aggregation box) and the southwest coast.

Harmful Algal Bloom Occurrence Risk

The PCA allowed the identification of areas that shared temporal dynamics, and the role of seasonality in regulating the

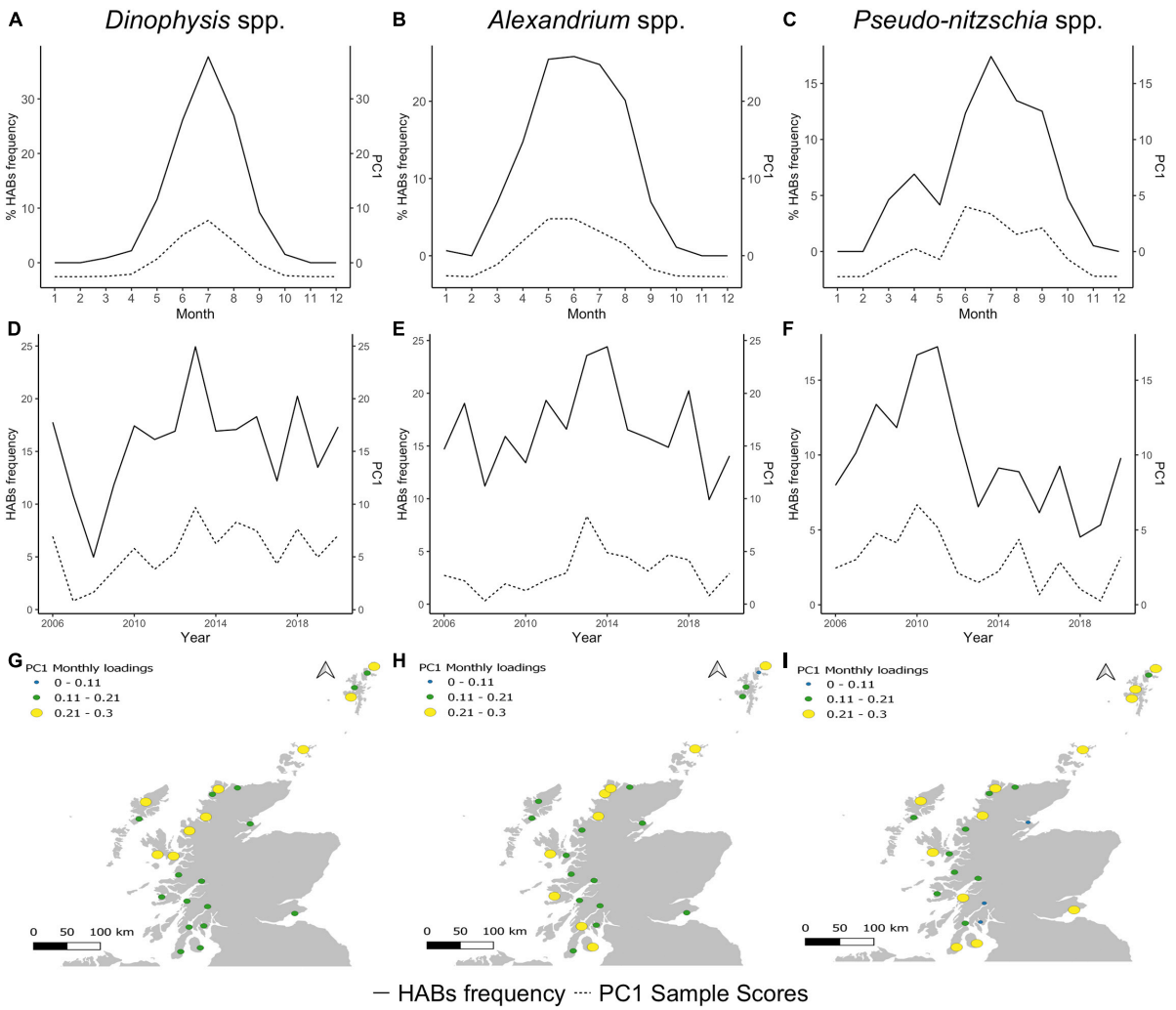

FIGURE 5 | First principal component (PC1) of *Dinophysis* spp., *Alexandrium* spp. and *Pseudo-nitzschia* spp. **(A–C)** Monthly sample scores, **(D–F)** annual sample scores, **(G–I)** monthly factor loadings per aggregation box.

different HAB genera. However, PCA results are independent of the magnitude of blooms, and hence to evaluate spatial trends in abundance we used the K-means test to cluster aggregation boxes that showed similar bloom size and timing, hence identifying similar levels of risk on a monthly and annual scale. In all cases, the elbow plot suggested using four clusters for analyses of monthly data. The K-means clustering explained almost ∼70% of variance in monthly *Dinophysis* and *Alexandrium* HAB frequencies (between_SS/total_SS = 71.9%, between_SS/total_SS = 68.2%, respectively) and *Pseudo-nitzschia* ∼50% (between_SS/total_SS = 52.1%). The monthly clusters of *Dinophysis* followed a similar trend, peaking in July (**Figure 7A**). However, bloom occurrence across the year varies between clusters with the "very-high" cluster exhibiting elevated risk both "early" (in April) and "late" (in October) in the year. In contrast to *Dinophysis* where clusters rarely overlapped, *Alexandrium* (**Figure 7B**) and *Pseudo-nitzschia* (**Figure 7C**) exhibited similar frequency of "early" and "late" blooms for all clusters. The "high" cluster exhibited "early" blooms by the increase of K-means from March to a peak in May for *Alexandrium* and April for *Pseudo-nitzschia*. The "very-high" cluster rapidly increased later in the year than the "high cluster" but then markedly exceeded it and all other clusters from June to September. *Alexandrium* "moderate" and "low" clusters showed similar seasonal patterns, but at different magnitudes. An increase in *Pseudo-nitzschia* risk was noted for the "very-high" and "high" clusters in spring (March-April), with the "moderate" cluster also being somewhat elevated in April. All clusters decreased in May, before a further summer increase during which bloom patterns differed amongst all clusters from June to October. For all genera, there was a distinct "low" cluster that exhibited consistently lower K-means peaking in July for *Dinophysis*, May and June for *Alexandrium* and June for *Pseudo-nitzschia*, remaining somewhat elevated until September for the latter genus. Thus *Dinophysis* blooms followed a similar temporal occurrence across clusters while *Alexandrium* and *Pseudo-nitzschia* showed a shift between "early" and "summer" blooms from low to high risk clusters.

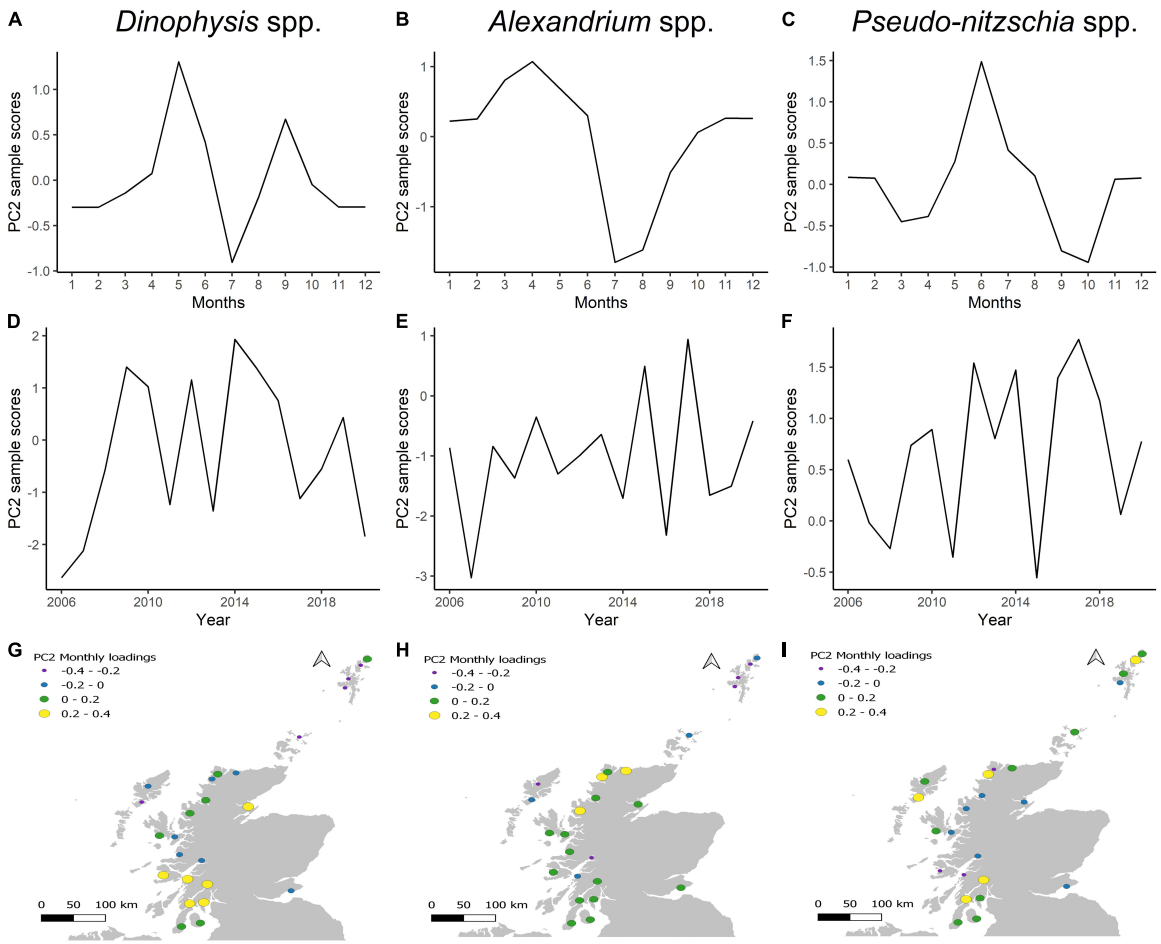

FIGURE 6 | Second principal component (PC2) of *Dinophysis* spp., *Alexandrium* spp., and *Pseudo-nitzschia* spp. **(A–C)** Monthly sample scores. **(D–F)** Annual sample scores. **(G–I)** Monthly factor loadings per aggregation box.

Members of "very-high" and "high" *Dinophysis* HAB-risk clusters were in the southwest, central west, northwest coast and south Shetland Islands (aggregation boxes: 3, 4, 9, 10, 12, 13, 15–17, 19–23, 25) (**Figure 7D**). The "low" risk cluster is scattered around the country, primarily on the Isle of Harris, Orkney Island, one area in the Shetland Islands, but also including the only east coast area and one mainland west coast location (aggregation boxes 2, 5, 6, 14, 18). For *Alexandrium*, the "very-high" HAB-risk cluster was only in one area in the west of Lewis and another in the south of the Shetland Islands; whilst the "high" cluster areas were more widespread, located in the southwest coast, central west coast, northwest coast, northeast and north of the Shetlands (**Figure 7E**). Areas assigned to the "low" *Alexandrium* HAB-risk cluster were in the southwest, southeast, Orkney and one in the Shetlands. The "very-high" risk cluster for *Pseudo-nitzschia* is located uniquely in two areas in the south of the Shetland Islands (**Figure 7F**). A high proportion of the areas correspond to the "low" cluster, the majority being in the southwest coast.

Clustering the annual data into four clusters explained a similar proportion of the variation to the clustering of monthly data: ∼60% of the variance in *Dinophysis* spp. (between_SS/total_SS = 63.5%), ∼50% for *Alexandrium* (between_SS/total_SS = 50.8%) and ∼60% for *Pseudo-nitzschia* (between_SS/total_SS = 61.1%). Risk varied from year to year, *Dinophysis* clusters displayed similar annual K-means patterns across the years (**Figure 8A**), but the relative level or risk remains consistent (i.e., "Very-high" risk areas had consistently higher risk than "high" risk areas). A noticeable difference was observed for the annual trends of *Alexandrium* (**Figure 8B**) and *Pseudo-nitzschia* (**Figure 8C**), with K-means showing considerable interannual variability for all clusters. Despite the "very-high" cluster scoring the highest risk in the majority of years, the "high" cluster exhibited similar risk levels from 2011 onward for *Alexandrium*, and exceeded "very high" cluster risk levels in 2015 for *Pseudo-nitzschia*. The distribution of clusters, in general, follows the monthly *Dinophysis* (**Figure 8D**) and *Pseudo-nitzschia* (**Figure 8F**) K-means analysis. For *Dinophysis*, the "very-high" and "high" clusters were mostly on the southwest coast, the islands of the central and northern west coast and the Shetland Islands, with "low" risk clusters on the east coast and Orkney Islands. For *Pseudo-nitzschia*, the "very-high" cluster is

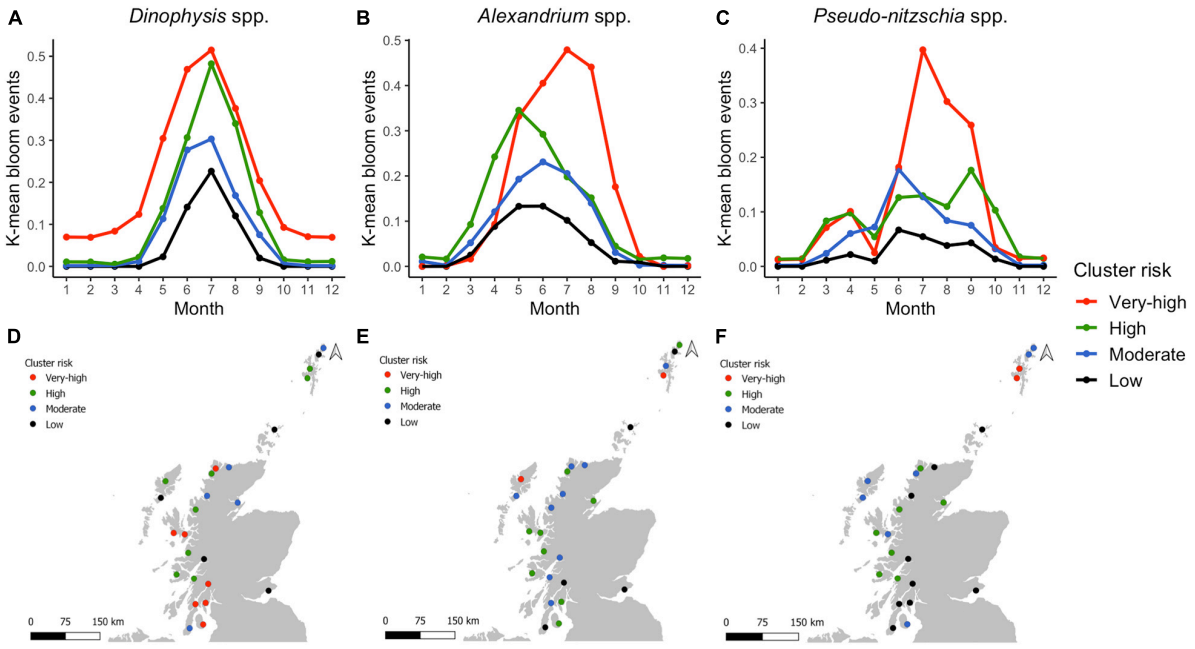

FIGURE 7 | *Dinophysis* spp., *Alexandrium* spp., and *Pseudo-nitzschia* spp. **(A–C)** Monthly K-means for each cluster. **(D–F)** Monthly K-means according to the HAB risk per aggregation box distributed in Scotland.

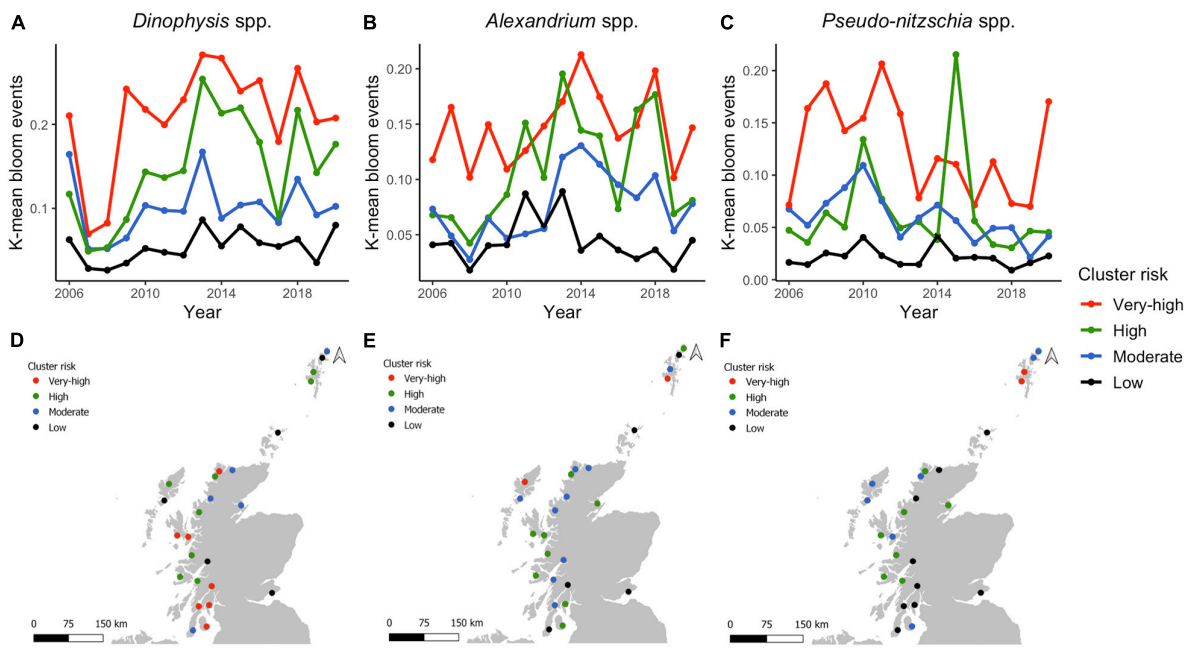

FIGURE 8 | *Dinophysis* spp., *Alexandrium* spp., and *Pseudo-nitzschia* spp. **(A–C)** Annual K-means for each cluster. **(D–F)** Annual K-means according to the HAB risk per aggregation box distributed in Scotland.

only in the south of Shetland Islands, with the "low risk cluster mainly on the southwest coast. The location of the *Alexandrium* clusters differed between monthly and annual values, "very-high and "high" risk is scattered in the west coast, west and Northern Isles (**Figure 8E**).

The spatial risk of the aggregation boxes used the monthly K-means classification, this was averaged and classified in a cluster rank (**Supplementary Table 1**). The total average risk was 2.36, with a maximum value of 3.67 in the south of the Shetland Islands and a minimum of 1.00 in the Orkney Islands

and the southeast coast. The highest combined risk locations (average above 3) were scored by the south Shetlands Island (box 4) and the South Isle of Skye (box 16). High scores (average of 3) included seven locations: the southwest of the Shetland Islands (box 3), the northwest coast (box 9), the north of the Isle of Lewis (box 13), southeast of Skye (box 15), Loch Ailort (box 17), the Isle of Mull (box 19) and the Isle of Arran (box 25). Five locations were identified as the lowest combined risk (average below 1.50), located in the south of the Kintyre Peninsula (box 24), central west inner loch-Loch Linnhe (box 18), the south east coast (box 6), the Orkney Islands (box 5) and the northwest Shetland Islands (box 2). High and low risk locations were significantly associated for *Dinophysis* spp. and *Alexandrium* spp. (correlation among risk scores, $r = 0.44$, $p < 0.05$), and *Alexandrium* spp. with *Pseudo-nitzschia* spp. (0.48, $p < 0.05$), but risk scores for *Dinophysis* spp. showed only a weak non-significant correlation with those for *Pseudo-nitzschia* spp. (0.29, $p > 0.05$).

Harmful Algal Bloom Relationships With Environmental Variables

Correlation was applied to evaluate any possible association between HABs annual frequency and annual mean of environmental variables (**Table 2**). This was conducted at a countrywide level as environmental information is not collected with sufficient spatial resolution for a regional analysis. The only positive significant correlation was found between the NAO index and the genus *Alexandrium* and corresponding PSTs toxins. *Dinophysis* spp. and SST were correlated negatively significant on an annual basis. There were no significant relationships between other taxa or biotoxins with SST or wind (intensity and direction).

TABLE 2 | Analyses of relationships of annual incidence of HABs and toxic events above the safety threshold with annual averages of environmental variables from 2006 to 2018.

Species/Biotoxin	SST	NAO index	Wind
Dinophysis spp.	–0.59*	0.18	0.23
DSTs	–0.52	0.48	0.66
Alexandrium spp.	–0.19	0.58*	0.69
PSTs	–0.34	0.68*	0.75
Pseudo-nitzschia spp.	–0.04	–0.48	0.39
DA	0.01	–0.49	0.67

*Correlation analyses was used to evaluate relationships with annual SST and annual North Atlantic Oscillation (NAO) index, using the rcorr() function in R. Linear regression was used to evaluate relationships with the annual wind values, using the directional north-south component [windspeed × sine(direction angle)] and east-west component [windspeed × cosine(direction angle)] as two terms in the regression equation. The result of the wind analysis was reported as the square root of the regression R^2 for comparison with correlations. *Significance $p \leq 0.05$.*

DISCUSSION

Interannual Variability of Harmful Algal Blooms

The analysis of temporal-spatial patterns is crucial for determining the risk of phytoplankton species of major concern to shellfish aquaculture in Scotland. Over the 15 years of the time series, we observed high interannual variability between years with no statistically significant trend in harmful bloom or shellfish biotoxin frequency for all taxa and toxins. This is consistent with other site specific case-studies (Moore et al., 2009; Díaz et al., 2016) and agrees with the recent analysis of global data series (Hallegraeff et al., 2021), which attributed the perceived increase in HAB events to intensified monitoring.

Furthermore, the frequencies of annual blooms and toxic events were found not to be correlated across years, suggesting annual HAB occurrences are independent and are not influenced by the previous year. The only exception was observed at a lag of 1 year for *Pseudo-nitzschia* spp. Given that this taxon is not thought to form resting stages (Azanza et al., 2018) this observation could potentially be related to a common biological response in consecutive years to similar environmental conditions. An earlier study (Rowland-Pilgrim et al., 2019) did not find a correlation between *Pseudo-nitzschia* spp. cell density and DA concentration in the same time series from 2008 to 2018.

The annual frequency of blooms of the dinoflagellates *Dinophysis* spp. and *Alexandrium* spp. were similar and significantly correlated. Hence, although the temporal and spatial dynamics of blooms of the two taxa within and between years differ, the data suggest that on a countrywide basis "good" and "bad" years exist for harmful dinoflagellate blooms. However, no correlation with readily available environmental drivers (SST, wind) were found. *Dinophysis* is a holoplanktonic genus with blooms having been described to develop offshore with advective transport to the coast (Whyte et al., 2014). In contrast, *Alexandrium* spp. forms cysts that are deposited in the benthos and hatch under the right conditions. Hence, the observed dynamics could be related to the group trait or succession pattern described by Smayda and Reynolds (2001), overcoming life cycle differences. A deeper understanding of the role of environmental variables is needed to determine the triggers for blooms of these harmful taxa.

Temporal and Spatial Bloom Dynamics

HAB occurrence in general followed the well-known seasonal pattern, with most blooms occurring from March to October. *Dinophysis* spp. and *Pseudo-nitzschia* spp. blooms reached a peak in July, and *Alexandrium* spp. exhibited a plateau from May to July. *Pseudo-nitzschia*, similarly to *Alexandrium*, exhibited two peaks throughout the year in spring and summer associated with specific locations. This confirms, countrywide, the characteristic temporal profile for this taxon demonstrated from local monitoring by Fehling et al. (2006). The crucial role of seasonality in regulating bloom dynamics was confirmed by the temporal patterns and significant autocorrelation between monthly occurrences for all genera. Seasonality is considered as a key driver of the phytoplankton composition, including dinoflagellate and diatom species in the west and east coast of Scotland (Bresnan et al., 2015). The environmental conditions during winter hinder the development of blooms, since Scottish waters are exposed to frequent storms leading to intense mixing of the water column; with light intensity and water

temperature being below the optimal conditions of growth. During spring, increasing irradiance intensity and duration, and an increase of water temperature and general decrease of storms result in ideal conditions for phytoplankton cell growth and higher incidence of blooms. Initially these are primarily diatom dominated, and then as nutrient concentrations decrease and stratification intensifies dinoflagellates become more prevalent (Davidson et al., 2011). These patterns are associated with Scottish transitional waters being regulated by the seasonal heating and cooling cycle (Edwards et al., 2013). However, despite the critical role of seasonality, its influence varied for the different HAB taxa. Greatest control was observed for *Dinophysis* spp. with seasonality, reflected in PC1, explaining over 50% of variance, perhaps because of its heterotrophic nature and the requirement for ciliate prey that are most prevalent in summer months (Reguera et al., 2012). In contrast, the lower proportion of variance explained and number of monthly lags autocorrelated for *Pseudo-nitzschia* spp. suggest seasonality is not as crucial factor for the development of blooms of this genus, with other factors such as local environmental conditions making dissolved silica available or stochastic effects being more important. As noted above, the differences in the seasonal peaks of the *seriata* and *delicatissima* groups of *Pseudo-nitzschia* are also responsible for the relative lack of seasonality of the genus as a whole.

Dinophysis presented the greatest bloom frequency. The countrywide interannual patterns observed are consistent with abundance observations at two targeted locations on the west coast of Scotland (Swan et al., 2018) and offshore patterns found in the Northeast Atlantic from Continuous Plankton Recorder data (Dees et al., 2017), and do not confirm the model based predictions of Gobler et al. (2017) of a climate driven increase in the abundance of *Dinophysis acuminata* in the region. The monthly and annual *Dinophysis* analysis using K-means categories, determined that the blooms respond similarly between clusters at a regional scale, but with varying levels of risk. The "very-high" cluster was predominantly located in the southwest coast, particularly in the Firth of Clyde, and was associated with "early" and "late" season blooms, as well as the highest mid-summer bloom frequency. The spatial distribution of the two highest K-means clusters was located predominantly on the west coast and the south of the Shetland Islands for both monthly and annual data series. Whereas the central west, northwest, Isle of Lewis and Shetland Islands are likely to respond to seasonal conditions in a shorter season, according to the principal components. These areas could be susceptible to the advective transportation of cells, since this has been attributed as the main reason of *Dinophysis* blooms rather than the *in situ* growth of cells (Smayda and Reynolds, 2001). Conditions such as local seasonal stratification or the development of frontal regions have previously been shown to regulate *Dinophysis* blooms at the species level with late summer *Dinophysis acuta* blooms occurring only in some years in two hydrologically different locations (Firth of Clyde and Loch Ewe) (Swan et al., 2018).

For *Alexandrium*, the spatial statistical tests indicated a shift of bloom location between "early" and "late" (summer) occurrence. "Early" blooms corresponding to the "high" risk cluster are geographically dispersed, predominantly on the west coast (south, central, north), while summer blooms portrayed by the "very-high" risk cluster are predominantly in the northeast of the Isle of Lewis and south of the Shetland Islands. The use of different cluster numbers ($k = 5, 4, 3$) consistently identified these areas as high-risk areas. These results confirm earlier observational studies that identified Orkney and Shetland Islands as *Alexandrium* "hotspots" in June and July (Bresnan et al., 2006). A decade-long time series (1996–2005) showed high densities in the Western Isles, Orkney and Shetland Islands; the location reaching the highest average annual cell densities and PSP levels amongst all areas (Brown et al., 2010). The "low" risk clusters located in two southwest locations, the east coast and the Orkney Islands differed from another study that found low maximum cell densities in lochs in the central west coast (Brown et al., 2010). Furthermore, the lowest combined risk for all taxa, including *Alexandrium*, is located in the south of the Kintyre Peninsula; however, the nearby area of Campbeltown recorded the highest PSTs value within the 2007–2020 data series (27,822 μg/kg) in April 2015.

Pseudo-nitzschia bloom occurrence showed, as did *Alexandrium*, a temporal-spatial shift between "early" and "summer" blooms. The monthly occurrence of all clusters increased during spring, commonly associated with the increase of nutrient availability, light intensity and duration. "Very-high" and "high" risk clusters exhibited similar K-means levels early in the year. A decrease of bloom events was observed after the spring bloom (March-April), showing low levels in May. This decreasing trend has been previously associated with the depletion of nutrients in the water column (Fehling et al., 2006). The spatial statistics identified the shift of bloom dynamics, with a higher occurrence during summer, especially for the "very-high" cluster, focusing on the south of the Shetlands (aggregation box 4). The increase in bloom occurrence during summer in our results is consistent with another study using the FSS data series, that identified an increasing trend of the taxon's cell abundance during summer and rare events of domoic acid above the permitted levels in shellfish tissue (Rowland-Pilgrim et al., 2019).

Spatially, high and low-risk areas are mainly differentiated by their orientation rather than geographical proximity, but also varying according to the taxa. The "high-risk" locations mainly face in a southwest direction. On the Scottish west shelf, water flows in a predominantly northwards direction governed by the Scottish Coastal Current (Hill and Simpson, 1988). The advection of cells from offshore waters, driven by this current has previously been identified as a means of transportation of *Alexandrium tamarense* (Hill et al., 2008) and *Karenia mikimotoi* (Hill et al., 2008; Gillibrand et al., 2016). The advection from offshore waters has also been associated with the transport of *Pseudo-nitzschia* spp. (Fehling et al., 2012) and *Dinophysis* spp. cells (Paterson et al., 2017). This potentially explains the "very-high" risk of *Dinophysis* in southwest facing sea lochs in the South of the country.

Phytoplankton and Biotoxin Relationship

Contamination of shellfish with DST is related to the presence of *Dinophysis* cells in the water column, with the shellfish toxin

concentration gradually increasing until it potentially surpasses the MPL. The high incidence and seasonal trend observed for *Dinophysis* and DSTs occurrence above the safety threshold and the significant correlation of such annual frequencies demonstrated the close link between this phytoplankter and shellfish toxicity. *Dinophysis* cells exhibit diverse levels of toxicity through the presence of different species with different toxin profiles (Swan et al., 2018). *Dinophysis acuminata* (linked with the production of okadaic acid and dinophysistoxin-1) has been found to be the predominant species in late spring and summer (June-August) in Scottish waters (Stern et al., 2014; Swan et al., 2018), whilst *D. acuta* (producer of dinophysistoxin-2) is found occasionally from July onward, but can be associated with extended toxic events (Swan et al., 2018). Our study found a prolonged toxicity of DSTs in shellfish events in late autumn (September-October) when the occurrence of *Dinophysis* above the safety threshold is low, likely demonstrating the slow depuration of these toxins from shellfish flesh (Svensson, 2003). Similar temporal dynamics of *D. acuminata* and *D. acuta* have also been found in Iberia (Moita et al., 2016).

Previous studies have demonstrated that a number of toxic and non-toxic species of *Alexandrium* exist in Scottish waters. PST shellfish toxicity in Scotland is thought to be primarily related to toxic *Alexandrium catenella* (formerly identified as *Gonyaulax excavata*, *Alexandrium fundyense*, and/or Group I ribotype/North American *Alexandrium tamarense*). However, monitoring identifies cells to genus only and the morphologically indistinguishable non-toxic *A. tamarense* can co-occur (Touzet et al., 2010) and hence be enumerated in the monitoring program. The presence of non-toxic strains of *A. minutum* in Scottish waters has been also detected (Lewis et al., 2018). In an ideal scenario, regulatory monitoring would enumerate only toxic *Alexandrium*. However, difficulty in discriminating between species on a rapid routine basis within a monitoring program has led the regulator to take a precautionary approach for the monitoring of *Alexandrium* (and our other genera of interest). Observations of high concentration of cells but low or absent toxicity exist (Higman et al., 2001). Moreover, temperature (and other environmental drivers) may impact excystment (Collins et al., 2009), competition (Davidson et al., 1999; Eckford-Soper et al., 2016) and toxicity (Flynn et al., 1994). However, our study found a correlation between the annual frequency of *Alexandrium* cells above the safety threshold and toxicity levels above the MPL. This concurs with other studies of cell abundance and PST concentrations (Bresnan et al., 2006; Stobo et al., 2008; Brown et al., 2010) and hence confirms the suitability of identifying *Alexandrium* to genus level as a means of ensuring shellfish safety.

When viewed as a time series, the annual frequency of *Pseudo-nitzschia* events above the safety threshold and domoic acid did not correlate, consistent with studies using cell densities and biotoxin levels (Hinder et al., 2011; Bresnan et al., 2017; Rowland-Pilgrim et al., 2019). Conversely, another study limited to two locations in Scotland for a period of 2 years (2001–2003) found a significant correlation using a 1.5 week temporal lag, associated with the fast uptake and depuration of the biotoxin by *M. edulis* (Bresnan et al., 2017). The non-correlation between *Pseudo-nitzschia* cells densities and domoic acid has been attributed to the variation in toxin content according to the group, species within the group, and size of the cells (Smayda, 2006). The rare occurrence of domoic acid events above the MPL during spring *Pseudo-nitzschia* spp. blooms could be explained by the presence of *P. delicatissima* group species containing low levels of DA per cell, or non-toxic members of the *P. delicatissima* group, predominant during spring (Fehling et al., 2006). Toxic events in late summer could be explain by the presence of the *P. seriata* group which contains species known to synthesize high levels of domoic acid (Smayda, 2006) and which are mostly found during the summer months (Fehling et al., 2006) and are infrequently observed during spring in Scottish waters (Paterson et al., 2017). A further confounding factor is that the decrease of the frequency of biotoxins above the maximum permitted level, specifically for PSTs, might be due to the high number of site closures for DSTs predominantly in July and August. Sampling is suspended, even if *Alexandrium* was still present in the water samples, hence the presence of a single biotoxin above the regulatory limit will cause under-sampling for the others.

Harmful Algal Blooms and Environmental Relationship

A range of conceptual models have been published to explain the relationship between different HAB genera and environmental conditions (see reviews of Reguera et al., 2012; Anderson, 2015; Bates et al., 2018). However, such models typically relate blooms to local environmental conditions that are not surveyed with the same fine temporal and spatial resolution as phytoplankton and biotoxins. Hence, to further evaluate the relationship between HAB events and those "large scale" environmental variables that are available in accessible databases, we used the correlation function to identify the direction and strength between these at a countrywide scale. At a climatological level, we found a significant positive correlation between the NAO index and the frequency of PSTs and producing genus *Alexandrium*. Positive NAO index leads to windier and turbulent conditions in the column water. Reports have suggested dinoflagellate blooms are enhanced under calm conditions (Smayda and Reynolds, 2001; Hinder et al., 2012). In contrast, the positive correlation between *Alexandrium* and PSTs could suggest turbulent conditions are strongly related to coastal bloom development. This again suggests HAB occurrences are not limited to regular seasonal environmental conditions; but that local conditions and atmospheric anomalies are likely to play a more important role in regulating these. The differences in correlation between the NAO index and the other environmental variables suggest the effect of the climatological system is not straightforward in that the NAO index is related to more climatological effects than just wind variation, and other variables are likely to be important in HAB development. The significant negative correlation between SST and *Dinophysis* blooms is consistent with another study that assessed the relationship between several dinoflagellate genera and this environmental variable (Hinder et al., 2012). The weak relationship between SST, wind and HAB events for most taxa and biotoxins might also be

explained by the large geographical scale used and high variability of the values in the time series. While genus based monitoring is thought to be suitable to safeguard human health within regulatory shellfish safety monitoring, the results strongly suggest cell enumeration to the group or species level in combination with higher resolution environmental monitoring would enhance the potential for phytoplankton counts to provide the early warning of shellfish toxicity that the shellfish industry require to minimize the economic losses associated with HABs.

CONCLUSION

The frequency of phytoplankton and biotoxin events above the safety threshold sampled by the Scottish shellfish safety monitoring programme did not show a significant increasing or decreasing trend in the last 15 years. HABs exhibited considerable variability, with non-correlation between annual frequencies of event indicating that blooms are not interannually related. A traditional seasonal pattern is observed for all taxa, reaching a monthly peak in July for *Dinophysis* spp. and *Pseudo-nitzschia* spp., with a plateau of blooms from May to July for *Alexandrium* spp. DSTs surpassed the MPL every year in the time series, PSTs in fewer years. The annual frequency of bloom and toxic events were significantly correlated with *Dinophysis* and *Alexandrium* and their respecting toxins. DA in contrast showed rare toxic events throughout the time series and correlation with *Pseudo-nitzschia* annual frequencies were non-significant. This has been attributed to the presence of non-toxic organisms, different factors regulating cell growth and biotoxin production and mussels' biotoxin assimilation rates. *Dinophysis* spp. and DSTs showed the highest frequency of events surpassing safety thresholds, representing the highest risk to the shellfish aquaculture in Scotland. The temporal analysis and spatial statistics (PCA and K-means) evidenced the crucial role seasonality plays on regulating timing, duration, intensity and location of HABs. But even with this consistent trend, known to be regulated by the cyclical Scottish waters, HAB dynamics vary according to the taxa and across the country. Relatively few countrywide relationships between HABs and environmental factors were found. Only the NAO index was significantly related to the HAB events of *Pseudo-nitzschia* spp. and PSTs. Despite this variable's influence on environmental conditions in the water column, the non-correlation between blooms and SST and wind (direction, intensity) demonstrates the relationship between the NAO index and blooms is not straightforward and HAB events are regionally controlled.

DATA AVAILABILITY STATEMENT

The raw data supporting the conclusions of this article will be made available by the authors, without undue reservation. Phytoplankton and biotoxin data can be accessed through the Food Standards Scotland (FSS).

AUTHOR CONTRIBUTIONS

FG, KD, and MB contributed to the design, statistical tests used, analysis and writing. SS contributed to the data analysis, interpretation and writing. AT contributed to the writing, especially the toxin analysis. All authors reviewed the results and approved the final version of the manuscript.

FUNDING

FG was funded by an Ocean Risk Ph.D. Scholarship from AXA XL. Additional support (KD) was received from the RCUK projects CAMPUS (NE/R00675X/1) and Off-Aqua (BB/s004246/1).

ACKNOWLEDGMENTS

All phytoplankton and biotoxin data were accessed through the Food Standards Scotland funded regulatory marine biotoxin monitoring program.

SUPPLEMENTARY MATERIAL

The Supplementary Material for this article can be found online at: https://www.frontiersin.org/articles/10.3389/fmars.2021.785174/full#supplementary-material

REFERENCES

Anderson, D. (2015). HABs in a changing world: a perspective on harmful algal blooms, their impacts, and research and management in a dynamic era of climatic and environmental change. *Harmful Algae* 2012, 3–17. doi: 10.1038/nature13478

Anderson, D. M., Boerlage, S. F. E., and Dixon, M. B. (2017). in *Harmful Algal Blooms (HABs) and Desalination: A Guide to Impacts, Monitoring and Management*, Vol. 78, eds D. M. Anderson, S. F. E. Boerlage, and M. B. Dixon (Paris: Intergovernmental Oceanographic Commission of UNESCO), 539.

Anderson, D. M., Stock, C. A., Keafer, B. A., Bronzino Nelson, A., McGillicuddy, D. J., Keller, M., et al. (2005). *Alexandrium fundyense* cyst dynamics in the Gulf of Maine. *Deep. Res. Part II* 52, 2522–2542. doi: 10.1016/j.dsr2.2005.06.014

Azanza, R. V., Brosnahan, M. L., Anderson, D. M., Hense, I., and Montresor, M. (2018). "The role of life cycle characteristics in harmful algal bloom dynamics," in *Global Ecology and Oceanography of Harmful Algal Blooms. Ecological Studies (Analysis and Synthesis)*, Vol. 232, eds P. Glibert, E. Berdalet, M. Burford, G. Pitcher, and M. Zhou (Cham: Springer). doi: 10.1007/978-3-319-70069-4_8

Báez, J. C., Real, R., López-Rodas, V., Costas, E., Salvo, A. E., García-Soto, C., et al. (2014). The North Atlantic Oscillation and the Arctic Oscillation favour harmful algal blooms in SW Europe. *Harmful Algae* 39, 121–126. doi: 10.1016/j.hal.2014.07.008

Barth, A., Walter, R. K., Robbins, I., and Pasulka, A. (2020). Seasonal and interannual variability of phytoplankton abundance and community composition on the Central Coast of California. *Mar. Ecol. Prog. Ser.* 637, 29–43. doi: 10.3354/meps13245

Bates, S. S., Hubbard, K. A., Lundholm, N., Montresor, M., and Leaw, C. P. (2018). Pseudo-nitzschia, Nitzschia, and domoic acid: new research since 2011. *Harmful Algae* 79, 3–43. doi: 10.1016/j.hal.2018.06.001

Belgrano, A., Lindahl, O., and Hernroth, B. (1999). North Atlantic Oscillation primary productivity and toxic phytoplankton in the Gullmar Fjord, Sweden (1985-1996). *Proc. R. Soc. B Biol. Sci.* 266, 425–430. doi: 10.1098/rspb.1999.0655

Berdalet, E., Fleming, L. E., Gowen, R., Davidson, K., Hess, P., Backer, L. C., et al. (2016). Marine harmful algal blooms, human health and wellbeing: challenges and opportunities in the 21st century. *J. Mar. Biol. Assoc. United Kingdom* 96, 61–91. doi: 10.1017/S0025315415001733

Bresnan, E., Arévalo, F., Belin, C., Branco, M. A. C., Cembella, A. D., Clarke, D., et al. (2021). Diversity and regional distribution of harmful algal events along the Atlantic margin of Europe. *Harmful Algae* 102:101976. doi: 10.1016/j.hal.2021.101976

Bresnan, E., Cook, K. B., Hughes, S. L., Hay, S. J., Smith, K., Walsham, P., et al. (2015). Seasonality of the plankton community at an east and west coast monitoring site in Scottish waters. *J. Sea Res.* 105, 16–29. doi: 10.1016/j.seares.2015.06.009

Bresnan, E., Fryer, R. J., Fraser, S., Smith, N., Stobo, L., Brown, N., et al. (2017). The relationship between *Pseudo-nitzschia* (Peragallo) and domoic acid in Scottish shellfish. *Harmful Algae* 63, 193–202. doi: 10.1016/j.hal.2017.01.004

Bresnan, E., Turrell, E., and Fraser, S. (2006). "Monitoring PSP toxicity and *Alexandrium* hotspots in Scottish waters," in *Proceedings Of the 12th HAB Meeting*, Copenhagen, 76–79.

Brown, L., Bresnan, E., Graham, J., Lacaze, J., Turrell, E., Collins, C., et al. (2010). Distribution, diversity and toxin composition of the genus *Alexandrium* (Dinophyceae) in Scottish waters. *Eur. J. Phycol.* 45, 375–393. doi: 10.1080/09670262.2010.495164

Chapelle, A., Gac, M., Le Labry, C., Siano, R., Quere, J., Caradec, F., et al. (2015). The Bay of Brest (France), a new risky site for toxic *Alexandrium minutum* blooms and PSP shellfish contamination (complete issue). *Harmful Algae News* 51, 4–5.

Coates, L., Parks, R., Swan, S., Davidson, K., Turner, A., Maskrey, B., et al. (2020). *Annual Report on the Results of the Shellfish Official Control Monitoring Programmes for Scotland–2019*. Aberdeen: Food Standards Scotland.

Collins, C., Graham, J., Brown, L., Bresnan, E., Lacaze, J. P., and Turrell, E. A. (2009). Identification and toxicity of *Alexandrium tamarense* (dinophyceae) in Scottish waters. *J. Phycol.* 45, 692–703. doi: 10.1111/j.1529-8817.2009.00678.x

Cowpertwait, P. S. P., and Metcalfe, A. V. (2008). *Introductory Time Series with R*. New York, NY: Springer.

Cusack, C., Dabrowski, T., Lyons, K., Berry, A., Westbrook, G., Salas, R., et al. (2016). Harmful algal bloom forecast system for SW Ireland. Part II: are operational oceanographic models useful in a HAB warning system. *Harmful Algae* 53, 86–101. doi: 10.1016/j.hal.2015.11.013

Davidson, K., Anderson, D. M., Mateus, M., Reguera, B., Silke, J., Sourisseau, M., et al. (2016). Forecasting the risk of harmful algal blooms. *Harmful Algae* 53, 1–7. doi: 10.1016/j.hal.2015.11.005

Davidson, K., and Bresnan, E. (2009). Shellfish toxicity in UK waters: a threat to human health? *Environ. Health* 8, 2–5. doi: 10.1186/1476-069X-8-S1-S12

Davidson, K., Tett, P., and Gowen, R. (2011). "Harmful algal blooms," in *Marine Pollution & Human Health*, eds R. Hester and R. Harrison (Cambridge: Royal Society of Chemistry), 95–127. doi: 10.1039/9781849732871-00095

Davidson, K., Whyte, C., Aleynik, D., Dale, A., Gontarek, S., Kurekin, A. A., et al. (2021). HABreports: online early warning of harmful algal and biotoxin risk for the Scottish Shellfish and finfish aquaculture industries. *Front. Mar. Sci.* 8:631732. doi: 10.3389/fmars.2021.631732

Davidson, K., Wood, G., John, E. H., and Flynn, K. J. (1999). An investigation of non-steady-state algal growth. I. An experimental model ecosystem. *J. Plankton Res.* 21, 811–837. doi: 10.1093/plankt/21.5.811

Dees, P., Bresnan, E., Dale, A. C., Edwards, M., Johns, D., Mouat, B., et al. (2017). Harmful algal blooms in the Eastern North Atlantic Ocean. *Proc. Natl. Acad. Sci. U.S.A.* 114, E9763–E9764. doi: 10.1073/pnas.1715499114

Dhanji-Rapkova, M., O'Neill, A., Maskrey, B. H., Coates, L., Teixeira Alves, M., Kelly, R. J., et al. (2018). Variability and profiles of lipophilic toxins in bivalves from Great Britain during five and a half years of monitoring: okadaic acid, dinophysis toxins and pectenotoxins. *Harmful Algae* 77, 66–80. doi: 10.1016/j.hal.2018.05.011

Díaz, P. A., Ruiz-Villarreal, M., Pazos, Y., Moita, T., and Reguera, B. (2016). Climate variability and *Dinophysis acuta* blooms in an upwelling system. *Harmful Algae* 53, 145–159. doi: 10.1016/j.hal.2015.11.007

Eckford-Soper, L. K., Bresnan, E., Lacaze, J. P., Green, D. H., and Davidson, K. (2016). The competitive dynamics of toxic *Alexandrium fundyense* and non-toxic *Alexandrium tamarense*: the role of temperature. *Harmful Algae* 53, 135–144. doi: 10.1016/j.hal.2015.11.010

Edwards, M., Bresnan, E., Cook, K., Heath, M., Helaouet, P., Lynam, C., et al. (2013). Impacts of climate change on plankton. *MCCIP Sci. Rev.* 2013, 1–10.

Fehling, J., Davidson, K., Bolch, C., and Tett, P. (2006). Seasonally of *Pseudo-nitzschia* spp. (Bacillariophyceae) in western Scottish waters. *Mar. Ecol. Prog. Ser.* 323, 91–105. doi: 10.3354/meps323091

Fehling, J., Davidson, K., Bolch, C. J. S., Brand, T. D., and Narayanaswamy, B. E. (2012). The relationship between phytoplankton distribution and water column characteristics in north west european shelf sea waters. *PLoS One* 7:e34098. doi: 10.1371/journal.pone.0034098

Fehling, J., Green, D. H., Davidson, K., Botch, C. J., and Bates, S. S. (2004). Domoic acid production by *Pseudo-nitzschia* seriata (Bacillariophyceae) in Scottish waters. *J. Phycol.* 40, 622–630. doi: 10.1111/j.1529-8817.2004.03200.x

Fischer, A. D., Brosnahan, M. L., and Anderson, D. M. (2018). Quantitative response of *Alexandrium catenella* cyst dormancy to cold exposure. *Protist* 169, 645–661. doi: 10.1016/j.protis.2018.06.001

Flynn, K., Franco, J. M., Fernandez, P., Reguera, B., Zapata, M., Wood, G., et al. (1994). Changes in toxin content, biomass and pigments of the dinoflagellate *Alexandrium minutum* during nitrogen refeeding and growth into nitrogen or phosphorus stress. *Mar. Ecol. Prog. Ser.* 111, 99–110. doi: 10.3354/meps111099

Fraga, S., Anderson, D. M., Bravo, I., Reguera, B., Steidinger, K. A., and Yentsch, C. M. (1988). Influence of upwelling relaxation on dinoflagellates and shellfish toxicity in Ria de Vigo, Spain. *Estuar. Coast. Shelf Sci.* 27, 349–361. doi: 10.1016/0272-7714(88)90093-5

Gillibrand, P. A., Siemering, B., Miller, P. I., and Davidson, K. (2016). Individual-based modelling of the development and transport of a *Karenia mikimotoi* bloom on the North-west European continental shelf. *Harmful Algae* 53, 118–134. doi: 10.1016/J.HAL.2015.11.011

Glibert, P. M., Anderson, D. M., Gentien, P., Graneli, E., and Sellner, K. (2005). The global, complex phenomena of Harmful Algal blooms. *Oceanography* 18, 136–147. doi: 10.5860/choice.28-0163

Gobler, C. J., Doherty, O. M., Hattenrath-Lehmann, T. K., Griffith, A. W., Kang, Y., and Litaker, R. W. (2017). Ocean warming since 1982 has expanded the niche of toxic algal blooms in the North Atlantic and North Pacific oceans. *Proc. Natl. Acad. Sci. U.S.A.* 114, 4975–4980. doi: 10.1073/pnas.1619575114

Hallegraeff, G. (1993). A review of harmful algal blooms and their appearante global increase. *Phycologia* 32, 79–99.

Hallegraeff, G. M. (2010). Ocean climate change, phytoplankton community responses, and harmful algal blooms: a formidable predictive challenge. *J. Phycol.* 46, 220–235. doi: 10.1111/j.1529-8817.2010.00815.x

Hallegraeff, G. M., Anderson, D. M., Belin, C., Bottein, M.-Y. D., Bresnan, E., Chinain, M., et al. (2021). Perceived global increase in algal blooms is attributable to intensified monitoring and emerging bloom impacts. *Commun. Earth Environ* 2:117. doi: 10.1038/s43247-021-00178-8

Herrera, L., and Escribano, R. (2006). Factors structuring the phytoplankton community in the upwelling site off El Loa river in northern Chile. *J. Mar. Syst.* 61, 13–38. doi: 10.1016/j.jmarsys.2005.11.010

Higman, W. A., Stone, D. M., and Lewis, J. M. (2001). Sequence comparisons of toxic and non-toxic *Alexandrium tamarense* (Dinophyceae) isolates from UK waters. *Phycologia* 40, 256–262. doi: 10.2216/i0031-8884-40-3-256.1

Hill, A. E., Brown, J., Fernand, L., Holt, J., Horsburgh, K. J., Proctor, R., et al. (2008). Thermohaline circulation of shallow tidal seas. *Geophys. Res. Lett.* 35:L11605. doi: 10.1029/2008GL033459

Hill, A. E., and Simpson, J. H. (1988). Low-frequency variability of the Scottish coastal current induced by along-shore pressure gradients. *Estuar. Coast. Shelf Sci.* 27, 163–180. doi: 10.1016/0272-7714(88)90088-1

Hinder, S. L., Hays, G. C., Brooks, C. J., Davies, A. P., Edwards, M., Walne, A. W., et al. (2011). Toxic marine microalgae and shellfish poisoning in the British isles: history, review of epidemiology, and future implications. *Environ. Health* 10:54. doi: 10.1186/1476-069X-10-54

Hinder, S. L., Hays, G. C., Edwards, M., Roberts, E. C., Walne, A. W., and Gravenor, M. B. (2012). Changes in marine dinoflagellate and diatom abundance under climate change. *Nat. Clim. Chang.* 2, 271–275. doi: 10.1038/nclimate1388

Kane, J. (2011). Multiyear variability of phytoplankton abundance in the Gulf of Maine. *ICES J. Mar. Sci.* 68, 1833–1841. doi: 10.1093/ICESJMS

Kassambara, A., and Mundt, F. (2020). factoextra: Extract and Visualize the Results of Multivariate Data Analyses. [WWW Document]. R Packag. version 1.0.7.

Available online at: https://CRAN.R-project.org/package=factoextra (accessed September 16, 2021).

Lever, J., Krzywinski, M., and Altman, N. (2017). Principal component analysis. *Nat. Methods* 14, 641–642. doi: 10.1038/nmeth.4346

Lewis, A. M., Coates, L. N., Turner, A. D., Percy, L., and Lewis, J. (2018). A review of the global distribution of *Alexandrium minutum* (Dinophyceae) and comments on ecology and associated paralytic shellfish toxin profiles, with a focus on Northern Europe. *J. Phycol.* 54, 581–598. doi: 10.1111/jpy.12768

Macqueen, J. (1967). "Some methods for classification and analysis of multivariate observations," in *Proceedings of the 5th Berkeley Symposium Mathematical Statistics and Probability*, Los Angeles, CA: University of California 1, 281–297.

Marchese, C., Castro de la Guardia, L., Myers, P. G., and Bélanger, S. (2019). Regional differences and inter-annual variability in the timing of surface phytoplankton blooms in the Labrador Sea. *Ecol. Indic.* 96, 81–90. doi: 10.1016/j.ecolind.2018.08.053

Mardones, J. I., Holland, D. S., Anderson, L., Bihan, V. L., Gianella, F., Clement, A., et al. (2020). "Estimating and mitigating the economic costs of harmful algal blooms on commercial and recreational shellfish harvesters," in *GlobalHAB. Evaluating, Reducing and Mitigating the Cost of Harmful Algal Blooms: A Compendium of Case Studied*, Vol. 59, ed. V. L. Trainer (Sidney, BC: PICES Scientific Report), 66–83.

Martino, S., Gianella, F., and Davidson, K. (2020). An approach for evaluating the economic impacts of harmful algal blooms: the effects of blooms of toxic *Dinophysis* spp. on the productivity of Scottish shellfish farms. *Harmful Algae* 99:01912. doi: 10.1016/j.hal.2020.101912

Met Office (2019). *MIDAS Open: UK hourly weather observation data, v201901 [WWW Document]*. Chilton, WI: Centre for Environmental Data Analysis. doi: 10.5285/8d85f664fc614ba0a28af3a2d7ef4533

Moita, M. T., Pazos, Y., Rocha, C., Nolasco, R., and Oliveira, P. B. (2016). Toward predicting *Dinophysis* blooms off NW Iberia: a decade of events. *Harmful Algae* 53, 17–32. doi: 10.1016/j.hal.2015.12.002

Moore, S. K., Mantua, N. J., Hickey, B. M., and Trainer, V. L. (2009). Recent trends in paralytic shellfish toxins in Puget Sound, relationships to climate, and capacity for prediction of toxic events. *Harmful Algae* 8, 463–477. doi: 10.1016/j.hal.2008.10.003

NOAA/National Weather Service (2021). *Climate Prediction Center. North Atlantic Oscillation [WWW Document]. Natl. Centers Environ. Predict*. Available online at: https://www.cpc.ncep.noaa.gov/products/precip/CWlink/pna/nao.shtml (Accessed January 12, 2018)

Paterson, R. F., McNeill, S., Mitchell, E., Adams, T., Swan, S. C., Clarke, D., et al. (2017). Environmental control of harmful dinoflagellates and diatoms in a fjordic system. *Harmful Algae* 69, 1–17. doi: 10.1016/j.hal.2017.09.002

Peperzak, L. (2003). Climate change and harmful algal blooms in the North Sea. *Acta Oecologica* 24, 139–144. doi: 10.1016/S1146-609X(03)00009-2

Philippart, C. J. M., Cadée, G. C., Van Raaphorst, W., and Riegman, R. (2000). Long-term phytoplankton-nutrient interactions in a shallow coastal sea: algal community structure, nutrient budgets, and denitrification potential. *Limnol. Oceanogr.* 45, 131–144. doi: 10.4319/lo.2000.45.1.0131

Phillips, M. R., Rees, E. F., and Thomas, T. (2013). Winds, sea levels and North Atlantic Oscillation (NAO) influences: an evaluation. *Glob. Planet. Change* 100, 145–152. doi: 10.1016/j.gloplacha.2012.10.011

PO.DAAC (2020). *National Centers for Environmental Information. Daily L4 Optimally Interpolated SST (OISST) In situ and AVHRR Anal. Ver. 2.1*. Pasadena, CA: PO.DAAC.

R Core Team (2021). *R: A Language and Environment for Statistical Computing*. Vienna: R Foundation for Statistical Computing.

Reguera, B., Riobó, P., Rodríguez, F., Díaz, P. A., Pizarro, G., Paz, B., et al. (2014). *Dinophysis* toxins: causative organisms, distribution and fate in Shellfish. *Mar. Drugs* 12, 394–461. doi: 10.3390/md12010394

Reguera, B., Velo-Suárez, L., Raine, R., and Park, M. G. (2012). Harmful *Dinophysis* species: a review. *Harmful Algae* 14, 87–106. doi: 10.1016/j.hal.2011.10.016

Rowland-Pilgrim, S., Swan, S. C., O'Neill, A., Johnson, S., Coates, L., Stubbs, P., et al. (2019). Variability of Amnesic Shellfish Toxin and *Pseudo-nitzschia* occurrence in bivalve molluscs and water samples–analysis of ten years of the official control monitoring programme. *Harmful Algae* 87:101623. doi: 10.1016/j.hal.2019.101623

Ruiz-Villarreal, M., García-García, L. M., Cobas, M., Díaz, P. A., and Reguera, B. (2016). Modelling the hydrodynamic conditions associated with *Dinophysis* blooms in Galicia (NW Spain). *Harmful Algae* 53, 40–52. doi: 10.1016/j.hal.2015.12.003

Siemering, B., Bresnan, E., Painter, S. C., Daniels, C. J., Inall, M., and Davidson, K. (2016). Phytoplankton distribution in relation to environmental drivers on the North West European Shelf Sea. *PLoS One* 11:e0164482. doi: 10.1371/journal.pone.0164482

Smayda, T. (2002). Adaptive ecology, growth strategies and the global bloom expansion of Dinoflagellates. *J. Oceanogr.* 58, 281–294.

Smayda, T. J. (1990). Novel and nuisance phytoplankton blooms in the sea: evidence for a global epidemic. *Toxic Mar. Phytoplankton* 40, 29–40.

Smayda, T. J. (2006). *Harmful Algal Bloom Communities in Scottish Coastal Waters: Relationship to Fish Farming and Regional Comparisons — A Review. Scottish Executive Environment Group Report*. Kingston, RI: University of Rhode Island.

Smayda, T. J., and Reynolds, C. S. (2001). Community assembly in marine phytoplankton: application of recent models to harmful Dinoflagellate blooms. *J. Plankton Res.* 23, 447–461. doi: 10.1093/plankt/23.5.447

Solic, M., Krstulovic, N., Marasovic, I., Baranovic, A., Pucherpetkovic, T., and Vucetic, T. (1997). Analysis of time series of planktonic communities in the Adriatic Sea: distinguishing between natural and man-induced changes. *Ocean. Acta* 20, 131–143.

Stern, R. F., Amorim, A. L., and Bresnan, E. (2014). Diversity and plastid types in *Dinophysis acuminata* complex (Dinophyceae) in Scottish waters. *Harmful Algae* 39, 223–231. doi: 10.1016/j.hal.2014.07.013

Stobo, L., Lacaze, J.-P. L., Scott, A., Petrie, J., and Turrell, E. (2008). Surveillance of algal toxins in shellfish from Scottish waters. *Toxicon* 51, 635–648. doi: 10.1016/j.toxicon.2007.11.020

Svensson, S. (2003). Depuration of Okadaic acid (Diarrhetic Shellfish Toxin) in mussels, *Mytilus edulis* (Linnaeus), feeding on different quantities of nontoxic algae. *Aquaculture* 218, 277–291.

Swan, S. C., Turner, A. D., Bresnan, E., Whyte, C., Paterson, R. F., McNeill, S., et al. (2018). *Dinophysis acuta* in scottish coastal waters and its influence on diarrhetic shellfish toxin profiles. *Toxins* 10, 1–20. doi: 10.3390/toxins10100399

Touzet, N., Davidson, K., Pete, R., Flanagan, K., McCoy, G. R., Amzil, Z., et al. (2010). Co-occurrence of the West European (Gr.III) and North American (Gr.I) ribotypes of *Alexandrium tamarense* (Dinophyceae) in Shetland, Scotland. *Protist* 161, 370–384. doi: 10.1016/j.protis.2009.12.001

Turner, A. D., Stubbs, B., Coates, L., Dhanji-Rapkova, M., Hatfield, R. G., Lewis, A. M., et al. (2014). Variability of paralytic shellfish toxin occurrence and profiles in bivalve molluscs from Great Britain from official control monitoring as determined by pre-column oxidation liquid chromatography and implications for applying immunochemical tests. *Harmful Algae* 31, 87–99. doi: 10.1016/j.hal.2013.10.014

Van Dolah, F. M. (2000). Marine algal toxins: origins, health effects, and their increased occurrence. *Environ. Health Perspect.* 108:133. doi: 10.2307/345463

Wells, M. L., Karlson, B., Wulff, A., Kudela, R., Trick, C., Asnaghi, V., et al. (2019). Future HAB science: directions and challenges in a changing climate. *Harmful Algae* 91, 1–18. doi: 10.1016/j.hal.2019.101632

Whyte, C., Swan, S., and Davidson, K. (2014). Changing wind patterns linked to unusually high *Dinophysis* blooms around the Shetland Islands, Scotland. *Harmful Algae* 39, 365–373. doi: 10.1016/j.hal.2014.09.006

Conflict of Interest: The authors declare that the research was conducted in the absence of any commercial or financial relationships that could be construed as a potential conflict of interest.

Publisher's Note: All claims expressed in this article are solely those of the authors and do not necessarily represent those of their affiliated organizations, or those of the publisher, the editors and the reviewers. Any product that may be evaluated in this article, or claim that may be made by its manufacturer, is not guaranteed or endorsed by the publisher.

frontiers | Frontiers in Marine Science

ORIGINAL RESEARCH
published: 14 April 2022
doi: 10.3389/fmars.2022.791329

Novel Methodologies for Providing *In Situ* Data to HAB Early Warning Systems in the European Atlantic Area: The PRIMROSE Experience

Manuel Ruiz-Villarreal[1], Marc Sourisseau[2], Phil Anderson[3], Caroline Cusack[4], Patricia Neira[5], Joe Silke[5], Francisco Rodriguez[6], Begoña Ben-Gigirey[6†], Callum Whyte[3], Solene Giraudeau-Potel[3], Loic Quemener[7], Gregg Arthur[8] and Keith Davidson[3]*

[1] Centro Oceanográfico de A Coruña, Instituto Español de Oceanografía (IEO, CSIC), A Coruña, Spain, [2] Ifremer, French Research Institute for Exploitation of the Sea, DYNECO PELAGOS, Plouzané, France, [3] Scottish Association for Marine Science (SAMS), Scottish Marine Institute, Oban, United Kingdom, [4] Ocean, Climate and Information Services, Marine Institute, Galway, Ireland, [5] Marine Environment and Food Safety Services, Marine Institute, Galway, Ireland, [6] Centro Oceanográfico de Vigo, Instituto Español de Oceanografía (IEO, CSIC), Vigo, Spain, [7] Ifremer, French Research Institute for Exploitation of the Sea, REM/RDT/DCM, Plouzané, France, [8] Shetland UHI, Shetland, United Kingdom

Harmful algal blooms (HABs) cause harm to human health or hinder sustainable use of the marine environment in Blue Economy sectors. HABs are temporally and spatially variable and hence their mitigation is closely linked to effective early warning. The European Union (EU) Interreg Atlantic Area project "PRIMROSE", Predicting Risk and Impact of Harmful Events on the Aquaculture Sector, was focused on the joint development of HAB early warning systems in different regions along the European Atlantic Area. Advancement of the existing HAB forecasting systems requires development of forecasting tools, improvements in data flow and processing, but also additional data inputs to assess the distribution of HAB species, especially in areas away from national monitoring stations, usually located near aquaculture sites. In this contribution, we review different novel technologies for acquiring HAB data and report on the experience gained in several novel local data collection exercises performed during the project. Demonstrations include the deployment of autonomous imaging flow cytometry (IFC) sensors near two aquaculture areas: a mooring in the Daoulas estuary in the Bay of Brest and pumping from a bay in the Shetland Islands to an inland IFC; and several drone deployments, both of Unmanned Aerial Vehicles (UAV) and of Autonomous Surface vehicles (ASVs). Additionally, we have reviewed sampling approaches potentially relevant for HAB early warning including protocols for opportunistic water sampling by coastguard agencies. Experiences in the determination of marine biotoxins in non-traditional vectors and how they could complement standard routine HAB monitoring are also considered.

Keywords: harmful algal blooms (HABs), HAB early warning, HAB observing system, autonomous imaging flow cytometry (IFC), drones, remotely piloted aircraft systems (RPAS), unmanned aerial vehicles (UAV), autonomous surface vehicles (ASVs)

OPEN ACCESS

Edited by:
Tomaso Fortibuoni, Istituto Superiore per la Protezione e la Ricerca Ambientale (ISPRA), Italy

Reviewed by:
Johan Robbens, Institute for Agricultural, Fisheries and Food Research (ILVO), Belgium
Aletta T. Yñiguez, University of the Philippines Diliman, Philippines
Holly Bowers, Moss Landing Marine Laboratories, United States
Raphael M. Kudela, University of California, Santa Cruz, United States

****Correspondence:***
Manuel Ruiz-Villarreal
manuel.ruiz@ieo.es;
manuel.ruiz@ieo.csic.es

†Present address:
Begoña Ben-Gigirey, European Union Reference Laboratory for Monitoring of Marine Biotoxins, Vigo, Spain

Specialty section:
This article was submitted to Marine Fisheries, Aquaculture and Living Resources, a section of the journal Frontiers in Marine Science

Received: *08 October 2021*
Accepted: *01 March 2022*
Published: *14 April 2022*

Citation:
Ruiz-Villarreal M, Sourisseau M, Anderson P, Cusack C, Neira P, Silke J, Rodriguez F, Ben-Gigirey B, Whyte C, Giraudeau-Potel S, Quemener L, Arthur G and Davidson K (2022) Novel Methodologies for Providing In Situ Data to HAB Early Warning Systems in the European Atlantic Area: The PRIMROSE Experience. Front. Mar. Sci. 9:791329. doi: 10.3389/fmars.2022.791329

1 INTRODUCTION

Harmful algal blooms (HABs) are increases in the density of certain phytoplankton species that cause harm to human health or hinder sustainable use of the marine environment in blue economy sectors (Wenhai et al., 2019). Some HAB species generate "shellfish poisoning syndromes" in humans, usually following the consumption of shellfish that have ingested the harmful cells and concentrated the toxin within their flesh (Berdalet et al., 2016). Other HABs can impact the health of farmed fish with significant economic consequences (Davidson et al., 2020). A variety of protists and prokaryotic photosynthetic organisms may be responsible for HAB episodes (Hallegraeff, 2004), including toxic and non-toxic species mainly from dinoflagellates, haptophytes, raphidophyceae, diatoms, pelagophyceans and cyanobacteria, among others, as detailed in the IOC-UNESCO taxonomic reference list of harmful microalgae (Lundholm et al., 2009). Their populations thrive under diverse environmental conditions and display different characteristics (e.g. morphological, chemotaxonomical and genetic), which enables their detection by multiple means depending on the applied technique (Stauffer et al., 2019).

HABs are temporally and spatially variable and hence their mitigation is closely linked to effective early warning. This is primarily achieved by a network of sampling sites located in the vicinity of aquaculture operations. According to the European Union (EU) Regulation No 853/2004 (European Parliament and Council, 2004) and its amendments, typically samples (water and shellfish) are collected on a weekly basis. Water samples are analysed by light microscopy to identify harmful organisms. Shellfish samples are investigated for marine biotoxins by using different instrumental techniques depending on the target analytes. In terms of shellfish safety, should concentration of HABs or their biotoxins in shellfish flesh exceed regulatory thresholds then harvesting restrictions are applied until the biotoxins depurate and the shellfish are safe for human consumption. The spatial and temporal changes of HAB species in the region are reviewed and discussed extensively elsewhere in the literature, for example Trainer et al. (2010), Belin et al. (2021), Bresnan et al. (2021), Fernandes-Salvador et al. (2021), this issue, or Gianella et al. (2021), this issue. In the case of shellfish biotoxin producing species, some monitoring networks consider alert threshold densities to trigger toxin monitoring based on historical data, like e.g. 100 cells l^{-1} for *Dinophysis* in Scotland (Swan et al., 2018) or if present whatever the *Dinophysis* species in France (Belin et al., 2021), while higher threshold densities (1,000-300,000 cells l^{-1}) are defined also in the case of the REPHY network for *Alexandrium, Protoceratium, Pseudo-nitzschia* and others. Measures to take management actions to minimize damage on farmed fish are possible if ichthyotoxic HAB densities rise significantly, though no threshold densities are established for fish killing HABs (Davidson et al., 2021). In both cases early warning of developing HABs is key to effective mitigation (e.g. Maguire et al., 2016).

High biomass blooms can be carried by advection from offshore areas to the coast. For these near surface bloom events, satellite detection is possible with algorithms developed to discriminate some HAB species from benign phytoplankton (Stumpf et al., 2009; Kurekin et al., 2014; Jordan et al., 2021). Such HAB detection approaches are particularly powerful if coupled to a numerical model that can predict the likely trajectory of the bloom over the following days and hence provide an early warning for at risk aquaculture sites (Davidson et al., 2016; Maguire et al., 2016). Low biomass blooms like those of the shellfish toxin producing dinoflagellates, in the genera *Dinophysis*, are difficult to monitor since they often present as subsurface blooms that are undetectable in satellite imagery. In addition, they are harmful at low cell densities ($<10^3$ cells l^{-1}), which comprise a small proportion of the full microphytoplankton community, and are therefore difficult to detect with conventional monitoring sampling methods (Escalera et al., 2012). Moreover, the frequency of conventional weekly monitoring, usually sampling inshore sites, is insufficient to raise an alert should wind reversals rapidly advect dense shelf populations into aquaculture sites within a matter of days (Escalera et al., 2010; Raine et al., 2010; Whyte et al., 2014). Anyway, hydrodynamical model runs combined with Lagrangian particle tracking simulations can give information on HAB transport along-shore or cross-shore in and out of harvesting areas (Maguire et al., 2016).

Today, the main limitation to the enhancement of HAB warning systems is the availability of high frequency, real or near-real-time, HAB data and relevant parameters in their ecosystem. These data are essential to constrain initiation, movement and growth of the blooms in numerical forecast models, to validate/confirm satellite detections and add value to the human interpretation of how the ecosystem is evolving. Future more sophisticated modelling systems will benefit from "nudging" as new observational *in-situ* data streams are available to enhance model estimations, a technique known as data assimilation forecasting. The European Union Interreg Atlantic Area project PRIMROSE, Predicting Risk and Impact of Harmful Events on the Aquaculture Sector[1], involved partners from the EU Atlantic Area (Spain, Portugal, France, Ireland and the UK) in an effort to improve early warning systems in the partners' regions building on improved data management and flow from existing HAB and biotoxin monitoring programmes and on coordination and development of HAB sampling and modelling systems (Mateus et al., 2019; Fernandes-Salvador et al., 2021). During PRIMROSE, which ran from 2018 to 2021, we reviewed and demonstrated novel methodologies for HAB sampling through the following activities: 1) deployment of autonomous imaging flow cytometry sensors on moorings near two aquaculture areas: the Daoulas Estuary in French Brittany and the Scottish Shetland Islands to demonstrate a dataflow pipeline, data processing and data sharing, 2) deployment of a suite of cheap, near-shore, autonomous surface vehicles capable of collecting water samples for shore-based assays, 3) evaluating protocols for opportunistic water sampling by coastguard agencies and 4) reviewing the performance of other opportunistic sampling approaches and how they augment standard routine HAB monitoring.

[1] https://www.shellfish-safety.eu/

2 AUTONOMOUS FLOW CYTOMETER SENSORS

Autonomous flow cytometers are a useful tool with fast sample throughput by comparison to traditional optical microscopy. The latter is the reference methodology for most national HAB monitoring programmes (Karlson et al., 2010) but requires time for transport of water samples, for sample preparation (up to 24 hours) and for taxonomic specialists to analyze and report the results (First and Drake, 2012) as well as correct sample preservation methods to prevent changes of morphology for some species during transport. This limits the sample processing throughput rate (Dunker, 2019) and the coupling of these data with information coming from other sensors in a HAB warning system. To address this problem a range of research tools have been developed, with some now being sufficiently mature and available on the market for application within automated mooring systems.

A major development was the emergence of Imaging Flow Cytometry (IFC) (Dashkova et al., 2017), an enhancement of a previous in-flow cytometric system that uses fluorescence and optical cell scatter measurements to discriminate planktonic cells, typically at the "functional group" level (Thyssen et al., 2008). The incorporation of imaging technology along with machine learning identification and classification of the resulting image data library has markedly advanced phytoplankton discrimination and enumeration capabilities in the field. Results from this application are promising (Campbell et al., 2010; Campbell et al., 2013; Dunker et al., 2018). While an IFC is still relatively expensive, cost reductions through product development are making this technology more widely accessible to users, with a recent increase in the number of deployments in a wide range of sensitive marine areas including the east and west coasts of the US (Fischer et al., 2020), a number of locations in Scandinavia (Kraft et al., 2021) and Hong Kong (Guo et al., 2021). Like all instruments, autonomous IFCs have significant cost and time constraints related to training, servicing, data management and subsequent data processing. At present, real-time analysis requires a physical link to land (cables) or a wide bandwidth network connection and access to significant data processing capability. Continuous sampling may require two or three autonomous flow cytometer units, with one deployed while the other units remain in the laboratory undergoing maintenance, calibration, service and training.

During PRIMROSE, the use of autonomous IFCs for HAB assessments have been tested and demonstrated in two sites: one IFC installed on a mooring at the Daoulas Estuary in the Bay of Brest, France and one IFC land based with water being continuously pumped from an adjacent bay in the Scottish Shetland islands.

2.1 Autonomous Flow Cytometer Sensor Installed in a Mooring

A platform with a frame to support a Cytosense flow cytometer (Cytobuoy product) was moored during PRIMROSE (**Figure 1**) in the Daoulas estuary in the Bay of Brest, an area that experiences regular *Alexandrium minutum* bloom events since 2012 (Chapelle et al., 2015). Water depth at the mooring site was more than three metres at spring-tide low water to avoid sea-bed contact (station C, **Figure 2**). The two time periods in 2019

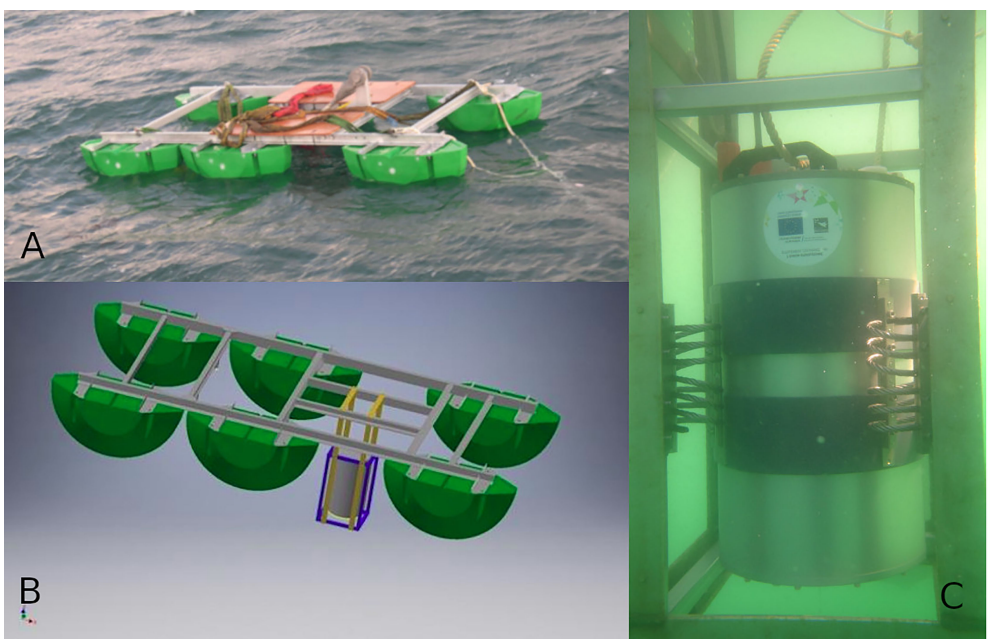

FIGURE 1 | Picture of the deployment of the PRIMROSE mooring platform at Anse du Roz in the Daoulas estuary **(A)** and scheme **(B)** showing details of the floating structure frame designed for carrying the autonomous flow cytometer, IFC **(C)**, its associated tools (batteries, etc) and other additional sensors.

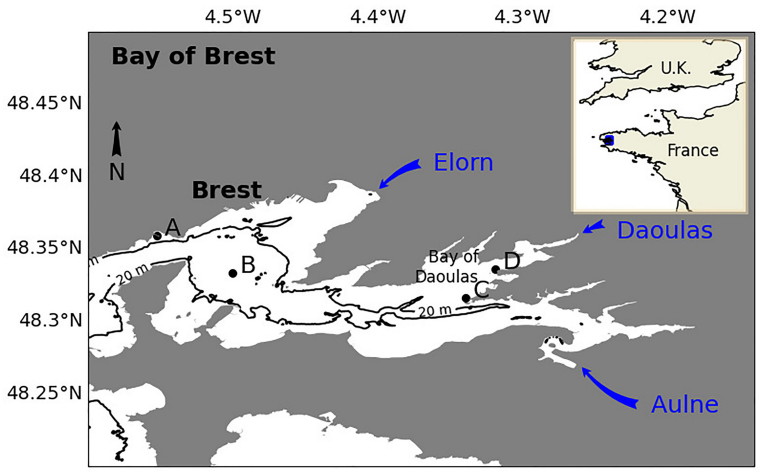

FIGURE 2 | Positions of the monitoring stations in the Bay of Brest: (Station A): Ste Anne du Portzic station from SOMLIT program (Observatory in the coastal environment, http://www.somlit.fr); (Station B): Lanveoc from REPHY national program; (Station C): PRIMROSE IFC mooring at Anse du Roz in the Daoulas estuary; (Station D): Alex Breizh mooring and sampling site at Pointe du Château in the Daoulas estuary.

investigated during PRIMROSE were 28th June to 10th July and 14th to 26th August 2019. The site position was 200 m from another established monitoring site (project Alex Breizh) with a mooring measuring temperature, fluorescence, salinity and turbidity (station D) where once per week samples for plankton community characterization are obtained 2 hours around high water (HW) using a kayak or a zodiac. A third station from the national monitoring program REPHY where weekly microscope based phytoplankton enumeration are obtained is located in the Bay of Brest (station B) at a distance of 2 km from the IFC mooring. REPHY samples are also taken during high water and data are available from 2016 (REPHY, 2021). To be in agreement with the microscopic dataset obtained in the existing monitoring in the Bay of Brest and due to the macrotidal characteristic of the Daoulas estuary, the IFC water sampling was also set to occur once during the day (during high water). Our data can also be compared to more oceanic waters analyzed at the entrance of the Bay of Brest (Station A), where a long term environmental monitoring station within the SOMLIT (Service d'Observation en Milieu Littoral) is established[2]. The environmental variables acquired since 1998 and the availability of phytoplankton samples taken weekly at high tide from 2009 allow the comparison between incoming waters and the Daoulas estuarine waters.

The ability to classify cells through the identification of collected images and/or the clustering or gating of fluorescence or cell scatter signals is the essential step in the analysis of IFC data. To permit comparisons with other data sets, the clusters were made in agreement with the protocol from other monitoring stations along the French coast (SOMLIT). Based on the size proxy (FSS, Forward Size Scatter) and the red/orange fluorescence ratio, five large clusters were made: *Synechococcus*-like, Picoeukaryotes, Nanophytoplankton, Cryptophyceae-like and Microphytoplankton. Cluster names, vocabulary and file format agree with the best practice followed in well-established European projects like SeadataCloud and Jerico Next (Artigas et al., 2019) to permit comparison and a larger diffusion of the data set. In this way, the IFC setup and data quality were evaluated in 2018 by comparing estimated abundances from fixed water samples with densities provided by two different flow cytometry platforms (Roscoff laboratory and Brest University). It should be noted that typical flow cytometry platforms do not provide estimates of the microphytoplankton cluster due to the size of their tubes and the volumes analyzed. The comparison was thus limited to the four smallest clusters. The first-round showed that the IFC set-up produced highly correlated abundances for the same clusters. A further quality control was undertaken in 2019 by comparing *in-situ* time series of autonomous sampling (counting of living cells without calibration beads) with cell densities estimated from chemically fixed samples (with calibration beads) that were manually collected at the same station and time period. Calibration beads were also used to check fluorescence stability and IFC alignment was checked before and after each deployment. The data of both sampling strategies were highly correlated (>0.99) and the data set from our *in-situ* IFC sampling was deemed sufficiently consistent to be used as a reliable monitoring tool.

The first output from our IFC data analysis was to highlight the strong spatial and temporal variability of the phytoplankton community in the Daoulas Estuary (**Figures 3A, B**). For such an area, the daily resolution that IFC provides is required to describe the trends of the evolution of cell density whereas the weekly frequency of existing monitoring is clearly inappropriate to make short term forecasts like those required in HAB warning systems. For example, local microphytoplankton blooms occurred at the Daoulas Estuary for 4 to 5 days after some high river runoff

[2]https://www.somlit.fr/brest/

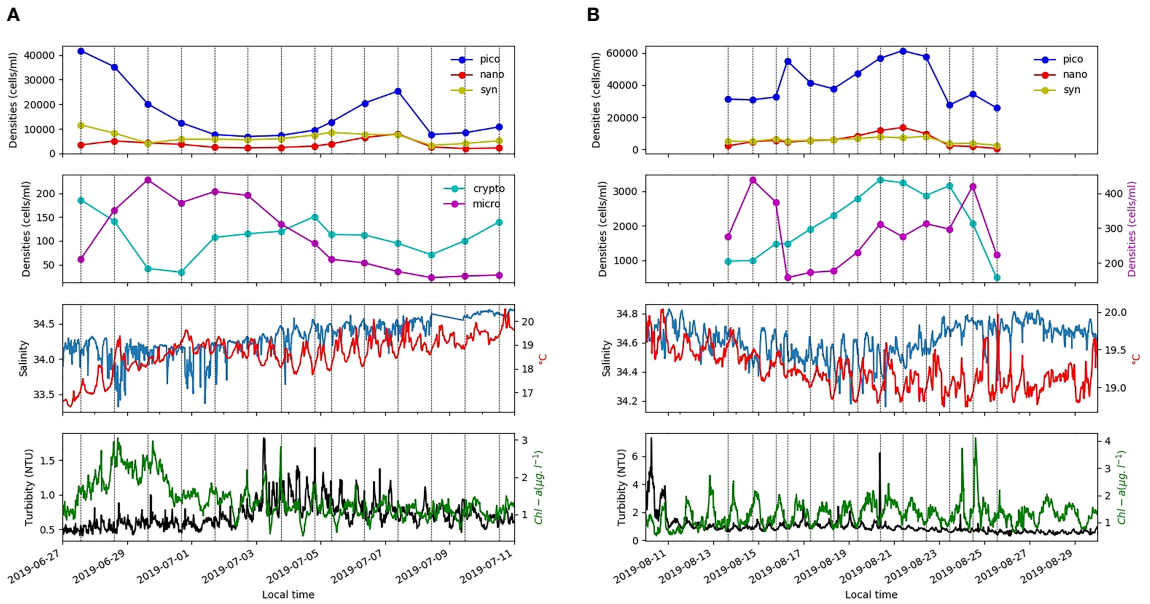

FIGURE 3 | Time series of variables obtained from the IFC and other sensors on the autonomous mooring in the Daoulas estuary (station C) from 28th June to 10th July 2019 **(A)** and from 13th August to 25th August 2019 **(B)**. Abundances of five regular clusters (*Synechococcus*, Picoeukaryotes, Nanophytoplankton, Microphytoplankton and Cryptophyceae) obtained from the IFC are plotted. IFC sampling was done at high water during the day (dotted vertical lines).

events (e.g. in the period 27th June to 1st July, **Figure 3A**). In the same way, an upstream movement of the maximum phytoplankton concentration occurred during nutrient-limited periods in the middle of the summer; note that in general, due to the estuarine dynamics of the macrotidal Daoulas estuary, HW sampling was associated with low Chl-a concentrations (**Figure 3B**). This displacement is illustrated by low cell densities at HW from 17th to 27th August 2019 (**Figure 3B**). The sets of daily microphytoplankton images produced during the IFC measurements are highly relevant to characterize the variability of the phytoplankton community and eventually to provide alerts of the presence of HAB species. An illustration is provided in **Figure 4** where IFC images from two days (29th June and 9th July) in the fortnight shown in **Figure 3A** are plotted. **Figure 4A** reveals that the microplankton peak coinciding with the chlorophyll maximum on 29th June is composed of chain diatoms (*Chaetoceros* spp.). After this peak, microplankton concentration is observed to decrease quickly in parallel to salinity increase. Picoplankton, which was high at the beginning of the period, decreases during the microplankton peak and attains a relative maximum on 7th July, when salinities are again higher. The 9th July image (**Figure 4B**) shows that plankton community is then composed of solitary dinoflagellate species, including *Alexandrium* spp. and *Ceratium* spp., which were also detected in the weekly sampling of the Alex Breizh project at Point du Château (station D).

The methodology for cluster processing of IFC data allowed the comparison of the plankton community at the Daoulas Estuary site (station C) with that at the entrance of the Bay of Brest measured in the weekly SOMLIT sampling (station A). The average seasonal evolution (**Figure 5**) shows that nanophytoplankton and Cryptophyceae densities are significantly higher in the Daoulas Estuary but that is not the case for picoeukaryotes and *Synechococcus*. Note that, as pointed out above, the microphytoplankton cluster was not computed at SOMLIT stations. Despite the high tidal mixing and the small residence time of water masses, separate monitoring stations are required to describe local growth and/or accumulation. Therefore, with the IFC mooring data set, we were able to demonstrate the significant difference in the phytoplankton community composition. This observation is based on a global approach to functional groups that remains limited to the macro scale description of the phytoplankton community and cannot yet be directly related to variability of HABs. The nanoflagellate cluster however includes the main part of the *Alexandrium* spp. populations due to the size limit between nano- and micro-phytoplankton clusters. The threshold was set to 20 µm whereas *Alexandrium* cell size can vary from 5 to 20 µm. Not all toxic species are included in one cluster (i.e. microphytoplankton).

With the settings used during these deployments (the speed of the water, analysis duration, minimal Equivalent Spherical diameter, etc.) and the *in-situ* cell densities, the number of recorded images were limited to between 100 to 300 per sample in 2019. This prevented a quantitative estimate of several image clusters, but the information gathered was still useful to support identification of the predominant species, as illustrated in **Figure 4**. Some modifications of the IFC hardware and setting were made to increase the number of images, and it is expected that a quantitative estimate can be achieved. New classifiers for automatic clustering of HAB species were

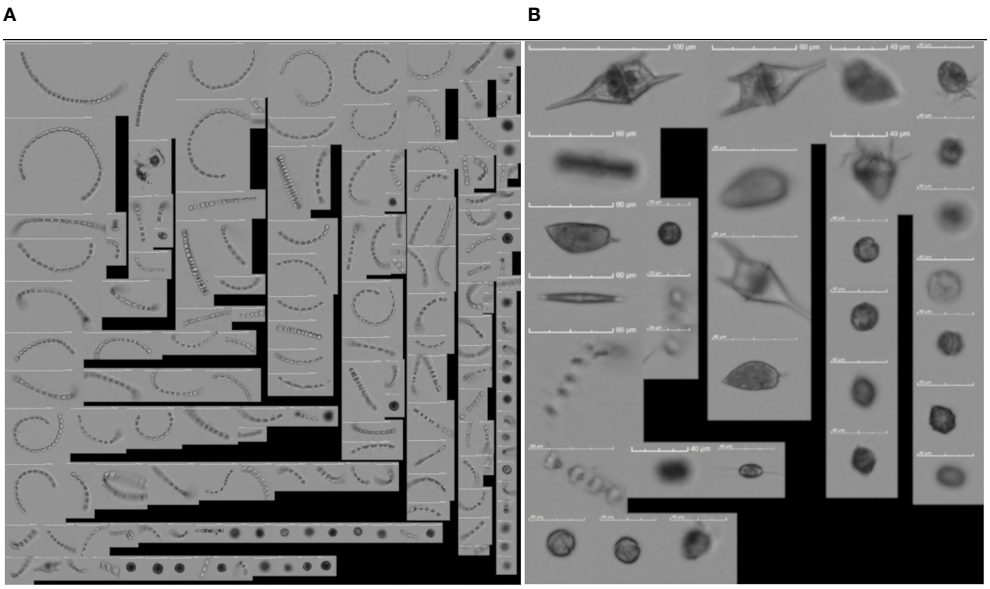

FIGURE 4 | Microphytoplankton images recorded during daylight high water at the IFC moored in the Daoulas estuary on 29th June **(A)** and on 9th July 2019 **(B)**.

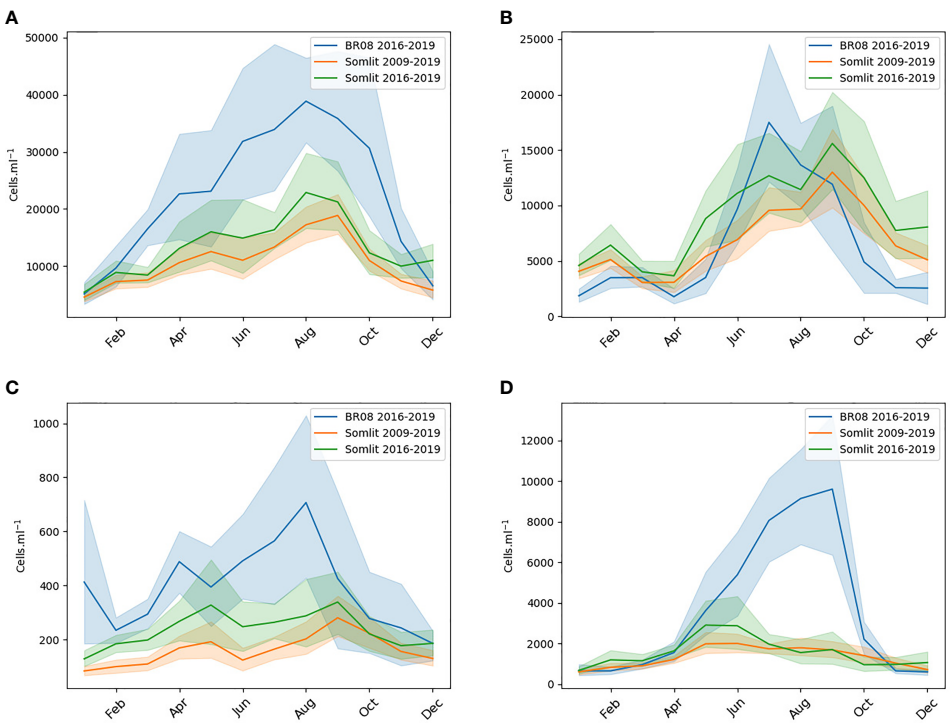

FIGURE 5 | Seasonal patterns of monthly average and standard deviation) observed by the IFC in the Daoulas Estuary (station D, **Figure 2**, blue line) during 2016-2019 for the Picoeukaryotes, *Synechococcus*, Cryptophyceae and Nanophytoplankton clusters **(A–D)**. The seasonal pattern at the entrance of the Bay was estimated from the SOMLIT-Brest station (station A) for the same and a longer period (green and red line respectively).

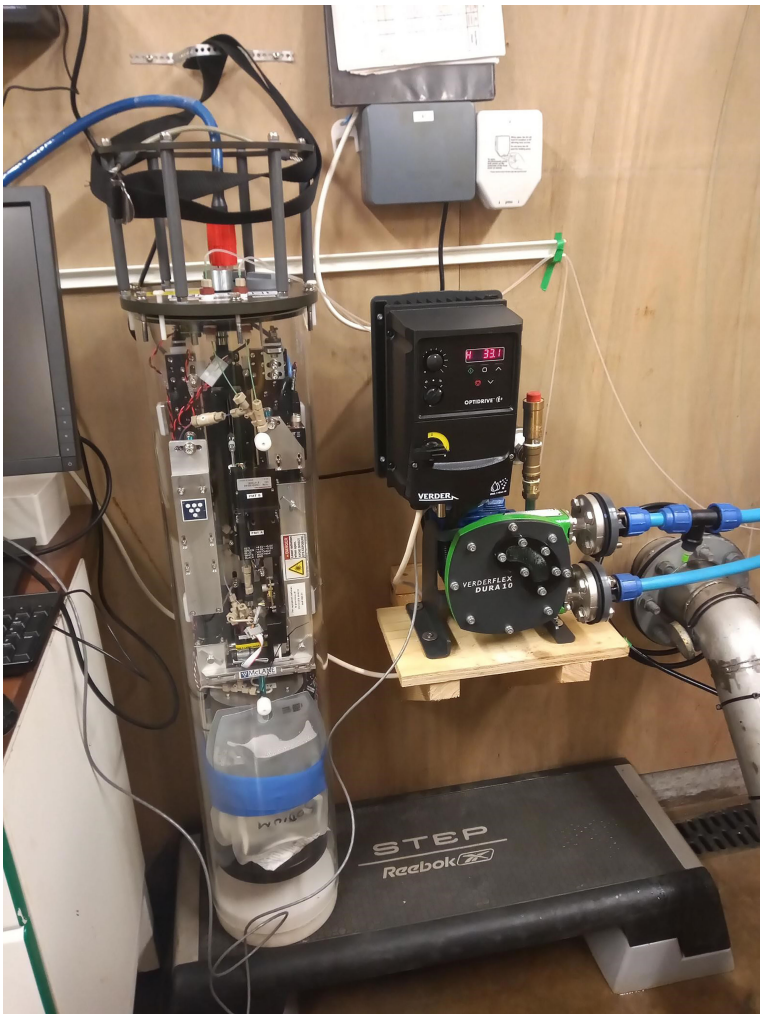

FIGURE 6 | FlowCytoBot (IFCB) deployed in Scalloway in the Shetland Islands during PRIMROSE. The IFCB is land based with seawater being continuously pumped from an adjacent bay.

constructed based on specific learning sets of > 1000 images obtained from cultivated strains of two toxic lineages (*Alexandrium minutum* and *Pseudo-nitzschia* spp.). Data has been sent in real time by 4G to an internal server since 2020, but the full automatic processing for dissemination is not yet operational.

2.2 Autonomous Flow Cytometer Sensor Installed on Land

Another deployment of an IFC was made in the Scottish Shetland islands in the form of a FlowCytoBot (IFCB). IFCBs have been used previously for HAB monitoring, for example in Texas, where harmful blooms of the shellfish biotoxin producing dinoflagellate *Dinophysis* were revealed (Campbell et al., 2010). The Shetland Islands are an important centre for Scottish aquaculture, with HAB monitoring by microscopy occuring at a number of aquaculture sites. The relative expense of these instruments prevents their wide deployment, hence, our IFCB has been located at a sentinel location (Scalloway) to provide high temporal frequency regional risk assessment. While not a shellfish harvesting site, the location coincides with the Marine Scotland Science Scottish Coastal Observatory monitoring site that provides parallel environmental information to aid in the understanding of HAB dynamics. In contrast to the French deployment the Scottish instrument is land based, with water being continuously pumped from the adjacent bay (**Figure 6**). This provides additional monitoring flexibility with the potential for hand collected samples from other aquaculture sites to be manually analyzed. HAB data from Scotland are made publicly available on the web in real time [via www.HABreports.org, (Davidson et al., 2021), this issue]. IFCB images can be displayed in near-real time or in delayed mode in the HABreports web page (**Figure 7A**). The 31th August 2021 IFC image shows the presence of *Pseudo-nitzschia* spp. The HABreports website

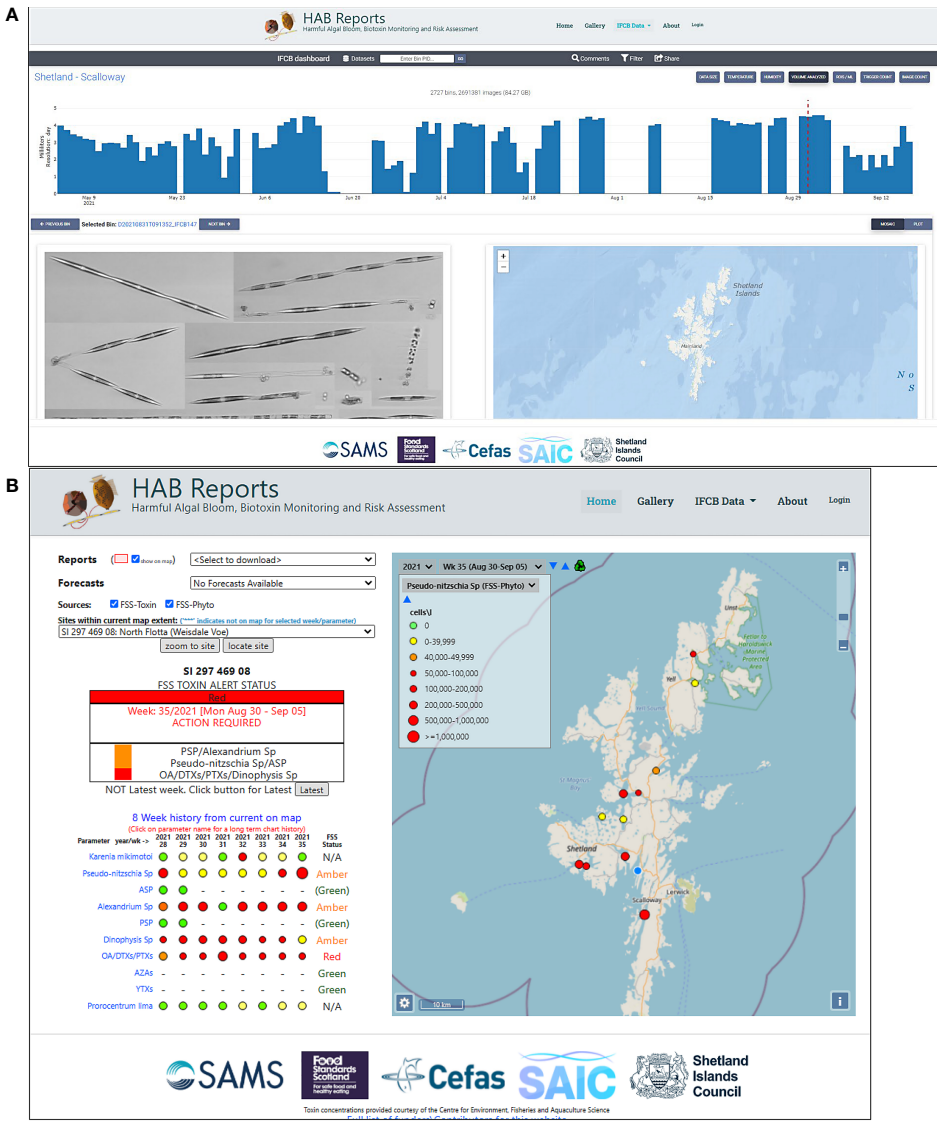

FIGURE 7 | HABreport portal (https://www.habreports.org/) snapshots: **(A)** interface for viewing and interrogating IFC data from Scalloway, showing the 31st August 2021 IFC image of largest phytoplankton (mainly Pseudo-nitzschia spp.) and **(B)** HABreports display (see Davidson et al., 2021) showing alert levels based on HAB species concentrations and toxin analysis for the current (week 35, Aug 30 - Sep 05) and previous weeks at the North Flotta HAB monitoring site (blue circle). Green/amber/red are Food Standards Scotland (FSS) "Toxin Traffic Light Guidance" levels that indicate the harvesting action and testing considerations that should follow (N/A, no action).

displayed alert levels for week 35 (Aug 30 - Sep 05) and previous weeks at the North Flotta (Weisdale Voe) monitoring site (**Figure 7B**), indicating an "amber" alert caused by the presence of *Pseudo-nitzschia*, although Amnesic Shellfish Poisoning (ASP) toxin concentration was below toxic levels. The presence of *Alexandrium* (rather abundant) and *Dinophysis* (scarce) was also detected in other IFC images for the same day (not shown). The HABreport bulletin therefore generated an alert that week due to the presence of these harmful taxa. In combination with Okadaic acid (OA)/Dinophysis Toxins (DTXs)/Pectenotoxins (PTXs) that were over regulatory limits an overall "red" alert was generated. There were also a few cells of *Karenia mikimotoi* in the IFC images although they were not detected in microscope monitoring.

Similar to the French IFC, operation of the Scottish instrument for plankton community characterisation, and therefore for use in HAB early warning, requires reliable image classification. Typically an IFCB image classifier is built using identifiable characteristics of training images. These characteristics, usually based on shape or texture descriptors, are then input to classifiers like Random Forest Algorithms (RFAs), or Supported Vector Machines (SVMs). Initial operation with a RFA classifier has proved promising in Shetland. However, Deep learning and Convolutional Neural

Networks (CNNs) in particular have shown superior performance for image classification tasks (Sharma et al., 2018) and classifiers are currently being developed using these approaches.

3 ROBOTIC PLATFORMS

Fully autonomous vehicles as either instrument platforms or as sample collection platforms for pure science research are becoming commonplace but are still far from a mature technology. Science is willing to take the risk of equipment failing to meet expectations given the returns-benefit of novel and unprecedented data. Forecasting for commerce requires a higher level of Technology Readiness Level (TRL) to give continual and dependable data for the end user to make reliable planning decisions; at present, mobile and static marine robotics are making little impact on aquaculture commerce in general, and HAB detection and analysis in particular. That said, the wish to automate, reduce cost and reduce risk is driving rapid progress in this arena.

We present here an overview of existing technologies that are commercially set to make a significant impact on HAB forecasting, which fall into two broad categories: airborne and surface autonomous vehicles. We review:

- Water landable quadcopter Remotely Piloted Aircraft System (RPAS) for very local sampling
- 100 km range Beyond Visual Line Of Sight (BVLOS) copter-wing RPAS
- 2 m scale Autonomous Surface Vehicle (ASV) for in-shore sampling and ocean color detection
- 300 nautical miles autonomy USV-Mar II ASV for automatic oceanographic sampling in the Galician rias

3.1 Remotely Piloted Aircraft Systems (RPAS) or 'Drones'

Commercial airborne robotic platforms are becoming commonplace for terrestrial work, predominantly for photography or video capture supporting different applications in an increasing variety of fields. Their use is curtailed to an extent due to the high consequence hazards involved with any aircraft in civil airspace. The term for robotic aircraft preferred by all national aviation authorities is "Remotely Piloted Aircraft System" to reflect that the legal responsibility of the 'operator' is identical to that of a pilot in a normal aircraft. The platform, even if fully robotic, must be capable of returning control to the operator at all times, and they must be capable of piloting the aircraft. Most commercial ventures have focused on operating within "Visual Line Of Sight" (VLOS) which legally[3] limits the craft to a radius of 500 m from the operator. VLOS limitation has a technical consequence, in that most VLOS operations use multi-copter style RPAS, that is the archetypal four-propeller 'drone'. The extreme flight inefficiency of this design coupled to the poor energy density of ca. 2020 batteries means flights are of the order of 10 - 20 minutes. The simplicity of operation and lack of need for a runway, coupled to the legal limit to range, however, make this the design of choice for the mass market.

A compromise design to get similar take off/landing simplicity, termed Vertical Take Off and Landing (VTOL) whilst still using efficient wings for lift, is now available. Both are considered below.

3.1.1 Water Landable Quadcopter RPAS

TetraDrone's TD7 hexacopter platform (**Figure 8**) was trialled during PRIMROSE for local sampling in Scotland. This aircraft is designed to land upon and to sample the sea surface, and is capable of making airborne measurements of variables such as temperature, humidity and CO2.

The TD7 floats act to an extent as a safety net: when operating over water the craft will not sink irretrievably if forced to land. The aircraft is flown within VLOS either from shore or small boats but water-landing capability is limited to fair weather surface conditions. Initial plans to modify the wet payload bay (visible under the aircraft fuselage) for HAB sampling was postponed following results of studies to assess the capability of RPAS-based measurement of ocean color, itself used within the PRIMROSE project to identify HAB signature. An intention was to combine airborne visible spectral data with land-and-sample; however, the airborne ability to detect HAB is limited due to the effects of sunlight 'glint' (Weeks, 2019). Further, the limited range and dependency on placid sea-state have put further focus on ASV (see below) as a solution to near-shore detection and sampling of HABs.

3.1.2 Vertical Take-Off and Landing (VTOL) RPAS Operating Beyond Visual Line Of Sight (BLVOS)

The standard commercial quadcopter style of 'drone' used in VLOS, with a legal operating radius of 500 m results in a flight time in the tens of minutes, reported in the previous section is quite unsuited to the scales of most marine applications. Fully robotic airborne platforms used as physical transport and delivery infrastructure were demonstrated in Argyll in 2020 and 2021, showing that integration of BVLOS RPAS in civilian airspace is legally possible and VTOL by fixed wing aircraft is technically possible. This UK first of a 'proof of feasibility' was conducted in Scotland by the London-based company, Skyports Ltd. Daily for two weeks in Argyll during the Covid-19 crisis medical supplies and test samples were transported, with circa six flights per day between the hospitals in Oban and on the island of Mull.

Full BVLOS, with permission from the UK Civil Aviation Authority (CAA), involves months of preparation and discussion, both with the relevant UK and local authorities, land-owners and other local interested parties such as other, piloted aircraft operators. This is the case even when operating in Argyll with a lower inherent risk compared to air-space above London, it is merely simpler and less complex in Argyll, and this was the main basis for Skyports initial interest in the area.

A more technical issue, but still essential, is the ability for VTOL. The familiar quad (or hexo or octo) -copter can, of course, take off and land vertically and do not need a runway.

[3] VLOS is set out in the UK under CAP722 and similar international regulation exists in all International Civil Aviation Organization (ICAO) countries

FIGURE 8 | TD7 water-landable UAV under trial on a near calm and sheltered embayment at Dunstaffnage Peninsula, Argyll, Scotland.

Such helicopter-style aircraft are far less efficient than those termed 'fixed-winged' and with electrical batteries much less energy-dense than fossil fuels, airtime for 'copters are 15 -30 minutes, even without payload. For BVLOS to be viable, therefore, the aircraft must fly, in the main, like a fixed-wing. An important feature of the Skyports aircraft Wingcopter (**Figure 9**) is the four swivel-mounted propellers; these rotate with a vertical axis at take-off and landing but rotate to a more familiar horizontal axis for winged flight (the aft propellers cease turning and fold back). This greatly increased payload/flight time, whilst still operating from a small field or (in this case) a helipad.

3.2 Autonomous Surface Vehicles (ASV)

3.2.1 ImpYak: A Fully Autonomous Small Surface Vehicle

ImpYak is a prototype impeller driven kayak initially conceived as a student practical demonstrator for the SAMS Marine Robotics course (**Figure 10**). ImpYak uses the "ArduPilot" family of autopilot software, an open-source initiative initiated in 2016 with "ArduRover", running on specialized Arduino-like microcontroller + sensor hardware. More specifically, ImpYak uses the ArduBoat branch of ArduPilot running on the PixHawk 4 platform. Using ArduPilot and relevant hardware such as PixHawk offers a rapid and economic route to developing autonomous platforms, and there are versions for rovers (land vehicles), fixed-wing aircraft, quad and multi copters and even submersibles such as AUVs and ROVs.

ImpYak comprises of:

- A standard river-surfing kayak, which is laterally stable, has no keel.
- Avionics ('autopilot') based on the Pixhawk 4 and sensor suite (GPS, compass and accelerometers)
- Off-the-shelf air-cooled motor controllers (Electronic Speed Controllers: ESC)
- A pair of 600W (=1.6 HP) underwater remotely operated vehicle (ROV) impellers
- Battery set (18V): LiPo or lead-acid

Two significant inherent benefits to this system design are, firstly, that all versions have similar 'front ends' with mission planning (again *via* free source software, such as Mission Planner and Q Ground Control), so operating the ImpYak is a simple transition if already familiar with ArduPilot aircraft. Secondly, the communication protocol between mission planning software and platform avionics is *via* MAVlink, a full-duplex communication protocol specifically designed for UAVs. MAVlink commands and system data are exchanged continually between platform and ground station, but can also be exchanged between vehicles. This already embedded protocol opens the capability of not just swarm behavior (such as multi-kayak fleets), but heterogeneous swarm control, such as an aircraft and boat acting in coordination, and sampling a vertical profile of the ocean atmospheric boundary layer.

Initial trials of these platforms show that they are capable of making pre-planned waypoint surveys or acting as stationary temporary surface mooring, which is a command mode called 'loiter'. Instrument packages can be included either externally or through-the-hull. The ImpYak has been equipped with a meteorological station and also with a through-the-hull solar spectrometer for zero-glint HAB spectroscopy. A sea-surface sampling system based around an Arduino microcontroller and a suite of peristaltic pumps have been proven using an 80cm boat, and will be installed on an ImpYak system.

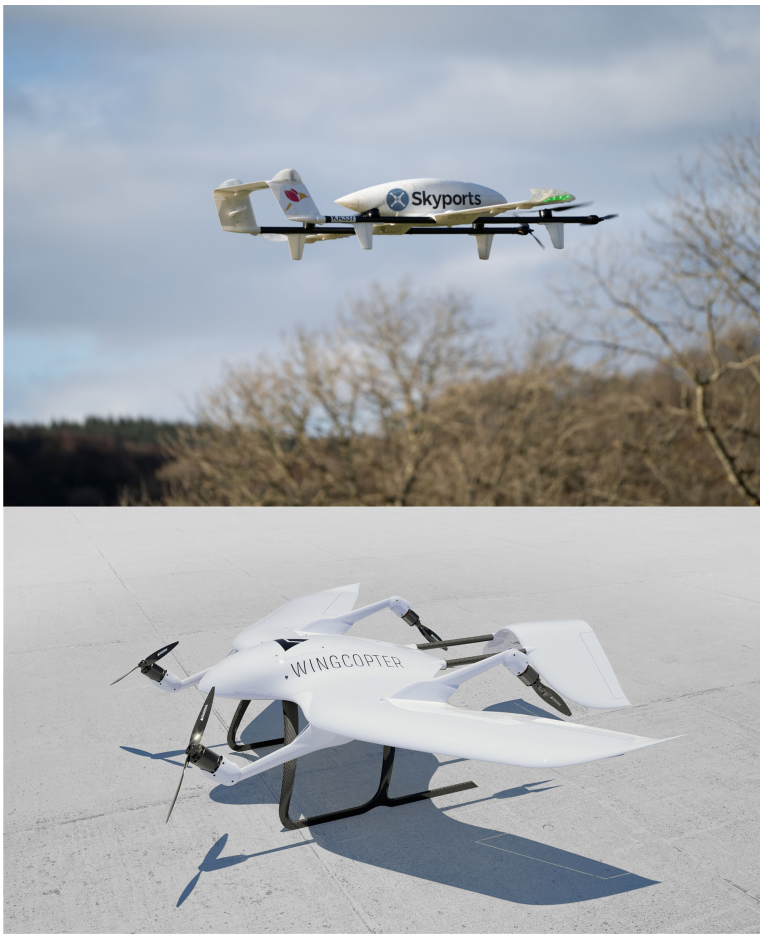

FIGURE 9 | The Skyports aircraft (Wingcopter VTOL winged aircraft) showing the swivel-mounted forward motors in take-off/landing mode. The under-slung payload 'pod' is visible. Reproduced with permission of Wingcopter.

3.2.2 The Galician CIVIL UAV Initiative for Automatic Oceanographic Sampling

In 2017 the Galician government launched a public procurement initiative for unmanned vehicles to address a set of technological challenges[4]. One of the projects was 'Automatic oceanographic sampling service using unmanned vehicles' (MAR-2). The contract was financed in 80% with FEDER funds corresponding to the smart growth operational program (POCInt) 2014-2020 and a collaboration agreement signed between the Ministry of Economy and Competitiveness, the Axencia Galega de Innovación (GAIN) and the Axencia para a Modernización Tecnolóxica de Galicia (AMTEGA) for the development of the Civil UAVs Initiative. The main purpose of the MAR-2 project was to find a technological solution using UAVs resulting in oceanographic sampling to significantly reduce costs of water quality control assessments and other monitoring programs, to enable high frequency data collection and to operate in adverse weather conditions. One of the agencies involved in the design of the technical requirements was INTECMAR, the regional government organization in charge of the Galician HAB monitoring service.

In summer 2020, the consortium of companies that won the public procurement tender presented the USV-Mar II prototype[5] (**Figure 11**). The USV-Mar II prototype is an Environmental Surveillance vessel, 10.5 m in length, made of naval steel with a reinforced fibreglass superstructure. It has a double pilot system, with operations possible from the boat or remotely following a predefined route autonomously. On board, it carries a robotic system with instruments to collect samples from water columns at different depths in predefined geographical points and has a system for data transmission to an operation room in land. The autonomy is more than 300 nautical miles. The operation of the prototype was tested in unmanned and manned mode in autumn 2020-winter 2021 and included taking water samples for nutrient

[4]https://www.civiluavsinitiative.com/en/programmes/solutions-program/

[5]https://seadrone.es/mar-2/

FIGURE 10 | ImpYak ASV in loiter mode on Loch Linnhe in north east Scotland on 9th July 2021 **(A)**, whilst working in conjunction with the FAAM aircraft (Facility for Airborne Atmospheric Measurements, https://www.faam.ac.uk) **(B)**.

analysis and phytoplankton identification and deploying the multiparametric sonde for oceanographic variables used in the weekly Galician HAB monitoring (Conductivity-Temperature-Depth (CTD) profiler equipped with a WETStar fluorescence sensor) in the Galician rias de Pontevedra and Vigo. The sampling system was found to be able to collect, classify, label, store and automatically conserve all samples.

4 OPPORTUNISTIC SAMPLING

In this section, we review examples of opportunistic approaches to sample collection outside of the usual coastal monitoring at aquaculture sites.

4.1 HAB Data Sampling by Coastguards

During PRIMROSE, we evaluated how the detection of a harmful bloom could be enhanced by opportunistic sampling, in this section through coordination with the Irish Coast Guard and the Irish Naval Service to collect water samples. A protocol was prepared and distributed (see **Supplementary Material**: Phytoplankton bloom sampling: Quick guide for Coastguard). Some examples of HAB *in- situ* sampling by coastguards, from selected years (2013 and 2017) when large biomass blooms occurred, are presented below.

On 27th May 2013, a phytoplankton bloom was detected in surface waters of the Irish Sea by the Marine Institute with the help of a Chl-a satellite data product developed by Ifremer/DYNECO and CERSAT in Brest (France) and NASA in the USA. The causative organism was the prymnesiophyte *Phaeocystis*. The satellite data allowed visualization of the spatial extent of the bloom with continued daily monitoring. The bloom was evident all along the east to southeast coasts of Ireland from Dublin to Wexford and was associated with cooler waters (**Figure 12**). After detection by satellite, field samples were taken by the Irish Environmental Protection Agency (EPA) who observed globular

FIGURE 11 | The USV Mar II prototype, developed in the Galician CIVIL UAV Initiative for Automatic oceanographic sampling, operating in the Galician Rias in manned and unmanned mode. Pictures provided by GAIN, Xunta de Galicia, Spain.

Phaeocystis colonies in the water, very evident against the Secchi disk at the surface (**Figure 12C**). Photographic images of the bloom were taken by a commercial airline pilot on 5th June 2013 ~ 18.5 Km off the Irish coast. Beaches on the east coast of Ireland were affected by this algal bloom, and the presence of *Phaeocystis pouchetii* was confirmed with water samples taken by the Irish Phytoplankton Monitoring Program the Marine Institute operates. *Phaeocystis pouchetii* is a common species and is known to have caused blooms along the east coast several times in previous years. The species causes water discoloration and foaming on beaches in windy conditions.

In September 2017, a blue green algal bloom was reported in bathing areas of Galway Bay, west Ireland. Samples taken were analyzed and cells of the cyanobacteria, genus *Anabaena*, were predominant and observed in clusters and chains. On 8th September, an opportunity to observe the extent of the bloom was facilitated by the Irish Coastguard Rescue 115 Sikorsky S-92 Helicopter with a number of aerial passes over the affected area in Galway Bay. Photos (**Figure 12D**) revealed the bloom extended throughout the inner part of the bay and along the north shore; information previously unavailable from shoreline observations.

In 2013, an offshore phytoplankton bloom was detected off the Irish northwest coast in satellite imagery. After detecting the bloom, a report was sent to the Irish Coast Guard on 20th July with information on the geographic extent of the bloom zone. Samples collected by MV Heather Jane II on 26th July were delivered to the Mulroy Coast Guard Unit on return to port. Samples mailed to the Marine Institute were manually analyzed and confirmed a non-harmful coccolithophore bloom that did not require management action. **Figure 13** presents the station position and temporal changes of the spatial extent of the bloom over a few days. Coccolithophorids were present at low cell densities (surface = ~6,000 cells l^{-1}; 3.7 m = 3,400 cells l^{-1}) and no toxic or harmful species were present. It is likely that the bloom was at the end stage. Between the 20th and 26th July, the bloom position shifted in an eastward direction away from the targeted sampling region. This may explain the low cell counts in the fixed water samples analyzed.

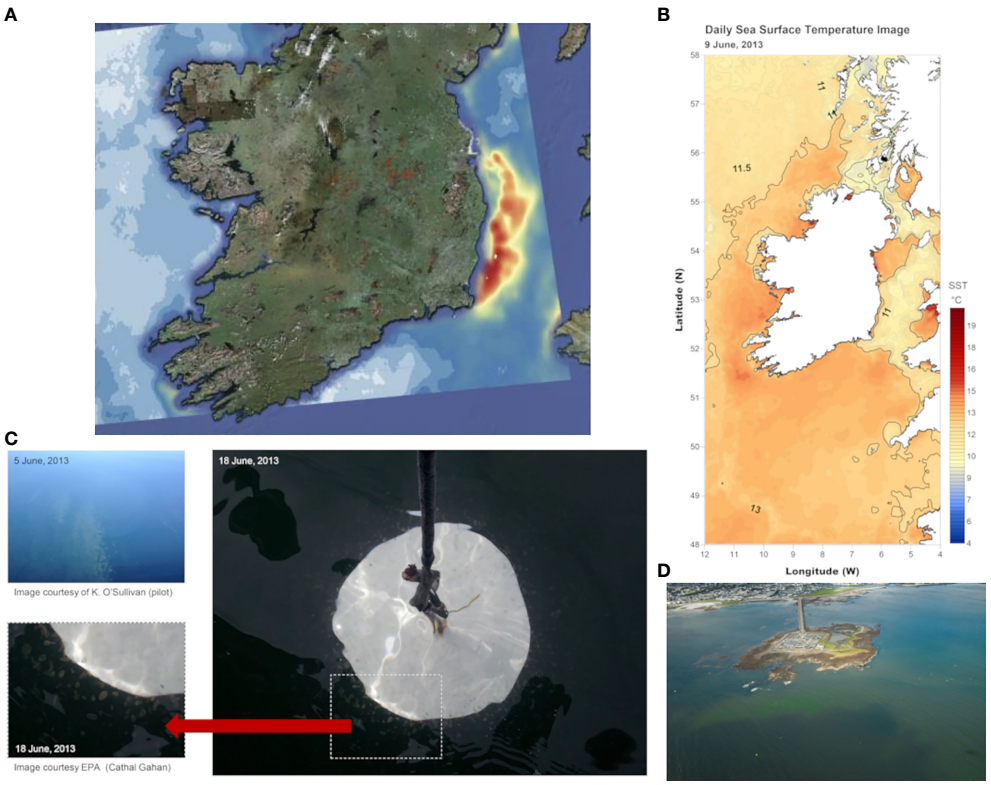

FIGURE 12 | **(A)** Satellite Chlorophyll image showing the extend of an exceptional *Phaeocystis* bloom in the Irish Sea, June 2013, **(B)** Satellite derived sea surface temperature data (CMEMS ODYSSEA SST data product) shows colder water evident at the bloom position **(C)** photographic images of dense *Phaeocystis* colonies in surface waters off the north Dublin Irish coastline on 18th June, 2013. The large globular *Phaeocystis* colonies are visible to the human eye in the water against the Secchi disk at the surface; aerial photograph of the bloom on 5th June taken by a pilot ~ 18.5 Km off the Irish east coast. **(D)** Bloom of cyanobacteria in Galway Bay, west coast of Ireland, in 2017 taken from a Coastguard Search and Rescue Helicopter revealing the extent of the bloom within the bay.

4.2 Coastal Opportunistic Sampling

In summer 2018, an exceptional Paralytic Shellfish Poisoning (PSP) outbreak occurred in the Rías Baixas (Ría de Vigo and Ría de Pontevedra, both southern Galician Rías), northwest Spain (**Figure 14**). This event was caused by an intense and prolonged (around one month) *Alexandrium minutum* bloom. The bloom caused prolonged shellfish harvesting closures at mussel rafts and infaunal seabeds due to PSP levels exceeding regulatory limits mainly in Ría de Vigo but also in Pontevedra. *Alexandrium minutum* has previously been found in Galicia in spring and summer during the upwelling season associated with water stability and stratification, but only in embayments like the Baiona Bay in the Ria de Vigo and the inner part of the Ria de Ares (Bravo et al., 2010). This was the first time that *Alexandrium* affected a larger area like the Rias de Vigo and Pontevedra. The high concentrations caused water discoloration: at the end of June, red waters appeared in the Ria de Vigo, which were still visible a month later. The Galician monitoring system (INTECMAR) detected the presence of *Alexandrium minutum* and PSP toxins above regulatory levels and harvesting areas in Vigo and Pontevedra were closed.

The spatial variability of water discoloration outside the monitoring stations and the presence of toxins in marine fauna not sampled in the biotoxin regulatory monitoring in shellfish could be studied with opportunistic sampling during this event (Rodríguez et al., 2018). The location of the sampling stations of INTECMAR and of the places where opportunistic monitoring was performed are provided in **Figure 14**. On 28th June, a call from the rescue services to the Oceanographic Centre of Vigo (IEO) raised the alarm that Samil Beach waters were discolored, probably due to a red tide. The authorities sought to identify the causative agent and were evaluating whether to restrain bathing until the nature of the phenomenon was clarified. Samil, the most popular urban beach in Vigo, is a few kilometres away from IEO and shore samples were collected rapidly (**Figure 15**). Reddish-brown patches, likely advected by water currents with the onset of very mild northwesterly winds, formed a bloom strip parallel to the shore visible from the mid-beach to the southern limit of the shore at the mouth of the Lagares River. At the IEO samples were analyzed and *Alexandrium* cell counts ranged between 30 to 48 $x10^6$ cells l^{-1}. *Alexandrium* became so dominant that the water samples resembled a monospecific culture (**Figure 15**, see right panel), with only minor presence of other dinoflagellates. The bloom cell densities were somewhat lower (10 $x10^6$ cells l^{-1}) in a sample taken 200 m offshore by a rescue boat. Observations of calcofluor-stained samples under the epifluorescence microscope soon identified the species as *A. minutum*. A detailed description of this summer 2018 A. *minutum* bloom and an analysis of the environmental factors that triggered this episode is in preparation by Nogueira et al.

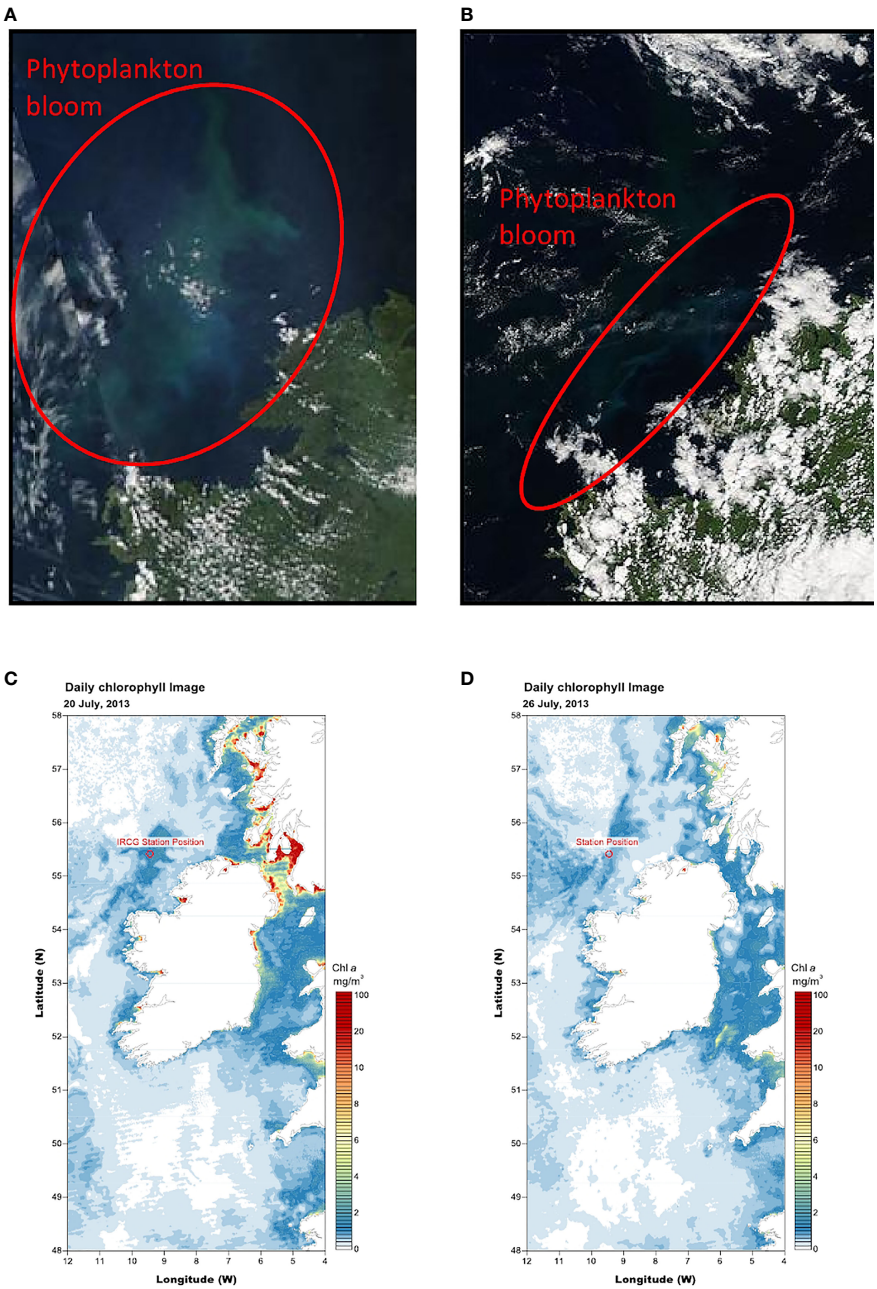

FIGURE 13 | **(A)** 20th July 2013 phytoplankton bloom off northwest Ireland NASA (MODIS: Aqua); **(B)** 26th July 2013 NASA (MODIS Aqua); **(C)** 20th July 2013 modelled Chlorophyll data and **(D)** 26th July 2013. Where **(C, D)** is derived from a data product from Ifremer DYNECO and CERSAT in Brest, France and NASA in the USA. The position of the station where samples were taken by the Irish Coast Guard (IRCG) is indicated in **(C, D)**.

Further opportunistic sampling during the *A. minutum* bloom event in summer 2018 is reported by Ben-Gigirey et al. (2020). Paralytic Shellfish Toxins (PSTs) were analyzed in marine fauna non-traditional vectors (invertebrates, fish and dolphins), collected at several locations in the Ria de Vigo. Invertebrate and fish samples were collected by scuba divers and local fishermen. In July and August 2018, samples from stranded dolphin (*Delphinus delphis*) individuals were taken by local research groups (CEMMA, "Coordinadora para o Estudo dos Mamíferos Mariños", http://www.cemma.org and the Marine Mammals Department at IEO Vigo). Highest PST levels were quantified in bivalve molluscs, however, PSTs were also found in mullet, mackerel, starfish, squids and ascidians. These results highlight the potential for the accumulation of PSTs in marine invertebrates other than shellfish that can potentially act as food web vectors and/or pose a serious risk for human health upon consumption.

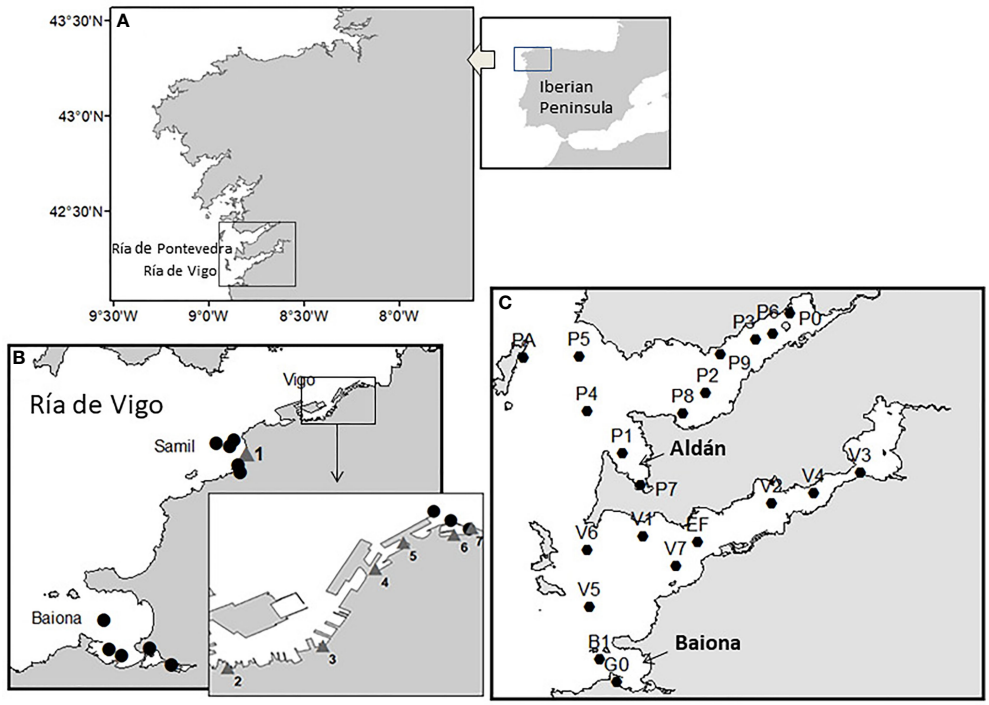

FIGURE 14 | Area of study for the *Alexandrium minutum* bloom in summer 2018 (Galicia, NW Spain). **(A)** Rías Baixas. **(B)** Sampling stations for cyst mapping (circles) and bloom seawater sampling locations (numbered triangles) in Vigo marina and Samil Beach. Fish and invertebrate samples for PSTs analyses were obtained from individuals collected next to 3 and 6. **(C)** Sampling stations of the Galician monitoring programme (INTECMAR) in the Rías de Vigo and Pontevedra.

FIGURE 15 | PhD student María García-Portela (IEO Vigo) sampling the *Alexandrium minutum* red tide in Samil Beach, June 28th, 2018. (left). *A. minutum*: light microscopy micrograph (400X) of the bloom sample from Samil Beach, June 28th (right). Figure reproduced from Rodríguez et al., 2018, Harmful Algae News.

5 DISCUSSION

5.1 Use of Drones (RPAS and UAVs) for HAB Monitoring

In the last decade, commercial airborne robotic platforms have become commonplace in the form of UAVs or 'drones'. Several recent reviews confirm the growing number of applications and developments in aquatic environments (Lally et al., 2019), including experiences in algal bloom monitoring (Kislik et al., 2018; Wu et al., 2019). The flexibility in flight scheduling, the high spatial and temporal resolution of the sampling and the cost effectiveness are the main reported advantages of UAVs, and thus it is expected that UAVs can provide a means of assisting HAB managers and monitoring agencies.

UAVs can collect both images and water samples. The collection of images is promoted by the development of lightweight sensors and allows the acquisition of images in high spatial and temporal resolution (several times per day)

with relatively low cost. UAVs in harmful algal research can be more flexible than satellite or airborne sampling and permit adapting to the high spatial and temporal variability of phytoplankton (Kislik et al., 2018). The applications of algal bloom detection with image sensors in UAVs also note that correction and calibration of images can overcome some of the problems of weather, sun glint or aerosols that cause inconsistent optical environments (Kislik et al., 2018; Wu et al., 2019; Cheng et al., 2020), although further testing in real operations is required the generalization of the use of UAVs in algal bloom studies.

Additionally, water samples can be collected by UAVs and drones. Several studies review that water sampling with drones having VTOL capability is feasible (Lally et al., 2019). As described above, during PRIMROSE we were able to prove BVLOS operations of RPAS, opening an opportunity for a step-change in rapid survey and sampling. The technical capability to operate BVLOS has been used in the polar regions for over a decade, but this has relied on the inherent zero risks to air-traffic (as there was no air traffic). The issue with BVLOS when integrating into civilian airspace is to demonstrate that at all times, and during every flight, the aircraft is under complete control, even with intermittent communication or partial system failure; the issue is trust in the aircraft and the operational procedures. These are not yet sufficiently mature for BVLOS to be currently commercially viable.

For the HAB monitoring applications, this dual capability (BVLOS and VTOL) means that aquaculture sites in the Scottish islands and inshore area around the Hebrides are now accessible to the SAMS laboratory at Oban with flight times of under one hour, and a payload capability of 2 -5 kg (depending on flight time required). Delivery of samples from aquaculture sites is essentially identical to a hospital delivery service proven in 2020; water (or other) samples can be transported rapidly from aquaculture sites to the mainland for assay. On the other hand, drones can collect validation data for forecast modelling since they can either fly instrumentation in the pod, rather than deliver physical samples, but also could hover-and-collect sea-surface samples on demand in places outside aquaculture sites, which was the intention of the water-landable quadcopter TD7.

5.2 ASVs in HAB Monitoring

Although not constrained by an equivalent to a Civil Aviation Authority and VLOS rules, the range for ASV operation is limited by the physics of scale. Smaller boats are slower than larger ones, with the hull speed increasing with the square root of the length of the waterline. The volume available for fuel (whether battery or combustion) will also tend to increase with the cube of the waterline length. It is over-simplifying, but a boat four times the length will travel twice as fast for 64x the time (the power requirements will also increase). Boat scale to wave scale also limits the operational limit of upper wind strength. All indicate that for an ASV, bigger is better, and thereby any advantages over existing traditional boats with people on board are diminished.

The Galician development shows how a regional government in the Atlantic Area used public procurement as a tool to advance the TRL of unmanned vehicles towards the demonstration in real conditions of the potential use of this technology in supporting public services. This process requires a high level of preparation effort of the initial procurement documents and concept of the desired development, as well as a high level of financing. A call for tenders was launched in 2017 after a preparation project and a robust prototype is in the demonstration phase. The prototype has been able to collect water samples and operate a CTD in unmanned and manned mode, and further testing is ongoing to ensure that samples can be properly used for phytoplankton identification.

The ImpYak system demonstrated in PRIMROSE benefits from Arduino microcontroller and other technologies affordable to research groups or monitoring programs having limited budget and clearly illustrate the cost-effectiveness of autonomous vehicles. ImpYak can be practically used at the 10 km scale of local aquaculture monitoring, and has been invited to Norway for trials in Svalbard fjords. Although not capable of deep-ocean surveys, these units are proving viable in the intermediate zone between shore-side access with, say, wellington boots or waders, and a large ocean-going vessel: this is the realm of the sea-loch or inner archipelago, which are notoriously difficult to view with satellite or forecast with existing resolution models. Therefore, cost-effective ASVs based on open source solutions like ImpYak are complementary in near coast measurements of HABs, which we have illustrated in this review that are still a necessary complement to HAB monitoring to be able to sample and analyze the presence of harmful algae or toxins.

5.3 Opportunistic and Non-Conventional Sampling

Marine biotoxins are natural compounds mainly produced by marine microalgae, dinoflagellates, and diatoms (Martínez et al., 2015). In terms of their evaluation, it is essential to analyze the toxins in relation to maximum permitted levels defined in the EU Regulation No 853/2004 (European Parliament and Council, 2004) and its amendments: Paralytic Shellfish Toxins, Amnesic Shellfish Toxins, Okadaic acid and Dinophysistoxins, Azaspiracids and Yessotoxins. It is also desirable to evaluate emerging toxins such as Spirolides, Pinnatoxins, Tetrodotoxin, Gymnodimines, etc. In the case of non-traditional vectors, evaluation of these compounds would provide an indication of the presence of marine biotoxins, and their potential accumulation and transfer in the food web, allowing appropriate further monitoring or action to be taken.

The detection of marine biotoxins in non-traditional vectors (rarely covered by the monitoring programs) has been already reported in European countries such as Portugal, UK, Croatia and Spain (Ben-Gigirey et al., 2012; Silva et al., 2013; Silva et al., 2018; Dean et al., 2020). Some of those vectors are consumed by humans and could cause intoxications (Roje-Busatto and Ujevic, 2014). The results from our activity in PRIMROSE demonstrate the need to contemplate non-conventional monitoring to complement traditional monitoring in order to prevent seafood intoxications. For example, the possible presence of PSTs in non-bivalve mollusc species, such as cephalopods, echinoderms and tunicates and the increased interest in the exploitation of marine

live resources other than bivalves have promoted a revision of monitoring strategies introducing non-traditional vectors. EU Regulation (EC) No 853/2004 (European Parliament and Council, 2004) sets the maximum PSTs concentrations not only in bivalve molluscs, but also in echinoderms, tunicates and marine gastropods. However, published data relating to these organisms so far are scarce and more studies are needed to evaluate the potential risks they could pose for human health as well as their impacts in the trophic chain. On top of that, more data on the presence of emerging marine toxins in the EU marine invertebrates are also necessary in order to perform risk assessment evaluations studies on these non-traditional vectors.

5.4 IFCs in a HAB Monitoring Context

Traditional light microscopy based HAB monitoring is typically undertaken for shellfish safety on a weekly basis. Given the potential for rapid harmful bloom development under some environmental conditions, this presents a risk to human health. IFCs offer a solution due to their hugely more rapid sample throughput, allowing multiple samples to be analyzed in a day. Finfish farms are not typically supported by such regulatory monitoring and hence often undertake on site microscopy based cell counts on a daily basis. This is labor and time intensive, and while the cost of an IFC is substantial, over the period of a number of years it is likely to be cost effective.

We have shown in our IFC demonstrations that the development of classifiers capable of automatically and reliably identifying and enumerating target phytoplankton cells is critical for use of such instruments in any assessment of phytoplankton communities including HAB species. In the PRIMROSE experience in the Daoulas estuary, the construction of large clusters from daily IFC data in agreement with the protocol for plankton identification from other monitoring stations along the French coast allowed the comparisons with the other data sets, demonstrating that the capacity of IFC for sustained daily monitoring of plankton and an improvement in the assessment of plankton variability. This tool will enlarge the available data set for statistical models [(Fernandes-Salvador et al., 2021), this issue] with new data of primary importance to describe phytoplankton community dynamics. The development of specific classifiers using images is also required but several problems are encountered: while many HAB genera are of concern in multiple countries, the morphological variability of cells requires the development of regional rather than global classifiers. Such developments hinge on the manual identification and annotation of phytoplankton images by trained taxonomists. Ideally many thousand images are required to account for variability in cell size, shape and orientation.

Ongoing improvement of image characterization is the next essential step towards a HAB warning system based on existing classifiers with well-known methods like RFAs, SVMs or CNNs. Typically an IFC image classifier utilizes feature or image characteristic vectors calculated from the labelled images. These characteristics, based on shape or texture descriptors, provide a reduced representation of an image. These vectors are then input to classifiers like RFAs or SVMs that have experienced considerable success in cell classification [e.g. (Sosik and Olson, 2007; Campbell et al., 2010) for SVM (Harred and Campbell, 2014) for RFA]. CNNs are suitable for processing grid-like data such as images and hence may be particularly suitable for IFC data. In fact, deep learning and Convolutional Neural Networks (CNNs) in particular have shown superior performance for image classification tasks (Sharma et al., 2018) and are now being applied to IFC data (Orenstein and Beijbom, 2017; González et al., 2019; Guo et al., 2021). CNNs do not need to specify feature vectors as input because the network itself learns them from the images during the training process called deep features, and may eventually become the method of choice for IFC image classification. For HAB applications, new classifiers for automatic clustering of HAB species need to be specifically constructed based on new data sets like those presented here in the IFC mooring demonstration in the Daoulas estuary for *Alexandrium minutum* and *Pseudo-nitzschia* spp. In addition to image recognition for species identification, machine-learning models allow estimation of biovolume from images using distance maps (Moberg and Sosik, 2012). Therefore, IFC have not only a potential to identify HAB species but also to characterize phytoplankton biomass and community composition.

Finally, methods to rapidly disseminate IFC data to stakeholders are required. The IFCB includes a dashboard that is capable of providing data to the user in real time. The interface for discovering and viewing IFC data in the HABreports website (Davidson et al., 2021) is a demonstration of an online user interface system being developed to best characterize and synthesize IFC data for non-expert users to allow them to evaluate HAB risk in their location. The standard clustering and the export flow tested during the deployment of the French IFC mooring follows international standards so that generated data files can be exported in European infrastructures like SeaDataNet, allowing them to be merged with other IFC repositories. Rapid data processing and access, especially of images for clustering, which is the key to an early warning system, remains under construction. The pipelines for data processing and their storage follow the FAIR principles (Findability, Accessibility, Interoperability, and Reusability; Wilkinson et al., 2016).

6 CONCLUSIONS AND OUTLOOK

The activities undertaken during PRIMROSE clearly show the potential of novel monitoring techniques, especially with autonomous devices, to characterize the high temporal and spatial variability of HABs and open new ways to develop early warning systems that use a larger set of biological data. In the same way, UAVs operating in Beyond Visual Line Of Sight (BVLOS) with Vertical Take-off and Landing (VTOL) and ASVs showed great potential to deliver assay samples and acquire data for model validation.

The examples from France and Scotland demonstrate the potential for IFC based monitoring in locations threatened by HABs, providing markedly enhanced temporal resolution compared to the, typically weekly, regulatory monitoring that

currently occurs to ensure shellfish safety. However, the cost of such instruments remains preventative to their wide deployment, at least within the relatively low financial margin shellfish industry. It is therefore important that comparative spatial studies be undertaken to best understand the sphere of influence of regional sentinel sites at which IFCs are deployed. A second IFCB will soon be deployed in Shetland to facilitate such studies in Scottish waters. In the Atlantic Area, a further IFC (Cytobuoy) is also expected to be installed in Galicia by IEO. In France, PRIMROSE partners are now a part of a French national consortium developing an international platform including phytoplankton images. This consortium is supported by the ODATIS Ocean Cluster (Ocean DAta Information and Services, https://www.odatis-ocean.fr/en/). In this way, we envisage participating in developments of pipelines devoted to toxic algae indexes.

Combined monitoring of HABs with the determination of marine biotoxins in non-traditional vectors would enhance the detection of toxic episodes and help to prevent food safety issues. The opportunistic sampling of non-traditional vectors has the advantage of getting very valuable information about the levels of regulated toxins present in those matrices in the production areas. These production areas may be different from those that are currently regularly monitored. Knowing the toxin levels in those vectors, offers the potential to apply measures to prevent human and animal (Dean et al., 2021) intoxications. The information gathered could also guide the design of future monitoring plans. The main drawback is the need for more resources: staff, laboratories equipment, sampling tools, vehicles (i.e. oceanographic vessels), sampling plans in rocky shore areas, etc. Therefore these would add extra-costs to the regular monitoring. The evaluation of emergent toxins in these vectors would additionally provide data for the risk assessment evaluation of those compounds. Therefore they should be reinforced in the near future. Additional studies, supported by PRIMROSE, that aim to evaluate the potential presence of emergent toxins, Cyclic Imines such as Spirolides, Gymnodimine and Pinnatoxins (Villar-González et al., 2006; Davidson et al., 2015; Otero et al., 2019; Lamas et al., 2021) and Tetrodotoxins (Blanco L. et al., 2019) by High Performance Liquid Chromatography coupled to High Resolution Mass Spectrometry in non-traditional vectors from the Galician Rias Baixas remain on-going.

In offshore or non-easily accessible areas, where some HABs initiate, identification relies mainly on satellite observations, limited by cloud cover. However, the potential exists to obtain oceanographic information and plankton samples on the surface from FerryBox devices in commercial vessels (Hartman et al., 2014) or in the water column from autonomous moorings or glider cruises (Stumpf et al., 2010; Seegers et al., 2015). Improving the coordination of oceanographic vessel operators can facilitate the acquisition of samples if the HAB alert happens to coincide with an oceanographic cruise. An illustration of this coordination is reported in Jordan et al., (2021), this issue. *Karenia* spp. risk was detected by satellite off the south coast of Ireland in July 2019 while an oceanographic cruise was in the area and samples could therefore be taken, confirming the presence of *K. mikimotoi*. However, most of the time HAB data sampling by coastguards is one of the few methods to acquire HAB *in situ* data in offshore areas on request. Our experience has shown that elaboration of protocols can improve the capacity of water sampling by coastguards in areas far from monitoring sites, and consequently can complement the HAB detection by satellite, in particular to assess the extent of high biomass blooms in areas of recreation or aquaculture importance. A potential step forward to coordination and protocol sharing initiatives are quick HAB screening approaches like HABscope (Hardison et al., 2019) since it is easy to train non scientists (e.g. fishers, coastguard personnel, aquaculture operators) on its use. This relatively inexpensive, ~ $500, robust microscope is attached to an iPod touch and uses Artificial Intelligence (AI) image detection software to isolate the swimming pattern of specific HAB taxa. This facilitates the automatic identification and cell enumeration of the target species with a direct upload and transfer of images *via* Wi-Fi for verification and integration into HAB early warning systems. Ireland is in the process of testing the NOAA developed HABscope in coastal and shelf waters (Jordan and Cusack, Marine Institute, ongoing work[6]) to see if *Karenia* spp. can be detected using the same AI that NOAA uses for *K. brevis* (Hardison et al., 2019).

Novel monitoring for HABs has the potential to improve the cost-effectiveness of early warning systems. Strategies and obligations vary among countries but HAB monitoring is focused on safeguarding human health rather than on managing aquaculture business risk (Fernandes-Salvador et al., 2021). Since the financial cost of HAB and biotoxin monitoring at all aquaculture sites is prohibitive, the currently regulatory HAB network in a particular country is typically based at a subset of shellfish harvesting sites, with the specific locations and frequency of sampling dictated by local and national risk assessments. Higher frequency autonomous monitoring potentially offers the opportunity to decrease the size of the traditional monitoring network, but will require the identification of sentinel sites that allow the identification of a developing bloom, potentially followed by triggering local sampling at risk aquaculture areas. However, since the current regulatory monitoring of HABs and toxins in regions like the EU is very effective in safeguarding human health (Blanco J. et al., 2019; Belin et al., 2021; Davidson et al., 2021), changes in the monitoring network also require a careful evaluation of the eventual health risk increase associated with the relocation or reduction of sampling sites.

The cost of maintaining HAB monitoring and early warning systems is clearly lower than the cost of HAB induced effects in human health and of socio economic impacts in the aquaculture sector. However, an accurate assessment of the actual effect of short term forecasts mitigation and consequently of their economical impact is very difficult to achieve because the estimation of the real cost of HAB is complex. For fish aquaculture, the economic loss is clear in extreme events

[6] https://www.marine.ie/Home/site-area/news-events/press-releases/irish-scientists-collaborate-noaa-test-new-habscope

causing fish mortality (Karlson et al., 2021) but the losses due to minor fish kills and sub-lethal events require careful evaluation of the mitigation strategies and a cost assessment would involve reviewing aquaculture business planning as well as sharing of monitoring and potentially sensitive commercial information between industry and scientists (Davidson et al., 2020). For shellfish aquaculture, economical evaluation of costs is more difficult since biogeography, seasonal variability, regularity of the bloom, type of shellfish and commercialisation issues can strongly modulate the cost of HAB (Rodriguez et al., 2011; Martino et al., 2020; Guillotreau et al., 2021; Karlson et al., 2021).

Anyway, advancement of existing forecasting approaches requires additional inputs to provide a better understanding and monitoring of the distribution of HAB species and microbiological contamination. We have seen that novel methodologies exist and have potential to complement existing monitoring by improving spatial and temporal coverage of observations. The methodologies we have presented can enhance the capacity of sampling in areas outside the monitoring sites, provide earlier detection of the presence of HAB species and allow higher temporal monitoring and cost-efficient sampling in the period between consecutive samplings in the regulatory monitoring. Thus, the higher temporal frequency provided by these approaches can improve the forecasts as data becomes hourly/daily rather than weekly. Therefore, we believe that novel techniques will lead to improved prediction and early warning of future events resulting in an enhanced mitigation capacity, which will benefit aquaculture producers. The PRIMROSE experience shows that advances can be achieved through cooperation and sharing of knowledge, experiences and demonstrations.

Finally, for all novel monitoring, despite some unavoidable time-consuming constraints associated with sensor servicing or administrative processes like permissions or limitations for flight, the emerging bottleneck appearing now is the data flow. There remains a lot of technical development and further testing is required to obtain these new data sets in real or near real time. Early warning systems for HABs and microbiological risk in aquaculture are expected to be able to make a strong step forward when these pipelines are fully implemented.

DATA AVAILABILITY STATEMENT

The raw data supporting the conclusions of this article will be made available by the authors upon request. Any requests for Marine Institute Digital Data, please go to this link: https://www.marine.ie/Home/marine-institute-request-digital-data. The data set from the Somlit monitoring used in section 2.1 has been obtained from a third party. Requests to access these datasets should be directed to Lambert C., christophe.lambert@univ-brest.fr.

AUTHOR CONTRIBUTIONS

All authors participated in the research and discussion of the potential of novel methodologies for providing in situ data to HAB early warning systems. MS and LQ deployed and analysed IFC in the Bay of Brest. KD, CW, SG-P and GA deployed and analysed IFC in Scotland. PA coordinated drone development and demonstrations in Scotland. CC and JS designed HAB data sampling by coastguards. FR and BB-G participated in samplings of harmful algae and marine biotoxins in Galicia. MR-V coordinated research and writing of the manuscript and produced the first draft together with MS, PA, KD, CC and PN and all authors, who approved it for publication.

FUNDING

This work has been funded by the European Union Interreg Atlantic Area project PRIMROSE EAPA182_2016, an IOC-SCOR GlobalHAB endorsed project. KD and CW were also funded by the UKRI grants NE/T008571/1 and BB/S004246/1 and SG-P was funded by a PhD studentship funded by Marine Scotland Science and the Data Lab. Sampling in Ría de Vigo had support from the Spanish National Project DIANAS (CTM2017-86066-R, MICINN, Spain) and Project IN607A 2019/04 (GRC, Xunta de Galicia, Spain).

ACKNOWLEDGMENTS

We thank Paola Arce of SAMS for her contribution to the Scottish IFCB development work. We also thank Marie Latimier and Julien Quere for their contributions to the Ifremer flow cytometer deployments and the data analyses. Special thanks to Alex Brown from Wingcopter for providing and allowing the reproduction of pictures in **Figure 9**, to the Departamento de Xestión de Innovación, Área de Programas of the Axencia Galega de Innovacion for providing pictures of the demonstration of the MAR2 prototype in **Figure 11**, and to Cathal Gahan (Environmental Protection Agency, Ireland) and Kevin O'Sullivan (Irish pilot) for providing photographic evidence of phytoplankton blooms in **Figure 12**.

SUPPLEMENTARY MATERIAL

The Supplementary Material for this article can be found online at: https://www.frontiersin.org/articles/10.3389/fmars.2022.791329/full#supplementary-material

REFERENCES

Artigas, F., Créach, V., Houliez, E., Karlson, B., Lizon, F., Seppälä, J., et al. (2019). *Novel Methods for Automated in Situ Observations of Phytoplankton Diversity and Productivity: Synthesis of Exploration, Inter Comparisons and Improvements. JERICO-NEXT WP3, Deliverable 3.2. Version 5* (Brest, France: IFREMER), 88pp. JERICO-NEXT-WP3-D3.2-120819-V5. doi: 10.25607/OBP-945

Belin, C., Soudant, D., and Amzil, Z. (2021). Three Decades of Data on Phytoplankton and Phycotoxins on the French Coast: Lessons From REPHY and REPHYTOX. *Harmful Algae* 102, 101733. doi: 10.1016/j.hal.2019.101733

Ben-Gigirey, B., Rodríguez-Velasco, M. L., Otero, A., Vieites, J. M., and Cabado, A. G. (2012). A Comparative Study for PSP Toxins Quantification by Using MBA and HPLC Official Methods in Shellfish. *Toxicon* 60, 864–873. doi: 10.1016/j.toxicon.2012.05.022

Ben-Gigirey, B., Rossignoli, A. E., Riobó, P., and Rodríguez, F. (2020). First Report of Paralytic Shellfish Toxins in Marine Invertebrates and Fish in Spain. *Toxins* 12 (11), 723. doi: 10.3390/toxins12110723

Berdalet, E., Fleming, L. E., Gowen, R., Davidson, K., Hess, P., Backer, L. C., et al. (2016). Marine Harmful Algal Blooms, Human Health and Wellbeing: Challenges and Opportunities in the 21st Century. *J. Mar. Biol. Assoc. U.K.* 2015, 61–91. doi: 10.1017/S0025315415001733

Blanco, J., Arévalo, F., Correa, J., and Moroño, Á. (2019). Lipophilic Toxins in Galicia (NW Spain) Between 2014 and 2017: Incidence on the Main Molluscan Species and Analysis of the Monitoring Efficiency. *Toxins* 11 (10), 612. doi: 10.3390/toxins11100612

Blanco, L., Lago, J., González, V., Paz, B., Rambla-Alegre, M., and Cabado, A. G. (2019). Occurrence of Tetrodotoxin in Bivalves and Gastropods From Harvesting Areas and Other Natural Spaces in Spain. *Toxins (Basel)* 11, 1–9. doi: 10.3390/toxins11060331

Bravo, I., Fraga, S., Figueroa, R. I., Pazos, Y., Massanet, A., and Ramilo, I. (2010). Bloom Dynamics and Life Cycle Strategies of Two Toxic Dinoflagellates in a Coastal Upwelling System (NW Iberian Peninsula). *Deep Sea Res. Part II Top. Stud. Oceanogr.* 57, 222–234. doi: 10.1016/j.dsr2.2009.09.004

Bresnan, E., Arévalo, F., Belin, C., Branco, M. A., Cembella, A. D., Clarke, D., et al. (2021). Diversity and Regional Distribution of Harmful Algal Events Along the Atlantic Margin of Europe. *Harmful Algae* 102, 101976. doi: 10.1016/j.hal.2021.101976

Campbell, L., Henrichs, D. W., Olson, R. J., and Sosik, H. M. (2013). Continuous Automated Imaging-In-Flow Cytometry for Detection and Early Warning of *Karenia Brevis* Blooms in the Gulf of Mexico. *Environ. Sci. Pollut. Res.* 20, 6896–6902. doi: 10.1007/s11356-012-1437-4

Campbell, L., Olson, R. J., Sosik, H. M., Abraham, A., Henrichs, D. W., Hyatt, C. J., et al. (2010). First Harmful *Dinophysis* (Dinophyceae, Dinophysiales) Bloom In the Us Is Revealed By Automated Imaging Flow Cytometry. *J. Phycol.* 46, 66–75. doi: 10.1111/j.1529-8817.2009.00791.x

Chapelle, A., Le Gac, M., Labry, C., Siano, R., Quere, J., Caradec, F., et al. (2015). The Bay of Brest (France), a New Risky Site for Toxic *Alexandrium Minutum* Blooms and PSP Shellfish Contamination. *Harmful Algae News* 51, 4–5. doi: 10.5281/zenodo.5110019

Cheng, K. H., Chan, S. N., and Lee, J. H. W. (2020). Remote Sensing of Coastal Algal Blooms Using Unmanned Aerial Vehicles (UAVs). *Mar. Pollut. Bull.* 152, 110889. doi: 10.1016/j.marpolbul.2020.110889

Dashkova, V., Malashenkov, D., Poulton, N., Vorobjev, I., and Barteneva, N. S. (2017). Imaging Flow Cytometry for Phytoplankton Analysis. *Methods San Diego Calif.* 112, 188–200. doi: 10.1016/j.ymeth.2016.05.00

Davidson, K., Anderson, D. M., Mateus, M., Reguera, B., Silke, J., Sourisseau, M., et al. (2016). Forecasting the Risk of Harmful Algal Blooms. *Harmful Algae* 53, 1–7. doi: 10.1016/j.hal.2015.11.005

Davidson, K., Baker, C., Higgins, C., Higman, W., Swan, S., Veszelovszki, A., et al. (2015). Potential Threats Posed by New or Emerging Marine Biotoxins in UK Waters and Examination of Detection Methodologies Used for Their Control: Cyclic Imines. *Mar. Drugs* 13, 7087–7112. doi: 10.3390/md13127057

Davidson, K., Jardine, S., Martino, S., Myre, G., Peck, L., Raymond, R., et al. (2020). "The Economic Impacts of Harmful Algal Blooms on Salmon Cage Aquaculture," in *GlobalHAB. Evaluating, Reducing and Mitigating the Cost of Harmful Algal Blooms: A Compendium of Case Studies*. Ed. V. L. Trainer, (Sidney, BC, Canada: PICES Press) 84–94+.

Davidson, K., Whyte, C., Aleynik, D., Dale, A., Gontarek, S., Kurekin, A. A., et al. (2021). HABreports: Online Early Warning of Harmful Algal and Biotoxin Risk for the Scottish Shellfish and Finfish Aquaculture Industries. *Front. Mar. Sci.* 8, 631732. doi: 10.3389/fmars.2021.631732

Dean, K. J., Alexander, R. P., Hatfield, R. G., Lewis, A. M., Coates, L. N., Collin, T., et al. (2021). The Common Sunstar Crossaster Papposus—A Neurotoxic Starfish. *Mar. Drugs* 19, 695. doi: 10.3390/md19120695

Dean, K. J., Hatfield, R. G., Lee, V., Alexander, R. P., Lewis, A. M., Maskrey, B. H., et al. (2020). Multiple New Paralytic Shellfish Toxin Vectors in Onshore North Sea Benthos, a Deep Secret Exposed. *Mar. Drugs* 18, 400. doi: 10.3390/md18080400

Dunker, S. (2019). Hidden Secrets Behind Dots: Improved Phytoplankton Taxonomic Resolution Using High-Throughput Imaging Flow Cytometry. *Cytometry A* 95, 854–868. doi: 10.1002/cyto.a.23870

Dunker, S., Boho, D., Waeldchen, J., and Maeder, P. (2018). Combining High-Throughput Imaging Flow Cytometry and Deep Learning for Efficient Species and Life-Cycle Stage Identification of Phytoplankton. *BMC Ecol.* 18, 51. doi: 10.1186/s12898-018-0209-5

Escalera, L., Pazos, Y., Dolores Doval, M., and Reguera, B. (2012). A Comparison of Integrated and Discrete Depth Sampling for Monitoring Toxic Species of *Dinophysis*. *Mar. Pollut. Bull.* 64 (1), 106–113. doi: 10.1016/j.marpolbul.2011.10.015

Escalera, L., Reguera, B., Moita, T., Pazos, Y., Cerejo, M., Cabanas, J. M., et al. (2010). Bloom Dynamics of *Dinophysis Acuta* in an Upwelling System: *In Situ* Growth Versus Transport. *Harmful Algae* 9 (3), 312–322. doi: 10.1016/j.hal.2009.12.002

European Parliament and Council (2004). Regulation No 853/2004 of 29 April 2004 Laying Down Specific Hygiene Rules for Food of Animal Origin. *J. Eur. Union* L 139, 55–205. 2004.

Fernandes-Salvador, J. A., Davidson, K., Sourisseau, M., Revilla, M., Schmidt, W., Clarke, D., et al. (2021). Current Status of Forecasting Toxic Harmful Algae for the North-East Atlantic Shellfish Aquaculture Industry. *Front. Mar. Sci.* 8, 666583. doi: 10.3389/fmars.2021.666583

First, M. R., and Drake, L. A. (2012). Performance of the Human "Counting Machine": Evaluation of Manual Microscopy for Enumerating Plankton. *J. Plankton Res.* 34, 1028–1041. doi: 10.1093/plankt/fbs068

Fischer, A. D., Hayashi, K., McGaraghan, A., and Kudela, R. M. (2020). Return of the "Age of Dinoflagellates" in Monterey Bay: Drivers of Dinoflagellate Dominance Examined Using Automated Imaging Flow Cytometry and Long-Term Time Series Analysis. *Limnol. Oceanogr.* 65, 2125–2141. doi: 10.1002/lno.11443

Gianella, F., Burrows, M. T., Swan, S. C., Turner, A. D., and Davidson, K. (2021). Temporal and Spatial Patterns of Harmful Algae Affecting Scottish Shellfish Aquaculture. *Front. Mar. Sci.* 8, 785174. doi: 10.3389/fmars.2021.785174

González, P., Castaño, A., Peacock, E. E., Díez, J., Del Coz, J. J., and Sosik, H. M. (2019). Automatic Plankton Quantification Using Deep Features. *J. Plankton Res.* 41 (4), 449–463. doi: 10.1093/plankt/fbz023

Guillotreau, P., Le Bihan, V., Morineau, B., and Pardo, S. (2021). The Vulnerability of Shellfish Farmers to HAB Events: An Optimal Matching Analysis of Closure Decrees. *Harmful Algae*. 101, 101968. doi: 10.1016/j.hal.2020.101968

Guo, J., Ma, Y., and Lee, J. H. (2021). Real-Time Automated Identification of Algal Bloom Species for Fisheries Management in Subtropical Coastal Waters. *J. Hydro-Environ. Res.* 36, 1–32. doi: 10.1016/j.jher.2021.03.002

Hallegraeff, G. M. (2004). "Harmful Algal Blooms: A Global Overview," in *Manual on Harmful Marine Microalgae*, *2nd revised edition*. Eds. G. M. Hallegraeff, D. M. Anderson, A. D. Cembella and H. O. Enevoldsen (Paris, France: UNESCO), 793. (Monographs on Oceanographic Methodology, 11).

Hardison, D. R., Holland, W. C., Currier, R. D., Kirkpatrick, B., Stumpf, R., Fanara, T., et al. (2019). HABscope: A Tool for Use by Citizen Scientists to Facilitate Early Warning of Respiratory Irritation Caused by Toxic Blooms of *Karenia Brevis*. *PloS One* 14 (6), e0218489. doi: 10.1371/journal.pone.0218489

Harred, L. B., and Campbell, L. (2014). Predicting Harmful Algal Blooms: A Case Study With *Dinophysis ovum* in the Gulf of Mexico. *J. Plankton Res.* 36, 1434–1445. doi: 10.1093/plankt/fbu070

Hartman, S. E., Hartman, M. C., Hydes, D. J., Smythe-Wright, D., Gohin, F., and Lazure, P. (2014). The Role of Hydrographic Parameters, Measured From a Ship of Opportunity, in Bloom Formation of Karenia Mikimotoi in the English Channel. *J. Mar. Syst.* 140, 39–49. doi: 10.1016/j.jmarsys.2014.07.001

Jordan, C., Cusack, C., Tomlinson, M. C., Meredith, A., McGeady, R., Salas, R., et al. (2021). Using the Red Band Difference Algorithm to Detect and Monitor a Karenia Spp. Bloom Off the South Coast of Ireland, June 2019. *Front. Mar. Sci.* 8. doi: 10.3389/fmars.2021.638889

Karlson, B., Andersen, P., Arneborg, L., Cembella, A., Eikrem, W., John, U., et al. (2021). Harmful Algal Blooms and Their Effects in Coastal Seas of Northern Europe. *Harmful Algae* 102, 101989. doi: 10.1016/j.hal.2021.101989

Karlson, B., Cusack, C., and Bresnan, E. (Eds.) (2010). *Microscopic and Molecular Methods for Quantitative Phytoplankton Analysis (Intergovernmental Oceanographic Commission Manuals and Guides; 55)*. (Paris, France: UNESCO). doi: 10.25607/OBP-1371

Kislik, C., Dronova, I., and Kelly, M. (2018). UAVs in Support of Algal Bloom Research: A Review of Current Applications and Future Opportunities. *Drones* 2, 35. doi: 10.3390/drones2040035

Kraft, K., Seppälä, J., Hällfors, H., Suikkanen, S., Ylöstalo, P., Anglès, S., et al. (2021). First Application of IFCB High-Frequency Imaging-In-Flow Cytometry to Investigate Bloom-Forming Filamentous Cyanobacteria in the Baltic Sea. *Front. Mar. Sci.* 8, 594144. doi: 10.3389/fmars.2021.594144

Kurekin, A. A., Miller, P. I., and van der Woerd, H. J. (2014). Satellite Discrimination of *Karenia mikimotoi* and *Phaeocystis* Harmful Algal Blooms in European Coastal Waters: Merged Classification of Ocean Colour Data. *Harmful Algae* 31, 163–176. doi: 10.1016/j.hal.2013.11.003

Lally, H. T., O'Connor, I., Jensen, O. P., and Graham, C. T. (2019). Can Drones be Used to Conduct Water Sampling in Aquatic Environments? A Review. *Sci. Total Environ.* 670, 569–575. doi: 10.1016/j.scitotenv.2019.03.252

Lamas, J. P., Arévalo, F., Moroño, Á., Correa, J., Rossignoli, A. E., and Blanco, J. (2021). Gymnodimine A in Mollusks From the North Atlantic Coast of Spain: Prevalence, Concentration, and Relationship With Spirolides. *Environ. Pollut.* 279, 116919. doi: 10.1016/j.envpol.2021.116919

Lundholm, N., Churro, C., Fraga, S., Hoppenrath, M., Iwataki, M., Larsen, J., et al. (Eds.) (2009). *IOC-UNESCO Taxonomic Reference List of Harmful Micro Algae*. (Paris, France: UNESCO). Available at: https://www.marinespecies.org/hab on 2022-03-14. doi: 10.14284/362

Maguire, J., Cusack, C., Ruiz-Villarreal, M., Silke, J., McElligott, D., and Davidson, K. (2016). Applied Simulations and Integrated Modelling for the Understanding of Toxic and Harmful Algal Blooms (ASIMUTH): Integrated HAB Forecast Systems for Europe's Atlantic Arc. *Harmful Algae* 53, 160–166. doi: 10.1016/j.hal.2015.11.006

Martínez, A., Garrido-Maestu, A., Ben-Gigirey, B., Chapela, M. J., González, V., Vieites, J. M., et al. (2015). "Marine Biotoxins," in *Springer Handbook of Marine Biotechnology*. Ed. S.-K. Kim (Heidelberg, Germany: Springer), 869–904. doi: 10.1007/978-3-642-53971-8_37

Martino, S., Gianella, F., and Davidson, K. (2020). An Approach for Evaluating the Economic Impacts of Harmful Algal Blooms: The Effects of Blooms of Toxic Dinophysis spp. on the Productivity of Scottish Shellfish Farms. *Harmful Algae*. 99, 101912. doi: 10.1016/j.hal.2020.101912

Mateus, M., Fernandes, J., Revilla, M., Ferrer, L., Villarreal, M. R., Miller, P., et al. (2019). Early Warning Systems for Shellfish Safety: The Pivotal Role of Computational Science, in Proceedings of the International Conference on Computational Science (Cham: Springer) 361–375. doi: 10.1007/978-3-030-22747-0_28

Moberg, E. A., and Sosik, H. M. (2012). Distance Maps to Estimate Cell Volume From Two-Dimensional Plankton Images. *Limnol. Oceanogr. Methods* 10, 278–288. doi: 10.4319/lom.2012.10.278

Orenstein, E. C., and Beijbom, O. (2017). "Transfer Learning and Deep Feature Extraction for Planktonic Image Data Sets," in *IEEE Winter Conference on Applications of Computer Vision (WACV)*,, 2017. 1082–1088. doi: 10.1109/WACV.2017.125

Otero, P., Miguéns, N., Rodríguez, I., and Botana, L. M. (2019). LC–MS/MS Analysis of the Emerging Toxin Pinnatoxin-G and High Levels of Esterified OA Group Toxins in Galician Commercial Mussels. *Toxins (Basel)* 11, 394. doi: 10.3390/toxins11070394

Raine, R.McDermott, G.Silke, J.Lyons, K.Nolan, G.Cusack, C. (2010). A Simple Short Range Model for the Prediction of Harmful Algal Events in the Bays of Southwestern Ireland. *J. Mar. Syst.* 83 (3–4), 150–157. doi: 10.1016/j.jmarsys.2010.05.001

REPHY – French Observation and Monitoring program for Phytoplankton and Hydrology in coastal waters (2021). *REPHY Dataset - French Observation and Monitoring Program for Phytoplankton and Hydrology in Coastal Waters. Metropolitan data* (SEANOE). doi: 10.17882/47248

Rodríguez, F., Escudeiro, A., and Reguera, B. (2018). Red Waters in Ría De Vigo (NW Spain). *Harmful Algae News* 61, 1–4. doi: 10.5281/zenodo.5109858

Rodríguez, G. R., Villasante, S., and García-Negro, M. C. (2011). Are Red Tides Affecting Economically the Commercialization of the Galician (NW Spain) Mussel Farming?. *Mar. Policy* 35 (2), 252–257. doi: 10.1016/j.marpol.2010.08.008

Roje-Busatto, R., and Ujevic, I. (2014). PSP Toxins Profile in Ascidian *Microcosmus Vulgaris* (Heller 1877) After Human Poisoning in Croatia (Adriatic Sea). *Toxicon* 79, 28–36. doi: 10.1016/j.toxicon.2013.12.014

Seegers, B. N., Birch, J. M., Marin, R.III, Scholin, C. A., Caron, D. A., Seubert, E. L., et al. (2015). Subsurface Seeding of Surface Harmful Algal Blooms Observed Through the Integration of Autonomous Gliders, Moored Environmental Sample Processors, and Satellite Remote Sensing in Southern California. *Limnol. Oceanogr.* 60, 754–764. doi: 10.1002/lno.10082

Sharma, N., Jain, V., and Mishra, A. (2018). An Analysis of Convolutional Neural Networks for Image Classification. *Proc. Comput. Sci.* 132, 377–384. doi: 10.1016/j.procs.2018.05.198

Silva, M., Barreiro, A., Rodriguez, P., Otero, P., Azevedo, J., Alfonso, A., et al. (2013). New Invertebrate Vectors for PST, Spirolides and Okadaic Acid in the North Atlantic. *Mar. Drugs* 11, 1936–1960. doi: 10.3390/md11061936

Silva, M., Rey, V., Barreiro, A., Kaufmann, M., Neto, A. I., Hassouani, M., et al. (2018). Paralytic Shellfish Toxins Occurrence in non-Traditional Invertebrate Vectors From North Atlantic Waters (Azores, Madeira, and Morocco). *Toxins* 10, 362. doi: 10.3390/toxins10090362

Sosik, H. M., and Olson, R. J. (2007). Automated Taxonomic Classification of Phytoplankton Sampled With Imaging-in-Flow Cytometry. *Limnol. Oceanogr. Methods* 5, 204–216. doi: 10.4319/lom.2007.5.204

Stauffer, B. A., Bowers, H. A., Earle, B., Davis, T. W., Johengen, T. H., Kudela, R., et al. (2019). Considerations in Harmful Algal Bloom Research and Monitoring: Perspectives From a Consensus-Building Workshop and Technology Testing. *Front. Mar. Sci.* 6, 399. doi: 10.3389/fmars.2019.00399

Stumpf, S., Fleming-Lehtinen, V., and Granéli, E. (2010). "Integration of Data for Nowcasting of Harmful Algal Blooms," In: J. Hall, D. E. Harrison and D. Stammer, editors. *Proceedings of OceanObs'09: Sustained Ocean Observations and Information for Society*, 21–25 September 2009 (Venice, Italy: ESA Publication WPP-306). doi: 10.5270/OceanObs09.36

Stumpf, R. P., Tomlinson, M. C., Calkins, J. A., Kirkpatrick, B., Fisher, K., Nierenberg, K., et al. (2009). Skill Assessment for an Operational Algal Bloom Forecast System. *J. Mar. Syst.* 76 (1-2), 151–161. doi: 10.1016/j.jmarsys.2008.05.016

Swan, S. C., Turner, A. D., Bresnan, E., Whyte, C., Paterson, R. F., McNeill, S., et al. (2018). *Dinophysis Acuta* in Scottish Coastal Waters and Its Influence on Diarrhetic Shellfish Toxin Profiles. *Toxins* 10, 399. doi: 10.3390/toxins10100399

Thyssen, M., Tarran, G. A., Zubkov, M. V., Holland, R. J., Gregori, G., Burkill, P. H., et al, et al. (2008). The Emergence of Automated High-Frequency Flow Cytometry: Revealing Temporal and Spatial Phytoplankton Variability. *J. Plankton Res.* 30, 333–343. doi: 10.1093/plankt/fbn005

Trainer, V. L., Pitcher, G. C., Reguera, B., and Smayda, T. J. (2010). The Distribution and Impacts of Harmful Algal Bloom Species in Eastern Boundary Upwelling Systems. *Prog. Oceanogr.* 85, 33–52. doi: 10.1016/j.pocean.2010.02.003

Villar-González, A., Rodríguez-Velasco, M. L., Ben-Gigirey, B., and Botana, L. M. (2006). First Evidence of Spirolides in Spanish Shellfish. *Toxicon* 48, 1068–1074. doi: 10.1016/j.toxicon.2006.09.001

Weeks, R. (2019). *Use of Multi- and Hyper-Spectral Techniques for Examining Ocean Reflectance From Remotely Piloted Aircraft Platforms* (Aberdeen University).

Wenhai, L., Cusack, C., Baker, M., Tao, W., Mingbao, C., Paige, K., et al. (2019). Successful Blue Economy Examples With an Emphasis on International Perspectives. *Front. Mar. Sci.* 6. doi: 10.3389/fmars.2019.00261

Whyte, C., Swan, S., and Davidson, K. (2014). Changing Wind Patterns Linked to Unusually High *Dinophysis* Blooms Around the Shetland Islands, Scotland. *Harmful Algae* 39, 365–373. doi: 10.1016/j.hal.2014.09.006

Wilkinson, M. D., Dumontier, M., Aalbersberg, I. J., Appleton, G., Axton, M., Baak, A., et al. (2016). The FAIR Guiding Principles for Scientific Data Management and Stewardship. *Sci. Data* 3, 160018. doi: 10.1038/sdata.2016.18

Wu, D., Li, R., Zhang, F., and Liu, J. (2019). A Review on Drone-Based Harmful Algae Blooms Monitoring. *Environ. Monit. Assess.* 191, 211. doi: 10.1007/s10661-019-7365-8

Conflict of Interest: The authors declare that the research was conducted in the absence of any commercial or financial relationships that could be construed as a potential conflict of interest.

the publisher, the editors and the reviewers. Any product that may be evaluated in this article, or claim that may be made by its manufacturer, is not guaranteed or endorsed by the publisher.

frontiers | Frontiers in Marine Science

ORIGINAL RESEARCH
published: 14 July 2022
doi: 10.3389/fmars.2022.914909

Advection and Composition of *Dinophysis* spp. Populations Along the European Atlantic Shelf

Saeed Hariri[1], *Martin Plus*[1], *Mickael Le Gac*[1], *Véronique Séchet*[2], *Marta Revilla*[3] *and Marc Sourisseau*[1*]

[1] IFREMER, DYNECO, Pelagos Laboratory, Plouzané, France, [2] IFREMER, DYNECO, Phycotoxins Laboratory, Nantes, France, [3] AZTI, Marine Research Division, Basque Research and Technology Alliance (BRTA), Pasaia, Spain

The main objective was to study relationships between the regional biogeography of *Dinophysis* species and water masses circulation along the European Atlantic coast. Hydrodynamic connectivities were estimated with a Lagrangian approach. Available and validated physical hindcasts from regional hydrodynamical models, with different resolutions were used. The target area is the Bay of Biscay (NE Atlantic) and connectivity was evaluated between a set of spatially distributed stations and during temporally specified periods. Different indexes related to connectivity properties such as mean, median, most frequent transit times were calculated. To illustrate the dispersion pattern, a molecular approach was jointly set-up to describe the species composition of this genus. At the seasonal scale, a high connectivity within the Bay of Biscay was observed with a slight northward connectivity from Galicia coastal waters to the Shelf of the Bay of Biscay. By comparison to the connectivity between shelf waters of French Brittany and English Channel waters, a higher connectivity between shelf waters of French Brittany and the Celtic Sea shelf was observed. The species mixing in the Bay of Biscay from Galicia waters to the Celtic Sea was confirmed by the genetic analyses despite the absence of *Dinophysis sacculus* in natural samples. The molecular methodology developed for this work, permitting at least the description of the species composition, also highlights, at the European scale, an unexpected low genetic variability which echoes the complex taxonomic classification inside the genus and the difficulties encountered by national monitoring programs to reach a taxonomic resolution at species level. It is now necessary to start some monitoring at the species level before realizing mid- or long-term forecasts.

Keywords: community, diversity, transcriptome, connectivity, biogeography, Atlantic

OPEN ACCESS

Edited by:
Joe Silke,
Marine Institute, Ireland

Reviewed by:
Wonho Yih,
Kunsan National University, South Korea
Carmela Caroppo,
National Research Council (CNR), Italy

***Correspondence:**
Marc Sourisseau
Marc.Sourisseaul@ifremer.fr

Specialty section:
This article was submitted to Marine Fisheries, Aquaculture and Living Resources, a section of the journal Frontiers in Marine Science

Received: *07 April 2022*
Accepted: *24 May 2022*
Published: *14 July 2022*

Citation:
Hariri S, Plus M, Le Gac M, Séchet V, Revilla M and Sourisseau M (2022) Advection and Composition of Dinophysis spp. Populations Along the European Atlantic Shelf. Front. Mar. Sci. 9:914909. doi: 10.3389/fmars.2022.914909

1 INTRODUCTION

Marine protists form a large part of microbial communities situated at the base of marine food webs but, within the several thousands known species, a small number produce biotoxins that can affect human health and/or induce severe economical losses. *Dinophysis* genus [including more than 120 phototrophic and heterotrophic species, Jensen and Daugbjerg (2009)] has several toxic species [≈

11, Zingone and Larsen (2022)] and due to its high economical impact on the worldwide coastal fishing and aquaculture activities, understanding its biogeography and the connectivities between coastal areas appears of primary importance. This genus is widely distributed, and seems to exhibit highly variable preferendums among species, *Dinophysis acuminata* surviving across a wide temperature range (Kamiyama et al., 2010) while other species have restricted environmental tolerances, as for example *D. norvegica* limited to boreal regions or *D. tripos* typically found in tropical-temperate waters (Reguera et al., 2012). To our knowledge, despite these differences, it is also possible to underline similarities in their life cycles: they are planktonic without known cyst stage, mixotrophic and kleptoplastidic. Their toxicity is due to the production of several lipophilic toxins such as the okadaïc acid and dinophysistoxins that cause diarrheic syndromes in humans (DSP, Diarrheic Shellfish Poisoning). *Dinophysis* spp. usually do not bloom at very high densities (rarely over 100 000 cells/L), but even when they constitute a small proportion of the microplankton community, they can contaminate seafood. Another relevant point is the apparent difficulty of taxonomic identification using optical microscopy. At least, nine species were observed along the European Atlantic coast (Bresnan et al., 2021), but various reports and publications detailed morphological variation among species that can be greater than initially described, specifically for the *Dinophysis acuminata* complex (Lassus and Bardouil, 1991; Bravo et al., 1995; Raho et al., 2013; Wolny et al., 2020; Séchet et al., 2021). Monitoring programs thus provide some historical and well distributed dataset to identify areas with recurrent blooms of this genus but the interpretation of the time series remains difficult at the species level and probably introduced bias in our perception of their ecology. For example, Bresnan et al. (2021) consider members of the *Dinophysis acuminata* complex are coastal species but according to their long growing season (occurring from spring to early autumn) and life duration, a coastal limitation of these species seems unlikely.

Like other marine species, their biogeography remains primarily constrained by environmental selection and connectivity between each environment through the advection of water parcels. Two different hypotheses are put forward to assess population connectivity and community composition. One idea is that 'everything is everywhere but the environment selects' (Bass Becking, 1934; Fenchel and Finlay, 2004; de Wit and Bouvier, 2006), whereas the other concept assumes that 'the regions of the oceans are not so well connected' (Martiny, 2006; Casteleyn, 2010) leading to local populations with their own ecological niches and physiological capacities. However, due to the fluid properties in marine environment, each parcel of water can reach any other part of the ocean, it's just a matter of time. There is thus no opposition between the two hypotheses, as suggested by Jonsson and Watson (2016). Neither concept is entirely accurate excluding the other, as species biogeography depends on the organisms observed, the efficiency of the selection process, the rate of the evolution processes as well as their transport velocities by ocean currents. As an example, it has been observed that some microbial communities have strong genetic differentiation at small spatial scales (Godhe et al., 2013). In the same way, investigating the physical transport pathways that can potentially facilitate the migration of harmful algal blooms (HABs) species between different coastal regions along the Atlantic coast, will enhance our ability to respond adequately to such events occurring in a changing marine environment, e.g., to get monitoring programs climate-ready in advance of major changes and eventually to highlight potential new hazards.

The main objective of this work was to investigate the composition and distribution of the *Dinophysis* community along the European Atlantic Area. A methodology based on two complementary approaches was used: a single nucleotide polymorphism (SNP) approach to attempt a description of the *Dinophysis* community at least at the species level, in synergy with a Lagrangian approach to investigate the seasonal and inter-annual variability of hydrodynamical connectivity patterns of shelf waters. Additionally, the variability of connectivity matrices obtained by different hydrodynamic models is examined.

2 MATERIAL AND METHODS

2.1. Selection of Target Areas and *In-Situ* Samples

To study seasonal connectivities between water masses with some potential presence and due to the large distribution of the species, 8 large targets (**Figure 1**) were well distributed along the north Atlantic margin. The target areas also correspond to water masses where this genus has been regularly observed (Delmas et al., 1992; Xie et al., 2007; Farrell et al., 2012;

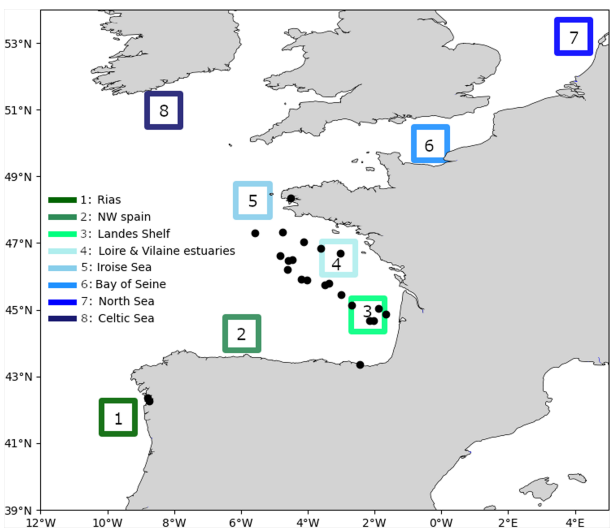

FIGURE 1 | Positions of the target areas defined for the connectivities (boxes from 1 to 7) and *in-situ* samples. *In-situ* samples of the surface water (0-5m) were made in Ria de Vigo (July 2018), coastal Basque waters (2019 and 2020), Bay of Brest (May to July 2013, 2014 and 2015) and over the continental shelf (May 2018 and 2019).

Batifoulier et al., 2013; Diaz et al., 2013). Reversely, to describe community composition, *in-situ* samples were not so well distributed. Due to the methodological development, an opportunistic *in-situ* sampling strategy based on scientific cruises or bloom events in waters close to Marine stations were used during the study. Some surface water (0-5m) was randomly sampled (**Figure 1**). When some *Dinophysis* cells were significantly observed in microplankton samples (> 500 cells/liters), a large volume of seawater (between 2 and 16 liters) was collected. The sea water was next gravity filtered through nylon filters between 20 and 200 μm and the intermediate fraction was conserved. Cells were next resuspended in seawater and the volume was set to 200 ml. The 200 ml sample was next divided in two parts. A 20 ml fraction was fixed with Lugol for microscopic observations and the 180 ml remaining was re-filtered on a polycarbonate filter (5, 10 or 20 μm mesh size). After filtration, filters were rolled in cryotubes with an addition of RNAlater, flash-frozen in liquid nitrogen and conserved in -80°C. At the end of the project, 23 samples were collected from Spain to North of the Bay of Biscay (**Figure 1**) but unfortunately no sample was obtained for the English channel, Celtic Sea and North Sea.

2.2. Water Masses Connectivity

Lagrangian methods in ocean models are commonly used for connectivity purposes and this approach makes it possible to study, in time and space, all ocean connections [e.g., Blanke and Raynaud (1997); Alberto et al. (2011); Watson (2011); Mora (2012); Van Sebille (2018)]. It should be indicated that within this general framework, biological connectivity is usually described as the "realised" exchange of individuals (or genes) between marine populations (taking into account the initial populations size) whereas the hydrological connectivity describes the potential exchange of individuals between water masses (i.e. potential individual exchanges between populations without taking into account any of the selection processes occurring during advection neither any difference between populations size).

2.2.1. Particle Properties

Connectivities being highly sensitive to particle properties (life duration, vertical position, …) estimates from fish larvae provided by previous work in this area (Huret et al., 2010) can't be used. Setting biological parameters characterizing the focused organisms, is a key step when studying the hydrological connectivity and this work constitutes a first attempt for *Dinophysis* populations. These species are slow-growing dinoflagellates (Stolte and Garcés, 2006; Velo-Suarez et al., 2010b), nutritionally versatile to inherit the ability to photosynthesis (such species are klepto-chloroplastida, i. e. they use the chloroplasts of their preys to perform photosynthesis), many are obligate mixotrophs, and some are solely heterotrophic in nature (Hansen, 1991; Jacobson and Andersen, 1994; Kim et al., 2008). Due to these traits, cells are able to survive several months and their densities remain low compared to other plankton species in their size fraction. Thus, the duration of the particle advection was fixed to 3 months, without any mortality even if the particles spend a long period in aphotic deep waters. The main part of living protists biomass being located in near surface waters, because autotrophic cells (including *Dinophysis* prey) need sufficient light to perform photosynthesis, releasing cells in the mixed surface water layer was considered as a pragmatic methodology. It was also considered, as a first approximation and even if *Dinophysis* cells have some motility capacities (vertical migrations, gyrotaxis, …), that they are transported within water masses without any specific buoyancy, i.e. the particles buoyancy was assigned to neutral. Finally, assuming that *Dinophysis* populations spend their whole life cycle in the pelagic environment without an overwintering strategy, the simulation duration spanned two seasons: spring-summer (from April to August) and autumn-winter (October to February) to study the potential transport during contrasted hydrodynamical conditions.

2.2.2. Lagrangian Model

The position of the numerical particles during each time step was calculated using the off-line tool Ichthyop (Lett et al. (2008), https://www.ichthyop.org/) which is regularly used to describe fish larvae dispersion. Velocity, temperature, and salinity fields were obtained from hydrodynamic models as input time series. The process of particle dispersion by turbulent phenomena is perfectly explained and predicted by the Lagrangian modelling approach introduced by Taylor (1921). This approach was widely used for turbulent flows (e.g., (Pope, 1985; Pope, 1994; Pope, 2000; Mitarai et al., 2003). A total of 100 000 virtual particles were deployed (1 100 particles per day at a random initial time of the day) in the surface layer of each square station. Overall in this study, more than 8.10^6particles were used. The position of each particle was obtained by interpolating U (velocity fields) between grid points and integrating the following equation:

$$\frac{\partial X_n(\tau, a)}{\partial t} = U_n(\tau, a) \quad (1)$$

Here, $U_n(\tau, a)$ is the velocity of the nth Lagrangian particle and $X_n(\tau, a)$ is the position of nth fluid particle. The particle velocity is related to the Eulerian flow at the particle location:

$$U_n(\tau, a) = u[X_n(\tau, a), t_n + \tau] \quad (2)$$

$u(x,t)$ is the Eulerian velocity at a given location x and time t respectively, and t_n is the release time of the nth Lagrangian particle. Noting that the transport of particles is based on 3D simulations, it is important to keep in mind that the calculated velocity fields are both in the horizontal and vertical directions (some trajectories of numerical particles are presented in **Figure S1**).

2.2.3. Velocity Fields

Ocean circulation from the Iberian Peninsula to Celtic sea (**Figure 2**) was generated with the state-of-the-art ocean general circulation model MARS3D. The MARS3D model uses a free surface primitive equation designed to describe hydrodynamics from regional to local scales. The sigma coordinates are used on the vertical dimension to resolve

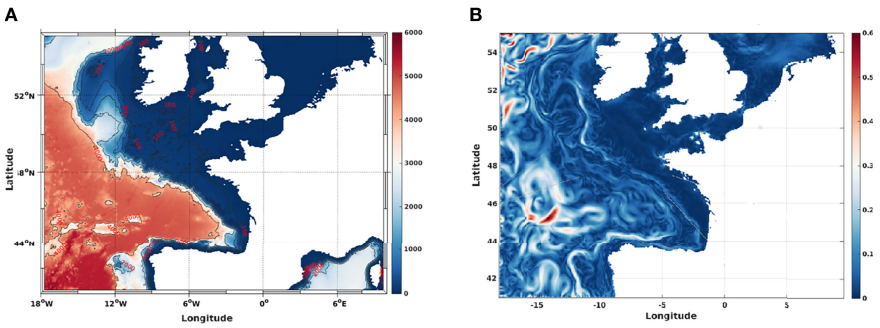

FIGURE 2 | **(A)** Bathymetry of the modelled region, **(B)** Sample daily averaged surface current in the Bay of Biscay in the particle tracking modelling exercise.

simultaneously shallow and deep waters. In our study, two different configurations of the MARS3D model in the Bay of Biscay (M4000 and M1000 with different resolutions and external forcing) were used to cover several decades.

The first configuration (M4000 i.e. MARS3D-MANGAE4000, 1958-2014) describes circulation in the Bay of Biscay and its extension to the western English Channel. It was already validated using hydrology analyses of the French continental shelf (Lazure et al., 2009). The horizontal resolution was of 4 km with 30 vertical levels in sigma coordinates and the domain covered from 4.68°E to 14.25°W, and 40.96°N to 52.48°N. The bathymetry was provided by the SHOM (Hydrological and Oceanographic Service of the French Navy). A resolution of 0.15m at the surface and 3.5 m in the middle of a 100m water column corresponded to the grid spacing in sigma coordinate. It should be noted that the period of simulation ranges from 1958 to 2014 and daily averaged outputs were used. The DFS4.3 [Drakkar Forcing Set; Brodeau et al. (2010)] model was used for atmospheric fields. This model was based on ERA40 ECMWF reanalysis (Uppala et al., 2005) from 1958 to 1989 and ERA-Interim ECMWF reanalysis (Dee et al., 2011) from 1989 to 2014. The turbulence closure scheme was based on the equation of the evolution of the turbulent kinetic energy (Gaspar et al., 1990). The global ORCA025 simulation, which was an application of the NEMO model (Madec et al., 1998), was used to provide data on temperature, salinity, SSH and currents at the open boundaries of the model as initial condition. Tides are important because they play a major role in the mixing of temperature and salinity at the shelf break, in the bottom friction over the shelf, and in the currents close to the coast. For our simulation, the FES2004 solution (Lyard et al., 2006) providing 14 tidal constituents (M2, S2, K2, N2, 2N2, O1, P1, K1, Q1, Mf, Mtm, Mm, Msqm and M4) were used. The second configuration (M1000 i.e. BACH1000_100lev Configuration, 2001-2010) also extended from the Bay of Biscay to the English Channel from 41.00 to 52.50°N, and from 14.30°W to 4.50°E but with a 1 km spatial horizontal resolution and a time step of 60 seconds (Theetten et al., 2017). This configuration had 1449 × 1282 grid points and used 100 vertical sigma levels. The outputs were also daily averaged. The bathymetry was a composite of several IFREMER digital terrain models (DTMs) and the interpolated topographies were smoothed using a local filter of below 0. which echoes the low value of 25 (Haidvogel and Beckmann, 1999). River runoffs were provided from 95 chronological records located on the Spanish, French, Dutch, British and Irish coasts. One of the major differences between the previous configuration was related to initial conditions for temperature, salinity, sea surface height and, baroclinic and barotropic velocities. In this configuration the initial conditions were derived from a DRAKKAR global configuration named ORCA12_L46-MJM88 (Molines et al., 2014). Another difference was the use of a sponge layer (Marchesiello et al., 2001) on the North, South and West boundaries. The same tide, with 14 components was imposed at the model boundaries, and the same atmospheric forcing as the M4000 were used. To estimate interannual variability of velocity fields, Lagrangian particle transport exercises were performed for 5 years (from 2010 to 2014).

2.2.4. Lagrangian Indices

Based on Lagrangian integration, different approaches have been used to quantitatively describe the connectivity between marine areas. These include Lagrangian probability density functions (PDFs) (Mitarai et al., 2009), graph theory (Rossi et al., 2014) and characteristic time scales associated with surface ocean connectivity (Jonsson and Watson, 2016). Most of these methods are based on the general definition of a "connectivity timeT^m_{min}," which depends on oceanographic distances and is defined as the mean time required for particles to move from one location to another (Cowen et al., 2007; Mitarai et al., 2009). Jonsson and Watson (2016) proposed to use the "minimum connectivity time" (T_{min}), defined as the fastest travel time from source to destination for numerical particles, inferred from a Dijkstra algorithm (Dijkstra, 1959). This minimum connection time also shows usually a better agreement and correspondence with genetic dispersal in marine connectivity Alberto et al. (2011). Following this idea, Costa et al. (2017) used graph theory and transfer probabilities to calculate "betweeness", i.e., the shortest paths between different sites within variable ocean dynamics. The benefit of using the minimum connection time rather than the average transit time has been addressed in some empirical work (e.g., Doos (1995); Cowen et al. (2007); Mora

(2012). Consequently, in our study, we chose to estimate the minimum, mean, median and most frequent value of the "minimum connectivity time" (T^m_{min}, $T^{'}_{min}$,T^d_{min}, and T^f_{min} respectively) for all particles traveling from one station to another.

2.3. SNP Based *Dinophysis* Diversity

Due to the impossibility to consistently discriminate between several species by morphological criteria and usual molecular approach (Park et al., 2019; Séchet et al., 2021), a SNP approach was used due to its strong resolutive capacity down to the populations scale. Biological samples were sonicated on ice for 30 s in LBP buffer (Macherey-Nagel) and RNA extraction was performed using NucleoSpin ®RNA Plus kit (Macherey-Nagel) following the manufacturer's protocol. Extracted RNA was quantified using a Biotek Epoch spectrophotometer and the quality estimated on RNA 6000 nanochips using a Bioanalyzer (Agilent). Library preparation was performed using the Illumina mRNA TruSeq stranded kit starting from 0.5 µg of total RNA. Library quality was assessed on a Bioanalyzer using high-sensitivity DNA analysis chips and quantified using Kappa Library Quantification Kit. Paired-end sequencing was performed using 2 x 150 bp cycles on Illumina Hiseq3000 at the GeT-PlaGe France Genomics sequencing platform (Toulouse, France). Read quality was assessed using FastQC (http://ww.w.bioinformatics.bbsrc.ac.uk/projects/fastqc/), and Trimmomatic Bolger et al. (2014); Metegnier et al. (2020) (V. 0.33) was used to trim ambiguous, low quality reads and sequencing adapters with parameters ILLUMINACLIP: Adapt.fasta: 2:30:10 LEADING: 3 TRAILING: 3 MAXINFO: 135: 0,8 MINLEN: 80. Two strategies were investigated to obtain *Dinophysis* reference transcriptomes from the 14 *Dinophysis* strains available in **Table 1**. (excluding the US strain). First one per species was obtained using Trinity Haas et al. (2013) by pooling the reads of the different strains belonging to the same species. Second, a single genus wide *de novo* assembly was obtained by pooling the reads from the 14 strains. Only transcripts longer than 200 bp were retained. When several isoforms were identified, only the longest one was retained. The reads from each strain were individually mapped to the seven reference transcriptomes using the BWA-MEM aligner Li (2013) and the percentage of remapping on each reference calculated. As the percentage of remapping on the genus wide reference was higher than 99% for all strains for a total size of 802 660 transcripts (to be compared to the sum of the six species specific reference transcriptomes: 1 921 084 transcripts), the genus wide reference transcriptome was selected for the analyses presented below. As described previously Metegnier et al. (2020), all the MMETSP reference transcriptomes Keeling et al. (2014) were downloaded from Cyverse (http://www.cyverse.org). All references corresponding to unknown species were discarded. The reference corresponding to *Dinophysis acuminata* reference was replaced by the one obtained from the present study. Within each transcriptome, for each transcript, only the longest isoform was considered. When several transcriptomes per species were available (several strains or culture conditions), they were merged into a single reference, and CD-HIT-EST Li and Godzik (2006) was used to remove homologous sequences within each reference. A total of 313 species specific reference transcriptomes, representing 213 unique genus, were considered and concatenated to build the meta-reference. Reads from the 14 *Dinophysis* strains described above as well as from another *D. acuminata* strain obtained from the MMETSP database were aligned to the genus wide *Dinophysis* reference transcriptome. Reads from the 120 meta-transcriptomic datasets were aligned to the meta-reference. Alignments were performed using the BWA-MEM aligner Li (2013). Samtools Li and Godzik (2006) was used to discard reads displaying low quality alignments (MapQ<10) as well as the ones mapping to several transcripts (FLAGS < 1,000). For each meta-transcriptomic dataset, the relative abundance of the transcripts for each gene in each sample was calculated Metegnier et al. (2020). SNPs from the strains were identified using Freebayes (Garrison and Marth, 2012) as described in Le Gac et al. (2016). VCFTOOLS (Danecek et al., 2011) was used to keep SNPs with two alleles, a quality criterion higher than 40,

TABLE 1 | List of the *Dinophysis* strains.

Strain	Species	Date	Locality	Library
D_sacculus_D13	*D. sacculus*	May-15	Meyran/Arcachon Bay	PRIM37[1]
D_sacculus_D14	*D. sacculus*	May-16	Loscolo/Vilaine Bay	PRIM38[1]
D_sacculus_D15	*D. sacculus*	Oct-17	Crique angle/Thau lagoon	PRIM39[1]
D_sacculus_D77	*D. sacculus*	Marc-18	Massame/Berre lagoon	PRIM40[1]
D_acuminta_REM	*D. acuminata*	Oct-17	Ria de Vigo	PRIM32[2]
D_acuminta_V1	*D. acuminata*	Jun-18	Ria de Vigo	PRIM42[2]
D_acuminta_V2	*D. acuminata*	Nov-17	Ria de Vigo	PRIM43[2]
D_acuta_V4	*D. acuta*	Oct-10	Ria de Pontevedra	PRIM44[2]
D_acuta_V6	*D. acuta*	Nov-17	Ria de Pontevedra	PRIM45[2]
D_caudata_V7	*D. caudata*	Jul-17	Ria de Vigo	PRIM46[2]
D_caudata_V8	*D. caudata*	Aug-17	Ria de Vigo	PRIM47[2]
D_caudata_V9	*D. caudata*	Aug-17	Ria de Vigo	PRIM48[2]
D_fortii_V10	*D. fortii*	Nov-18	Ria de Vigo	PRIM49[2]
D_tripos_V11	*D. tripos*	Jul-16	Ria de Vigo	PRIM50[2]
D_acuminata_MME TSP (DAEP01)	*D. acuminata*	Sept-06	Eel Pond, Woods hole, MS, US	SRX551108[3]

They were isolated by Ifremer/Phyc[1], IEO/Vigo[2] and Woods Hole Oceanographic Institution[3].

and covered more than 10 times in each strain. It corresponded to a total of 296,887 SNPs. Nucleotide divergence was calculated for each pair of strains as the number of variant sites divided by the total number of sites covered more than ten times in each strain. Strains were clustered based on nucleotide divergence using hclust in R. The allelic frequencies of the natural populations based on the meta-transcriptomic samples were obtained using FreeBayes (Garrison and Marth, 2012) enforcing diploidy, and extracting coverage for each of the two alleles at the various SNP positions identified in the strain datasets. PLINK (Purcell et al., 2007) was used to prune SNPs displaying strong linkage disequilibrium (10 kb windows, 10 bp window step size, 0.1 r^2 threshold), leaving 73,318 SNPs after pruning. These SNPs were used to perform a PCA analysis as a first exploratory investigation of the *Dinophysis* community composition in the meta-transcriptomic samples. Median proportion at diagnostic SNPs, i.e. SNPs displaying a given allele in all strains from a given species and the alternative allele in all the other strains, were used to estimate the relative proportion of the *Dinophysis* species in the *in-situ* samples.

3 RESULTS

3.1. Hydrodynamic Connectivity

In order to avoid redundant information, some correlations between the Lagrangian indices (T^m_{min}, $T^{'}_{min}$,T^d_{min}, and T^f_{min}) were performed. As expected, the indices were highly correlated and only the index showing the highest correlations was thus presented hereafter ($T^{'}_{min}$, see **Table 2**). In the same way, in order to describe the maximum inter-annual variability of connectivity patterns, correlations for $T^{'}_{min}$ between years were performed and the years showing the most different patterns were retained (years 2011 and 2013, **Table 3**). This simple analysis also showed the high stability of the connectivity patterns in spring an autumn (**Figure 3**) but also that inter-annual variability appeared as global trend affecting all stations in a similar way (by increasing or reducing the connectivity times due to a more energetic circulation). For the sake of simplification, the global seasonal patterns are thus described hereafter based on the network based on $T^{'}_{min}$ for 2011.

During the spring-summer (April to August) period, the water masses from English Channel and North Sea appeared not connected to other areas with our setting, and the Celtic Sea weakly connected to the Bay of Biscay and Iberian coast. A $T^{'}_{min}$ of approximately 88 days was calculated for particles traveling in a northward direction from Galicia (Station 1) to the English Channel entrance (Station 5). A duration longer than 3 months is thus required for cells to go further north and to reach Celtic Sea. A global northward advection along the coast was shown, with short calculated $T^{'}_{min}$ between coastal waters of the north Iberian shelf (station 2) and stations 3, 4 and 5. The fastest transit pathway for particles in spring-summer, was found between station 2 and 3 with $T^{'}_{min}$ estimated to be 12 and 11 days in 2011 and 2013 respectively (**Figures 3A, B**). It is even quicker during the winter period with $T^{'}_{min}$ between these two stations being 11 and 10 days in 2011 and 2013 respectively (**Figures 3C, D**). Several transit are also unidirectional. Particles released in Galician waters and North-West Spain (stations 1 and 2) travelled towards stations in the Bay of Biscay while a significant reverse connectivity flow was not observed (**Figure 3**). In the same idea, the $T^{'}_{min}$ from station 4 to station 5 is estimated to be around 32 days in summer 2011 (respectively 23 days in winter), while the inverse particle movement can take almost twice (respectively four times longer in winter). As a general pattern, simulations show the particles were transported on further distances during the autumn-winter period compared to spring-summer ((**Figures 3A, C**). It is illustrated by the increase of the number of edge per node in the winter. Stations 6 and 7 are also connected to the other stations. The fastest connectivity pathways calculated were however roughly the same than during the summer in the Bay of Biscay. All the described patterns shown a low inter-annual variability with some differences shorter than a week in many cases. The water masses from the Bay of Biscay appear thus strongly connected with a general circulation oriented slightly Northward.

To analyze the results consistency, a comparison was made between two models (**Figure 4**) with different model resolution and configuration. The 4 km resolution flow fields are more

TABLE 2 | Correlation between the transit time indices from all years (the mean, median, most frequent value and minimum, of the "minimum connectivity time": $T^{'}_{min}$,T^d_{min}, and T^f_{min} and T^m_{min}respectively).

Correlation	$T^{'}_{min}$	T^d_{min}	T^f_{min}	T^m_{min}
$T^{'}_{min}$	–	0.954	0.915	0.962
T^d_{min}	–	–	0.888	0.925
T^f_{min}	–	–	–	0.883

TABLE 3 | Correlation of $T^{'}_{min}$ (mean "minimum connectivity time") between different years.

Correlation	2010	2011	2012	2013	2014
2010	–	0.949	0.934	0.911	0.929
2011	–	–	0.964	0.925	0.968
2012	–	–	–	0.915	0.929
2013	–	–	–	–	0.917

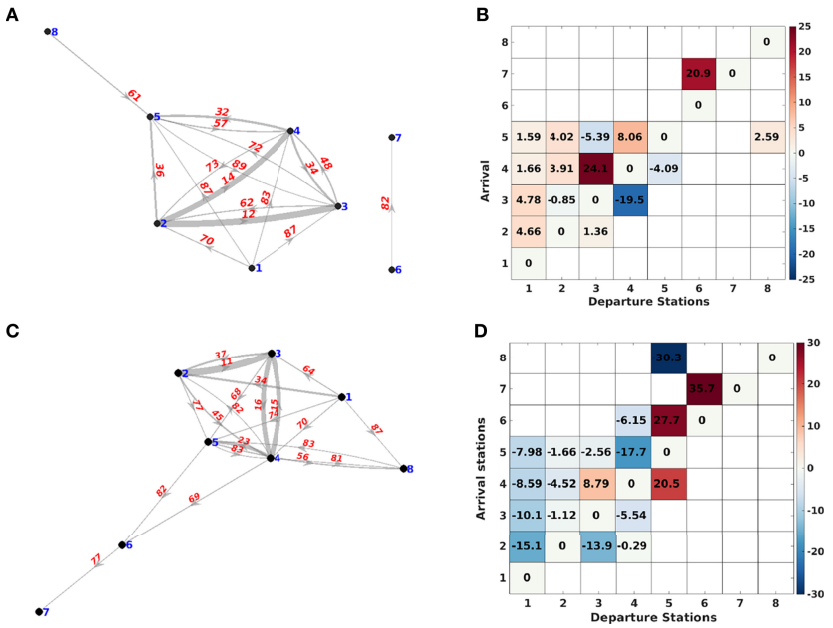

FIGURE 3 | **(A)** Dinophysis connectivity network showing the mean "min transit time" (days) between the departure stations and the arrival stations in spring 2011, **(B)** Difference between the "mean transit time" values during spring 2011, 2013 (2011-2013), **(C)** Dinophysis connectivity network showing the "mean transit time" (days) between the departure stations and the arrival stations in winter 2011, **(D)** Difference between the "mean transit time" values during winter 2011, 2013 (2011-2013). A graphical representation of connectivity times keeping geographical distances between node is illustrated in **Figure S4**.

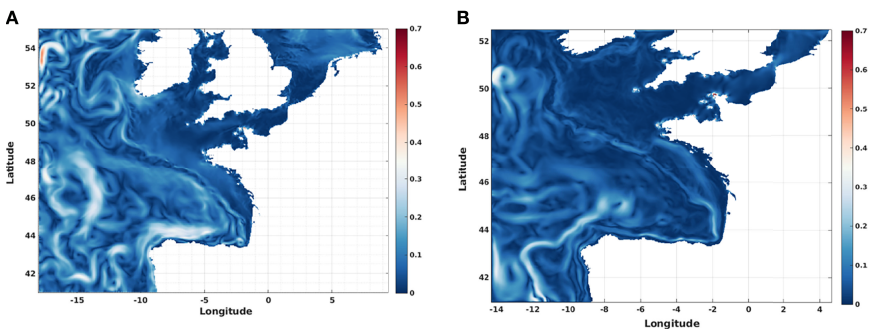

FIGURE 4 | Sample surface flow fields of the hydrodynamical models in November 2010. **(A)** The 4 km horizontal resolution model and **(B)** The 1 km horizontal resolution model.

energetic than in the 1 km resolution model, whatever the considered year. Implicitly, some lower transit time were expected but this dynamic also leads to the generation of a large number of (sub) mesoscale eddies (cyclonic and anticyclonic) in the centre of Bay of Biscay (out of the shelf) which can greatly influence the particles retention. The presence of eddies, resulting from the continental margin current instabilities interacting with the bottom topography, is also more frequent with the 4 km resolution model. These dynamic conditions indeed reduce the calculated transit times for any *Dinophysis* cells present in these currents (**Figure 5**). These differences are however moderate because it affects mainly the movement of numerical particles in the central (oceanic) part of the Bay of Biscay. Over the shelf, the main ocean circulation drivers remains wind and density gradients caused by rivers plumes.

3.2. Dinophysis Community

SNP analyses of the fifteen *Dinophysis* strains belonging to six different species enabled a clear distinction among the six species (**Figure 6**). Three strongly divergent species pairs were identified. The two species *D. acuminata* and *D. sacculus*, that are difficult

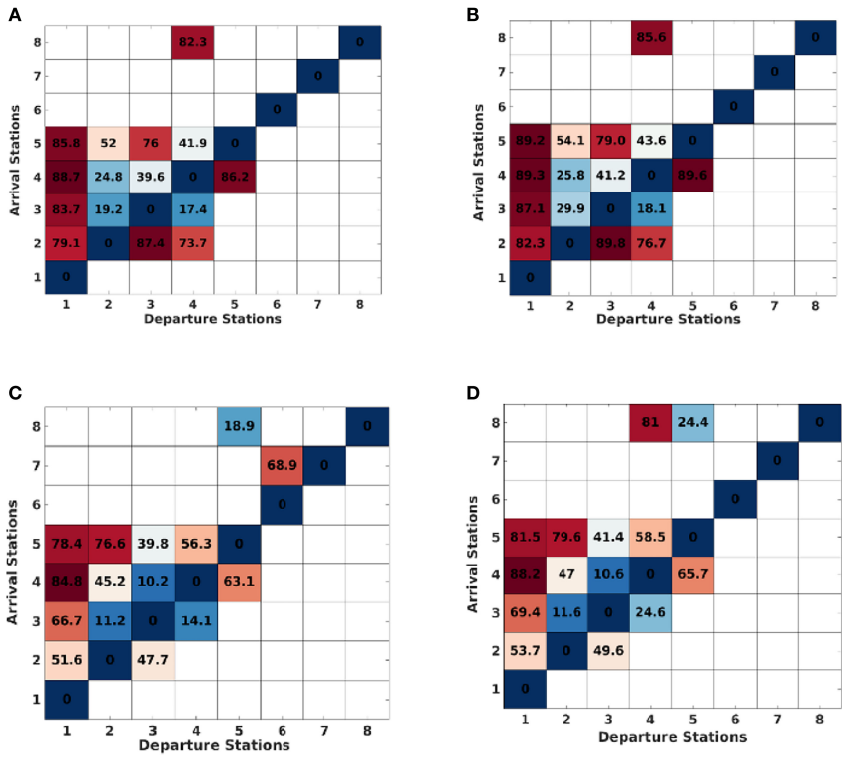

FIGURE 5 | Dinophysis connectivity matrix showing the "mean transit time" (days) in spring 2010, **(A)** Model resolution = 4km, **(B)** Model resolution = 1km, and in winter 2010, **(C)** Model resolution = 4km, **(D)** Model resolution = 1km.

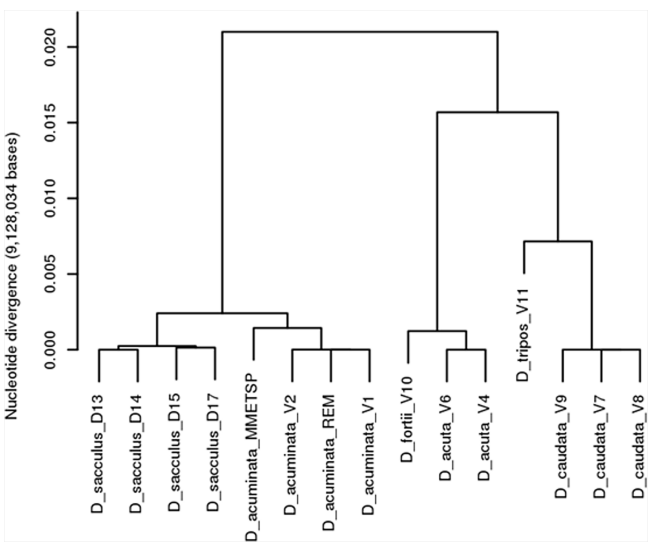

FIGURE 6 | Clustering of Dinophysis spp. strains based on genetic variation (296 887 SNPs).

to distinguish morphologically or by using regular genetic markers Séchet et al. (2021), displayed low levels of nucleotide divergence (< 0.0025, corresponding to ≈ 20 000 SNPs displaying genetic differences among strains of the two species). Two other species, *D. acuta* and *D. fortii* were even less divergent (< 0.0012, ≈ 11 000 SNPs). The two other sister species *D. caudata* and *D. tripos* displayed a higher level of nucleotide divergence level around 0.007 (≈ 60 000 SNPs). Within each of the four species represented by at least two strains, the level of intraspecific variability was extremely low, with a nucleotide divergence of 2.6 10^{-6} (20 SNPs) and 2.96 $10.^{-6}$ (30 SNPs) within *D. acuta* and *D. caudata*, respectively. Between the three european *D. acuminata*, nucleotide divergence was around 5 10^{-6} (< 100 SNPs), but raised to 1.4 10^{-3} (≈ 13 000 SNPs) between the European and American strains (on the same order scale than the observed inter-specific differences). Finally, we note a genetic divergence of 2 10^{-4} (≈ 1 500 SNPs) between the two *D. sacculus* strains from the Mediterranean sea (D15 and D17) and the two *D. sacculus* strains from the Atlantic ocean (D13 and D14), while nucleotide divergence was 10^{-4} and 2 10^{-7} among strains from the Mediterranean sea and the Atlantic ocean, respectively. This very low level of intraspecific variability precluded the analysis of genetic structure within each species but the identification of species specific SNPs enabled us to investigate the relative proportion of the various species in the *in-situ* samples from Galicia waters to the entrance of the Channel.

Following Metegnier et al. (2020), environmental reads obtained from 120 *in-situ* samples were aligned to a metareference database composed of 313 species specific reference transcriptomes (**Figure S2**). A large proportion of environmental reads did not align to the metareference (20 to 80%), probably because several species abundant in the natural samples were not represented in the metareference database. *Dinophysis* genus, which is assumed to be oceanic, only represented a very small proportion of environmental reads (< 5%) despite the differential filtration used and the samples pre-selection based on microscopic observations. This observation was in agreement with the microscopic observations of our samples. Despite the significant presence of *Dinophysis* cells, they were never the most abundant fraction of the samples. The analysis was thus restricted to 59 environmental samples with more than 20 000 reads aligning to the *Dinophysis* reference transcriptome. Samples corresponded to samples from the Bay of Brest (prefix label: RB), Bay of Vigo (prefix label: Remedios), Bay of Arcachon (prefix label: Arcachon), Basque waters (prefix label: Azti), Iroise Sea (prefix label: Mascoet) and waters over the continental shelf in the Bay of Biscay (prefix label: Pelgas). The relative abundance of the resolved *Dinophysis* species across natural populations can be compared with the strain genotypes inferred above (**Figure 7**). The Bay of Brest and Vigo samples are mainly composed of the *D. acuminata*/*D. sacculus* complex (not resolved using this graph). *D. acuta, caudata and fortii* were never the dominant among *Dinophysis* community. Few samples from the continental shelf and Basque waters had a significant fraction of *D. tripos*. To improve the taxonomic resolution of our approach, the analysis was restricted to the SNPs diagnostic of

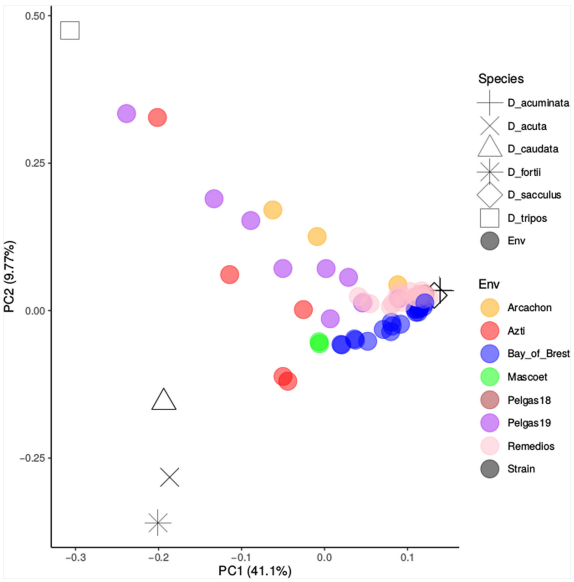

FIGURE 7 | PCA analysis of species composition in Dinophysis spp. populations. The in-situ samples are represented by colored dots and the strains by black symbols.

the various species, only considering the 15 *in-situ* samples with more than 5 diagnostic SNPs for each species each covered by more than 10 reads (**Figure 8**). It indicated clearly that the two *Dinophysis* species from our cultivated set often co-occured in the natural communities from Galicia to the Bay of Biscay. *D. acuminata* is often well represented, except in a few samples where *D. tripos* tends to dominate. Due to the low number of samples, the analysis of specific environmental factors was not realised. A significant fraction of one or several *Dinophysis* species, which were not included in our reference transcriptome, is also observed. The species composition tends to vary at the same locality, and there is no clear geographical pattern of co-occurence.

4 DISCUSSIONS

From all hydrodynamics configurations, the connectivity pattern described in autumn-winter is in agreement with the general cyclonic circulation previously reported for the region Charria et al. (2017). It is mostly influenced by the eastward Iberian Poleward Current in deep ocean Le Cann and Serpette (2009) and by the northwestward current over the continental shelf Lazure et al. (2008). At the annual scale, without any specific behaviour and selection, populations should be well mixed at the European scale involving potential migrations between all water masses over the shelf. Reversely during the summer, connectivities indicate that the English Channel and the North Sea seems seasonally isolated from the other areas. During the summer, the advection of some blooms occurring over the Atlantic Shelf to the English channel is thus unlikely. An

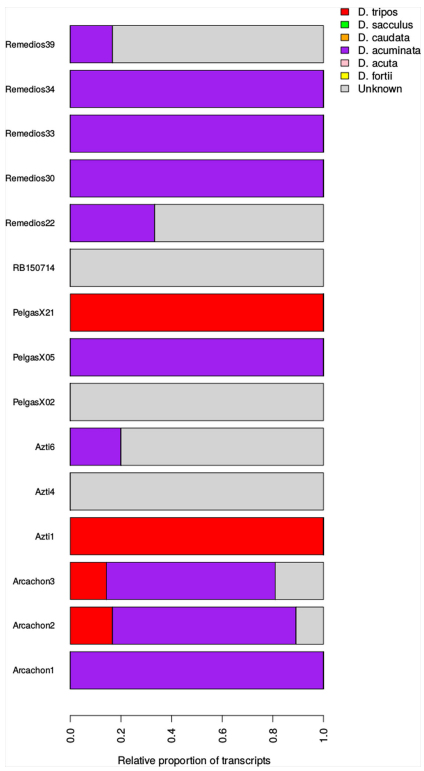

FIGURE 8 | Relative proportion of Dinophysis species based on diagnostic SNPs at the species level (7 taxonomic groups).

environmental selection should lead to a species composition different from those observed in the Bay of Biscay. *D. norvegica* could illustrate such a process with some observations typically distributed in northerly waters of the Atlantic (Bresnan et al., 2021). Unfortunately, this assumption cannot be verified because we were not able to sampled this northern part of the coast and no reference transcriptome of this species was available. We must also indicate that the porosity of this barrier is probably underestimated by the Lagrangian methodology that assumed only three limited areas for particle departure in the Bay of Biscay. By increasing their sizes or slightly change their positions, a small connection could appear over the summer. This boundary is then only a seasonal semi-permeable barrier.

Reversely, all the water masses from the Bay of Biscay are well connected (high number of edges per nodes with some exchanges in both directions) and this result helps in the analysis of the observed species composition. Despite the limitation associated to the low number of reads from *in-situ* samples, probably due to the large part of the other plankton community also retained on the filters, only two identified species were detected in the Bay of Biscay without any spatial pattern. A dominance of *D. acuminata* is observed over the Bay of Biscay but *D. tripos* can also constitute a significant fraction of the community (over the French shelf and along the Basque country). The variability of the relative abundances thus appears more related to some local dynamics or to a patchy distribution of cells. The unknown fraction (**Figures 8**, **S3**) is due to one or several *Dinophysis* species without reference transcriptome. From microscopic observation, some round cells were observed in our samples. Due to the regular observations of *Phalacroma rotundatum* or *D. ovum* in the area (Reguera et al., 2014), they represent probably a large fraction of this unknown group. It should be noted that there was no specific strategy (period, geographical position, etc…) for conducting the *in-situ* sampling, which can be considered as random. The species absence could be bias by the relatively "small" number of retained samples (15) but it should also indicates the global trend. A second analyse was thus made to increase the number of retained samples (47) by using a lower taxonomic resolution (**Figure S3**). The same trend was highlighted with a dominance *D. acuminata* and only one detection of *D. acuta/fortii* in Basque waters. At the species level, the absence of detection for *D. sacculus* in all our samples is finally surprising because it was relatively easily isolated and cultivated from French coastal waters. This observation raises two questions. The first one is the porosity used for the filtration but, to be meaningful, almost all of the cells of this species must be lower than (20 μm). The second question is a coastal adaptation for this species, because with some high migration and invasion capacities along the coast, all the six species could grow in this area when favorable conditions would be encountered. These high potential migration rates also shown that to describe ecological niches at a species level (i.e. to understand species biogeography and to forecast some scenarii) implementing monitoring programs with an higher taxonomic resolution is highly required.

Connectivity between Galicia (Rias) and the South of the Bay of Biscay is mostly impacted by the general oceanic circulation and the continental slope current. Weak anticyclonic (clockwise) circulation can become cyclonic (anticlockwise) close to the continental margin but the populations flow, at the seasonal scale, appears unidirectional from Galacia waters to the Bay of Biscay. In the same way, we simulated rather short travel times from Asturias waters (station 2) towards the Arcachon area (station 3) than in the opposite direction. This pattern during the spring-summer is slightly different from the described general circulation. Summer circulation of the surface layer is considered as anticyclonic (southward over the abyssal plain and along the Basque coast, Valencia et al. (2004)) or weak and highly variable by being windy driven over the French shelf Charria et al. (2017). Here, particles tend to move northward even if inverse movement remains possible. This observations is likely related to the vertical mixing that brings some cells below surface layers where advection processes can be different. Coastal jets, which refer in the North hemisphere to alongshore flows caused by the horizontal density gradient made by tidal mixing, is a such process occurring at depth of the neighbouring pycnocline where highest cell densities are very often observed and with a northward direction. This process can occurred over the French shelf, as observed in Celtic Sea Raine (2014), and leads to a northward advection, regardless of the weather conditions. Some other and fast windy driven processes also occurs in this area

such as western winds leading to a fast (up to 19 cm.s-1) northward advection circulation Batifoulier et al. (2013) but these processes are not resolved with our model configurations and the position of our releasing stations.

The relatively long connectivity time (2-3 months) from Galicia to the Bay of Biscay also indicates that the positive correlation of the inter-annual variability between cell abundances monitored in these two areas Diaz et al. (2013) is more related to favorable environmental conditions to *Dinophysis* spp. at large scale than to population advection. From Galicia (Remedios samples) to the entrance of the English Channel (Bay of Brest, RB), *D. acuminata* appears as dominant, followed by the unknown species group and several observation of *D. tripos* and *D. acuta/fortii*. There is, once again, no northward trend in the community composition from Galicia to the English Channel. Moreover, due to the low genetic variability observed at the European scale it was not possible to analyze the intra-specific variability. However, some significant differences between *D. acuminata* strains isolated over different years and from North America and Europe seems to indicate the existence of biogeographic patterns at the global scale. This very low genetic variability is thus significant and highlights some unexpected properties that echo the Lewontin's paradox (Filatov, 2019).

As indicated previously for the summer barrier, a possible drawback of our methodology is its sensitivity to the setting of the particles parameters. For example, the highest cell concentrations of *Dinophysis* spp. are regularly observed at marked density gradients, related to a sudden vertical change in temperature and/or salinity in the water column Maestrini S. Y. (1998). *Dinophysis* blooms (when cell densities become significant in the whole sampled community) are thus frequently observed in species-specific horizontal thin layers related to physical shear and vertical swimming behavior (Moita et al., 2006; Velo-Suarez et al., 2010a). These distributions could have an impact on the populations advection over short time scales. Nonetheless, due to their presence at low density in the other layers and the transport duration longer (three month here) than the life duration of these thin layers, it is unlikely that some significant differences in the described seasonal patterns of connectivity time could be expected. The last uncertainty is related to the settings of the hydrodynamic configurations. Unresolved mixing processes can change significantly the simulated movement of particles (McWilliams, 2016;)?. By increasing the horizontal resolution, connectivity times should decrease and the average number of edge per node in the connectivity network increase. In our case, these effects are however strongly masked by the more energetic circulation simulated with the coarser resolution. As a reminder, apart from the horizontal resolution, boundaries conditions and vertical resolution were the main differences. Of these two differences, the lower vertical resolution of the 4km configuration appears as the main driver of the energy difference by creating an overestimation of the vertical mixing along strong bathymetry gradient (slopes), which is a regular problem for models using a sigma grid. Particles remaining in the surface water layer or in a subsurface layer move then more rapidly in the coarse model configuration due to (sub) mesoscale eddies generated by continental slope currents in the Bay of Biscay. Nevertheless, the same general patterns are conserved in both configurations with: a confirmed simulated northward connectivity from Galicia to the Bay of Biscay, a high connectivity within the Bay of Biscay and a higher connectivity between shelf waters of French Brittany and Celtic Sea shelf sea than from shelf waters of French Brittany and English Channel and North Sea. According to the network stability over a decade from different configurations, we tried to evaluate it over a longer period by reproducing this methodology with some velocity fields from other scenarios [from 1975 to 2100, POLCOMS-ERSEM on the Northeast Atlantic, Kay et al. (2018)]. This investigation was however dismissed due to the differences between the hydrodynamic solutions used in this work and those provided.

5 CONCLUSIONS

This study allowed us to characterise the main connectivity patterns along the European northeast Atlantic coast for water masses with some *Dinophysis* populations, and its stability during the last decade. At the populations scale, some mixing of *Dinophysis* populations from the Western Iberian shelf, the Bay of Biscay and the Celtic Sea are likely with a northward trend (especially in the Celtic Sea) throughout the year. A significant boundary, that could limit biological flows during the summer, occurs at the entrance of the English Channel. The study also points out the interest of following the specific dynamics because, if nowadays a strong dominance of *Dinophysis acuminata* is observed, all species can migrate and bloom all along the European coast. Despite the unsolved problem of low proportions for *Dinophysis* cells in the sample, this work provides a methodology in that way with some references sequences to clearly identify and describe the species dynamics.

DATA AVAILABILITY STATEMENT

Sequencing reads were deposited to the European Nucleotide Archive and are accessible under the accessions PRJEB53578 (metaT reads) and PRJEB53438 (Dinophysis RNAseq reads).

AUTHOR CONTRIBUTIONS

SH, MS, MP, and ML contributed to the initial idea, data analysis, and the manuscript writing. VS, and MR contributed to the cultures and water sampling. All authors contributed to the article and approved the submitted version.

FUNDING

This study was funded by PRIMROSE (EC Interreg Atlantic Area EAPA 182/2016. MR was also funded by the Basque Government

(Spain), through the project "BIOTOX" from the European Maritime and Fisheries Fund (EMFF-00002-INA2021-33).

ACKNOWLEDGMENTS

We thank Rodriguez Francisco, Pilar Rial (IEO, Vigo) and Liliane Carpentier (IFREMER, Nantes) for the isolation and source of biological material belonging to Dinophysis strains from NW Spain and France. We also thank Marivi Lucero (AZTI), Pascale Malestroit and Marie-Madeleine Danielou (IFREMER) for their contributions to the sampling and samples selection.

SUPPLEMENTARY MATERIAL

The Supplementary Material for this article can be found online at: https://www.frontiersin.org/articles/10.3389/fmars.2022.914909/full#supplementary-material

REFERENCES

Alberto, F., Raimondi, P., Reed, D., Coelho, N., Leblois, R., Whitmer, A., et al. (2011). Isolation by Oceanographic Distance Explains Genetic Structure for Macrocystis Pyrifera in the Santa Barbara Channel. *Mol. Ecol.* 20, 2543–2554. doi: 10.1111/j.1365-294X.2011.05117.x

Bass Becking, L. (1934). *Geobiologie of Inleiding Tot De Milieukunde* (The Hague, The Netherlands: W. P. Van Stockum & Zoon).

Batifoulier, F., Lazure, P., Velo-Suarez, L., Maurer, D., Bonneton, P., Charria, G., et al. (2013). Distribution of Dinophysis Species in the Bay of Biscay and Possible Transport Pathways to Arcachon Bay. *J. Mar. Syst.*, 109–110. doi: 10.1016/j.jmarsys.2011.12.007

Blanke, B., and Raynaud, S. (1997). Kinematics of the Pacific Equatorial Undercurrent: An Eulerian and Lagrangian Approach From GCM Results. *J. Phys. Oceanog.* 27, 1038–1053. doi: 10.1175/1520-0485

Bolger, A. M., Lohse, M., and Usadel, B. (2014). Trimmomatic: A Flexible Trimmer for Illumina Sequence Data. *Bioinformatics* 30, 2114–2120. doi: 10.1093/bioinformatics/btu170

Bravo, I. I., Reguera, B. B., and Fraga, S. S. (1995). *Description of Different Morphotypes of D. Acuminata Complex in the Galician Rias Bajas in 1991* (Lavoisier Publishing Inc).

Bresnan, E., Arévalo, F., Belin, C., Branco, M. A. C., Cembella, A. D., Clarke, D., et al. (2021). Diversity and Regional Distribution of Harmful Algal Events Along the Atlantic Margin of Europe. *Harm. Algae.* 102, 101976. doi: 10.1016/j.hal.2021.101976

Brodeau, L., Barnier, B., Tréguier, A.-M., Penduff, T., and Gulev, S. K. (2010). An ERA40-Based Atmospheric Forcing for Global Ocean Circulation Models. *Ocean. Model.* 31, 88–104. doi: 10.1016/j.ocemod.2009.10.005

Casteleyn, G. (2010). Itlimits to Gene Flow in a Cosmopolitan Marine Planktonic Diatom. *Proc. Natl. Acad. Sci. U.S.A.* 107, 12952–12957. doi: 10.1073/pnas.1001380107

Charria, G., Theetten, S., Vandermeirsch, F., Yelekci, O., and Audiffren, N. (2017). Interannual Evolution of (Sub)Mesoscale Dynamics in the Bay of Biscay. *Ocean. Sci.* 13, 777–797. doi: 10.5194/os-13-777-2017

Costa, A., Petrenko, A., Guizien, K., and Doglioli, A. (2017). On the Calculation of Betweenness Centrality in Marine Connectivity Studies Using Transfer Probabilities. *PLos One* 12, 0189021. doi: 10.1371/journal.pone.0189021

Cowen, R., Gawarkiewicz, G., Pineda, J., Thorrold, S., and Werner, F. (2007). Enpopulation Connectivity in Marine Systems. *Oceanography* 20, 14–20. doi: 10.5670/oceanog.2007.26

Danecek, P., Auton, A., Abecasis, G., Albers, C. A., Banks, E., DePristo, M. A., et al. (2011). Engthe Variant Call Format and VCFtools. *Bioinf. (Oxford. England).* 27, 2156–2158. doi: 10.1093/bioinformatics/btr330

Dee, D. P., Uppala, S. M., Simmons, A. J., Berrisford, P., Poli, P., Kobayashi, S., et al. (2011). the ERA-Interim Reanalysis: Configuration and Performance of the Data Assimilation System. *Q. J. R. Meteorol. Soc.* 137, 553–597. doi: 10.1002/qj.828

Delmas, D., Herbland, A., and Maestrini, S. (1992). Environmental-Conditions Which Lead to Increase in Cell-Density of the Toxic Dinoflagellates Dinophysis Spp in Nutrient-Rich and Nutrient-Poor Waters of the French Atlantic Coast. *Mar. Ecol. Prog. Ser.* 89, 53–61. doi: 10.3354/meps089053

de Wit, R., and Bouvier, T. (2006). 'Everything Is Everywhere, But, the Environment Selects'; What Did Baas Becking and Beijerinck Really Say? *Environ. Microbiol.* 8, 755–758. doi: 10.1111/j.1462-2920.2006.01017.x

Diaz, P. A., Reguera, B., Ruiz-Villarreal, M., Pazos, Y., Velo-Suarez, L., Berger, H., et al. (2013). Climate Variability and Oceanographic Settings Associated With Interannual Variability in the Initiation of Dinophysis Acuminata Blooms. *Mar. Drugs* 11, 2964–2981. doi: 10.3390/md11082964

Dijkstra, E. W. (1959). A Note on Two Problems in Connexion With Graphs. *Numer. Math.* 1, 269–271. doi: 10.1007/BF01386390

Doos, K. (1995). Inter Ocean Exchange of Water Masses. *J. Geophys. Res. Ocean.* 100, 13499–13514. doi: 10.1029/95jc00337

Farrell, H., Gentien, P., Fernand, L., Lunven, M., Reguera, B., González-Gil, S., et al. (2012). Scales Characterising a High Density Thin Layer of Dinophysis Acuta Ehrenberg and Its Transport Within a Coastal Jet. *Harm. Algae.* 1536–46. doi: 10.1016/j.hal.2011.11.003

Fenchel, T., and Finlay, B. (2004). The Ubiquity of Small Species: Patterns of Local and Global Diversity. *Bioscience* 54, 777–784. doi: 10.1641/0006-3568(2004)054[0777:TUOSSP]2.0.CO;2

Filatov, D. A. (2019). Extreme Lewontin's Paradox in Ubiquitous Marine Phytoplankton Species. *Mol. Biol. Evol.* 36, 4–14. doi: 10.1093/molbev/msy195

Garrison, E., and Marth, G. (2012). Haplotype-Based Variant Detection From Short-Read Sequencing. *arXiv:1207.3907*, ArXiv: 1207.3907.

Gaspar, P., Grégoris, Y., and Lefevre, J.-M. (1990). A Simple Eddy Kinetic Energy Model for Simulations of the Oceanic Vertical Mixing: Tests at Station Papa and Long-Term Upper Ocean Study Site. *J. Geophys. Res.: Ocean.* 95, 16179–16193. doi: 10.1029/JC095iC09p16179

Godhe, A., Egardt, J., Kleinhans, D., Sundqvist, L., Hordoir, R., and Jonsson, P. R. (2013). Seascape Analysis Reveals Regional Gene Flow Patterns Among Populations of a Marine Planktonic Diatom. *Proc. R. Soc. B.: Biol. Sci.* 280, 20131599. doi: 10.1098/rspb.2013.1599

Haas, B. J., Papanicolaou, A., Yassour, M., Grabherr, M., Blood, P. D., Bowden, J., et al. (2013). eng*De Novo* Transcript Sequence Reconstruction From RNA-Seq Using the Trinity Platform for Reference Generation and Analysis. *Nat. Protoc.* 8, 1494–1512. doi: 10.1038/nprot.2013.084

Haidvogel, D. B., and Beckmann, A. (1999). *Numerical Ocean Circulation Modeling.*

Hansen, P. (1991). DXinophysis - a Planktonic Dinoflagellate Genus Which can Act Both as a Prey and a Predator of a Ciliate. *Mar. Ecol. Prog. Ser.* 69, 201–204. doi: 10.3354/meps069201

Huret, M., Petitgas, P., and Woillez, M. (2010). Dispersal Kernels and Their Drivers Captured With a Hydrodynamic Model and Spatial Indices: A Case Study on Anchovy (Engraulis Encrasicolus) Early Life Stages in the Bay of Biscay. *Prog. Oceanog.* 87, 6–17. doi: 10.1016/j.pocean.2010.09.023

Jacobson, D., and Andersen, R. (1994). The Discovery of Mixotrophy in Photosynthetic Species of Dinophysis (Dinophyceae) - Light and Electron-Microscopic Observations of Food Vacuoles in Dinophysis-Acuminata, D-Norvegica and 2 Heterotrophic Dinophysoid Dinoflagellates. *Phycologia* 33, 97–110. doi: 10.2216/i0031-8884-33-2-97.1

Jensen, M. H., and Daugbjerg, N. (2009). Molecular Phylogeny of Selected Species of the Order Dinophysiales (Dinophyceae)—Testing the Hypothesis of a Dinophysioid Radiation1. *J. Phycol.* 45, 1136–1152. doi: 10.1111/j.1529-8817.2009.00741.x

Jonsson, B., and Watson, J. (2016). The Timescales of Global Surface- Ocean Connectivity. *Nat. Commun.* 7, 1-6. doi: 10.1038/ncomms11239

Kamiyama, T., Nagai, S., Suzuki, T., and Miyamura, K. (2010). Effect of Temperature on Production of Okadaic Acid, Dinophysistoxin-1, and Pectenotoxin-2 by Dinophysis Acuminata in Culture Experiments. *Aquat. Microb. Ecol.* 60, 193–202. doi: 10.3354/ame01419

Kay, S., Andersson, H., Catalán, I. A., Drinkwater, K. F., Eilola, K., Jordà, G., et al. (2018). *Projections of Physical and Biogeochemical Parameters and Habitat Indicators for European Seas, Including Synthesis of Sea Level Rise and Storminess. Public 1.3*.

Keeling, P. J., Burki, F., Wilcox, H. M., Allam, B., Allen, E. E., Amaral-Zettler, L. A., et al. (2014). The Marine Microbial Eukaryote Transcriptome Sequencing Project (MMETSP): Illuminating the Functional Diversity of Eukaryotic Life in the Oceans Through Transcriptome Sequencing. *PLos Biol.* 12, e1001889. doi: 10.1371/journal.pbio.1001889

Kim, S., Kang, Y., Kim, H., Yih, W., Coats, D., and Park, M. (2008). Growth and Grazing Responses of the Mixotrophic Dinoflagellate Dinophysis Acuminata as Functions of Light Intensity and Prey Concentration. *Aquat. Microb. Ecol.* 51, 301–310. doi: 10.3354/ame01203

Lassus, P., and Bardouil, M. (1991). Le Complexe Dinophysis Acuminata: Identification Des Espèces Le Long Des Côtes Françaises. *Cryptogam. Algol.* 12, 1–9.

Lazure, P., Dumas, F., and Vrignaud, C. (2008). Circulation on the Armorican Shelf (Bay of Biscay) in Autumn. *J. Mar. Syst.* 72, 218–237. doi: 10.1016/j.jmarsys.2007.09.011

Lazure, P., Garnier, V., Dumas, F., Herry, C., and Chifflet, M. (2009). Development of a Hydrodynamic Model of the Bay of Biscay, Validation of Hydrology, Cont. *Shelf. Res.* 29, 985–997. doi: 10.1016/j.csr.2008.12.017

Le Cann, B., and Serpette, A. (2009). Intense Warm and Saline Upper Ocean Inflow in the Southern Bay of Biscay in Autumn-Winter 2006-2007. *Continent. Shelf. Res.* 29, 1014–1025. doi: 10.1016/j.csr.2008.11.015

Le Gac, M., Metegnier, G., Chomérat, N., Malestroit, P., Quéré, J., Bouchez, O., et al. (2016). Evolutionary Processes and Cellular Functions Underlying Divergence in Alexandrium Minutum. *Mol. Ecol.* 25, 5129–5143. doi: 10.1111/mec.13815

Lett, C., Verley, P., Mullon, C., Parada, C., Brochier, T., Penven, P., et al. (2008). A Lagrangian Tool for Modelling Ichthyoplankton Dynamics. *Environ. Model. Soft.* 23, 1210–1214. doi: 10.1016/j.envsoft.2008.02.005

Li, H. (2013). Aligning Sequence Reads, Clone Sequences and Assembly Contigs With BWA-MEM. *arXiv:1303.3997*, ArXiv: 1303.3997.

Li, W., and Godzik, A. (2006). Cd-Hit: A Fast Program for Clustering and Comparing Large Sets of Protein or Nucleotide Sequences. *Bioinformatics* 22, 1658–1659. doi: 10.1093/bioinformatics/btl158

Lyard, F., Lefevre, F., Letellier, T., and Francis, O. (2006). Modelling the Global Ocean Tides: Modern Insights From FES2004. *Ocean. Dynam.* 56, 394–415. doi: 10.1007/s10236-006-0086-x

Madec, G., Delecluse, P., Imbard, M., and Lévy, C. (1998). OPA 8.1 Ocean General Circulation Model Reference Manual. 91.

Maestrini, S. Y. (1998). Bloom Dynamics and Ecophysiology of Dinophysis Spp. pp. 243-65.

Marchesiello, P., McWilliams, J., and Shchepetkin, A. (2001). Open Boundary Conditions for Long-Term Integration of Regional Oceanic Models. *Ocean. Model.* 3, 1–20. doi: 10.1016/S1463-5003(00)00013-5

Martiny, J. (2006). Microbial Biogeography: Putting Microorganisms on the Map. *Nat. Rev. Microbiol.* 4, 102–112. doi: 10.1038/nrmicro1341

McWilliams, J. (2016). Submesoscale Currents in the Ocean. *Proc. R. Soc A.* 472, 20160117. doi: 10.1098/rspa.2016.0117

Metegnier, G., Paulino, S., Ramond, P., Siano, R., Sourisseau, M., Destombe, C., et al. (2020). Species Specific Gene Expression Dynamics During Harmful Algal Blooms. *Sci. Rep.* 10, 6182, 1–14. doi: 10.1038/s41598-020-63326-8

Mitarai, S., Riley, J. J., and Kosály, G. (2003). A Lagrangian Study of Scalar Diffusion in Isotropic Turbulence With Chemical Reaction. *Phys. Fluid.* 15, 3856–3866. doi: 10.1063/1.1622950

Mitarai, S., Siegel, D., Watson, J., Dong, C., and Mc Williams, J. (2009). Quantifying Connectivity in the Coastal Ocean With Application to the Southern California Bight. *J. Geophys. Res.* 114, 10026. doi: 10.1029/2008JC005166

Moita, M., Sobrinho-Gonçalves, L., Oliveira, P., Palma, S., and Falcão, M. (2006). A Bloom of Dinophysis Acuta in a Thin Layer Off North-West Portugal. *Afr. J. Mar. Sci.* 28, 265–269. doi: 10.2989/18142320609504160

Molines, J., Barnier, B., Penduff, T., Treguier, A., and Le Sommer, J. (2014). "Orca12.L46 Climatological and Interannual Simulations Forced With DFS4.4: GJM02 and MJM88," in *Drakkar Group Experiment Report GDRI-DRAKKAR-2014-03-19*.

Mora, C. (2012). High Connectivity Among Habitats Precludes the Relationship Between Dispersal and Range Size in Tropical Reef Fishes. *Ecography* 35, 89–96. doi: 10.1111/j.1600-0587.2011.06874.x

Park, J. H., Kim, M., Jeong, H. J., and Park, M. G. (2019). Revisiting the Taxonomy of the "Dinophysis Acuminata Complex" (Dinophyta)'. *Harm. Algae.* 88, 101657. doi: 10.1016/j.hal.2019.101657

Pope, S. (1985). PDF Methods for Turbulent Reactive Flows. *Prog. Energy Combust. Sci.* 11, 119–192. doi: 10.1016/0360-1285(85)90002-4

Pope, S. (1994). Lagrangian PDF Methods for Turbulent Flows. *Annu. Rev. Fluid. Mech.* 26, 23–63. doi: 10.1146/annurev.fl.26.010194.000323

Pope, S. (2000). *Turbulent Flows* (New York: Cambridge Univ. Press).

Purcell, S., Neale, B., Todd-Brown, K., Thomas, L., Ferreira, M. A. R., Bender, D., et al. (2007). PLINK: A Tool Set for Whole-Genome Association and Population-Based Linkage Analyses. *Am. J. Hum. Genet.* 81, 559–575. doi: 10.1086/519795

Raho, N., Rodríguez, F., Reguera, B., and Marín, I. (2013). Are the Mitochondrial Cox1 and Cob Genes Suitable Markers for Species of Dinophysis Ehrenberg? *Harm. Algae.* 28, 64–70. doi: 10.1016/j.hal.2013.05.012

Raine, R. (2014). A Review of the Biophysical Interactions Relevant to the Promotion of HABs in Stratified Systems: The Case Study of Ireland. *Deep. Sea. Res. Part II.: Top. Stud. Oceanog.* 101, 21–31. doi: 10.1016/j.dsr2.2013.06.021

Reguera, B., Riobó, P., Rodríguez, F., Díaz, P. A., Pizarro, G., Paz, B., et al. (2014). Dinophysis Toxins: Causative Organisms, Distribution and Fate in Shellfish. *Mar. Drugs* 12, 394–461. doi: 10.3390/md12010394

Reguera, B., Velo-Suarez, L., Raine, R., and Park, M. G. (2012). Harmful Dinophysis Species: A Review. *Harm. Algae.* 14, 87–106. doi: 10.1016/j.hal.2011.10.016

Rossi, V. E., Ser-Giacomi, C. L., and Hernández-G arcía, E. (2014). Hydrodynamic Provinces and Oceanic Connectivity From a Transport Network Help Designing Marine Reserves. *Geophys. Res. Lett.* 41, 2883–2891. doi: 10.1002/2014GL059540

Séchet, V., Sibat, M., Billien, G., Carpentier, L., Rovillon, G.-A., Raimbault, V., et al. (2021). Characterization of Toxin-Producing Strains of Dinophysis Spp. (Dinophyceae) Isolated From French Coastal Waters, With a Particular Focus on the D. Acuminata-Complex. *Harm. Algae.* 101974, 1–14. doi: 10.1016/j.hal.2021.101974

Stolte, W., and Garcés, E. (2006). "Ecological Aspects of Harmful Algal In Situ Population Growth Rates," in *Ecology of Harmful Algae*. Eds. E. Granéli and J. T. Turner (Berlin, Heidelberg: Springer), 139–152. doi: 10.1007/978-3-540-32210-8_11

Taylor, G. (1921). Diffusion by Continuous Movements. *Proc. Lond. Math. Soc.* 20, 196–202.

Theetten, S., Vandermeirsch, F., and Charria, G. (2017). BACH1000_100lev-51 : A MARS3D Model Configuration for the Bay of Biscay, SEANOE. doi: 10.17882/43017

Uppala, S. M., KÅllberg, P. W., Simmons, A. J., Andrae, U., Bechtold, V. D. C., Fiorino, M., et al. (2005). The ERA-40 Re-Analysis. *Q. J. R. Meteorol. Soc.* 131, 2961–3012. doi: 10.1256/qj.04.176

Valencia, V., Franco, J., Borja, Á., and Fontán, A. (2004). "Chapter 7 - Hydrography of the Southeastern Bay of Biscay," in *Elsevier Oceanography Series*, vol. 70 . Eds. Á. Borja and M. Collins (Elsevier), 159–194. doi: 10.1016/S0422-9894(04)80045-X

Van Sebille, E. (2018). Lagrangian Ocean Analysis: Fundamentals and Practices. *Ocean. Model.* 121, 49–75. doi: 10.1016/j.ocemod.2017.11.008

Velo-Suarez, L., Fernand, L., Gentien, P., and Reguera, B. (2010a). Hydrodynamic Conditions Associated With the Formation, Maintenance and Dissipation of a Phytoplankton Thin Layer in a Coastal Upwelling System. *Continent. Shelf. Res.* 30, 193–202. doi: 10.1016/j.csr.2009.11.002

Velo-Suarez, L., Reguera, B., Gonzalez-Gil, S., Lunven, M., Lazure, P., Nezan, E., et al. (2010b). Application of a 3D Lagrangian Model to Explain the Decline of a Dinophysis Acuminata Bloom in the Bay of Biscay. *J. Mar. Syst.* 83, 242–252. doi: 10.1016/j.jmarsys.2010.05.011

Watson, J. (2011). Currents Connecting Communities: Nearshore Community Similarity and Ocean Circulation. *Ecology* 92, 1193–1200. doi: 10.1890/10-1436.1

Wolny, J. L., Egerton, T. A., Handy, S. M., Stutts, W. L., Smith, J. L., Whereat, E. B., et al. (2020). Characterization of Dinophysis Spp. (Dinophyceae, Dinophysiales) From the Mid-Atlantic Region of the United States1. *J. Phycol.* 56, 404–424. doi: 10.1111/jpy.12966

Xie, H., Lazure, P., and Gentien, P. (2007). Small Scale Retentive Structures and Dinophysis. *J. Mar. Syst.* 64, 173–188. doi: 10.1016/j.jmarsys.2006.03.008

Zingone, A., and Larsen, J. (2022). "Dinophysiales," in *IOC-UNESCO Taxonomic Reference List of Harmful Micro Algae (HABs)*. Available at: http://www.marinespecies.org/hab on 2022-05-01.

Conflict of Interest: The authors declare that the research was conducted in the absence of any commercial or financial relationships that could be construed as a potential conflict of interest.

Publisher's Note: All claims expressed in this article are solely those of the authors and do not necessarily represent those of their affiliated organizations, or those of the publisher, the editors and the reviewers. Any product that may be evaluated in this article, or claim that may be made by its manufacturer, is not guaranteed or endorsed by the publisher.

frontiers | Frontiers in Marine Science

ORIGINAL RESEARCH
published: 25 July 2022
doi: 10.3389/fmars.2022.749071

Assessing the Performance and Application of Operational Lagrangian Transport HAB Forecasting Systems

Michael Bedington[1]*, *Luz María García-García*[2], *Marc Sourisseau*[3] *and Manuel Ruiz-Villarreal*[2]*

[1] Plymouth Marine Laboratory (PML), Plymouth, United Kingdom, [2] Instituto Español de Oceanografía (IEO, CSIC), Centro Oceanográfico da Coruña, A Coruña, Spain, [3] IFREMER, French Research Institute for Exploitation of the Sea, DYNECO PELAGOS, Plouzané, France

OPEN ACCESS

Edited by:
Marcos Mateus,
Universidade de Lisboa, Portugal

Reviewed by:
Clarissa Anderson,
University of California, San Diego, United States
Joe Silke,
Marine Institute, Ireland

***Correspondence:**
Michael Bedington
mbe@pml.ac.uk
Manuel Ruiz-Villarreal
manuel.ruiz@ieo.csic.es

Specialty section:
This article was submitted to Marine Fisheries, Aquaculture and Living Resources, a section of the journal Frontiers in Marine Science

Received: 28 July 2021
Accepted: 23 May 2022
Published: 25 July 2022

Citation:
Bedington M, García-García LM, Sourisseau M and Ruiz-Villarreal M (2022) Assessing the Performance and Application of Operational Lagrangian Transport HAB Forecasting Systems. Front. Mar. Sci. 9:749071. doi: 10.3389/fmars.2022.749071

Availability of operational regional hydrodynamic models and near real time Harmful Algal Bloom (HAB) alerts from monitoring stations and remote sensing products have allowed the proliferation of short term advective HAB forecasts. However, their predictive ability in simulating HAB transport needs to be continuously evaluated in events of different HAB species to assess their applicability to different domains and the impacts of the choices made in model setup. Here we review the performance of three different modelling systems which were part of the PRIMROSE project against historical bloom events in different regions in the European Atlantic Area. The objectives are to understand their predictive ability and to demonstrate some aspects of Lagrangian model setup that are relevant to HAB early warning systems; in particular the use of advection-diffusion only models (without a biological component) and the effects of model configuration, especially model resolution. Hindcast and forecast simulations have been run in examples of high biomass blooms detected in satellite imagery; in the western English Channel, several events of potentially toxic species like *Karenia mikimotoi* and *Prorocentrum cordatum (minimum)* were simulated and in Western France a bloom of *Mesodinium rubrum*, prey of the toxic *Dinophysis* spp. Additionally, some simulations for studying the evolution of low biomass *Dinophysis* spp. blooms in Galicia-North Portugal were undertaken with models of different setup. Several metrics have been used to quantify the model performance and to compare the results of the different model configurations, showing that differences in hydrodynamical model configuration (initiation, resolution, forcing, and simulation domain) result in differences in the predicted transport of HABs. We find that advection only is a reasonable approximation but that it may do worse in an early (onset) phase than later on, and we find transport is generally increases with increasing resolution. Our results confirm that Lagrangian particle tracking tools can be integrated operationally in HAB early warning systems providing useful information on potential HAB evolution to users.

Keywords: harmful algal bloom (HAB), HAB forecast, HAB advection, lagrangian modelling, *Dinophysis acuta*, *Karenia mikimotoi*

1 INTRODUCTION

HABs occur seasonally in shelf seas due to favourable conditions promoting local growth or as a result of advection from other areas. When this happens, shell and fin aquaculture might be damaged either indirectly, in case of high biomass HABs which cause oxygen depletion events (O'Boyle et al., 2016) or fish kills (Lee and Qu, 2004), or directly from the toxins, which might result in a food security hazard. The current economic impact of HABs is considerable; one estimate for Scottish aquaculture alone is £1.2 million per year out of a turnover of £12 million (Martino et al. 2020), and the incidence is considered likely to increase with climate change (Paerl and Huisman 2008; Elliott 2012; Wells et al. 2020), making the problem even more important. Beyond aquaculture, HAB forecasts may be of interest for beaches, where they impact human health (Anderson et al., 2016) and provision of ecosystem services.

Monitoring for HABs now encompasses routine *in situ* measurements, field campaigns, and detection from remote sensing, which uses algorithms based on reflectance and other parameters to determine the likelihood that harmful species are present (Kutser et al., 2006; Kurekin et al., 2014; Sourisseau et al., 2016). However, these provide snapshots in the present or recent past. Forecasts for the likelihood of algal bloom incursions on sites of interest in the future provide the most value to end-users since they can allow mitigation actions to be taken. The critical time frame for these predictions depends on the needs of the end-user, but can be on the order of days (Cusack et al., 2016).

HAB forecasting is complex since, whilst the mechanism of triggering a bloom might be understood, e.g. from upwelling variability (Pitcher et al.,2010; Ruiz-Villarreal et al., 2016), the onset of thermal stratification (Simpson and Sharples, 2012; Hartman et al., 2014), or stratification in river plumes (Glibert et al., 2010; Velo-Suárez et al., 2010), diagnosing when these are likely to occur and particularly whether a particular bloom will comprise harmful species, is very uncertain. Once initiated, advection is a significant driver in bloom evolution (Lee and Qu, 2004; Davidson et al., 2009; Velo-Suárez et al., 2010; Aoki et al., 2012; Gillibrand et al., 2016) but continued development, with either more cells growing or dying off, can be as significant, leaving a process which is neither fully physically or biologically determined.

Here we restrict our focus to short term forecasts from operational physics models using Lagrangian drift approaches only. Different reviews of HAB early warning systems (Davidson et al., 2016; Maguire et al., 2016; Ralston and Moore, 2020; Fernandes-Salvador et al., 2021, this issue) cover the range of other approaches, including statistical and machine learning approaches. The increase in availability of regional scale operational models has made near term operational advection-only forecasts feasible in a wide range of areas. These hydrodynamic forecast models typically have a forecast window of 2-7 days and the outputs are used to drive a Lagrangian drift model representing the HAB (e.g. Aleynik et al., 2016; Pinto et al., 2016; Ruiz-Villarreal et al., 2016; Silva et al., 2016). Despite being broadly similar in the size of the region they cover and the length of forecasts, there is considerable heterogeneity of setups.

During the EU funded project ASIMUTH, it was demonstrated that HAB forecast systems showed skill in predicting HAB transport and in assessing the area affected by the blooms (Maguire et al., 2016). The hydrodynamic model configurations developed and demonstrated during the project provided information on the variability of cross-shore and along-shore flows that move HAB populations towards (or away from) harvesting places. The hydrodynamical model runs combined with Lagrangian particle tracking simulations showed skill in predicting along-shore transport of HABs (Gillibrand et al., 2016; Pinto et al., 2016; Ruiz-Villarreal et al., 2016; Silva et al., 2016) as well as cross-shelf transport in and out of harvesting areas (Aleynik et al., 2016; Cusack et al., 2016; Ruiz-Villarreal et al., 2016).

The physical models used for the HAB forecasts are run at different scales, both spatially and temporally, and on either regular (e.g. Ruiz-Villarreal et al., 2016) or unstructured or telescopic grids (e.g. Aleynik et al., 2016), which are becoming more popular in bathymetrically complex areas. Short term HAB predictions usually use these models to force a Lagrangian drift model that is generally run offline (using current velocities stored from a previously run hydrodynamic model) since this allows faster computation and the possibility of re-using the hydrodynamic fields. However, the frequency at which the forcing is saved is a balance between space needed for the forcing files and temporally resolving the most relevant features of the flow.

In this paper we describe three different operational coastal HAB drift forecast systems in operation under the Interreg Atlantic Area Predicting Risk and Impact of Harmful Events on the Aquaculture Sector (PRIMROSE) project (2018-2021), which brought together partners from across the European Atlantic seaboard to improve capacity and tools for HAB prediction (Mateus et al., 2019). In this contribution, we compare these models to several bloom events, both historical and during the project period, to understand the efficacy of advection-only models for short term forecasts and to show the impact of different model choices on the results. We also discuss how their performance impacts on how they might provide value for forecast users, what considerations are important for implementing such a system, and where there is scope for future improvement.

2 METHODS

2.1 Models

The three demonstrated HAB modelling systems are from three different partners in PRIMROSE : Plymouth Marine Laboratory (PML), Institut Français de Recherche pour l'Exploitation de la Mer (IFREMER), and Instituto Español de Oceanografia (IEO), and will be referred to by the respective institute initials throughout. Whilst the domains of these models intersect, they are primarily focused on different areas: the Western Channel

and Celtic Sea (PML), the Western Channel and the eastern Bay of Biscay (IFREMER) and NW and N Iberia (IEO) (**Figure 1**). All the model systems are formed of an operational hydrodynamic model with a separate particle tracking model which is run offline utilising the output from the hydrodynamic model. None of the particle tracking models include explicit biological behaviours (e.g. diurnal migration, life cycle, nutrient limitation) and are purely passively advecting particles.

2.1.1 South West UK Model - PML

An unstructured grid hydrodynamic model FVCOM; (Chen et al. 2003) is run operationally for a domain covering the SW of the UK, producing 3-day forecasts. An operational atmospheric downscaling model [Weather Research and Forecasting model (WRF)] is also run to provide high resolution surface forcing, downscaling the NCEP GFS model (Lien et al. 2016). Lateral boundary data for the hydrodynamic model comes from CMEMS AMM15 model [1.5 km horizontal resolution, (Tonani et al. 2019)], and river input is modelled from the WRF temperature and precipitation using regression and deep-learning models, respectively. The Lagrangian model PyLAG; (Uncles et al. 2020) is run offline on saved hourly outputs from the hydrodynamic model. The Lagrangian model uses a Milstein scheme for advection and diffusion, with the diffusivities provided directly from the hydrodynamic model.

In the operational product, particles are seeded based on output from a HAB-risk product which uses ocean colour (Kurekin et al. 2014). This product uses the multiple bands of ocean colour [6 for MODIS (412, 443, 488, 531, 547 and 667 nm)] with a Linear Discriminant Analysis classifier which was trained on an image set identified by *in-situ* sampling or feature identification. It was assessed to have an 88% accuracy rate for *Karenia mikimotoi* blooms in the Western English Channel; full details are in (Kurekin et al. 2014). Particles are released in a 200 m radius area around the identified high risk locations with 10,000 particles per location. Particles are advected using only the surface layer currents until the end of the forecast period. The results of the model are served both as a gridded particle density and as a probability field, which takes into consideration uncertainty both from the identification algorithm and from the drifting particles.

2.1.2 Bay of Biscay and Western Channel - IFREMER

The Lagrangian Particle tracking model Ichthyop (Lett et al. 2008) is forced using hourly, or daily (de-tided with a Demerliac filter) velocity fields from the hydrodynamic model MARS3D [finite difference, mode splitting model in a sigma-coordinate framework (Lazure and Dumas 2008). It runs on grids of differing resolution (4 km, 2.5 km and 1 km) in an operational way (MARC project: http://marc.ifremer.fr/en/) and produces 4-day forecasts. Wind forcing is Meteo- France product (ARPEGE or AROME according to the configuration and period considered, resolution of 30 km and 1.3 km, respectively). River discharges of the at least 5 main rivers are provided on a daily frequency by River Basin Agencies through the Operational Data Center (http://en.data.ifremer.fr/). Some flow rates of additional rivers are deduced from the measured flow rate of the nearest main river by linear regression.

The Lagrangian model is run only on an *ad-hoc* basis in response to individual events of concern. Most of the time, the model is used to define the bloom advection for some biological reanalysis. HAB cells are represented as passive particles and are introduced in the mixed surface layer. For the two selected events in the English Channel (2003 and 2020), 100,000 and 91, 200 particles were respectively released over the first ten and twenty meters. The horizontal resolution of velocity field was 4 km at hourly temporal resolution. For the *Mesodinium* event in the Bay

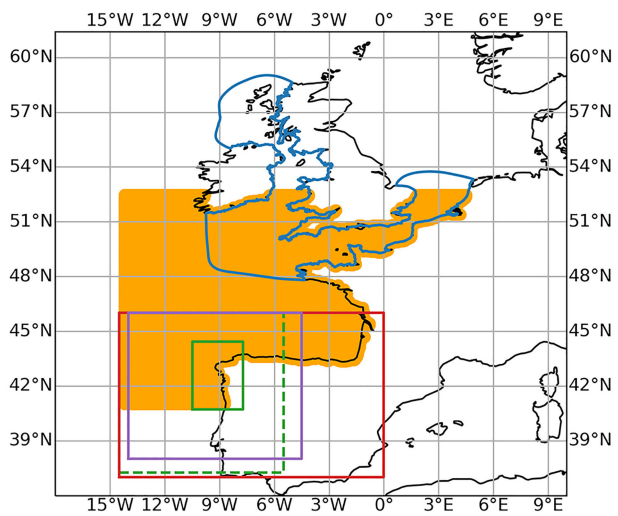

FIGURE 1 | The model domains of the models in the study PML (blue), IFREMER (orange), MeteoGalicia (purple), IEO BIO (red) and IEO RAIA (green) which has a parent grid (dashed line) and nested high resolution grid (solid line).

of Biscay in June 2020, a total of 115,000 particles were released within the first ten meters. Daily velocity fields with a horizontal resolution of 2.5 km were used. Only the vertical dispersion was considered in all simulations and advection equations were solved with a fourth order Runge-Kutta numerical scheme.

2.1.3 Western Iberian Shelf: North Portugal and Galicia - IEO

The Lagrangian particle tracking model Ichthyop (Lett et al. 2008) is forced offline by the saved hourly results of different ROMS hindcast, nowcast and forecast model configurations in the area run by IEO and MeteoGalicia.

MeteoGalicia is a regional meteorological agency that runs meteorological and oceanographic forecasts to support the government and stakeholders in Galicia (NW Spain), a region where the marine sector is of large socioeconomic importance. The MeteoGalicia ROMS model forecast configuration runs on a 2 km resolution grid covering Galicia and is forced at the surface by the operational configuration of the WRF model and at the open boundary by CMEMS (Copernicus Marine Environment Monitoring Service) global model output (horizontal resolution of 1/12°) (Mercator 2016). Tides and the input of several rivers are included. River discharges consist of daily averaged flow and temperature of the main rivers in Galicia obtained from runs of a configuration of the river basin-scale model Soil Water Assessment Tool (SWAT). Further details of the model configuration and validation can be found in (Costa et al. 2012; Venâncio et al. 2019).

Two IEO hydrodynamic model configurations were used in this study: IEO RAIA and IEO BIO. IEO RAIA is based on the ROMS-Agrif realistic model configuration developed during the RAIA Interreg POCTEP Galicia-Portugal project and has a resolution of 4 km in a parent grid (IEO RAIA) and of 1.3 km in a child grid (IEO RAIA nested) centered on Galicia-North Portugal. IEO RAIA is forced by the atmospheric model WRF operationally run by MeteoGalicia (12 km resolution with hourly output). Open boundaries are obtained from the results of a previous climatological run covering the northeast Atlantic. The effect of tides and rivers (11 rivers in the model domain) are included. This configuration has been compared to different *in situ* and satellite data sets and has shown skill in simulating the relevant oceanographic processes in the area (river plumes, shelf and slope current, surface circulation) and their spatial and temporal variability (Otero and Ruiz-Villarreal, 2008; Otero et al., 2008; Otero et al., 2009; Otero et al., 2013). It has been run coupled to dispersion models to demonstrate marine services such as HAB early warning (Ruiz-Villarreal et al., 2016) or pollution dispersion (Marta-Almeida et al., 2013; Otero et al., 2014).

The IEO BIO configuration, described in (García-García et al. 2016), was set up with the ROMS Rutgers version in a domain enlarged to the east to cover the whole northern Iberian shelf. This configuration is similar to the IEO RAIA, but open boundary conditions are taken from the operational MyOcean forecasting and analysis system for the North Atlantic running at Mercator Ocean at the time of the simulations (Lellouche et al., 2013), and additional rivers are included. The IEO BIO configuration has been used coupled to particle-tracking models for simulations of along-shore transport of *D. acuta* for several autumns in Galicia (Ruiz-Villarreal et al., 2016) and in a coupled hydrodynamical-biochemical model configuration to force an Individual Based Model of Early Life Stages of sardine in the Atlantic stock (García-García et al., 2016).

In the Lagrangian model HAB cells are treated as passive particles. Horizontal dispersion is considered, with a fixed dissipation rate of 10^{-9} m^2 s^{-3}. A fourth order Runge-Kutta numerical scheme is used to solve the advection equations. For the operational model run of the early warning system demonstrated in PRIMROSE and previously in ASIMUTH (Ruiz-Villarreal et al., 2016), daily forecasts (3-day window) are run and particles are randomly released in the first 20m of the water column at six locations/configurations. These have been selected to assess the eventual alongshore transport from the northern Portuguese shelf to the Galician Rías Baixas (Vigo, Pontevedra, Arousa and Muros), where the harvesting areas are located, and to explore water exchange between the rías and the across-shore transport to the adjacent shelf.

2.2 Events and Observations

We have identified various bloom events of different HAB species to understand factors involved in the design of a HAB forecast system (see **Table 1**). When different model configurations with different spatial and temporal resolutions were available, i.e. blooms in the Western Channel in 2003 and 2020 and in *Dinophysis* spp. bloom in Iberia in autumn 2013, different particle tracking simulations were run forced by those models and compared. Two events in the Western Channel in 2010 and 2015 had remote sensing data available over a period of weeks, and this allowed the investigation of the period over which an advection-only forecast might be applicable, and how the location of the triggering area affects the results. Examples from 2013 and 2020 of Iberian *Dinophysis* spp. blooms demonstrate the integration with *in-situ* measurements of HAB species, biotoxins and closures at aquaculture monitoring sites. Finally, an event in 2020 in the Channel shows the factors to consider in a nearshore advection event and the importance of wind forcing, which is also discussed in the other events in the Western Channel.

To understand the spatial development of high biomass blooms in the Channel we have used remote sensing measurements of chlorophyll-a, in particular, daily composites retrieved from the Ocean Colour component of the European Space Agency (ESA) Climate Change Initiative (CCI) project (Sathyendranath et al. 2019). The remote sensing product has a spatial resolution of 4 km and combines observations from multiple sensors (MERIS, MODIS Aqua, SeaWiFS LAC & GAC, VIIRS, OLCI). These have been compared with the particles advected in the Lagrangian models to understand the change in spatial extent and location of the blooms. *In-situ* plankton observations from various sources have been included to allow species identification for the chosen blooms.

TABLE 1 | Summary of the simulations.

Year	Model	HAB species	Area
2003 (June-August)	MARS3D	*Karenia mikimotoi*	Western Channel
2010 (June)	FVCOM	*Karenia mikimotoi*	Western Channel
2013 (September-October)	ROMS	*Dinophysis acuta* and *acuminata*	West Iberia
2015 (September)	FVCOM	*Prorocentrum cordatum*	Western Channel
2020 (April)	MARS3D	*Mesodinium rubrum*, prey of *Dinophysis* spp.	West France
2020 (June)	MARS3D, FVCOM	*Karenia mikimotoi* risk	Western Channel
2020 (September-October)	ROMS	*Dinophysis acuta* and *acuminata*	West Iberia

2.3 Metrics

Several metrics have been used to quantify the model performance with respect to the satellite observations (in the case of high biomass blooms), and to compare the results of the different model configurations.

For the high biomass blooms that can be identified from satellite observations, the polygons representing the blooms have been automatically identified as the areas above a threshold of 5 mg/l, corresponding to the threshold used in Mishra and Mishra (2012) to define a 'severe bloom' on their index: all points on the grid of remote sensed data were determined whether they were above or below the threshold, and those above were connected to form polygons outlining the areas which were entirely above the threshold. The same has been performed on gridded data of particle counts obtained from the Lagrangian model for purposes of comparison with the satellite data, using a threshold number of particles scaled to the total number of particles run. In all cases, days with high cloud cover (>30%) were omitted, and for the days the calculations were performed, the model data was masked to omit data corresponding to areas covered by clouds in the observations. The centre of mass is defined as the mean longitude and latitude, weighted by chlorophyll concentration (particle count) of the observations (model). These centres of mass were compared to the centroids of the observed and modelled polygons and found to give very similar results, so centroids are not shown. Another metric is the percentage of model particles which lie within the observation polygons for a particular day. The dispersion is calculated for both the observed and modelled polygons by taking the change in total polygon area between two snapshots and dividing by the time (the time spacing between snapshots varies depending on which days have been omitted due to cloud cover). The final metric is the percentage overlap between the two polygons, defined as the percentage of the observed polygon which intersects with the modelled polygon.

The *D. acuta* and *D. acuminata* blooms that occurred in Portugal and Galicia in 2013 were not high biomass blooms that could be detected from remote sensing. In this case, we compared the results of the different model configurations by using as metric some of the Dispersal Kernel indices described in (Woillez et al. 2009). In particular, the *Centre of Gravity (CG)*, which represents the mean location of the particles at a certain time; the *Positive Area (PA)*, which is the sum of the area units that contain, at least, one particle; the *Equivalent Area (EA)*, which is the area that the particles would occupy if they were distributed at homogeneous densities; the *Coefficient of Variation (CV)* defined as CV=PA/EA and the *mean distance* between the mean start and mean end particle positions. These indices, among others, have been used in previous studies to estimate dispersion patterns associated with Lagrangian models e.g. (Huret et al. 2010; García-García et al. 2016).

3 RESULTS

3.1 Western Channel Hindcasts: PML Model

The PML setup was compared to two historical blooms which occurred in the Western Channel region in 2010 and 2015. The blooms were selected on the following criteria: blooms within the available model period, availability of recorded HAB species from *in-situ* sampling and with enough cloud free remote sensing data to be able to compare the model predictions to the development apparent in the observations. The model setup was identical to the operational setup, with underlying currents and diffusion coefficients from the FVCOM hydrodynamic model, the only change being the lateral boundary forcing came from the reanalysis version of prior lower resolution CMEMS model (AMM7 - O'Dea et al. 2012), since historical forecasts for AMM15 were not available.

A bloom of *K. mikimotoi* in the Western Channel, identified from FerryBox data (Smythe-Wright et al. 2014; Barnes et al. 2015) occurred in summer 2010. The bloom was evident on satellite chlorophyll data (**Figure 2**, column A) for a considerable period (July 5th - August 4th). Regions of high chlorophyll (threshold 5mg/l as above) in the remote sensing were identified to define the start locations for the model runs. Since the bloom was long lived, and to disentangle advection from evolution, two separate start times 2010-07-05 (**Figure 2**, column B) and 2010-07-15 (**Figure 2**, column C) were used, which correspond to points of clear remote sensing images. The second release was chosen for the 15th of July because at this date the particles released during the initial seeding (the 5th of July) had significantly diverged from the observed bloom.

The model shows limited ability in representing the evolution of the bloom at the early stages; particles move southwards in the model and this only matches one part of the observed bloom, since it extends considerably further to the east and north. This is reflected in the rapid drop in particles in polygon and polygon overlap metrics (**Figure 3**), though the spatial split means the centres of mass diverge in a more linear manner. Initiating a second release 10 days later results in a better performance for

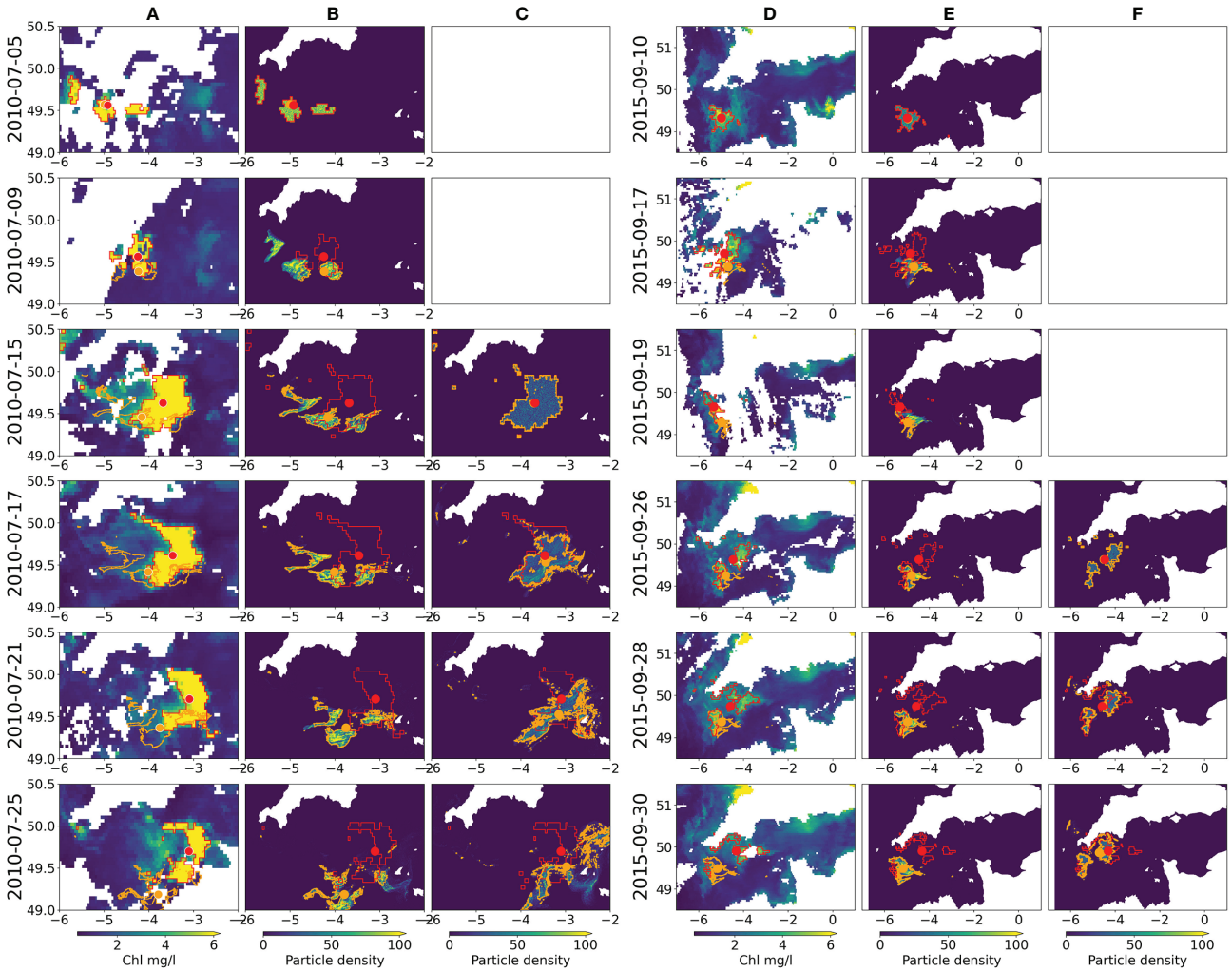

FIGURE 2 | Remote sensing Chl **(A, D)**, and particle densities from the first release **(B)** and re-release **(C)** in the July 2010 **(A–C)** and September 2015 **(D–F)** events. The selected images, which show the progression of each bloom, are chosen for being the clearest remote sensing data, hence the uneven date distribution. Identified areas of high Chl from the remote sensing are marked inside red polygons with the centre of mass marked by a red spot. Areas of high particle density are shown in orange with the corresponding centre of mass shown by orange spots.

the first 5 days (improved across all statistics, **Figure 3**) after which the model shows faster nearshore advection than the observations close to Brittany (**Figure 2**). In this latter part of the second release the model is no better than the original release, with observed and model polygons having low overlaps and increasing centre of mass separations. Dispersion for both runs is similar to the observations, but with considerable variability (**Supplementary Material: Figure 1**). Sensitivity to initial release time on shorter time scales was also studied by running experiments at hourly intervals across a six hour period but found not to significantly affect the results (**Supplementary Material: Figure 2**).

The second event considered is a bloom in September 2015 of the small HAB dinoflagellate *Prorocentrum cordatum (minimum)* that can form extremely dense blooms. *P. cordatum* is detected quite commonly in some monitoring areas along the southern coast of England, but with variable cell densities from year to year (Turner et al. 2017), data available in (UK Food Standards Agency 2020) and it is also commonly found in the summer in the western English Channel at the L4 time series station (Widdicombe et al. 2010). Observations from the Western Channel Observatory (WCO) in September 2015 report concentrations of >5,000,000 cells per litre (Hiscock et al. 2016). The bloom is clearly visible on the remote sensing data as a high chlorophyll-a patch between the 10th of September and the 3rd of October (**Figure 2**, column D) and our particle tracking simulations of the evolution of a potential HAB were run. Again, two separate starting points based on a high chlorophyll threshold in the remote sensing were used to initiate the particle tracking model: 2015-09-10 (**Figure 2**, column E) and 2015-09-26 (**Figure 2**, column F). The performance of the model in the 2015 event was broadly similar to the 2010 event. The

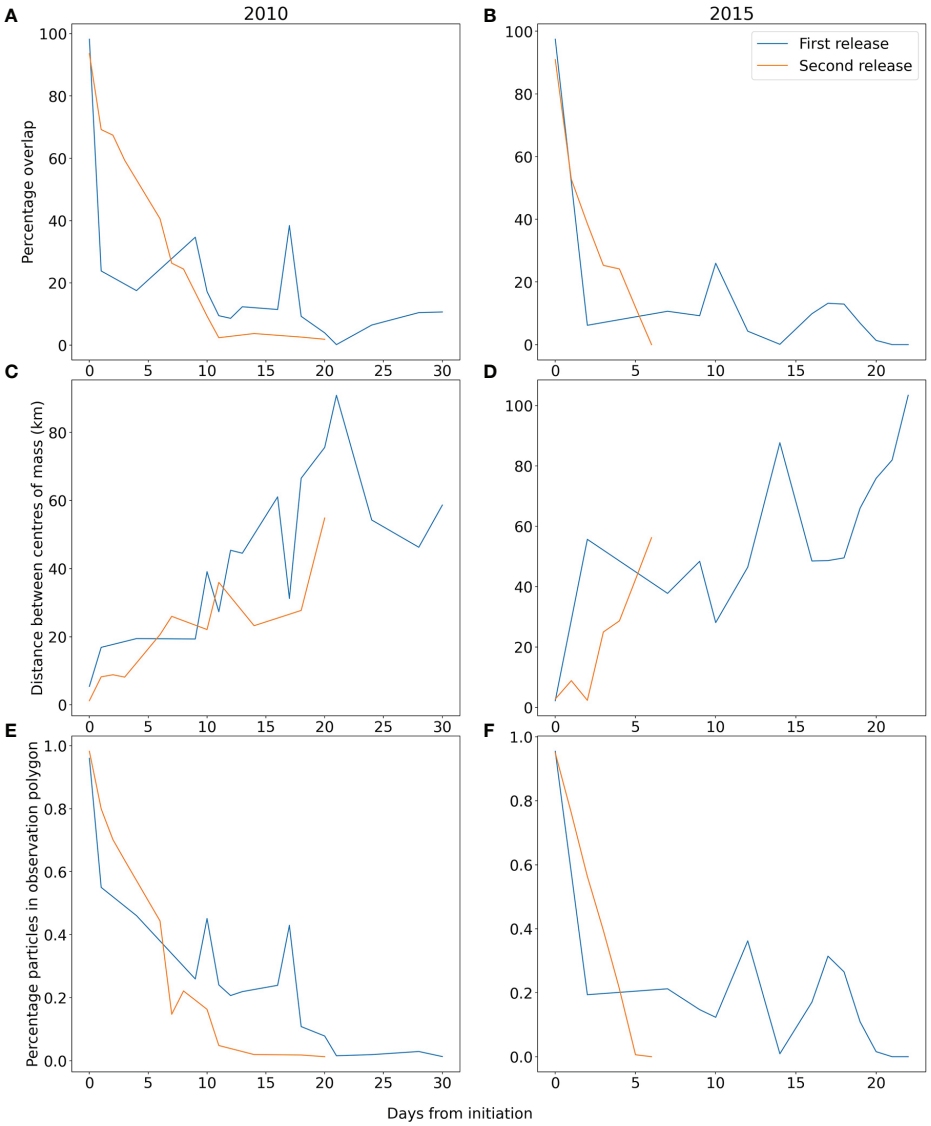

FIGURE 3 | Percentage overlap of polygons **(A, B)**, Distance between centres of mass **(C, D)**, and percentage of modelled particles within observation polygon **(E, F)** for each day after initiation for first (blue) and second release (orange) in 2010 **(A, C, E)** and 2015 **(B, D, F)**.

initial seeding failed to recreate the north and eastward evolution of the bloom, leading to swift drops in the overlap metrics and a separation in the centre of mass too (**Figure 3**). The model was also reseeded later in the bloom (26th September) and showed better agreement with the advection over the first few days (reduced centre of mass separation and less steep decline in particles in polygon percentage). However, by the fifth day the statistics were similar for both runs. The simulations show that particles reach the English southern coast, and this is in accordance with *in situ* observations: *P. cordatum* cells were measured in HAB monitoring samples taken along the southern coast of England in late summer 2015 (Turner et al. 2017), and high numbers (>1,000,000 cells per litre) were recorded at the end of September in St. Austell Bay, Cornwall (Hiscock et al. 2016; UK Food Standards Agency 2020).

3.2 Western Channel Hindcast: IFREMER Model

The IFREMER model was used to simulate two events: one historical (2013) described in this section and one during the PRIMROSE project in 2020 (see section 3.6). A well documented bloom of *K. mikimotoi* occurred in the Channel in 2003, which resulted in mortality of many wild fish species. (Vanhoutte-Brunier et al. 2008) used an Eulerian passive tracer model to simulate this event with an older MARS3D configuration and concluded that apparent transport towards the coast must have

been driven by progressive occurrence of favourable conditions for growth, and not by advection (since the tracer took a northward path). In this work, the new operational IFREMER model is used, which is an upgrade of the MARS3D system with several key improvements: increase in spatial resolution, thirty vertical layers (instead of twelve), a wider geographical domain and more rivers. Tracer transport is simulated with a Lagrangian instead of an Eulerian approach. The IFREMER model was initiated from and compared to the tracers released in (Vanhoutte-Brunier et al. 2008) (**Figure 4A**) In the IFREMER model (**Figure 4B**), from the initial release on 23 June, particles are transported westwards (see particle positions on the 7th of July) and then eastwards (see position of the particles on the 21st of July). The remote sensing data for the period shows the westward extension of the bloom matched by the particles (**Figure 4C**), but also bloom activity to the east. Unfortunately, cloud cover after the 13th of July hampered satellite imagery, which therefore could not provide information on the subsequent transport of the bloom. Comparing the overlap with the bloom area and the distance between the centroids of the shapes, the new model demonstrates that the separation between the centroids was much less than the estimate for the (Vanhoutte-Brunier et al. 2008) model (**Figure 4** and **Supplementary Material: Figure 3**), since it captures the western movement, but the overlap of the polygons is not much greater since it does not capture the expansion to the east. The new run is also not able to reproduce the bloom reaching the French coast of Brittany by the beginning of August. The French Phytoplankton and Phycotoxin Monitoring Network (REPHY) counted 405 000 cells l^{-1} in the Saint-Brieuc Bay on the 15th of August 2003 (REPHY 2021). As suggested by (Vanhoutte-Brunier et al. 2008), our simulation also indicates that the *Karenia* cells found at Saint-Brieuc result from a coastal event related to local growth and not to the advection of the bloom observed offshore.

3.3 PRIMROSE Western France Hindcast: IFREMER Model

In the second event explored with the IFREMER model, a bloom of *Mesodinium rubrum* occurred in the Bay of Biscay during PRIMROSE. *Mesodinium* spp. is associated with blooms nearshore, in estuaries and embayments (Johnson et al. 2013; Trowbridge et al. 2017) and can persist for considerable periods (Crawford et al. 1997). A bloom was observed in spring 2020 at two local harbours (Oleron and Sables, **Figures 5A, B** respectively) and created considerable public concern due to water discolouration during the period of confinement due to COVID. The presence of *M. rubrum* was confirmed by the French HAB monitoring system REPHY, and this bloom was followed by the detection of *Dinophysis* spp. The *ad-hoc* operational model was run during this event to investigate the potential connection between the two sites. Particles were released at two locations on two different start dates: at Sables harbour where discolored waters were observed first to assess if there was an advective connection to the later observation at Oleron (05/04/2020 12:00). The second drift was initiated from Oleron, to estimate displacement of the bloom. Locations of particle release at Oleron were estimated from a satellite index of bloom (Normalized Difference Chlorophyll Index, NDCI as defined by (Mishra and Mishra 2012), values over 0.5 are considered as a blooming area) computed from a satellite product (Copernicus Sentinel 1A, 18/04/2020 10:56) (**Figure 5D**). Hydrodynamics were provided by a MARS3D configuration (horizontal resolution of 2.5 km) forced by ARPEGE-HR solutions (hourly, 0.1°, Meteo France).

Particles released at Sables were not advected to Oleron area (**Figure 5C**), which suggests the bloom was spread over a larger area. In the same figure panel, we can see that particles released from Oleron strongly drifted offshore after 8 days, possibly driven by a short period of strong offshore winds after the 18th of March (**Figures 5E, F**).

3.4 West Iberia Hindcast: IEO Model

The autumn 2013 *Dinophysis acuta* event on the northern Portuguese coast and Galician rías was the most intense since 2005 (Díaz et al. 2016), and *D. acuta* appeared together with *D. acuminata*. The HAB caused the closures of most of the harvesting polygons in the area for several months including the Christmas period, one of the most profitable of the year. The along-shore transport of *D. acuta* from the Portuguese shelf to the Galician rías has been described as the cause of sudden autumn blooms (Escalera et al., 2010; Pitcher et al., 2010; Díaz et al., 2016). *D. acuta* blooms usually occur in the summer in the shelf off Aveiro and get transported northwards. Several events of *D. acuta* autumn transport to the Galician Rías have been described, particularly those in 2005 and 2013 (Díaz et al., 2016). **Table 2** summarizes the timeline of the sequence of closures from Portugal to the Galician bivalve harvesting polygons in 2013.

Lagrangian modelling studies of the 2013 event have been previously carried out (Ruiz-Villarreal et al. 2016; Silva et al. 2016; Moita et al. 2016) to try to elucidate if advection could explain the transport of *D. acuta* and the timing of closures from Portugal to the Galician rías. All model exercises predicted northwards transport, although no detailed analysis of the impact of the model configuration in the predicted particle transport was performed. In this paper we revisit this HAB event to evaluate the impact of using hydrodynamic models of different resolutions and configurations to force the Lagrangian model. We used four different model configurations: the IEO RAIA in the parent 4 km grid (IEO RAIA) and the child 1 km grid (IEO RAIA nested); the IEO BIO 3.5 km grid and the MeteoGalicia 2 km operational forecast configurations. Model set ups differ in the extent of the model domain (see **Figure 1**) and also in forcing at the open boundary (RAIA is forced with a climatology and IEO BIO and MeteoGalicia with Mercator), and river input.

Figure 6B shows the release of particles at the Portuguese polygon close to Aveiro the 17 th of September 2013 (blue particles), the date for which the maximum concentration of *D. acuta* was detected at Aveiro (**Table 2**). One week later (the 24 th of September 2013), the particles were mostly located to the south

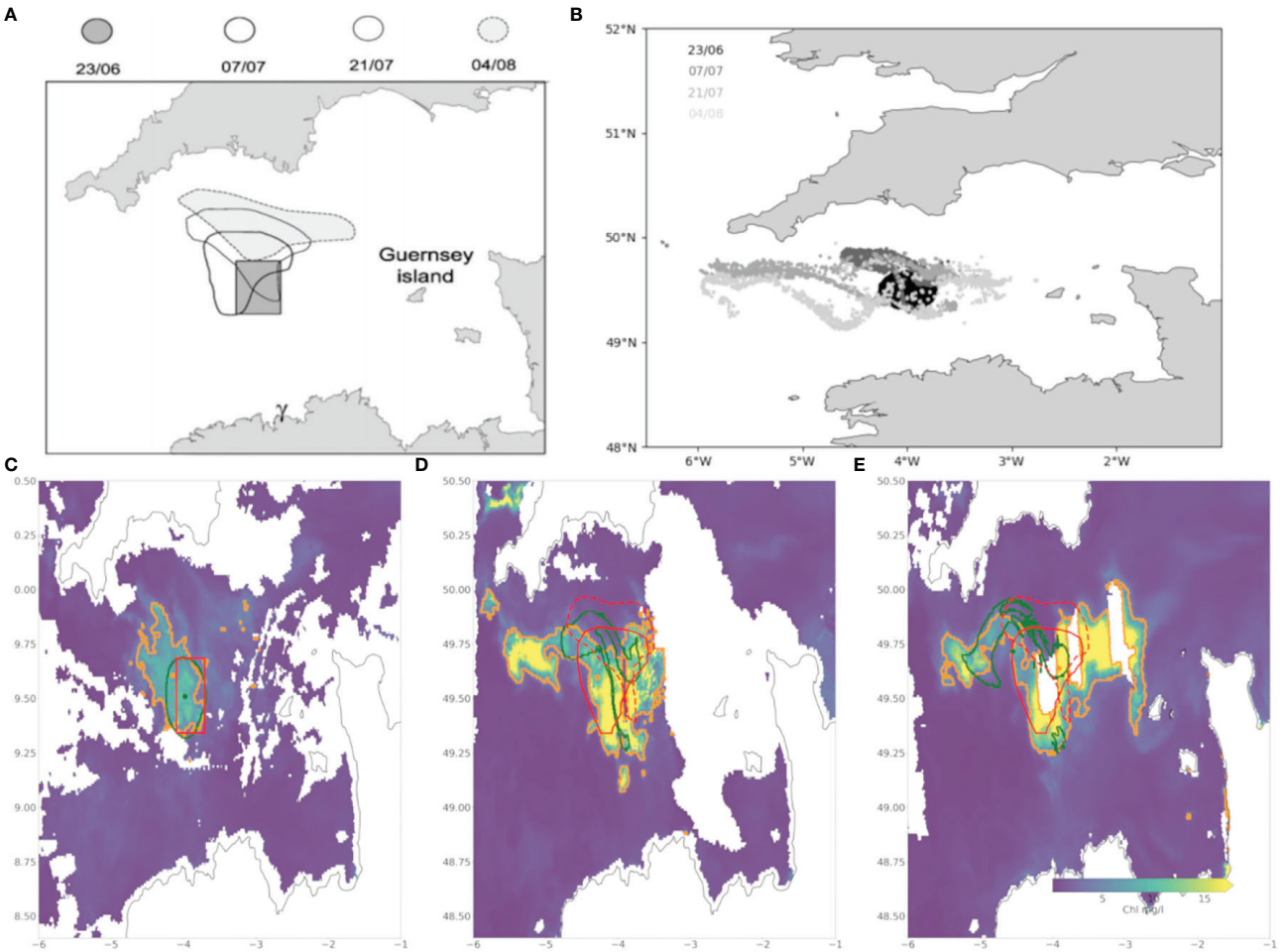

FIGURE 4 | Advection of passive tracer in the 2003 K. *mikimotoi* bloom **(A)** represented with isolines of modelled tracer concentration plotted every two weeks (reproduced from (Vanhoutte-Brunier et al. (2008)). The MARS3D model configuration had a 4x4 km resolution and 12 sigma levels from the south of Brittany (47.5N, 5.6W) to north of the Rhine river plume (52.5N, 5.0W). Lagrangian advection from the same period **B**) observed with a configuration using a larger geographical domain and a higher vertical resolution (30 sigma layers). CCI remote sensing chlorophyll from the same period, showing three days when cloud cover was least (**C** - 2003/06/23, **D** - 2003/07/09, **E** - 2003/07/13). The positive area for the particle run is shown in green, tracer from (Vanhoutte-Brunier et al. (2008) are shown in red for 07/07 (solid) and 21/07 (dashed).

and offshore the initial release position (red dots), due to the dominant upwelling winds (**Figure 6A**). This dispersion to the south is higher in the coarser resolution models (**Figure 6B**, IEO BIO and IEO RAIA). Note that in the case of the finest model resolution (**Figure 6B**, IEO RAIA nested) the particles did not displace further south because of the size of the model domain (see **Figure 1**).

After the 24th of September 2013, strong downwelling conditions prevailed in the area (**Figure 6A**), which explains the northward transport of particles that reached the south of Ría de Vigo on the 30th of September 2013 (green particles in **Figure 6B**) in the case of the IEO RAIA configuration, and further north in the case of the IEO BIO, MeteoGalicia and the high-resolution configuration (IEO RAIA nested). The average transport northward is higher in the case of the mid-resolution model MeteoGalicia (as shown by the trajectory of the CG (black line) in 6B) because the transport to the south under upwelling conditions the previous week was less intense than in the coarse resolution models IEO RAIA and IEO BIO. The same happened in the case of the high-resolution model IEO RAIA nested, but in this case it was affected by the limits of the model domain.

Finally, on the 4th of October, when the polygons started to close in the north of Portugal and the southern Galician Rias, we can see that all the models show particles (yellow in **Figure 6**) located at the mouth of every ria and even further northwards in the case of the IEO BIO, MeteoGalicia and IEO RAIA nested models. Hence, the results shown here are compatible with the sequence of events compiled in **Table 2**.

Figure 6C illustrates the position of the particles in the first and second weeks after their release close to Aveiro the 24th of September (blue particles). In this case, downwelling conditions were dominant (**Figure 6A**), and just one week later (30th of

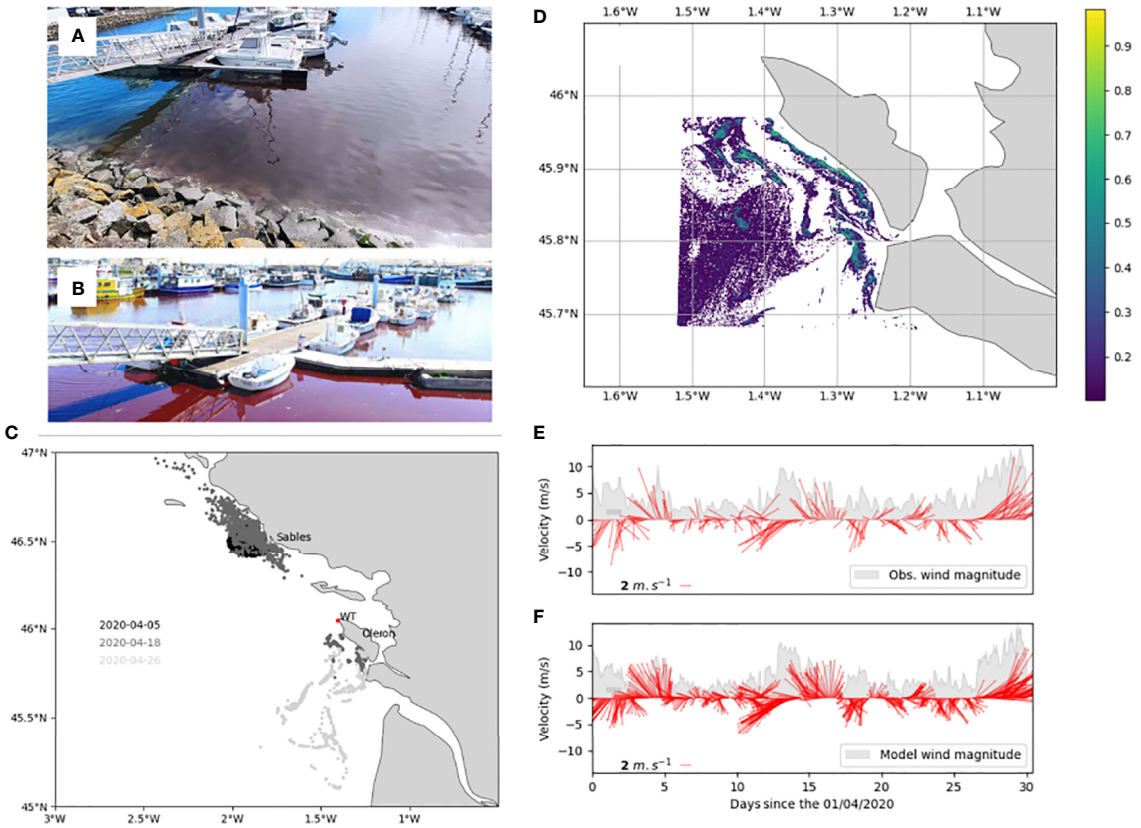

FIGURE 5 | *Mesodinium rubrum* observed in the harbours at Sables **(A)** and Oleron **(B)** on 05/04/2020 and 11/04/2020 respectively. The simulated advection **(C)** from each of these start locations and dates is shown. The first release was from a point source in front of the Sables d'Olonne harbour (05/04) to see if there was a connective pathway between the events, and the second release (18/04 10:56) was based on a satellite index of bloom **(D)** Observed winds from the meteorological station Chassiron (WT) [10 min average, **(E)**] are compared to forcing winds [minute frequency, **(F)**] for the same location. Forcing winds were interpolated from ARPEGE-HR solutions (hourly frequency).

September, red particles), the particles are close to the mouth of the ria de Vigo for the IEO RAIA model (**Figure 6C**, second column), up to ria de Arousa for the IEO BIO and the MeteoGalicia models (**Figure 6C**, first and third columns) and up to ria de Muros in the case of the IEO RAIA nested domain (**Figure 6C**, fourth column). The 4th of October (two weeks later, green particles), the particles are occupying the mouths of all the rías, except Muros, when using the IEO RAIA model as forcing. With the IEO BIO configuration, particles move further north (up to Malpica) and, in the case of the MeteoGalicia and IEO RAIA nested models, the particles reach up to the Artabro Gulf. These results are also compatible with the sequence of events described in **Table 2** and do not differ much from those for the 30th of September and 4th of October in **Figure 6B**, although in the latter case, the density of particles reaching the Galician Rías would be higher, since the transport was always in the same direction and confined onshore. This is clear in the trajectory of the CG (black line), which shows a northward transport for all the configurations, with the MeteoGalicia model showing the longest transport and the IEO RAIA the shortest. **Figure 6** illustrates that the mechanism of northward transport from Portugal persisted over several weeks.

The effect of the different hydrodynamic model configurations on the particle transport is summarized by means of some Dispersal Kernel indices in **Table 3** for the 17th and the 24th of September 2013 releases. These indices give an idea of the particle dispersion. For instance, if we consider the simulations starting the 17th of September, we see that the IEO RAIA configuration is the one producing the highest dispersion of particles (highest PA=13,750 km^2), followed by the IEO BIO (PA=13,575 km^2) and the IEO RAIA nested (PA= 6,850 km^2) and MeteoGalicia (PA= 6,800 km^2) models. This is clearly reflected in **Figure 6B**, where we can see that the IEO BIO and IEO RAIA configurations produce a southward transport of particles first, followed by a northward transport, which results in a larger area occupied by the particles. The MeteoGalicia configuration, which is run in a model domain as large as IEO RAIA (**Figure 1**), does not produce the initial movement of particles southwards, which results in a smaller occupied area and an overall transport further away from the mean initial

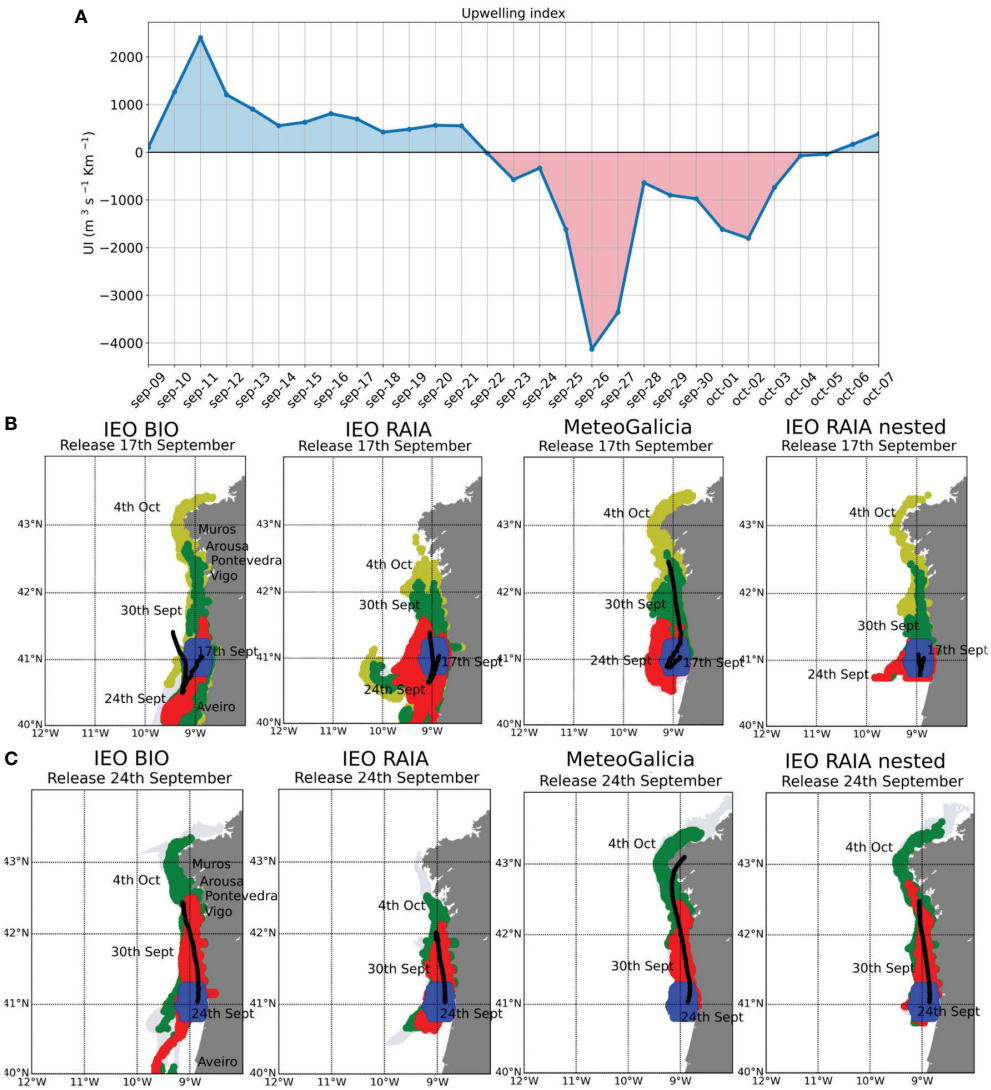

FIGURE 6 | Upwelling index for the September 2013 hindcast **(A)**. Particle positions at different dates after being released in different areas on the 17th of September **(B)** and on the 24th of September **(C)**. Black lines mark the trajectories of the Center of Gravity (CG). Column 1: IEO BIO model, 3.5 km resolution; Column 2: IEO RAIA model, 4 km resolution; Column 3: MeteoGalicia model, 2 km resolution and Column 4: IEO RAIA nested model, 1 km resolution.

TABLE 2 | Sequence of events: *D. acuta* event 2013 and *D. acuta* and *D. acuminata* event 2020 at Portugal and Galician Rias.

Date	Location	Event
9th Sept. 2013	Aveiro (Portugal)	Initiation of the *D. acuta* bloom (>200 cell/l detected)
17th Sept. 2013	Aveiro (Portugal)	Maximum concentration of *D. acuta* (4,640 cell/l)
27th Sept. 2013	North of Portugal (L1 and L2 polygons)	Low numbers of *D. acuta*
30th Sept.2013	Bueu, Ria de Pontevedra	Some cells detected (80 cell/l) at one harvesting polygon
4th Oct. 2013	North of Portugal (L1 and L2 polygons)	Closure of polygons
4th - 5th Oct. 2013	Rias de Vigo and Pontevedra	First polygon closures
8th - 9th Oct. 2013	Rias de Vigo, Pontevedra, Arousa and Muros	Closures extend to all the rias and most polygons
4th Sept. 2020	North of Portugal (L1 and L2 polygons)	Polygon closures (DSP)
7th Sept. 2020	North of Portugal	*D. acuminata*: 200 cell/l at L1 and 600 cell/l at L3
8th Sept. 2020	North of Portugal L3	*D. acuta*: 160 cell/l
16th Sept. 2020	Rías de Vigo and Pontevedra	Polygon closures (DSP)
19th - 26th Sept. 2020	Ría de Arousa	Polygon closures (DSP)
25th Sept. 2020	Ria de Muros	Polygon closures (DSP)

Data from the INTECMAR and IPMA Galician and Portuguese HAB monitoring.

TABLE 3 | Dispersal Kernel indices [Mean Distance, Positive Area (PA), Equivalent Area (EA) and Coefficient of Variation (CV)] for the different model configurations run in the 2013 HAB event in W Iberia.

Simulations starting the 17th of September 2013				
Model Configuration	Mean distance (km)	PA (km^2)	EA (km^2)	CV
IEO BIO	65	13575	360.29	6.1
IEO RAIA	42.5	13750	644.16	4.51
MeteoGalicia	159.8	6800	411.48	3.94
IEO RAIA nested	10.78	6850	63.49	10.34
Simulations starting the 24th of September 2013				
Model Configuration	Mean distance (km)	PA (km^2)	EA (km^2)	CV
IEO BIO	157.6	12650	783.14	3.89
IEO RAIA	129.2	6625	582.59	3.22
MeteoGalicia	229.4	7825	576.74	3.54
IEO RAIA nested	160.33	9225	757.40	3.34

location in the northward direction (compare the trajectories of the CG, black lines in **Figure 6**). The particles are also more homogeneously distributed when using the IEO RAIA configuration (highest EA). The CV indicates the existence of more homogeneous densities (lower values) or aggregates (higher values), meaning that the IEO BIO configuration produced more aggregates (CV=6.1), followed by the IEO RAIA (CV=4.51) and the MeteoGalicia (CV=3.94) configurations. In terms of mean distance between the mean particle origin and the mean particle end, it is the MeteoGalicia model the one that shows higher values (159.8 km), followed by the IEO BIO (65 km) and the IEO RAIA (42.5 km). The indices for the IEO RAIA nested model are influenced by the fact that the particles get accumulated in the southern limit of its domain (see **Figure 1**) during the first days of the simulation, which results in a PA similar to the MeteoGalicia model, but with much higher aggregation (CV=10.34).

For the simulations starting the 24th of September 2013, the IEO BIO shows the highest dispersion (PA=12,650 km^2) due to a number of particles being transported southwards. In the remaining configurations, this southward transport is minimal (IEO RAIA, IEO RAIA nested) or non-existent (MeteoGalicia) and the dispersion area increases with resolution. The degree of aggregation is similar in all the configurations (CV around 3), although slightly higher for IEO BIO. The longest mean transport (229.4 km) corresponded to the MeteoGalicia configuration (which did not show southward transport at all), followed by the highest resolution model (IEO RAIA nested, 160.33 km), for which the mean distance was similar to the IEO BIO model (157.63 km).

3.5 PRIMROSE Forecasts in Galicia

During PRIMROSE, a transboundary event involving a proliferation of *Dinophysis acuta* and *Dinophysis acuminata* that lead to harvesting polygon closures in North Portugal and the Galician Rías in September 2020 was investigated using the IEO early warning system, forced by the ROMS MeteoGalicia forecast model. **Table 2** summarizes the time sequence of toxic phytoplankton and biotoxin measurements during this event, together with the dates when closures were enforced by the regulatory authorities. **Figures 7A, B** show the evolution of the concentration of *D. acuminata* and *D. acuta*, respectively, during the month of September 2020, and **Figure 7C** depicts the concentration of DSP biotoxin. The DSP toxin was already above regulatory threshold permissible level (160 μg/kg) in the first week of September in Portugal (caused by *D. acuminata*), as well as in some polygons in Ría de Pontevedra, which were already affected for several weeks due to the presence of both species of *Dinophysis* (**Table 2**). The second week of September (second column **Figure 7**), some polygons at the mouth of Ría de Vigo exceeded the DSP threshold, but it is during the third week (third column) when high concentrations were measured inside the ría causing most of the polygon to be closed due to the accumulation of both species. In the following week (fourth column), *D. acuminata* and *D. acuta* blooms closed polygons in the Rías de Arousa and Muros.

The IEO early warning system was used to investigate whether: a) there was a potential transport from the Portuguese shelf to the Galician Rías and this caused the closures of harvesting areas and b) the sequence of closures from south to north in the Galician Rías was caused by exchange between adjacent rías.

The upwelling index evolution from the 4th of September, when the first polygons were closed in North Portugal, shows that winds were upwelling favourable and relaxed around the 8th of September (**Figure 8B**) during neap tides (**Figure 8A**). The Lagrangian model forecasts for the 4th of September do not suggest northward transport on the Portuguese shelf (**Figure 7D**), and neither do the forecasts for the subsequent days before the closures in Ria de Vigo after the 16th of September (not shown), probably due to the rather calm wind conditions. Polygon closures extended from Vigo to Arousa from the 16th of September onward, just a few days after the occurrence of neap tides and still under rather calm wind conditions (**Figures 8A, B**). The results of the Lagrangian forecasts for the 16th of September at Ría de Vigo (**Figure 7E**) show that particles mostly remained confined inside the ría, and that the exchange with Ría de Pontevedra and the rías further northwards was unlikely, based on the model results.

Just a few weeks after the polygon closures, conditions changed and most of the closed polygons in Rías de Vigo, Arousa and Muros reopened between the 9th and the 17th of

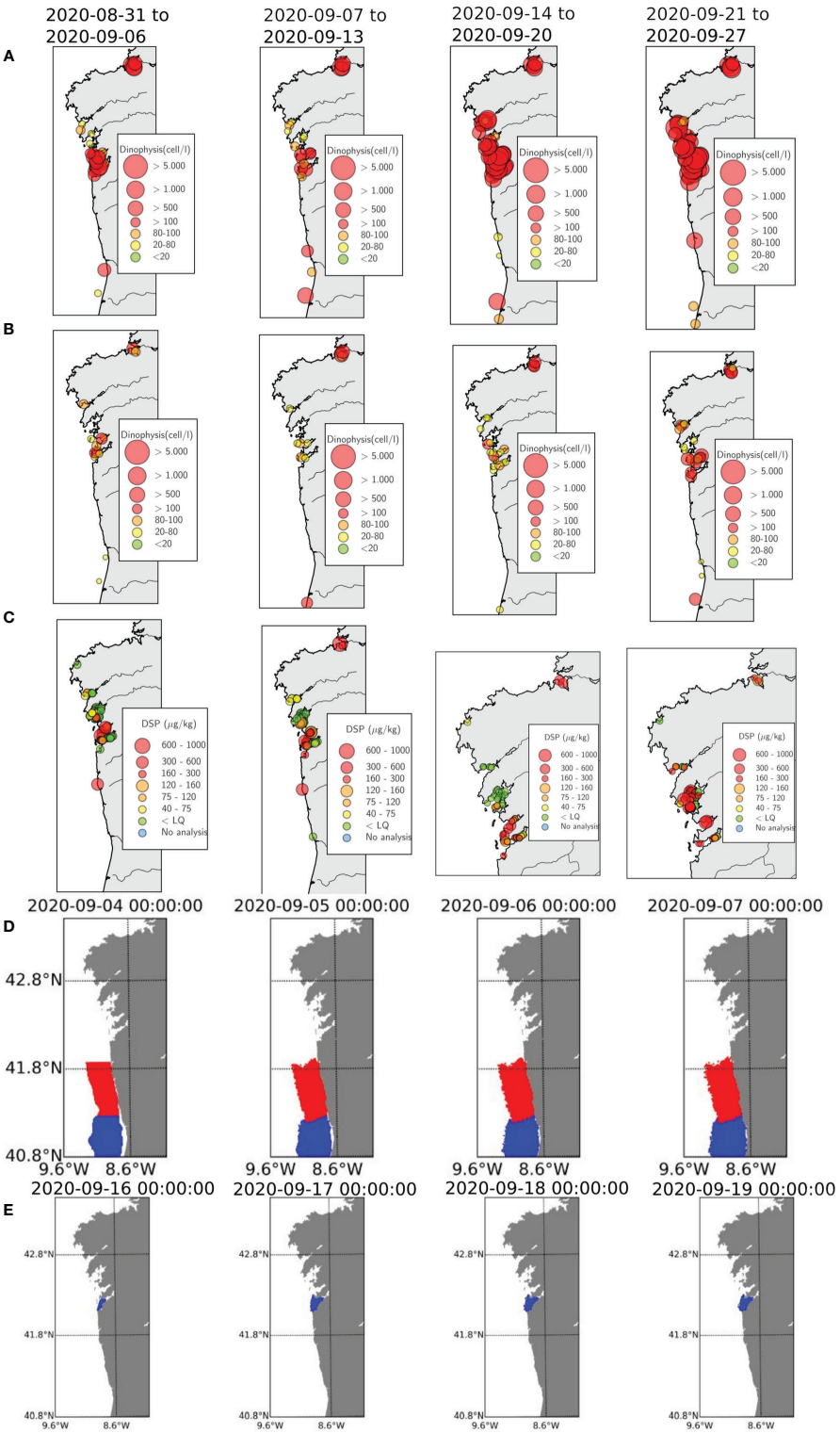

FIGURE 7 | Results of the PRIMROSE forecast and data from the weekly Galician and Portuguese monitoring programs in September 2020: **(A)** *Dinophysis acuminata* **(B)** *Dinophysis acuta* and **(C)** DSP toxins (no data available in Portugal during the last two weeks). **(D)** Particles released in Portuguese areas from 4-7 September **(E)** Particles released in the Ria de Vigo from 16-19 September.

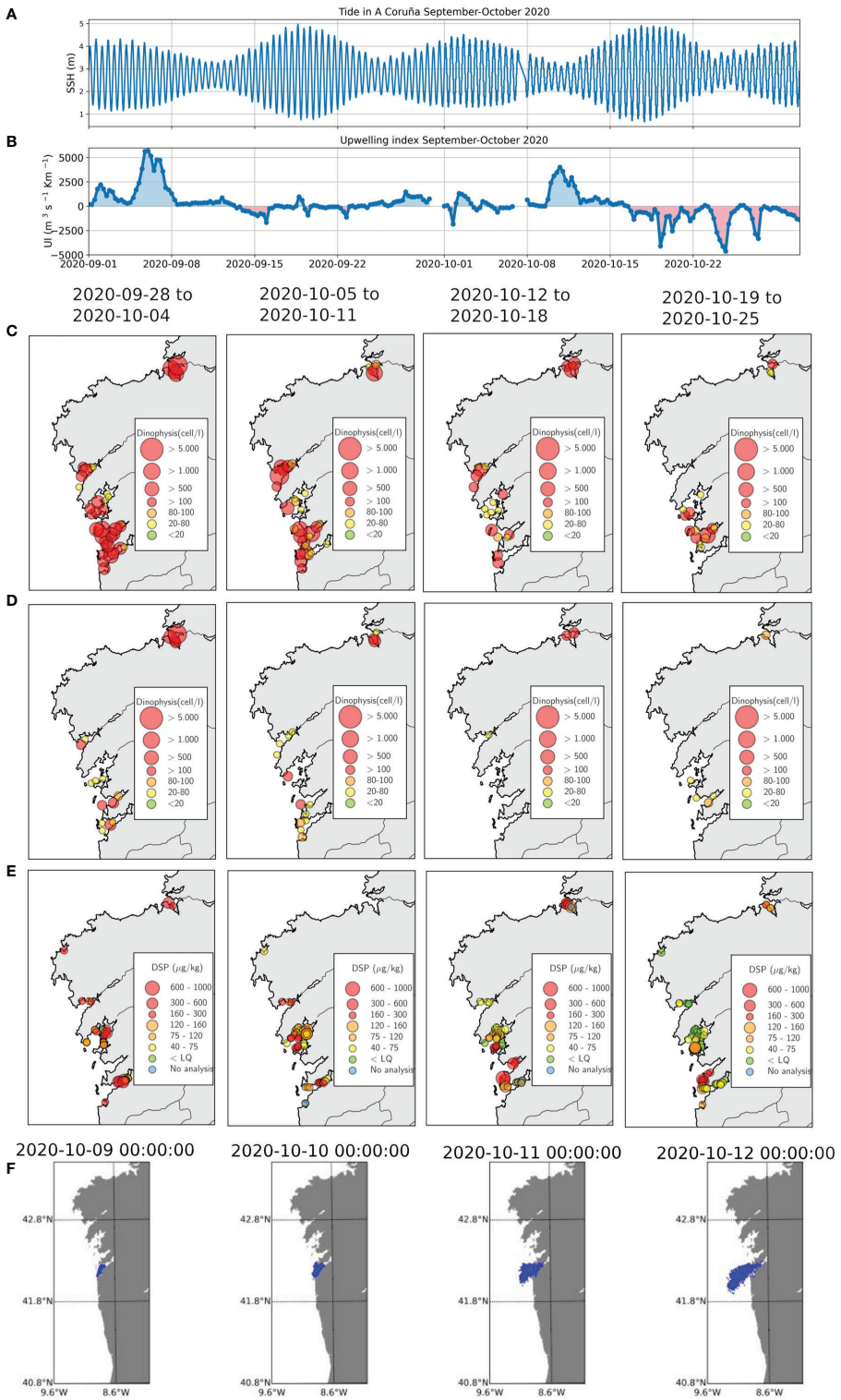

FIGURE 8 | Results of the PRIMROSE forecasts and data from the weekly Galician monitoring program in October 2020: **(A)** Tides at A Coruña in September-October 2020, **(B)** Upwelling index in September-October 2020 **(C)** *Dinophysis acuminata* **(D)** *Dinophysis acuta* and **(E)** DSP toxins **(F)** Particles released in the Ria de Vigo from 9-12 October.

October. **Figures 8A, B** show that this was a period of neap tides under strong upwelling conditions. Upwelling conditions are favourable for the offshore transport, and hence the outflow and exportation of toxic cells, which would produce a "cleaning effect". **Figures 8C, D** show that *D. acuminata* and *D. acuta* concentrations reduced during that period, except for Ría de Pontevedra, where *D. acuminata* persisted. The reduction in the DSP biotoxin throughout October is clear in **Figure 8E** for all the rías, except Pontevedra. The IEO early warning system predicted conditions of transport outside the rías (see **Figure 8F** for Ría de Vigo), and concluded that polygon re-openings were likely. Forecasts of trends to open/close of harvesting areas are another service provided by the forecasting system, already demonstrated in ASIMUTH project (Maguire et al., 2016; Ruiz-Villarreal et al., 2016; Silva et al., 2016).

3.6 PRIMROSE Forecasts in the Channel: PML-IFREMER Model Comparison

A potential large bloom was spotted in the Channel region in June 2020 during PRIMROSE and since it incurred on both PML and IFREMER model domains, model runs using both the PML and IFREMER (2.5 km) model frameworks were undertaken. The full operational setups as described in section 2.1 were used. The identification of the bloom came from the algorithmic *Karenia* spp. risk identification from satellite images based on algorithm by (Kurekin et al. 2014) introduced in the section 2.1.1. The HAB risk map in the PML HAB Risk portal[1] shows the composite image over several days. However, for sensible comparison to the higher time frequency involved with advection, the respective model runs were compared to the algorithm output from individual passes of the satellite products (**Figure 9**). Unfortunately, whilst the initial satellite images were clear and the algorithm was able to identify a HAB, the following days were affected by cloud coverage. In any case, the eastern part of the bloom remained in the visible part of the images and thus, the satellite could be used to assess the skill of the two models.

Both models were started from points the operational HAB risk algorithm deemed as high risk. The PML model shows a much greater spread of particles from the western starting positions, where they reach the higher velocity currents around the Channel Islands, and also a closer incursion towards the coast from the eastern starting points. The significant difference driving this is that the offline forcing of the IFREMER Lagrangian model in this case is saved at a daily resolution, so tidal frequency is not resolved (though will include underlying tidal features in the hydrodynamical model).

4 DISCUSSION

The Lagrangian drift models presented here attempt to fulfill the need of short term forecasting of HAB blooms primarily aimed at aquaculture users (Cusack et al., 2016; Ruiz-Villarreal et al., 2016; Silva et al., 2016). We have looked at operational HAB models from the PRIMROSE project and compared them to observed blooms, in particular to see how applicable advection alone is to the short term prediction of HAB movement and how model setup might impact on the results of transport models.

4.1 Advection of High Biomass Blooms Simulated With Lagrangian Particle Tracking Models: Strengths and Uncertainties

Several case studies were focused on high biomass blooms such as those of *K. mikimotoi* in the Western Channel with the objective of evaluating how a short term advective only forecast performs. *K. mikimotoi* is frequently present in the summer phytoplankton community in the Channel (Widdicombe et al., 2010) and it is thought to be responsible for occasional mass finfish and benthic mortalities (Barnes et al., 2015). In sections 3.1, 3.2 and 3.6, Lagrangian particle trajectories were compared to satellite imagery following the metrics described in section 2.3.1.

Remote sensing products have several challenges for direct use in model comparison. Firstly, remote sensing is not a perfect measure of a bloom, especially for toxic species. *K. mikimotoi* for example is known to produce a thin layer which may not show up on satellite imagery (McManus et al. 2008; Brand et al. 2012), and nearshore chlorophyll measurements will be affected by sediments (Le et al. 2013). Also, *Karenia* species cell colouring imply that they have reduced reflectance, which makes it hard to identify species and will likely under count concentrations, especially once cell concentrations are above 10^4 cells 1^{-1} (Hu et al. 2005; Cannizzaro et al. 2008). Whilst studies have used chlorophyll products to study *K. brevis* blooms e.g. (Redalje et al. 2008), the Normalized Fluorescence Line Height (NFLH) product was shown to give better results (Hu et al. 2005; Cannizzaro et al. 2008; Tomlinson et al. 2009). In a review of various different approaches, (Soto et al. 2015) found further improvements when combined with other products, determining the Rrs - NFLH method using NFLH and the 555nm reflectance to perform best for identifying *Karenia* blooms. However, for these events coverage with chlorophyll-a products was better than the NFLH and 555nm product, and when comparing to available scenes from NFLH and Rrs - NFLH (**Supplementary Material: Figures 4, 5**), the chlorophyll product shows a very similar bloom evolution. In this study, since we have identified the species from available *in-situ* observations and we are concerned with the bloom shape and movement rather than absolute concentrations, the use of a chlorophyll product is less problematic.

Another issue related to remote sensing is that data availability is variable due to cloud cover. This can be mitigated with the use of composites of several days together or interpolation between days of data availability. Here we are concerned with short time scale advection and hence, products composited over a longer period of time will average out this movement. Interpolated products should not have this problem, but must use some extra technique to fill in the gaps, for example

[1] https://www.s3eurohab.eu/portal/?state=cf0d81 - retrieved 2022/03/15

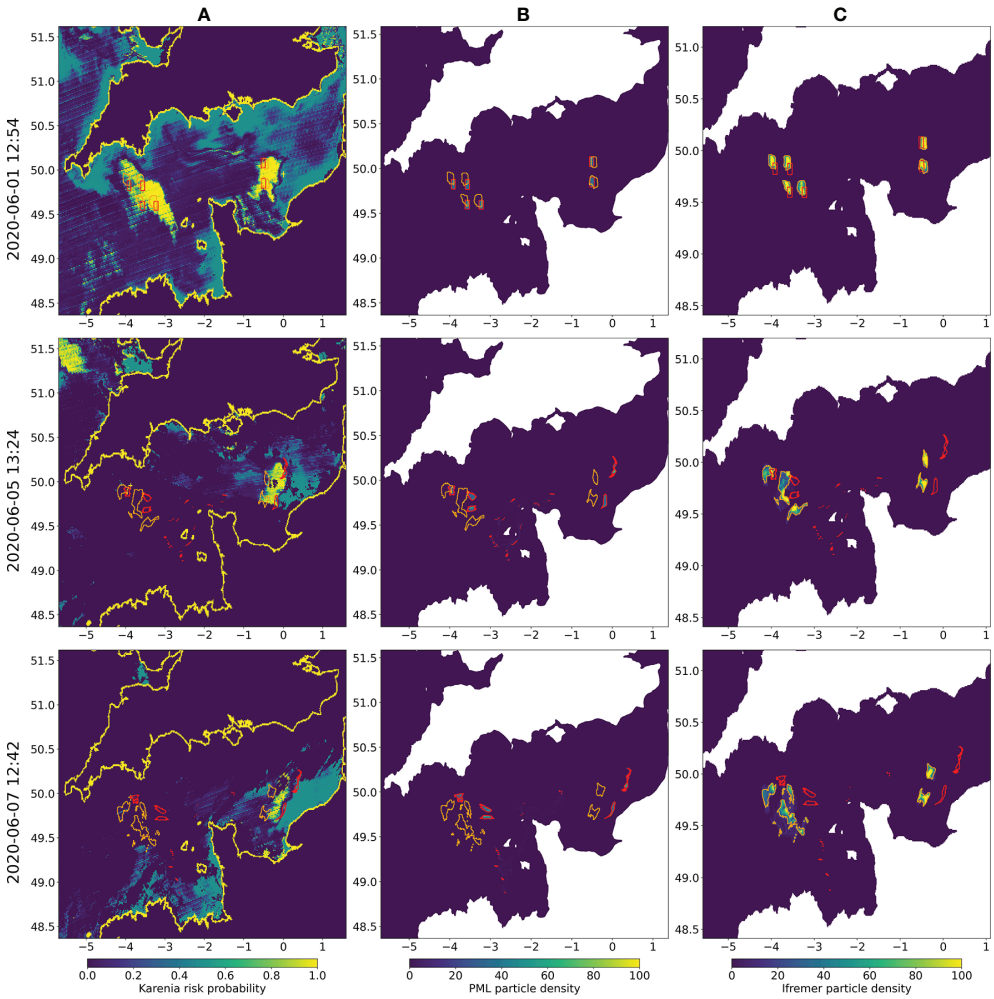

FIGURE 9 | Comparison of HAB risk from remote sensing **(A)** and particle densities for PML model **(B)** and IFREMER **(C)**, on selected days with clearer satellite image of *Karenia* risk (2020/06/01 12:54, 2020/06/05, 2020/06/07). The polygons of high particle density for PML model (red) and IFREMER (orange) are shown in each panel.

using a hydrodynamic model [(Lin et al. 2021), this issue] or machine learning (Vandal and Nemani 2019) to produce intermediate images, which may itself introduce spurious movement. Here we decided to be conservative and only use products which are either daily composites or individual scenes, omitting days with high cloud cover (>30%), to ensure we are comparing to actual bloom development.

Despite these concerns, remote sensing products provide a spatial and temporal coverage of potential HAB events that cannot be achieved by alternative methods. For example, *in-situ* sampling requires structured field campaigns e.g. (Velo-Suárez et al. 2010) and has to be fortunate enough to coincide with a bloom [e.g. Jordan et al. 2021, this issue]. Opportunistic measurements, such as FerryBoxes provide only limited spatial resolution (Qurban 2009; Hartman et al. 2014), which is not sufficient to understand the advective component of mid-channel blooms. In future it is possible these limitations will be overcome by responsive sampling by unmanned platforms [e.g. as demonstrated by Ruiz-Villarreal et al. 2022, this issue].

If we assume that the remote sensing data provided an accurate representation of bloom development, then in both examples from the PML model (sections 3.1 and 3.6) the latter part of the bloom evolution was better forecast than the initial movement. In both cases the efficacy of the forecast dropped rapidly in the first five days after initialisation, as demonstrated by the various metrics applied for comparing particle model results and satellite data. The difference between the initial and latter movement could represent a period of rapid growth followed by advection, which would fit with rapid onset in the order of a few days followed by a maintenance phase that has been observed in some HAB species (Redalje et al. 2008; Aoki et al. 2012), and with the apparent change in surface area of the bloom during this period, though the latter could also be a consequence of diffusive processes. Onset here refers to onset

visible on the remote sensing data; there may be prior activity at the subsurface or with a low chlorophyll content and hence not detected by the satellite, but this would be beyond the scope of a remote sensing triggered forecast system. If this scenario of growth during the early stage of a bloom followed by advection was the case, it would suggest that a forecast system based only on the advection of passive particles such as the one described here would not account for all the processes involved, and that adding some biological behaviour to the particles would improve the representation of the bloom evolution. In this respect, the individual-based modelling of the development and transport of the strong 2006 K. *mikimotoi* bloom in Scotland reported in (Gillibrand et al. 2016) showed the potential benefit from better parameterisation of temperature dependence of both growth and mortality, albeit over a longer time frame. Their simulations clearly also showed the importance of advection in HAB transport and they conclude that their results would be improved by improvement of spatial and temporal resolution of the underlying hydrodynamical model, which agrees with our conclusions. Additionally, models aimed at predicting the onset of blooms using sea surface temperature and wind indices (Cusack et al. 2015; Karki et al. 2018) could be included to indicate the reliability of a short term advective forecast at a particular time.

Another possibility is that the advection was poorly forecast in the initial stages compared to the latter, due to some change in the physical conditions. Wind conditions can play an important role both for onset - for mid channel blooms low wind speeds are a factor in *K. mikimotoi* bloom formation (Gentien et al. 2007) - but also for its impact on advection itself. Direct and indirect wind forcing (the latter *via* wind waves) are key to predict surface advection (Röhrs et al. 2021). The PML model does not account for the Stokes drift, the resultant Lagrangian transport from surface waves, and this can be a significant component of drift. The highest frequency components drive the largest drift effect at the surface of the water, and are often wind waves (Röhrs et al. 2014; Tamtare et al. 2021). The wind speeds during both years were modest, though in the latter portion of both years after the second release, wind speeds were lower than during the initial period (**Figure 10**), which could suggest that either the advection is less well predicted during higher wind or the bloom dynamics are different.

4.2 Impact of Hydrodynamic Model Configuration in Particle Transport

We have presented several examples in which differences in model resolution and in other details of model configuration strongly influence particle dispersion and consequently HAB transport forecasts. The analysis of the autumn 2013 *D. acuta* event (section 3.4) clearly illustrates that different model configurations result in different trajectories of Lagrangian particles. We were able to compare four different model set-ups that differ in spatial resolution, model domain and model forcing (river input and open boundary forcing). Although there are some published results of particle tracking simulations of that 2013 event (Moita et al. 2016; Ruiz-Villarreal et al. 2016; Silva et al. 2016), the hydrodynamical conditions driving particle transport are only described in detail in (Ruiz-Villarreal et al. 2016), who report a northwards current on the shelf coinciding with the relaxation of upwelling winds around neap tides, which can be responsible of the along-shore transport of *D. acuta* from Portugal to Galicia. Surface currents and surface salinity at relevant dates during this event in our four different model configurations are plotted in **Figure 11**, where it is noticeable that shelf circulation off the rias and representation of rivers differs. Shelf currents are directed northwards in all configurations although there are differences in speed and current location on the shelf, note especially the strong northwards velocities in the MeteoGalicia results. These differences in model configurations result in the differences in particle transport evident in **Figure 6** and in Dispersal kernel indices, which we have seen in section 3.4. It is interesting to note that, in general, particles get advected more often to the north coast (longer mean transport) in the higher resolution configurations (MeteoGalicia and IEO RAIA nested), and this is especially clear when comparing IEO RAIA (4 km resolution) and IEO RAIA nested (1 km resolution). It is difficult to evaluate against observations the extent of the northwards transport in this event. The only available information is that *D. acuta* was not observed in the north coast HAB monitoring stations in the

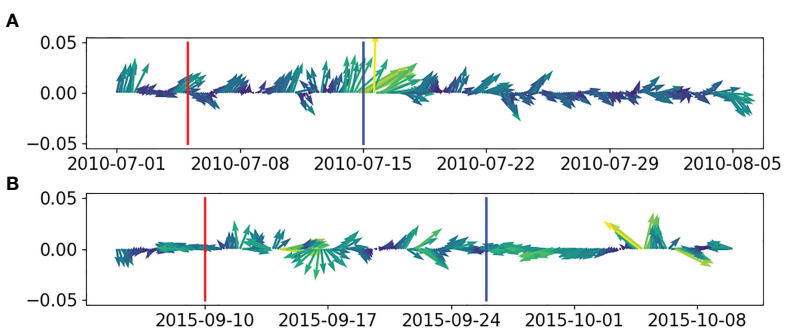

FIGURE 10 | Wind velocities during the PML model drifts in 2010 **(A)** and 2015 **(B)**. In both years the red line indicates the first particle release and the blue the second.

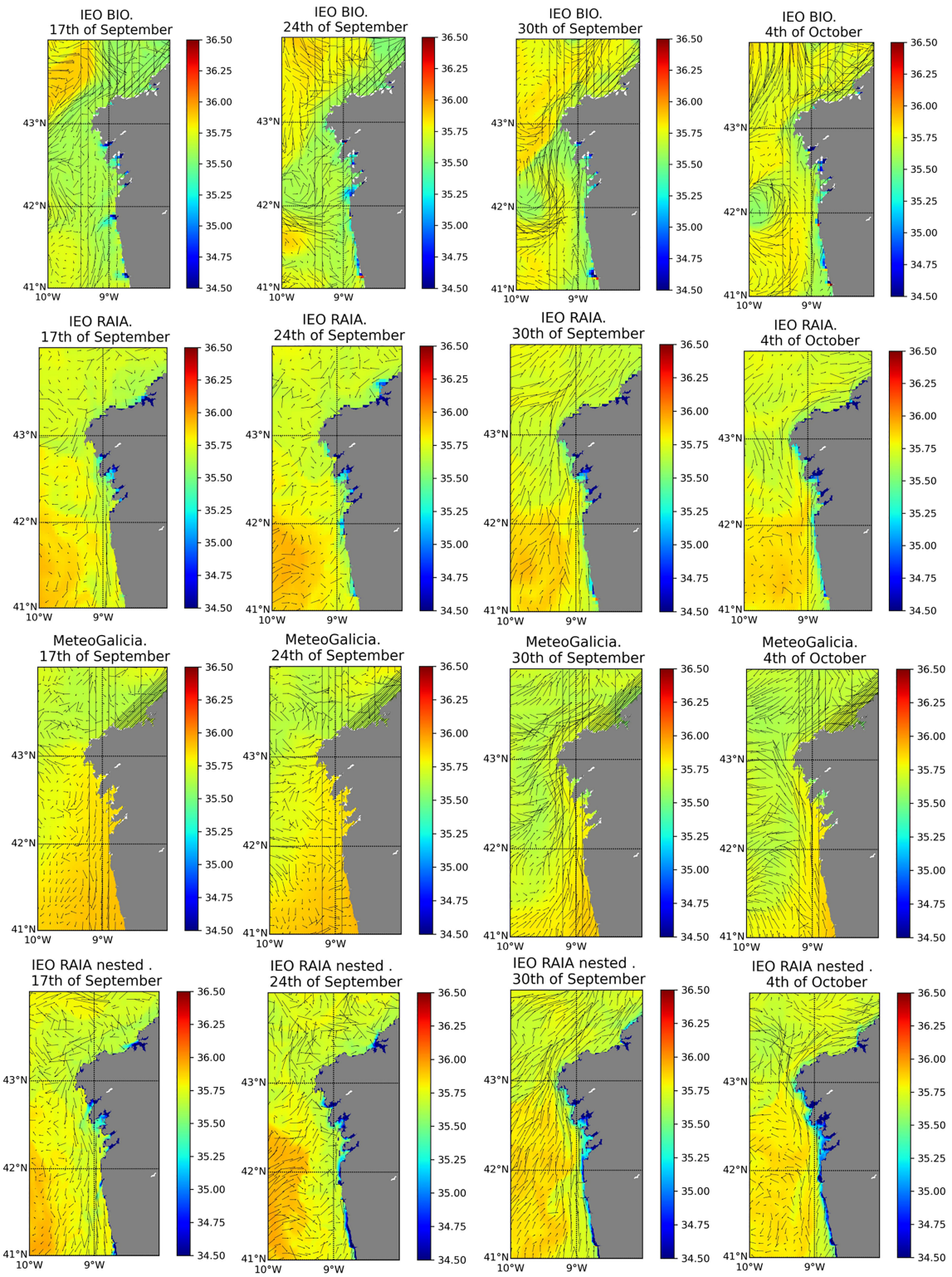

FIGURE 11 | Surface current velocities and surface salinities at relevant dates during the 2013 HAB event for the model configurations: IEO BIO, IEO RAIA, MeteoGalicia and IEO RAIA nested.

Ria de Ares, which could suggest that northwards advection was not so strong. The dependence on the resolution of the forcing hydrodynamic model has already been recognised in the literature, e.g. (Kvile et al. 2018; Nooteboom et al. 2020), who also report higher resolution appears to lead to greater transport, possibly from smaller scale effects being represented rather than diffused out. The impact of changing model resolution is also clear in the IFREMER 2003 model run (section 3.2), although the use of Eulerian and Lagrangian transport models in the two simulations does not allow us to isolate the impact of resolution in those results.

Differences in shelf circulation and dispersion of particles off the rias among the different IEO/MeteoGalicia model configurations could be partly attributable to the differences in river input, which are evident in surface salinity (**Figure 11**). IEO RAIA and IEO BIO configurations consider river run off from all rivers in Galicia and in the Portuguese shelf. MeteoGalicia configuration is forced by model predictions from SWAT for Galician rivers including Miño, but on the northern Portuguese shelf it only includes a climatological monthly average run-off from Douro river. Moreover, in these hindcast simulations, IEO RAIA and IEO BIO configurations are forced by real daily river run-off data, while MeteoGalicia includes river run-offs from the SWAT forecasts, which tends to underestimate peak flows (Venâncio et al., 2019). In addition, IEO RAIA and IEO BIO configurations are free runs, resulting in the freshwater budget on the shelf being well represented, while in MeteoGalicia configuration, the re-initialization with MyOcean model (Costa et al., 2012) implies that the freshwater budget at scales longer than the forecast cycle comes only from the rivers considered in the MyOcean model (Minho and Douro). The lower influence of river plumes in the dynamics could explain the fact that the higher resolution MeteoGalicia (2km) configuration, run in a model domain similar to IEO RAIA and with open boundaries from an operational model (as IEO BIO), seems to favour the underestimation of southwards transport of particles and the overestimation of northwards currents as seen in **Figure 11**, with the consequence that particles are mainly transported northwards in that model configuration.

The comparison of the IFREMER to PML model in the summer 2020 event (section 3.6) suggests that temporal resolution of the underlying hydrodynamic model used to force the Lagrangian model also has an effect. Whilst other studies have found temporal resolution to be potentially less important than spatial resolution (Qin et al. 2014; Kvile et al. 2018), here it meant that tidal currents were not included in the IFREMER Lagrangian simulations, and hence the physical forcing of the particle tracking was not represented equally. In spite of this, the limited evidence from the remote sensing suggests that the IFREMER model has done a better job in this case, at least on the eastern portion of the bloom, which was not advected onshore. This could indicate that tides were not the most relevant driver of particle transport in this particular case. There is also a difference in approach to diffusion, with the IFREMER model using an advective only setup in the horizontal and the PML model having spatially varying diffusion based on the underlying hydrodynamic model. However, for the short term forecasts, which are the aim of these operational systems, it is not expected that diffusion will have a great impact.

Our results showing divergence between models highlight the importance of the spatial and temporal variability of the model that forces the particle transport model. All these forcing models have lateral boundary conditions provided by coarser resolution models, the setup of which has an impact on the forecasts. In the September 2013 event in NW Iberia, we used different model set-ups and we could show that differences in model resolution, domain and river input impacted the transport model. Forcing at the open boundary was also different in models (climatology, one-way nesting or a larger operational model) and the comparison of IEO BIO and IEO RAIA results, showing that IEO BIO demonstrating higher variability offshore, indicates that forcing with an operational larger scale model impacts the resultant transport. A detailed sensitivity study of the impact of changes in lateral forcing in forecast models and in the associated particle transport is beyond the scope of this paper, since setting up operational boundary conditions for different upstream models is a complex process. Our results confirm however that it is necessary to evaluate the differences that model-set up (including resolution, freshwater input, and open boundary conditions) may induce in the dynamics predicted by the different hydrodynamic models, since the description of currents, frontal structures and well mixed/stratified areas may differ between circulation model setups and consequently have an impact on particle transport.

4.3 Use of Lagrangian Particle Tracking Simulations Within HAB Alert Systems

Early warning of the presence, location and subsequent evolution of HABs is the objective of a HAB alert system. A Lagrangian model based HAB alert system comprises three components: an initial detection component, for example from *in-situ* measurements or remote sensing; a Lagrangian model component to turn this into a forecast, the efficacy of which has been the focus of this study; and a dissemination component, to inform aquaculture producers and managers in charge of protection of human health of the risk that a HAB may affect aquaculture areas.

For HAB alert systems of high biomass species such as *Karenia* spp., which usually appear offshore in areas not routinely sampled by existing *in-situ* monitoring (concentrated in aquaculture production areas on the coast), detection of HAB risk to initiate the Lagrangian model comes from satellite imagery. The approach of *Karenia* spp. risk detection from remote sensing and then execution of particle tracking simulations is in use in the eastern Gulf of Mexico (Stumpf et al., 2009), and was demonstrated in the Scottish coast during ASIMUTH (Gillibrand et al., 2016). In this manuscript, we have illustrated in Section 3.6 that this approach has utility for assessing the advection of potential HAB species in the English Channel, especially *K. mikimotoi*, which appears frequently in the summer (Widdicombe et al., 2010; Barnes et al., 2015). This HAB forecast method is affected by the accuracy of the satellite

products to detect a bloom and discriminate the particular species, which can be harmful or not. In the example in Section 3.6 although the alert was activated by the *Karenia* spp. risk and models were run to provide forecast of an eventual HAB, no bloom of *Karenia* spp. at the *in situ* monitoring sites were observed see (Atkinson et al. 2021). HAB detection algorithms are being constantly improved to distinguish harmful from non-harmful high chlorophyll blooms (Cannizzaro et al. 2008; Tomlinson et al. 2009; Sourisseau et al. 2016), but there are still considerable challenges in species discrimination (Kurekin et al. 2014; Feng et al. 2022) and in distinguishing high turbidity from high chlorophyll concentrations of HAB species (Martinez-Vicente et al. 2020), this issue, and this will remain a source of error independent of the errors from the Lagrangian model.

We have also shown in this study (Sections 3.1) that remote sensing combined with Lagrangian particle modelling is useful to follow blooms of other potential HAB species like *Prorocentrum cordatum (minimum)*, which can form highly dense monospecific blooms. Blooms of *P. cordatum (minimum)* have been associated with anoxic/hypoxic events causing fish kills (Heil et al., 2005). Although there is debate about its toxicity (Heil et al., 2005; Turner et al., 2017), *P. cordatum* is currently monitored in bivalve aquaculture areas in Europe. Interestingly the HAB risk map aimed at *Karenia* spp. also indicated high likelihood of a bloom during this event[2], this could indicate a misidentification of species in this case and work discriminating the two, as has been done for *K. mikimotoi* and another *Prorocentrum* species (*P. donghaiense*) in (Feng et al. 2022), might be valuable for future HAB prediction. Finally, we have also demonstrated in section 3.3 that the Lagrangian particle simulations are a tool for tracking the evolution of high biomass blooms of the non-toxic *Mesodinium rubrum*, prey of *Dinophysis* spp.

For low biomass blooms like those of *Dinophysis* spp., initiation in the alert system relies only on the observations of the monitoring systems. If the monitoring systems detect the presence of the toxic species, it is an indication of the risk that a HAB could affect aquaculture sites. However, the monitoring only takes measurements of toxic species and toxins in aquaculture sites (located near the coast), but the bloom might be developing offshore, and then be transported to the sites. Therefore, the strategy chosen for HAB alerts of these species in the Galician early warning system is the constant release of particles in selected areas in Galicia as well as in Portugal as described in section 2.1.3. Our evaluation of the Galician system in September 2020 (section 3.5) confirmed that the Lagrangian-hydrodynamical coupled simulations provide predictions of favorable conditions of along-shore advection, exchanges between rías or flows in and out of the rías, and this is useful for characterising *Dinophysis* spp. HAB transport, confirming (Ruiz-Villarreal et al. 2016) conclusions. However, the results of the coupled hydrodynamical-Lagrangian simulations did not explain fully the sequence of events, which might be attributed to model uncertainties (misrepresentation of shelf dynamics, i.e river plumes, resolution not being high enough to resolve rías and fluxes between them, etc.), but also to the possibility of the HAB event being caused by local growth of *D.* acuminata and *D. acuta* and not by advective alongshore transport of *D. acuta* like in other autumns. The analysis of this HAB event clearly shows that although models are an important element of the early warning system, a HAB alert can only be issued in light of the measurements of the HAB monitoring system. When transnational alongshore transport is relevant, as in the presented simulations of *Dinophysis* spp. in Galicia and N Portugal (sections 3.4 and 3.5), transboundary exchange of information on HAB species and toxins between different HAB monitoring systems is crucial.

The final part of a HAB alert system is the dissemination to end-users. Hydrodynamic model simulations in the different areas are currently distributed *via* THREDDS (Thematic Realtime Environmental Distributed Data Services), a web data server that provides metadata and data access for scientific datasets using different remote data access protocols including Open Geospatial Consortium (OGC) standard protocols. The availability of model output in the THREDDS server allows us to obtain data *via* OPENDAP, HTTPserver or NetcdfSubset, but also *via* OGC Web Map Service (WMS) or Web Coverage Service (WCS) Interface Standards. However, a THREDDS server is not the best option for distributing non-gridded data, such as the Lagrangian model outputs. At IEO, the Lagrangian particle output files are transformed into shapefiles in order to be served through a GeoServer, which serves data using standard OGC protocols. In the GeoServer, the latest Lagrangian particle output from the daily run of the Lagrangian particle tracking simulations is served for visualization in viewers and data portals, including PRIMROSE data viewer. A similar approach is followed at IFREMER for distributing Lagrangian particle trajectories.

Presentation is a part of dissemination. Two differing presentations of Lagrangian trajectories for use in HAB forecast systems are shown in **Figure 12**. The IEO model runs regularly using the same starting locations, which have been identified as possible sources (see section 2.1.3). These are presented in a portal with the individual tracks shown, which allows rapid visualization of trajectories (**Figure 12A**). The PML model is initiated from remote sensing HAB algorithms, which as above come with an associated uncertainty (Kurekin et al. 2014). Also, all the advection models include a diffusion term which adds an element of stochasticity to the results which represents sub-grid scale processes. The PML output combines both sources of uncertainty (from the detection algorithm and from the diffusion of the particles). In this way, each particle is associated with the probability from the detection algorithm, then kernel density estimates are fitted to each particle release to give the probability distribution from advection component. These two probabilities are combined using a simple Bayesian approach to produce a single map of HAB probability (**Figure 12B**). Whilst this attempts to include the available information on uncertainty from all inputs to the model, the result is less clearly a drift product, which makes it less easily interpretable, possibly resulting in less uptake by, and thus value, to end users. However, given the uncertainties of the drift, either presentation is improved by an accompanying interpretation. These

[2]https://www.s3eurohab.eu/portal/?state=cf0d81 - accessed 2022/03/15.

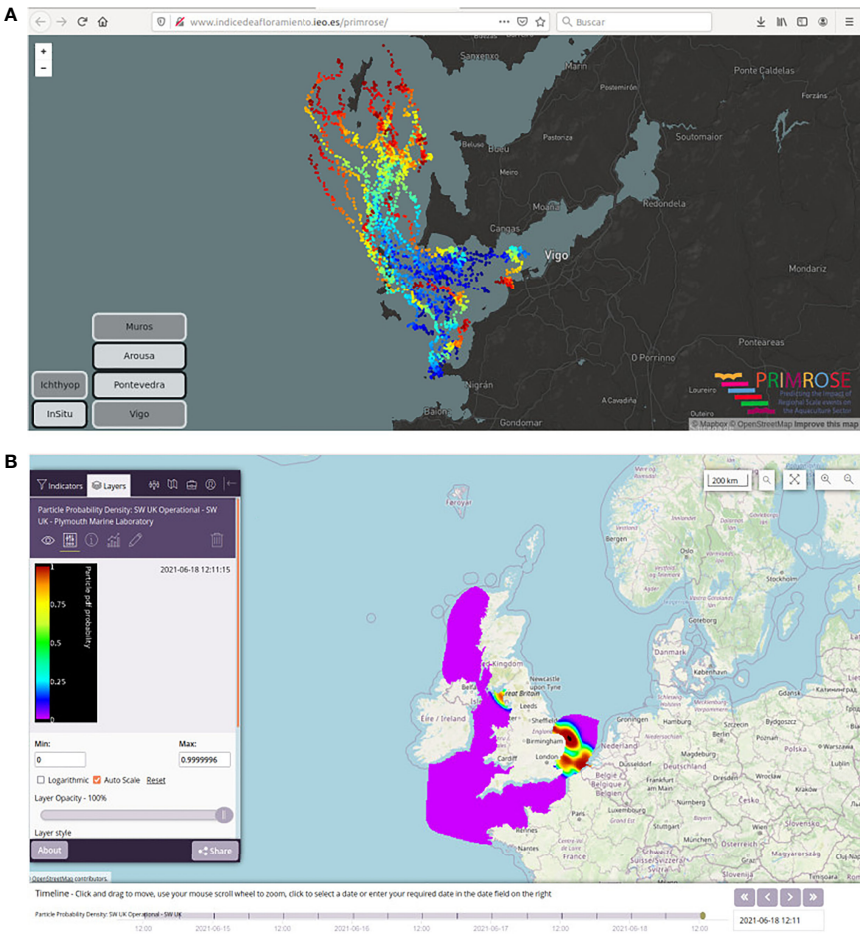

FIGURE 12 | Presentation of Lagrangian particle tracking operational results demonstrated during the PRIMROSE project. **(A)** Lagrangian particle forecast for Ría de Vigo corresponding to 29th September 2020 run as served by the IEO data viewer (http://www.indicedeafloramiento.ieo.es/primrose), also available at the PRIMROSE portal (https://primrose.eofrom.space/?state=ae63b8). Time is represented in the plot as colour for the particle positions, from blue at the start through to red three days after. **(B)** Lagrangian particle forecast from PML model corresponding to 18th June 2021 as served by the PRIMROSE portal (http://primrose.eofrom.space). The probability density field shows the probability of a bloom incurring on a particular location at a particular time step, considering both the probability of an accurate identification from the remote sensing algorithm and from the uncertainty in the predicted particle tracks.

forecasts are not usually presented in isolation; they more often form part of HAB bulletins or HAB report web sites, such as those produced in ASIMUTH (Cusack et al. 2016; Maguire et al. 2016; Ruiz-Villarreal et al. 2016; Silva et al. 2016) and PRIMROSE projects (Davidson et al. 2021; Fernandes-Salvador et al. 2021), this issue. HAB early warning system presentations add in local measurements, general oceanographic conditions and expert advice, along with advective forecasts, which help to mitigate the problems of interpretation and user uptake identified above.

5 SUMMARY AND CONCLUSIONS

- Particle tracking models have shown utility within an alert system to track movement of identified HABs between and around coastal areas over short timescales even when run with advection only, with models being easily run "offline" on saved hydrodynamic fields
- HAB early warning systems are based on the availability of information about the presence of HAB and on tools that predict the transport. The availability of routine forecasts is paramount for an early warning system, but our results clearly show that differences and limitations of the hydrodynamic model configurations strongly affect the simulated transport. Several metrics have been used to quantify the model performance with respect to satellite observations (in the case of high biomass blooms) and to compare the results of different model configurations run for the same event. We have illustrated in several events how differences in resolution, forcing and simulation domain cause differences in the predicted transport of HABs.
- For high biomass HAB blooms of *K. mikimotoi* and *P. cordatum (minimum)* such as those identified and simulated

in the Western Channel, there appeared to be distinct periods of growth and advection with the forecast model performing well only in the latter period. Reseeding and rerunning a forecast model during the initial period of a bloom is therefore of importance to provide forecasts of HAB advection.
- The analysis of *Dinophysis* spp. HAB events in West Iberia clearly shows that models are an important element of the early warning system, since Lagrangian-hydrodynamical coupled simulations provide predictions of favorable conditions of along-shore advection, exchanges between rías or flows in and out of the rías, and this is useful for characterising *Dinophysis* spp. HAB transport. However, HAB alert and evaluation of the forecast rely on the measurements of HAB monitoring systems. In areas like Galicia and N Portugal where transnational alongshore transport can be relevant, we have seen that transboundary exchange of information between different HAB monitoring systems is crucial.
- In future, short-term advective forecasts might be improved by adding a biological model or machine learning component to improve the prediction during the onset of blooms. Another direction for which these advective models might be important is the cross boundary, to alert between different currently discrete regional modelling systems (Maguire et al., 2016; Anderson et al., 2019). Nevertheless our results have shown that the choices underlying the hydrodynamic model setup also have a significant effect on the results and improvements to the understanding and implementation of these models is as important as adding extra features.
- Further improvement of HAB transport tools requires continuous improvements in hydrodynamic coastal models and further effort in analysing past events in order to improve the alert systems and of our understanding of HAB transport.

DATA AVAILABILITY STATEMENT

The raw data supporting the conclusions of this article will be made available by the authors, without undue reservation.

AUTHOR CONTRIBUTIONS

Each author ran their respective institutes models and initially collated the observations and supporting data relevant to their own model runs. All authors contributed to the analysis and discussion of the results and to manuscript preparation and writing.

FUNDING

This work has been funded by European Union Interreg Atlantic Area project PRIMROSE (EAPA182_2016). The development and execution of forecast model configurations as well as the distribution of model results in web services has received support from Interreg Atlantic Area project MyCoast (EAPA285_2016). IEO acknowledges complementary support for the development of a HAB early warning system in Galicia from project MarRISK (Interreg POCTEP Spain Portugal, 0262_MARRISK_1_E) and from Axencia Galega de Innovación (GAIN, Xunta de Galicia, Spain).

ACKNOWLEDGMENTS

Computations presented by IEO were performed at CESGA – Centro de Supercomputación de Galicia. We thank MeteoGalicia, especially Pedro Costa and Anabela Venâncio, for their assistance in efficiently accessing MeteoGalicia model output. We thank Alexandra Silva (IPMA) for providing *D. acuta* and *D. acuminata* data of N Portugal monitoring stations for September 2020. We thank Andrey Kurekin for provision of the raw HAB risk data for model comparison.

SUPPLEMENTARY MATERIAL

The Supplementary Material for this article can be found online at: https://www.frontiersin.org/articles/10.3389/fmars.2022.749071/full#supplementary-material

REFERENCES

Aleynik, D., Dale, A. C., Porter, M., and Davidson, K. (2016). A High Resolution Hydrodynamic Model System Suitable for Novel Harmful Algal Bloom Modelling in Areas of Complex Coastline and Topography. *Harmful Algae* 53, 102–117. doi: 10.1016/j.hal.2015.11.012

Anderson, C. R., Berdalet, E., Kudela, R. M., Cusack, C. K., Silke, J., O'Rourke, E., et al. (2019). Scaling Up From Regional Case Studies to a Global Harmful Algal Bloom Observing System. *Front. Mar. Sci.* 6. doi: 10.3389/fmars.2019.00250

Anderson, C. R., Kudela, R. M., Kahru, M., Chao, Y., Rosenfeld, L. K., Bahr, F. L., et al. (2016). Initial Skill Assessment of the California Harmful Algae Risk Mapping (C-HARM) System. *Harmful Algae* 59, 1–18. doi: 10.1016/j.hal.2016.08.006

Aoki, K., Onitsuka, G., Shimizu, M., Kuroda, H., Matsuyama, Y., Kimoto, K., et al. (2012). Factors Controlling the Spatio-Temporal Distribution of the 2009 *Chattonella Antiqua* Bloom in the Yatsushiro Sea, Japan. *Estuarine Coast. Shelf Sci.* 114, 148–155. doi: 10.1016/j.ecss.2012.08.028

Atkinson, A., McEvoy, A., Widdicombe, C., and Hiscock, K. (2021). "Plankton Observations," in *South-West Marine Ecosystems Report for 2020*. Eds. K. Hiscock and B. Earll (Plymouth, UK: Marine Biological Association of the UK), 12–18. doi: 10.17031/p2hc-rg17

Davidson, K., Whyte, C., Aleynik, D., Dale, A., Gontarek, S., Kurekin, A. A., et al. (2021). HAB Reports: Online Early Warning of Harmful Algal and Biotoxin Risk for the Scottish Shellfish and Finfish Aquaculture Industries. *Front. Mar. Sci.* 8, 631732. doi: 10.3389/fmars.2021.631732

Barnes, M. K., Tilstone, G. H., Smyth, T. J., Widdicombe, C. E., Gloël, J., Robinson, C., et al. (2015). Drivers and Effects of *Karenia Mikimotoi* Blooms in the Western English Channel. *Prog. Oceanography* 137, 456–469. doi: 10.1016/j.pocean.2015.04.018

Brand, L. E., Campbell, L., and Bresnan, E. (2012). Karenia: The Biology and Ecology of a Toxic Genus. *Harmful Algae* 14, 156–178. doi: 10.1016/j.hal.2011.10.020

Cannizzaro, J. P., Carder, K. L., Chen, F. R., Heil, C. A., and Vargo, G. A. (2008). A Novel Technique for Detection of the Toxic Dinoflagellate, *Karenia Brevis*, in

the Gulf of Mexico From Remotely Sensed Ocean Color Data. *Continental Shelf Res.* 28, 137–158. doi: 10.1016/j.csr.2004.04.007

Chen, C., Liu, H., and Beardsley, R. (2003). An Unstructured Grid, Finite-Volume, Three-Dimensional, Primitive Equations Ocean Model: Application to Coastal Ocean and Estuaries. *J. Atmospheric Oceanic Technol.* 20, 159–186. doi: 10.1175/1520-0426(2003)020<0159:AUGFVT>2.0.CO;2

Costa, P., Gómez, B., Venâncio, A., Pérez, E., and Pérez-Muñuzuri, V. (2012). Using the Regional Ocean Modelling System (ROMS) to Improve the Sea Surface Temperature Predictions of the MERCATOR Ocean System. *Scientia Marina* 76, 165–175. doi: 10.3989/scimar.03614.19E

Crawford, D., Purdie, D., Lockwood, A., and Weissman, P. (1997). Recurrent Red-Tides in the Southampton Water Estuary Caused by the Phototrophic Ciliate *Mesodinium Rubrum*. *Estuarine Coast. Shelf Sci.* 45, 799–812. doi: 10.1006/ecss.1997.0242

Cusack, C., Dabrowski, T., Lyons, K., Berry, A., Westbrook, G., Salas, R., et al. (2016). Harmful Algal Bloom Forecast System for SW Ireland. Part II: Are Operational Oceanographic Models Useful in a HAB Warning System. *Harmful Algae* 53, 86–101. doi: 10.1016/j.hal.2015.11.013

Cusack, C., Mouriño, H., Moita, M. T., and Silke, J. (2015). Modelling *Pseudo-Nitzschia* Events Off Southwest Ireland. *J. Sea Res.* 105, 30–41. doi: 10.1016/j.seares.2015.06.012

Davidson, K., Anderson, D. M., Mateus, M., Reguera, B., Silke, J., Sourisseau, M., et al. (2016). Forecasting the Risk of Harmful Algal Blooms. *Harmful Algae* 53, 1–7. doi: 10.1016/j.hal.2015.11.005

Davidson, K., Miller, P., Wilding, T. A., Shutler, J., Bresnan, E., Kennington, K., et al. (2009). A Large and Prolonged Bloom of Karenia Mikimotoi in Scottish Waters in 2006. *Harmful Algae* 8, 349–361. doi: 10.1016/j.hal.2008.07.007

Díaz, P. A., Ruiz-Villarreal, M., Pazos, Y., Moita, T., and Reguera, B. (2016). Climate Variability and *Dinophysis Acuta* Blooms in an Upwelling System. *Harmful Algae* 53, 145–159. doi: 10.1016/j.hal.2015.11.007

Elliott, J. A. (2012). Is the Future Blue-Green? A Review of the Current Model Predictions of How Climate Change Could Affect Pelagic Freshwater Cyanobacteria. *Water Res.* 46, 1364–1371. doi: 10.1016/j.watres.2011.12.018

Escalera, L., Reguera, B., Moita, T., Pazos, Y., Cerejo, M., Cabanas, J., et al. (2010). Bloom Dynamics of *Dinophysis Acuta* in an Upwelling System: *In Situ* Growth Versus Transport. *Harmful Algae* 9, 312–322. doi: 10.1016/j.hal.2009.12.002

Feng, C., Ishizaka, J., and Wang, S. (2022). A Simple Method for Algal Species Discrimination in East China Sea, Using Multiple Satellite Imagery. *Geosci. Lett.* 9, 1–9. doi: 10.1186/s40562-022-00222-1

Fernandes-Salvador, J. A., Davidson, K., Sourisseau, M., Revilla, M., Schmidt, W., Clarke, D., et al. (2021). Current Status of Forecasting Toxic Harmful Algae for the North-East Atlantic Shellfish Aquaculture Industry. *Front. Mar. Sci.* 8. doi: 10.3389/fmars.2021.666583

García-García, L. M., Ruiz-Villarreal, M., and Bernal, M. (2016). A Biophysical Model for Simulating Early Life Stages of Sardine in the Iberian Atlantic Stock. *Fisheries Res.* 173, 250–272. doi: 10.1016/j.fishres.2015.10.002

Gentien, P., Lunven, M., Lazure, P., Youenou, A., and Crassous, M.-P. (2007). Motility and Autotoxicity in *Karenia Mikimotoi* (Dinophyceae). *Philos. Trans. R. Soc. B: Biol. Sci.* 362, 1937–1946. doi: 10.1098/rstb.2007.2079

Gillibrand, P., Siemering, B., Miller, P., and Davidson, K. (2016). Individual-Based Modelling of the Development and Transport of a *Karenia Mikimotoi* Bloom on the North-West European Continental Shelf. *Harmful Algae* 53, 118–134. doi: 10.1016/j.hal.2015.11.011

Glibert, P. M., Allen, J. I., Bouwman, A., Brown, C. W., Flynn, K. J., Lewitus, A. J., et al. (2010). Modeling of HABs and Eutrophication: Status, Advances, Challenges. *J. Mar. Syst.* 83, 262–275. doi: 10.1016/j.jmarsys.2010.05.004

Hartman, S., Hartman, M., Hydes, D., Smythe-Wright, D., Gohin, F., and Lazure, P. (2014). The Role of Hydrographic Parameters, Measured From a Ship of Opportunity, in Bloom Formation of *Karenia Mikimotoi* in the English Channel. *J. Mar. Syst.* 140, 39–49. doi: 10.1016/j.jmarsys.2014.07.001

Heil, C. A., Glibert, P. M., and Fan, C. (2005). *Prorocentrum Minimum* (Pavillard) Schiller: A Review of a Harmful Algal Bloom Species of Growing Worldwide Importance. *Harmful Algae* 4, 449–470. doi: 10.1016/j.hal.2004.08.003

Hiscock, K., Earll, B., Smyth, T., Atkinson, A., Hiscock, K., Herdson, D., et al. (2016) *South-West Marine Ecosystems in 2015*. Available at: https://swmecosystems.co.uk/wp-content/uploads/2016/02/SWME-2015-collated_reports_final_December.pdf.

Hu, C., Muller-Karger, F. E., Taylor, C. J., Carder, K. L., Kelble, C., Johns, E., et al. (2005). Red Tide Detection and Tracing Using MODIS Fluorescence Data: A Regional Example in SW Florida Coastal Waters. *Remote Sens. Environ.* 97, 311–321. doi: 10.1016/j.rse.2005.05.013

Huret, M., Petitgas, P., and Woillez, M. (2010). Dispersal Kernels and Their Drivers Captured With a Hydrodynamic Model and Spatial Indices: A Case Study on Anchovy (*Engraulis Encrasicolus*) Early Life Stages in the Bay of Biscay. *Prog. Oceanogr.* 87, 6–17. doi: 10.1016/j.pocean.2010.09.023

Johnson, M. D., Stoecker, D. K., and Marshall, H. G. (2013). Seasonal Dynamics of *Mesodinium Rubrum* in Chesapeake Bay. *J. Plankton Res.* 35, 877–893. doi: 10.1093/plankt/fbt028

Jordan, C., Cusack, C., Tomlinson, M. C., Meredith, A., McGeady, R., Salas, R., et al. (2021). Using the Red Band Difference Algorithm to Detect and Monitor a Karenia Spp. Bloom Off the South Coast of Ireland, June 2019. *Front. Mar. Sci.* 8. doi: 10.3389/fmars.2021.638889

Karki, S., Sultan, M., Elkadiri, R., and Elbayoumi, T. (2018). Mapping and Forecasting Onsets of Harmful Algal Blooms Using MODIS Data Over Coastal Waters Surrounding Charlotte County, Florida. *Remote Sens.* 10, 1656. doi: 10.3390/rs10101656

Kurekin, A., Miller, P., and van der Woerd, H. (2014). Satellite Discrimination of *Karenia Mikimotoi* and *Phaeocystis* Harmful Algal Blooms in European Coastal Waters: Merged Classification of Ocean Colour Data. *Harmful Algae* 31, 163–176. doi: 10.1016/j.hal.2013.11.003

Kutser, T., Metsamaa, L., Vahtmäe, E., and Strömbeck, N. (2006). Suitability of MODIS 250 M Resolution Band Data for Quantitative Mapping of Cyanobacterial Blooms. Proceedings of the Estonian Academy of Sciences. Biology. *Ecology* 55, 318–328. doi: 10.3176/biol.ecol.2006.4.04

Kvile, K.Ø., Romagnoni, G., Dagestad, K.-F., Langangen, Ø., and Kristiansen, T. (2018). Sensitivity of Modelled North Sea Cod Larvae Transport to Vertical Behaviour, Ocean Model Resolution and Interannual Variation in Ocean Dynamics. *ICES J. Mar. Sci.* 75, 2413–2424. doi: 10.1093/icesjms/fsy039

Lazure, P., and Dumas, F. (2008). An External–Internal Mode Coupling for a 3d Hydrodynamical Model for Applications at Regional Scale (MARS). *Adv. Water Resour.* 31, 233–250. doi: 10.1016/j.advwatres.2007.06.010

Lee, J. H., and Qu, B. (2004). Hydrodynamic Tracking of the Massive Spring 1998 Red Tide in Hong Kong. *J. Environ. Eng.* 130, 535–550. doi: 10.1061/(ASCE)0733-9372(2004)130:5(535

Le, C., Hu, C., Cannizzaro, J., English, D., Muller-Karger, F., and Lee, Z. (2013). Evaluation of Chlorophyll-a Remote Sensing Algorithms for an Optically Complex Estuary. *Remote Sens. Environ.* 129, 75–89. doi: 10.1016/j.rse.2012.11.001

Lellouche, J.-M., Le Galloudec, O., Drévillon, M., Régnier, C., Greiner, E., Garric, G., et al. (2013). Evaluation of Global Monitoring and Forecasting Systems at Mercator Océan. *Ocean Sci.* 9, 57–81. doi: 10.5194/os-9-57-2013

Lett, C., Verley, P., Mullon, C., Parada, C., Brochier, T., Penven, P., et al. (2008). A Lagrangian Tool for Modelling Ichthyoplankton Dynamics. *Environ. Model. Software* 23, 1210–1214. doi: 10.1016/j.envsoft.2008.02.005

Lien, G.-Y., Kalnay, E., Miyoshi, T., and Huffman, G. J. (2016). Statistical Properties of Global Precipitation in the NCEP GFS Model and TMPA Observations for Data Assimilation. *Monthly Weather Rev.* 144, 663–679. doi: 10.1175/MWR-D-15-0150.1

Lin, J., Miller, P. I., Jönsson, B. F., and Bedington, M. (2021). Early Warning of Harmful Algal Bloom Risk Using Satellite Ocean Color and Lagrangian Particle Trajectories. *Front. Mar. Sci.* 8. doi: 10.3389/fmars.2021.736262

Maguire, J., Cusack, C., Ruiz-Villarreal, M., Silke, J., McElligott, D., and Davidson, K. (2016). Applied Simulations and Integrated Modelling for the Understanding of Toxic and Harmful Algal Blooms (ASIMUTH): Integrated HAB Forecast Systems for Europe's Atlantic Arc. *Harmful Algae* 53, 160–166. doi: 10.1016/j.hal.2015.11.006

Marta-Almeida, M., Ruiz-Villarreal, M., Pereira, J., Otero, P., Cirano, M., Zhang, X., et al. (2013). Efficient Tools for Marine Operational Forecast and Oil Spill Tracking. *Mar. pollut. Bull.* 71, 139–151. doi: 10.1016/j.marpolbul.2013.03.022

Martinez-Vicente, V., Kurekin, A., Sá, C., Brotas, V., Amorim, A., Veloso, V., et al. (2020). Sensitivity of a Satellite Algorithm for Harmful Algal Bloom Discrimination to the Use of Laboratory Bio-Optical Data for Training. *Front. Mar. Sci.* 7. doi: 10.3389/fmars.2020.582960

Martino, S., Gianella, F., and Davidson, K. (2020). An Approach for Evaluating the Economic Impacts of Harmful Algal Blooms: The Effects of Blooms of Toxic *Dinophysis* Spp. On the Productivity of Scottish Shellfish Farms. *Harmful Algae* 99, 101912. doi: 10.1016/j.hal.2020.101912

Mateus, M., Fernandes, J., Revilla, M., Ferrer, L., Villarreal, M. R., Miller, P., et al. (2019). "Early Warning Systems for Shellfish Safety: The Pivotal Role of Computational Science," in *Computational Science – ICCS 2019*. Eds. J. M. F. Rodrigues, P. J. S. Cardoso, J. Monteiro, R. Lam, V. V. Krzhizhanovskaya, M. H. Lees, J. J. Dongarra and P. M. Sloot (Cham: Springer International Publishing), 361–375. doi: 10.1007/978-3-030-22747-0_28

McManus, M. A., Kudela, R. M., Silver, M. W., Steward, G. F., Donaghay, P. L., and Sullivan, J. M. (2008). Cryptic Blooms: Are Thin Layers the Missing Connection? Estuaries and Coasts 31, 396–401. doi: 10.1007/s12237-007-9025-4

Mercator (2016). *Global Ocean 1/12° Physics Analysis and Forecast Updated Dail.* (Mercator Ocean, France: Copernicus Marine Service). doi: 10.48670/MOI-00016

Mishra, S., and Mishra, D. R. (2012). Normalized Difference Chlorophyll Index: A Novel Model for Remote Estimation of Chlorophyll-a Concentration in Turbid Productive Waters. *Remote Sens. Environ.* 117, 394–406. doi: 10.1016/j.rse.2011.10.016

Moita, M. T., Pazos, Y., Rocha, C., Nolasco, R., and Oliveira, P. B. (2016). Toward Predicting *Dinophysis* Blooms Off NW Iberia: A Decade of Events. *Harmful Algae* 53, 17–32. doi: 10.1016/j.hal.2015.12.002

Nooteboom, P. D., Delandmeter, P., van Sebille, E., Bijl, P. K., Dijkstra, H. A., and von der Heydt, A. S. (2020). Resolution Dependency of Sinking Lagrangian Particles in Ocean General Circulation Models. *PLoS One* 15, e0238650. doi: 10.1371/journal.pone.0238650

O'Boyle, S., McDermott, G., Silke, J., and Cusack, C. (2016). Potential Impact of an Exceptional Bloom of *Karenia Mikimotoi* on Dissolved Oxygen Levels in Waters Off Western Ireland. *Harmful Algae* 53, 77–85. doi: 10.1016/j.hal.2015.11.014

O'Dea, E., Arnold, A., Edwards, K., Furner, R., Hyder, P., Martin, M., et al. (2012). An Operational Ocean Forecast System Incorporating NEMO and SST Data Assimilation for the Tidally Driven European North-West Shelf. *J. Operational Oceanography* 5, 3–17. doi: 10.1080/1755876X.2012.11020128

Otero, P., and Ruiz-Villarreal, M. (2008). Wind Forcing of the Coastal Circulation Off North and Northwest Iberia: Comparison of Atmospheric Models. *J. Geophysical Research-Oceans* 113, C10019. doi: 10.1029/2008JC004740

Otero, P., Ruiz-Villarreal, M., Allen-Perkins, S., Vila, B., and Cabanas, J. (2014). Coastal Exposure to Oil Spill Impacts From the Finisterre Traffic Separation Scheme. *Mar. Pollut. Bull.* 85, 67–77. doi: 10.1016/j.marpolbul.2014.06.020

Otero, P., Ruiz-Villarreal, M., García-García, L., González-Nuevo, G., and Cabanas, J. M. (2013). Coastal Dynamics Off Northwest Iberia During a Stormy Winter Period. *Ocean Dynamics* 63, 115–129. doi: 10.1007/s10236-012-0585-x

Otero, P., Ruiz-Villarreal, M., and Peliz, A. (2008). Variability of River Plumes Off Northwest Iberia in Response to Wind Events. *J. Mar. Syst.* 72, 238–255. doi: 10.1016/j.jmarsys.2007.05.016

Otero, P., Ruiz-Villarreal, M., and Peliz, A. (2009). River Plume Fronts Off NW Iberia From Satellite Observations and Model Data. *ICES J. Mar. Sci.* 66 (9), 1853–64. doi: 10.1093/icesjms/fsp156

Paerl, H. W., and Huisman, J. (2008). CLIMATE: Blooms Like It Hot. *Science* 320, 57–58. doi: 10.1126/science.1155398

Pinto, L., Mateus, M., and Silva, A. (2016). Modeling the Transport Pathways of Harmful Algal Blooms in the Iberian Coast. *Harmful Algae* 53, 8–16. doi: 10.1016/j.hal.2015.12.001

Pitcher, G., Figueiras, F., Hickey, B., and Moita, M. (2010). The Physical Oceanography of Upwelling Systems and the Development of Harmful Algal Blooms. *Prog. Oceanogr.* 85, 5–32. doi: 10.1016/j.pocean.2010.02.002

Qin, X., van Sebille, E., and Gupta, A. S. (2014). Quantification of Errors Induced by Temporal Resolution on Lagrangian Particles in an Eddy-Resolving Model. *Ocean Model.* 76, 20–30. doi: 10.1016/j.ocemod.2014.02.002

Qurban, M. A. B. (2009). *An Investigation of Factors Influencing the Spatial and Temporal Distribution of Surface Phytoplankton in the English Channel and Bay of Biscay in 2003 and 2004* (Doctoral dissertation, University of Southampton).

Ralston, D. K., and Moore, S. K. (2020). Modeling Harmful Algal Blooms in a Changing Climate. *Harmful Algae* 91, 101729. doi: 10.1016/j.hal.2019.101729

Redalje, D. G., Lohrenz, S. E., Natter, M., Tuel, M., Kirkpatrick, G., Millie, D., et al. (2008). The Growth Dynamics of *Karenia Brevis* Within Discrete Blooms on the West Florida Shelf. *Continental Shelf Res.* 28, 24–44. doi: 10.1016/j.csr.2007.04.011

REPHY (2021). REPHY Dataset - French Observation and Monitoring Program for Phytoplankton and Hydrology in Coastal Waters. *Metropolitan data. SEANOE*. doi: 10.17882/47248

Röhrs, J., Christensen, K. H., Vikebø, F., Sundby, S., Saetra, Ø., and Broström, G. (2014). Wave-Induced Transport and Vertical Mixing of Pelagic Eggs and Larvae. *Limnology Oceanography* 59, 1213–1227. doi: 10.4319/lo.2014.59.4.1213

Röhrs, J., Sutherland, G., Jeans, G., Bedington, M., Sperrevik, A. K., Dagestad, K.-F., et al. (2021). Surface Currents in Operational Oceanography: Key Applications, Mechanisms, and Methods. *J. Operational Oceanogr.* 0, 1–29. doi: 10.1080/1755876X.2021.1903221

Ruiz-Villarreal, M., García-García, L. M., Cobas, M., Díaz, P. A., and Reguera, B. (2016). Modelling the Hydrodynamic Conditions Associated With *Dinophysis* Blooms in Galicia (NW Spain). *Harmful Algae* 53, 40–52. doi: 10.1016/j.hal.2015.12.003

Ruiz-Villarreal, M., Sourisseau, M., Anderson, P., Cusack, C., Neira, P., Silke, J., et al. (2022). Novel Methodologies for Providing *in Situ* Data to HAB Early Warning Systems in the European Atlantic Area: The Primrose Experience. *Front. Mar. Sci.* 9. doi: 10.3389/fmars.2022.791329

Sathyendranath, S., Brewin, R. J., Brockmann, C., Brotas, V., Calton, B., Chuprin, A., et al. (2019). An Ocean-Colour Time Series for Use in Climate Studies: The Experience of the Ocean-Colour Climate Change Initiative (OC-CCI). *Sensors* 19, 4285. doi: 10.3390/s19194285

Silva, A., Pinto, L., Rodrigues, S., de Pablo, H., Santos, M., Moita, T., et al. (2016). A HAB Warning System for Shellfish Harvesting in Portugal. *Harmful Algae* 53, 33–39. doi: 10.1016/j.hal.2015.11.017

Simpson, J. H., and Sharples, J. (2012). *Introduction to the Physical and Biological Oceanography of Shelf Seas* (Cambridge: Cambridge University Press).

Smythe-Wright, D., Daniel, A., Boswell, S., Purcell, D., Hartman, M., Hartman, S., et al. (2014). Phytoplankton and Pigment Studies in the Bay of Biscay and English Channel. *Deep Sea Res. Part II: Topical Stud. Oceanography* 106, 76–86. doi: 10.1016/j.dsr2.2013.12.015

Soto, I. M., Cannizzaro, J., Muller-Karger, F. E., Hu, C., Wolny, J., and Goldgof, D. (2015). Evaluation and Optimization of Remote Sensing Techniques for Detection of *Karenia Brevis* Blooms on the West Florida Shelf. *Remote Sens. Environ.* 170, 239–254. doi: 10.1016/j.rse.2015.09.026

Sourisseau, M., Jegou, K., Lunven, M., Quere, J., Gohin, F., and Bryere, P. (2016). Distribution and Dynamics of Two Species of Dinophyceae Producing High Biomass Blooms Over the French Atlantic Shelf. *Harmful Algae* 53, 53–63. doi: 10.1016/j.hal.2015.11.016

Stumpf, R. P., Tomlinson, M. C., Calkins, J. A., Kirkpatrick, B., Fisher, K., Nierenberg, K., et al. (2009). Skill Assessment for an Operational Algal Bloom Forecast System. *J. Mar. Syst.* 76, 151–161. doi: 10.1016/j.jmarsys.2008.05.016

Tamtare, T., Dumont, D., and Chavanne, C. (2021). The Stokes Drift in Ocean Surface Drift Prediction. *J. Operational Oceanogr.* 0, 1–13. doi: 10.1080/1755876X.2021.1872229

Tomlinson, M., Wynne, T., and Stumpf, R. (2009). An Evaluation of Remote Sensing Techniques for Enhanced Detection of the Toxic Dinoflagellate *Karenia Brevis*. *Remote Sens. Environ.* 113, 598–609. doi: 10.1016/j.rse.2008.11.003

Tonani, M., Sykes, P., King, R. R., McConnell, N., Péquignet, A.-C., O'Dea, E., et al. (2019). The Impact of a New High-Resolution Ocean Model on the Met Office North-West European Shelf Forecasting System. *Ocean Sci.* 15, 1133–1158. doi: 10.5194/os-15-1133-2019

Trowbridge, C., Davenport, J., Plowman, C., Harman, L., and McAllen, R. (2017). Marine Aloricate Ciliate Red Tides in a Temperate Irish Sea Lough. *Mar. Biodiversity* 47, 869–878. doi: 10.1007/s12526-016-0520-3

Turner, A. D., Dhanji-Rapkova, M., Coates, L., Bickerstaff, L., Milligan, S., O'Neill, A., et al. (2017). Detection of Tetrodotoxin Shellfish Poisoning (TSP) Toxins and Causative Factors in Bivalve Molluscs From the UK. *Mar. Drugs* 15 (9), 277. doi: 10.3390/md15090277

UK Food Standards Agency (2020) *Phytoplankton Results for England and Wales*. Available at: https://data.gov.uk/dataset/9a86b044-58a3-46d0-8455-5046f5769627/phytoplankton-results-for-england-and-wales.

Uncles, R., Clark, J., Bedington, M., and Torres, R. (2020). "Chapter 31 - On Sediment Dispersal in the Whitsand Bay Marine Conservation Zone: Neighbour to a Closed Dredge-Spoil Disposal Site," in *Marine Protected Areas*. Eds. J. Humphreys and R. W. Clark (Amsterdam, Netherlands: Elsevier), 599–629. doi: 10.1016/B978-0-08-102698-4.00031-9

Vandal, T., and Nemani, R. (2019). "Temporal Interpolation of Geostationary Satellite Imagery With Task Specific Optical Flow," in *Arxiv Preprint Arxiv*, vol. 1907, 12013. doi: 10.48550/ARXIV.1907.12013

Vanhoutte-Brunier, A., Fernand, L., Ménesguen, A., Lyons, S., Gohin, F., and Cugier, P. (2008). Modelling the *Karenia Mikimotoi* Bloom That Occurred in the Western English Channel During Summer 2003. *Ecol. Model.* 210, 351–376. doi: 10.1016/j.ecolmodel.2007.08.025

Velo-Suárez, L., Reguera, B., González-Gil, S., Lunven, M., Lazure, P., Nézan, E., et al. (2010). Application of a 3D Lagrangian Model to Explain the Decline of a *Dinophysis Acuminata* Bloom in the Bay of Biscay. *J. Mar. Syst.* 83, 242–252. doi: 10.1016/j.jmarsys.2010.05.011

Venâncio, A., Montero, P., Costa, P., Regueiro, S., Brands, S., and Taboada, J. (2019). "An Integrated Perspective of the Operational Forecasting System in Rías Baixas (Galicia, Spain) With Observational Data and End-Users," in *Computational Science – ICCS 2019*. Eds. J. M. F. Rodrigues, P. J. S. Cardoso, J. Monteiro, R. Lam, V. V. Krzhizhanovskaya, M. H. Lees, J. J. Dongarra and P. M. Sloot (Cham: Springer International Publishing). doi: 10.1007/978-3-030-22747-0_18

Wells, M. L., Karlson, B., Wulff, A., Kudela, R., Trick, C., Asnaghi, V., et al. (2020). Future HAB Science: Directions and Challenges in a Changing Climate. *Harmful Algae* 91, 101632. doi: 10.1016/j.hal.2019.101632

Widdicombe, C. E., Eloire, D., Harbour, D., Harris, R. P., and Somerfield, P. J. (2010). Long-Term Phytoplankton Community Dynamics in the Western English Channel. *J. Plankton Res.* 32, 643–655. doi: 10.1093/plankt/fbp127

Woillez, M., Rivoirard, J., and Petitgas, P. (2009). Notes on Survey-Based Spatial Indicators for Monitoring Fish Populations. *Aquat. Living Resour.* 22, 155–164. doi: 10.1051/alr/2009017

Conflict of Interest: The authors declare that the research was conducted in the absence of any commercial or financial relationships that could be construed as a potential conflict of interest.

Advantages of publishing in Frontiers

OPEN ACCESS
Articles are free to read for greatest visibility and readership

FAST PUBLICATION
Around 90 days from submission to decision

HIGH QUALITY PEER-REVIEW
Rigorous, collaborative, and constructive peer-review

TRANSPARENT PEER-REVIEW
Editors and reviewers acknowledged by name on published articles

Frontiers
Avenue du Tribunal-Fédéral 34
1005 Lausanne | Switzerland

Visit us: www.frontiersin.org
Contact us: frontiersin.org/about/contact

REPRODUCIBILITY OF RESEARCH
Support open data and methods to enhance research reproducibility

DIGITAL PUBLISHING
Articles designed for optimal readership across devices

FOLLOW US
@frontiersin

IMPACT METRICS
Advanced article metrics track visibility across digital media

EXTENSIVE PROMOTION
Marketing and promotion of impactful research

LOOP RESEARCH NETWORK
Our network increases your article's readership